分子磁性の超分子的制御

（研究課題番号　13640575）

平成 13～15 年度科学研究費補助金（基盤研究 (C)(2)）

研究成果報告書

平成１６年３月

研究代表者　石 田 尚 行

（電気通信大学電気通信学部助教授）

はしがき

分子磁性という学問分野は我国が世界に誇れる基幹物理化学の一つである。これまでに有機強磁性体や超高スピン分子の開発において世界のリードを取ってきたことはあらためて言うまでもない。ところで、基礎的研究面での多大な成功の一方で、残念ながら分子磁性材料の応用面への研究は立ち後れている。本研究では、分子性磁性材料開発に、分子性物質ならではといったような特性を付与することを目指した。すなわち、分子性磁性材料の将来は、旧来の無機材料系磁性体の用途とは異なる指向を持たねばならない、と位置づけた。その結果、研究題目にあるとおり、超分子化学の適用により磁気的相転移温度を変化させることが可能な化合物等を開発することができ、一定の成果が得られたと思う。

本補助金の交付に対して、文部科学省に心より感謝申し上げる。

研究組織

研究代表者：　石田尚行（電気通信大学電気通信学部助教授）
研究分担者：　野上　隆（電気通信大学電気通信学部教授）

研究経費

平成１３年度：　１，９００千円
平成１４年度：　１，０００千円
平成１５年度：　　７００千円
計　　３，６００千円

研究報告

学会誌等

1) 「超分子的に制御できる分子磁性」(**M**olecule-Based **M**agnets Tunable by **M**eans of Supra**m**olecular Che**m**istry) 石田尚行・野上　隆、日本応用磁気学会誌〜トピックス〜、27, 811-816 (2003).
2) "Pressure Effects of Genuine Organic Crystalline Ferromagnet Possessing Intermolecular Contacts between Nitroxide Oxygen and Methyl Hydrogen Atoms," M. Mito, T. Kawae, M. Hitaka, K. Takeda, T. Ishida, and T. Nogami, *Chem. Phys. Lett.,* **333**, 69-75 (2001).
3) "Single-Component Organic Semiconductors Based on Novel Radicals that Exhibit Electrochemical Amphotericity: Preparation, Crystal Structures, and Solid-State Properties of *N,N'*-Dicyanopyrazinonaphthoquinodiiminides Substituted with an *N*-Alkylpyrimidinium Unit," T. Suzuki, S. Miyanari, Y. Tsubata, T. Fukushima, T. Miyashi, Y. Yamashita, K. Imaeda, T. Ishida, and T. Nogami, *J. Org. Chem.*, **66**, 216-224 (2001).
4) "Dipyrimidine-Cu(II) Dinitrate Complexes Showing Magnetic Interactions," M. Yasui, Y. Ishikawa, N. Akiyama, T. Ishida, T. Nogami, and F. Iwasaki, *Acta Crystallogr., Sect. B*, **57**, 288-295 (2001).
5) "Radical-Copper Wheels: Structure and Magnetism of Hexanuclear Hybrid Arrays," J. Omata, T. Ishida, D. Hashizume, F. Iwasaki, and T. Nogami, *Inorg. Chem.*, **40**, 3954-3958 (2001).
6) "Ferromagnetic Exchange Coupling of Vanadium(IV) dπ Spins across Pyrimidine Rings: Dinuclear Complexes of Oxovanadium(IV) Bis(1,1,1,5,5,5-hexafluoropentane-2,4-dionate) Bridged by Pyrimidine Derivatives," T. Ishida, S. -i. Mitsubori, T. Nogami, N. Takeda, M. Ishikawa, and H. Iwamura, *Inorg. Chem.*, **40**, 7059-7064 (2001).
7) "Bis(hfac)-Copper(II) Complexes Bridged by Pyrimidines Showing Magnetic Interactions," M. Yasui, Y. Ishikawa, T. Ishida, T. Nogami, and F. Iwasaki, *Acta Crystallogr., Sect. B*, **57**, 772-779 (2001).
8) "Synthesis and Properties of New Oxygen-Containing Fulvalene Derivatives: Dibenzo- and Dinaphthotetraoxafulvalenes and Dibenzodioxadithiafulvalene," T. Nogami, K. Tanaka, T. Ishida, and A. Kobayashi, *Synth. Met.*, **120**, 755-756 (2001).
9) "Zero-Field Muon Spin Rotation Study on TEMPO-Based Magnets, Ar-CH=N-TEMPO," T. Ishida, S. Ohira, I. Watanabe, T. Nogami, and K. Nagamine, *Polyhedron*, **20**, 1545-1549 (2001).
10) "Ferromagnetic $S = 1$ Chain Formed by a Square Ni_2S_2 Motif in $Ni(qt)_2$ (qt = Quinoline-8-thiolate). Magnetic Properties of Related Compounds," T. Miyake, T. Ishida, D. Hashizume, F. Iwasaki, and T. Nogami, *Polyhedron*, **20**, 1551-1555 (2001).
11) "Radical-Copper Hexanuclear Arrays Showing Ferromagnetic Interactions," J. Omata, T. Ishida, D. Hashizume, F. Iwasaki, and T. Nogami, *Polyhedron*, **20**, 1557-1561 (2001).
12) "Anomalous Magnetism in Organic Radical Ferromagnets, 4-Arylmethyleneamino-2,2,6,6-tetramethylpiperidin-1-yloxyl just above *Tc* Studied by μSR Method," S. Ohira, T. Ise, K. Nakayama, T. Ishida, T. Nogami, I. Watanabe, and K. Nagamine, *Polyhedron*, **20**, 772-779 (2001).
13) "Novel Organic-Inorganic Molecular Assembly: a Copper(I) and Copper(II) Mixed-Valent Cluster with Bromide Bridges and Paramagnetic Ligands." T. Katayama, T. Ishida, and T. Nogami, *Inorg. Chim. Acta*, **329**, 31-35 (2002).

14) "Low-Temperature Heat Capacity and One-Dimensional Ferromagnetic Behavior of the Organic Free Radical, 4-Benzylideneamino-2,2,6,6-tetramethylpiperidin-1-oxyl (BATMP)," T. Sakakibara, Y. Miyazaki, T. Ishida, T. Nogami, and M. Sorai, *J. Phys. Chem. B*, **106**, 6390-6394 (2002).
15) "Antiferromagnetic Coupling of Transition Metal Spins across Pyrimidine and Pyrazine Bridges in Dinuclear Manganese(II), Cobalt(II), Nickel(II), and Copper(II) 1,1,1,5,5,5-Hexafluoropentane-2,4-dionate Complexes," T. Ishida, T. Kawakami, S.-i. Mitsubori, T. Nogami, K. Yamaguchi, and H. Iwamura, *J. Chem. Soc., Dalton Trans.*, **2002**, 3177-3186.
16) "Convenient Synthesis and Host-Guest Compounds of 9,9'(10*H*,10'*H*)-Spirobiacridines," M. Ooishi, M. Seino, R. Imachi, T. Ishida, and T. Nogami, *Tetrahedron Lett.*, **43**, 5521-5524 (2002).
17) "Metal-Azide-Pyrimidine Complexes $M(N_3)_2$(pm) with a Three-Dimensional Network Showing Weak Ferromagnetism for M = Mn and Fe and Antiferromagnetism for M = Co and Ni," Y. Doi, T. Ishida, and T. Nogami, *Bull. Chem. Soc. Jpn.*, **75**, 2455-2461 (2002).
18) "Crystal Structures and Magnetic Properties of Copper(II) Hexafluoroacetylacetonate Complexes with hnn and hin and Manganese(II) Hexafluoroacetylacetonate Complexes with hin (hnn = 4,4,5,5-Tetramethylimicazolin-1-oxyl 3-Oxide; hin = 4,4,5,5-Tetramethylimidazolin-1-oxyl)," T. Ise, T. Ishida, and T. Nogami, *Bull. Chem. Soc. Jpn.*, **75**, 2463-2468 (2002).
19) "Radical-Copper Macrocycles and Related Compounds," J. Omata, T. Ishida, D. Hashizume, F. Iwasaki, and T. Nogami, *Mol. Cryst. Liq. Cryst.*, **376**, 455-462 (2002).
20) "Magnetic Phase Transition of Fe^{II}, Co^{II}, and Ni^{II} Complexes Bridged by Pyrimidine and Dicyanamide," T. Kusaka, T. Ishida, D. Hashizume, F. Iwasaki, and T. Nogami, *Mol. Cryst. Liq. Cryst.*, **376**, 463-468 (2002).
21) "Solvated Magnets of $Fe[N(CN)_2]_2$(pyrimidine): Transition Phenomena Tuned by Guests," T. Kusaka, T. Ishida, and T. Nogami, *Mol. Cryst. Liq. Cryst.*, **379**, 259-264 (2002).
22) "First Isolation and Characterization of an HIN Complex, $CdCl_2(HIN)_4$ (HIN = 4,4,5,5-Tetramethylimidazolin-1-oxyl)," T. Ise, T. Ishida, and T. Nogami, *Mol. Cryst. Liq. Cryst.*, **379**, 147-152 (2002).
23) "Nitronyl Nitroxide Substituted Aniline *o*-APNN with a Three-Dimensional Hydrogen Bond Network Showing Ferromagnetic Interaction," K. Doi, T. Ishida, and T. Nogami, *Chem. Lett.*, **32**, 544-545 (2003).
24) "Metamagnetic Behavior of $[Ni(4ImNNH)_2(NO_3)_2]$ Having a Ground High-Spin State (4ImNNH = 4-Imidazolyl Nitronyl Nitroxide)," C. Aoki, T. Ishida, and T. Nogami, *Inorg. Chem. Commun.*, **6**, 1122-1125 (2003).
25) "Rectangular Tetragadolinium Complex Ion with a Ground *S* = 27/2 State Containing Bis(dimethylglyoximato)copper(II) as a Ferrimagnetic Exchange Coupler," Y. Kobayashi, S. Ueki, T. Ishida, and T. Nogami, *Chem. Phys. Lett.*, **378**, 337-342 (2003).
26) "Ferro- and Ferrimagnetic Chains of hin-Bridged Copper(II) and Manganese(II) and hnn-Bridged Manganese(II) Complexes (hin = 4,4,5,5-Tetramethylimidazolin-1-oxyl; hnn = 4,4,5,5-Tetramethylimidazolin-1-oxyl 3-Oxide)," T. Ise, T. Ishida, D. Hashizume, F. Iwasaki, and T. Nogami, *Inorg. Chem.*, **42**, 6106-6113 (2003).
27) "A Self-Assembled Helix from 4,6-Dimethylpyrimidine and Copper(II) Bromide," T. Ishida, L. Yang, and T. Nogami, *Chem. Lett.*, **32**, 1018-1019 (2003).

28) "Molecular Metamagnet [Ni(4ImNNH)$_2$(NO$_3$)$_2$] (4ImNNH = 4-Imidazolyl Nitronyl Nitroxide) and the Related Compounds Showing Supramolecular H-Bonding Interaction," C. Aoki, T. Ishida, and T. Nogami, *Inorg. Chem.,* **42**, 7616-7625 (2003).
29) "Magnetic Properties of 9,9-Disubstituted 9,10-Dihydroacridine-10-yloxyls," M. Seino, Y. Akui, T. Ishida, and T. Nogami, *Synth. Met.*, **133-134**, 581-583 (2003).
30) "Hybrid Magnetic Solids of Radical-Substituted Heteroaromatic Compounds with Metal Halides," T. Matsuyama, Y. Iwata, T. Ishida, and T. Nogami, *Synth. Met.*, **133-134**, 611-613 (2003).
31) "Low Temperature Deuterium NMR Studies on Magnetism of TEMPO Derivatives," G. Maruta, S. Takeda, M. Ooishi, R. Imachi, T. Ishida, and T. Nogami, *Synth. Met.*, **133-134**, 577-579 (2003).
32) "Hydroiminonitroxide Complexes with Metal Hexafluoroacetylacetonates," T. Ise, T. Ishida, and T. Nogami, *Synth. Met.*, **137**, 1281-1282 (2003).
33) "Host-Guest Chemistry of Radical-Copper Wheels. A Supramolecular Control of Magnetic Exchange Coupling," T. Ishida, J. Omata, and T. Nogami, *Polyhedron,* **22**, 2133-2138 (2003).
34) "*meta*-Phenylene-Bridged Bis(imino Nitroxide) Biradicals as Potential High-Spin Ligands," T. Ichimura, K. Doi, C. Mitsuhashi, T. Ishida, and T. Nogami, *Polyhedron*, **22**, 2557-2564 (2003).
35) "Effect of Staggered Field in S = 1/2 Antiferromagnetic Chain: Copper Pyrimidine," T. Asano, D. Nomura, Y. Inagaki, Y. Ajiro, H. Nojiri, Y. Narumi, K. Kindo, T. Ishida, and T. Nogami, *Physica B: Cond. Matter,* **329**, 1006-1007 (2003).
36) "Supramolecular Triangular and Linear Arrays of Metal-Radical Solids Using Imino-Nitroxide-Substituted Pyrazolate Bridges," S. Yamada, T. Ishida, and T. Nogami, *Dalton Trans.*, **2004**, 898-903.
37) "Weak Ferromagnetism with Very Large Canting in a Chiral Lattice: Fe(pyrimidine)$_2$Cl$_2$," R. Feyerherm, A. Loose, T. Ishida, T. Nogami, J. Kreitlow, D. Baabe, F. J. Litterst, S. Süllow, H.-H. Klauss, and K. Doll, *Phys. Rev. B*, **69**, 134427[1]-134427[8] (2004).
38) "Single-Crystal Magnetic Study on Guest-Tunable Weak Ferromagnets [M{N(CN)$_2$}$_2$(pyrimidine)](guest) (M = Fe, Co)," N. Takagami, T. Ishida, and T. Nogami, *Bull. Chem. Soc. Jpn.*, **76**, 1125-1134 (2004).
39) "Remarkably Strong Intermolecular Antiferromagnetic Couplings in the Crystal of Biphenyl-3,5-diyl Bis(*tert*-butyl Nitroxide)," G. Kurokawa, T. Ishida, and T. Nogami, *Chem. Phys. Lett.*, **392**, 74-79 (2004).
40) "Crystal Structure of a Molecular Complex from Native β-Cyclodextrin and Copper(II) Chloride," G. Kurokawa, M. Sekii, T. Ishida, and T. Nogami, *Supramol. Chem.* in press (2004).

口頭発表等

1) 「固体高分解能 NMR でみた有機強磁性体 Ar–CH=N–TEMPO の電子スピン密度分布」丸田悟朗・武田　定・大石征弘・石田尚行・野上　隆・川上貴資・山口　兆、日本化学会北海道支部、2001 年夏期研究会発表会、2001 年 7 月 15 日、室蘭。
2) 「ピリミジン・[VO(hfac)$_2$]$_2$ 錯体の磁性」野上　隆、石田尚行、文部省「特定領域研究(B)」(730)、「分子スピン制御による新機能伝導体・磁性体の構築」第四回研究会、2001 年 5 月 18–19 日、福岡。
3) "Structures and Magnetic Properties of Several Transition-Metal Pyrimidine Complexes," T.

Nogami and T. Ishida「分子スピン制御による新機能伝導体・磁性体の構築」第二回公開シンポジウム、2001 年 9 月 7–8 日、東工大。

4) "Magnetic Properties of 9,9-Disubstituted 9,10-Dihydroacridine-10-yloxyls," M. Seino, Y. Akui, T. Ishida, and T. Nogami, The Fourth International Symposium on Crystalline Organic Metals, Superconductors and Ferromagnets, 10-14, Sept. 2001, Rusutsu, Japan.

5) "Hybrid Magnetic Solids of Radical-Substituted Heteroaromatic Compounds with Metal Halides," T. Matsuyama, Y. Iwata, J. Sata, J. Omata,, T. Ishida, and T. Nogami, The Fourth International Symposium on Crystalline Organic Metals, Superconductors and Ferromagnets, 10-14, Sept. 2001, Rusutsu, Japan.

6) "Low Temperature Deuterium NMR Studies on Magnetism of TEMPO Derivatives," G. Maruta, S. Takeda, M. Ooishi, R. Imachi, T. Ishida, T. Nogami, The Fourth International Symposium on Crystalline Organic Metals, Superconductors and Ferromagnets, 10-14, Sept. 2001, Rusutsu, Japan.

7) 「純有機フェリ磁性体を目指したトリラジカル化合物の合成とその磁性」野上　隆、伊瀬智章、市村剛幸、石田尚行、２００１年分子構造総合討論会、2001 年 9 月 24–27 日、札幌市。

8) 「イミノニトロキシドラジカルを配位子として用いた金属錯体」伊瀬智章、野上　隆、石田尚行、２００１年分子構造総合討論会、2001 年 9 月 24–27 日、札幌市。

9) 「ジアザナフタレン架橋銅(II)錯体の合成と構造」小金民造、石田尚行、野上　隆、第 51 回錯体化学討論会、2001 年 9 月 28–30 日、松江市。

10) "Solvated Magnets of $Fe[N(CN)_2]_2$(pyrimidine): Transition Phenomena Tuned by Guests," T. Kusaka, T. Ishida, and T. Nogami, International Symposium on Cooperative Phenomena of Assembled Metal Complexes, 15-17, Nov. 2001, Osaka, Japan.

11) "First Isolation and Characterization of an HIN Complex, $CdCl_2(HIN)_4$ (HIN = 4,4,5,5-tetramethylimidazolin-1-oxyl," T. Ise, T. Ishida, and T. Nogami, International Symposium on Cooperative Phenomena of Assembled Metal Complexes, 15-17, Nov. 2001, Osaka, Japan.

12) "Structures and Magnetic Properties of Pyrimidine-Bridged Transition-Metal Complexes," T. Nogami and T. Ishida, The 7th Japan-China Joint Symposium on Conduction and Photo-conduction in Organic Solids and Related Phenomena, 19-22, Nov. 2001, Wusan, Guangzhou (広州), PRC.

13) 「ピリミジンと遷移金属とが集積する磁性体」石田尚行、理研セミナー、2001 年１２月１０日、和光（理化学研究所）。

14) "Magnetic structure of $Mn(dca)_2$(pyz-d_8) and other molecular magnets," R. Feyerherm, A. Loose, P. Smeibidl, S. Raasch, D. Többens, J. L. Manson, and T. Ishida, BENSC Experimental Reports 2001, p. 66, Hahn-Meitner-Institut Berlin, Germany.

15) "Magnetic-field induced gap and staggered susceptibility in the S=1/2 chain $[PM.Cu(NO_3)_2(H_2O)_2]_n$ (PM = pyrimidine)," R. Feyerherm, M. Meissner, and T. Ishida, Frühjahrstagung des Arbeitskreises Festkörperphysik der Deutsche Physikalische Gesellschaft e. V. (DPG), 26-30, Mar. 2001, Hamburg, Germany.

16) "Magnetische ordnung molekularer übergangsmetallkomplexe," R. Feyerherm, A. Loose, C. Mathoniére, O. Kahn, and T. Ishida, Frühjahrstagung des Arbeitskreises Festkörperphysik der Deutsche Physikalische Gesellschaft e. V. (DPG), 26-30, Mar. 2001, Hamburg, Germany.

17) "Single crystal studies of the 1-D systems $PMCu(NO_3)_2(H_2O)_2$ and $MnNi(NO_2)_4$(en)," R.

Feyerherm, A. Loose, T. Ishida, T. Nogami, C. Mathoniére, and O. Kahn, Conference on the European Science Foundation Programme "Molecular Magnets," 10-15, Mar. 2001, Davos, Switzerland.

18) "Crystal and magnetic structures of $FePM_2Cl_2$, Co(ox)(bpy) and MCl2(bpy), M = Co, Ni, determined by neutron powder diffraction mid-term," A. Loose, R. Feyerherm, T. Ishida, M. A. Lawandy, and J. Li, Conference on the European Science Foundation Programme "Molecular Magnets," 10-15, Mar. 2001, Davos, Switzerland.

19) 「磁場誘起ギャップ系 Cu pyrimidine の磁性と ESR」浅野貴行、野村大輔、稲垣裕次、網代芳民、野尻浩之、鳴海康雄、金道浩一、石田尚行、野上　隆、日本物理学会第５７年次大会、2002 年 3 月 24–27 日、草津市（立命館大）。

20) 「遷移金属アジ化物とピリミジンからなる転移温度 50 K 級の弱強磁性体」土肥芳隆、石田尚行、野上　隆、日本化学会第 81 春季年会、2002 年 3 月 26–29 日、東京。

21) 「立体障害のあるピリミジンを用いたらせん構造を持つ銅錯体」楊 立名、石田尚行、野上　隆、日本化学会第 81 春季年会、2002 年 3 月 26–29 日、東京。

22) 「$M^{II}[N(CN)_2]_2$(pyrimidine)におけるゲスト分子による磁性の制御」日下高治、石田尚行、野上　隆、日本化学会第 81 春季年会、2002 年 3 月 26–29 日、東京。

23) 「ニトロニルニトロキシドを有するピリミジンやピラジン誘導体を用いた金属錯体の構造と磁性」松山喬洋、岩田吉史、石田尚行、野上　隆、日本化学会第 81 春季年会、2002 年 3 月 26–29 日、東京。

24) 「ヒドロイミノニトロキシドラジカル錯体の構造と磁性」伊瀬智章、石田尚行、野上　隆、日本化学会第 81 春季年会、2002 年 3 月 26–29 日、東京。

25) 「基底 3 重項を目指したキレート配位能を有するビスイミノニトロキシド化合物とその誘導体の合成と磁性」土井健太郎、市村剛幸、三橋知恵美、石田尚行、野上　隆、日本化学会第 81 春季年会、2002 年 3 月 26–29 日、東京。

26) "Hydroiminonitroxide Complexes with Metal Hexafluoroacetylacetonates," T. Ise, T. Ishida, and T. Nogami, International Conference on Science and Technology of Synthetic Metals, June 29 - July 5, 2002, Shanghai, China.

27) "Preparation and Characterization of Bis(1,1,1,5,5,5-hexafluoro-2,4-pentanedionato)copper(II) Complexes with Diazanaphthalenes," T. Kogane, T. Ishida, and T. Nogami, 35th International Conference on Coordination Chemistry, ICCC35, July 21-26, 2002, Heidelberg, Germany.

28) "Effect of Staggered Field in S = 1/2 Antiferromagnetic Chain: Copper Pyrimidine," T. Asano, D. Nomura, Y. Inagaki, Y. Ajiro, H. Nojiri, Y. Narumi, K. Kindo, T. Ishida, and T. Nogami, The 23rd International Conference on Low Temperature Physics (LT23), Aug. 20 - 27, 2002, Hiroshima.

29) 「有機強磁性体 BATMP ラジカルの熱容量と磁気構造の次元性」宮崎裕司，榊原　武，石田尚行，野上　隆，徂徠道夫、分子構造総合討論会、平成１４年１０月１～４日、神戸。

30) 「ニッケル錯体を原料とするコンプレックスクラウンの構造および磁性の研究」中林崇･石田尚行･野上　隆、第 16 回基礎有機化学連合討論会、2002 年 10 月 3 日、東京（駒場）。

31) 「p–フェニレンで繋げた３つのニトロキシドラジカル部位を有する有機化合物の合成と磁性」黒川源太郎･石田尚行･野上　隆、第 16 回基礎有機化学連合討論会、2002 年 10 月 3 日、東京（駒場）。

32) 「ヒドロイミノニトロキシドラジカル錯体の構造と磁性」伊瀬智章･石田尚行･野上　隆、第 16 回基礎有機化学連合討論会、2002 年 10 月 3 日、東京（駒場）。
33) "Meta-Phenylene-Bridged Bis(iminonitroxide) Biradicals as Potential High-Spin Ligands," T. Ishida, T. Ichimura, and T. Nogami, VIIIth International Conference on Molecule-Based Magnets, Oct. 5-10, 2002, Valencia, Spain.
34) "Host-Guest Chemistry of Radical-Copper Wheels. A Supramolecular Control of Magnetic Exchange Coupling," T. Ishida, J. Omata, and T. Nogami, VIIIth International Conference on Molecule-Based Magnets, Oct. 5-10, 2002, Valencia, Spain.
35) "Canted Antiferromagnetism in TPM_2X_2: a Microscopic Study," J. Kreitlow, A. Wolter, D. Baabe, H.-H. Klauss, S. Süllow, D. Mienert, J. Litterst, R. Feyerherm, K. Doll, T. Ishida, M. A. C. de Melo, and A. Amato, VIIIth International Conference on Molecule-Based Magnets, Oct. 5-10, 2002, Valencia, Spain.
36) "Magnetic Structures of Transitiion Metal Complex Compounds Determined by Neutron Diffraction," R. Feyerherm, A. Loose, T. Ishida, J. Li, and P. Rabu, VIIIth International Conference on Molecule-Based Magnets, Oct. 5-10, 2002, Valencia, Spain.
37) 「ホストゲスト化学を利用した分子磁性の制御」石田尚行、野上　隆、分子科学研究所（後期）研究会、2003 年 3 月 3－5 日（岡崎）。
38) 「小さなラジカル配位子を有する新型遷移金属錯体の合成、構造、磁気物性」伊瀬智章、石田尚行、野上　隆、分子科学研究所（後期）研究会、2003 年 3 月 3－5 日（岡崎）。
39) "Rectangular Tetralanthanide Ln_4Cu_1 Complexes (Ln = Nd, Gd) Containing Bis(dimethylglyoximato)copper(II) as a Template in Synthesis and a Coupler in Magnetic Exchange," Y. Kobayashi, T. Ishida, and T. Nogagmi, Nano-Science of Advanced Metal Complexes, Mar. 22 - 24, 2003, Okazaki.
40) 「弱強磁性体 Fe(II)−ジシアナミド−ピリミジンの単結晶磁化率」高上直美、石田尚行、野上　隆、日本化学会第 83 春季年会、2003 年 3 月 18−21 日、東京（早稲田大）。
41) 「銅ジメチルグリオキシム錯イオンをテンプレートに用いたガドリニウム四核環状錯体」小林泰子、石田尚行、野上　隆、日本化学会第 83 春季年会、2003 年 3 月 18−21 日、東京（早稲田大）。
42) 「基底 3 重項キレート配位子ビスイミノニトロキシドを用いた遷移金属錯体の磁性と構造」土井健太郎、石田尚行、野上　隆、日本化学会第 83 春季年会、2003 年 3 月 18−21 日、東京（早稲田大）。
43) 「４－イミダゾリルあるいはピラジルニトロニルニトロキシドと金属ハロゲン化物からなる錯体の磁性」青木千草、松山喬洋、石田尚行、野上　隆、日本化学会第 83 春季年会、2003 年 3 月 18−21 日、東京（早稲田大）。
44) 「9−(5−ピリミジニル)アクリジンおよび、その 10−オキシドを用いた金属錯体の構造と磁性」清野　充、石田尚行、野上　隆、日本化学会第 83 春季年会、2003 年 3 月 18−21 日、東京（早稲田大）。
45) 「ヒドロニトロニルニトロキシドやヒドロイミノニトロキシドを用いた一次元磁性体の構築」伊瀬智章、石田尚行、野上　隆、日本化学会第 83 春季年会、2003 年 3 月 18−21 日、東京（早稲田大）。
46) 「2,2'−ビピリジルの 5 位にニトロキシドラジカルを持つ配位子を用いた錯体の構造と磁性」嶌田友和、石田尚行、野上　隆、日本化学会第 83 春季年会、2003 年 3 月 18−21

日、東京（早稲田大）。

47) 「多様な積層構造をもつフタロシアニンπ－d系導電体の構築」稲辺　保・野上　隆・石田尚行、文部科学省科学研究費特定領域「分子性導体」キックオフミーティング、2003年7月２８，２９日、東京（学習院）。

48) 「銅ジメチルグリオキシム錯イオンをテンプレートに用いたガドリニウム錯体の構造と磁性」石田尚行、小林泰子、上木創平、Muhamad Sahlan、野上　隆、分子構造総合討論会、2003年9月24–27日、京都。

49) 「置換基がπ共役系のみで構成されているニトロキシドラジカルの合成と磁性」黒川源太郎、柳　賢治、石田尚行、野上　隆、分子構造総合討論会、2003 年 9 月 24–27日、京都。

50) 「ラジカル置換ピラゾールを用いた銀錯体の磁性と構造」山多 晋、石田尚行、野上　隆、第３３回構造有機化学討論会、2003年10月3、4日、富山。

51) 「クラウンエーテルを置換基にもつニッケル錯体のカチオン包摂」中林　崇、石田尚行、野上　隆、第３３回構造有機化学討論会、2003年10月3、4日、富山。

52) 「高スピン分子へのアプローチ：制御された自己集合による３ｄ／４ｆ錯イオン形成」石田尚行、理研シンポジウム「モレキュラー・アンサンブル2003」、2003年12月1、２日、和光。

53) 「Chiral な結晶構造をもつ磁性体の開発」石田尚行・野上　隆、電気通信大学２１世紀COEプログラム第一回 公開シンポジウム「コヒーレント光科学の展開」、2003年 12月12日、調布。

54) 「Synthesis of dioxadiselenafulvalene derivatives」石田尚行・野上　隆、文部科学省科学研究費特定領域「分子性導体」第一回 シンポジウム、2004年 1月19,20日、東京（東工大）。

55) 「グリオキシマートを架橋配位子に用いた３ｄ／４ｆヘテロ金属多核錯体と鎖状錯体の構造と磁性」石田尚行、上木創平、Muhamad Sahlan、小林泰子、野上　隆、日本化学会第84春季年会、2004年3月26–29日、西宮（関西学院大）。

56) 「鉄(II)–ピリミジン–アジド系錯体の構造、弱強磁性挙動、および光誘起磁化」土肥芳隆、石田尚行、野上　隆、日本化学会第84春季年会、2004年3月26–29日、西宮（関西学院大）。

57) 「ラジカル置換ピラゾールを用いた遷移金属錯体の磁性と構造」山多 晋、石田尚行、野上　隆、日本化学会第84春季年会、2004年3月26–29日、西宮（関西学院大）。

58) 「オキシマート架橋をもつランタノイドと遷移金属イオンからなる錯体の構造と磁性」森　文仁、野上　隆、石田尚行、日本化学会第 84 春季年会、2004 年 3 月 26–29 日、西宮（関西学院大）。

59) 「ラジカル置換分子グリッドを目指した含ピリミジン架橋配位子の合成と錯形成の試み」柳　賢治、石田尚行、野上　隆、日本化学会第 84 春季年会、2004 年 3 月 26–29日、西宮（関西学院大）。

60) 「DBOSF（dibenzodioxadiselenafulvalene）の合成とその物性評価」小島崇寛、石田尚行、野上　隆、日本化学会第 84 春季年会、2004 年 3 月 26–29 日、西宮（関西学院大）。

研究成果

分子性磁性材料に強磁性的カップリングを付与し、さらに磁気的高次元ネットワークを構築するという研究命題は、結晶構造の中で望んだ分子配列をとらせることができるかという結晶設計・結晶工学の問題に帰せられる。結晶工学で一定の成果を与えている分野は配位結合を巧みに用いた「集積型金属錯体」である。超分子という言葉は、弱い結合を用いて、原子と原子から分子を作るのと同様に、分子と分子から分子システムを構築するという場合に用いられる。この定義に従えば、本課題で取り上げる集積型金属錯体は、その構造自体が超分子である。しかし、生体関連分子を思い起こすと、分子の機能性は、分子を認識する、分子の反応場を提供する、可逆的に分子を着脱するという動的な超分子科学である。本研究課題では、有機・分子性強磁性体を題材にして、超分子手法を用いて強磁性的–反強磁性的相互作用をスイッチしたり、分子の基底スピン多重度を変化させたり、スピンを発生あるいは消滅させるといったような、動的に磁性を制御することを目指した。

本研究グループでは従来より、ピリミジン架橋錯体の開発研究を強力に推進している。具体的な研究対象のうち二種の錯化合物に関する成果は、解説論文（文献１）に詳しく解説してある。以下に要点を簡単に述べる。略称等は原著論文に示してある。

ピリミジン(PM) および $N(CN)_2^-$ の架橋配位子を用いた錯体では、ゲスト分子が結晶の格子の間に取り込まれることがわかった。$[Fe\{N(CN)_2\}_2PM]\cdot$ (guest) の結晶構造は、ゲスト分子がエタノール、プロパノール、ブタノールおよびピリミジンのときに同形結晶を与え、磁気的相転移温度はそれぞれ 3.3, 4.4, 3.6, 5.6 K であった。液体ヘリウム温度領域における２Ｋの差はかなり大きいものであった。これらは弱強磁性挙動を示し、その傾角もゲスト分子に大きく依存した。つまり、この系では、磁性体を特徴付けるパラメータ（臨界温度、臨界磁場、自発磁化）をゲストにより変えることができた。

$[4PMNN\cdot CuX_2]_6$ (X = Cl, Br) は、12 スピン系大員環状の分子構造を有し、結晶中ではカラムを形成する（4PMNN は４位にニトロニルニトロキシドラジカル基を有するピリミジンである)。チューブ状空間にゲスト分子として有機分子やハロゲン化アルカリ金属塩を取り込ませたところ、強磁性的相互作用が増大した。ゲストとして水を用いたものは、減圧による脱水の前後で、磁性を大きく変化させることができた。この系は磁気相転移を示す物質ではなかったが、磁気的相互作用をゲストにより変えられることがわかった。この成果は日刊工業新聞 2002 年８月１日「ナノテクで新産業革命」の記事に取り上げられた（本項末尾に添付)。

これらの研究の過程で、数々の新規な超分子構造や磁性体を開発した。たとえば、$[Fe\{N(CN)_2\}_2PM]$ の五原子架橋アニオンを三原子架橋性アジ化物イオンに置き換えることにより転移温度を一桁向上させた（Tc ５０Ｋ程度)。らせんキラリティを有する錯化合物を開発し、そのなかからスピン傾角が 16 度という大きな自発磁化をもつ弱強磁性体 $[Fe(PM)_2Cl_2]$ が得られた。

純粋な有機ラジカル強磁性体として、すでに我々は TEMPO ラジカル系を開発済みであった。この強磁性の発現機構の解明のために、熱容量やゼロ磁場μＳＲなどの実験を行った。本研究課題では有機ラジカル類を超分子構造体へと展開し、金属–ラジカル–ハイブリッド系磁性体の開発も推進した。架橋配位子として複素芳香族類に着目し、円環状、鎖状といった超分子構造をもつハイブリッド磁性体を幾つか得ることができた。たとえば $[4ImNNH\cdot MX_2]$ （4ImNNH は 4–位にニトロニルニトロキシドラジカルを有するイミダゾール）においては、水素結合が巧みに利用され、それが構造体の構築のみならず磁気的カップリングの経路にも役に立っているということもわかった。また、最も立体的かさが小さい架橋性ラジカルとして HNN および HIN に着目した（水素置換のニトロニルニトロキシドやイミノニトロキシドラジカル)。これを用いた錯体では期待されたように従来のものよりも強い磁気的カップリングが得られた。実際、この系は低次元物質ながら強磁性体やフェリ磁性体になるものが得られた。

以上、超分子構造の利用による磁性体の開発ならびに超分子化学の利用による磁性のチューニングについては、一応の評価できる成果を挙げたと考えられる。しかし、題目にある『制御』という観点では、ここで説明した実験以上に今後スイッチング挙動や可逆性の検証を進めていく必要がある。これらの結果を基礎として、さらに産業上へ応用することが可能な物質群の開発が、今後の課題になると考えている。

新 ナノテク 産業革命 先端研究室の挑戦 45

電気通信大学・野上・石田研究室

分子磁石の研究／「六角穴」新錯体生む

電気通信大学量子・物質工学科の野上隆教授、石田尚行助教授の研究室は分子を構成単位とした有機磁石（分子磁石）の実現を目指して研究を進めてきた。ところが研究の方向は二転三転し、直径1・1ナノメートルの六角形の穴が開いた新しい錯体の作製という思わぬ展開になっている。「研究というのはどこでどうつながるか分からない」（野上教授）と実感した様子だ。

純粋な有機化合物は磁石（強磁性体）にならないのか―。このテーマは長年の疑問だった。有機化合物は本来、磁性を全く持たない。電子は一つひとつが磁性を持つが、原子同士が結合する際に逆向きの磁性同士が対になって打ち消し合い、分子全体として磁性を持たなくなるからだ。

磁性を持たせるには対にならない余分な電子（不対電子）をつくる必要がある。人為的に不対電子を形成すると化学的に不安定になるが、この部分で再び反応が起こらぬよう、周辺に置換基をつけるなどの化学修飾を施す。こうすると1分子中に一つの不対電子が形成される。

ところが、分子中の不対電子の磁性は原子同士の場合と同様、分子間で対になって打ち消し合い、結局、固体全体として磁性がなくなる場合がほとんどだ。

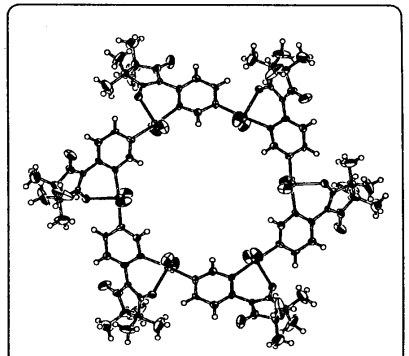

作製した錯体の化学構造

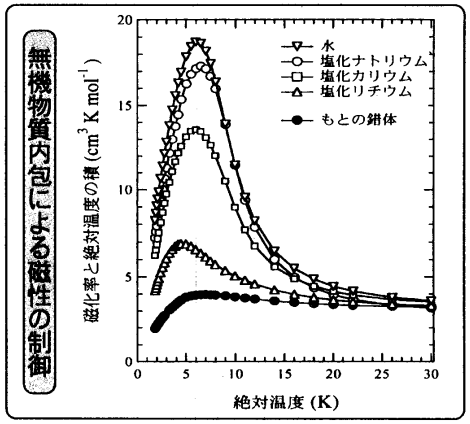

約10年前、この常識は破られた。「日本の研究者（東京大学物性研究所と岡崎国立共同研究機構分子科学研究所のグループ）が磁石になる物質を見つけた」（同）のだ。後に仏のグループも別の物質で発見。野上・石田研究室は3番目の発見者となった。「有機化合物の強磁性体は今、20ぐらいある。我々は2年ぐらいの間に八つ見つけた」（同）と説明する。

だがいずれの強磁性体も磁性を失う温度（転移温度）が低いのが課題。分子同士を近づけ、分子間の磁性の相互作用を強めれば転移温度は上がる理屈だが、皮肉にも不対電子周辺の置換基が邪魔だ。こうして純粋な有機化合物で強磁性体をつくる研究は「今でもやっているが、前ほどの熱意はなくなった」（同）。

代わりに最近、研究室では有機化合物と遷移金属イオンの複合物質の研究に力を入れている。「置換基も要らない。純粋有機化合物のジレンマがなくなる」（同）と転移温度の上昇を狙った。

1年ほど前、ピリミジンと二トロニルニトロキシドが結合した分子と銅の塩化物（もしくは臭化物）を混ぜ、直径1・1ナノメートルの六角形の穴が開いた錯体を作製した。「中が空洞で、美しい形が保たれているのが珍しい」（同）という。

この錯体は全体としては磁性を持たないが、銅の不対電子は銅の近くにあるニトロニルニトロキシドの不対電子と磁性の向きがそろっていて、隣の銅の不対電子とは磁性の向きが反対だ。しかも六角形の部分は積層構造をしており、縦方向に同じ位置の不対電子をたどると磁性の向きはそろっている。

穴の中に無機物を入れると磁性が劇的に変化することを実験で確かめた。とくに水を入れると、何も入れないときより6倍磁化しやすくなった（5000㌅の磁場中で測定）。水を抜くと元に戻るという可逆性もある。

野上教授は「有機物を入れたらどうなるかなどもっと詳しく調べたい。穴の開いた別のタイプの錯体にも目を向けていきたい」と新しい錯体への思い入れを示している。

論　文　集

超分子的に制御できる分子磁性

Molecule-Based Magnets Tunable by Means of Supramolecular Chemistry

石田尚行・野上　隆　電気通信大学量子・物質工学科
T. Ishida and T. Nogami, Department of Applied Physics and Chemistry, The University of Electro-Communications

Supramolecular techniques such as host–guest complex formation have been used to tune molecule-based magnetic materials. We will present two nano-porous magnetic materials, whose magnetic properties were changed by inclusion of small diamagnetic molecules. The first are low-temperature magnets derived from iron(II), $N(CN)_2^-$, and pyrimidine, which have guest molecules incorporated in the clearance of the 3-D framework. The T_C ranges from 3.3 K to 5.6 K, depending on the guest molecules. They are characterized as canted antiferromagnets below T_C. The second are hexanuclear wheel-shaped copper(II) complexes, whose crystals have a channel structure in a direction perpendicular to the molecular plane. The ferromagnetic interaction, which is ascribed to intermolecular contacts between the radical substituents, was remarkably enhanced by guest inclusion within a channel.

Key words: molecule-based magnets, supramolecular chemistry, transition metal complex, host–guest chemistry, porous material, weak ferromagnet, free radical, pyrimidine, iron(II), copper(II)

1. はじめに

題目を模式的に描けばFig. 1のようになる．用語に対して戸惑いのないように，初めに分子磁性と超分子に関する説明とそれにまつわるいくつかの話題を提供して，本稿の序としたい．

1.1 分子磁性[1]

分子性固体においてバルクの強磁性相は発現するかどうかという疑問に対して明確な回答を与えたのは，β相*p*-NPNNという有機強磁性体の発見であった[2]．従来の無機化合物材料であれば，磁性体といえば金属結晶や共有結合結晶であったから，磁気的相互作用は化学結合を通してのものであった．それに対して分子性結晶では空間を通して磁気的に相互作用せねばならない．そのことは強磁性相転移温度(T_C)が低いという欠点を必然的に伴う．現在の純有機磁石のT_Cの最高記録はTMAOの1.48 Kである[3]．

隣接分子間でラジカルスピン同士が強磁性的あるいは反強磁性的にカップルするかを決める要因は，それぞれのカップリングに望ましい配置で特定の原子や原子団で接触

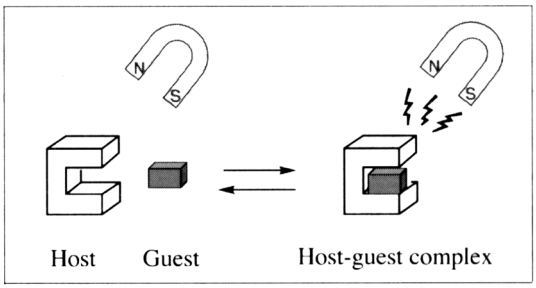

Fig. 1 A strategy of supramolecular control of molecule-based magnets.

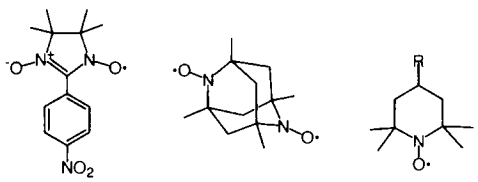

が行われるかどうかである．もし分子間で強磁性的カップリングが欲しければ，それはとりもなおさず結晶構造の中で望んだ分子配列をとらせることができるかという結晶工学の問題となる．水素結合，静電的双極子–双極子，電荷移動相互作用などを駆使して有機強磁性結晶の構築が提案されている．筆者らはTEMPOラジカル類から有機強磁性体を得たが，そこにはC–H…O水素結合が結晶を構築する相互作用であると同時に強磁性的相互作用の経路を与えるという説を唱えた[4]．しかし，希望どおりの結晶を得たいという問題の解決は，有機結晶では現在でも難しい．

ところで，結晶工学で一定の成果を与えている分野は配位結合を巧みに用いた「集積型金属錯体」[5]である．遷移金属イオンを用いた場合には，d, f軌道の電子スピンも磁性に関与させることができる．特に，有機ラジカルと遷移金属イオンからなる集積は，metal-radicalアプローチ[6]として広範な実例がある．磁性体へ適用した系では転移温度が室温を超えたものもある[7]．

1.2 超分子[8]

情報記録材料をはじめとする現代のテクノロジーには磁性体は不可欠であるが，分子磁性の開発のゴールは，従来の無機材料の磁性体を分子磁性材料に単純に置き換えるというものではない．この研究開発に携わる者は，その新規

な材料を開発して提供するのと平行して，将来のテクノロジーにおける分子磁性材料の新しい利用方法を提案する必要がある．例えば，MChD (magnetochiral dichromism; 磁気不斉二色性) は注目すべき分野である[9]．分子磁性材料は光に対して透明な材料が提供でき，しかも光学的不斉材料は有機合成手法あるいは自然分晶法により導入できる．筆者らもキラルならせん構造を有する弱強磁性体[10]を開発している．注目すべきもう一つの分野は，SMM (single-molecule magnet; 単分子磁石) である[11]．本来の磁気的相転移現象はバルクの物性であるが，ある条件を満たした多核遷移金属錯体は，磁気ヒステリシスを描き，これが単分子由来であることが明らかにされている．基底高スピン分子の開発はSMMを含めて磁性材料開発の一つの方針であり，筆者らも$S=27/2$錯イオンなどを合成している[12]．

超分子という言葉は，弱い結合を用いて，原子と原子から分子を作るのと同様に，分子と分子から分子システムを構築するという場合に用いられる[8]．この定義に従えば，本稿で取り上げる多孔質集積型金属錯体は，その構造自体が超分子である．しかし，生体関連分子を思い起こすと，分子の機能性は，分子を認識する，分子の反応場を提供する，可逆的に分子を着脱するという動的な超分子科学である．分子性材料ならではという機能の一つを磁性体開発に適用できないだろうか，磁性体のスイッチ，演算，情報記録に対する外的刺激の一つにゲスト分子の付加・脱離・ケージ内反応を提案できるのではないか，これが筆者らの研究動機である (Fig. 1)．

これまでにも，層状の金属水酸化物あるいはハロゲン化物が二次元磁性挙動を示し，いろいろなインターカレーターにより磁気転移温度を変えられる物質の報告例はあった[13]．これらの化合物では厳密な結晶構造を決定しにくいという難点があったが，筆者らの用いた集積型金属錯体における優位な点は，単結晶によるX線結晶構造解析の手法が用いられ，磁性-構造相関の議論に向くことである．

2. 超分子的に制御できる分子磁性

配位結合のもつ「共有結合性」は結晶工学から見て重要である．共有結合には方向性があるからである．ここでは，金属イオンの結合角 (90°か180°，つまり六配位八面体型のシスかトランス) と配位子の非共有結合電子対の方向性 (架橋性二座配位子の形状により，109.5°，120°，180°など) を比較的剛直だとするモデルで考えることができ，分子・結晶構造の予測を立てやすい．多核錯体を構築すれば，磁性材料としては超高スピン分子の構築や[14]，機能性材料としては分子カプセル[15]などに応用できる．三次元構造体は気体吸蔵材料や反応触媒[16]として展開されている．分子模型を玉と竹ひごで組み立てた経験があるだろうか．通常の分子では竹ひご部分が結合性電子対を意味するのだが，超分子の分野では，竹ひご部分に架橋性の分子を置く．したがって分子は非常に大きくなり，それに比例して隙間も大きい．本稿で意図する超分子科学はこのナノサイズの隙間を利用する科学のことである．以下に筆者らの開発した2種の超分子磁性体を紹介する．ホストがネットワーク構造をもった磁性体であり，非磁性のゲスト分子によりホストの磁性を調節する．

2.1 鉄-ピリミジン-ジシアナミド錯体

この化合物 ($[Fe\{(NC)_2N\}_2(pm)]\cdot(guest)_n$; $(guest)_n$ = $(pm)_1$ (**1**), $(EtOH)_1$ (**2**), $(PrOH)_1$ (**3**), $(BuOH)_{0.5}$ (**4**); 以下，太数字を用いて化合物を番号で表すものとする) の結晶構造[17]はFig. 2(a, b)に示すとおりに，Fe(II)イオン (d^6, $S=2$) をジシアナミド陰イオン $[(NC)_2N^-]$ が卍型に架橋してまず二次元構造ができ，このシート構造をピリミジンがアキシャル位からトランスジグザグに架橋して三次元構造となっている．ジシアナミドは末端の窒素だけが配位結合に寄与するので，5原子架橋だが，ピリミジンは3原子架橋なので，磁気的相互作用はピリミジン架橋側の方が強いと予想される．

この格子の隙間にはゲスト分子が入る[18]．エタノール，プロパノール，ブタノールから結晶を析出させるとそれぞ

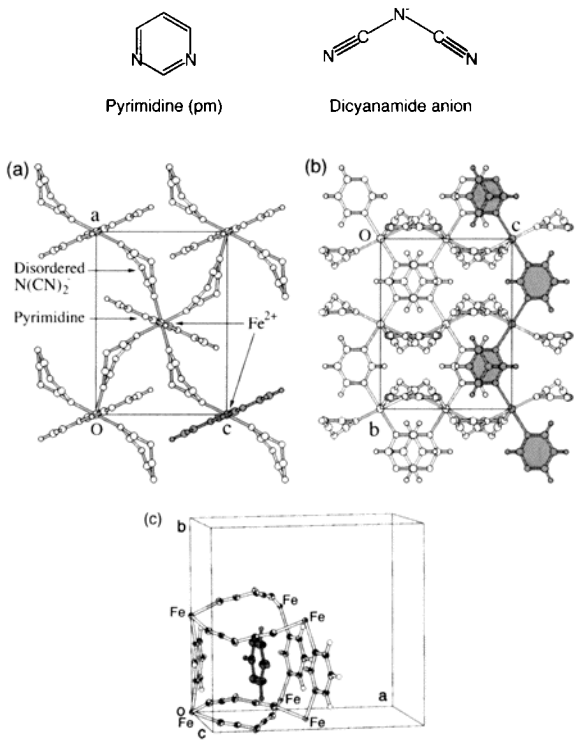

Fig. 2 (a,b) Crystal structure of **2** viewed along the b axis (a) and along the a axis (b). The $(NC)_2N$ moieties are disordered. One pm-Fe zig-zag chain is shaded. Guest molecules (EtOH) are not shown. (c) Crystal structure of **1**. A guest pm molecule is shaded. Only a quarter of cell is drawn for clarity.

れその溶媒分子が，また水から析出させるとピリミジンが閉じ込められる．なお，Fig. 2(a, b) ではジシアナミドが2本ずつ見えるが，これはディスオーダーである．ゲスト分子もディスオーダーしているが，**1** だけはゲストもホストもディスオーダーはない (Fig. 2(c))．

Fig. 3 に **1**〜**4** の多結晶試料の磁化曲線を示す．これらは磁化曲線の原点付近の自発磁化の存在から弱強磁性体ということができる．さらに興味深いことには，反強磁性構造から強磁性構造へ磁場誘起によりスピンが反転する現象（メタ磁性転移）も見せる．このメタ磁性転移を起こすことが幸いして，この磁性体がキャント磁性体として説明することできた (Fig. 4)．つまり，キャント角が非常に小さい物質はスピンが反転することにより磁化がほぼ飽和する (Fig. 3 の **1**)．一方，キャント角が大きい物質は，canted 反強磁性相からスピンが反転して canted 強磁性相へ転移

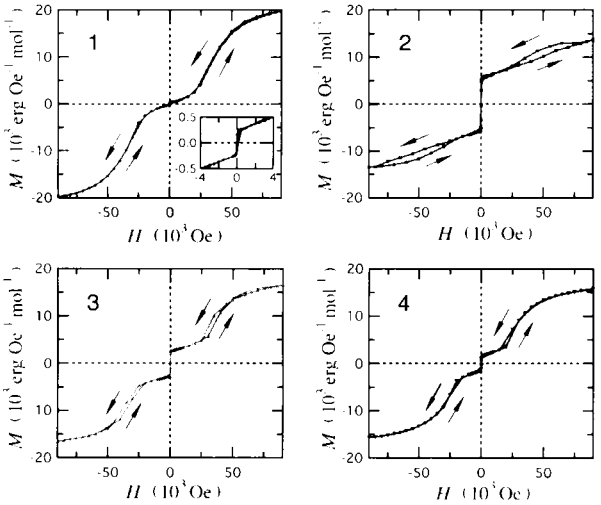

Fig. 3 M–H curves of **1**–**4** measured at 2.0 K.

Fig. 4 Spin structure of canted antiferromagnets. Spontaneous magnetization grows to the right direction.

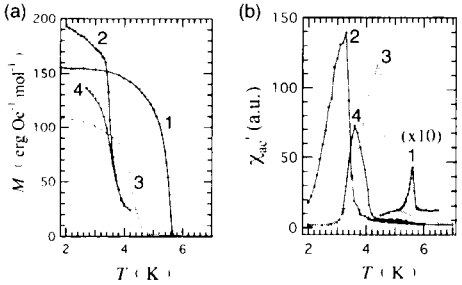

Fig. 5 (a) Field-cooled magnetization of **1**–**4** (H= 5 Oe). (b) Temperature dependence of χ_{ac}' for **1**–**4** (ν= 100 Hz).

すると考えられる（Fig. 3 の **2**〜**4**）．**1** と **2** の自発磁化の大きさからキャント角を見積もるとそれぞれ 0.6° と 14° となった．また，メタ磁性転移を起こす臨界磁場もゲストによってやや異なることもわかった．

磁気転移温度を求めた結果を Fig. 5 に示す．この物質群は自発磁化を有するので，弱い磁場中で温度を下げていくと，磁気相転移温度を迎えたところで急激に磁化が増大する．また，交流磁場中の磁化率は，基底反強磁性体の場合には転移温度付近でピークが見られる．この二つの独立した測定で求められた磁気転移温度はよく一致する．ピリミジンをゲストに有する物質 (**1**) とエタノールをゲストに有する物質 (**2**) は，転移温度がそれぞれ 5.6 K と 3.3 K と求められた．たかだか 2.3 K の差ではあるが，液体ヘリウム温度領域におけるこの差は相対的にかなり大きい．結晶構造上のディスオーダーが転移温度の低下を招いた可能性がある．

以上のことから，ゲストによりこの磁性体を特徴づける三つのパラメータ，転移温度，自発磁化（つまりキャント角），メタ磁性転移臨界磁場，を変えることができた．**1**〜**4** は，すべて単結晶 X 線結晶構造解析を済ませてあり，セル定数や Fe(II) の配位環境のわずかな違いのあることがわかっている．最近，単結晶を用いて弱強磁性の詳細な測定を行い，磁化容易軸が Fe(II) イオンのアキシャル結合軸を含む方向にあり，キャントによる自発磁化成分の発生する方向がピリミジン–Fe(II) のトランスジグザグ構造を含む面内（Fig. 2 の bc 面内）にあることを明らかにした[19]．この物質におけるスピンキャントは Fe(II) イオンが本来単独で有する異方性 (single-ion anisotropy) と関係が深いことがわかった．そのアキシャル異方性を与える結晶場，あるいは実効的なゼロ磁場分裂パラメータ D が負で十分に大きければ，交換相互作用 J と拮抗してキャント磁性体を与えるというモデルを提案できる．すなわち，後者はモーメントを交互に 180° に向けようとするのに，前者が 120° に向けようとしてキャントが発生する．この単結晶の測定は，ゲストによって single-ion anisotropy が違ってくることも明らかにした．つまり，わずかな Fe(II) 周辺の構造の違いがバルクの磁性に大きく影響している．

金属イオンに Co(II) や Ni(II) を用いた場合も Fe(II) と同型の結晶を与え，弱強磁性体となることがわかっており[17),20)]，これらを対象とする研究も今後の課題である．ピリミジン架橋を用いるとしばしば弱強磁性体が得られるのは[10),17),20)]，ピリミジンの 120° の角度で結合する方向性が隣接イオンの結晶場をジグザグと傾けさせる構造[21)]と関連があるだろう．

2.2 磁気的ナノチューブ

有機配位子はさまざまな化学修飾が可能であり，筆者らはさまざまなピリミジンを用いた錯体を合成してきた．ここではピリミジンの 4 位に分子磁性の研究対象として有

名なニトロニルニトロキシドと呼ばれる安定ラジカル置換基を導入して，新規な架橋配位子 4PMNN を開発した[22]．塩化または臭化銅(II) (Cu(II) は $d^9, S=1/2$) を用いて錯形成させたところ，ピリミジンが 120° の方向に非共有電子対を突き出していることを反映して大員環六核錯体 $[CuX_2 \cdot 4PMNN]_6$ (X=Cl (**5**), Br (**6**)) を与えた (Fig. 6)[23]．この分子では結晶学的に独立なのは金属と配位子の一組であり，分子全体としては 12 スピン系である．隣接分子は c 軸 1 並進の関係にある．つまり分子が鉛直に積み重なって，結果としてチューブ状の空孔ができる．向き合った Cu(II) 間の距離でチューブの直径を定義すると，約 1.1 nm である．

分子内には重要な交換相互作用の経路が 2 種類ある．最も強く働くと予想されるのはラジカルの酸素原子が直接 Cu(II) イオンにアキシャル位から配位している構造に働く強磁性的相互作用である．つまりここに局所的な $S=1$ 単位が形成される．この相互作用は Cu(II) の磁性軌道 $d_{x^2-y^2}$ とラジカルの磁性軌道 π^* とが直交することに基づく[6]．次に働くのはピリミジンが Cu(II) イオン同士を架橋することによる反強磁性的相互作用である．両側の Cu(II) のエカトリアル位に配位して，ピリミジンの非共有電子対が両側で軌道の重なりを有することに基づく超交換相互作用である[24]．ところで，一見してこの描像では，分子内で 6 個の $S=1$ が上下上下上下と円周に沿って並ぶと予想されるのだが，以下に述べる三番目の経路が分子間にあり，磁性は複雑である．

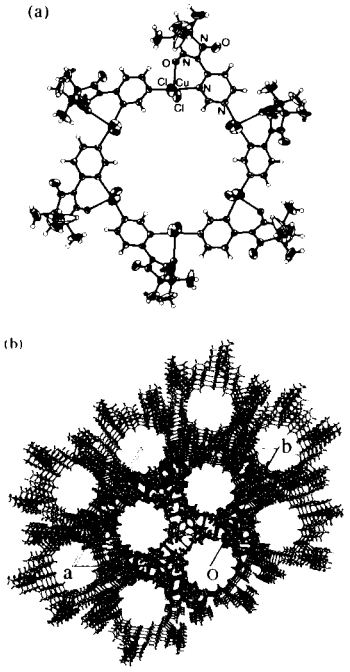

Fig. 6 (a) Molecular structure of **5**. For the chemical formula, see Fig. 7. (b) Molecular arrangement in the crystal of **5** viewed along the c axis.

分子が外側にラジカル部位を突き出しているおかげで，分子間の接触はラジカル同士で行われる．その分子間の重要なところだけを描いたのが Fig. 7 である．ここは専門外の読者には煩雑であるかもしれないので詳細を割愛する．有機磁性体の分野では著名な原理なのであるが[1), 25)]，SOMO (singly-occupied molecular orbital) の軌道の係数を有する原子と係数をもたない原子との接触は，強磁性的相互作用を与える．本系ではそのような状況がラジカル主骨格 ONCNO の末端 O が隣分子のラジカル骨格の中央 C へ T 字型に接触して達成されている[26]．この T 字型接触は，筒状構造の交点において 3_1 らせんの対称性により c 軸に沿って一次元的に連なっている．だから，Cu(II) とラジカルからなる $S=1$ 単位が一次元強磁性鎖を形成し，この鎖が六角格子状に束ねられ，鎖同士がお互い反強磁性的にカップルしているというのがこの物質の磁性の描像とな

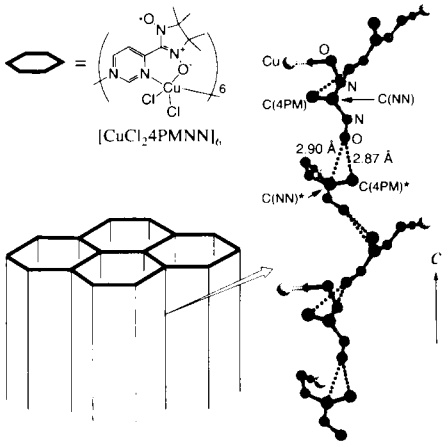

Fig. 7 (Left) Schematic drawing of the tube-like cavity in the crystal of **5**. (Right) Linear array of nitronyl nitroxide groups with a T-shaped configuration along the c axis. Six ONC(–C)NO–Cu fragments are drawn.

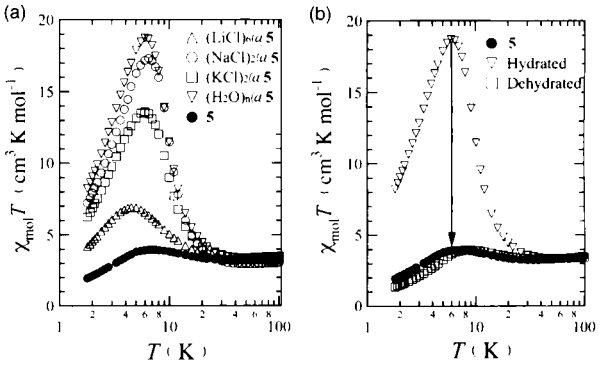

Fig. 8 (a) Temperature dependence of the product of χ_{mol} and T measured at 5000 Oe for $(MCl)_n$@**5** and $(H_2O)_n$@**5**, and **5**. (b) Temperature dependence of the product of χ_{mol} and T of freshly prepared $(H_2O)_n$@**5** and evacuated $(H_2O)_n$@**5** together with that of **5** measured at 5000 Oe.

る．

多結晶試料による磁気測定結果はFig. 8に示されている（ゲストのない場合の●データ）．磁化率と温度の積（$\chi_{mol}T$）を温度に対してプロットしたものである．この温度領域では常磁性体である．温度を下げるに従い，$\chi_{mol}T$値は一度減少したあと上昇に転じ，最後に再び減少する．近似的に表現するならば，途中の上昇部分が分子間の強磁性的相互作用に帰属できる．

分子構造をよく見ると，Cu(II)は5配位であり，内側の6番目の配位場所が空いている．この状況はクラウンエーテルやクリプタンドの状況の逆となっている．クラウンエーテル類はホストが非共有電子対を有するためにゲスト分子は金属イオンである．一方，本錯体はホストが非共有電子対を受け入れうるので，ゲストとしての候補は，ハロゲン化物イオン，水，酸素や窒素原子をもつ有機物となる．

5の合成の際に，塩化リチウム，ナトリウム，カリウム塩を共存させて六核錯体を析出させると[27]，元素分析結果は，それぞれ，$(LiCl)_6$@**5**, $(NaCl)_2$@**5**, $(KCl)_2$@**5**という組成を示した．これらのホスト-ゲスト錯体の磁気測定結果をFig. 8(a)に示した．7 K付近に観察される強磁性的相互作用が顕著に強められることがわかった．**6**と臭化アルカリ金属塩の組み合わせも同様の挙動を示した．また，有機ゲストを用いた場合にも強磁性的相互作用の増大が認められた[28]．水を加えた溶媒から析出させた結晶$(H_2O)_n$@**5**は，ゲスト分子として水が想定される[27]．合成直後の試料では，他のゲストの場合と同様に強磁性的相互作用の増大が見られたが，試料を減圧下乾燥し，再び同一の測定条件で磁化率を測定したところ，空のホストのときの強磁性的相互作用の強さに戻った(Fig. 8(b))．チューブ状の空隙から水分子を抜き取ることができたと考えられる．なお，X線結晶構造解析により結晶の空間群とセル定数を決定したところ，ホストだけの場合に見られた結晶構造を維持していたので，ゲストはチューブの中にある．チューブの中に電子密度を認めることはできたが，ディスオーダーのためにゲスト分子を描くことはできなかった．

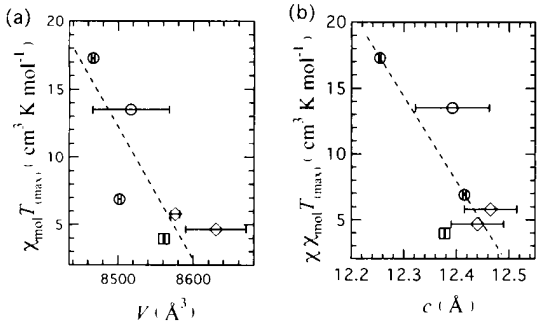

Fig. 9 Correlations between the $\chi_{mol}T$ maximum value and the cell volume (V) (a) and between the $\chi_{mol}T$ maximum value and the c length (b) for the host-guest compounds of **5**. Guest molecules are MCl (M=Li, Na, K) (circles), organic compounds (diamonds), and none (squares).

構造と磁性の相関を調べるために，セル体積と$\chi_{mol}T$の最大値との関係をプロットしたものがFig. 9(a)である．個々のセル定数との関係を調べると，c軸との関係が認められた(Fig. 9(b))．結論は，ゲスト包接がc軸の短縮を伴って強磁性的相互作用を増大させるということである．ゲスト分子が入ることにより，ハロゲン化金属塩ならばクーロン引力，有機芳香族分子ならπ-π相互作用，水ならば水素結合がc軸に異方的に働くのであろう．この結晶構造がゲストがなくてもつぶれることがないのは，ハニカム格子の力学的な強度が強いことを反映しているように思われるが，分子スタック方向では分子間力がゆるいのでこちらへ一方的に圧縮されやすいことにも原因があるだろう．

構造の変化による磁性の変化は次のように説明できる．ゲストが包接されると，分子スタック方向が近接する．この異方的なゆがみは，分子間の強磁性的相互作用を与える一次元鎖に対して，鎖を縮める方向の圧縮をもたらす．したがって，そこに働く強磁性的相互作用が増大する．この物質は磁気転移することはなかったが，強磁性的相互作用をゲストにより増減できることがわかった．

3. ま と め

以上，筆者らの開発した2種の超分子磁性体を紹介した．ゲスト分子によりホストの磁性を調整できることを示すことができた．題目にある『制御』という観点では，ここで説明した実験以上に今後スイッチング挙動や可逆性の検証を進めていく必要がある．ところで，情報記録材料をはじめとする電子物性材料は外部刺激に対する応答速度が重要であるが，ホスト-ゲスト化学という化学反応プロセスは本質的に反応速度定数に縛られていて，そのような用途に向くかどうかについて疑問をもつ向きもあるだろう．しかし先に述べたように，これまでのテクノロジーの枠にとらわれた磁性開発は分子磁性研究の目指すところではない．例えばDNA断片がコンピュータに使われることが取りざたされる時代である．たとえ化学反応をウェットなプロセスで行うにしても，演算素子，情報記録素子，表示材料，ナノテクノロジー以外にも，従来にない新しいテクノロジーへ展開される可能性は十分にある．新規な材料を開発していくには新規な用途の提案を伴わねばならない．

謝　辞　分子磁性を研究対象として仕事を進めてきたのは，岩村　秀教授（放送大学；東大理（当時））の示唆によっており，ピリミジン架橋配位子のアイディアは高スピン分子開発に携わらなければ決して発案できなかったものである．X線結晶構造解析では岩崎不二子教授，安井正憲助教授（電通大量子物質），橋爪大輔博士（理研）のお世話になった．磁気的相互作用の機構については，山口　兆教

授と川上貴資博士（阪大理），および吉澤一成教授（九大有基研）に理論的サポートをいただいた．合成と磁気測定は野上-石田研の学生であった日下高治君，小俣順一君，高上直美君の努力の賜物である．この場を借りてお礼申し上げる．

参考文献

1) J. A. Crayston, J. N. Devine, and J. C. Walton: *Tetrahedron*, **56**, 7829 (2000); H. Iwamura: *Adv. Phys. Org. Chem.*, **26**, 179 (1990); J. S. Miller and A. J. Epstein: *Angew. Chem. Int. Ed.*, **33**, 385 (1994).
2) M. Kinoshita, P. Turek, M. Tamura, K. Nozawa, D. Shiomi, Y. Nakazawa, M. Ishikawa, M. Takahashi, K. Awaga, T. Inabe, and Y. Maruyama: *Chem. Lett.*, 1225 (1991).
3) R. Chiarelli, M. A. Novak, A. Rassat, and J. L. Tholence: *Nature*, **363**, 147 (1993).
4) T. Nogami, T. Ishida, M. Yasui, F. Iwasaki, N. Takeda, M. Ishikawa, T. Kawakami, and K. Yamaguchi: *Bull. Chem. Soc. Jpn.*, **69**, 1841 (1996).
5) 北川　進著：「集積型金属錯体」講談社サイエンティフィク (2001).
6) A. Caneschi, D. Gatteschi, and R. Sessoli: *Acc. Chem. Res.*, **22**, 392 (1989).
7) J. M. Manriquez, G. T. Yee, R. S. McLean, A. J. Epstein, and J. S. Miller: *Science*, **252**, 1415 (1991).
8) 妹尾　学，荒木孝二，大月　穣著：「超分子化学」，東京化学同人 (1998).
9) G. L. J. A. Rikken and E. Raupach: *Nature*, **390**, 493 (1997); K. Inoue, H. Imai, P. S. Ghalsasi, K. Kikuchi, M. Ohba, H. Okawa, and J. V. Yakhmi: *Angew. Chem. Int. Ed.*, **40**, 4242 (2001); E. Coronado, C. J. Gomez-Garcia, A. Nuez, F. M. Romero, E. Rusanov, and H. Stoeckli-Evans: *Inorg. Chem.*, **41**, 4615 (2002).
10) K. Nakayama, T. Ishida, R. Takayama, D. Hashizume, M. Yasui, F. Iwasaki, and T. Nogami: *Chem. Lett.*, 497 (1998); K. Zusai, T. Kusaka, T. Ishida, R. Feyerherm, M. Steiner, and T. Nogami: *Mol. Cryst. Liq. Cryst.*, **343**, 127 (2000); R. Feyerherm, A. Loose, T. Ishida, T. Nogami, J. Kreitlow, D. Baabe, F. J. Litterst, S. Suellow, H.-H. Klauss, and K. Doll: *phys. Rev. B*, 投稿中.
11) D. Gatteschi and R. Sessoli: *Angew. Chem. Int. Ed.*, **42**, 268 (2003); G. Christou, D. Gatteschi, D. N. Hendrickson, and R. Sessoli: *MRS Bull.*, **25**, 66 (2000).
12) Y. Kobayashi, T. Ishida, and T. Nogami: 投稿準備中.
13) K. Awaga, E. Coronado, and M. Drillon: *MRS Bull.*, **25**, 52 (2000).
14) J. Larionova, M. Gross, M. Pilkington, H. Andres, H. Stoeckli-Evans, H. U. Güdel, and S. Decurtins: *Angew. Chem. Int. Ed.*, **39**, 1605 (2000).
15) M. Fujita, K. Umemoto, and M. Yoshizawa: *Chem. Commun.*, 509 (2001).
16) M. Eddaoudi, D. B. Moler, H. Li, B. Chem, T. M. Reineke, M. O'Keeffe, and O. M. Yaghi: *Acc. Chem. Res.*, **34**, 319 (2001); S. Kitagawa and M. Kondo: *Bull. Chem. Soc. Jpn.*, **71**, 1739 (1998).
17) T. Kusaka, T. Ishida, D. Hashizume, F. Iwasaki, and T. Nogami: *Chem. Lett.*, 1146 (2000).
18) T. Kusaka, T. Ishida, and T. Nogami: *Mol. Cryst. Liq. Cryst.*, **379**, 259 (2002).
19) N. Takagami, T. Ishida, and T. Nogami: 投稿準備中.
20) T. Kusaka, T. Ishida, D. Hashizume, F. Iwasaki, and T. Nogami: *Mol. Cryst. Liq. Cryst.*, **376**, 463 (2002).
21) R. Feyerherm, S. Abens, D. Günther, T. Ishida, M. Meissner, M. Meschke, T. Nogami, and M. Steiner: *J. Phys.: Condens. Matter*, **12**, 8495 (2000).
22) J. Omata, T. Ishida, D. Hashizume, F. Iwasaki, and T. Nogami: *Mol. Cryst. Liq. Cryst.*, **376**, 455 (2002).
23) J. Omata, T. Ishida, D. Hashizume, F. Iwasaki, and T. Nogami: *Inorg. Chem.*, **40**, 3954 (2001).
24) T. Ishida, T. Kawakami, S.-i. Mitsubori, T. Nogami, K. Yamaguchi, and H. Iwamura: *J. Chem. Soc., Dalton Trans.*, 3177 (2002); F. Mohri, K. Yoshizawa, T. Yamabe, T. Ishida, and T. Nogami: *Mol. Eng.*, **8**, 357 (1999).
25) H. M. McConnell: *J. Chem. Phys.*, **39**, 1910 (1963); 野上　隆：応用物理，**63**, 674 (1994).
26) K. Inoue and H. Iwamura: *Chem. Phys. Lett.*, **207**, 551 (1995); T. Kawakami, A. Oda, W. Mori, K. Yamaguchi, K. Inoue, and H. Iwamura: *Mol. Cryst. Liq. Cryst.*, **279**, 29 (1996).
27) J. Omata, T. Ishida, and T. Nogami: *Polyhedron*, in press.
28) J. Omata, T. Ishida, D. Hashizume, F. Iwasaki, and T. Nogami: *Polyhedron*, **20**, 1557 (2001).

（2003年3月31日受理）

石田尚行　いしだ　たかゆき
平3　東京大学大学院理学系研究科化学専攻博士課程修了，電気通信大学電気通信学部助手，同講師，同助教授，現在に至る．
専門　有機物理化学　（理博）

野上　隆　のがみ　たかし
昭46　東京大学大学院理学系研究科化学専攻博士課程修了，大阪大学工学部助手，同講師，同助教授，**平2**　電気通信大学電気通信学部教授，現在に至る．
専門　有機固体物性化学　（理博）

5 January 2001

ELSEVIER

Chemical Physics Letters 333 (2001) 69–75

CHEMICAL PHYSICS LETTERS

www.elsevier.nl/locate/cplett

Pressure effects of genuine organic crystalline ferromagnet possessing intermolecular contacts between nitroxide oxygen and methyl hydrogen atoms

M. Mito [a,*], T. Kawae [a], M. Hitaka [a], K. Takeda [a,b], T. Ishida [c], T. Nogami [c]

[a] *Department of Applied Quantum Physics, Faculty of Engineering, Kyushu University, Fukuoka 812-8581, Japan*
[b] *Institute of Environmental Systems, Faculty of Engineering, Kyushu University, Fukuoka 812-8581, Japan*
[c] *Department of Applied Physics and Chemistry, The University of Electro-Communications, Chofu, Tokyo 182-8585, Japan*

Received 29 August 2000; in final form 7 November 2000

Abstract

We have found the pressure-induced (1) periodical down–up variation of transition temperature (T_c), (2) ferro- to antiferro-magnetic transition and (3) reduction of the magnetic lattice dimensionality in a genuine organic crystalline bulk-ferromagnet *p*-Cl–C_6H_4–CH=N-TEMPO ($T_c = 0.28$ K) with spin polarizations on intermolecular contacts between the nitroxide oxygen and methyl hydrogen atoms (C–H $\cdots$ O–N contacts). These phenomena can be understood by the pressure-induced rotation of the methyl moiety relevant to the interaction-mechanism through C–H $\cdots$ O–N contacts.

1. Introduction

Since the discovery of bulk-ferromagnetic transition in β-phase *p*-nitrophenyl nitronyl nitroxide ($C_{13}H_{16}N_3O_4$, abbreviated as β-phase *p*-NPNN) [1], several genuine organic bulk-ferromagnets consisting of only light elements (e.g. H, C, N, O etc.) have been found [2–5]. In these systems, the unpaired electron is delocalized over the whole molecule, and their mechanisms for the ferromagnetic intermolecular interaction are very complicated (see, for example, [6]). Their transition temperatures (T_c's) have not exceeded 1.5 K yet, due to their complexity. In the case of β-phase *p*-NPNN ($T_c = 0.61$ K), spin polarizations on C, N and O are pointed out to be important in understanding the bulk-ferromagnetism [7]. However, the importance of the spin polarization on the lightest H atoms has not been recognized sufficiently.

We report the first experimental result indicating the importance of the spin polarization on H atom sites in realizing the genuine organic bulk-ferromagnetism. We investigated the pressure effects in a prototype of genuine organic bulk-ferromagnets with intermolecular contacts between the nitroxide oxygen and methyl hydrogen atoms (C–H $\cdots$ O–N contacts), 4-(*p*-chlorobenzylideneamino)-2,2,6,6-tetramethylpiperidin-1-yloxyl ($C_{16}H_{22}ClN_2O$, *p*-Cl–C_6H_4–CH=N-TEMPO, abbreviated as Cl-TEMPO here, see Fig. 1a) with $T_c = 0.28$ K [4]. The nitroxide oxygen atom in the

* Corresponding author. Fax: +81-92-633-6958.
E-mail address: mitohtap@mbox.nc.kyushu-u.ac.jp (M. Mito).

0009-2614/01/$ - see front matter
PII: S0009-2614(00)01344-0

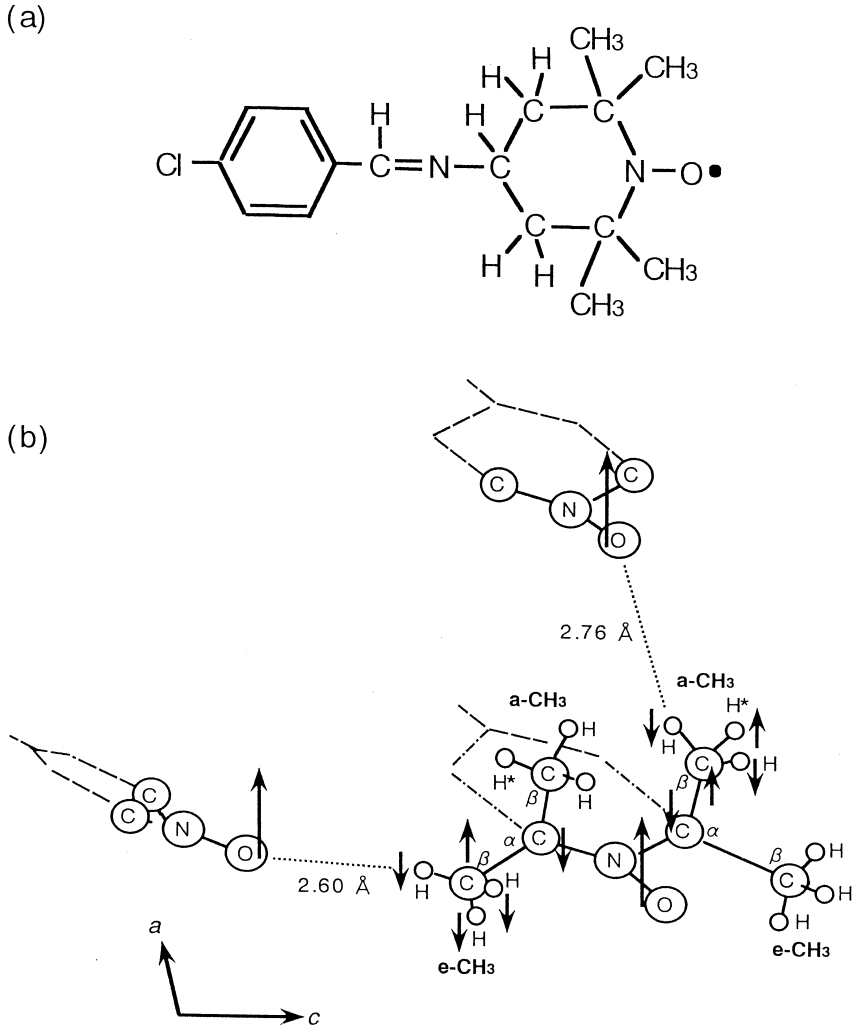

Fig. 1. (a) Molecular structure of Cl-TEMPO. (b) Space alignment of principal spin polarizations of Cl-TEMPO molecules. The carbon adjacent to the nitroxide nitrogen is called as α-carbon, and the carbon of the methyl moiety is called as β-carbon. Four methyl moieties linked to the TEMPO ring are classified to two equatorial methyl (e-CH_3) groups and two axial methyl (a-CH_3) ones.

TEMPO-based ferromagnets is always located near methyl- and/or methylene-hydrogen atoms at a β-position from an nitroxide group in adjacent molecules, and the interatomic distances (2.5–2.9 Å) are close to the sum of the van der Waals radii of H and O atoms [8]. The pressurization can bring about intramolecular transformation (e.g. a rotation of a molecular group) as well as intermolecular shrinkage, and we can artificially change the environment around the H atoms in Cl-TEMPO.

Prior to this experiment, the pressure effects of the prototype of genuine organic bulk-ferromagnet β-phase *p*-NPNN have been already investigated; the ferro- to antiferro-magnetic (F–AF) transition [9,10] and the reduction of the magnetic lattice dimensionality of dominant interactions from three into two [11] have been observed and these behaviors have been explained with the pressure-induced rotation of nitrophenyl moiety [12].

2. Experimental

The preparation of Cl-TEMPO has been described elsewhere [4]. The crystal structure of Cl-TEMPO belongs to monoclinic with the space group $P2_1/c$, and the lattice parameters $a = 5.909$ Å, $b = 24.475$ Å, $c = 11.421$ Å and $\beta = 103.84°$ [4,13]. The magnetism of this compound has already been investigated by the measurements of magnetic susceptibility, magnetization [4], heat capacity [14,15] and μSR [16]. Fig. 1 shows the principal spin polarizations along the path of magnetic interactions [4,8]. The polarized neutron diffraction experiment shows that an NO moiety of TEMPO ($C–CH_2–C(CH_3)_2–NO–C(CH_3)_2–CH_2–C$) ring has about 78% of spin density [17]. If we assign a positive spin on the NO portion, intramolecular spin polarization results in the slightly negative spin density on some hydrogens of methyl moieties (abbreviated as β-hydrogens), which couples magnetically with NO radical sites of the adjacent molecules (see Fig. 1b). This mechanism due to C–H···O–N contacts (β-hydrogen mechanism) makes an appearance of two-dimensional ferromagnetic alignment on the *ac*-plane in Cl-TEMPO [4,8,14,15]. The ferromagnetic planes are stacked along *b*-axis with the interplane distance of 10.86 Å (O···O), giving very weak interplane interaction. Recently in another TEMPO-based ferromagnetic compound possessing the two-dimensional network, it had been pointed out that the dipolar interaction plays the important role as the interplane interaction [18]. Furthermore we have to mention four methyl groups linked to the TEMPO ring, in explaining the ferromagnetism of Cl-TEMPO. They are classified into two groups; one is an equatorial methyl (e-CH_3) group on the TEMPO plane, and the other an axial methyl (a-CH_3) group with the C–C bond perpendicular to the averaged TEMPO plane. Solid state NMR measurements [19] and molecular orbital calculations clarified that all hydrogens of e-CH_3 have negative spin densities, whereas two hydrogens of a-CH_3 also have negative spin densities and only one hydrogen H^* of a-CH_3 has a positive spin density (see Fig. 1b). From a closer look at the crystal structure, the H^* atoms do not take part in the interaction paths between neighboring molecules at ambient pressure.

We have measured ac magnetic susceptibility (χ_{ac}), magnetization (M) and heat capacity (C) of Cl-TEMPO under hydrostatic pressures up to 14.4 kbar [11]. The hydrostatic pressure was attained with a Cu–Be clamp cell (13ø × 50 mm), and the polycrystalline sample of Cl-TEMPO (75.9 mg) mixed with the pressure transmission oil (Apiezon-K grease, 36.1 mg) and some tips of Al metal (3.9 mg) were enclosed in a small teflon cell. The real pressure at low temperatures was estimated from the superconducting transition temperature of Al [20]. Ac magnetic susceptibility (χ_{ac}) was measured by the ac-bridge ($H_{ac} = 0.1$ Oe and $f = 15.9$ Hz) in the temperature region from 0.14 to 2.0 K and external magnetic fields (H's) up to 300 Oe. The magnetization was obtained by integrating the in-phase component of ac magnetic susceptibility (χ'_{ac}) against the external magnetic field (H). With a small $H_{ac}(f)$ with a low frequency of $f = 15.9$ Hz, χ'_{ac} is almost identical with static dM/dH in this system. The heat capacity was measured by a quasi-adiabatic heat-pulse method in the temperature region from 0.13 to 4.5 K. The magnetic heat capacity of Cl-TEMPO is so dominant at low temperatures that the heat capacities of Apiezon-K grease, teflon cell, and lattice contribution of Cl-TEMPO could be ignored below 2.5 K.

3. Experimental results

Fig. 2 shows some experimental results of in-phase component (χ'_{ac}) in the pressure region up to 13.6 kbar at $H = 0$. The behavior of the out-of-phase is qualitatively the same as χ'_{ac}. The temperature with the peak of χ'_{ac} corresponds to the bulk-ferromagnetic transition temperature (T_c) [4]. Fig. 3 shows the pressure dependence of T_c of Cl-TEMPO up to 14.4 kbar. Pressure dependence of χ'_{ac} of Cl-TEMPO looks nonsystematic, but there are two regularities: (1) T_c repeats down–ups with a period of about 4 kbar for $P < 9$ kbar and eventually change turns to a monotonous and slight increase for $P \geqslant 9$ kbar. (2) The magnitude of χ'_{ac} monotonously decreases with increasing pressure. The latter means a suppression of the net

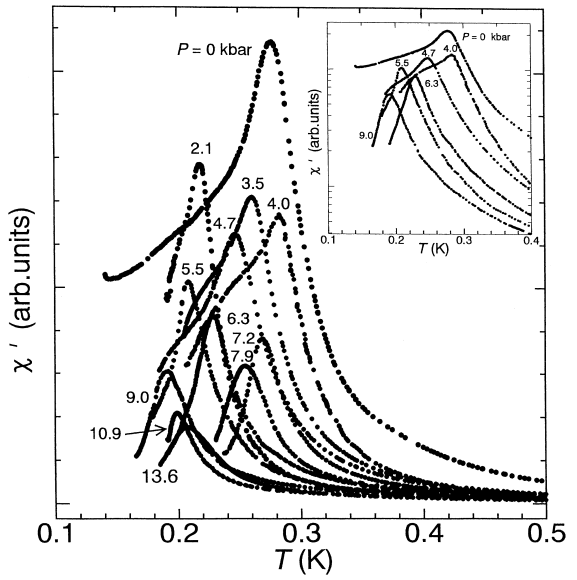

Fig. 2. Some results χ'_{ac} of Cl-TEMPO in the pressure region up to 13.6 kbar. The ordinate of the inset figure is plotted in a logarithmic scale.

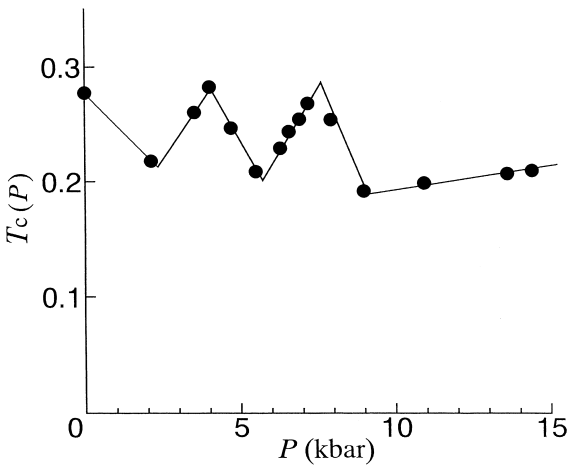

Fig. 3. Pressure dependence of $T_c(P)$ of Cl-TEMPO up to 14.4 kbar.

ferromagnetic interaction by the pressurization. In order to clarify these pressure effects of χ_{ac} in more detail, we have investigated the pressure effects on the magnetization and the heat capacity.

Fig. 4 shows the magnetization (M) curve in the pressure region up to 13.6 kbar at lower temperature than the corresponding T_c. Here M at each pressure is normalized with the saturated magnetization at $P = 0$ (M_s). At $P = 0$ kbar, the initial gradient of the magnetization is linear and rapid, and the magnetization shows a saturation in a small magnetic field of 150 Oe. The development of the magnetization is monotonously suppressed with increasing pressure. At $P = 4.0$ kbar, we can still see a ferromagnetic rapid increase of the magnetization. At $P \geqslant 6.9$ kbar, however, the magnetization shows a concave curve, or a behavior of the spin flopping peculiar to the bulk-antiferromagnetic ordering, and the flopping field becomes larger with increasing pressure. Coming back to the inset of Fig. 2, we notice the different temperature dependence of χ_{ac} below T_c; χ_{ac} at $P \leqslant 4.7$ kbar has a tendency to maintain a gradual decrease below T_c, but that at $P \geqslant 5.5$ kbar tends to drop rapidly below T_c. This difference of χ'_{ac} below T_c appears in the difference of the initial development of the magnetization. We estimated the critical pressure of pressure-induced F–AF transition to be about 5 kbar.

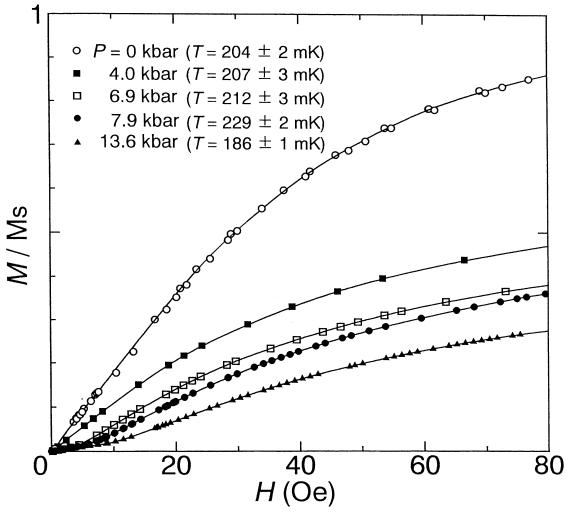

Fig. 4. Magnetization (M) curve of Cl-TEMPO at $P \leqslant 13.6$ kbar. These measurements have been performed at lower temperatures than the corresponding $T_c(P)$. M at each pressure is normalized with the saturated magnetization at $P = 0$ (M_s). Each solid curve is a guide for the eye.

The heat capacity gives us the information about the magnetic lattice dimensionality and the magnitude of dominant interactions as well as T_c.

Fig. 5 shows the low-temperature heat capacities (C's) at three representative pressures $P = 0$, 7.6 and 14.4 kbar, which correspond to the ferromagnetic region, the antiferromagnetic one just after the F–AF transition and the strongly restricted antiferromagnetic one, respectively. At $P = 0$ kbar, we observed a sharp anomaly of three-dimensional magnetic order at $T = 0.27$ K and a broad tail characteristic of short range ordering above $T = 0.5$ K, whose development is reproduced with the spin $S = 1/2$ two-dimensional Heisenberg ferromagnetic (2DHF) model with $J/k_B = 0.55 \pm 0.03$ K (curve (a)) [21,22]. This two-dimensional behavior of C at $P = 0$ kbar has been confirmed by Sorai et al. [14,15]. On the other hand, C at $P = 14.4$ kbar shows a plateau peculiar to the $S = 1/2$ one-dimensional Heisenberg ferromagnetic (1DHF) system [23] above $T = 0.5$ K, and the intrachain interaction is estimated to be $J/k_B = 0.63 \pm 0.07$ K (curve (b)). The three-dimensional magnetic order at $T = 0.17$ K is of the bulk-antiferromagnetic ordering, referring to the results of magnetization. It should be noticed that the system at $P = 14.4$ kbar has transformed to the quasi-one-dimensional ferromagnetic system. From the mean field theory for the quasi-one-dimensional system with the interchain coupling zJ' (z the number of the interchain interaction path; J' the interchain interaction) [24], we can estimate the one dimensionality at $P = 14.4$ kbar as $|zJ'/J| \simeq 4 \times 10^{-2}$. Meanwhile at $P = 7.6$ kbar, we can see both the characters of the 2DHF system (curve (c); $J/k_B = 0.27 \pm 0.02$ K [21,22]) and the 1DHF one (curve (d); $J/k_B = 0.75 \pm 0.07$ K [23]), but the overall behavior is closer to one-dimensional rather than two-dimensional. These experimental facts reveal that the reduction of the magnetic lattice dimensionality becomes an important factor in realizing the bulk-antiferromagnetic ordered state under high pressures. This phenomenon has been also seen in β-phase p-NPNN [9–12].

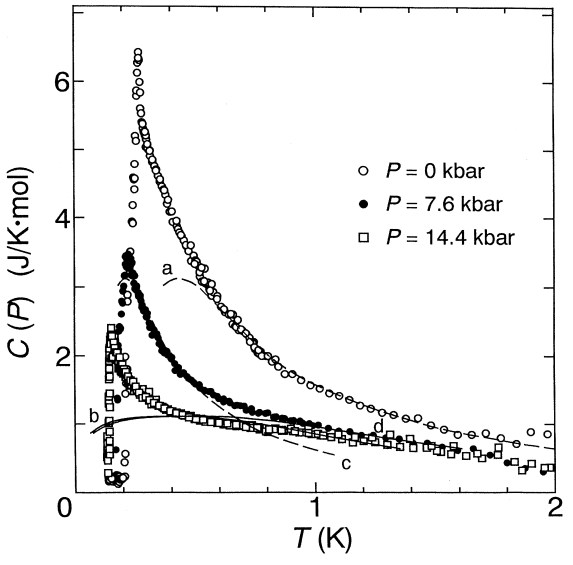

Fig. 5. Heat capacity of Cl-TEMPO at $P = 0$, 7.6 and 14.4 kbar. The broken curves of (a,c) show the theoretical curves of 2DHF system with $J/k_B = 0.55$ and 0.27 K. The solid curves (b,d) show the theoretical curves of 1DHF system with $J/k_B = 0.63$ and 0.75 K.

4. Discussion

We discuss the above interesting experimental facts based on the β-hydrogen mechanism. In explaining the periodical down–ups of T_c, we thought of intramolecular deformation of several atomic positions and/or rotation of a portion of molecule. Recently the pressure-induced molecular rotation has been experimentally indicated in the molecules with the hydrogen bonds (e.g. HCl, H_2S, NH_3) and CH_4 by the optical measurements [25]. In β-phase p-NPNN, the rotation of nitrophenyl group by the pressurization has been expected [12]. Theoretically the periodical increase and decrease of intermolecular interaction by the rotation of the methyl moiety have been already analyzed for C_6H_5–CH=N-TEMPO [26]. We have reached the following conclusion: In Cl-TEMPO, the pressure-induced rotation of the methyl moiety triggers the periodical decrease and increase of the ferromagnetic interaction on the ac-plane, which leads to the periodical change of T_c. The shrinkage between ac-planes is also possible by the pressurization. But this effect will be complementary when compared with above drastic changes by the rotation of the methyl moieties, since the interplane intermolecular distance is twice as large as intraplane one. It has been confirmed that the crystal

symmetry does not change within the present experimental pressure region by the powdered X-ray diffraction measurement [29].

In order to explain the overall pressure effects of Cl-TEMPO in detail, we must consider not only the movements of H atoms but also the existence of H^* and the change of the spin density by them. As we have already described, there are two types of β-hydrogen atoms in Cl-TEMPO; positively and negatively spin-polarized ones. The intermolecular interaction along a-axis is propagated through a-CH_3 with H^*, and on the other hand, that along c-axis is done through e-CH_3 without H^* (see Fig. 1b). At ambient pressure, the ferromagnetic interaction between neighboring molecules is realized by C–H$\cdots$O–N contacts with negatively spin-polarized H atom. However, under the pressure the another interaction path C–$H^*\cdots$O–N can also be take effect, and contributes as an antiferro-magnetic term. The effect of H^* by the methyl rotation leads to the change of the balance of ferro- and antiferromagnetic contributions, and consequently T_c would fall or rise. This effect is dominant in the intermolecular interaction path along a-axis. The strong restricted state at $P \geqslant 9$ kbar is probably the quasi one-dimensional system with the ferromagnetic intrachain interaction along c-axis and the antiferromagnetic interchain one along a-axis. Furthermore, methyl rotation gives rise to the change of spin density on the β-hydrogen atoms, since the magnitude of the spin density of β-hydrogen is sensitive to the conformation, especially, the dihedral angle around N–C(α)–C(β)–H(β) [27,28]. Thus, a few factors bring about the periodical down–ups of T_c, and these effects do not appear in β-phase p-NPNN.

Generally in a genuine two-dimensional Heisenberg system with $S = 1/2$, there is no long range magnetic order at finite temperatures [30], but weak interplane interactions and/or slight anisotropy trigger the magnetic order. In reality, T_c of Cl-TEMPO has a finite T_c due to these effects, even when it comes down to the lowest temperatures. Furthermore in the higher pressure than 9.0 kbar, T_c changes only slightly. In Cl-TEMPO, the nearest neighbor distances between oxygen and hydrogen in neighboring molecules at ambient pressure are 2.76 Å along a-axis and 2.60 Å along c-axis, which are quite close to the sum of the van der Waals radii of H and O atoms (1.20 Å + 1.40 Å). Under high pressures, the intramolecular transformations are restricted, and the large intermolecular shrinkage also cannot be expected, due to the effect of van der Waals force.

5. Conclusion

We have found the pressure-induced (1) periodical down–up variation of transition temperature, (2) ferro- to antiferromagnetic transition and (3) reduction of the magnetic lattice dimensionality in genuine organic bulk-ferromagnet Cl-TEMPO with spin polarizations on C–H$\cdots$O–N contacts. These phenomena can be understood by the pressure-induced rotation of the methyl moiety relevant to the interaction-mechanism through C–H$\cdots$O–N contacts. Our experimental results firstly indicates that the spin polarization on the H atom plays the important roles in realizing the genuine organic bulk-ferromagnetism.

Acknowledgements

This work was supported in part by Grant-in-Aid for Scientific Research (A) (12305022) and (C) (12640558), and a Grant-in-Aid for Scientific Research on Priority Areas (B) of Molecular Conductors and Magnets (Area No. 730/11224206) from the Ministry of Education, Science, Sports and Culture, Japan.

References

[1] M. Kinoshita, P. Turek, M. Tamura, K. Nozawa, D. Shiomi, Y. Nakazawa, M. Ishikawa, M. Takahashi, K. Awaga, T. Inabe, Y. Maruyama, Chem. Lett. (1991) 1225.
[2] R. Chiarelli, M.A. Novak, A. Rassat, J.L. Tholence, Nature 363 (1993) 147.
[3] T. Sugawara, M. Matushita, A. Izuoka, N. Wada, N. Takeda, M. Ishikawa, J. Chem. Soc. Chem. Commun. (1994) 1723.
[4] T. Nogami, T. Ishida, H. Tsuboi, H. Yoshikawa, H. Yamamoto, M. Yasui, F. Iwasaki, H. Iwamura, N. Takeda, M. Ishikawa, Chem. Lett. (1995) 635.

[5] S. Nakatsuji, H. Morimoto, H. Anzai, J. Kawashima, K. Maeda, M. Mito, K. Takeda, Chem. Phys. Lett. 296 (1998) 159.
[6] M. Kinoshita, Jpn. J. Appl. Phys. 33 (1994) 5718.
[7] M. Okumura, K. Yamaguchi, M. Nakano, W. Mori, Chem. Phys. Lett. 207 (1993) 1.
[8] T. Nogami, T. Ishida, M. Yasui, F. Iwasaki, N. Takeda, M. Ishikawa, T. Kawakami, K. Yamaguchi, Bull. Chem. Soc. Jpn. 69 (1996) 1841.
[9] M. Mito, T. Kawae, M. Takumi, K. Nagata, M. Tamura, M. Kinoshita, K. Takeda, Phys. Rev. B 56 (1997) 14255.
[10] K. Takeda, M. Mito, T. Kawae, M. Takumi, K. Nagata, M. Tamura, M. Kinoshita, J. Phys. Chem. B 102 (1998) 671.
[11] K. Takeda, K. Konishi, M. Tamura, M. Kinoshta, Phys. Rev. B 53 (1996) 3374.
[12] K. Takeda, M. Mito, T. Kawae, H. Deguchi, S. Takagi, M. Okumura, T. Kawakami, K. Yamaguchi, M. Kinoshita, Chem. Phys. Lett. 308 (1999) 181.
[13] F. Iwasaki, J.H. Yoshikawa, H. Yamamoto, E. Kan-nari, K. Takeda, M. Yasui, T. Ishida, T. Nogam, Acta. Cryst. B 55 (1999) 231.
[14] Y. Miyazaki, T. Matsumoto, T. Ishida, T. Nogami, M. Sorai, Bull. Chem. Soc. Jpn. 73 (2000) 67.
[15] M. Sorai, Y. Miyazaki, T. Hashiguchi, in: P.M. Lahti (Ed.), Magnetic Properties of Organic Materials, Marcel Dekker, New York, p. 475.
[16] R. Imachi, T. Ishida, T. Nogami, S. Ohira, K. Nishiyama, K. Nagamine, Chem. Lett. (1997) 233.
[17] Y. Pontillon, T. Ishida, E. Lelievre–Berna, T. Nogami, E. Ressouche, J. Schweizer, Mol. Cryst. Liq. Cryst. 334 (1999) 359.
[18] T. Ishida, S. Ohira, T. Ise, K. Nakayama, I. Watanabe, T. Nogami, K. Nagamine, Chem. Phys. Lett. 330 (2000) 110.
[19] G. Murata, S. Takeda, R. Imachi, T. Ishida, T. Nogami, K. Yamaguchi, J. Am. Chem. Soc. 121 (1999) 424.
[20] M. Levy, J.L. Olsen, Solid State Commun. 2 (1964) 137.
[21] G.A. Baker Jr., H.E. Gilbert, J. Eve, G.S. Rushbrooke, Phys. Lett. 25A (1967) 207.
[22] K. Yamaji, J. Kondo, J. Phys. Soc. Jpn. 35 (1973) 25.
[23] J.C. Bonner, H.E. Fisher, Phys. Rev. 135 (1964) A640.
[24] M. Steiner, J. Villain, C.G. Windson, Adv. Phys. 25 (1976) 87.
[25] H. Shimizu, K. Kamabuchi, T. Kume, S. Sasaki, Phys. Rev. B 59 (1999) 11727.
[26] T. Kawakami, A. Oda, S. Takeda, W. Mori, T. Ishida, M. Yasui, F. Iwasaki, T. Nogami, K. Yamaguchi, Mol. Cryst. Liq. Cryst. 306 (1997) 141.
[27] Y. Ellinger, R. Subra, J. Chem. Phys. 62 (1975) 10.
[28] D. Ondercin, T. Sandreczki, R.W. Kreilick, J. Mag. Reson. 34 (1979) 151.
[29] M. Takumi, K. Nagata, private communication.
[30] N.D. Mermin, H. Wagner, Phys. Rev. Lett. 17 (1966) 1133.

Single-Component Organic Semiconductors Based on Novel Radicals that Exhibit Electrochemical Amphotericity: Preparation, Crystal Structures, and Solid-State Properties of *N*,*N*′-Dicyanopyrazinonaphthoquinodiiminides Substituted with an *N*-Alkylpyridinium Unit

Takanori Suzuki*

Division of Chemistry, Graduate School of Science, Hokkaido University,Sapporo 060-0810, Japan

Setsuko Miyanari, Yoshiaki Tsubata, Takanori Fukushima, and Tsutomu Miyashi

Department of Chemistry, Graduate School of Science, Tohoku University, Aoba-ku, Sendai 980-8578, Japan

Yoshiro Yamashita

Department of Chemistry, Interdisciplinary Graduate School of Science and Engineering, Tokyo Institute of Technology, Midori-ku, Yokohama 226-8502, Japan

Kenichi Imaeda

Institute for Molecular Science, Myodaiji, Okazaki 444-8585, Japan

Takayuki Ishida and Takashi Nogami

Department of Applied Physics and Chemistry, The University of Electro-Communications, Chofugaoka, Chofu 182-8585, Japan

tak@sci.hokudai.ac.jp.

Received September 12, 2000

N,*N*′-Dicyanonaphthoquinodiimines fused with a pyrazine ring **1** were prepared from the corresponding quinones **4**. The new acceptors **1** have a planar π-system and undergo reversible two-stage 1e-reduction. Quaternization of the pyridyl substituent in **1d**−**f** gave pyridinium derivatives **2d**$^+$, **2e**$^+$, and R-**3**$^+$, respectively, which are stronger acceptors that undergo three-stage 1e-reduction. Upon electrochemical reduction of these cations, novel radicals **2d**$^\bullet$, **2e**$^\bullet$, and R-**3**$^\bullet$ were generated and isolated as stable solids. The molecular geometries determined by X-ray analysis indicated that these radicals adopt a zwitterionic structure, in which the unpaired electron is located on the quinodiimine unit but not on the pyridyl group. These novel radicals undergo facile and reversible 1e-oxidation as well as two-stage 1e-reduction. The observed amphotericity endows the radicals with electrical conductivities (10^{-5} to 10^{-9} S cm^{-1}), and these thus represent a new motif for single-component organic semiconductors.

Recently, much attention has been focused on multistage organic redox systems in the field of materials science. Among these, a series of compounds that show electrochemical amphotericity is of special interest,[1] where 1e-oxidation and reduction occur within an easily accessible potential window. Beside their potential application as NLO materials[2] or molecular electronic devices,[3] another unique property is their electrical conductivity[4] as a single component.[5−8] Although it is quite difficult to endow closed-shell species with high amphotericity,[1] this would be much easier to achieve with stable radicals. Furthermore, intrinsic conductivity is warranted in such open-shell species because the unpaired electron could become a carrier in the solid.[7,8] From this viewpoint, we previously studied a series of (A-π-D$^\bullet$)-type stable radicals **5** which have a pyrazino-TCNQ skeleton (Scheme 1). Form A can polarize to a zwitterionic structure, form B, by configuration interac-

(1) Nakasuji, K.; Yoshida, K.; Murata, I. *J. Am. Chem. Soc.* **1983**, *105*, 5136. Takahashi, K.; Suzuki, T. *J. Am. Chem. Soc.* **1989**, *111*, 5483. Bando, P.; Martín, N.; Segura, J. L.; Seoane, C.; Ortí, E.; Viruela, P. M.; Viruuela, R.; Albert, A.; Cano, F. H. *J. Org. Chem.* **1994**, *59*, 4618. Karikome, K.; Kitamura, C.; Tanaka, S.; Yamashita, Y. *J. Am. Chem. Soc.* **1995**, *117*, 6791.

(2) Marder, S. R.; Kippelen, B.; Jen, A. K.-Y.; Peyghambarian, N. *Nature* **1997**, *388*, 845.

(3) Petty, M. C.; Bryce, M. R.; Bloor, D. *Introduction to Molecular Electronics*; Oxford University Press: Oxford, 1995.

(4) Farges, J. P. *Organic Conductors: Fundamental and Applications*; Marcel Dekker: New York, 1994.

(5) Inokuchi, H.; Imaeda, K.; Enoki, T.; Mori, T.; Maruyama, Y.; Saito, G.; Okada, N.; Yamochi, H.; Seki, K.; Higuchi, Y.; Yasuoka, N. *Nature* **1987**, *329*, 39. Yamashita, Y.; Tanaka, S.; Imaeda, K.; Inokuchi, H. *Chem. Lett.* **1991**, 1213. Cordes, A. W.; Haddon, R. C.; Oakley, R. T.; Schneemeyer, L. F.; Waszczak, J. V.; Young, K. M.; Zimmerman, N. M. *J. Am. Chem. Soc.* **1991**, *113*, 582.

(6) Morimoto, K.; Inabe, T. *J. Mater. Chem.* **1995**, *5*, 1749. Kobayashi, A.; Tanaka, H.; Kumasaki, M.; Torii, H.; Narymbetov, B.; Adachi, T. *J. Am. Chem. Soc.* **1999**, *121*, 10763.

(7) Awaga, K.; Sugano, T.; Kinoshita, M. *Bull. Chem. Soc. Jpn.* **1985**, *58*, 1886.

(8) Tsubata, Y.; Suzuki, T.; Miyashi, T.; Yamashita, Y. *J. Org. Chem.* **1992**, *57*, 6749.

10.1021/jo001352r CCC: $20.00
Published on Web 12/16/2000

Scheme 1

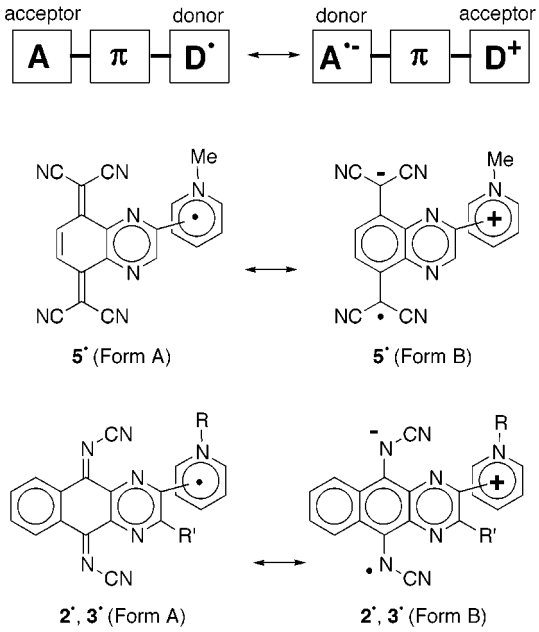

tion. In both forms, electron-donating and -accepting subunits are present to ensure electrochemical amphotericity, which forms the core of our molecular design. Radicals **5** were proven to be conductive as expected (10^{-5} to 10^{-9} S cm^{-1}),[8] yet the difficulty of obtaining single crystalline samples hampered the detailed measurement of their solid-state properties as well as the determination of their precise molecular geometries. In our continuing efforts to generate and characterize novel stable radicals with high electrical amphotericity,[9] we have found that *N*,*N*′-dicyanonaphthoquinodiimine (DCNNQI) fused with a pyrazine ring is a special skeleton that gives highly crystalline radicals of (A-π-D•) ↔ (A$^{-\bullet}$-π-D^{+})-type (Scheme 1). We report here the preparation, properties, and molecular and crystal structures of the title radicals **2**• and **3**•, which are new members of a rare class of semiconductors based on single-component pure organic materials.

Results and Discussion

Preparation, Structure, and Redox Behavior of Pyrazino-DCNNQIs (1). New DCNNQI derivatives fused with a pyrazine ring **1** were prepared by Hünig's method[10] from the corresponding pyrazinonaphthoquinones **4** and bis(trimethylsilyl)carbodiimide **6** under the influence of $TiCl_4$ or CsF. Probably due to the strong coordination of Ti to N atoms of pyrazine and/or pyridine rings, however, the reaction conditions had to be examined and adjusted for this series of quinones **4a**−**f**. Thus, the diphenyl derivative **1b** was obtained in 72% yield when quinone **4b**[11] was first complexed with $TiCl_4$ in CH_2Cl_2 and then heated with **6**. However, treatment of the parent quinone **4a**[11] by a similar procedure gave an intractable black tar. THF was shown to be a better

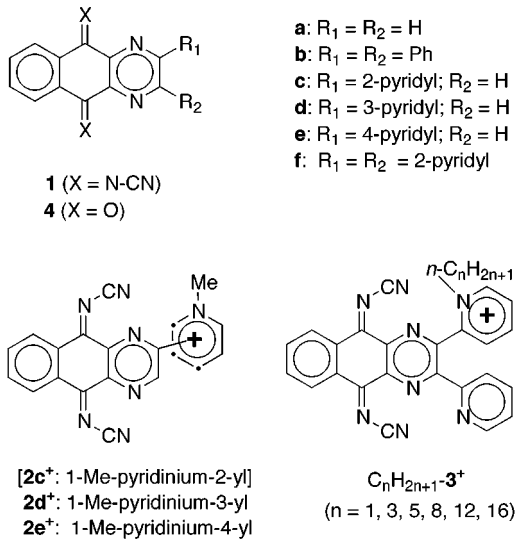

reaction medium in this case, and precomplexation of $TiCl_4$ with THF, but not with quinone, is effective for obtaining the unsubstituted pyrazino-DCNNQI **1a** in an acceptable yield (40%). The latter conditions also worked well for preparing compounds **1c**−**e** with a pyridil substituent from the corresponding quinones **4c**−**e**, which in turn were obtained by condensation reactions of 2,3-diaminonaphthoquinone[12] and bromoacetylpyridines in DMSO. Treatment of the diamine with 2,2′-pyridil gave quinone **4f** with two pyridine rings, which was converted to DCNNQI derivative **1f** by carbodiimide **6** in the presence of CsF but not $TiCl_4$. The DCNNQIs **1** thus prepared are stable orange crystals, but are sensitive to acid-catalyzed hydrolysis. They were best purified by recrystallization, since chromatographic separation caused partial decomposition of **1**.

A planar geometry is expected for the pyrazino-DCNNQI skeleton by considering the reported planarity for the parent DCNNQI[13] and pyrazino-TCNQ[8] skeletons. This idea was confirmed by an X-ray analysis of **1f**: the largest deviation of an atom from the least-squares plane is only 0.03 Å for the pyrazino-DCNNQI unit (Figure S1 in the Supporting Information). Due to the *o*-terphenyl-type structure, each of two pyridyl groups makes a dihedral angle of 49.3° or 30.6° with the pyrazine ring (Scheme 2). For comparison, an X-ray analysis was also conducted for **7f** with a tetracyanonaphthoquinodimethane (TCNNQ) skeleton (Figure S2), which was readily prepared by the condensation reaction of quinone **4f** with malononitrile. As shown in Scheme 2, the central six-membered ring of pyrazino-TCNNQ **7f** exhibits boat-form deformation, which is caused by steric repulsion between the *peri*-hydrogens and dicyanomethylene groups.[14,15] Two pyridyl groups are rotated against the pyrazine ring by 54.5° and 26.5° in **7f**, which are similar to the values observed in **1f**.

In accord with the planar π-system for the pyrazino-DCNNQI skeleton, **1a** undergoes reversible two-stage 1e-

(9) Amphoteric radicals exhibiting inverse polarization [(D-π−A•) ↔ (D$^{+\bullet}$-π−A^{-}); D = TTFs] were generated and characterized: Suzuki, T.; Yamada, M.; Ohkita, M.; Tsuji, T. *Heterocycles* **2001**, *54*, 387.

(10) Aumüller, A.; Hünig, S. *Angew. Chem., Int. Ed. Engl.* **1984**, *23*, 447; *Liebigs Ann. Chem.* **1986**, 142.

(11) Efimova, G. A.; Efros, L. S. *Zh. Org. Khim.* **1966**, *2*, 531 [*CA* **65**: 8910a].

(12) Winkelmann, E. *Tetrahedron* **1969**, *25*, 2427.

(13) Aumüller, A.; Hünig, S. *Angew. Chem., Int. Ed. Engl.* **1984**, *23*, 449.

(14) Schubert, U.; Hünig, S.; Aumüller, A. *Liebigs Ann. Chem.* **1985**, 1216.

(15) Iwasaki, F. *Acta Crystallogr.* **1971**, *B27*, 1360. Kabuto, C.; Fukazawa, Y.; Suzuki, T.; Yamashita, Y.; Miyashi, T.; Mukai, T. *Tetrahedron Lett.* **1986**, *27*, 925.

Table 1. Reduction Potentials[a] of Newly Prepared DCNNQIs 1a,b,f and Related Acceptors Measured in MeCN

compound	E_1^{red}/V	E_2^{red}/V
1a ($R_1 = R_2 = H$)	−0.14	−0.61
1b ($R_1 = R_2 = Ph$)	−0.15	−0.62
1f ($R_1 = R_2 = 2$-pyridyl)	−0.11	−0.59
7a	−0.25	−0.32
DCNQI	+0.18	−0.47
DCNNQI	+0.02	−0.56

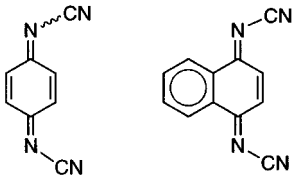

DCNQI DCNNQI

[a] E/V vs SCE, 0.1 mol dm^{-3} Et_4NClO_4 in MeCN, Pt electrode, scan rate 100 mV s^{-1}.

Scheme 2

Dihedral angles (°) in **1f** and **7f**

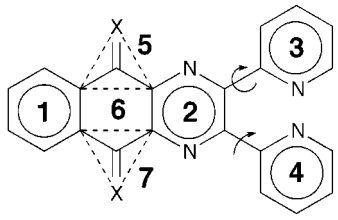

X =	N-CN	$C(CN)_2$
plane 1 and 2	13.3	23.6
plane 2 and 3	49.3	54.5
plane 2 and 4	30.6	26.5
plane 5 and 6	2.3	22.9
plane 6 and 7	3.4	21.4

reduction (Table 1). Essentially the same first and second reduction potentials (E_1^{red} and E_2^{red}) were observed for the diphenyl and bis(2-pyridyl) derivatives **1b** and **1f**, which shows that the bulky substituents on the pyrazine ring no longer affect the intrinsic redox properties of pyrazino-DCNNQI. As indicated by comparison of E_1^{red} values measured under the same conditions, **1** are weaker acceptors than DCNQI[10] and DCNNQI,[10] which obeys the general trend that annelation of an aromatic ring raises the LUMO level of Wurster-type acceptors.[16,17] In the case of pyrazino-TCNNQ **7a**, which has a deformed structure, the difference between E_1^{red} and E_2^{red} (ΔE) is so small that its anion radical easily undergoes disproportionation.[18,19] On the contrary, the large ΔE values of **1** indicate that their anion radicals are thermodynamically stable. In fact, **1b**$^{-\bullet}$ was isolated as a stable green-black salt [Et_4N^+(**1b**)$_2^{-\bullet}$: λ_{max} (DMF) 588 (log ϵ 4.32), 534 (4.14), 450 sh (4.01) nm] when **1b** was electrochemically reduced in CH_2Cl_2 containing 0.05 mol dm^{-3} Et_4NClO_4.

The observed planar geometry as well as stable anion radical formation support the use of a pyrazino-DCNNQI skeleton in constructing (A-π-D$^{\bullet}$) ↔ (A$^{-\bullet}$-π-D$^+$)-type stable radicals.

Preparation, Redox Properties, and Molecular Structure of Stable Radicals (2$^{\bullet}$ and 3$^{\bullet}$). Treatment of pyrazino-DCNNQIs possessing a 3-pyridyl or 4-pyridyl substituent (**1d** and **1e**) with CH_3OTf in CH_2Cl_2 gave quaternary salts, **2d**$^+$ and **2e**$^+$, as yellow powders in respective yields of 71 and 91%. Alkylation occurs selectively at the pyridine N atom, as shown by their NMR spectra. In the case of **1c** with a 2-pyridyl substituent, however, *N*-methylation did not proceed cleanly even under other conditions using Me_3OBF_4 or Me_2SO_4 as an alkylating reagent. Therefore, we could not obtain a pure salt of **2c**$^+$ although bis(2-pyridyl) derivative **1f** was easily converted to the monomethylated cation CH_3-**3**$^+$ in 82% yield.

Table 2. Redox Potentials[a] of Acceptors 1c−f, *N*-methylated Cations (2d$^+$, 2e$^+$, CH_3-3$^+$), and Radicals (2d$^{\bullet}$, 2e$^{\bullet}$, CH_3-3$^{\bullet}$) Measured in DMF along with the Electrical Conductivities[b] of Radicals

compound	E_1^{ox}/V	E_1^{red}/V	E_2^{red}/V	E_3^{red}/V	σ/S cm^{-1}
1c	−	+0.02	−0.51	−	−
1d	−	+0.01	−0.53	−	−
2d$^+$	−	+0.10	−0.41	−1.22[c]	−
2d$^{\bullet}$	+0.10	−0.39	−1.20[c]	−	5.9×10^{-6}
1e	−	+0.03	−0.50	−	−
2e$^+$	−	+0.12	−0.36	−1.01[c]	−
2e$^{\bullet}$	+0.12	−0.36	−1.01[c]	−	1.6×10^{-5}
1f	−	−0.06	−0.59	−	−
CH_3-**3**$^+$	−	+0.09	−0.45	−1.33[c]	−
CH_3-**3**$^{\bullet}$	+0.09	−0.44	−1.35[c]	−	6.5×10^{-6}

[a] E/V vs SCE, 0.1 mol dm^{-3} Et_4NClO_4 in DMF, Pt electrode, scan rate 100 mV s^{-1}. [b] Measured on compaction pellets by a two-probe method at room temperature. [c] Irreversible or quasi-reversible waves. Values are calculated as $E^{red} = E^{pc}$(cathodic peak potential) + 0.03 V.

According to voltammetric analyses on pyridinium derivatives (**2d**$^+$, **2e**$^+$, CH_3-**3**$^+$), they undergo three-stage 1e-reduction (Table 2). The slightly higher values of E_1^{red} and E_2^{red} compared with those for **1d**−**f** are due to the strong electron-withdrawing nature of the *N*-methylpyridinium substituent. The third reduction potentials (E_3^{red}) of these cations are close to E^{red} of *N*-methylpyridinium iodide (−1.27 V) measured under the same conditions. These results suggest that E_1^{red} and E_2^{red} of cations correspond to two-stage 1e-reduction of the pyrazino-DCNNQI unit, whereas the *N*-methylpyridinium moiety is reduced at E_3^{red} (Scheme 3). The positive shifts of E_2^{red} and E_3^{red} of **2e**$^+$ compared with those of **2d**$^+$ may be accounted for by smaller Coulombic repulsion in **2e**$^-$ due to the contribution of charge-annihilated form C. Considering these points, the main contributor to these radicals seems to be the zwitterionic structure, form B, in which the unpaired electron is located on the pyrazino-DCNNQI skeleton.

Electrochemical reduction of the quaternary salts (**2d**$^+$TfO$^-$, **2e**$^+$TfO$^-$, and CH_3-**3**$^+$TfO$^-$) in MeCN gave black-violet crystalline materials with a low solubility, which were assigned to the desired radicals (**2d**$^{\bullet}$, **2e**$^{\bullet}$, and CH_3-**3**$^{\bullet}$). Their cyclic voltammograms indicated that they undergo facile and reversible 1e-oxidation as well as two-stage 1e-reduction (Figure 1), demonstrating their electrochemical amphotericity. As shown in Table 2, the oxidation potentials (E_1^{ox}) of radicals correspond well to

(16) Deuchert, K.; Hünig, S. *Angew. Chem Int. Ed. Engl.* **1978** *17*, 875.
(17) Aumüller, A.; Hünig, S. *Liebigs Ann. Chem.* **1986**, 165.
(18) Yamashita, Y.; Suzuki, T.; Saito, G.; Mukai, T. *Chem. Lett.* **1986**, 715.
(19) Aumüller, A.; Hünig, S. *Liebigs Ann. Chem.* **1984**, 618.

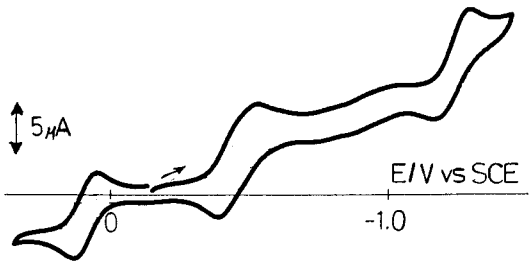

Figure 1. Cyclic voltammogram of **1d**• first scanned to negative (E/V vs SCE, 0.1 mol dm^{-3} Et_4NClO_4 in DMF, Pt electrode, scan rate 100 mV s^{-1}).

Scheme 3

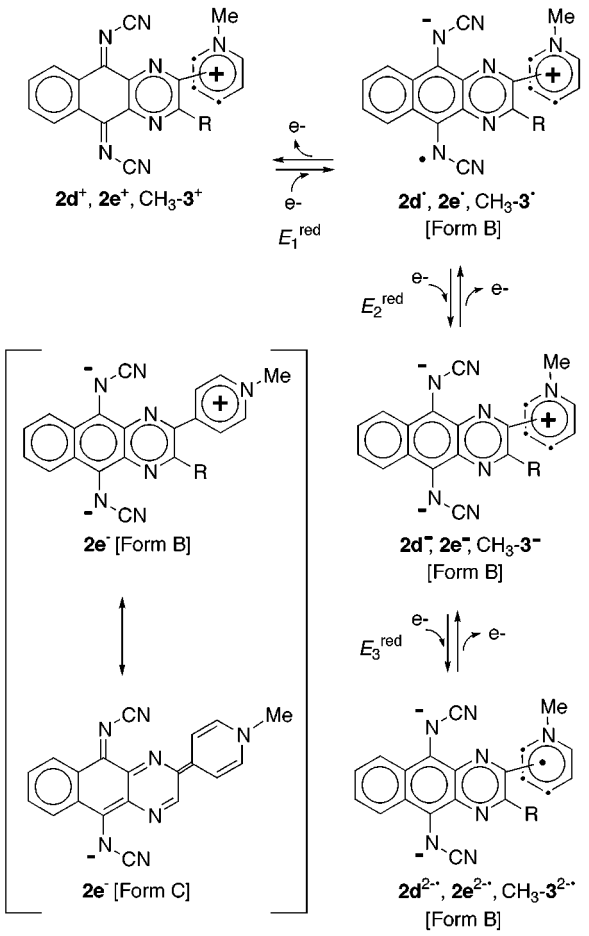

E_1^{red} of cations as expected, and E_1^{red} and E_2^{red} of radicals are nearly the same as E_2^{red} and E_3^{red} of cations, respectively. On the basis of the redox properties of **2d**•, **2e**•, and CH_3-**3**•, it was confirmed that these species exist as monomers rather than as covalently bound dimers.

The contribution of form B to the novel radical was indicated by the resemblance of the UV−vis spectra to that of **1b**$^{-\bullet}$ [CH_3-**3**•: λ_{max} (DMF) 596 (log ϵ 4.09), 550 (3.94), 460 (3.76) nm]. Such strong absorptions in the longer wavelength region are absent in cationic precursors or neutral DCNNQIs (Figure 2). An X-ray analysis of CH_3-**3**• confirmed that the radical adopts a zwitterionic structure, form B (Figure S3). Notably, the exocyclic imine bonds [av. 1.331(10) Å] are longer than those in **1f** [av. 1.297(3) Å]. The latter value is close to that found in the parent DCNQI [1.303(2) Å][20] whereas those found in CH_3-**3**• are comparable to that in the anion radical salt [Li$^+$(2,5-Me_2-DCNQI)$^{-\bullet}$: 1.323(3) Å].[21] Since this bond

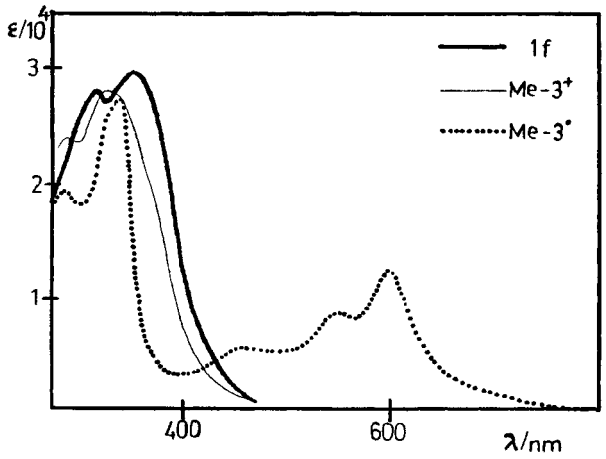

Figure 2. UV−vis spectra of **1f**, CH_3-**3**$^+$OTf$^-$, and CH_3-**3**• measured in DMF.

Scheme 4

Structural parameters in R-**3**•

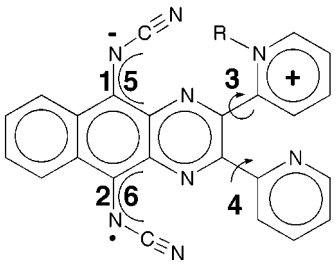

R =	CH_3	C_5H_{11}
bond length 1 / Å	1.329(10)	1.322(8)
bond length 2 / Å	1.332(9)	1.332(8)
dihedral angle 3 / °	78.8	69.7
dihedral angle 4 / °	30.3	27.6
torsion angle 5/ °	18.8	16.4
torsion angle 6/ °	7.4	7.2

length is sensitive to the degree of charge-transfer,[21] it is reasonable to assume that the DCNNQI unit in CH_3-**3**• is completely reduced to its anion radical despite the large experimental errors of the bond lengths. One of the N−C≡N units is slightly deviated from the planar naphtho[2,3-*b*]pyrazine unit, which is also in accord with the single-bond character of the exocyclic imine bonds and the reduced rotation barrier around them. On the other hand, the positive charge seems to localize on the *N*-methylpyridinium moiety, which is attached to the pyrazine ring with a larger dihedral angle (78.8°) than that of the neutral pyridyl group (30.3°) (Scheme 4).

Solid-State Properties and Crystal Structure of Stable Radicals (2• **and 3**•**).** The novel radicals studied here represent new single-component organic semiconductors (Table 2). Although the observed conductivities (ca. 10^{-5} S cm^{-1}) are lower than those of conventional multicomponent organic conductors or single-component solids of transition metal complexes,[6] they are among the highest values ever reported for pure organic materials.[5]

(20) Andreetti, G. D.; Bradamante, S.; Bizzarri, P. C.; Pagai, G. A. *Mol. Cryst. Liq. Cryst.* **1985**, *120*, 309.
(21) Kato, R.; Kobayashi, H.; Kobayashi, A. *J. Am. Chem. Soc.* **1989**, *111*, 5224.

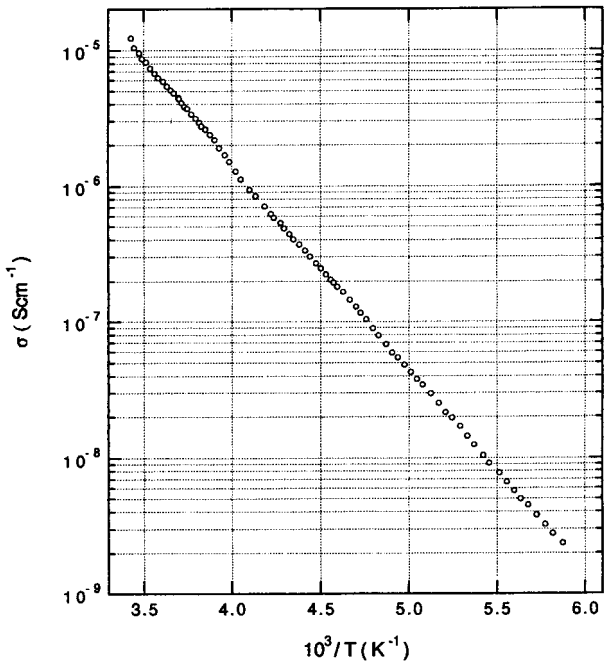

Figure 3. Temperature-dependence of conductivity for single crystalline CH_3-**3**• measured along the needle axis.

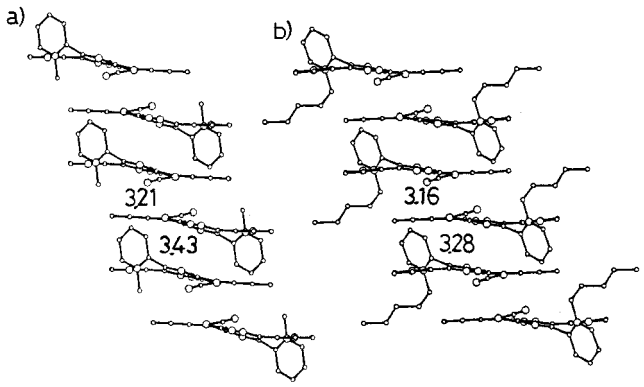

Figure 4. One-dimensional columnar stack in (a) CH_3-**3**• and (b) C_5H_{11}-**3**• crystals.

The temperature-dependence of the single-crystalline sample of CH_3-**3**• revealed that it is a semiconductor with a small activation energy of 0.30 eV, and a linear correlation was seen between the logarithm of the conductivity and $1/T$, as shown in Figure 3. Its room-temperature conductivity (1.2×10^{-5} S cm^{-1}) is only 1.8 times as large as the value obtained with the powder sample, suggesting a low anisotropy of conduction.

In the crystal of CH_3-**3**•, molecules are packed in a one-dimensional columnar stack (Figure 4a), which seems to be the main conduction path by face-to-face overlap of π-electrons. One of the two overlaps in the column is of "ring-over-double bond"-type[22] with a small interplanar distance of 3.21 Å (Figure 5a) and is thus suitable for orbital interaction between DCNNQI$^{-\bullet}$ moieties. In the other overlap (Figure 5b), however, molecules are greatly slipped with a wider separation of molecular planes (3.43 Å). Such dyad formation in the column may be one of the reasons for the limited conductivity of this radical. It should be noted that there are several short contacts

(22) Fritchie, C. J., Jr. *Acta Crystallogr.* **1966**, *20*, 892.

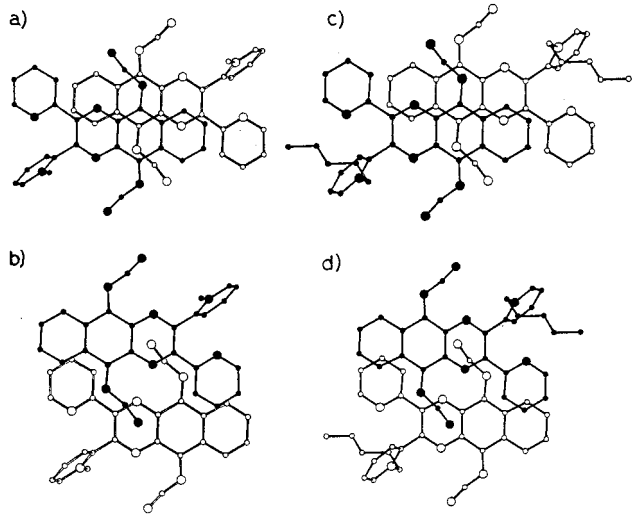

Figure 5. Two types of molecular overlaps in CH_3-**3**• [(a) in the dyad (interplanar distance, 3.21 Å); (b) between the dyads (3.43 Å)] and in C_5H_{11}-**3**• [(c) in the dyad (interplanar distance, 3.16 Å); (d) between the dyads (3.28 Å)]. Molecular planes are arranged parallel in all overlaps.

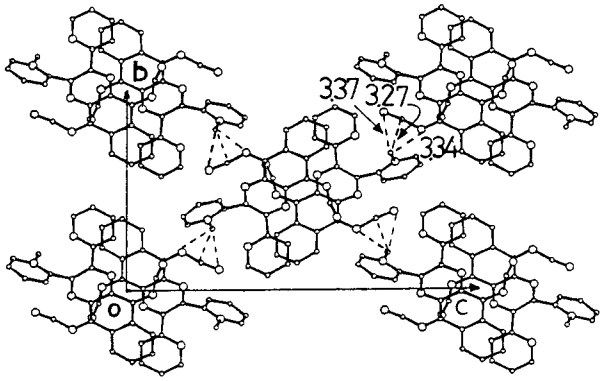

Figure 6. Packing arrangement in CH_3-**3**• crystal viewed along the *a* axis. Intermolecular Me···N (3.34, 3.37 Å) and Me•••C(sp) (3.27 Å) contacts are shown by dotted lines (sum of van der Waals radii: 3.50 Å for Me···N; 3.70 Å for Me···C).

(3.27, 3.34, 3.37 Å) between the N−C≡N moiety and Me group of neighboring columns (Figure 6). By considering the high acidity of C−H in Me of pyridinium, it is likely that such contacts induce C−H···N-type hydrogen bonding.[23] Thus, the suggested small anisotropy of conduction in CH_3-**3**• may be related to the proximity of columnar stacks in the crystal, which may induce conductivity in the transverse direction.

To confirm this idea, radicals C_nH_{2n+1}-**3**• which have a longer alkyl group on the pyridinium moiety were prepared, and their properties were investigated. By quaternization of **1f** with *n*-C_nH_{2n+1}OTf (n = 3, 5, 8, 12, and 16), the corresponding cations C_nH_{2n+1}-**3**$^+$ were obtained as stable yellow triflate salts in respective yields of 40−82% and were in turn converted to the desired radicals C_nH_{2n+1}-**3**• in yields of 46−87% by electrolyses in MeCN. The length of the alkyl group scarcely affects the redox properties of C_nH_{2n+1}-**3**$^+$ and C_nH_{2n+1}-**3**• in solution (Table 3). However, the electrical conductivities of powder samples of these radicals change over several

(23) Muscal, M. *Chem. Commun.* **1998**, 303. Steiner, T.; Desiraju, G. R. *Chem. Commun.* **1998**, 891. Calhorda, M. J. *Chem. Commun.* **2000**, 801.

Table 3. Redox Potentials[a] of Cationic Precursors C_nH_{2n+1}-3$^+$ and Radicals C_nH_{2n+1}-3$^\bullet$ Measured in DMF along with the Electrical Conductivities[b] of Radicals C_nH_{2n+1}-3$^\bullet$

compound	E_1^{ox}/V	E_1^{red}/V	E_2^{red}/V	E_3^{red}/V	σ/S cm^{-1}
C_3H_7-3$^+$	–	+0.09	−0.42	−1.34[c]	
C_3H_7-3$^\bullet$	+0.09	−0.43	−1.36[c]	–	1.8×10^{-6}
C_5H_{11}-3$^+$	–	+0.13	−0.41	−1.28[c]	
C_5H_{11}-3$^\bullet$	+0.14	−0.38	−1.26[c]	–	6.0×10^{-8}
C_8H_{17}-3$^+$		+0.09	−0.45	−1.32[c]	
C_8H_{17}-3$^\bullet$	+0.10	−0.43	−1.30[c]	–	8.3×10^{-8}
$C_{12}H_{25}$-3$^+$	–	+0.11	−0.43	−1.31[c]	
$C_{12}H_{25}$-3$^\bullet$	+0.07	−0.47	−1.33[c]	–	1.0×10^{-7}
$C_{16}H_{33}$-3$^+$	–	+0.09	−0.45	−1.32[c]	
$C_{16}H_{33}$-3$^\bullet$	+0.07	−0.47	−1.35[c]	–	1.0×10^{-9}

[a] E/V vs SCE, 0.1 mol dm^{-3} Et_4NClO_4 in DMF, Pt electrode, scan rate 100 mV s^{-1}. [b] Measured on compaction pellets by a two-probe method at room temperature. [c] Irreversible or quasi-reversible waves. Values are calculated as $E^{red} = E^{pc}$(cathodic peak potential) + 0.03 V.

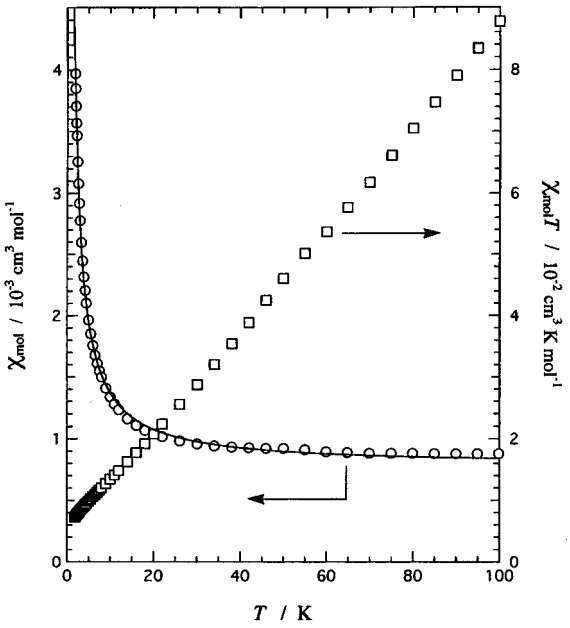

Figure 7. Temperature-dependence of magnetic susceptibility of CH_3-3$^\bullet$. The solid line represents the calculated χ_{mol} based on the modified Curie−Weiss equation (see text).

orders of magnitude (10^{-6} to 10^{-9} S cm^{-1}), indicating that the alkyl chain may affect the crystal packing. X-ray analysis of C_5H_{11}-3$^\bullet$ (Figure S4) revealed that the molecular geometry and two overlaps in the columnar stack closely resemble those in CH_3-3$^\bullet$ (Scheme 4 and Figures 4b, 5c, and 5d). The largest difference between the two packing patterns is that there is no short contact between columnar stacks in C_5H_{11}-3$^\bullet$, which may explain why its conductivity is less than that of CH_3-3$^\bullet$ by 2 orders of magnitude.

Finally, considering the recent interest in conducting magnetic multifunctional materials,[24] the magnetic properties of radical CH_3-3$^\bullet$ were also investigated by a SQUID magnetometer. Figure 7 shows the temperature-dependence of the molar magnetic susceptibility, which is obviously smaller than the value expected for a S = 1/2 species. The data satisfactorily fit the Curie−Weiss equation with temperature-independent paramagnetism [$\chi_{mol} = C/(T - \theta) + N\alpha$], where C, θ, and $N\alpha$ are the Curie constant, Weiss temperature, and temperature-independent paramagnetic term, respectively. We obtained $C = 5.94 \times 10^{-3}$ cm^3 K mol^{-1}, $\theta = -0.018$ K, and $N\alpha = 7.79 \times 10^{-4}$ cm^3 mol^{-1}. The C value corresponds to a spin concentration of 1.6%, indicating the presence of strong antiferromagnetic coupling to make this specimen practically diamagnetic just like TCNQ$^{-\bullet}$ compounds.[25] The Curie spins are likely to arise from lattice defects. The negligible θ value can be rationalized in view of the low spin concentration.

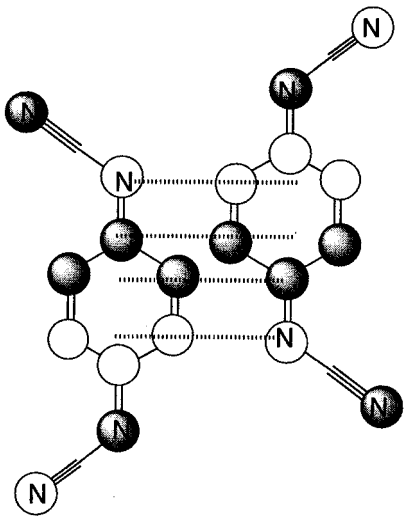

Figure 8. SOMO of DCNQI$^{-\bullet}$. Two molecules are shown to postulate the orbital interaction in the dyad of CH_3-3$^\bullet$ and C_5H_{11}-3$^\bullet$. The areas of the circles are arbitrary.

The crystal structure of CH_3-3$^\bullet$ shown in Figure 5a suggests that antiferromagnetic coupling takes place within a dyad. The singly occupied molecular orbital (SOMO) of DCNNQI$^{-\bullet}$ is calculated based on the semiempirical MO theory and schematically shown in Figure 8. The "ring-over-double bond"-type dimerization gives rise to a considerably large SOMO−SOMO overlap because they are facing each other in-phase. The interdyad magnetic interaction is not yet clear, but the interplanar distance of 3.43 Å also suggests the presence of SOMO−SOMO overlap between dyads. The intra- and interdyad orbital overlaps seem responsible for the observed temperature-independent paramagnetism as well as semiconducting properties.

Conclusion

These results have shown that the novel radicals 2$^\bullet$ and 3$^\bullet$ can be isolated as crystalline stable solids, which prefer a zwitterionic structure (form B) rather than a neutral radical form (form A). Due to their high electrochemical amphotericity with E_{sum} ($\equiv E_1^{ox} - E_1^{red}$) of 0.48−0.54 V, they exhibit electrical conductivities of 10^{-5} to 10^{-9} S cm^{-1}, and thus represent a new motif for a single-component organic semiconductor. These values, however, are much lower than those of conventional multi-

(24) Sugano, T.; Fukasawa, T.; Kinoshita, M. *Synth. Met.* **1991**, *41−43*, 3281. Sugimoto, T.; Yamaga, S.; Kakai, M.; Ohmori, K.; Tsujii, M.; Nakatsuji, H.; Fujita, H.; Yamauchi, J. *Chem. Lett.* **1993**, 1361. Kumai, R.; Izuoka, A.; Sugawara, T. *Mol. Cryst. Liq. Cryst.* **1993**, *232*, 151. Fujiwara, H.; Kobayashi, H. *Chem. Commun.* **1999**, 2417.

(25) Fritchie, C. J., Jr.; Arthur, P., Jr. *Acta Crystallogr.* **1966**, *21*, 139. Reis, A. H., Jr.; Preston, L. D.; Williams, J. M.; Peterson, S. W.; Candela, G. A.; Swartzendruber, L. J.; Miller, J. S. *J. Am. Chem. Soc.* **1979**, *101*, 2756.

component conductors, perhaps due to the adoption of unfavorable packing arrangements such as a nonuniform columnar stack. Another factor that limits the present conductivities seems to be the predominant contribution of form B to the radicals. When the contributions of forms A and B are nearly equal, fractional charge-transfer would be achieved on the DCNNQI skeleton, which leads to a half-filled band structure to achieve higher conductivity. Studies involving exchange of the pyridinium unit for other quaternary heterocycles with much stronger electron affinity are now in progress.

Experimental Section

Preparation of Pyrazino-DCNNQI Derivatives (1a−f). To an ice-cooled yellow solution of $TiCl_4$ (0.30 mL, 2.74 mmol) in dry THF (23 mL) were added a solution of bis(trimethylsilyl)carbodiimide **6** (696 mg, 3.68 mmol) in 2 mL of dry THF and then a suspension of finely powdered quinone **1a**[11] (100 mg, 0.476 mmol) in 15 mL of dry THF under N_2. After the mixture was stirred for 80 min, it was poured into an ice-cooled buffer solution (1/30 mol dm^{-3} $Na_2HPO_4-KH_2PO_4$, 120 mL) and extracted with cold CH_2Cl_2. The combined extracts were washed with brine and dried over Na_2SO_4. Evaporation of solvent and recrystallization from CH_2Cl_2−hexane gave *N*,*N*′-dicyanopyrazino[2,3-*b*]naphthoquinodiimine **1a** (49 mg) as orange crystals in 40% yield. 2-(2-Pyridyl)-, 2-(3-pyridyl)-, and 2-(4-pyridyl)-substituted derivatives, **1c**−**e**, were also obtained by similar procedures in respective yields of 42%, 28%, and 40%.

To a solution of quinone **4b**[11] (103 mg, 0.284 mmol) in 10 mL of dry CH_2Cl_2 was added $TiCl_4$ (0.12 mL, 1.09 mmol) under N_2. To the resultant suspension of the complex was then added dropwise a solution of **6** (685 mg, 3.80 mmol) in 2 mL of dry CH_2Cl_2 over 10 min. After the entire mixture was stirred at room temperature for 4 h and then heated at reflux for 2.5 h, it was poured into water (100 mL) and extracted with CH_2Cl_2. The combined extracts were washed with brine and dried over Na_2SO_4. Evaporation of solvent and recrystallization from CH_2Cl_2−MeOH gave *N*,*N*′-dicyano-2,3-diphenylpyrazino[2,3-*b*]naphthoquinodiimine **1b** (84 mg) as orange crystals in 72% yield.

To a suspension of quinone **4f** (751 mg, 2.06 mmol) and CsF (3.70 g, 24.4 mmol) in dry THF (150 mL) was added dropwise a solution of **6** (3.34 g, 18.6 mmol) in 5 mL of dry THF over 10 min under N_2. After the mixture was stirred for 2 h at room temperature, it was poured into an ice-cooled buffer solution (1/30 mol dm^{-3} $Na_2HPO_4-KH_2PO_4$, 175 mL) and extracted with cold CH_2Cl_2. The combined extracts were washed with brine and dried over Na_2SO_4. Evaporation of solvent and recrystallization from CH_2Cl_2−hexane gave 2,3-bis(2-pyridyl)-*N*,*N*′-dicyanopyrazino[2,3-*b*]naphthoquinodiimine **1f** (674 mg) as orange needles in 79% yield. This material is the CH_2Cl_2-solvate and is efflorescent when exposed to air.

Data for **1a**: mp 252−270 °C (dec); ^{1}H NMR (200 MHz, $CDCl_3$) δ/ppm 9.24 (2H, s), 8.64−8.59 (2H, m), 7.95 (2H, AA′XX′); IR (KBr) 2140 cm^{-1}; EI-MS *m*/*z* 258 (M^+). Anal. Calcd for $C_{14}H_6N_6$: C, 65.11; H, 2.34; N, 32.54. Found: C, 64.63; H, 2.58; N, 32.04. Data for **1b**: mp 280−287 °C (dec); ^{1}H NMR (90 MHz, $CDCl_3$) δ/ppm 8.57 (2H, AA′XX′), 7.90 (2H, AA′XX′), 7.80−7.60 (4H, m), 7.50−7.30 (6H, m); IR (KBr) 2143 cm^{-1}; UV−vis (DMF) λ_{max} 438 (sh, log ϵ 3.69), 368 (4.46), 358 (4.46), 314 (4.38), 306 (sh, 4.37) nm; EI-MS *m*/*z* (relative intensity) 410 (M^+, 100), 409 (29). Anal. Calcd for $C_{26}H_{14}N_6$: C, 76.09; H, 3.44; N, 20.48. Found: C, 75.62; H, 3.55; N, 20.32. Data for **1c**: orange powder (1,2-dichloroethane−hexane), mp 235−255 °C (dec); ^{1}H NMR (200 MHz, $CDCl_3$) δ/ppm 10.34 (1H, s), 9.06 (1H, ddd, J = 7.9, 1.1, 1.0 Hz), 8.65 (1H, ddd, J = 4.8, 1.8, 1.0 Hz), 8.65−8.60 (2H, m), 8.03 (1H, ddd, J = 7.9, 7.7, 1.8 Hz), 7.97−7.92 (2H, m), 7.52 (1H, ddd, J = 7.7, 4.8, 1.1 Hz); IR (KBr) 2137 cm^{-1}; EI-MS *m*/*z* 335 (M^+). Anal. Calcd for $C_{19}H_9N_7 \cdot 0.75H_2O$: C, 65.42; H, 3.03; N, 28.11. Found: C, 65.73; H, 2.98; N, 27.76. Data for **1d**: orange powder (CH_2Cl_2−hexane), mp 209.5−211 °C (dec); ^{1}H NMR (200 MHz, $CDCl_3$) δ/ppm 9.76 (1H, s), 9.57 (1H, dd, J = 2.1, 0.8 Hz), 9.08 (1H, ddd, J = 8.1, 2.1, 1.8 Hz), 8.87 (1H, dd, J = 5.0, 1.8 Hz) 8.65−8.50 (2H, m), 7.98−7.93 (2H, m), 7.65 (1H, ddd, J = 8.1, 5.0, 0.8 Hz); IR (KBr) 2138 cm^{-1}; EI-MS *m*/*z* 335 (M^+). Anal. Calcd for $C_{19}H_9N_7 \cdot H_2O$: C, 64.59; H, 3.14; N, 27.75. Found: C, 64.83; H, 3.12; N, 27.85. Data for **1e**: orange powder (CH_2Cl_2−hexane), mp 203−226 °C (dec); ^{1}H NMR (200 MHz, $CDCl_3$) δ/ppm 9.75 (1H, s), 8.97 (2H, AA′BB′), 8.66−8.61 (2H, m), 8.38 (2H, AA′BB′), 7.99−7.94 (2H, m); IR (KBr) 2138 cm^{-1}; EI-MS *m*/*z* (relative intensity) 335 (M^+, 63), 334 (100). Anal. Calcd for $C_{19}H_9N_7 \cdot 0.5H_2O$: C, 66.27; H, 2.93; N, 28.47. Found: C, 65.82; H, 2.90; N, 28.56. Data for **1f**: mp 254−268 °C (dec); ^{1}H NMR (200 MHz, $CDCl_3$) δ/ppm 8.75 (2H, ddd, J = 7.8, 1.0, 0.8 Hz), 8.62 (2H, AA′XX′), 8.31 (2H, ddd, J = 4.9, 1.7, 0.8 Hz), 8.01 (2H, ddd, J = 7.8, 7.7, 1.7 Hz), 7.94 (2H, AA′XX′), 7.33 (2H, ddd, J = 7.7, 4.9, 1.0 Hz); IR (KBr) 2143 cm^{-1}; UV−vis (DMF) λ_{max} 352 (log ϵ 4.47), 314 (4.45) nm, EI-MS *m*/*z* 412 (M^+). Anal. Calcd for $C_{24}H_{12}N_8 \cdot 0.5CH_2Cl_2$: C, 64.69; H, 2.88; N, 24.63. Found: C, 64.34; H, 3.04; N, 24.50.

Preparation of Anion Radical Salt of 1b. A dry CH_2Cl_2 solution of **1b** (18 mg, 0.043 mmol) containing Et_4NClO_4 (0.05 mol dm^{-3}) was electrochemically reduced by a constant current of 15 μA in an H-tube. Pt wires were used as the working and counter electrodes. Anion radical salt [Et_4N^+(**1b**)$_2^{-\bullet}$] was deposited as black needles, which were collected by suction (12 mg, yield 60%): mp 207−221 °C (dec), IR (KBr) 2096 cm^{-1}; UV−vis (DMF) λ_{max} 588 (log ϵ 4.32), 534 (4.14), 450 (sh, 4.01), 374 (sh, 4.60), 340 (4.77), 322 (sh, 4.68), 298 (sh, 4.61). Anal. Calcd for $C_{60}H_{48}N_{13} \cdot 2H_2O$: C, 73.00; H, 5.31; N, 18.45. Found: C, 73.45; H, 5.24; N, 18.23.

Preparation of Quaternary Salts (2d$^+$TfO$^-$, 2e$^+$TfO$^-$, and C_nH_{2n+1}-3$^+$TfO$^-$). To a solution of **1d** (26 mg, 0.0769 mmol) in dry CH_2Cl_2 (30 mL) was added CH_3OTf (0.050 mL, 0.44 mmol) under N_2. After the mixture was stirred for 14 h, filtration of the deposited precipitates gave 3-(*N*,*N*′-dicyanopyrazino[2,3-b]naphthoquinodiimin-2-yl)-1-methylpyridinium triflate **2d**$^+$TfO$^-$ (27 mg) as a yellow powder in 71% yield. Similarly, **2e**$^+$TfO$^-$ and CH_3-**3**$^+$TfO$^-$ were obtained from **1e** and **1f** in respective yields of 91% and 82%. By using *n*-C_nH_{2n+1}OTf[26] (n = 3, 5, 8, 12, and 16) in place of CH_3OTf, C_nH_{2n+1}-**3**$^+$TfO$^-$ salts were obtained from **1f** in respective yields of 82%, 79%, 50%, 40%, and 40%. In cases of cations with a long alkyl chain (n = 12 and 16), the addition of ether and hexane was necessary to deposit the quaternary salts before filtration.

Data for **2d**$^+$TfO$^-$: mp 139−161 °C (dec); ^{1}H NMR (200 MHz, CD_3CN) δ/ppm 9.97 (1H, br. s), 9.83 (1H, s), 9.44 (1H, d, J = 8.2 Hz), 8.81 (1H, d, J = 6.2 Hz) 8.62−8.57 (2H, m), 8.72 (1H, dd, J = 8.2, 6.2 Hz), 8.04−8.00 (2H, m), 4.47 (3H, s); IR (KBr) 2149, 1275, 1256 cm^{-1}; FAB-MS (relative intensity) *m*/*z* 351 (71), 350 (M^+, 100). Anal. Calcd for $C_{20}H_{12}N_7 \cdot CF_3SO_3 \cdot H_2O$: C, 48.74; H, 2.73; N, 18.95; S, 6.20. Found: C, 48.84; H, 2.77; N, 18.89; S, 6.21. Data for **2e**$^+$TfO$^-$: yellow powder, mp 227.5−246 °C (dec); ^{1}H NMR (200 MHz, CD_3CN) δ/ppm 9.93 (1H, s), 9.06 (2H, AA′BB′), 8.90 (2H, AA′BB′), 8.62−8.57 (2H, m), 8.04−8.00 (2H, m), 4.49 (3H, s); IR (KBr) 2144, 1160 cm^{-1}; FAB-MS (relative intensity) *m*/*z* 351 (64), 350 (M^+, 100). Anal. Calcd for $C_{20}H_{12}N_7 \cdot CF_3SO_3 \cdot 0.5H_2O$: C, 49.61; H, 2.58; N, 19.28; S, 6.31. Found: C, 49.50; H, 2.50; N, 19.06 S, 6.47. Data for CH_3-**3**$^+$TfO$^-$: yellow powder, mp 252−260 °C (dec); ^{1}H NMR (200 MHz, acetone-d_6) δ/ppm 9.48 (1H, dd, J = 6.4, 1.2 Hz), 9.13 (1H, ddd, J = 7.8, 1.2, 1.0 Hz), 8.82 (1H, ddd, J = 8.1, 7.3, 1.2 Hz), 8.68 (2H, m), 8.46 (1H, ddd, J = 7.3, 6.4, 1.2 Hz), 8.37 (1H, ddd, J = 4.6, 1.6, 1.0 Hz), 8.26 (1H, dd, J = 8.1, 1.2 Hz), 8.19 (2H, ddd, J = 7.8, 7.6, 1.6 Hz), 8.15 (2H, m), 7.59 (1H, ddd, J = 7.6, 4.6, 1.2 Hz), 5.63 (2H, s, CH_2Cl_2), 4.65 (3H, s); IR (KBr) 2152, 1258 cm^{-1}; UV−vis (DMF) λ_{max} 324 (log ϵ 4.45), 284 (4.38) nm; FAB-MS *m*/*z* 427 (M^+). Anal. Calcd for $C_{25}H_{15}N_8 \cdot CF_3SO_3 \cdot H_2O \cdot CH_2Cl_2$: C, 47.73; H, 2.82; N, 16.49. Found: C, 48.08; H, 2.63; N, 16.69. Data for C_3H_7-**3**$^+$TfO$^-$: yellow powder, mp 220.5−226 °C (dec); ^{1}H NMR (200 MHz,

(26) Beard, C. D.; Baum, K.; Grakauskas, V, *J. Org. Chem.* **1973**, *38*, 3673.

CD_3CN) δ/ppm 9.07 (1H, ddd, J = 7.9, 1.0, 1.0 Hz), 8.96 (1H, dd, J = 6.2, 1.4 Hz), 8.61 (2H, m), 8.53 (1H, ddd, J = 8.1, 7.8, 1.4 Hz), 8.24 (1H, ddd, J = 4.7, 1.7, 1.0 Hz), 8.17 (1H, ddd, J = 7.8, 6.2, 1.5 Hz), 8.09 (1H, ddd, J = 7.9, 7.7, 1.7 Hz), 8.06 (2H, m), 7.86 (1H, dd, J = 8.1, 1.5 Hz), 7.47 (1H, ddd, J = 7.7, 4.7, 1.0 Hz), 4.71 (1H, ddd, J = 14.0, 8.6, 6.6 Hz), 4.39 (1H, ddd, J = 14.0, 9.0, 6.6 Hz), 1.96−1.91 (2H, m), 0.85 (3H, t, J = 7.4 Hz); IR (KBr) 2148, 1260 cm^{-1}; FAB-MS m/z 455 (M^+). Anal. Calcd for $C_{27}H_{19}N_8{\cdot}CF_3SO_3{\cdot}H_2O$: C, 54.02; H, 3.40; N, 18.00. Found: C, 53.63; H, 3.31; N, 17.66. Data for C_5H_{11}-**3**$^+$-TfO^-: pale yellow powder, mp 256−267 °C (dec); ^1H NMR (200 MHz, CD_3CN) δ/ppm 9.07 (1H, ddd, J = 7.9, 1.0, 1.0 Hz), 8.95 (1H, dd, J = 6.3, 1.3 Hz), 8.64−8.59 (2H, m), 8.52 (1H, ddd, J = 8.1, 7.8, 1.3 Hz), 8.24 (1H, ddd, J = 4.8, 1.8, 1.0 Hz), 8.17 (1H, ddd, J = 7.8, 6.3, 1.4 Hz), 8.09 (1H, ddd, J = 7.9, 7.7, 1.8 Hz), 8.04−8.02 (2H, m), 7.85 (1H, dd, J = 8.1, 1.4 Hz), 7.47 (1H, ddd, J = 7.7, 4.8, 1.0 Hz), 4.84 (1H, ddd, J = 13.6, 9.2, 6.4 Hz), 4.52 (1H, ddd, J = 13.6, 8.9, 6.2 Hz), 1.96−1.91 (2H, m), 1.22−1.17 (4H, m), 0.80−0.73 (3H, m); IR (KBr) 2157, 1273 cm^{-1}; FAB-MS m/z 483 (M^+). Anal. Calcd for $C_{29}H_{23}N_8{\cdot}CF_3SO_3{\cdot}1.5H_2O$: C, 54.62; H, 3.97; N, 16.99. Found: C, 54.74; H, 3.66; N, 16.82. Data for C_8H_{17}-**3**$^+TfO^-$: pale yellow powder, mp 240.5−250 °C (dec); ^1H NMR (200 MHz, CD_3CN) δ/ppm 9.07 (1H, ddd, J = 7.8, 1.0, 0.8 Hz), 8.94 (1H, dd, J = 6.1, 1.0 Hz), 8.67−8.57 (2H, m), 8.52 (1H, ddd, J = 8.0, 7.9, 1.0 Hz), 8.23 (1H, ddd, J = 4.7, 1.7, 0.8 Hz), 8.17 (1H, ddd, J = 7.9, 6.1, 1.5 Hz), 8.09 (2H, ddd, J = 7.8, 7.7, 1.7 Hz), 8.07−8.03 (2H, m), 7.86 (1H, dd, J = 8.0, 1.5 Hz), 7.48 (1H, ddd, J = 7.7, 4.7, 1.0 Hz), 4.71 (1H, ddd, J = 13.8, 9.0, 6.2 Hz), 4.38 (1H, ddd, J = 13.8, 9.0, 6.4 Hz), 1.96−1.91 (2H, m), 1.01 (10H, m), 0.76 (3H, t, J = 5.5 Hz); IR (KBr) 2144, 1261 cm^{-1}; FAB-MS m/z 525 (M^+). Anal. Calcd for $C_{32}H_{29}N_8{\cdot}CF_3SO_3{\cdot}0.5H_2O$: C, 57.97; H, 4.42; N, 16.39. Found: C, 57.70; H, 4.45; N, 16.10. Data for $C_{12}H_{25}$-**3**$^+TfO^-$: yellow powder, mp 95−124 °C (dec); ^1H NMR (200 MHz, CD_3CN) δ/ppm 9.07 (1H, ddd, J = 7.9, 1.1, 0.9 Hz), 8.94 (1H, dd, J = 6.3, 1.2 Hz), 8.67−8.58 (2H, m), 8.52 (1H, ddd, J = 8.0, 7.9, 1.2 Hz), 8.23 (1H, ddd, J = 4.6, 1.8, 0.9 Hz), 8.17 (1H, ddd, J = 7.9, 6.3, 1.4 Hz), 8.09 (1H, ddd, J = 7.9, 7.7, 1.8 Hz), 8.10−8.02 (2H, m), 7.86 (1H, dd, J = 8.0, 1.4 Hz), 7.47 (1H, ddd, J = 7.7, 4.6, 1.1 Hz), 4.71 (1H, ddd, J = 13.8, 8.8, 6.2 Hz), 4.38 (1H, ddd, J = 13.8, 9.0, 6.2 Hz), 1.96−1.91 (2H, m), 1.16 (18H, m), 0.85 (3H, t, J = 6.6 Hz); IR (KBr) 2922, 2150, 1259 cm^{-1}; FAB-MS m/z 581 (M^+). Anal. Calcd for $C_{36}H_{37}N_8{\cdot}CF_3SO_3{\cdot}0.5H_2O$: C, 60.07; H, 5.18; N, 15.15; S, 4.33. Found: C, 60.36; H, 5.17; N, 14.78; S, 4.64. Data for $C_{16}H_{33}$-**3**$^+TfO^-$: yellow powder, mp 87−121 °C (dec); ^1H NMR (200 MHz, CD_3CN) δ/ppm 9.07 (1H, ddd, J = 8.0, 1.1, 1.0 Hz), 8.94 (1H, dd, J = 6.3, 1.3 Hz), 8.66−8.58 (2H, m), 8.52 (1H, ddd, J = 8.0, 7.8, 1.3 Hz), 8.23 (1H, ddd, J = 5.0, 1.8, 1.1 Hz), 8.17 (1H, ddd, J = 7.8, 6.3, 1.4 Hz), 8.08 (1H, ddd, J = 8.0, 7.7, 1.8 Hz), 8.04 (2H, m), 7.86 (1H, dd, J = 8.0, 1.4 Hz), 7.47 (1H, ddd, J = 7.5, 5.0, 1.0 Hz), 4.71 (1H, ddd, J = 13.8, 9.0, 6.0 Hz), 4.38 (1H, ddd, J = 13.8, 8.8, 6.2 Hz), 1.96−1.91 (2H, m), 1.30−1.11 (26H, m), 0.87 (3H, t, J = 6.4 Hz); IR (KBr) 2917, 2150, 1268 cm^{-1}; FAB-MS m/z 637 (M^+). Anal. Calcd for $C_{40}H_{45}N_8{\cdot}CF_3SO_3{\cdot}0.5H_2O$: C, 61.87; H, 5.83; N, 14.08. Found: C, 62.14; H, 5.69; N, 14.06.

Preparation of Stable Radicals (2d•, 2e•, and C_nH_{2n+1}-3•). A dry MeCN solution of **2d**$^+TfO^-$ (10 mg, 0.020 mmol) containing Et_4NTfO (0.05 mol dm^{-3}) was electrochemically reduced by a constant current of 15 μA in an H-tube. Pt wires were used as the working and counter electrodes. 3-(*N*,*N*′-Dicyanopyrazino[2,3-*b*]naphthoquinodiimin-2-yl)-1-methylpyridyl **2d•** was gradually deposited as black-violet crystals, which were collected by suction (6 mg, yield 77%). Similarly, **2e•** and C_nH_{2n+1}-**3•** (n = 1, 3, 5, 8, 12, and 16) were obtained from **2e**$^+TfO^-$ and C_nH_{2n+1}-**3**$^+TfO^-$ in respective yields of 88%, 72%, 71%, 87%, 46%, 68%, and 63%.

Data for **2d•**: mp 243−251 °C (dec); IR (KBr) 2092 cm^{-1}; FAB-MS (relative intensity) m/z 352 (100), 351 (36), 350 (M^+, 16). Anal. Calcd for $C_{20}H_{12}N_7{\cdot}1.5H_2O$: C, 63.65; H, 4.01; N, 25.97. Found: C, 63.78; H, 3.91; N, 25.46. Data for **2e•**: black-violet crystals, mp 260−273 °C (dec); IR (KBr) 2091 cm^{-1}; FAB-MS (relative intensity) m/z 352 (100), 351 (50), 350 (M^+, 18). Anal. Calcd for $C_{20}H_{12}N_7{\cdot}2H_2O$: C, 62.16; H, 4.17; N, 25.37. Found: C, 62.21; H, 3.86; N, 25.49. Data for CH_3-**3•**: black crystals, mp 190−198 °C (dec); IR (KBr) 2107 cm^{-1}; UV−vis (DMF) λ_{max} 596 (log ε 4.09), 550 (3.94), 460 (3.76), 336 (4.86), 326 (sh, 4.85), 284 (4.74) nm. Anal. Calcd for $C_{25}H_{15}N_8{\cdot}H_2O$: C, 67.41; H, 3.85; N, 25.15. Found: C, 67.09; H, 3.67; N, 24.74. Data for C_3H_7-**3•**: black crystals, mp 70−78 °C (dec); IR (KBr) 2107 cm^{-1}. Anal. Calcd for $C_{27}H_{19}N_8{\cdot}1.5H_2O$: C, 67.21; H, 4.60; N, 23.22. Found: C, 66.85; H, 4.60; N, 23.18. Data for C_5H_{11}-**3•**: black-violet crystals, mp 218−225 °C (dec); IR (KBr) 2107 cm^{-1}; UV−vis (DMF) λ_{max} 596 (log ε 4.17), 550 (4.03), 456 (3.82), 338 (4.48), 326 (sh, 4.45), 286 (4.29) nm. Anal. Calcd for $C_{29}H_{23}N_8{\cdot}2H_2O$: C, 67.04; H, 5.24; N, 21.57. Found: C, 66.50; H, 5.09; N, 21.32. Data for C_8H_{17}-**3•**: black-violet crystals, mp 100−108 °C (dec); IR (KBr) 2097 cm^{-1}; UV−vis (DMF) λ_{max} 598 (log ε 4.26), 550 (4.11), 460 (3.90), 338 (4.56), 326 (sh, 4.53), 286 (4.36) nm. Anal. Calcd for $C_{32}H_{29}N_8{\cdot}0.75H_2O$: C, 71.29; H, 5.70; N, 20.78. Found: C, 71.44; H, 5.70; N, 20.71. Data for $C_{12}H_{25}$-**3•**: black-violet crystals, mp 93−106 °C (dec); IR (KBr) 2100 cm^{-1}. Anal. Calcd for $C_{36}H_{37}N_8{\cdot}0.5H_2O$: C, 73.19; H, 6.48; N, 18.97. Found: C, 73.44; H, 6.40; N, 18.82. Data for $C_{16}H_{33}$-**3•**: black-violet crystals, mp 193−207 °C (dec); IR (KBr) 2101 cm^{-1}. Anal. Calcd for $C_{40}H_{45}N_8{\cdot}0.5H_2O$: C, 74.27; H, 7.17; N, 17.32. Found: C, 73.92; H, 7.24; N, 17.11.

Preparation of Quinones (4c−f). To a solution of 2,3-diaminonaphthoquinone[12] (2.00 g, 10.6 mmol) in dry DMSO (25 mL) was added 2-(bromoacetyl)pyridinium bromide[27] (3.59 g, 12.8 mmol). After the mixture was stirred at room temperature for 3 h, it was poured into water (250 mL) and extracted with CH_2Cl_2. The combined extracts were washed with water and dried over Na_2SO_4. Evaporation of solvent and chromatographic separation on Al_2O_3 (CH_2Cl_2) gave 2-(2-pyridyl)-pyrazino[2,3-*b*]naphthoquinone **4c** (913 mg) as pale yellow needles in 30% yield. 2-(3-Pyridyl) and 2-(4-pyridyl) derivatives, **4d** and **4e**, were obtained by similar condensation reactions of **6** with 3- and 4-(bromoacetyl)pyridinium bromide, respectively, in yields of 37% and 30%. In the latter two cases, crude products were purified by sublimation (0.01 Torr; 240−260 °C for **4d** and 260−270 °C for **4e**).

To a solution of 2,3-diaminonaphthoquinone (2.46 g, 13.1 mmol) in EtOH (170 mL) was added 2,2′-pyridil (3.15 g, 14.4 mmol), and the mixture was heated at reflux for 15 h. A tan powder precipitated on cooling, which was collected by suction. Recrystallization from CH_2Cl_2−EtOH gave 2,3-bis(2-pyridyl)-pyrazino[2,3-*b*]naphthoquinone **4f** (3.04 g) as pale yellow needles in 64% yield.

Data for **4c**: mp 265−266 °C; ^1H NMR (200 MHz, $CDCl_3$) δ/ppm 9.55 (1H, s), 9.47 (1H, dd, J = 2.6, 0.6 Hz), 8.85 (1H, dd, J = 4.8, 1.7 Hz), 8.65 (1H, ddd, J = 8.0, 2.0, 1.7 Hz), 8.47 (2H, m), 7.94 (2H, m), 7.57 (1H, ddd, J = 8.0, 4.8, 0.6 Hz); IR (KBr) 1686, 1677 cm^{-1}; EI-MS m/z 287 (M^+). Anal. Calcd for $C_{17}H_9N_3O_2{\cdot}0.25H_2O$: C, 69.98; H, 3.28; N, 14.40. Found: C, 70.28; H, 3.42; N, 14.36. Data for **4d**: yellow needles, mp 269−271.5 °C; ^1H NMR (200 MHz, $CDCl_3$) δ/ppm 9.55 (1H, s), 9.47 (1H, dd, J = 2.0, 0.6 Hz), 8.85 (1H, dd, J = 4.8, 1.7 Hz), 8.65 (1H, ddd, J = 8.0, 2.0, 1.7 Hz) 8.47 (2H, m), 7.94 (2H, m), 7.57 (1H, ddd, J = 8.0, 4.8, 0.6 Hz); IR (KBr) 1686, 1677 cm^{-1}; EI-MS m/z 287 (M^+). Anal. Calcd for $C_{17}H_9N_3O_2{\cdot}0.5H_2O$: C, 68.92; H, 3.40; N, 14.18. Found: C, 68.59; H, 3.39; N, 13.98 Data for **4e**: yellow needles, mp 299−300 °C ^1H NMR (200 MHz, $CDCl_3$) δ/ppm 9.57 (1H, s), 8.91 (2H, AA′BB′), 8.48 (2H, m), 8.18 (2H, AA′BB′), 7.95 (2H, m); IR (KBr) 1682 cm^{-1}; EI-MS m/z 287 (M^+). Anal. Calcd for $C_{17}H_9N_3O_2{\cdot}0.25H_2O$: C, 69.97; H, 3.28; N, 14.40. Found: C, 70.14; H, 3.39; N, 14.49. Data for **4f**: mp 289−292 °; ^1H NMR (200 MHz, $CDCl_3$) δ/ppm 8.47 (2H, AA′XX′), 8.31 (2H, ddd, J = 4.8, 1.2, 1.2 Hz), 8.26 (2H, ddd, J = 7.8, 1.2, 1.2 Hz), 7.98−7.85 (4H, m), 7.29 (2H, ddd, J = 7.8, 4.8, 1.2 Hz); IR (KBr) 1694, 1672 cm^{-1}; EI-MS m/z 364 (M^+). Anal. Calcd for $C_{22}H_{12}N_4O_2$: C, 72.52; H, 3.32; N, 15.38. Found: C, 72.24; H, 3.77; N, 15.40.

Preparation of Pyrazino-TCNNQ Derivatives (7f). To a solution of quinone **4f** (500 mg, 1.37 mmol) in 40 mL of dry

(27) Wingfield, H. N., Jr. *J. Org. Chem.* **1959**, *24*, 872.

CH_2Cl_2 was added $TiCl_4$ (0.60 mL, 5.47 mmol) under N_2. To the resultant suspension of the complex was then added dropwise a solution of malononitrile (458 mg, 4.93 mmol) and dry pyridine (4.5 mL, 55.6 mmol) in 20 mL of dry CH_2Cl_2 over 1 h at −20 °C. After the entire mixture was stirred at this temperature for 3 h, it was poured into water (200 mL) and extracted with CH_2Cl_2. The combined extracts were washed with brine and dried over Na_2SO_4. Evaporation of solvent and chromatographic separation on SiO_2 (AcOEt/CH_2Cl_2, 1:30) gave 2,3-bis(2-pyridyl)-11,11,12,12-tetracyanopyrazino[2,3-*b*]naphthoquinodimethane **7f** (343 mg) as a pale yellow powder in 54% yield: mp 246−258 °C (dec); ^{1}H NMR (200 MHz, $CDCl_3$) δ/ppm 8.58 (2H, AA′XX′), 8.36 (2H, ddd, J = 8.1, 1.1, 1.1 Hz),8.31 (2H, ddd, J = 4.9, 2.0, 1.1 Hz), 7.94 (2H, ddd, J = 8.1, 8.1, 2.0 Hz), 7.87 (2H, AA′XX′), 7.31 (2H, ddd, J = 8.1, 4.9, 1.1 Hz); IR (KBr) 2215 cm^{-1}; UV−vis (MeCN) λ_{max} 366 (log ϵ 4.56), 312 (4.45), 226 (4.52) nm, EI-MS m/z 460 (M^+). Anal. Calcd for $C_{28}H_{12}N_8 \cdot 0.75CH_2Cl_2$: C, 65.88; H, 2.60; N, 21.38. Found: C, 65.76; H, 2.79; N, 22.24.

Measurement of Redox Potentials. Oxidation potentials (E^{ox}) were measured by cyclic voltammetry in dry MeCN or dry DMF containing 0.1 mol dm^{-3} Et_4NClO_4 as a supporting electrolyte. Ferrocene undergoes 1e-oxidation at +0.38 V in MeCN or at +0.44 V in DMF under similar conditions. All of the values shown in the text are in E/V vs SCE, and Pt was used as the working electrode. In the case of irreversible waves, half-wave potentials were estimated from the cathodic peak potentials (E^{pc}) as $E^{red} = E^{pc}$ + 0.03 V.

X-ray Analyses. Crystal data for **1f**·CH_2Cl_2: $C_{25}H_{14}N_8Cl_2$, M 497.35, efflorescent orange needles by recrystallization from CH_2Cl_2, 0. 7 × 0.1 × 0.05 mm, triclinic $P\bar{1}$, a = 11.444(1), b = 16.371(3), c = 6.1366(6) Å, α= 96.219(2), β = 102.977(2), γ = 78.624(4)°, V = 1095.9(2) Å^3, ρ (Z = 2) = 1.507 g cm^{-1}. A total of 4453 unique data points ($2\theta_{max}$ = 55.6°) were measured at T = 120 K on a Rigaku Mercury CCD camera apparatus (Mo−Kα radiation, λ= 0.71069 Å). Numerical absorption correction was applied (μ = 3.30 cm^{-1}). The structure was solved by the direct method and refined by the full-matrix least-squares method on F with anisotropic temperature factors for non-hydrogen atoms. Hydrogen atoms were picked up from the D-map. The final R and Rw values are 0.043 and 0.057 for 3374 reflections with $I > 3\sigma I$ and 315 parameters. The maximum residual electron density is 0.35 e Å^{-3}.

Crystal data for **7f**: $C_{28}H_{12}N_8$, M 460.46, yellow plates from $CHCl_3$, 0.3 × 0.15 × 0.1 mm, triclinic $P\bar{1}$, a = 10.694(8), b = 13.104(7), c = 8.102(5) Å, α = 97.82(5), β = 101.07(6), γ = 76.35(5)°, V = 1077.8(12) Å^3, ρ (Z = 2) = 1.419 g cm^{-1}. A total of 3829 unique data points ($2\theta_{max}$ = 50°) were measured at T = 286 K by a Rigaku AFC-5R four-circle diffractometer with an ω−2θ scan mode (Mo−Kα radiation, λ = 0.71069 Å). No absorption correction was applied (μ = 0841 cm^{-1}). The structure was solved by the direct method and refined by the block-diagonal least-squares method on F with anisotropic temperature factors for non-hydrogen atoms. Hydrogen atoms were picked up from the D-map and included in the refinement with isotropic temperature factors. The final R value is 0.090 for 2054 reflections with $F > 3\sigma F$ and 374 parameters. The maximum residual electron density is 0.40 e Å^{-3}.

Crystal data for CH_3-**3**•: $C_{25}H_{15}N_8$, M 427.45, black plates by electrocrystallization from MeCN containing 0.05 M $Et_4N^+TfO^-$, 0.25 × 0.1 × 0.1 mm, monoclinic $P2_1/c$, a = 8.089-(3), b = 11.916(2), c = 20.983(3) Å, β = 97.96(3), V = 2003.0-(8) Å^3, ρ (Z = 4) = 1.417 g cm^{-1}. A total of 2983 unique data points ($2\theta_{max}$ = 120°) were measured at T = 286 K with an ω−2θ scan mode (Cu−Kα radiation, λ = 1.5418 Å). Absorption correction was applied by means of the empirical Ψ-scan method (μ = 6.87 cm^{-1}). The structure was solved by the direct method and refined by the block-diagonal least-squares method on F with anisotropic temperature factors for non-hydrogen atoms. Hydrogen atoms were located at the calculated positions and included in the refinement with isotropic temperature factors. The final R value is 0.079 for 1677 reflections with $F > 3\sigma F$ and 359 parameters. The maximum residual electron density is 0.38 e Å^{-3}.

Crystal data for n-C_5H_{11}-**3**••$2H_2O$: $C_{29}H_{27}N_8O_2$, M 519.59, black needles by electrocrystallization from MeCN containing 0.05 M $Et_4N^+TfO^-$, 0.25 × 0.05 × 0.05 mm, triclinic $P\bar{1}$, a = 11.987(2), b = 13.980(1), c = 7.679(1) Å, α= 92.30(1), β = 91.09(1), γ = 99.03(1)°, V = 1284.8(2) Å^3, ρ (Z = 2) = 1.343 g cm^{-1}. A total of 3529 unique data points ($2\theta_{max}$ = 115°) were measured at T = 286 K with ω−2θ scan mode (Cu−Kα radiation, λ = 1.5418 Å). Absorption correction was applied by means of the empirical Ψ-scan method (μ = 6.81 cm^{-1}). The structure was solved by the direct method and refined by the block-diagonal least-squares method on F with anisotropic temperature factors for non-hydrogen atoms. Hydrogen atoms were located at the calculated positions and included in the refinement with isotropic temperature factors. The final R value is 0.076 for 2183 reflections with $F > 3\sigma F$ and 445 parameters. The maximum residual electron density is 0.36 e Å^{-3}.

Measurement of Electrical Conductivity of Radicals. Powder conductivities were measured on compaction samples by a two-probe method at room temperature. The temperature-dependence measurement was conducted on a specimen of CH_3-**3**• (0.1 × 0.05 × 0.075 mm) by a two-probe method with a cooling rate of 2 K min^{-1} to 170 K. Anisotropy of the conductivity could not be measured since only tiny needlelike crystals were obtained. The values of σ and E_a for single-crystalline CH_3-**3**• are those along the needle axis.

Measurement of Magnetic Properties of Radical CH_3-3•. Magnetic susceptibility was measured on a Quantum Design MPMS SQUID magnetometer. A sample cell was filled with a polycrystalline sample of CH_3-**3**• (19.51 mg). The measurement was taken over the temperature range of 1.8 to 100 K at 0.5000 T. Background data of the cell were separately measured under the same conditions, and the diamagnetic contribution of the sample itself was estimated from Pascal's constants.

Acknowledgment. This work was supported by the Ministry of Education, Science and Culture, Japan (Grant Nos. 10146101 and 06243105). Financial support from the Casio Science Promotion Foundation and a Research Grant from the Iwatani Naoji Foundation (to T.S.) is gratefully acknowledged.

Supporting Information Available: Ortep drawings (Figures S1−S4) and structural data for the X-ray analyses (positional and thermal parameters; bond distances and angles) of **1f**·CH_2Cl_2, CH_3-**3**•, C_5H_{11}-**3**••$2H_2O$, and **7f**. This material is available free of charge via the Internet at http://pubs.acs.org.

JO001352R

Acta Crystallographica Section B
Structural Science
ISSN 0108-7681

Dipyrimidine–copper(II) dinitrate complexes showing magnetic interactions

Masanori Yasui, Yoshimitsu Ishikawa, Naoya Akiyama, Takayuki Ishida, Takashi Nogami and Fujiko Iwasaki*

Department of Applied Physics and Chemistry, The University of Electro-Communications, Chofu, Tokyo 182-8585, Japan

Correspondence e-mail: fuji@pc.uec.ac.jp

Received 14 September 2000
Accepted 8 February 2001

Crystals of $Cu^{II}(NO_3)_2(pm)_3$ (1), and two crystalline forms of $Cu^{II}(NO_3)_2(H_2O)_2(pm)_2$, (2) and (3), showed ferromagnetic, antiferromagnetic and paramagnetic interactions at extremely low temperatures, respectively. Crystal structure analyses revealed that the complexes were *catena*-dinitrato[μ-pyrimidine-κN^1:κN^3]-(pyrimidine-N^1)copper(II), $[Cu(NO_3)_2(pm)_2]_n$, *catena*-diaquadinitrato[μ-pyrimidine-κN^1:κN^3]copper(II), $[Cu(NO_3)_2(H_2O)_2(pm)]_n$, and diaquadinitratodipyrimidine-copper(II), $Cu(NO_3)_2(H_2O)_2(pm)_2$ for (1), (2) and (3), respectively. In (1) the Cu atom is coordinated by the two nitrates and N atoms of the non-bridging pyrimidine and bridging pyrimidine to form a one-dimensional coordination polymer. The complex is a five-coordinated square pyramid and can be regarded as a pseudo-seven-coordinated complex, since other short non-bonding Cu···O contacts are observed. In the crystals of (2) the pyrimidine bridges the Cu atoms to form a one-dimensional coordination chain. On the other hand, complex (3) is not a coordination polymer. It is important to form a coordination polymer for the appearance of the magnetic interactions. Types of coordination of the bridging organic moieties should also play an important role in magnetic properties. Magnetic measurements of (1) and (2) show that they are good examples of uniform $S = 1/2$ ferro- and antiferromagnetic Heisenberg chains with exchange parameters $2J/kB = +1.8$ and -36 K, respectively.

1. Introduction

Recently many organic coordination compounds containing transition metals as spin sources have been studied to develop magnetic interactions in organic compounds. Some copper(II) transition complexes coordinated with pyrimidines or related compounds which have *meta*-coordination positions showed magnetic interactions (Ishida *et al.*, 1995, 1996, 1997). Among them, complexes of $Cu^{II}(hfac)_2$ (hfac = 1,1,1,5,5,5-hexafluoropentane-2,4-dionate) coordinated by quinazoline, pyrimidine and 4-methylpyrimidine showed ferromagnetic interactions at extremely low temperatures. Structural studies revealed that these complexes formed one-dimensional coordination chains and the interactions between chains were van der Waals type (Ishida *et al.*, 1996; Yasui *et al.*, 2001). In order to improve the molecular interactions, $Cu^{II}(NO_3)_2$ complexes coordinated by pyrimidine (hereafter abbreviated by pm) were synthesized and their magnetic properties were measured (Ishida *et al.*, 1997). The complex $Cu(NO_3)_2(pm)_3$ (1) showed a ferromagnetic interaction. X-ray analysis revealed that the complex $Cu(NO_3)_2(H_2O)_2(pm)_2$ crystallized into two modifications, (2) and (3); the magnetic properties

measured on these crystals separately showed an antiferromagnetic interaction for (2) and a paramagnetic interaction for (3). Crystal structure analyses were performed on these $Cu^{II}(NO_3)_2$ complexes (1)–(3) in order to examine the relations between magnetic interactions and crystal structures.

2. Experimental

Complex (1) was synthesized from copper(II) nitrate trihydrate and pyrimidine, and crystallized from methanol solutions. Crystals of (1) were coated with epoxy resin soon after being produced from the solution, because they were very unstable in air. Crystals of (2) and (3) were obtained from copper(II) nitrate and pyrimidine in water. Two types of crystals were obtained from the same batch. The X-ray analysis revealed that crystals of $Cu(NO_3)_2(H_2O)_2(pm)_2$ showed two modifications, (2) and (3). The intensity data were measured using a Rigaku diffractometer AFC-7*R* with a graphite monochromator. The structures were solved by direct methods using the programs *SIR*88 (Burla *et al.*, 1989) and *DIRDIF*92 (Buerskens *et al.*, 1992). The H atoms were obtained from difference Fourier maps. The structures were refined by full-matrix least-squares with anisotropic temperature factors for non-H atoms and isotropic ones for H atoms.

For (1) intensity measurement was also carried out at 100 K with an N_2-extraction gas-flow device using a different crystal (1*b*) in order to analyze electron densities. For (1*b*), after the refinements with full-matrix least-squares using the program *SHELXL*97 (Sheldrick, 1997) [$R = 0.0366$ for 4958 reflections, $I > 2\sigma(I)$, $wR_2 = 0.1012$ for 7876 reflections with 197 parameters, flack parameter = 0.0350 (9), H atoms were treated as a riding model] and high-order refinements with $\sin\theta/\lambda > 0.6$, further refinements were carried out using the multipole expansion atomic scattering factors by the program *MOLLY*5 (Hansen & Coppens, 1978). Crystal data, details concerning data collection and structure refinements are listed in Table 1.[1]

3. Results and discussions

3.1. Structure of (1)

The molecular structure of (1) along with the atomic numbering and the crystal structure are shown in Figs. 1 and 2, respectively. Selected bond distances and angles are listed in Table 2. The Cu atom is coordinated by O1, O4, N3 and N5 equatorially, and N6^{i} [(i) $x-\frac{1}{2}, 1-y, z$] axially to form a five-coordinated square-pyramidal complex. The Cu atom is coordinated by two types of pyrimidines; one bridges Cu···Cu at the *meta* N atoms to form a one-dimensional chain along the *a* axis, while the other coordinates only at one N atom. In the pyrimidine-bridging chain, —Cu—N—C—N—Cu—N—C—N—, one N atom coordinates axially and the other coordinates equatorially. The axial Cu1—N6^{i} [2.303 (3) Å] is significantly longer than the equatorial Cu1—N3 and Cu1—N5 lengths [2.041 (3) and 2.036 (3) Å, respectively]. In the distorted octahedral complex, $Cu^{II}(hfac)_2(pm)_2$, pyrimidine moieties also bridge the Cu atoms from the axial and equatorial positions with Cu—N_{ax} 2.370 (7) Å and Cu—N_{eq} 2.104 (7) Å. Four other Cu complexes coordinated by pyrimidines were found from the Cambridge Structural Database (CSD; Allen *et al.*, 1991). Two of them are five-coordinated square pyramids with axially and equatorially bridging pyrimidines (Refcodes: LAYNAE; Chen, Fu *et al.*, 1994; ZATGOQ; Chen, Qiu *et al.*, 1994). In these complexes Cu—N_{ax} are 2.35–2.45 Å and

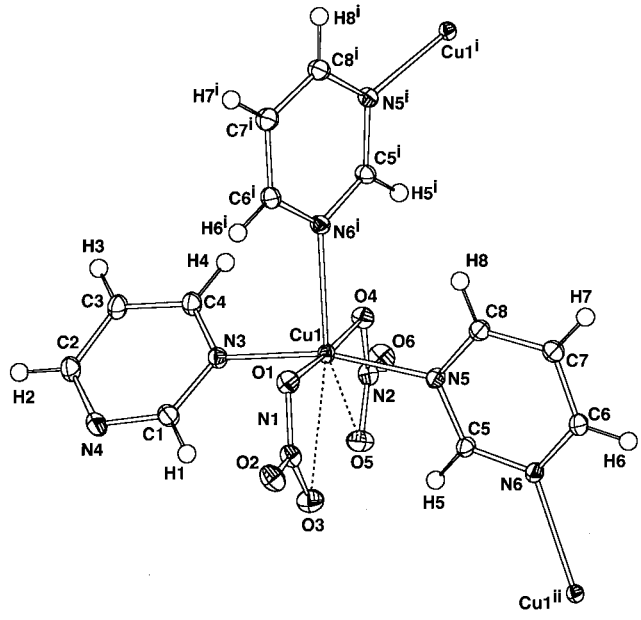

Figure 1
*ORTEP*II (Johnson, 1976) drawing of (1*b*) (100 K) with the atom-numbering. The displacement ellipsoids for non-H atoms are drawn at 50% probability and the H atoms are drawn as spheres with a radius of 0.1 Å. Symmetry codes: (i) $x-\frac{1}{2}, 1-y, z$; (ii) $x+\frac{1}{2}, 1-y, z$.

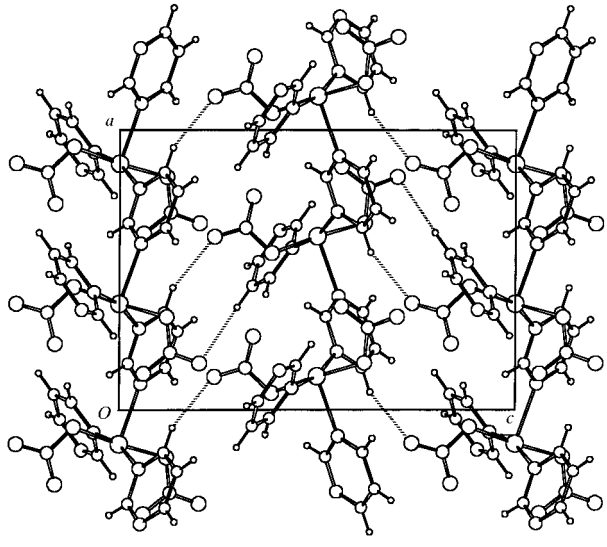

Figure 2
Crystal structure of (1*b*) viewed along the *b* axis. C—H···O contacts are shown with broken lines.

[1] Supplementary data for this paper are available from the IUCr electronic archives (Reference: OA0034). Services for accessing these data are described at the back of the journal.

Table 1
Experimental details.

	(1*a*)	(1*b*)	(2)	(3)
Crystal data				
Chemical formula	$Cu(NO_3)_2(C_4H_4N_2)_2$	$Cu(NO_3)_2(C_4H_4N_2)_2$	$Cu(C_4H_4N_2)(H_2O)_2$-$(NO_3)_2$	$Cu(C_4H_4N_2)_2(H_2O)_2$-$(NO_3)_2$
Chemical formula weight	347.74	347.74	303.68	383.78
Cell setting, space group	Orthorhombic, $Pca2_1$	Orthorhombic, $Pca2_1$	Monoclinic, C_2/c	Monoclinic, $P2_1/a$
a, b, c (Å)	9.991 (5), 8.531 (6), 14.359 (5)	10.000 (2), 8.4519 (2), 14.187 (2)	12.408 (8), 11.511 (9), 7.518 (9)	7.1658 (12), 14.105 (2), 7.5358 (14)
β (°)	90	90	114.99 (5)	114.324 (12)
V (Å^3)	1223.9 (11)	1199.1 (4)	973.2 (15)	694.1 (2)
Z	4	4	4	2
D_x (Mg m^{-3})	1.887	1.926	2.072	1.836
Radiation type	Mo $K\alpha$	Mo $K\alpha$	Mo $K\alpha$	Mo $K\alpha$
No. of reflections for cell parameters	25	25	25	25
θ range (°)	14.8–17.5	14.0–15.6	12.6–16.7	17.2–17.5
μ (mm^{-1})	1.827	1.865	2.289	1.630
Temperature (K)	295	100	294	296
Crystal form, color	Prism, blue	Prism, blue	Prismatic, light blue	Prism, blue
Crystal size (mm)	0.40 × 0.30 × 0.20	0.15 × 0.14 × 0.10	0.40 × 0.40 × 0.30	0.30 × 0.20 × 0.20
Data collection				
Diffractometer	Rigaku AFC-7*R*	Rigaku AFC-7*R*	Rigaku AFC-7*R*	Rigaku AFC-7*R*
Data collection method	ω–2θ scans	ω–2θ scans	ω–2θ scans	ω–2θ scans
Absorption correction	Psi-scan (North *et al.*, 1968)	Analytical (De Meulenaer & Tompa, 1965)	Psi-scan	Psi-scan
T_{min}	0.582	0.749	0.323	0.612
T_{max}	0.711	0.801	0.544	0.734
No. of measured, independent and observed parameters	1464, 1464, 1394	15 315, 7876, 5759	1162, 1113, 1076	1625, 1508, 1291
Criterion for observed reflections	$I > 2\sigma(I)$	$I > 3\sigma(F)$	$I > 2\sigma(I)$	$I > 2\sigma(I)$
R_{int}	0.0000	0.0685	0.0596	0.0427
θ_{max} (°)	27.50	60.0	27.50	26.94
Range of h, k, l	$0 \rightarrow h \rightarrow 12$ $0 \rightarrow k \rightarrow 11$ $-18 \rightarrow l \rightarrow 0$	$-24 \rightarrow h \rightarrow 24$ $-20 \rightarrow k \rightarrow 0$ $0 \rightarrow l \rightarrow 34$	$0 \rightarrow h \rightarrow 16$ $0 \rightarrow k \rightarrow 14$ $-9 \rightarrow l \rightarrow 8$	$0 \rightarrow h \rightarrow 9$ $0 \rightarrow k \rightarrow 17$ $-9 \rightarrow l \rightarrow 8$
No. and frequency of standard reflections	3 every 150 reflections	3 every 100 reflections	3 every 150 reflections	3 every 150 reflections
Intensity decay (%)	0.18	0.997	6.68	2.95
Refinement				
Refinement on	F^2	F	F^2	F^2
$R[F^2>2\sigma(F^2)]$, $wR(F^2)$, S	0.0286, 0.0782, 1.038	0.0384, 0.0339, 1.236	0.0285, 0.0821, 1.152	0.0517, 0.148, 1.079
No. of reflections and parameters used in refinement	1464, 199	5759, 535	1113, 97	1508, 130
H-atom treatment	Riding	Not refined	Refined	Refined
Weighting scheme	$w = 1/[\sigma^2(F_o^2) + (0.0619P)^2 + 0.1183P]$, where $P = (F_o^2 + 2F_c^2)/3$	$w = 1/[\sigma^2(F_o^2)]$	$w = 1/[\sigma^2(F_o^2) + (0.0538P)^2 + 0.8570P]$, where $P = (F_o^2 + 2F_c^2)/3$	$w = 1/[\sigma^2(F_o^2) + (0.1118P)^2 + 0.2222P]$, where $P = (F_o^2 + 2F_c^2)/3$
$(\Delta/\sigma)_{max}$	0.000	0.001	0.001	0.001
$\Delta\rho_{max}$, $\Delta\rho_{min}$ (e Å^{-3})	0.702, −0.598	1.34, −1.44	0.612, −0.866	1.54, −1.321
Extinction method	*SHELXL*97 (Sheldrick, 1997)	None	*SHELXL*97 (Sheldrick, 1997)	None
Extinction coefficient	0.0030 (12)	–	0.104 (4)	–

Computer programs used: *AFC Control Software* (Rigaku Corporation, 1994), *TEXSAN* (Molecular Science Corporation, 1992), *SIR*88 (Burla *et al.*, 1989), *SHELXL*97 (Sheldrick, 1997), *MOLLY*5 (Hansen & Coppens, 1978), *DIRDIF*92 (Beurskens *et al.*, 1992).

Cu—N_{eq} are 2.00–2.01 Å. However, these complexes showed strong antiferromagnetic interactions owing to the *trans*-oxamidato-bridged Cu dimers. The other complexes include one which has a three-dimensional network with tetrahedrally bridging pyrimidines (RIDKOE; Keller, 1997) and another which is an octahedral complex with four equatorial non-bridging pyrimidines (RIQNAG; Novak & Keller, 1997). The bond lengths of Cu—N for these complexes are 2.03–2.15 Å.

The planarity of the equatorial coordination is distorted, as shown from the angles of O1—Cu1—O4, N3—Cu1—N5, N3—Cu1—N6^{i} and N5—Cu1—N6^{i}, which are 175.56 (12), 165.81 (11), 94.09 (12) and 100.05 (11)°, respectively. The dihedral angles between the equatorial O1—O4—N3—N5 plane and the nitrate and pyrimidine planes are 81.24 (12), 89.08 (13), 40.81 (15), 81.96 (10) and 87.36 (10)° for O1—N1—O2—O3, O4—N2—O5—O6, N3—C1—N4—C2—C3—C4,

Table 2
Selected bond lengths and angles (Å, °).

	(1*a*) (295 K)	(1*b*) (100 K)
Cu1—O1	1.990 (3)	2.001 (2)
Cu1—O4	1.978 (3)	1.978 (2)
Cu1—N3	2.041 (3)	2.0268 (19)
Cu1—N5	2.036 (3)	2.0329 (18)
Cu1—N6^{i}	2.303 (3)	2.2928 (18)
O1—N1	1.296 (4)	1.298 (3)
O2—N1	1.232 (4)	1.225 (3)
O3—N1	1.226 (5)	1.245 (3)
O4—N2	1.298 (4)	1.302 (3)
O5—N2	1.230 (4)	1.233 (3)
O6—N2	1.229 (5)	1.229 (3)
Cu1—O3	2.776 (3)	2.799 (2)
Cu1—O5	2.751 (4)	2.742 (2)
O1—Cu1—O4	175.58 (11)	175.95 (9)
O1—Cu1—N3	91.10 (12)	90.81 (9)
O1—Cu1—N5	90.06 (12)	89.68 (8)
O1—Cu1—N6^{i}	90.06 (12)	90.17 (8)
O4—Cu1—N3	88.79 (12)	88.85 (8)
O4—Cu1—N5	91.12 (11)	91.66 (8)
O4—Cu1—N6^{i}	85.54 (11)	85.83 (8)
N3—Cu1—N5	165.84 (11)	165.58 (8)
N3—Cu1—N6^{i}	94.09 (12)	94.04 (7)
N5—Cu1—N6^{i}	100.05 (11)	100.37 (7)
Cu1—O1—N1	113.5 (2)	113.92 (17)
Cu1—O4—N2	112.8 (2)	112.01 (15)
O1—N1—O2	117.7 (3)	118.2 (2)
O1—N1—O3	118.3 (3)	118.2 (2)
O2—N1—O3	124.0 (3)	123.6 (2)
O4—N2—O5	118.0 (3)	118.4 (2)
O4—N2—O6	118.2 (3)	117.9 (2)
O5—N2—O6	123.8 (4)	123.7 (3)
Cu1—N3—C1	121.3 (3)	121.71 (16)
Cu1—N3—C4	121.7 (2)	121.47 (15)
Cu1—N5—C5	119.3 (2)	118.64 (14)
Cu1—N5—C8	123.7 (2)	123.92 (15)
C5—N6—Cu1^{ii}	120.6 (2)	120.00 (14)
C6—N6—Cu1^{ii}	123.0 (2)	122.31 (14)

Symmetry codes: (i) $x-\frac{1}{2}, 1-y, z$; (ii) $x+\frac{1}{2}, 1-y, z$.

N5—C5—N6—C6—C7—C8 and N6^{i}—C5^{i}—N5^{i}—C8^{i}—C7^{i}—C6^{i} planes, respectively.

In the molecule, short non-bonding Cu···O contacts are observed; the lengths of Cu1···O3 and Cu1···O5 are 2.776 (3) and 2.752 (4) Å, respectively. Therefore, (1) can be regarded as a pseudo-seven-coordinated complex. The angles of O—Cu···O are 50.80 (12), 51.43 (10) and 82.60 (11)° for O1—Cu1···O3, O4—Cu1···O5 and O3···Cu1···O5, respectively. The corresponding values at 100 K are 2.799 (2), 2.742 (2) Å, and 50.83 (9), 51.92 (8) and 81.67 (8)°, for Cu1···O3, Cu1···O5, O1—Cu1···O3, O4—Cu1···O5 and O3···Cu1···O5, respectively. Fig. 3 shows the model deformation maps of (1*b*). In Fig. 3(*a*) (the section of the equatorial plane), the lone-paired electrons of O and N atoms coordinated equatorially are clearly shown. The densities of the lone-paired electrons of O3 and O5 are shown in the plane defined by the axial N6^{i}, and equatorial O1 and O4 atoms (Fig. 3*b*). These electron densities point to the Cu atom showing pseudo-coordination. The accuracy of the intensity data, especially at higher θ angles, was inadequate for the detailed discussion of the *d* electrons of the Cu atom. In some Cu complexes with bidentate nitrate groups, found from the CSD, the coordination type is largely a distorted octahedron, where short Cu—O distances of bidentate nitrato groups are 1.959–2.102 Å and long Cu—O distances are 2.541–2.683 Å (COPFOC; Munno & Bruno, 1984; ZEQJIO, Martens *et al.*, 1995).

The lengths of O1—N1 [1.296 (4) Å] and O4—N2 [1.297 (4) Å] in the nitrates are significantly longer than the other N—O bonds [1.225 (5)–1.231 (4) Å], showing the polarizable effect for the strong coordination of Cu1—O1 [1.990 (3) Å] and Cu1—O4 [1.978 (3) Å].

The intrachain Cu1···Cu1^{i} distance is 6.008 (2) Å and the interchain Cu···Cu distances are 7.633 (2) and 8.274 (2) Å for Cu1···Cu1^{iii} [(iii) $\frac{3}{2}-x, y, \frac{1}{2}+z$] and Cu1···Cu1^{iv} [(iv) $1-x, 1-y, \frac{1}{2}+z$], respectively. The corresponding distances at 100 K are 5.9881 (4), 7.5535 (1) and 8.1826 (2) Å for Cu1···Cu1^{i}, Cu1···Cu1^{iii} and Cu1···Cu1^{iv}, respectively. These distances are similar to those of the pyrimidine complexes of Cu^{II}(hfac)$_2$. The contacts between coordination chains are of C—H···O type, of which the dimensions are listed in Table 3.

3.2. Structure of (2)

The molecular structure of (2) along with the atomic numbering is shown in Fig. 4 and the crystal structure is shown

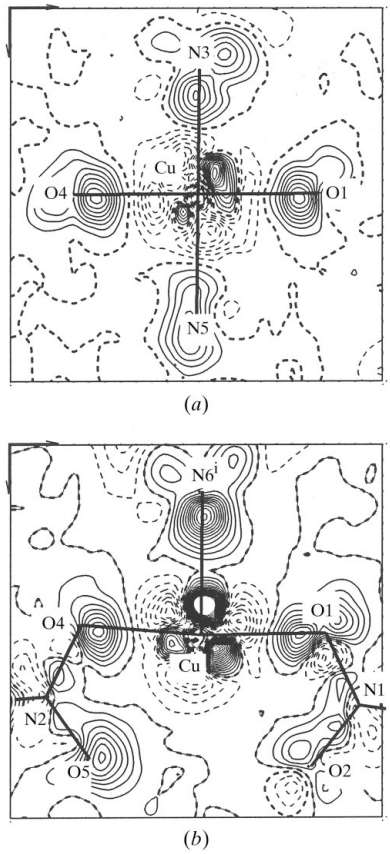

Figure 3
Model-deformation maps, $\Delta\rho$ = ρ[calc,multipole-atom] − ρ[calc, spherical-atom], of (1*b*). (*a*) Section of the equatorial plane; (*b*) section of the O3—Cu1—O5 plane. Solid lines denote positive contours, dashed and dotted lines represent zero and negative contours. Contour intervals: 0.1 e Å^{-3}.

Table 3
Geometry of the intermolecular hydrogen bonds (Å, °).

X—H$\cdots Y$	$X\cdots Y$	H$\cdots Y$	X—H$\cdots Y$
(1*a*)			
C8—H8$\cdots$O6^{iv}	3.310 (5)	2.42	160
C3—H3$\cdots$O2^{v}	3.409 (6)	2.48	178
(1*b*)			
C8—H8$\cdots$O6^{iv}	3.290 (3)	2.38	160
C3—H3$\cdots$O2^{v}	3.372 (3)	2.42	178
(2)			
O4—H41$\cdots$O3^{v}	2.759 (3)	1.93 (3)	176 (2)
O4—H42$\cdots$O3^{vi}	2.782 (4)	2.02 (4)	168 (3)
(3)			
O4—H41$\cdots$O3^{ii}	2.700 (4)	1.87 (5)	168 (4)
O4—H42$\cdots$N3^{iii}	2.769 (4)	1.94 (5)	170 (4)

Symmetry codes: For (1*a*) and (1*b*): (iv) $1-x, 1-y, z+\frac{1}{2}$; (v) $1-x, -y, z-\frac{1}{2}$. For (2): (v) $x, -y, z-\frac{1}{2}$; (vi) $x, y, z-1$. For (3): (ii) $x+1, y, z$; (iii) $x+\frac{1}{2}, \frac{1}{2}-y, z$.

in Fig. 5. Bond distances and angles are listed in Table 4. The Cu1 atom is located at the center of inversion of the crystals and coordinated by two pyrimidines and two water molecules equatorially, and two nitrate anions axially, forming a distorted six-coordinated octahedron. There are no examples of the Cu complexes coordinated with two NO_3 groups and two water molecules in the CSD. The pyrimidine bridges the Cu atoms at the *meta*-N positions to form a one-dimensional coordination chain. The pyrimidine moiety lies in the twofold symmetry of the crystals. In this case, an equatorial–equatorial coordination of pyrimidine is observed along the —Cu—N—C—N—Cu—N—C—N— chain. The length of the axial coordination with NO_3, Cu1—O1 [2.340 (2) Å], is longer than that of Cu—ONO_2 in (1). The lengths of the equatorial coordination with H_2O, Cu1—O4, and pyrimidine, Cu1—N2, are 2.0109 (16) and 2.0315 (18) Å, respectively. A large deviation of the angle of O4—Cu1—O1 [82.22 (8)°] from the right angle shows the

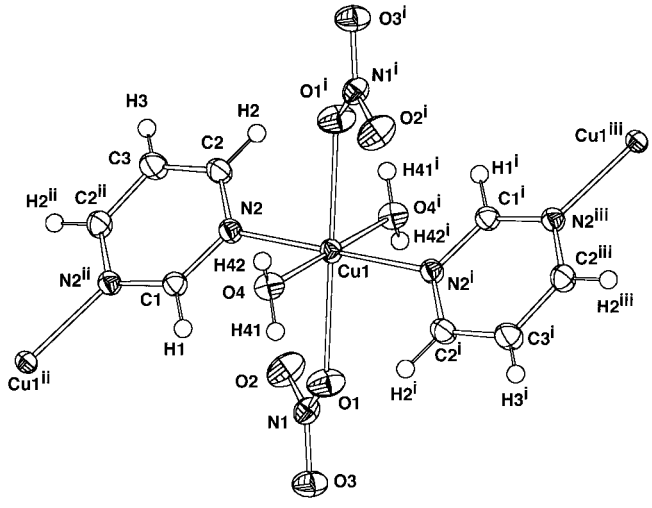

Figure 4
*ORTEP*II (Johnson, 1976) drawing of (2) with the atom numbering. The displacement ellipsoids for non-H atoms are drawn at 50% probability and the H atoms are drawn as spheres with a radius of 0.1 Å. Symmetry codes: (i) $\frac{1}{2}-x, \frac{1}{2}-y, -z$; (ii) $1-x, y, \frac{1}{2}-z$; (iii) $x-\frac{1}{2}, \frac{1}{2}-y, z-\frac{1}{2}$.

Table 4
Selected bond lengths and angles of (2) and (3).

(2)		(3)	
Cu1—O1	2.340 (2)	Cu1—O1	2.435 (3)
Cu1—O4	2.0109 (16)	Cu1—O4	1.973 (2)
Cu1—N2	2.0315 (18)	Cu1—N2	2.017 (2)
O1—N1	1.260 (2)	O1—N1	1.254 (4)
O2—N1	1.224 (2)	O2—N1	1.242 (4)
O3—N1	1.266 (2)	O3—N1	1.240 (4)
O1—Cu1—O4	82.22 (8)	O1—Cu1—O4	91.45 (10)
O1—Cu1—O4^{i}	97.78 (8)	O1—Cu1—O4^{i}	88.55 (10)
O1—Cu1—N2	91.78 (8)	O1—Cu1—N2	93.17 (10)
O1—Cu1—N2^{i}	88.22 (8)	O1—Cu1—N2^{i}	86.83 (10)
O4—Cu1—N2	87.71 (8)	O4—Cu1—N2	89.50 (9)
O4—Cu1—N2^{i}	92.29 (8)	O4—Cu1—N2^{i}	90.50 (9)
Cu1—O1—N1	125.60 (13)	Cu1—O1—N1	123.3 (2)
O1—N1—O2	121.54 (17)	O1—N1—O2	120.1 (3)
O1—N1—O3	117.46 (17)	O1—N1—O3	120.1 (3)
O2—N1—O3	121.00 (18)	O2—N1—O3	119.8 (3)
Cu1—N2—C1	118.55 (14)	Cu1—N2—C1	120.22 (19)
Cu1—N2—C2	123.64 (12)	Cu1—N2—C2	121.9 (2)

Symmetry codes: For (2): (i) $\frac{1}{2}-x, \frac{1}{2}-y, -z$. For (3): (i) $-x, 1-y, -z$.

distortion from the regular octahedron. The dihedral angles between the equatorial O4—N2—O4^{i}—N2^{i} [(i) $\frac{1}{2}-x, \frac{1}{2}-y, -z$] plane and the planes of NO_3, H_2O and the six-membered ring of pyrimidine are 87.44 (10), 80 (3) and 41.62 (8)°, respectively. In the nitrate, the lengths of the O1—N1 [1.260 (2) Å] and the O3—N1 [1.266 (2) Å] bonds are longer than the O2—N1 bond [1.224 (2) Å], but shorter than the N—O bonds related to the strong coordination in (1). The O1 and O3 atoms relate to the coordination and the intermolecular hydrogen bond (see later), respectively, while the O2 atom is free.

The Cu$\cdots$Cu distances are 5.737 (5) and 6.874 (5) Å for the intrachain Cu1$\cdots$Cu1^{ii} [(ii) $1-x, y, \frac{1}{2}-z$] and the interchain Cu1$\cdots$Cu1^{iv} [(iv) $x, 1-y, \frac{1}{2}+z$], respectively. The coordination chains are bound by the hydrogen-bonding network as shown in Fig. 5. Two types of hydrogen bonds are observed between H_2O and NO_3: O4—H41$\cdots$O3^{v} [(v) $x, -y, z-\frac{1}{2}$] and O4—H42$\cdots$O3^{vi} [(vi) $x, y, z-1$]. The geometry of the hydrogen bonds is listed in Table 3.

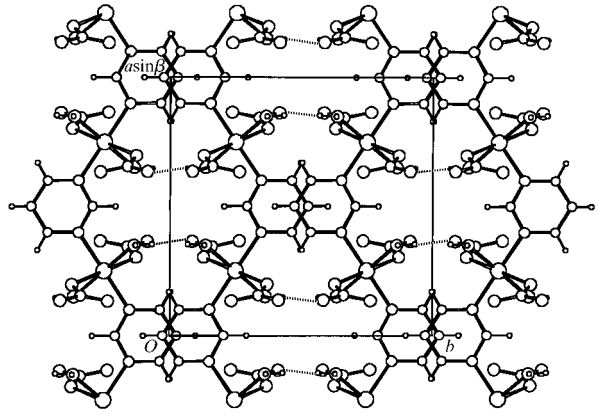

Figure 5
Crystal structure of (2) viewed along the *c* axis. Hydrogen bonds are shown with broken lines.

3.3. Structure of (3)

The molecular structure of (3) along with the atomic numbering is shown in Fig. 6. Bond distances and angles are listed in Table 4. Crystal structure is shown in Fig. 7.

The Cu atom is located at the center of inversion of the crystals and is coordinated by two N atoms of the pyrimidines and two O atoms of the water molecules at the equatorial positions, and two O atoms of the nitrate anions at the axial positions, forming a six-coordinated octahedron. In this instance, unlike (2), the complex is not a coordination polymer. One of the two N atoms of the pyrimidine moiety does not coordinate to the Cu atom. This N atom is used as an acceptor of the intermolecular hydrogen bonding. In the crystals two types of intermolecular hydrogen bond are formed; one is between the water molecule and the nitrate, O4—H41···O3^{ii} [(ii) $x+1, y, z$], and the other is between the water molecule and the pyrimidine, O4—H42···N3^{iii} [(iii) $x+\frac{1}{2}, -y+\frac{1}{2}, z$]. The network of the hydrogen bonds and the dimensions are shown in Fig. 7 and Table 3, respectively. The geometry of the octahedron of (3) is different from that of (2). The axial Cu1—O1 bond [2.435 (3) Å] of (3) is longer than that of (2) [2.340 (2) Å]. The deviations of the bond angles of O1—Cu1—O4 and O1—Cu1—N2 from 90° are less than those of (2), which reflects the weak coordination of Cu1—O1 in (3). The dihedral angles between the equatorial plane and NO_3, H_2O and pyrimidine planes are 35.05 (17), 55 (3) and 52.89 (10)°, respectively. These values are also quite different from those of (2). The deviation of the NO_3 moiety from the regular triangle is the smallest among these three complexes.

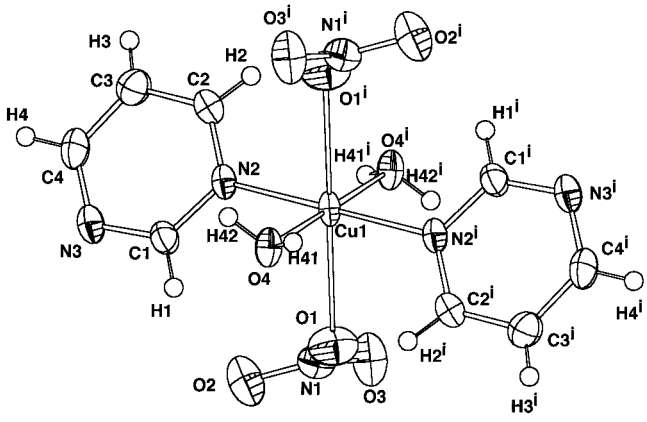

Figure 6
*ORTEP*II (Johnson, 1976) drawing of (3) with the atom numbering. The displacement ellipsoids for non-H atoms are drawn at 50% probability and the H atoms are drawn as spheres with a radius of 0.1 Å. Symmetry code: (i) $-x, 1-y, -z$.

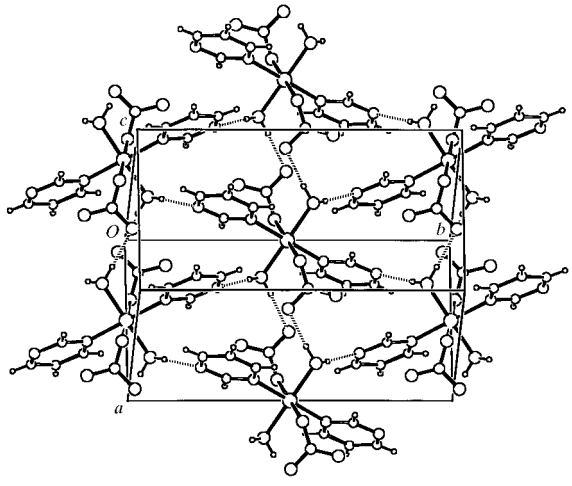

Figure 7
Perspective view of the crystal structure of (3). Hydrogen bonds are shown with broken lines.

3.4. Magnetism

Fig. 8 shows the temperature dependence of $\chi_{mol}T$ (χ_{mol} = molar magnetic susceptibility) for (1), (2) and (3), in which the data were collected on an MPMS-7 SQUID magnetometer (Quantum Design) down to 1.8 K at 0.5 T for the polycrystalline samples (Ishida *et al.*, 1997). The $\chi_{mol}T$ value is proportional to the square of the effective magnetic moment and consequently indicates magnetic interactions in the specimens especially at low temperatures. The $\chi_{mol}T$ value is almost constant for (3), indicating the absence of any appreciable magnetic interaction among the Cu^{II} spins. This paramagnetism agrees well with the isolated mononuclear structure of (3) described above.

A monotonous increase in the $\chi_{mol}T$ of (1) with a decrease in temperature clearly indicates the presence of ferromagnetic interactions. In order to confirm the presence of ferromagnetic interactions the magnetization curve was measured at 1.8 K up to 7 T. The data obtained exceeded the theoretical Brillouin function of $S = 1/2$ and fell between those of $S = 1$ and 3/2. The exchange parameter J (defined by a spin Hamiltonian $H = -2JS_i \cdot S_{i+1}$) between the neighboring Cu^{II} spins can be

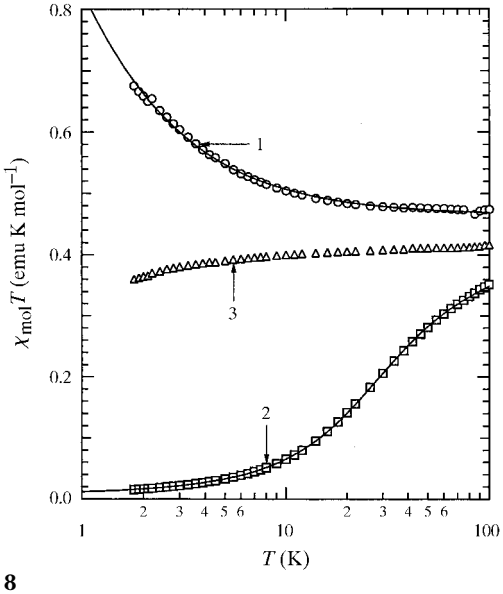

Figure 8
Temperature dependences of the product $\chi_{mol}T$ for (1) (circles), (2) (squares) and (3) (triangles). The solid lines are best-fit curves. See text for the parameters and equations.

estimated from the $\chi_{mol}T$ *versus* T plot. Positive and negative J imply ferro- and antiferromagnetic couplings, respectively. An expression of a high-temperature series (HTS) expansion of magnetic susceptibility as a function of temperature has been proposed for uniform $S = 1/2$ ferromagnetic Heisenberg chains (Baker *et al.*, 1964). A best fit to the above expression gave $2J/k_B = +1.78$ (2) K and $g = 2.23$ (1).

The antiferromagnetic behavior was found for (2), as indicated by a decrease in $\chi_{mol}T$ with a decrease in temperature. The general behavior for uniform $S = 1/2$ antiferromagnetic Heisenberg chains has been analyzed (Bonner & Fisher, 1964). However, fits of the data of (2) to the Bonner–Fisher equation alone gave unsatisfactory results, because of the presence of some additional contribution which is not expected from the ideal chain. The observed temperature dependence of $\chi_{mol}T$ can be well described by the sum of Bonner–Fisher and Curie terms, affording $2J/k_B = -36.8$ (2) K and $g = 2.12$ (1) with a 1.7 (1)% Curie contribution. An HTS expansion is valid for both positive and negative J (Kahn, 1993), and a fit of the data in a temperature range above 23 K (a peaking temperature of χ_{mol}) to this equation gave $2J/k_B = -35.3$ (2) K and $g = 2.13$ (1), assuming that the Curie term is negligible. The $|2J|/k_B = 36$ K of (2) is larger than those of the pyrazine-bridged antiferromagnetic compounds, $Cu(L)(NO_3)_2$ (L = pyrazine derivatives, $2J/k_B = -4$ to -18 K; Richardson & Hatfield, 1976). The molecular orbital calculation analysis suggests that the through-space interaction between two nitrogen lone pairs within a pyrimidine molecule plays an important role in the exchange mechanism for a pyrimidine-bridged dinuclear model compound (Mohri *et al.*, 1999). The large negative value of J of (2) is ascribed to a short N···N distance in pyrimidine compared with those of pyrazines.

Usually, Curie contributions found in antiferromagnetic chain compounds are attributed to impurity spins (such as chain defects). However, a single crystal of (2) showed the strong anisotropy of the Curie contribution by a factor as large as six (Feyerherm *et al.*, 1999). This finding indicates that the Curie contribution is intrinsic for the antiferromagnetic chain. A similar anisotropic Curie contribution has been reported for the one-dimensional antiferromagnetic compound, copper(II) benzoate (Date *et al.*, 1970). Furthermore, a field-induced spin-excitation gap has been extensively investigated in connection with the effective staggered magnetic field in copper(II) benzoate (Dender *et al.*, 1997; Oshikawa & Affleck, 1997). It is well known that the uniform $S = 1/2$ antiferromagnetic chains have a gapless continuum of spin excitations (Bonner & Fisher, 1964). The origin of the Curie contribution as well as a possible spin-excitation gap of the $S = 1/2$ chain in the crystal of (2) can be accounted for by the structural features in the chain: the relative canting g-tensor principal axes of the neighboring copper(II) ions. The Cu—O(nitrate) (Cu1—O1) bond is tilted from the octahedral axis by approximately 8°, as shown from the bond angles. The angle between the Cu1—O1 and the neighboring Cu—O bond along the chain [Cu1^{ii}—O1^{ii}, (ii) $1-x, y, \frac{1}{2}-z$] is 106.90 (11)° and the dihedral angle between the equatorial planes of neighboring Cu^{II} ions [O4—N2—O4^{i}—N2^{i}, (i) $\frac{1}{2}-x, \frac{1}{2}-y, -z$, and O4^{ii}—N2^{ii}—O4^{vii}—N2^{vii}, (vii) $x+\frac{1}{2}, \frac{1}{2}-y, z+\frac{1}{2}$] is 58.80 (8)°.

As shown by the solid lines in Fig. 8, the calculations with the optimized parameters reproduce well the experimental data. Therefore, (1) and (2) can be regarded as almost ideal one-dimensional ferromagnetic and antiferromagnetic chains, respectively. Although the networks of hydrogen bonding are found among the chains for both and seem important to construct the crystal structures, they did not function as magnetic couplers.

3.5. Relations between magnetic interactions and coordination structure

The pyrimidine bridge can work as both ferromagnetic and antiferromagnetic couplers. There are no significant differences in the C—N$_{pm}$(eq) lengths between complexes exhibiting different magnetic interactions. The dimensions of the pyrimidine moieties show no significant differences between bridging and non-bridging coordinations. The crucial difference is the coordination types of the *meta*-N atoms of the bridging pyrimidine: an axial–equatorial coordination was observed in (1), showing ferromagnetic interactions. Similarly, axial–equatorial coordination types were found in Cu^{II}(hfac)$_2$(qn), Cu^{II}(hfac)$_2$(pm) and Cu^{II}(hfac)$_2$(4-Me-pm), all of which show ferromagnetic interactions. On the other hand, an equatorial–equatorial coordination was observed in (2), showing antiferromagnetic interactions.

The superexchange mechanism is usually discussed concerning the atomic orbital(s) on a closed-shell bridging atom, but in the present study this mechanism should be applied to the molecular orbital on the bridging pyrimidine molecule. The magnetic orbital $d_{x^2-y^2}$ of the copper(II) ion is located on the equatorial plane. The magnetic coupling can be explained in terms of orbital overlaps between a molecular orbital of the pyrimidine and two Cu^{II} $d_{x^2-y^2}$ orbitals. With appreciable overlaps on both sides of the pyrimidine, the magnetic coupling is expected to be antiferromagnetic. When one N atom of pyrimidine is axially coordinated to the copper(II) ion, there is no orbital overlap between the Cu $d_{x^2-y^2}$ and N $n\sigma$ and $p\pi$ orbitals due to orthogonality. Thus, the axial–equatorial combination favors ferromagnetic interactions. A semi-empirical molecular orbital analysis is described elsewhere (Mohri *et al.*, 1999).

This work was supported in part by a Grant-in-Aid for Scientific Research (No. 08454180) and a Grant-in-Aid for Scientific Research on Priority Areas 'Molecular Conductors and Magnets' and 'Metal Assembled Complexes' (Area Nos. 730/11 224 204 and 401/11 136 212, respectively) from the Ministry of Education, Science, Sports and Culture.

References

Allen, F. H., Davies, J. E., Galloy, J. J., Johnson, O., Kennard, O., Macrae, C. F., Mitchell, E. M., Mitchell, G. F., Smith, J. M. & Watson, D. G. (1991). *J. Chem. Inf. Comput. Sci.* **31**, 187–204.

Baker, G. A. Jr, Rushbrooke, G. S. & Gilbert, H. E. (1964). *Phys. Rev. A*, **135**, 1272–1277.
Beurskens, P. T., Admiraal, G., Beurskens, G., Bosma, W. P., Garcia-Granda, S., Gould, R. O., Smits, J. M. M. & Smykalla, C. (1992). *DIRDIF*92. Technical Report, Crystallography Laboratory, University of Nijmegen, The Netherlands.
Bonner, J. C. & Fisher, M. E. (1964). *Phys. Rev. A*, **135**, 640–658.
Burla, M. C., Camalli, M., Cascarano, G., Giacovazzo, C., Polidori, G., Spagna, R. & Viterbo, D. (1989). *J. Appl. Cryst.* **22**, 389–303.
Chen, Z. N., Fu, D. G., Yu, K. B. & Tang, W. X. (1994). *J. Chem. Soc. Dalton Trans.* pp. 1917–1921.
Chen, Z. N., Qiu, J., Tang, W. X. & Yu, K. B. (1994). *Inorg. Chim. Acta*, **224**, 171–176.
Date, M., Yamazaki, H. & Motokawa, M. (1970). *Suppl. Prog. Theor. Phys.* **46**, 194–209.
De Meulenaer, J. & Tompa, H. (1965). *Acta Cryst.* **19**, 1014–1018.
Dender, D. C., Hammar, P. R., Reich, D. H., Broholm, C. & Aeppli, G. (1997). *Phys. Rev. Lett.* **79**, 1750–1753.
Feyerherm, R., Ishida, T., Nogami, T. & Steiner, M. (1999). *Mol. Cryst. Liq. Cryst.* **355**, 235–244.
Hansen, N. K. & Coppens, P. (1978). *Acta Cryst.* A**34**, 909–921.
Ishida, T., Mitsubori, S., Nogami, T., Ishikawa, Y., Yasui, M., Iwasaki, F., Iwamura, H., Takeda, N. & Ishikawa, M. (1995). *Synth. Met.* **71**, 1791–1792.
Ishida, T., Nakayama, K., Nakagawa, M., Sato, W., Yasui, M., Iwasaki, F. & Nogami, T. (1997). *Synth. Met.* **85**, 1655–1658.
Ishida, T., Nogami, T., Yasui, M., Iwasaki, F., Iwamura, H., Takeda, N. & Ishikawa, M. (1996). *Mol. Cryst. Liq. Cryst.* **279**, 87–96.
Johnson, C. K. (1976). *ORTEP*II, Report ORNL-5138. Oak Ridge National Laboratory, Tennessee, USA.
Kahn, O. (1993). *Molecular Magnetism*, ch.11, Section 11.1, pp. 251–257. Weinheim: VCH Publishers.
Keller, S. W. (1997). *Angew. Chem. Engl. Ed.* **36**, 247–248.
Martens, C. F., Schenning, A. P. H. J., Feiters, M. C., Berens, H. W., van der Linden, J. G. M., Admiraal, G., Beurskens, P. T., Kooijman, H., Spek, A. L. & Nolte, R. J. M. (1995). *Inorg. Chem.* **34**, 4735–4744.
Mohri, F., Yoshizawa, K., Yamabe, T., Ishida, T. & Nogami, T. (1999). *Mol. Engng.* **8**, 357–373.
Molecular Science Corporation (1992). *TEXSAN*. MSC, 3200 Research Forest Drive, The Woodlands, TX 77381, USA.
Munno, G. D. & Bruno, G. (1984). *Acta Cryst.* B**40**, 2030–2032.
North, A. C. T., Phillips, D. C. & Mathews, F. S. (1968). *Acta Cryst.* A**24**, 351–359.
Novak, B. & Keller, S. W. (1997). *J. Chem. Cryst.* **27**, 279–282.
Oshikawa, M. & Affleck, I. (1997). *Phys. Rev. Lett.* **79**, 2883–2886.
Richardson, H. W. & Hatfield, W. E. (1976). *J. Am. Chem. Soc.* **98**, 835–839.
Rigaku Corporation (1994). *AFC Control Software.* Rigaku Corporation, Tokyo, Japan.
Sheldrick, G. M. (1997). *SHELXL*97. University of Göttingen, Germany.
Yasui, M., Ishikawa, Y., Ishida, T., Nogami, T. & Iwasaki, F. (2001). To be published.

Radical−Copper Wheels: Structure and Magnetism of Hexanuclear Hybrid Arrays

Junichi Omata, Takayuki Ishida,*,† Daisuke Hashizume, Fujiko Iwasaki, and Takashi Nogami*

Department of Applied Physics and Chemistry, The University of Electro-Communications, Chofu, Tokyo 182-8585, Japan

Received December 27, 2000

Complexation of copper(II) bromide and chloride with 4-pyrimidinyl nitronyl nitroxide (4PMNN) as a bridging ligand gave discrete hexanuclear complexes carrying 12 spins, $[CuX_2\cdot(4PMNN)]_6$ [X = Br (**1**), Cl (**2**)], which crystallize in a trigonal space group $R\bar{3}$. The crystallographic parameters are $C_{11}H_{15}Br_2CuN_4O_2\cdot 0.3H_2O$, a = 28.172(2), c = 12.590(2) Å, V = 8653(2) Å^3, and Z = 18 for **1**, and $C_{11}H_{15}Cl_2CuN_4O_2\cdot 0.3H_2O$, a = 28.261(2), c = 12.378(1) Å, and Z = 18 for **2**. The hexanuclear arrays construct a perfect column perpendicular to the molecular plane. The diameter of the resultant honeycomblike channel is ca. 11.5 Å defined by the interatomic distance of two opposing copper ions. Their magnetic behavior is interpreted as the simultaneous presence of ferro and antiferromagnetic couplings. The ferromagnetic couplings are attributed to the interactions between a copper spin and the axially coordinated nitronyl nitroxide spin and between nitronyl nitroxide groups through van der Waals contacts. The antiferromagnetic coupling is due to the interaction between copper ions across the pyrimidine bridges.

Introduction

The metal−radical approach has been successful in the design of ferrimagnetic compounds that show magnetic order at low temperatures.[1,2] The synthesis and magnetic property of a hexanuclear compound containing six *cis*-Mn(hfac)$_2$ entities connected by phenyl nitronyl nitroxide have been reported.[3] Self-assembled oligonuclear complexes sometimes possess architectural beauty.[4−6] Such polynuclear discrete molecules have fascinated chemists owing especially to their mesoscopic physical properties (magnetic hysteresis of purely molecular origin, for instance).[7,8] We have reported the magnetism of pyrimidine-bridged transition metal complexes[9−12] in connection with the organic high-spin *m*-phenylene-bridged polycarbenes and radicals.[13] In the course of our study on the magnetic role of radical-substituted pyrimidine across μ-1,3-NCN bridges, we have found that hexanuclear arrays $[CuX_2\cdot(4PMNN)]_6$ (**1**: X = Br, **2**: X = Cl; 4PMNN = 4-pyrimidinyl nitronyl nitroxide[14]) exhibited ferromagnetic intermolecular interactions.

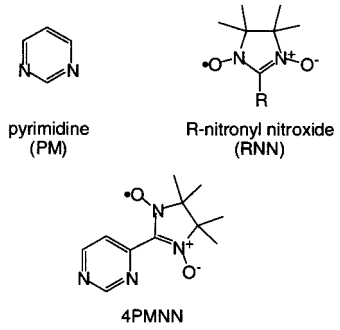

Experimental Section

The 4-pyrimidinecarboxaldehyde was prepared according to the method previously reported,[15] by using *N*,*N*-dimethylformamide diethyl acetal and pyruvic aldehyde dimethyl acetal as starting materials. The formyl group was converted to a nitronyl nitroxide group by Ullman's method,[16] giving blue plates of 4PMNN in 76% yield from 4-pyrimidinecarboxaldehyde (mp 128−131 °C, recrystallized from ether−hexane). Anal. Calcd for $C_{11}H_{15}N_4O_2$: C, 56.16; H, 6.43; N, 23.82%. Found: C, 56.64; H, 6.48; N, 23.63%. MS (EI, 70 eV) *m*/*z* 236 (68%, MH^+), 106 (100%). ESR (benzene, room temperature) g = 2.0065, a_N = 7.1 G (quintet).

The typical procedure of complexation is as follows. A methanol solution (10 mL) containing 34 mg (0.14 mmol) of 4PMNN and 35 mg (0.16 mmol) of $CuBr_2$ was allowed to stand at room temperature for a week. Dark green needles (18 mg, 0.039 mmol) of **1** were precipitated and collected on a filter; the crystals were suitable for X-ray

* To whom communication should be addressed.
† E-mail: ishi@pc.uec.ac.jp.

(1) Caneschi, A.; Gatteschi, D.; Rey, P.; Sessoli, R. *Acc. Chem. Res.* **1989**, *22*, 392.
(2) Inoue, K.; Hayamizu, T.; Iwamura, H.; Hashizume, D.; Ohashi, Y. *J. Am. Chem. Soc.* **1996**, *118*, 1803.
(3) Caneschi, A.; Gatteschi, D.; Laugier, J.; Rey, P.; Sessoli, R.; Zanchini, C. *J. Am. Chem. Soc.* **1988**, *110*, 2795.
(4) Taft, K. L.; Lippard, S. J., *J. Am. Chem. Soc.* **1990**, *112*, 9629.
(5) Abbati, G. L.; Cornia, A.; Fabretti, A. C.; Caneschi, A.; Gatteschi, D. *Inorg. Chem.* **1998**, *37*, 1430.
(6) Blake, A. J.; Grant, C. M.; Parsons, S.; Rawson, J. M.; Winpenny, E. P. *J. Chem. Soc., Chem. Commun.* **1994**, 2363.
(7) Friedman, J. R.; Sarachik, M. P.; Tejada, J.; Ziolo, R. *Phys. Rev. Lett.* **1996**, *76*, 3830.
(8) Thomas, L.; Lionti, F.; Ballow, R.; Gatteschi, D.; Sessoli, R.; Barbara, B. *Natrure* **1996**, *383*, 145.
(9) Ishida, T.; Nogami, T. *Recent Res. Devel. Pure Appl. Chem.* **1997**, *1*, 1.
(10) Ishida, T.; Nakayama, K.; Nakagawa, M.; Sato, W.; Ishikawa, Y.; Yasui, M.; Iwasaki, F.; Nogami, T. *Synth. Met.* **1997**, *85*, 1655.
(11) Nakayama, K.; Ishida, T.; Takayama, R.; Hashizume, D.; Yasui, M.; Iwasaki, F.; Nogami, T. *Chem. Lett.* **1998**, 497.
(12) Kusaka, T.; Ishida, T.; Hashizume, D.; Iwasaki, F.; Nogami, T. *Chem. Lett.* **2000**, 1146.
(13) Iwamura, H. *Adv. Phys. Org. Chem.* **1990**, *26*, 179.
(14) Systematic name: 2-(4-pyrimidinyl)-4,4,5,5-tetramethylimidazolin-1-yloxyl 3-oxide.
(15) Bredereck, H.; Sell, R.; Effenberger, F. *Chem. Ber.* **1964**, *97*, 3406.
(16) Ullman, E. F.; Osiecki, J. H.; Darcy, R. *J. Am. Chem. Soc.* **1972**, *94*, 7049.

10.1021/ic001462g CCC: $20.00
Published on Web 06/27/2001

Table 1. Crystallographic Data of **1** and **2**

formula	$C_{11}H_{15}Br_2CuN_4O_2{\cdot}0.3H_2O$	$C_{11}H_{15}Cl_2CuN_4O_2{\cdot}0.3H_2O$
fw	464.02	375.12
space group	$R\bar{3}$	$R\bar{3}$
a/Å	28.172(2)	28.261(2)
c/Å	12.590(2)	12.378(1)
V/Å^3	8653(2)	8561(1)
Z	18	18
D_{calc}/g cm^{-3}	1.605	1.312
μ(Mo Kα)/mm^{-1}	5.298	1.435
R^a ($I > 2\sigma(I)$)	0.0576	0.0605
$R_w{}^b$ ($I > 2\sigma(I)$)	0.102	0.118
T/K	296	296
λ/Å	0.71073	0.71073

$^a R = \sum||F_o| - |F_c||/\sum|F_o|$. $^b R_w = [\sum w(F_o^2 - F_c^2)^2/\sum w(F_c^2)^2]^{1/2}$.

diffraction and magnetic studies. Anal. Calcd for $C_{11}H_{15}Br_2CuN_4O_2$: C, 28.81; H, 3.30; N, 12.22%. Found: C, 28.77; H, 4.11; N, 11.94%. Green needle crystals of **2** were prepared by using of $CuCl_2$ in place of $CuBr_2$. Anal. Calcd for $C_{11}H_{15}Cl_2CuN_4O_2$: C, 35.74; H, 4.09; N, 15.15%. Found: C, 36.19; H, 4.39; N, 14.79%.

X-ray diffraction data were collected on a Raxis-Rapid IP diffractometer (Rigaku) with graphite monochromated Mo Kα radiation (λ = 0.71073 Å) at 296 K. The crystal sizes were 0.2 × 0.1 × 0.1 and 0.2 × 0.03 × 0.03 mm^3 for **1** and **2**, respectively. Numerical absorption correction was applied. The structure was solved with the program SAPI-91[17] and refined using all the independent reflections with the program SHELXL-97.[18] Anisotropic temperature factors were used for non-hydrogen atoms. Significant peaks found in the channel on difference maps were assigned to water molecules with a small occupancy of 0.3. Selected crystallographic data of **1**·(0.3H_2O)$_6$ and **2**·(0.3H_2O)$_6$ are listed in Table 1.

Magnetic properties were measured on an MPMS SQUID magnetometer (Quantum Design) equipped with a 7 T superconducting magnet over a temperature range 1.8−300 K. Diamagnetic contribution of the sample itself was estimated from Pascal's constants.

Results and Discussion

Structural Studies. As Table 1 shows, the crystals of **1** and **2** are isomorphous, belonging to a space group trigonal $R\bar{3}$. We focus on the molecular and crystal structures of **1** here. Figure 1(a) shows a crystallographically independent unit for **1**, one $CuBr_2$·(4PMNN) moiety and a water molecule with an occupancy of almost 0.3, together with atom labeling. As Figure 1(b) shows, a molecule consists of a wheel-like hexamer of $CuBr_2$·(4PMNN) in a head-to-tail fashion, in which the pyrimidine (PM) rings work as μ-N1−C1−N2 bridges. The resultant hexagonal array shapes a cavity with a nanosized diameter; the interatomic distance of the opposing Cu1···Cu1* is 11.497(3) Å (the symmetry operation code for * is $-x$, $-y$, $-z$).

Selected bond lengths and angles of **1** and **2** are listed in Table 2. The molecular structure of **2** is quite similar to that of **1**, and the atoms of **2** are similarly numbered. The copper ion is pentacoordinated to form a square-pyramidal structure and is slightly deviated upward from the basal plane. Two bromide ions and two PM nitrogen atoms are bonded at the *trans*-equatorial positions. One oxygen atom in the nitronyl nitroxide (NN) group is coordinated at an axial position with the Cu−O distance of 2.216(6) Å for **1**, which is somewhat longer than

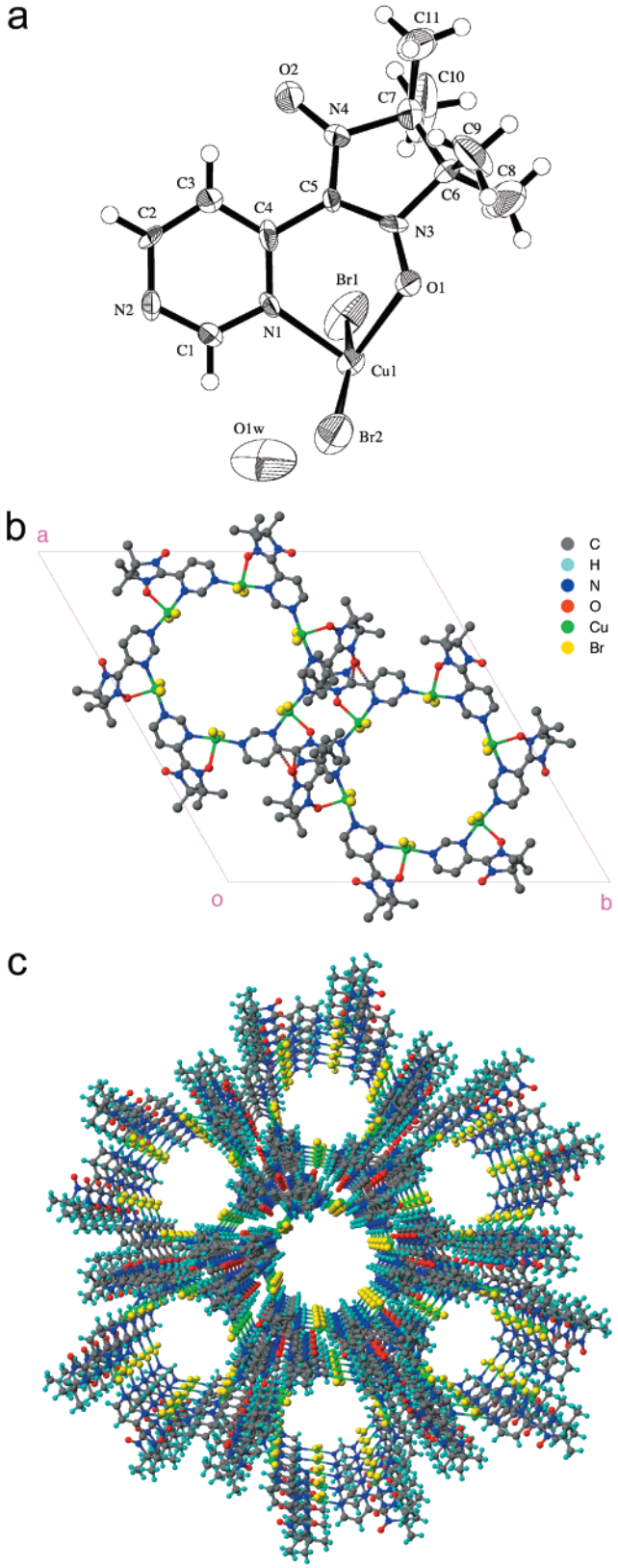

Figure 1. (a) Crystallographically independent unit of [$CuBr_2$·(4PMNN)]$_6$ (**1**) with atomic numbering. Thermal ellipsoids at the 50% level are shown for non-hydrogen atoms. Only oxygen atom (O1w) is shown for a water molecule with an occupancy of 0.3. (b) Two molecules of **1**. The hydrogen atoms and disordered water molecules are omitted. Intermolecular van der Waals contacts between O and C atoms are indicated with dotted lines. (c) Molecular arrangement in the crystal of **1** viewed along the c axis.

(17) Fan, H.-F. SAPI-91, Structure Analysis Program with Intelligent Control, Rigaku Corp., Tokyo, 1991.
(18) Sheldrick, G. M. Program for Crystal Structure Refinement, University of Göttingen, Germany, 1997.

Table 2. Selected Bond Lengths (Å) and Angles (Deg) of $[CuX_2 \cdot (4PMNN)]_6$ [X = Br (**1**), Cl (**2**)][a]

compound	**1**	**2**
Cu1 X1	2.3992(18)	2.249(2)
Cu1 X2	2.4010(18)	2.256(2)
Cu1 N1	2.020(7)	2.057(5)
Cu1 N2#	2.025(7)	2.030(5)
Cu1 O1	2.216(6)	2.262(4)
O1 N3	1.284(8)	1.286(6)
O2 N4	1.262(9)	1.269(6)
X1 Cu1 X2	162.39(7)	164.24(9)
N1 Cu1 N2#	175.6(3)	174.99(19)
N1 Cu1 O1	84.3(2)	83.38(16)
N2# Cu1 O1	91.4(3)	91.62(17)
O1 Cu1 X1	101.60(17)	100.86(13)
O1 Cu1 X2	95.97(17)	94.76(13)
N1 C4 C5 N3	−25.5(13)	−26.5(9)
O1 Cu1 N1 C1	−152.5(7)	−151.9(5)

[a] Symmetry code for #: $x - y, x, -z$.

the equatorial Cu1−N1 and Cu1−N2# distances (the symmetry code for # is $x - y, x, -z$). The C4−C5 bond between the two rings, PM and NN, is twisted by an angle of 26°, which is smaller than that of uncoordinated 4PMNN (44°).[19] The PM plane is largely canted from the Cu1 equatorial plane, as indicated by a dihedral angle between the PM ring and the axial Cu1−O1 bond. There are three molecules in a unit cell, and Figure 1(b) shows only two molecules in order to clarify intermolecular contacts between O2···C4§ and O2···C5§ (the symmetry code for § is $-y + 2/3, x - y + 1/3, z + 1/3$). Two contacts are drawn in Figure 1(b) with dotted lines. Each contact successively repeats, with a 3_1 screw symmetry along the *c* axis, and belongs to its individual magnetic chain. There are six chains running through a unit cell. Detailed intermolecular geometry of **1** and **2** will be discussed later.

As Figure 1(c) shows, the molecular hexanuclear arrays construct a column along the *c* axis, and consequently, a honeycomblike channel structure is formed. The intracolumnar neighboring molecular arrays are related by the translation along the *c* axis. No interatomic contact is found within a column, whereas intercolumnar atomic distances are relatively short. Note that the elemental analysis and X-ray diffraction study of **1** and **2** indicate that the channels are almost empty. Crystal solvents are supposed to be easily removed from the channel during usual evacuation process prior to the analysis.

Magnetic Properties. Figure 2 shows the temperature dependence of the product of magnetic susceptibility and temperature ($\chi_{mol}T$) for **1** and **2** measured at 500 Oe. The spin-only $\chi_{mol}T$ value of a molecule having twelve paramagnetic $S = 1/2$ spins is 4.5 cm^3 K mol^{-1}, assuming $g_{av} = 2.0$, being in apparent agreement with the experimental values. With decreasing temperature the $\chi_{mol}T$ values gradually decreased, but below ca. 40 K they turned to increase. Such a temperature dependence of $\chi_{mol}T$, showing a broad minimum, is often characterized for ferrimagnetic materials. However, **1** and **2** consist of two doublet species from copper(II) and an organic radical 4PMNN with a 1/1 molar ratio, and all of the copper(II) ions and radicals are crystallographically equivalent. Complexes **1** and **2** can hardly be regarded as ferrimagnetic materials. The "ferrimagnetic-like" behavior of **1** and **2** strongly suggests the simultaneous presence of ferro and antiferromagnetic interactions in their crystals.

With decreasing temperature below 40 K, the $\chi_{mol}T$ values increased and reached maxima of 35.6 and 22.6 cm^3 K mol^{-1} for **1** and **2**, respectively, and finally decreased again below ca. 3 K. The maximum values correspond to spin-only values of *S* of ca. 8 for **1** and *S* of slightly larger than 6 for **2**, suggesting that the ferromagnetic coupling should be attributed to interactions among the hexameric molecular arrays. The difference between the $\chi_{mol}T$ vs *T* profiles of **1** and **2** (Figure 2) do not seem to be intrinsic. Actually, the peak of the $\chi_{mol}T$ value was somewhat sample dependent. The magnetic properties may be changed in relation to the occupancy of the crystal solvent molecules included.

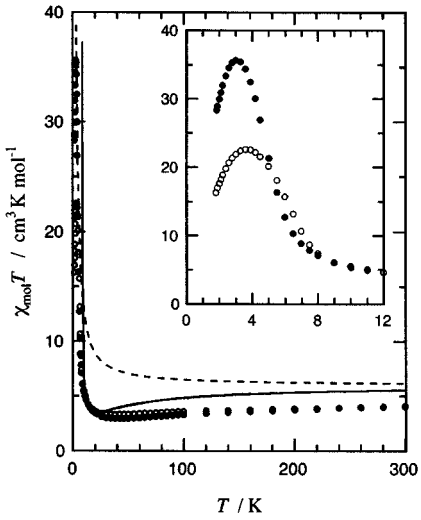

Figure 2. Temperature dependence of the product of χ_{mol} and *T* for $[CuX_2 \cdot (4PMNN)]_6$ [**1**: X = Br (filled circles), **2**: X = Cl (open circles)] measured at 500 Oe. Solid and Broken lines correspond to calculated curves based on a modified hexagonal model and the Fisher model, respectively. For the equations and parameters, see the text. Inset shows the magnification of the plot in a low-temperature region.

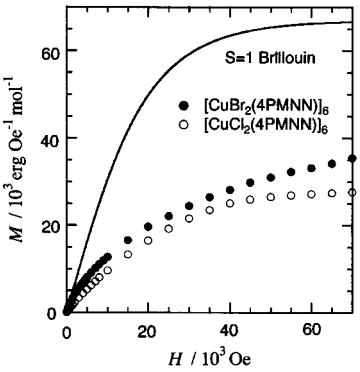

Figure 3. Magnetization curves of **1** and **2** measured at 2 K. The solid line represents a theoretical curve based on Brillouin function with $g_{av} = 2.0$ and $S = 1$.

The final decrease below ca. 3 K is more remarkable, and the maximum value is more suppressed in the measurements at larger applied fields. This finding indicates that the decrease is partly due to a saturation effect. To check whether antiferromagnetic phase transition occurs at around the peaking temperature, we measured the magnetization curves of **1** and **2** at 1.8 K (Figure 3). The magnetizations are very small and fall below the $S = 1$ Brillouin function with $g_{av} = 2.0$, clearly indicating the presence of dominant antiferromagnetic interaction. No inflection point was found in detailed d*M*/d*H* analysis in the *M*−*H* curves at 1.8 K. No anomaly was found in the measurements of field-cooled (5 Oe) or zero-field-cooled magnetization down to 1.8 K. Though **1** and **2** are paramagnets, the antiferromagnetic behavior is rationalized from the following discussion of the magnetic structure.

(19) Omata, J.; Ishida, T.; Hashizume, D.; Iwasaki, F.; Nogami, T. *Mol. Cryst. Liq. Cryst.*, in press.

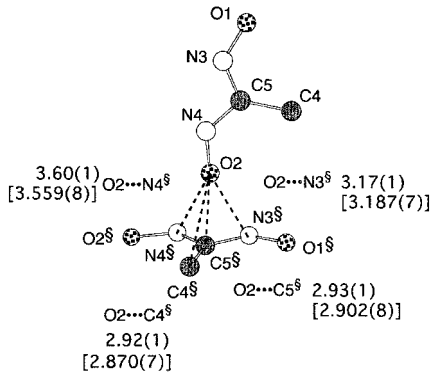

Figure 4. Intercolumnar atomic contacts for the crystal of **1** are shown in Å with dotted lines. Those values for the crystal of **2** are shown in square brackets. Only the ONCNO moiety and the C4 atom of the pyrimidinyl 4-position are drawn for the sake of clarity. The symmetry code for § is $-y + 2/3, x - y + 1/3, z + 1/3$.

Mechanisms of Magnetic Coupling. We can find a chelate structure in the repeating unit CuX_2·(4PMNN), in which the NN oxygen atom is axially coordinated to the copper ion. The orthogonality of Cu $3d_{x^2-y^2}$ and O $2p_z$ orbitals favors ferromagnetic interaction between the Cu and NN spins, as previously clarified for the one-dimensional Cu(II) complex bridged by methyl−NN.[1,20] The hexanuclear arrays are regarded as involving six local triplets at low temperatures.

On the other hand, we can also find that the PM bridges two copper ions. We have reported that the coordination structures of PM-bridged copper(II) complexes are simply classified into three types: axial−equatorial, equatorial−equatorial, and axial−axial coordinations of two nitrogen atoms in a PM ring.[9,10,21,22] The corresponding superexchange interactions are ferromagnetic, antiferromagnetic, and paramagnetic, respectively, through the PM ring.[9,10,21,22] In the present case, the PM bridge should be an antiferromagnetic coupler, since every PM nitrogen atom is coordinated at an equatorial position. Accordingly, the magnetism is expected to show antiferromagnetic coupling among six triplet units within a molecular array, and the experimental results above 40 K (Figure 2) agree with this interpretation. The increase of $\chi_{mol}T$ below 40 K must be attributed to intermolecular ferromagnetic interactions.

There is no interatomic contact within a column. As indicated with a dotted line in Figure 1(b), however, relatively short contacts can be pointed out between columns. Figure 4 shows selected atoms of adjacent 4PMNN groups. The shortest distance is found between a terminal NN oxygen atom and a carbon atom of the PM 4-position in a neighboring molecule. The O2···C4§ distances of 2.92(1) and 2.870(7) Å for **1** and **2**, respectively, are shorter than the sum of the van der Waals radii (3.2 Å).[23] The second shortest distance is found between a terminal NN oxygen atom and a central NN carbon atom (O2···C5§). Almost vertical spatial arrangement of two NN units forms a T-shaped configuration. We performed a semiempirical molecular orbital calculation of 4PMNN,[24] confirming that the NN group has a node of the singly occupied molecular orbital (SOMO) at the central carbon atom, and that none of the atoms of the PM group have appreciable coefficients of the SOMO. The O2···C5§ contact gives rise to ferromagnetic coupling on the basis of McConnell's theory.[25] Similar proximities were reported on ferromagnetic crystals of lithium *p*-NN-substituted benzoate[26,27] and 1,2,4-triazole-3-yl-NN,[28] and the ab initio calculation of exchange interaction demonstrated that such O···C(NN) contacts favored ferromagnetic interaction. Furthermore, Awaga has proposed that a large SOMO−NHOMO overlap due to contact between an NN group and an α-substituent (bonded to the central carbon atom) is required for appreciable ferromagnetic interaction.[29,30] Therefore, the first and second shortest contacts in the present complexes are both responsible for the observed ferromagnetic interaction. Figures 1b and 1c show that the intermolecular van der Waals contacts can be found to be surrounded by three columns, and this geometry successively repeats with a 3_1 screw symmetry along the *c* axis, forming a uniform linear chain. Along this interpretation, the crystals of **1** and **2** can be regarded as ferromagnetic chains accompanied by antiferromagnetic coupling among the chains.

Semiquantitative Analysis. To estimate semiquantitatively the exchange parameters (*J*'s),[31] J_{Cu-NN}, J_{Cu-Cu}, and J_{NN-NN} are defined between the copper(II) and axially coordinated NN spins, between two copper(II) spins across the PM ring, and between two NN spins through the van der Waals contacts, respectively. Below 40 K the ferromagnetic interaction was dominantly observed, which is due to the one-dimensional structure along the *c* axis with J_{NN-NN}. We applied the data of the $\chi_{mol}T$ upsurge region to the Curie−Weiss law, $\chi_{mol} = C/(T - \theta)$, to give positive Weiss temperatures; $\theta = 4.0$ and 3.8 K for **1** and **2**, respectively. The exchange parameters of several copper(II)−NN complexes in which the nitroxide oxygen is located in an axial site have been reported to possess $2J/k = 14-100$ K,[1] which is much larger than the θ obtained here. Actually, extrapolated values of $\chi_{mol}T$ at higher temperatures than 300 K seem to be larger than 4.5 cm^3 K mol^{-1}, indicating that J_{Cu-NN} is relatively large and positive (ferromagnetic). To simplify models, the Cu−NN unit is set to form a local triplet in a low-temperature region; i.e., $J_{Cu-NN} \gg J_{NN-NN}$ and $J_{Cu-NN} \gg |J_{Cu-Cu}|$. We adopt the following models to the present system. One is a hexagonal cluster model and the other a linear chain model. When the intramolecular interactions, J_{Cu-NN} and J_{Cu-Cu}, are predominantly opperative, rather than J_{NN-NN}, we choose a hexagonal cluster model.

Only the nearest-neighboring interaction is defined in a regular hexagonal arrangement of $S = 1$ sites. This model is expected to exhibit a monotonic increase or decrease in a $\chi_{mol}T$ versus *T* plot. Thus, we applied the van Vleck equation to this cluster model with modification of a Weiss mean field parameter θ', giving

$$\chi_{mol} = \frac{Ng^2\mu_B{}^2}{k(T-\theta')}\left[\frac{A}{B}\right]$$

with

$$A = 182 + 550\exp(12x) + 900\exp(22x) + 812\exp(30x) + 400\exp(36x) + 72\exp(40x)$$

$$B = 13 + 55\exp(12x) + 135\exp(22x) + 203\exp(30x) + 200\exp(36x) + 108\exp(40x) + 15\exp(42x)$$

(20) Caneschi, A.; Gatteschi, D.; Laugier, J.; Rey, P. *J. Am. Chem. Soc.* **1987**, *109*, 2191.
(21) Mohri, F.; Yoshizawa, K.; Yamabe, T.; Ishida, T.; Nogami, T. *Mol. Eng.* **1999**, *8*, 357.
(22) Yasui, M.; Ishikawa, Y.; Akiyama, N.; Ishida, T.; Nogami, T.; Iwasaki, F. *Acta Crystallogr., B* **2001**, *57*, 288.
(23) Bondi, A. *J. Phys. Chem.* **1964**, *68*, 441.
(24) Stewart, J. J. P. MOPAC version 6.0, *QCPE* #455. Stewart, J. J. P. *J. Comp. Chem.* **1989**, *10*, 209.
(25) McConnell, H. M. *J. Chem. Phys.* **1963**, *39*, 1910.
(26) Inoue, K.; Iwamura, H. *Chem. Phys. Lett.* **1995**, *207*, 551.

and

$$x = -J_{Cu-Cu}/kT$$

We estimated $J_{Cu-Cu}/k = -5$ K and $\theta' = +8.5$ K, and the calculated curve is superposed with a solid line in Figure 2. A broad minimum is reproduced, but upward deviation from the data is found in a high temperature region. This deviation is reasonably assigned to the disregard of thermal population of the Cu−NN singlets. The positive θ' value is related to ferromagnetic J_{NN-NN}.

To estimate J_{NN-NN}, the data are fit to the Fisher equation[32] for a uniform infinite chain of $S = 1$ classical spins

$$\chi_{mol} = \frac{Ng^2\mu_B{}^2S(S+1)}{3kT}\left[\frac{1+u}{1-u}\right]$$

$$u = \coth\left[\frac{2J_{NN-NN}S(S+1)}{kT}\right] - \left[\frac{kT}{2J_{NN-NN}S(S+1)}\right]$$

We obtained $J_{NN-NN}/k = +6$ K from the fit to the $\chi_{mol}T$ upsurge region, and the calculated curve is also shown with a dotted line in Figure 2. The larger discrepancy in a high-temperature region is due to the disregard of interchain antiferromagnetic interaction (J_{Cu-Cu}) and thermal population of the Cu−NN singlets. Although in this treatment J_{NN-NN} is probably underestimated because the antiferromagnetic interaction is not excluded from the data, the obtained J_{NN-NN} is roughly compatible with the positive θ' obtained by the analysis on the hexagonal model.

The magnetic behavior of the present complexes is rationalized by the competitive magnitudes of J_{NN-NN} and $|J_{Cu-Cu}|$. The final decrease of the $\chi_{mol}T$ values is explained as follows. The hexagonal molecule has a ground singlet state due to the negative J_{Cu-Cu}. The crystal becomes antiferromagnetic despite the presence of intermolecular ferromagnetic interaction. Even when the ferromagnetic correlation preferentially grows along the column, the triplet Cu−NN spin pairs are arranged completely in alternate rows in a hexagonal lattice, and consequently the antiferromagnetic behavior was observed as an indication of a possible antiferromagnetic order below 1.8 K.

Concluding Remarks

Discrete hexanuclear complexes **1** and **2** construct a perfect column perpendicular to the macrocyclic molecular plane. The ferromagnetic couplings observed are attributed to the interactions between a copper spin and the axially coordinated nitronyl nitroxide spin and also between nitronyl nitroxide groups through the van der Waals contacts. The diameters of the honeycomblike channel structures are ca. 11.5 Å, and they form ferromagnetic one-dimensional structures in the column direction. Thus, we can think of these complexes as "magnetic nanotubes". We have attempted the synthesis of host−guest complexes of **1** and **2**, because the inner vacant axial sites are available for further coordination, and found that the magnetic properties changed depending on guest molecules. Details will be reported separately.

Acknowledgment. This work was supported by Grants-in-Aid for Scientific Research on Priority Areas of "Molecular Conductors and Magnets" (No. 730/11224204) and "Creation of Delocalized Electronic Systems" (No. 297/12020219) from the Ministry of Education, Science, Sports and Culture, Japan.

Supporting Information Available: Crystallographic data (excluding structure factors) for the structures of **1**·$(0.3H_2O)_6$ and **2**·$(0.3H_2O)_6$, in CIF format. This material is available free of charge via the Internet at http://pubs.acs.org.

IC001462G

(27) Kawakami, T.; Oda, A.; Mori, W.; Yamaguchi, K.; Inoue, K.; Iwamura, H. *Mol. Cryst. Liq. Cryst.* **1996**, *279*, 29.
(28) Kawakami, T.; Yamaguchi, K.; Matsuoka, F.; Yamashita, Y.; Kahn, O. *Polyhedron,* in press.
(29) Awaga, K.; Inabe, T.; Maruyama, Y. *Chem. Phys. Lett.* **1992**, *190*, 349.
(30) Awaga, K. In *Magnetic Properties of Organic Materials*; Lahti, P. M., Ed.; Marcel Decker: New York, 1999; Chapter 25, pp 519−534.
(31) The exchange parameter J between two spins S_i and S_j is defined by the spin Hamiltonian $H = -2J\,S_i{\cdot}S_j$.
(32) Fisher, M. E. *Am. J. Phys.* **1964**, *32*, 343.

Ferromagnetic Exchange Coupling of Vanadium(IV) dπ Spins across Pyrimidine Rings: Dinuclear Complexes of Oxovanadium(IV) Bis(1,1,1,5,5,5-hexafluoropentane-2,4-dionate) Bridged by Pyrimidine Derivatives

Takayuki Ishida,*,† Shin-ichi Mitsubori,† Takashi Nogami,† Naoya Takeda,‡ Masayasu Ishikawa,‡ and Hiizu Iwamura§

Department of Applied Physics and Chemistry, The University of Electro-Communications, Chofu, Tokyo 182-8585, Japan, Institute for Solid State Physics, The University of Tokyo, Kashiwa, Chiba 277-8581, Japan, and The University of the Air, Wakaba, Mihama-ku, Chiba 261-8586, Japan

Received July 10, 2001

Dinuclear oxovanadium(IV) complexes bridged by pyrimidine derivatives, $L[VO(hfac)_2]_2$ [L = pyrimidine (PM), 4-methylpyrimidine (MPM), 4,6-dimethylpyrimidine, 4-aminopyrimidine, and quinazoline; hfac = 1,1,1,5,5,5-hexafluoropentane-2,4-dionate], were synthesized and characterized. All of them showed intramolecular ferromagnetic interaction, and the magnetic susceptibilities were analyzed on the basis of the singlet−triplet model, giving $2J/k_B = 2.2-5.5$ K. $PM[VO(hfac)_2]_2$ crystallized in a monoclinic space group $C2/c$ with $a = 34.092(2)$, $b = 6.9783(4)$, and $c = 16.4940(9)$ Å, $\beta = 109.104(1)°$, $V = 3707.8(4)$ Å^3, and $Z = 4$ for $C_{24}H_8F_{24}N_2O_{10}V_2$, and $MPM[VO(hfac)_2]_2$ gave isomorphous crystals. A semiempirical calculation study based on the determined structure suggests the presence of dπ−pπ interaction between vanadium and pyrimidine nitrogen atoms. Ferromagnetic coupling is explained in terms of a spin-polarization mechanism across the pyrimidine bridge. The intermolecular ferromagnetic interaction of $PM[VO(hfac)_2]_2$ can be interpreted by the contact between the spin-polarized pyrimidine moiety and the oxovanadium oxygen atom in an adjacent molecule.

Introduction

A wide variety of complexes with three-dimensional networks have been developed in which π-conjugated N-donor ligands are used for bridges (cyanide and dicyanamide anions for instance).[1−3] Control of magnetic interactions in polynuclear complexes is a key for building molecule-based magnets.[4] High-spin organic molecules (**A** and its analogues with spin sources of radicals, carbenes, or nitrenes) are accessible when nonbonding molecular orbitals are present due to π-topological symmetry of the alternant hydrocarbon skeletons.[5] Application of this strategy to transition-metal complexes is not sufficiently understood, and only a few complexes have been exploited along this approach.[6−9] Francesconi and co-workers revealed that the dinuclear titanium(III) complexes containing 2,4-dimercaptopyrimidine or its selenium analogue as a bridge exhibited ferromagnetic coupling between the titanium spins.[7] McCleverty and co-workers demonstrated that the dinuclear molybdenum(V) complexes bridged by bipyridyls showed magnetic couplings which were consistent with an anticipation from the spin polarization mechanism.[8] We planned to investigate dinuclear vanadium(IV) complexes as a prototype of ground high-spin (triplet) molecules (**B**) because all of the unpaired electron configurations of Ti^{III}, Mo^{V}, and V^{IV} are d^1 and the dπ−pπ orbital overlap seems to be essential for realization of ferromagnetic interaction based on the spin polarization effect.

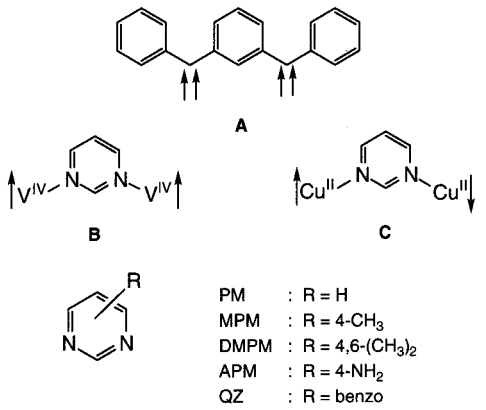

We synthesized pyrimidine-bridged dinuclear vanadium(IV) complexes $L[VO(hfac)_2]_2$ [L = pyrimidine (PM), 4-methyl-

* Corresponding author. Tel: +81-424-43-5490. Fax: +81-424-43-5501. E-mail: ishi@pc.uec.ac.jp.
† The University of Electro-Communications.
‡ The University of Tokyo.
§ The University of the Air.

(1) Ferlay, S.; T. Mallah, T.; Ouahés, R.; Veillet, P.; Verdaguer, M. *Nature* **1995**, *378*, 701. Sato, O.; Iyoda, T.; Fujishima, A.; Hashimoto, K. *Science* **1997**, *272*, 704.
(2) Batten, S. R.; Jensen, P.; Moubaraki, B.; Murray, K. S.; Robson, R. *Chem. Commun*. **1998**, 439. Kurmoo, M.; Kepert, C. J. *New J. Chem*. **1998**, *22*, 1515. Manson, J. L.; Kmety, C. R.; Huang, Q. Z.; Lynn, J. W.; Bendele, G. M.; Pagola, S.; Stephens, P. W.; Liable-Sands, L. M.; Rheingold, A. L.; Epstein, A. J.; Miller, J. S. *Chem. Mater*. **1998**, *10*, 2552.
(3) Kusaka, T.; Ishida, T.; Hashizume, D.; Iwasaki, F.; Nogami, T. *Chem. Lett*. **2000**, 1146.
(4) Kahn, O. *Molecular Magnetism*; VCH: New York, 1993.
(5) Iwamura, H. *Adv. Phys. Org. Chem*. **1990**, *26*, 179. Rajca, A. *Chem. Rev*. **1994**, *94*, 871. Mataga, N. *Theor. Chim. Acta* **1967**, *10*, 372. Longuet-Higgins, J. C. *J. Chem. Phys*. **1950**, *18*, 265. Crayston, J. A.; Devine, J. N.; Walton, J. C. *Tetrahedron* **2000**, *56*, 7829.
(6) Ishida, T.; Mitsubori, S.-i.; Nogami, T.; Iwamura, H. *Mol. Cryst. Liq. Cryst*. **1993**, *233*, 345. Ishida, T.; Nogami, T. *Recent Res. Devel. Pure Appl. Chem*. **1997**, *1*, 1.

10.1021/ic010730n CCC: $20.00
Published on Web 11/13/2001

pyrimidine (MPM), 4,6-dimethylpyrimidine (DMPM), 4-aminopyrimidine (APM), and quinazoline (QZ); hfac = 1,1,1,5,5,5-hexafluoropentane-2,4-dionate] and preliminarily reported their magnetic properties.[10−12] On the other hand, pyrimidine rings can also work as antiferromagnetic couplers in manganese(II),[6] iron(II),[3,13] cobalt(II),[3,6,14] nickel(II),[6,13] and copper(II)[6,15−17] complexes (**C**). A few theoretical analyses have been reported on the roles of pyrimidine as an exchange coupler.[18,19] We describe here the X-ray crystal structures of PM[VO(hfac)$_2$]$_2$ (**1**) and MPM[VO(hfac)$_2$]$_2$ (**2**) and discuss mechanisms of their intra- and intermolecular ferromagnetic exchange couplings. Spin distribution onto the pyrimidine ligands is proposed to play an important role in both intra- and intermolecular magnetic interactions.

Experimental Section

Materials. Pyrimidine ligands were purchased from TCI, Aldrich, or Wako and used without further purification. VO(hfac)$_2$ was prepared according to the literature method.[20] The following complexation of VO(hfac)$_2$ and PM is typical.

To a dichloromethane solution (15 mL) containing VO(hfac)$_2$ (0.4 mmol) was added PM (0.2 mmol) with a microsyringe. After being refluxed for 1 h, the mixture was concentrated to ca. 2 mL by a rotary evaporator and diluted with hexane (5 mL). The crude product of **1** crystallized after standing at room temperature and collected on a filter. The product was purified by repeated recrystallizations from dichloromethane−hexane.

1: yield 64%, brown plates. Anal. Calcd for $C_{24}H_8N_2O_{10}F_{24}V_2$: C, 27.66; H, 0.77; N, 2.69. Found: C, 27.36; H, 0.87; N, 2.79. **2**: yield 54%, brown plates. Anal. Calcd for $C_{25}H_{10}N_2O_{10}F_{24}V_2$: C, 28.43; H, 0.95; N, 2.65. Found: C, 28.32; H, 1.09; N, 2.80. DMPM[VO(hfac)$_2$]$_2$: yield 21%, brown powder. Anal. Calcd for $C_{26}H_{12}N_2O_{10}F_{24}V_2$: C, 29.18; H, 1.13; N, 2.62. Found: C, 28.92; H, 1.40; N, 2.61. APM[VO(hfac)$_2$]$_2$: yield 52%, brown powder. Anal. Calcd for $C_{24}H_9N_3O_{10}F_{24}V_2$: C, 27.27; H, 0.86; N, 3.98. Found: C, 27.40; H, 1.08; N, 4.05. QZ[VO(hfac)$_2$]$_2$: yield 71%, fine black plates, mp 149.5 °C. Anal. Calcd for $C_{28}H_{10}N_2O_{10}F_{24}V_2$: C, 30.79; H, 0.92; N, 2.57. Found: C, 30.68; H, 1.15; N, 2.84. The crystals were sublimed or decomposed above 140 °C during melting-point measurements except for QZ[VO(hfac)$_2$]$_2$.

X-ray Crystallographic Analysis. Diffraction data for **1** and **2** were collected on a Rigaku R-axis RAPID diffractometer with graphite-monochromated Mo Kα radiation (λ = 0.710 69 Å) at 293 K. Numerical absorption correction was applied. The initial structures were directly solved by a heavy-atom Patterson method in the teXsan program package.[21] All of the atoms including hydrogens could be found in difference Fourier maps for **1**. The atomic coordinates and thermal displacement parameters were refined anisotropically for non-hydrogen atoms and isotropically for hydrogen atoms. In the case of **2** parameters of hydrogen atoms are not included for the refinement. Full-matrix least-squares methods were applied using all of the independent diffraction data for **1** and **2**. Each trifluoromethyl group was found to possess two conformations, and these occupancies were determined by disordered models.

The crystallographic data of **1** are as follows: $C_{24}H_8F_{24}N_2O_{10}V_2$; monoclinic, *C*2/*c*; a = 34.092(2), b = 6.9783(4), c = 16.4940(9) Å; β = 109.104(1)°; V = 3707.8(4) Å^3; Z = 4; d_{calcd} = 1.867 g cm^{-3}; μ(Mo Kα) = 6.77 cm^{-1}; R_{int} = 0.032, R = 0.050 ($I > 2.0\sigma(I)$), and R_w = 0.139 (all data) for 4218 observed reflections ($R = \Sigma||F_o| - |F_c||/\Sigma|F_o|$ and $R_w = [\Sigma w(F_o^2 - F_c^2)^2/\Sigma w(F_c^2)^2]^{1/2}$). The crystal size was 0.2 × 0.08 × 0.08 mm^3. Figure 1a shows a crystallographically independent unit for **1**, in which only major conformations of the trifluoromethyl groups were drawn for the sake of clarity. The occupancies of the major conformations were 0.55, 0.78, 0.53, and 0.50 for C4, C8, C9, and C13 trifluoromethyl groups, respectively.

The crystallographic data of **2** are as follows: $C_{25}H_{10}F_{24}N_2O_{10}V_2$; monoclinic, *C*2/*c*; a = 33.866(8), b = 7.455(2), c = 16.119(4) Å; β = 109.627(4)°; V = 3833(1) Å^3; Z = 4; d_{calcd} = 1.830 g cm^{-3}; μ(Mo Kα) = 6.56 cm^{-1}; R_{int} = 0.064, R = 0.083 ($I > 2.0\sigma(I)$), and R_w = 0.192 (all data) for 4314 observed reflections. The crystal size was 0.15 × 0.15 × 0.05 mm^3. Since the cell constants of **2** were very close to those of **1**, the structure was solved by the model in which the methyl group of MPM had an occupancy of 0.5 due to the symmetry. Although the refinement for **2** was converged properly with a conformational analysis on trifluoromethyl groups similarly to the case of **1**, the *R* factors are poorer than those of **1**. The additional methyl group was found on the C2 position with an occupancy of 0.5, but four hydrogen atoms on the methyl group and on the C2 atom could not be determined. The molecular framework, symmetry, and the cell constants of **2** are sufficiently reliable for discussion.

Magnetic Measurements. Magnetic susceptibilities of polycrystalline specimens were measured on a Quantum Design MPMS SQUID magnetometer at 0.5 T in a temperature range down to 1.8 K. Magnetization curves were obtained on an Oxford Instruments Faraday balance equipped with a 7 T coil. The magnetic responses were corrected with diamagnetic blank data of the sample holder obtained separately. The diamagnetic contribution of sample itself was estimated from Pascal's constants.

The ac susceptibility was measured down to about 40 mK in a ^{3}He−^{4}He dilution refrigerator at the ac magnetic field of about 4 μT with a frequency of 127 Hz. The $M-H$ curve was recorded by an integration technique in which the difference of the voltages induced on pickup and reference coils by sweeping the magnetic field is integrated over time by a computer.[22]

Molecular Orbital Calculation. Semiempirical UHF (unrestricted Hatree−Fock) calculation on INDO (intermediate neglect of differential overlap) approximation were done on a ZINDO module in the CAChe program package.[23] The atomic coordinates were available from the X-ray crystallographic analysis. A hypothetical molecule, PM·VO(hfac)$_2$, has 40 atoms, 147 atomic orbitals, and 191 electrons in the valence shell. The surface of the molecular orbitals was drawn at the 0.05 e Å^{-3} level. In calculation on the twist angle dependence of the

(7) Francesconi, L. C.; Corbin, D. R.; Clauss, A. W.; Hendrickson, D. N.; Stucky, G. D. *Inorg. Chem.* **1981**, *20*, 2078.
(8) Ung, V. A.; Couchman, S. M.; Jeffery, J. C.; McCleverty, J. A.; Ward, M. D.; Totti, F.; Gatteschi, D. *Inorg. Chem.* **1999**, *38*, 365.
(9) Oshio, H.; Ichida, H. *J. Phys. Chem.* **1995**, *99*, 3294. Oshio, H. *J. Chem. Soc., Chem. Commun.* **1991**, 240.
(10) Mitsubori, S.-i.; Ishida, T.; Nogami, T.; Iwamura, H. *Chem. Lett.* **1994**, 285.
(11) Mitsubori, S.-i.; Ishida, T.; Nogami, T.; Iwamura, H.; Takeda, N.; Ishikawa, M. *Chem. Lett.* **1994**, 685.
(12) Ishida, T.; Mitsubori, S.-i.; Nogami, T.; Ishikawa, Y.; Yasui, M.; Iwasaki, F.; Iwamura, H.; Takeda, N.; Ishikawa, M. *Synth. Met.* **1995**, *71*, 1791.
(13) Zusai, Z.; Kusaka, T.; Ishida, T.; Feyerherm, R.; Steiner, M.; Nogami, T. *Mol. Cryst. Liq. Cryst.* **2000**, *343*, 127.
(14) Nakayama, K.; Ishida, T.; Takayama, R.; Hashizume, D.; Yasui, M.; Iwasaki, F.; Nogami, T. *Chem. Lett.* **1998**, 497.
(15) Yasui, M.; Ishikawa, Y.; Akiyama, N.; Ishida, T.; Nogami, T.; Iwasaki, F. *Acta Crystallogr. B* **2001**, *57*, 288. Feyerherm, R.; Abens, S.; Günther, D.; T. Ishida, T.; Meissner, M.; Meschke, M.; Nogami, T.; Steiner, M. *J. Phys.: Condens. Matter* **2000**, *12*, 8495.
(16) Ezuhara, T.; Endo, K.; Matsuda, K.; Aoyama, Y. *New J. Chem.* **2000**, *24*, 609.
(17) Omata, J.; Ishida, T.; Hashizume, D.; Iwasaki, F.; Nogami, T. *Inorg. Chem.* **2001**, *40*, 3954.
(18) Mohri, F.; Yoshizawa, K.; Yamabe, T.; Ishida, T.; Nogami, T. *Mol. Eng.* **1999**, *8*, 357.
(19) Takano, Y.; Onishi, T.; Kitagawa, Y.; Soda, T.; Yoshioka, Y.; Yamaguchi, K. *Int. J. Quantum Chem.* **2000**, *80*, 681.
(20) Su, C.-C.; Reed, J. W.; Gould, E. S. *Inorg. Chem.* **1973**, *12*, 337. Selbin, J.; Maus, G.; Johnson, D. L. *J. Inorg. Nucl. Chem.* **1967**, *29*, 1735.
(21) *teXsan*: *crystal structure analysis package*; Molecular Structure Corp.: The Woodlands, TX, 1985, 1999.
(22) Nakazawa, Y.; Tamura, M.; Shirakawa, N.; Shiomi, D.; Takahashi, M.; Kinoshita, M.; Ishikawa, M. *Phys. Rev. B* **1992**, *46*, 8906.
(23) *ZINDO*, CAChe 3.9; Oxford Molecular Group; Oxford, U.K., 1996. Zerner, M. C.; Loew, G. H.; Kirchner, R. F.; Mueller-Westerhoff, U. T. *J. Am. Chem. Soc.* **1980**, *102*, 589 and references therein.

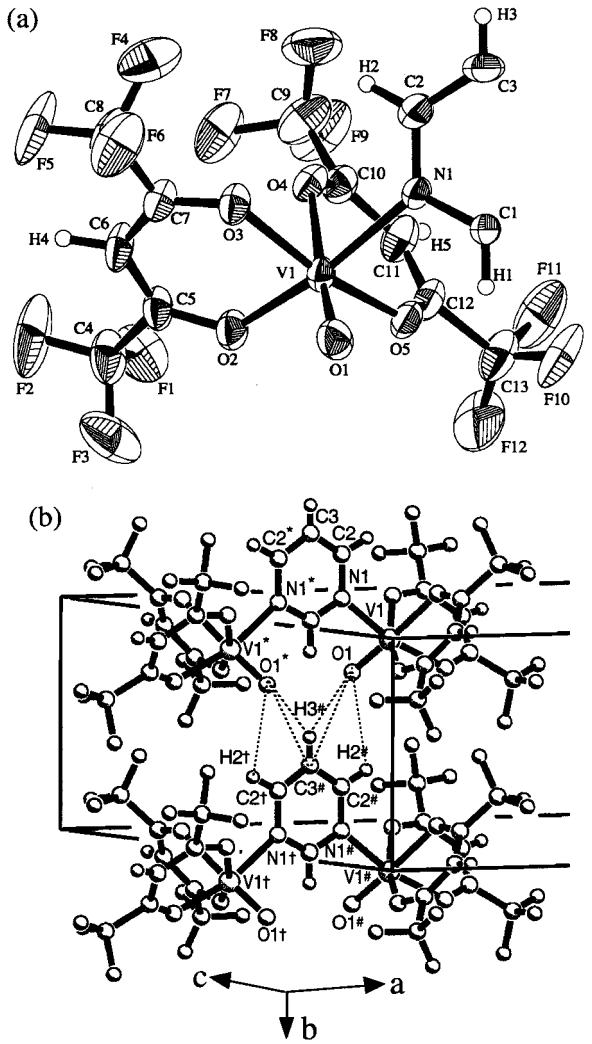

Figure 1. (a) ORTEP drawing of PM[VO(hfac)$_2$]$_2$ (**1**) with thermal ellipsoids at the 30% probability level. Only major conformations of the trifluoromethyl groups are drawn for the sake of clarity. Atomic numberings are also shown. (b) Nearest neighboring molecular arrangement of **1**. Relatively short interatomic distances are shown with dotted lines. The distances are 3.04(4), 3.03(4), and 3.582(5) Å for O1···H2$^{\#}$, O1···H3$^{\#}$, and O1···C3$^{\#}$, respectively. Symmetry operation codes: for *, $-x, -y, -z + 1/2$; #, $x, y + 1, z$; †, $-x, y + 1, -z + 1/2$.

spin density distribution around the V1−N1 bond, the rigid structures of the PM and VO(hfac)$_2$ moieties were used.

Results

Structures of 1 and 2. We obtained single crystals of **1** and **2** which are suitable for X-ray structure analysis. The analysis reveals that the two molecular structures are essentially identical with the same symmetry, except for the additional methyl group in **2**. The difference of molecular arrangements will be discussed later in connection with the presence or absence of intermolecular magnetic interaction. The crystallographically independent unit and atomic numbering of **1** are shown in Figure 1a. A half of **1** is crystallographically independent with a 2-fold axis through C1−C3. Selected interatomic distances and angles are listed in Table 1. The vanadium ion has an octahedral coordination sphere, and the oxovanadium oxygen and PM nitrogen atoms are located in a cis configuration. The crystal consists of a racemic mixture of $\Delta-\Delta$ and $\Lambda-\Lambda$ enantiomers, which are related by inversion symmetry in a *C*2/*c* space group.

It is crucial for the analysis of magnetic interaction which site, axial or equatorial, each PM nitrogen is coordinated to.

Table 1. Selected Bond Lengths (Å) and Angles (deg) for PM[VO(hfac)$_2$]$_2$ (**1**)

V1−N1	2.163(2)	C1−N1	1.326(3)
V1−O1	1.583(3)	N1−C2	1.325(4)
V1−O2	2.010(2)	C2−C3	1.369(4)
V1−O3	1.985(2)	O2−C5	1.253(4)
V1−O4	2.159(2)	O3−C7	1.255(4)
V1−O5	1.999(2)	O4−C10	1.244(4)
		O5−C12	1.248(4)
N1−V1−O1	93.5(1)	O1−V1−O2	101.2(1)
N1−V1−O2	165.1(1)	O1−V1−O3	100.6(1)
N1−V1−O3	90.82(9)	O1−V1−O4	176.2(1)
N1−V1−O4	83.02(9)	O1−V1−O5	96.0(1)
N1−V1−O5	86.29(9)		
O1−V1−N1− C1	42.3(2)	O3−V1−N1−C1	142.9(2)
$\phi_{1,4}$[a]	42.6(2)	$\phi_{3,4}$[a]	98.3(2)
$\phi_{2,4}$[a]	47.4(2)		

[a] Dihedral angles between two least-squares planes. The suffixes 1−4 denote the planes defined by the following atoms: 1, V1, O1, O2, O4, and N1; 2, V1, O5, O2, O3, and N1 (equatorial plane); 3, V1, O1, O3, O4, and O5; 4, C1, N1, C2, and C3 (pyrimidine plane).

Although the V−N distance is 2.163(2) Å which is largest among the coordination distances, we cannot distinguish which is axial or equatorial only from the distances, because the covalent and ion radii of each atom are different. The direction of the oxovanadium oxygen (O1) and O4 is usually assigned to be axial from the ligand field theory under octahedral symmetry. Actually, the coordination bond of V1−O4 (2.159(2) Å) is significantly longer than those of V1−O2, −O3, and −O5 (1.99−2.01 Å). The PM nitrogen is assigned to be at an equatorial position, and the magnetic orbital is d_{xy}.

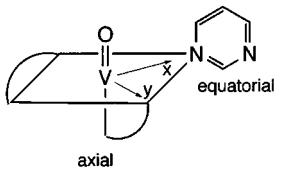

Two related mononuclear compounds, (pyridine)VO(acac)$_2$[24] and (γ-picoline)VO(acac)$_2$,[25] were reported previously, where acac denotes pentane-2,4-dionate. In contrast to the case of **1** and **2**, the nitrogen atoms are coordinated at the axial position, i.e., the trans position to the oxovanadium oxygen. The V−N bond lengths are 2.45−2.48 Å in the acac complexes, which is fairly longer than that of **1**, because of the distortion of an elongated octahedron. However, the geometrical arguments of the acac compounds also concluded the magnetic orbital to be d_{xy}.

The PM plane in **1** is located almost perpendicular to the O1−O3−O4−O5 plane as indicated by the dihedral angles of 98.3(2)° (Table 1). The dihedral angles between the PM bridge and two coordination planes, O1−O2−O4−N1 and O5−O2−O3−N1, are also important for the interpretation of magnetic interaction. As Table 1 shows, the PM plane is largely canted from the V1−O1−O2−O4−N1 and V1−O5−O2−O3−N1 planes with an angle of 42.6(2)°.

Compounds **1** and **2** are isomorphous, and the cell constants are very close to each other. The additional methyl group does not affect the coordination structure. Since the PM moiety has a staggered conformation around V1−N1 bond in the original

(24) Shao, M.; Wang, L.; Tang, Y. *Kexue Tongbao* **1984**, *29*, 759.
(25) Shao, M.; Wang, L.; Tang, Y. *Huaxue Xuebao (Acta Chim. Shinica)* **1983**, *41*, 985.

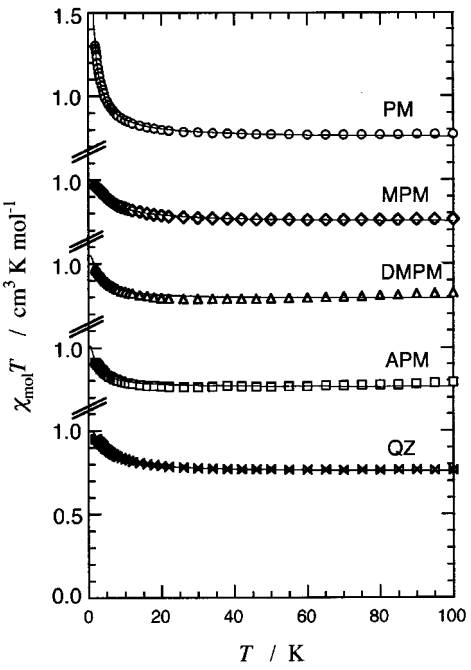

Figure 2. Temperature dependence of the product $\chi_{mol}T$ for L[VO(hfac)$_2$]$_2$ containing various pyrimidines. For abbreviation of the ligands, see the text. The solid lines represent the fits to the equation based on the singlet−triplet model.

form of **1**, the methyl group in **2** can be accommodated into an open space without any cost of geometrical deformation. Therefore, it is reasonably understood that the crystal of **2** has an only slightly larger (3.4%) cell volume.

However, the *b* axis of **2** is significantly longer (6.8% or Δb = 0.48 Å) than that of **1**. Several intermolecular contacts within 3 Å are found between fluorine atoms in these crystals. The hfac groups can hardly act as a magnetic coupler. Caneschi and co-workers reported that various metal bis(hfac) salts bridged with imidazoline-1-oxyl 3-oxide radicals formed one-dimensional magnetic structure,[26] in which interchain metal−metal exchange interaction is prohibited by intervening trifluoromethyl groups. In this study we have to focus on short interatomic distances with respect to VO−PM−VO cores. As Figure 1b shows, the nearest neighboring molecules are related by the *b*-axis translation. Relatively short distances are found between oxovanadium oxygen atom (O1) and pyrimidine hydrogen (H2, H3) and carbon atoms (C3), as indicated by dotted lines in Figure 1b. No other meaningful contacts were found. In the case of **2**, the methyl group on C2 separates these contacts, as evidenced by the anisotropic elongation in the *b* direction.

The molecular structures of L[VO(hfac)$_2$]$_2$ (L = DMPM, APM, and QZ) could not be determined because of their poor crystalline nature. Their V^{IV}−PM−V^{IV} skeleton and the coordination spheres may be similar to those of **1** and **2** viewing from the magnetic properties as shown below.

Magnetic Properties of Pyrimidine-Bridged Complexes. Figure 2 shows the temperature dependence of the product of temperature and molar magnetic susceptibility per a dinuclear molecule ($\chi_{mol}T$) for the five pyrimidine-bridged complexes obtained here. In a high-temperature region, the $\chi_{mol}T$ values are close to 0.75 cm^3 K mol^{-1} for all complexes. Although precise *g* values are calculated from theoretical fitting, these $\chi_{mol}T$ values indicate that the *g* values of the vanadium(IV) ions are very close to 2.0, suggesting that orbital contribution is negligible. We apply the Bleaney−Bowers formula[27] to the present system, similarly to the analysis of the magnetic properties of isomeric pyrazine (PZ) bridged complex, PZ[VO(hfac)$_2$]$_2$, which was proposed to possess an identical coordination sphere.[28]

Table 2. Best-Fit Parameters for the Magnetic Measurements of L[VO(hfac)$_2$]$_2$[a]

L	g	$2Jk_B^{-1}$/K	Θ/K	ref
PM	1.99	4.46	0.49	this work
MPM	1.99	5.48		this work
DMPM	2.05	2.88		this work
APM	2.01	2.22		this work
QZ	2.00	4.50		this work
PZ[b]	1.92	−55.0		ref[e]
MPZ[c]	1.99	−19.4		ref[e]
DMPZ[d]	1.93	−11.6		ref[e]

[a] For the fitting equations and abbreviations, see the text. [b] Pyrazine. [c] Methylpyrazine. [d] 2,5-Dimethylpyrazine. [e] Haddad, M. S.; Hendrickson, D. N.; Cannady, J. P.; Drago, R. S.; Bieksza, D. S. *J. Am. Chem. Soc.* **1978**, *101*, 898.

pyrazine

The $\chi_{mol}T$ values increased with decreasing temperature for all of the complexes investigated here, indicating that the S = 1/2 spins of vanadium(IV) ions are ferromagnetically coupled. The experimental $\chi_{mol}T$ values approached from the isolated S = 1/2 spin-only value (0.75 cm^3 K mol^{-1}) to the S = 1 spin-only value (1.00 cm^3 K mol^{-1}) with g = 2. Assuming that the temperature dependence of the $\chi_{mol}T$ is ascribable only to the spin−spin coupling, we analyze these data by the following formula:[27]

$$\chi_{mol} = \frac{2Ng^2\mu_B^2}{k_BT}\frac{1}{3+\exp(-2J/k_BT)} \quad (1)$$

where the singlet−triplet energy gap corresponds to 2*J*. The best fit *J* parameters are summarized in Table 2, and the calculated curves are superposed in Figure 2. Positive *J* values imply the presence of ferromagnetic interaction within a molecule; i.e., the molecule is a ground high-spin (triplet) species. The $2J/k_B$ values are 2.2−5.5 K.

In the case of **1**, the $\chi_{mol}T$ value exceeded the theoretical triplet value at 1.8 K. The data were analyzed on eq 2 by introducing a Weiss mean field parameter Θ to eq 1. We obtained Θ = +0.49 K together with g = 1.99 and $2J/k_B$ = 4.46 K for **1**.

$$\chi_{mol} = \frac{2Ng^2\mu_B^2}{k_B(T-\Theta)}\frac{1}{3+\exp(-2J/k_BT)} \quad (2)$$

To clarify whether the spins are coupled in an intramolecular fashion, we measured the magnetization curves. Figure 3a shows that the magnetization of **2** at 3.0 K fell exactly on the Brillouin function with S = 1, clearly demonstrating that the molecule has a ground triplet state without any appreciable intermolecular magnetic interaction.

(26) Caneschi, A.; Gatteschi, D.; Lalioti, N.; Sangregorio, C.; Sessoli, R. *J. Chem. Soc., Dalton Trans.* **2000**, 3907. Caneschi, A.; Gatteschi, D.; Lalioti, N.; Sangregorio, C.; Sessoli, R.; Venturi, G.; Vindigni, A.; Rettori, A.; Pini, M. G.; Novak, M. A. *Angew. Chem. Int. Ed. Engl.* **2001**, *40*, 1760.

(27) Bleaney, B.; Bowers, K. D. *Proc. R. Soc. London, Ser. A* **1952**, *214*, 451.

(28) Haddad, M. S.; Hendrickson, D. N.; Cannady, J. P.; Drago, R. S.; Bieksza, D. S. *J. Am. Chem. Soc.* **1978**, *101*, 898.

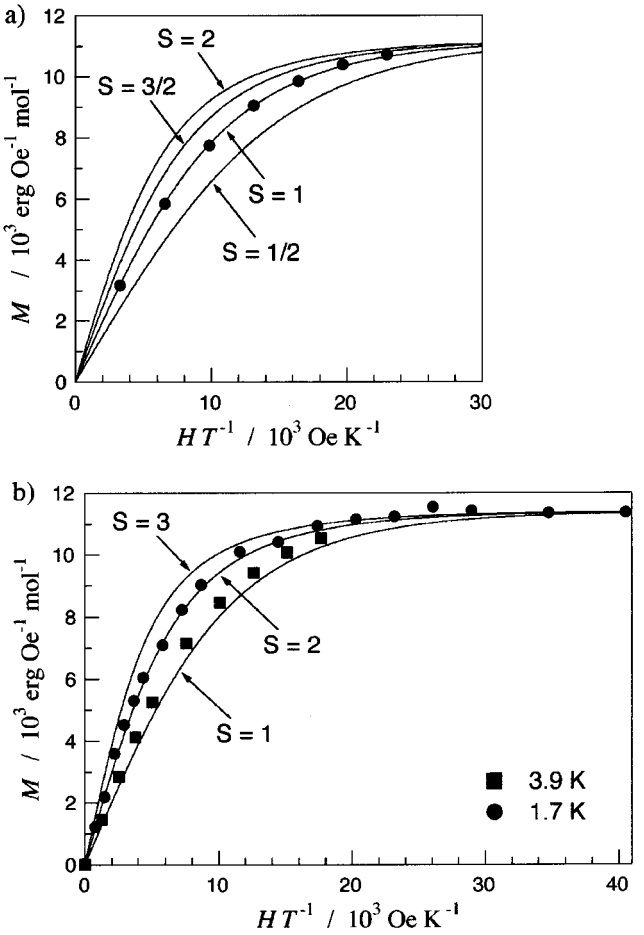

Figure 3. (a) Magnetization curves of MPM[VO(hfac)$_2$]$_2$ at 3.0 ± 0.1 K. The solid lines represent theoretical curves with S = 1/2, 1, 3/2, and 2 (g = 2.0). (b) Magnetization curves of PM[VO(hfac)$_2$]$_2$ at 1.7 ± 0.1 K (circles) and at 3.9 ± 0.1 K (squares). The solid lines represent theoretical curves with S = 1, 2, and 3 (g = 2.0).

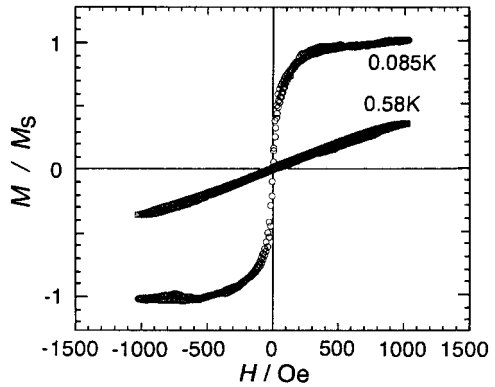

Figure 4. Magnetization curves of PM[VO(hfac)$_2$]$_2$ at 0.085 and 0.58 K.

On the other hand, the magnetization curves of **1** exceeded that of the Brillouin function with S = 1 and the saturation was more remarkable at lower temperature (Figure 3b). This finding is consistent with the positive Θ obtained above (Table 2). These facts indicate the presence of intermolecular ferromagnetic interaction as well as intramolecular one. In fact, as the magnetic measurements below 1.8 K revealed, the ac magnetic susceptibility starts to diverge at around 0.14 K.[11] The $M-H$ curve at 0.085 K shows an S-shaped curve (Figure 4) whereas a paramagnetic feature was observed at 0.58 K. The S-shaped curve strongly suggests that ferromagnetic ordering takes place. The coercive field at 0.085 K was very small (<5 Oe). From the crystal structure analysis, we can only find a uniform one-dimensional chain structure consisting of the dinuclear complexes along the b axis (Figure 1b). The intermolecular magnetic interaction along the b axis is safely assumed to be ferromagnetic. However, interchain interaction is hardly explained by the crystal structure. Since the vanadium(IV) spins have practically no magnetic anisotropy as indicated by the g values close to 2.0, the bulk magnetism may depend on the low-dimensional structure leading to a possible dipolar interaction among the chains.

We have to make some argument regarding other contributions (e.g. zero-field splitting) to the temperature dependence of $\chi_{mol}T$. We proved the exact S = 1 Curie behavior of **2** as shown by the Brillouin curve in Figure 3a and the plateau of the $\chi_{mol}T$ value around 2 K in Figure 2. Figure 2 also shows stepwise behavior from the exact S = 1/2 spin-only value to the exact S = 1 spin-only value for **2** with a decrease of temperature. These findings indicate that the main contribution of this temperature dependence should be attributed to spin−spin coupling interaction. However, a small contribution of zero-field splitting which may be operative below 1.8 K cannot be eliminated.

To compare the function of isomeric pyrazine (PZ) as a magnetic exchange coupler, we also measured magnetic properties of PZ[VO(hfac)$_2$]$_2$ and found the intramolecular antiferromagnetic coupling with $2J/k_B = -67$ K.[10] This finding is in good agreement with those reported by Hendrickson and coworkers;[28] L[VO(hfac)$_2$]$_2$ (L = pyrazine, methylpyrazine, 2,5-dimethylpyrazine) showed antiferromagnetic coupling between vanadium(IV) spins across the pyrazine ring (Table 2), and the pyrazine nitrogen atom was suggested to be located at an equatorial position from the X-ray powder diffraction study. Therefore, we can conclude that pyrimidine and pyrazine bridges can work as ferromagnetic and antiferromagnetic couplers, respectively, in which the bridging bases are located at equatorial positions of VO(hfac)$_2$ in common.

Discussion

The present conclusion is entirely compatible to the organic compounds, xylylenes; *m*- and *p*-xylylenes are ground high-spin and low-spin molecules, respectively.[5] For further discussion on the detailed exchange mechanism in the bis-VO(hfac)$_2$ system, we performed a semiempirical molecular orbital calculation on these complexes on the basis of the geometry determined by the X-ray crystal structure analysis. We calculated on a hypothetical mononuclear species, PM·VO(hfac)$_2$. The UHF treatment in INDO[23] calculation of PM·VO(hfac)$_2$ gave the singly occupied molecular orbital (SOMO) with the orbital energy of −8.007 eV (Figure 5). The SOMO resides on the O5−O2−O3−N1 equatorial plane, which justifies the geometrical definition from the structural analysis. Apparently the SOMO is mainly contributed from a t_{2g} dπ (d_{xy}) orbital of the vanadium ion, whose symmetry is preferable for the V−PM conjugation.

The coefficients of the atomic orbitals in the PM moiety are so small that their lobes could not appear in Figure 5. Instead, calculated spin density may give valuable information about what happens in the vanadium−PM conjugation. The spin densities at V1, N1, C1, N1*, C2*, C3, and C2 are calculated to be +1.150, −0.182, +0.197, −0.178, +0.190, −0.214, and +0.194, respectively (symmetry operation code for *: $-x$, y, $-z + 1/2$). The UHF treatment tends to overestimate polarized

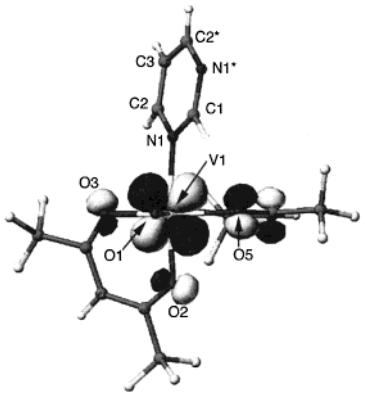

Figure 5. Surface of the singly occupied molecular orbital of PM•VO(hfac)$_2$ based on UHF calculation in the INDO method. The atomic coordinates determined by the X-ray crystallographic study were used.

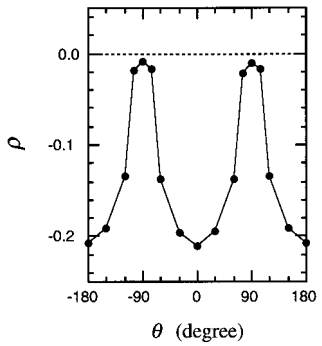

Figure 6. Spin density (ρ) on N1* as a function of dihedral angle (θ) of O1−V1−N1−C1 calculated with UHF/INDO. The solid line is drawn for a guide to the eye.

spin densities.[29] The sign of the spin densities in the present study is confirmed to alternate throughout the PM π-electron network. The ferromagnetic coupling in the present complexes can be understood as follows. Once a negative spin density is induced at the coordinated nitrogen atom (N1), alternating spin densities are induced on the π-electron network of a six-membered PM ring. In the real dinuclear compounds, N1* which carries polarized negative spin density is coordinated to an adjacent vanadium ion, and consequently, the vanadium ion is positively spin polarized. On the other hand, when a pyrazine ring is used as a bridge, a neighboring vanadium ion is negatively spin polarized, i.e., antiferromagnetically correlated.

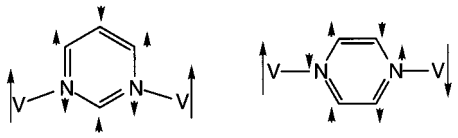

To check the role of the dπ−pπ conjugation between V and PM, we calculated the variation of the spin density distribution as a function of the twist angle around the V−N bond. Calculated spin densities will give reliable comparison within calculation study despite the overestimation. The twist angle θ is defined by the dihedral angle of O1−V1−N1−C1. The experimental angle in **1** is 42.3(2)°. As Figure 6 shows, the calculated spin density on N1* oscillates twice in a cycle. The molecule has no symmetrical element around V1−N1 (2-fold axis or mirror plane) and therefore the calculated density must not be the same between −180 and 0° and 0 and 180°. However the profiles of the two area are quite similar to each other, indicating the presence of a local π-type overlap through the V1−N1 bond on the MO level. A parallel arrangement between the vanadium d_{xy} and nitrogen p_z orbitals ($\theta = 0$ and $\pm$ 180°) is ideal for the maximum orbital overlap, while practically no spin density is polarized when $\theta = \pm 90°$. In the present system, medium overlap is expected from the staggered conformation (θ = ca. 45°) and, therefore, the π-electron system of PM moderately participates in the SOMO.

As described above, the crystals of **1** and **2** have an isostructure but the intermolecular magnetic interactions are different. Assuming that the pyrimidine ring has an appreciable polarized spin density, the different interactions are reasonably explained as follows. The UHF/INDO calculation indicates the presence of positive and negative spin densities at H3 and O1, respectively. The crystal structure analysis reveals the interatomic distances of 3.03(3) and 3.582(5) Å for H3$^{\#}$···O1 and C3$^{\#}$···O1, respectively (symmetry operation code for #: x, $y + 1$, z). Nonzero atomic orbital overlap between O1 and H3$^{\#}$ can be expected because the O1···H3 distances are only slightly larger than the sum of the van der Waals radii. Such a contact gives rise to a weak hydrogen bond, i.e., local antiferromagnetic coupling between small spin densities on O1 and H3$^{\#}$ atoms. Thus, a spin polarization scheme can be drawn as V1(↑)-N1-(↓)-C2(↑)-C3(↓)-H3(↑)···O(↓)═V(↑). Two vanadium spins are ferromagnetically correlated. In the crystal of **2**, the methyl group on C2 prohibit the H3$^{\#}$···O1 interaction due to the steric hindrance. Compound **2** behaves as an ideal paramagnet with $S = 1$.

As mentioned in Introduction, there are several instances of pyrimidine-bridged complexes showing antiferromagnetic interactions. The copper(II) nitrate complexes containing PM bridges are extensively investigated.[15,18] The equatorial−equatorial coordination was found in the antiferromagnetic PM-bridged complex, $[PM{\cdot}Cu(NO_3)_2{\cdot}(H_2O)_2]_n$.[15] The σ-type orbital overlaps between copper $d_{x^2-y^2}$ and nitrogen n orbitals on both sides give rise to an antiferromagnetic superexchange through the PM orbital(s).[18] A similar σ pathway is proposed also in copper(II)−pyrazine complexes.[30] In sharp contrast to the copper case, complexes **1** and **2** possessing a symmetrical equatorial−equatorial coordination structure show ferromagnetic interaction through a π pathway. Yamaguchi and co-workers suggested that the exchange interaction should be divided into two terms: the spin polarization effect and superexchange mechanism (spin delocalization effect).[19] The π- and σ-pathways are theoretically explained in connection with the spin polarization and superexchange mechanism, respectively; the spin polarization effect controls the magnetic coupling of the V^{IV} complexes with only dπ spins, whereas the superexchange is dominantly operative in the Cu^{II} complexes having dσ spins.

Acknowledgment. This work was supported by a Grant-in-Aid for Scientific Research on Priority Areas of "Molecular Conductors and Magnets" (No. 730/11224204) and by a Grant-in-Aid for Scientific Research (No. 13640575) from the Ministry of Education, Culture, Sports, Science, and Technology of Japan.

Supporting Information Available: Crystallographic data (excluding structure factors) for the structures of **1** and **2**, in CIF format. This material is available free of charge via the Internet at http://pubs.acs.org.

IC010730N

(29) Zheludev, A.; Barone, V.; Bonnet, M.; Delley, B.; Grand, A.; Ressouche, E.; Rey, P.; Subra, R.; Schweizer, J. *J. Am. Chem. Soc.* **1994**, *116*, 2019.

(30) Kuramoto, H.; Inoue, M.; Emori, S.; Sugiyama, S. *Inorg. Chem. Acta* **1979**, *32*, 209.

Acta Crystallographica Section B
Structural Science
ISSN 0108-7681

Bis(hfac)-copper(II) complexes bridged by pyrimidines showing magnetic interactions

Masanori Yasui, Yoshimitsu Ishikawa, Takayuki Ishida, Takashi Nogami and Fujiko Iwasaki*

Department of Applied Physics and Chemistry, The University of Electro-Communications, Chofu, Tokyo 182-8585, Japan

Correspondence e-mail: fuji@pc.uec.ac.jp

Received 13 March 2001
Accepted 14 August 2001

Crystals of bis(1,1,1,5,5,5-hexafluoropentane-2,4-dionato)bis-pyrimidinecopper(II) (1), bis(1,1,1,5,5,5-hexafluoropentane-2,4-dionato)bis(4-methylpyrimidine)copper(II) (2), bis-(1,1,1,5,5,5-hexafluoropentane-2,4-dionato)bis(quinazoline)-copper(II) (3) showed ferromagnetic interactions at extremely low temperature. Crystal structure analyses revealed that these complexes were *catena*-bis(1,1,1,5,5,5-hexafluoropentane-2,4-dionato)[μ-pyrimidine-N^1:N^3]copper(II), $[Cu(hfac)_2(pm)_2]_n$, *catena*-bis(1,1,1,5,5,5-hexafluoropentane-2,4-dionato)-[μ-4-methylpyrimidine-N^1:N^3]copper(II), $[Cu(hfac)_2(4\text{-Mepm})]_n$, and *catena*-bis(1,1,1,5,5,5-hexafluoropentane-2,4-dionato)[μ-pyrimidine-N^1:N^3]copper(II), $[Cu(hfac)_2(qz)]_n$, for (1), (2) and (3), respectively. In (1) and (2) the pyrimidines bridge the Cu atoms with an axial–equatorial mode to form one-dimensional spiral chains. Complex (3) also forms a one-dimensional chain structure. The coordination mode of (3) is axial–axial at room temperature, while axial–equatorial at 120 K. On the other hand, the structure of the other modification of the 4-methylpyrimidine complex (4), showing paramagnetic properties, was revealed to be a trinuclei complex bridged by two 4-methylpyrimidines, tris[bis-(1,1,1,5,5,5-hexafluoropentane-2,4-dionato)copper(II)][bis-μ-4-methyl-pyrimidine-N^1:N^3]. The chain structures with an axial–equatorial coordination mode of the bridging organic moieties should play an important role in the appearance of the ferromagnetic interactions.

1. Introduction

Many organic coordination compounds containing transition metals as spin sources have been studied to develop magnetic interactions in organic compounds. Some copper(II) transition complexes, coordinated pyrimidines or related compounds which have *meta*-coordination positions, showed magnetic interactions (Ishida *et al.*, 1995, 1996, 1997). The dipyrimidine-copper(II) dinitrate complexes $Cu^{II}(NO_3)_2(pm)_3$ and $Cu^{II}(NO_3)_2(H_2O)_2(pm)_2$ (pm = pyrimidine) showed ferromagnetic and antiferromagnetic interactions, respectively. Crystal structure analyses revealed that these complexes formed one-dimensional coordination polymers bridged by pyrimidines (Yasui, Ishikawa *et al.*, 2001). The differences between the magnetic interactions depend on the coordination types of the *meta*-N atoms of the bridging pyrimidine: the axial–equatorial coordination for $Cu^{II}(NO_3)_2(pm)_3$ shows ferromagnetic interactions and the equatorial–equatorial coordination for $Cu^{II}(NO_3)_2(H_2O)_2(pm)_2$ shows antiferromagnetic interactions. Complexes of $Cu^{II}(hfac)_2$ (hfac = 1,1,1,5,5,5-hexafluoropentane-2,4-dionate) coordinated by pyrimidine (1), 4-methylpyrimidine (2) and quinazoline (3)

showed ferromagnetic interactions at extremely low temperature. In this paper structure analyses were performed on these complexes in order to elucidate the relationships between crystal structures and magnetic characters. Structural studies at low temperatures (100/120 K) were also carried out owing to the large thermal displacements of trifluoromethyl groups at room temperature. X-ray analysis revealed that the complex with 4-methylpyrimidine crystallized into two modifications, (2) and (4); the magnetic properties measured on these crystals separately showed paramagnetic properties for (4), in contrast to ferromagnetic for (2).

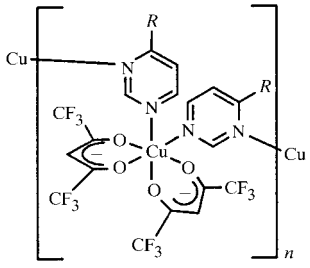

(1) R = H
(2) R = CH_3

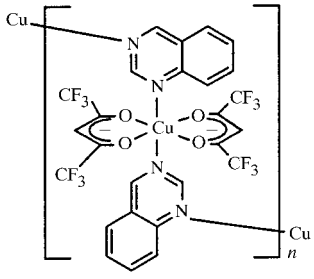

(3)

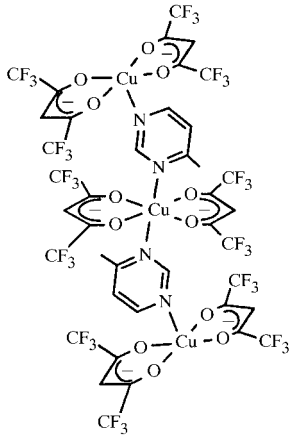

(4)

2. Experimental

Complexes (1), (2) and (3) were prepared by refluxing a dichloromethane solution of $Cu(hfac)_2$ and the bridging ligands in a stoichiometric ratio (Ishida *et al.*, 1995, 1996). The polycrystalline samples were recrystallized from dichloromethane–hexane solutions. Crystals of (2) and (4) were obtained in the same crystallization batch with different habits. These crystals were separated under the microscope and were subjected to the X-ray diffraction and magnetic studies separately. Intensity data were measured using a Rigaku AFC-7*R* diffractometer with a graphite monochromator. Intensity measurements at 120 or 100 K were carried out with an N_2 extraction gas-flow device using different crystals. The structures were solved by direct methods using the programs listed in Table 1. The H atoms at low temperatures were obtained from difference-Fourier maps. The structures were refined by full-matrix least-squares with anisotropic temperature factors for non-H atoms and isotropic ones for H atoms. For the refinements using intensity data at room temperatures, most H atoms were treated as riding models. No refinements of the disordered structures were performed, although thermal displacements of the F atoms at room temperature were very large. In the case of (1*a*) and (1*b*) refinements with the space group $I4_1/acd$, which is the higher space group of $I4_1cd$, failed. The space group $I4_1/acd$ shows a systematic abscence in the $hk0$ zone as h or $k = 2n + 1$. These reflections were rather weak, but significantly observed

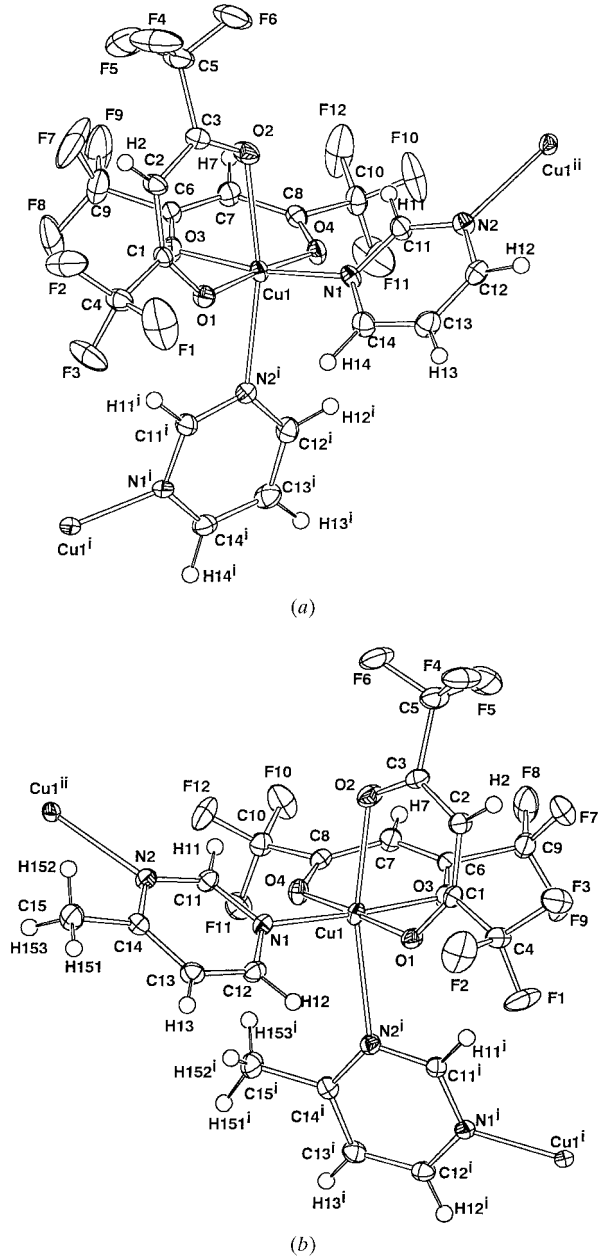

(*a*)

(*b*)

Figure 1
*ORTEP*II (Johnson, 1976) drawings of the complexes (1*b*) and (2*b*) with atom numbering. The displacement ellipsoids for the non-H atoms are drawn at 50% probability and the H atoms are drawn as spheres with a radius of 0.1 Å. (*a*) (1*b*), symmetry codes: (i) $y, \frac{1}{2} - x, \frac{1}{4} + z$; (ii) $\frac{1}{2} - y, x, z - \frac{1}{4}$. (*b*) (2*b*), symmetry codes: (i) $\frac{3}{4} - y, \frac{1}{4} + x, \frac{1}{4} + z$; (ii) $y - \frac{1}{4}, \frac{3}{4} - x, z - \frac{1}{4}$.

Table 1
Experimental details.

	(1*a*) (296 K)	(1*b*) (120 K)	(2*a*) (294 K)	(2*b*) (100 K)	(3*a*) (296 K)
Crystal data					
Chemical formula	$Cu(C_5HF_6O_2)_2$-$(C_4H_4N_2)$	$Cu(C_5HF_6O_2)_2$-$(C_4H_4N_2)$	$Cu(C_5HF_6O_2)_2$-$(C_5H_6N_2)$	$Cu(C_5HF_6O_2)_2$-$(C_5H_6N_2)$	$Cu(C_5HF_6O_2)_2$-$(C_8H_6N_2)$
Chemical formula weight	557.75	557.75	571.78	571.78	607.8
Cell setting, space group	Tetragonal, $I4_1cd$	Tetragonal, $I4_1cd$	Tetragonal, $I4_1/a$	Tetragonal, $I4_1/a$	Monoclinic, $P2_1/n$
a, b, c (Å)	18.586 (3), 18.586, 22.345 (4)	18.3757 (17), 18.3757, 22.137 (3)	19.253 (8), 19.253, 22.380 (9)	18.808 (2), 18.80, 22.182 (4)	12.300 (2), 12.1233 (18), 15.1545 (19)
β (°)	90	90	90	90	102.464 (12)
V (Å^3)	7718.9 (19)	7474.9 (12)	8296 (5)	7846.5 (16)	2206.5 (6)
Z	16	16	16	16	4
D_x (Mg m^{-3})	1.920	1.982	1.831	1.936	1.830
Radiation type	Mo $K\alpha$	Mo $K\alpha$	Mo $K\alpha$	Mo $K\alpha$	Mo $K\alpha$
No. of reflections for cell parameters	25	25	25	24	25
θ range (°)	13.3–17.4	13.2–17.4	13.5–17.4	13.1–18.7	12.5–17.3
μ (mm^{-1})	1.271	1.312	1.185	1.253	1.120
Temperature (K)	296	120	294	100	296
Crystal form, color	Pillar, green	Pillar, green	Prism, green	Prism, green	Pillar, green
Crystal size (mm)	0.35 × 0.25 × 0.25	0.330 × 0.250 × 0.250	0.20 × 0.20 × 0.20	0.30 × 0.20 × 0.20	0.30 × 0.15 × 0.10
Data collection					
Diffractometer	Rigaku AFC-7*R*	Rigaku AFC-7*R*	Rigaku AFC-7*R*	Rigaku AFC-7*R*	Rigaku AFC-7*R*
Data collection method	ω–2θ scans	ω–2θ scans	ω–2θ scans	ω–2θ scans	ω–2θ scans
Absorption correction	Psi-scan (North *et al.*, 1968)	Numerical (Coppens *et al.*, 1965)	Psi-scan	Numerical	Psi-scan
T_{min}	0.729	0.724	0.764	0.879	0.827
T_{max}	0.737	0.753	0.795	0.907	0.888
No. of measured, independent and observed parameters	2282, 2282, 1759	4317, 2210, 2008	5031, 4747, 2602	9495, 4517, 3920	5433, 5063, 2806
Criterion for observed reflections	$I > 2\sigma(I)$	$I > 2\sigma(I)$	$I > 2\sigma(I)$	$I > 2\sigma(I)$	$I > 2\sigma(I)$
R_{int}	0.0000	0.0294	0.0280	0.0253	0.0512
θ_{max} (°)	27.50	27.49	27.48	27.50	27.50
Range of h, k, l	$0 \rightarrow h \rightarrow 24$ $0 \rightarrow k \rightarrow 17$ $0 \rightarrow l \rightarrow 29$	$0 \rightarrow h \rightarrow 23$ $0 \rightarrow k \rightarrow 23$ $0 \rightarrow l \rightarrow 28$	$0 \rightarrow h \rightarrow 24$ $0 \rightarrow k \rightarrow 24$ $0 \rightarrow l \rightarrow 29$	$0 \rightarrow h \rightarrow 24$ $0 \rightarrow k \rightarrow 24$ $-28 \rightarrow l \rightarrow 28$	$-15 \rightarrow h \rightarrow 15$ $0 \rightarrow k \rightarrow 15$ $0 \rightarrow l \rightarrow 19$
No. and frequency of standard reflections	3 every 150 reflections	3 every 150 reflections	3 every 150 reflections	3 every 150 reflections	3 every 150 reflections
Intensity decay (%)	0.12	0.93	−2.41	2.06	−0.96
Refinement					
Refinement on	F^2	F^2	F^2	F^2	F^2
$R[F^2>2\sigma(F^2)]$, $wR(F^2)$, S	0.045, 0.1388, 1.071	0.0296, 0.0827, 1.055	0.0527, 0.1796, 1.028	0.0273, 0.0838, 1.082	0.0447, 0.1622, 1.023
No. of reflections and parameters used in refinement	2282, 304	2210, 322	4747, 315	4517, 339	5063, 369
H-atom treatment	Riding	Refined	Riding	Refined	Refined
Weighting scheme	$w = 1/[\sigma^2(F_o^2) + (0.0671P)^2 + 16.8141P]$, where $P = (F_o^2 + 2F_c^2)/3$	$w = 1/[\sigma^2(F_o^2) + (0.0433P)^2 + 8.5189P]$, where $P = (F_o^2 + 2F_c^2)/3$	$w = 1/[\sigma^2(F_o^2) + (0.0781P)^2 + 8.0262P]$, where $P = (F_o^2 + 2F_c^2)/3$	$w = 1/[\sigma^2(F_o^2) + (0.0456P)^2 + 3.8089P]$, where $P = (F_o^2 + 2F_c^2)/3$	$w = 1/[\sigma^2(F_o^2) + (0.0757P)^2 + 0.3712P]$ where $P = (F_o^2 + 2F_c^2)/3$
$(\Delta/\sigma)_{max}$	0.014	0.003	0.001	0.001	0.046
$\Delta\rho_{max}$, $\Delta\rho_{min}$ (e Å^{-3})	0.67, −0.378	0.595, −0.36	0.546, −0.367	0.351, −0.494	0.481, −0.414
Extinction method	None	None	None	None	Not applied

	(3*b*) (120 K)	(4*a*) (294 K)	(4*b*) (100 K)
Crystal data			
Chemical formula	$Cu(C_5HF_6O_2)_2(C_8H_6N_2)$	$Cu_3(C_5HF_6O_2)_6(C_5H_6N_2)_2$	$Cu_3(C_5H_6O_2)_6(C_5H_6N_2)_2$
Chemical formula weight	607.8	1621.2	1621.2
Cell setting, space group	Monoclinic, $P2_1/n$	Triclinic, $P\bar{1}$	Triclinic, $P\bar{1}$
a, b, c (Å)	12.023 (5), 11.920 (4), 15.065 (4)	11.728 (4), 13.621 (5), 10.919 (2)	11.552 (3), 13.397 (4), 10.505 (3)
α, β, γ (°)	90, 102.42 (2), 90	94.46 (3), 113.78 (2), 65.02 (2)	95.48 (2), 112.982 (19), 64.503 (18)

Table 1 (continued)

	(3*b*) (120 K)	(4*a*) (294 K)	(4*b*) (100 K)
V (Å^3)	2108.4 (13)	1437.8 (7)	1345.8 (6)
Z	4	1	1
D_x (Mg m^{-3})	1.915	1.872	2.000
Radiation type	Mo $K\alpha$	Mo $K\alpha$	Mo $K\alpha$
No. of reflections for cell parameters	25	24	25
θ range (°)	12.9–15.9	10.1–13.8	12.7–16.3
μ (mm^{-1})	1.172	1.275	1.362
Temperature (K)	120	294	100
Crystal form, color	Pillar, green	Pillar, green	Pillar, green
Crystal size (mm)	0.210 × 0.20 × 0.10	0.250 × 0.130 × 0.10	0.250 × 0.120 × 0.10
Data collection			
Diffractometer	Rigaku AFC-7*R*	Rigaku AFC-7*R*	Rigaku AFC-7*R*
Data collection method	ω–2θ scans	ω–2θ scans	ω–2θ scans
Absorption correction	Numerical	Psi-scan	Numerical
T_{min}	0.799	0.811	0.823
T_{max}	0.894	0.883	0.895
No. of measured, independent and observed parameters	5064, 4838, 3317	6904, 6586, 3590	6750, 6185, 5044
Criterion for observed reflections	$I > 2\sigma(I)$	$I > 2\sigma(I)$	$I > 2\sigma(I)$
R_{int}	0.0382	0.0167	0.0165
θ_{max} (°)	27.50	27.48	27.50
Range of h, k, l	$0 \rightarrow h \rightarrow 15$ $-15 \rightarrow k \rightarrow 0$ $-19 \rightarrow l \rightarrow 19$	$0 \rightarrow h \rightarrow 15$ $-16 \rightarrow k \rightarrow 17$ $-14 \rightarrow l \rightarrow 12$	$-11 \rightarrow h \rightarrow 14$ $-15 \rightarrow k \rightarrow 17$ $-13 \rightarrow l \rightarrow 12$
No. and frequency of standard reflections	3 every 150 reflections	3 every 150 reflections	3 every 150 reflections
Intensity decay (%)	2.28	8.13	2.79
Refinement			
Refinement on	F^2	F^2	F^2
$R[F^2 > 2\sigma(F^2)]$, $wR(F^2)$, S	0.0454, 0.1346, 1.023	0.0561, 0.1967, 1.028	0.0345, 0.0932, 1.026
No. of reflections and parameters used in refinement	4838, 369	6586, 430	6185, 466
H-atom treatment	Refined	Fixed	Refined
Weighting scheme	$w = 1/[\sigma^2(F_o^2) + (0.0599P)^2 + 2.1059P]$, where $P = (F_o^2 + 2F_c^2)/3$	$w = 1/[\sigma^2(F_o^2) + (0.0942P)^2 + 0.5397P]$, where $P = (F_o^2 + 2F_c^2)/3$	$w = 1/[\sigma^2(F_o^2) + (0.0418P)^2 + 1.0143P]$, where $P = (F_o^2 + 2F_c^2)/3$
$(\Delta/\sigma)_{max}$	0.000	0.007	0.008
$\Delta\rho_{max}$, $\Delta\rho_{min}$ (e Å^{-3})	1.236, −1.004	0.736, −0.426	0.62, −0.584
Extinction method	None	None	None

Computer programs used: *AFC* (Rigaku Corporation, 1994), *TEXSAN* (Molecular Structure Corporation, 1992), *SIR*92 (Altomare *et al.*, 1994), *SAPI*91 (Fan, 1991), *SHELXL*97 (Sheldrick, 1997), *ORTEP*II (Johnson, 1976).

with $I/\sigma(I) > 10$. Crystal data, details concerning data collection and structure refinements are listed in Table 1.[1]

3. Results and discussion

3.1. Structures of (1) and (2)

The molecular structures of (1*b*) at 120 K and (2*b*) at 100 K, along with the atomic numbering, are shown in Fig. 1. Selected bond distances and angles at low temperatures are listed in Table 2. For each complex, the Cu atom is coordinated by O1, O3, O4 and N1 equatorially, and N2^i [(i) $y, \frac{1}{2} - x, \frac{1}{4} + z$ for (1) and (i) $\frac{3}{4} - y, \frac{1}{4} + x, \frac{1}{4} + z$ for (2)] and O2 axially to form a six-coordinated octahedral complex. Therefore, two hfac groups coordinate the Cu atom with a *cis* configuration. The pyrimidine moiety bridges the Cu···Cu at the *meta* N atoms with equatorial and axial positions to form a one-dimensional chain. In (1*b*) the axial Cu1—O2 and Cu1—N2^i distances are 2.346 (3) and 2.387 (3) Å, respectively. The corresponding values for (2*b*) are 2.2861 (13) and 2.4957 (15) Å for Cu1—O2 and Cu1—N2^i, respectively. The longer Cu1—N^i distance of (2*b*) than (1*b*) is due to the steric effect of the methyl group. Dihedral angles related to the pyrimidine planes are also listed in Table 2. The inclination of the pyrimidine plane to the equatorial plane of (1*b*) is slightly different from that of (2*b*).

Stereoscopic views of the coordination polymer chains of (1*b*) and (2*b*) are shown in Fig. 2. In the crystals of (1) the pyrimidine groups bridge the Cu atoms to form a 4_3 spiral chain along the *c* axis. The 4_1 spiral chain is also generated from the symmetry operation of the space group. The spiral chain of (2) shown in Fig. 2 has a 4_1 symmetry. These

[1] Supplementary data for this paper are available from the IUCr electronic archives (Reference: OA0036). Services for accessing these data are described at the back of the journal.

complexes are the first bis(hfac)-Cu complexes having polymer chain structures bridged by N atoms from the result of the search of the Cambridge Structural Database (CSD; Allen & Kennard, 1993).

3.2. Structure of (3)

In the crystals of (3), two independent Cu atoms, Cu1 and Cu2, occupy the inversion centers. The structures of these complexes along with the atomic numbering are shown in Fig. 3. Selected bond distances and angles at 296 and 120 K are listed in Table 3. The coordination around the Cu atom is two *trans* hfac groups and two quinazolines. The quinazoline molecule bridges Cu1 and Cu2 at the *meta* N atoms to form a one-dimensional chain. A stereoscopic view of the coordination polymer chain of (3*b*) is shown in Fig. 4. At room temperature, the coordination lengths of Cu1—O1, Cu1—O2 and Cu1—N1 are 2.002 (2), 2.070 (3) and 2.182 (4) Å, respectively. The coordination lengths of Cu2—O3, Cu2—O4 and Cu2—N2 are 1.963 (2), 1.965 (3) and 2.464 (3) Å, respectively. For both Cu1 and Cu2 atoms, the two hfac groups coordinate equatorially and two quinazoline moieties coordinate axially. That is, the quinazoline ring bridges Cu atoms with the axial–axial coordination. The complexes showing ferromagnetic interactions with bridging *meta*-N atoms in the polymer chains, analyzed so far, have shown the axial–equatorial coordination type.

However, the coordination mode changed drastically at 120 K. The length of Cu1—N1 reduced to 2.043 (3) from 2.182 (4) Å and the length of Cu1—O2 increased to 2.189 (3) from 2.070 (3) Å. That is, the coordination of the quinazoline changes from an axial position to an equatorial one at 120 K. On the other hand, the coordination type around the Cu2

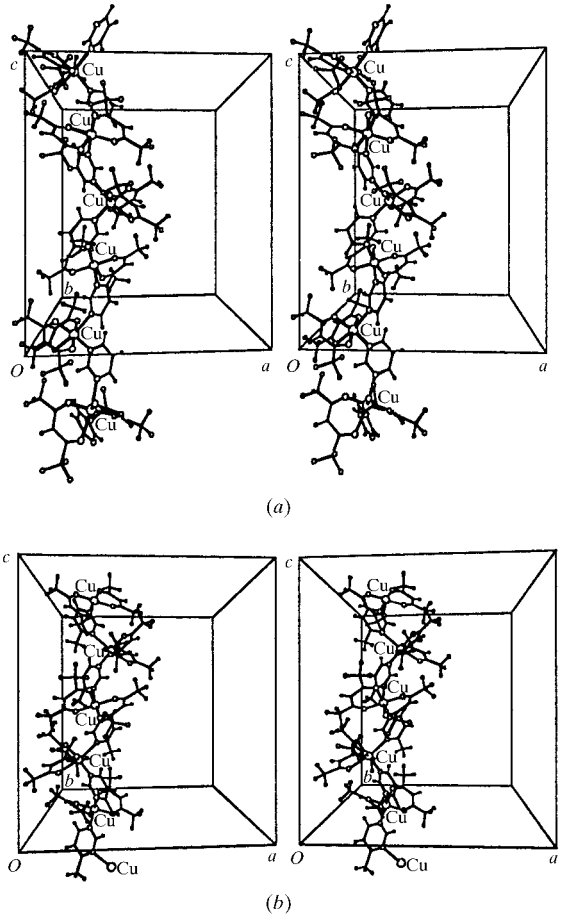

Figure 2
Stereoscopic views of the coordination polymers of (*a*) (1*b*) and (*b*) (2*b*).

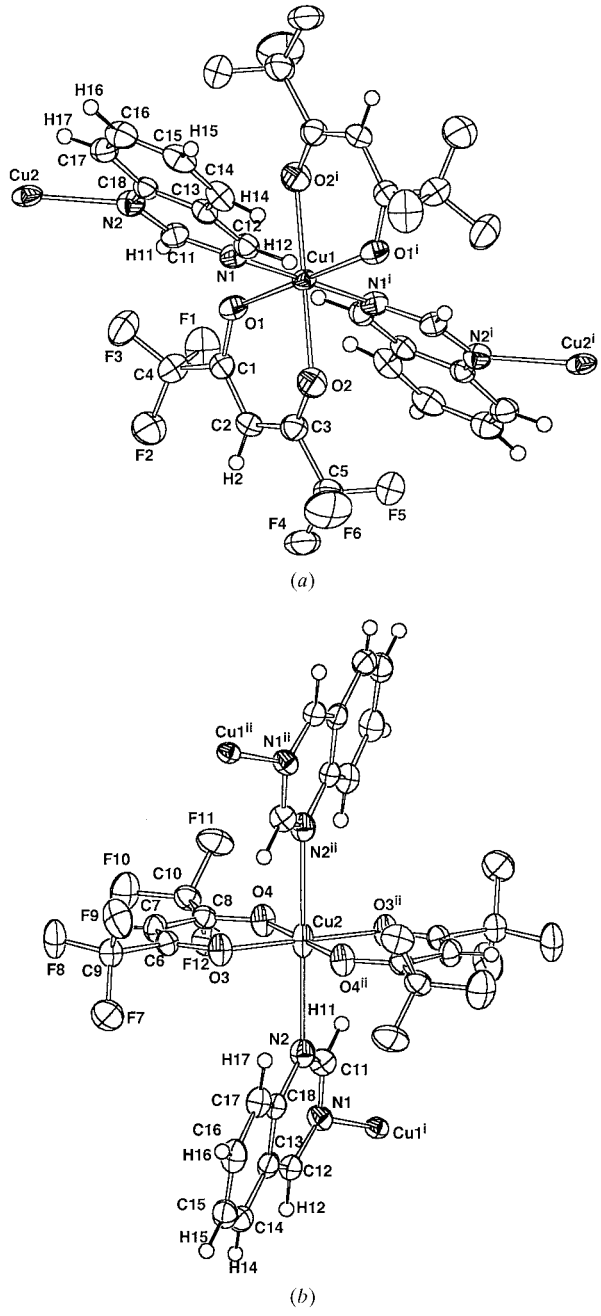

Figure 3
*ORTEP*II (Johnson, 1976) drawings of the complexes of (3*b*) with atom numbering. The displacement ellipsoids for non-H atoms are drawn at 50% probability and the H atoms are drawn as spheres with a radius of 0.1 Å. (*a*) Complex of Cu1; (*b*) complex of Cu2. Symmetry codes: (i) $-x, -y, -z$; (ii) $-x, 1-y, -z$.

Table 2
Selected bond lengths and angles (1*b*) and (2*b*) (Å, °).

	(1*b*)	(2*b*)
Cu1—O1	1.952 (3)	1.9558 (12)
Cu1—O2	2.346 (3)	2.2861 (13)
Cu1—O3	1.989 (3)	1.9970 (13)
Cu1—O4	1.949 (3)	1.9558 (12)
Cu1—N1	2.029 (4)	2.0212 (15)
Cu1—N2^{i}	2.387 (3)	2.4957 (15)
O1—Cu1—O2	86.25 (12)	87.20 (5)
O1—Cu1—O3	91.29 (12)	90.70 (5)
O1—Cu1—O4	176.22 (11)	178.24 (5)
O1—Cu1—N1	91.33 (13)	91.63 (6)
O1—Cu1—N2^{i}	84.84 (13)	82.95 (5)
O2—Cu1—O3	82.04 (11)	84.19 (5)
O2—Cu1—O4	97.24 (12)	94.49 (5)
O2—Cu1—N1	89.58 (13)	93.02 (6)
O2—Cu1—N2^{i}	167.66 (12)	166.81 (5)
O3—Cu1—O4	90.62 (13)	89.98 (5)
O3—Cu1—N1	171.04 (14)	176.28 (6)
O3—Cu1—N2^{i}	89.63 (12)	87.17 (5)
O4—Cu1—N1	87.27 (13)	87.77 (5)
O4—Cu1—N2^{i}	91.92 (13)	95.46 (5)
N1—Cu1—N2^{i}	99.14 (11)	96.00 (5)
Plane 1–pm	80.56 (11)	82.87 (4)
Plane 2–pm	37.12 (15)	31.56 (7)
Plane 3–pm	40.28 (14)	35.17 (6)
Plane 1–pm^{i}	29.44 (16)	38.29 (6)
Plane 2–pm^{i}	88.22 (10)	86.89 (12)
Plane 3–pm^{i}	78.11 (9)	76.41 (11)
pm–pm^{i}	84.82 (12)	86.52 (5)

Plane 1: Cu1—O1—C1—C2—C3—O2; plane 2: Cu1—O3—C6—C7—C8—O4; plane 3: Cu1—O1—O3—O4—N1. Symmetry codes: (i) $y, \frac{1}{2}-x, \frac{1}{4}+z$ for (1*b*); (i) $-y+\frac{3}{4}, x+\frac{1}{4}, z+\frac{1}{4}$ for (2*b*).

atom was kept during the temperature change. These facts show that the quinazoline ring bridges Cu atoms with an axial–equatorial coordination mode at 120 K and an axial–axial mode at room temperature. The axial–equatorial coordination is favored to the appearance of the ferromagnetic interaction observed at extremely low temperature.

Preliminary measurements showed gradual changes of the lattice constants from 296 to 100 K. The lattice constants, measured with some crystals which were obtained in the same crystallization batch, showed no significant change compared with the results in Table 1. Thus, all crystals in this batch are identical to each other. Detailed examinations of the structural changes and a possibility of the phase transition are in progress.

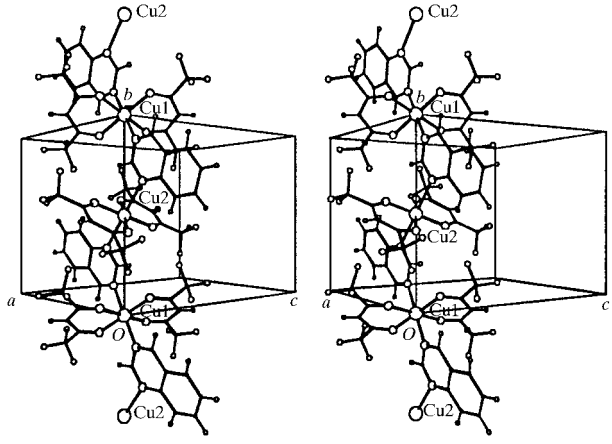

Figure 4
Stereoscopic view of the coordination polymer of (3*b*).

Table 3
Selected bond lengths and angles (3*a*) and (3*b*) (Å, °).

	(3*a*) (296 K)	(3*b*) (120 K)
Cu1—O1	2.002 (2)	2.011 (2)
Cu1—O2	2.070 (3)	2.189 (3)
Cu1—N1	2.182 (4)	2.043 (3)
Cu2—O3	1.963 (2)	1.957 (2)
Cu2—O4	1.965 (3)	1.968 (2)
Cu2—N2	2.464 (3)	2.439 (3)
O1—C1	1.247 (4)	1.272 (4)
O2—C3	1.241 (5)	1.248 (4)
O3—C6	1.245 (4)	1.260 (4)
O4—C8	1.253 (5)	1.258 (4)
N1—C11	1.363 (5)	1.364 (4)
N1—C12	1.318 (5)	1.325 (4)
N2—C11	1.295 (5)	1.308 (4)
N2—C18	1.403 (5)	1.397 (4)
O1—Cu1—O2	88.73 (11)	87.37 (9)
O1—Cu1—O2^{i}	91.27 (11)	92.64 (9)
O1—Cu1—N1	88.77 (11)	88.76 (11)
O1—Cu1—N1^{i}	91.23 (11)	91.24 (11)
O2—Cu1—N1	96.71 (13)	96.29 (11)
O2—Cu1—N1^{i}	83.29 (13)	83.71 (11)
O3—Cu2—O4	91.78 (11)	92.08 (10)
O3—Cu2—O4^{ii}	88.22 (11)	87.92 (10)
O3—Cu2—N2	91.35 (12)	91.32 (11)
O3—Cu2—N2^{ii}	88.65 (12)	88.67 (10)
O4—Cu2—N2	88.36 (11)	88.68 (10)
O4—Cu2—N2^{ii}	91.64 (11)	91.32 (10)

Symmetry codes: (i) $-x, -y, -z$; (ii) $-x, -y+1, -z$.

Table 4
Selected bond lengths and angles (4*b*) (Å, °).

Cu1—O1	1.9715 (17)	Cu2—O4	1.9393 (18)
Cu1—O2	1.9509 (17)	Cu2—O5	1.9379 (17)
Cu1—N1	2.437 (2)	Cu2—O6	1.9727 (18)
Cu2—O3	1.9578 (18)	Cu2—N2	2.225 (2)
O1—Cu1—O2	92.21 (7)	O4—Cu2—O5	169.08 (8)
O1—Cu1—O2^{i}	87.79 (7)	O5—Cu2—O6	91.82 (7)
O1—Cu1—N1	90.23 (7)	O3—Cu2—N2	100.68 (8)
O2—Cu1—N1	87.14 (7)	O4—Cu2—N2	95.99 (8)
O3—Cu2—O4	92.00 (8)	O5—Cu2—N2	94.94 (8)
O3—Cu2—O5	86.24 (7)	O6—Cu2—N2	93.66 (7)
O3—Cu2—O6	165.64 (8)		

Symmetry code: (i) $-x, -y+1, -z$.

3.3. Structure of (4)

The molecular structure of (4) along with the atomic numbering is shown in Fig. 5. Bond distances and angles are listed in Table 4. Two types of Cu atoms are located in complex (4). The Cu1 atom is located at the center of inversion of the crystals and is coordinated by two hfac groups equatorially and two bridging 4-methylpyrimidines axially, forming a six-coordinated octahedron. On the other hand, the Cu2 atom

Table 5
Summary of the structural features of Cu complexes coordinated with hfac/NO_3 and pyrimidines showing magnetic interactions.

Complexes	Structure	$(hfac)_2$ coordination	*meta*-N coordination	Magnetic interaction	Atoms in eq. plane	Bond lengths (Å)			
						eq. Cu—N	eq. Cu—O	ax. Cu—N	ax. Cu—O
(1) $(hfac)_2(pm)_2$[a]	Polymer	*Cis*	Ax.–eq.	Ferromagnetic	3O 1N	2.029	1.963	2.387	2.346
(2) $(hfac)_2$(4-Me-pm)$_2$[a]	Polymer	*Cis*	Ax.–eq.	Ferromagnetic	3O 1N	2.021	1.970	2.496	2.286
(3) $(hfac)_2(qz)_2$ [a]	Polymer	*Trans*	Ax.–eq.	Ferromagnetic	2O 2N	2.043	2.011		2.189
		Trans			4O		1.963	2.439	
(4) $(hfac)_2$(4-Me-pm)$_2$[a]	Trinuclei	*Trans*	Ax.–ax.	Paramagnetic	4O		1.961	2.437	
		Trans			4O		1.952	2.225	
$(NO_3)_2(pm)_3$[b]	Polymer		Ax.–eq.	Ferromagnetic	2O 2N	2.030	1.990	2.293	
$(NO_3)_2(pm)_2(H_2O)_2$[b]	Polymer		Eq.–eq.	Antiferromagnetic	2O 2N	2.032	2.011		2.340
$(NO_3)_2(pm)_2(H_2O)_2$[b]	Mononucleus		Unbridged	Paramagnetic	2O 2N	2.017	1.973		2.435

References: (*a*) this work; (*b*) Yasui, Ishikawa *et al.* (2001).

occupying a general position is located at the center of the base of the five-coordinated square pyramid, formed by two equatorial hfac groups and a bridging pyrimidine. The Cu2 atom deviates from the plane formed by the four O atoms of the hfac groups to the N2 atom by 0.2149 (9) Å. This deviation is also shown from the large bond angles of N2—Cu2—O. The whole structure of the complex is a trinuclei metal complex bridged by two pyrimidines. The lengths of axial Cu—N bonds are 2.437 (2) and 2.225 (2) Å for Cu1—N1 and Cu2—N2, respectively. The plane formed by Cu1 and O atoms of two hfac groups (plane 1), the plane formed by Cu2 and O atoms of two hfac groups (plane 2) and the pyrimidine plane (plane 3) are orthogonal to each other with dihedral angles of 73.10 (6), 79.27 (7) and 83.51 (7)°, for planes 1–2, 1–3 and 2–3, respectively.

The crystal structure of (4) is shown in Fig. 6. In the crystals, plane 2, the base of the square pyramid, overlaps face-to-face to that at (ii) $1-x, -y, 1-z$. The mean distance between planes is 3.725 (3) Å and the distance of Cu2···Cu2^{ii} is 4.8273 (15) Å. The corresponding values at 300 K are 3.996 (6) and 5.326 (19) Å. The appearance of the paramagnetic property of (4) can be ascribed to the segregated arrangement of trinuclei Cu complexes.

Similar trinuclei Cu complexes bridged by two 5-methylpyrimidines and two 2,3,5-trimethylpyradines were searched from the CSD. The structural feature of the 5-methylpyrimidine complex is very close to that of (4), including the packing mode (Kogane *et al.*, 1994). The length of the central Cu—N bond (2.051 Å) is shorter than that of (4) and the intermolecular Cu···Cu distance (5.885 Å) is longer than that of (4). In the case of the pyradine derivative, the coordination of the hfac groups is *cis* at both terminal sides with five-coordinated square pyramids (Kogane *et al.*, 1994). The packing mode of the crystals is quite different from that of (4).

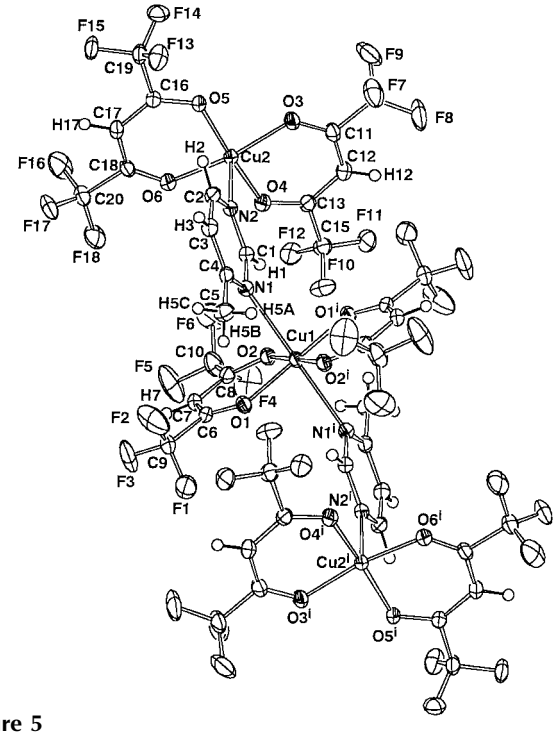

Figure 5
*ORTEP*II (Johnson, 1976) drawing of (4*b*) with atom numbering. The displacement ellipsoids for non-H atoms are drawn at 50% probability and the H atoms are drawn as spheres with a radius of 0.1 Å. Symmetry codes: (i) $-x, 1-y, -z$.

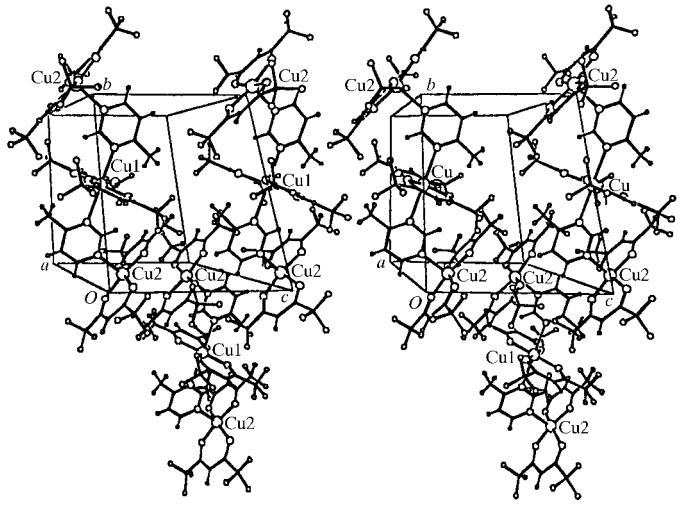

Figure 6
Stereoscopic view of the crystal structure of (4*b*).

3.4. Relations between magnetic interactions and coordination structure

The structural features of $(hfac)_2Cu^{II}$ complexes with bridging pyrimidines, as well as those of $(NO_3)_2Cu^{II}$ complexes, showing magnetic interactions are summarized in Table 5. In the crystals of the complexes showing ferromagnetic interactions (1), (2), (3) and $Cu^{II}(NO_3)_2(pm)_3$, coordination polymer chains are formed and the coordination mode of the bridging *meta* N atoms of the pyrimidine moieties is axial–equatorial. On the other hand, the coordination type of the complex, $Cu^{II}(NO_3)_2(H_2O)_2(pm)_2$, showing an antiferromagnetic interaction, is equatorial–equatorial, although the structure is a one-dimensional polymer chain. These facts indicate that the pyrimidine bridge can work as both ferromagnetic and antiferromagnetic couplers. It can be concluded that the coordination modes of the bridging *meta* N atoms play important roles to determine the differences between magnetic interactions. The electron density study on $Cu^{II}(NO_3)_2(H_2O)_2(pm)_2$ shows that an unpaired electron of the Cu^{II} ion is located in the $d_{x^2-y^2}$ orbital (Yasui, Takayama *et al.*, 2001). The magnetic coupling can be explained in terms of orbital overlaps between a molecular orbital of the pyrimidine and two Cu^{II} $d_{x^2-y^2}$ orbitals. With appreciable overlaps on both sides of the pyrimidine, the magnetic coupling is expected to be antiferromagnetic. When one N atom of pyrimidine is axially coordinated to the copper(II) ion, there is no orbital overlap between the Cu^{II} $d_{x^2-y^2}$ and N $n\sigma$ and $p\pi$ orbitals due to orthogonality (Ishida & Nogami, 1997). Thus, the axial–equatorial combination favors the ferromagnetic interaction. Therefore, it is very important that the coordination mode of (3) changes from axial–axial at room temperature to axial–equatorial at low temperature, since the magnetic interactions appear at extremely low temperature.

This work was supported in part by a Grant-in-Aid for Scientific Research (No. 08454180) and a Grant-in-Aid for Scientific Research on Priority Areas 'Molecular Conductors and Magnets' and 'Metal Assembled Complexes' (Area Nos. 730/11 224 204 and 401/11 136 212, respectively) from the Ministry of Education, Science, Sports and Culture.

References

Allen, F. H. & Kennard, O. (1993). *Chem. Des. Autom. News*, **8**, 31–37.
Altomare, A., Cascarano, M., Giacovazzo, C., Guagliardi, A., Burla, M. C., Polidori, G. & Camalli, M. (1994). *J. Appl. Cryst.* **27**, 435.
Coppens, P., Leiserowitz, L. & Rabinovich, D. (1965). *Acta Cryst.* **18**, 1035–1038.
Fan, H.-F. (1991). *SAPI*91. Rigaku Corporation,Tokyo, Japan.
Ishida, T., Mitsubori, S., Nogami, T., Ishikawa, Y., Yasui, M., Iwasaki, F., Iwamura, H., Takeda, N. & Ishikawa, M. (1995). *Synth. Met.* **71**, 1791–1792.
Ishida, T., Nakayama, K., Nakagawa, M., Sato, W., Yasui, M., Iwasaki, F. & Nogami, T. (1997). *Synth. Met.* **85**, 1655–1658.
Ishida, T. & Nogami, T. (1997). *Recent Res. Dev. Pure Appl. Chem.* **1**, 1–15.
Ishida, T., Nogami, T., Yasui, M., Iwasaki, F., Iwamura, H., Takeda, N. & Ishikawa, M. (1996). *Mol. Cryst. Liq. Cryst.* **279**, 87–96.
Johnson, C. K. (1976). *ORTEP*II. Report ORNL-5138. Oak Ridge National Laboratory, Tennessee, USA.
Kogane, T., Kobayashi, K., Ishii, M., Hirota, R. & Nakahara, M. (1994). *J. Chem. Soc. Dalton Trans.* pp. 13–18.
Molecular Structure Corporation (1992). *TEXSAN*. MSC, 3200 Research Forest Drive, The Woodlands, TX 77381, USA.
North, A. C. T., Phillips, D. C. & Mathews, F. S. (1968). *Acta Cryst.* A**24**, 351–359.
Rigaku Corporation (1994). *AFC Control Software*. Rigaku Corporation, Tokyo, Japan.
Sheldrick, G. M. (1997). *SHELXL*97. University of Göttingen, Germany.
Yasui, M., Ishikawa, Y., Akiyama, N., Ishida, T., Nogami, T. & Iwasaki, F. (2001). *Acta Cryst.* B**57**, 288–295.
Yasui, M., Takayama, R., Akiyama, N., Hashidume, D. & Iwasaki, F. (2001). *Mol. Cryst. Liq. Cryst.* In the press.

ELSEVIER

Synthetic Metals 120 (2001) 755–756

SYNTHETIC METALS

www.elsevier.com/locate/synmet

Synthesis and properties of new oxygen-containing fulvalene derivatives: dibenzo- and dinaphthotetraoxafulvalenes and dibenzodioxadithiafulvalene

Takashi Nogami[a]*, Kohtaro Tanaka[a], Takayuki Ishida[a], Akiko Kobayashi[b]

[a]*Department of Applied Physics and Chemistry, University of Electro-Communications, Chofugaoka, Chofu, Tokyo 182-8585, Japan*

[b]*Research Center for Spectrochemistry, Graduate School of Science, University of Tokyo, Hongo, Bunkyo-ku, Tokyo 113-0033, Japan*

Abstract

Novel oxygen-containing fulvalene-derivatives, DBTOF, DNTOF, and DBOTF, were synthesized as donor molecules for highly conducting organic complexes. *Cis-* and *trans*-forms of DBOTF could be separated, and their molecular and crystal structures were determined by X-ray crystallography. From cyclic voltammetries and molecular orbital calculations of these donor molecules, the order of donor abilities of DBTXF series and DBOTF were established. *Trans*-DBOTF-TCNQ complex was an insulator.

Keywords: Heterocyclic synthesis, Coupling reactions, X-ray emission, diffraction and scattering

1. Introduction

Since TTF was recognized as a donor molecule affording 1D metallic conducting organic complex, a large number of TTF-derivatives have been synthesized [1]. Replacement of the sulfur of TTF-derivatives with Se and Te has also given TST- and TTeF-derivatives. TMTSF and BEDT-TTF are the most successful donor molecules affording organic superconducting salts [2]. Replacement of one sulfur atom of DBTTF with oxygen has been achieved in 1996 [3]. However, replacement of more than one sulfur atoms of TTF-skeleton with oxygen has not been reported until our report on the synthesis of DBTOF and DNTOF [4], which have four oxygen atoms in fulvalene skeleton. We have also succeeded in the synthesis of DBOTF (*cis-* and *trans*-forms), having two oxygen and two sulfur atoms in the fulvalene skeleton. Synthesis, X-ray structure analysis, cyclic voltammetry, and MO calculation of these new oxygen-containing fulvalene derivatives, together with *trans*-DBOTF-TCNQ salts, will be reported in this paper.

2. Synthesis

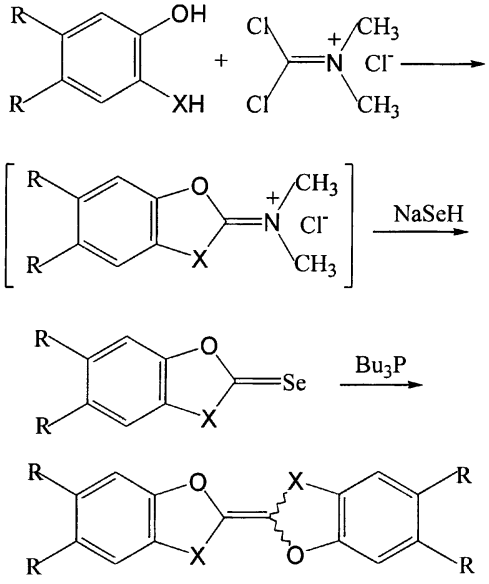

DBTOF (X = O, R = H)
DNTOF (X = O, R-R = -CH=CH-CH=CH-)
DBOTF (X = S, R = H)

Scheme 1

* Corresponding author. Tel +81-424-43-5483; fax +81-424-43-5501;
E-mail: nogami@pc.uec.ac.jp

PII: S0379-6779(00)00748-7

DBTOF, DNTOF and DBOTF were synthesized by Scheme 1. Detailed synthetic procedures of DBTOF and DNTOF have already been reported [4]. Applying similar reaction conditions, two isomers, *cis*- and *trans*- forms of DBOTF, were obtained [5]. They could be separated by an HPLC, followed by recrystallizations from CH_2Cl_2/ hexane for *cis*-form (yield 22%) and from CH_2Cl_2/ acetonitrile for *trans*-form (yield 11%), respectively. ^{1}H-NMR measurements revealed that the *cis*- form converts to the *trans*-form in solution at room temperature in several days. DBTOF gradually decomposes to catechol in the air. Thus, it should be stored in an inert atmosphere.

3. X-Ray Crystallography of DBOTF

Molecular and crystal structures of DBTOF and DNTOF were reported previously [4]. Fig. 1(a) shows the molecular structure of *cis*-DBOTF determined by X-ray crystallography [6]. Owing to the *cis*-form, the molecule has a slightly bent structure. Fig. 1(b) shows the molecular structure of *trans*-DBOTF [7].

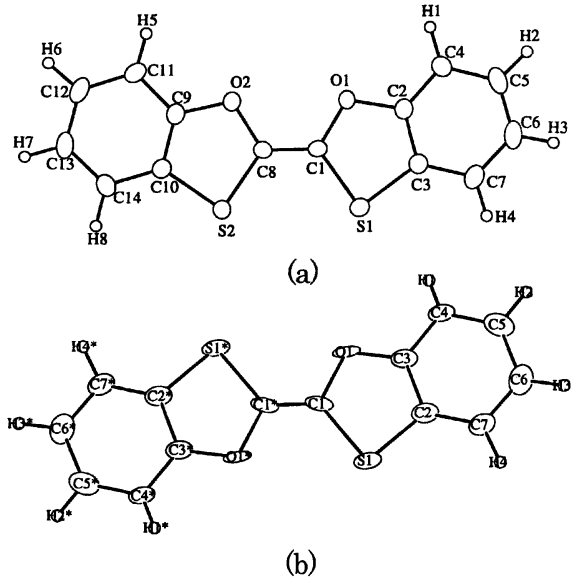

Fig. 1 Molecular structures of DBOTF. (a) *cis*-form, (b) *trans*-form.

4 Cyclic Voltammetry and MO Calculation

The cyclic voltammetry (CV) of DBTOF, *trans*-DBOTF, *cis*-DBOTF and DBTTF gave anodic peaks ($E_{ox}^{P}(1)$) at 0.61, 0.56, 0.47 and 0.49 V (*vs* Ag/Ag^+) in CH_2Cl_2.[8]. CV of DNTOF could not be measured due to its poor solubility.

The orbital energies of the highest occupied molecular orbitals (HOMO) of DBTOF, *trans*-DBOTF, *cis*-DBOTF and DBTTF were obtained by a semi-empirical PM3 calculation [9], based on the determined molecular structures, and they are –8.33, -8.20, -8.13 and –7.99 eV, respectively. In view of the reported CV results of related donor molecules [10], together with the CV results and MO calculations in this study, the electron donating abilities of DBTXF series and DBOTF are: DBTTeF ~ DBTTF > DBTSF ~ *cis*-DBOTF > *trans*-DBOTF > DBTOF [11].

5. *Trans*-DBOTF-TCNQ Complex

Single crystals of *trans*-DBOTF-TCNQ complexes (1:1 composition) were obtained from CH_2Cl_2 / acetonitrile solutions as black plates. IR spectra (KBr) of the complex showed a CN-stretching at 2213 cm^{-1}, which suggests the degree of charge-transfer to be 0.8; CN-stretching of Li^+TCNQ^- and TCNQ are 2209 and 2225 cm^{-1}, respectively. The *trans*-DBOTF-TCNQ complex was an insulator.

References

[1] G. Schukat, E. Fanghanel, Sulfur Rep. 14 (1993) 245.

[2] T. Ishiguro, K. Yamaji, G. Saito, Organic Superconductors, Springer, Berlin, Heidelberg, New York, Barcelona, Budapest, Hong Kong, London, Milan, Paris, Singapore, Tokyo, 1998.

[3] S. T. D'Arcangelis, D. O. Cowan, Tetrahedron Lett. 37 (1996) 2931.

[4] K. Tanaka, K. Yoshida, T. Ishida, A. Kobayashi, T. Nogami, Adv. Mater. 12 (2000) 661.

[5] Melting points: *cis*-form 115 °C (dec); *trans*-form 208-210 °C.

[6] *cis*-DBOTF: pale yellow plate, orthorhombic, $P2_12_12_1$, a = 10.9(3), b = 27.5(4), c = 3.9(5) Å, V = 1181.2(4) Å^3, Z = 4, D_{calc} = 1.531 g/cm^3, μ(MoK_α) = 4.38 cm^{-1}, R = 0.038 for 1124 reflections.

[7] *trans*-DBOTF: colorless plate, monoclinic, $P2_1/c$, a = 9.31(1), b = 5.83(1), c = 11.632(8) Å, β = 111.83(7)°, V = 586(1) Å^3, Z = 2, D_{calc} = 1.542 g/cm^3, μ(MoK_α) = 4.41 cm^{-1}, R = 0.088 for 402 reflections

[8] First anodic ($E_{ox}^{P}(1)$) and corresponding cathodic peaks were observed for *cis*-DBOTF. Only anodic peaks could be observed for DBTOF, *trans*-DBOTF and DBTTF due to decompositions of cation radicals.

[9] J. J. P. Stewart, MOPAC 6.0, QCPE No. 455, Department of Chemistry, Indiana University, Bloomington, IN 1990.

[10] K. Lerstrup, D. Talham, A. Bloch, T. Poehler, D. Cowan, J. Chem. Soc. Chem. Commun., (1982) 336.

[11] The contradictory results of $E_{ox}^{P}(1)$ and HOMO levels between *cis*-DBOTF and DBTTF may arise from the uncertainty of the $E_{ox}^{P}(1)$ value of DBTTF due to decomposition of cation radicals.

PERGAMON

Polyhedron 20 (2001) 1545–1549

POLYHEDRON

www.elsevier.nl/locate/poly

Zero-field muon spin rotation study on TEMPO-based magnets, Ar-CH=N-TEMPO

Takayuki Ishida [a,*], Seiko Ohira [b,c], Isao Watanabe [c], Takashi Nogami [a], Kanetada Nagamine [b,c]

[a] *Department of Applied Physics and Chemistry, The University of Electro-Communications, Chofu, Tokyo 182-8585, Japan*
[b] *Muon Science Laboratory, The Institute of Physical and Chemical Research (RIKEN), Wako, Saitama 351-0198, Japan*
[c] *Meson Science Laboratory, Institute of Materials Structure Science, High Energy Accelerator Research Organization, Tsukuba, Ibaraki 305-0801, Japan*

Received 17 September 2000; accepted 12 October 2000

Abstract

Long-range magnetic orderings are demonstrated by zero-field muon spin rotation/relaxation measurements on the genuine organic free radical crystals, 4-(*p*-chlorobenzylideneamino)-, 4-(*p*-phenylbenzylideneamino)-, and 4-(benzylideneamino)-TEMPOs (TEMPO = 2,2,6,6-tetramethylpiperidin-1-yloxyl) with T_C values of 0.28, 0.22, and 0.17 K, respectively, and 4-(4-pyridylmethyleneamino)-TEMPO with T_N of ≈ 0.07 K. From comparison between the crystal structures and internal fields at the muon sites, dominant two-dimensional ferromagnetic interaction is confirmed and inter-sheet dipolar interaction is proposed for bulk magnetism.

Keywords: Magnetic phase transition; Organic ferromagnet; Antiferromagnet; Ferromagnetic interaction; Free radical

1. Introduction

In the last decade, the quest for purely organic ferromagnets has been the subject of intensive research [1]. The first purely organic radical ferromagnet was discovered for β-phase *p*-nitrophenyl nitronyl nitroxide (*p*-NPNN) [2]. Muon spin rotation/relaxation/resonance (μSR) is a versatile technique for determining the magnetic ground state of organic crystals, since zero-field measurements prove directly the local magnetic field in the specimen, and it has been used to study a number of nitronyl nitroxide radicals [3–6].

2,2,6,6-Tetramethylpiperidin-1-yloxyl (TEMPO) derivatives are also an interesting class of molecular crystals showing a variety of magnetic ground states [7,8]. We reported the zero-field muon spin rotation/relaxation (ZF-μSR) studies of Cl- [9–11], Biph- [9,11], and Ph-TEMPOs [11]. The bulk ferromagnetisms below T_C were demonstrated by $M-H$ curves [12–14] and the heat capacity measurement [15]. The antiferromagnetism of 4Py-TEMPO was also revealed by the ZF-μSR [11] and $M-H$ curves [16]. We overview here the results of magnetism, ZF-μSR, and crystal structure. We propose a possible mechanism for their bulk magnetic orderings based on the ab initio calculation of the internal magnetic field [17,18], and rationalize the intra-sheet exchange mechanism previously proposed [7,8].

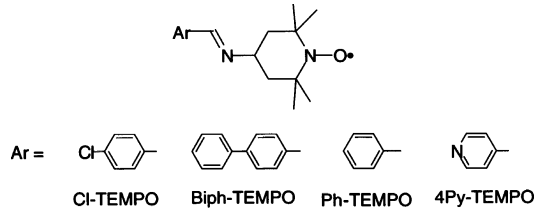

2. Experimental

The materials were prepared by a condensation reaction of 4-amino-TEMPO with the corresponding aromatic aldehydes [19,20] and purified by recrystallization

* Corresponding author. Tel.: +81-424-43-5490; fax: +81-424-43-5501.
E-mail address: ishi@pc.uec.ac.jp (T. Ishida).

0277-5387/01/$ - see front matter
PII: S0277-5387(01)00652-0

from ethanol. For instrumentation details see Refs. [9–11].

3. Results

Fig. 1(a) shows typical time spectra of ZF-μSR signals of Biph-TEMPO for an instance. Above 250 mK, slowly relaxing signals without oscillation were obtained, which correspond to a paramagnetic phase. At 220 mK rather rapid depolarization was found, and the appearance of a clear oscillation below 220 mK indicates the presence of an appreciable internal magnetic field due to spontaneous magnetization, suggesting the presence of long-range magnetic ordering. A single frequency component indicates that every injected muon resides at a particular position and experiences a similar internal magnetic field. With decreasing temperature the frequency increased, indicating that the spontaneous magnetization increased.

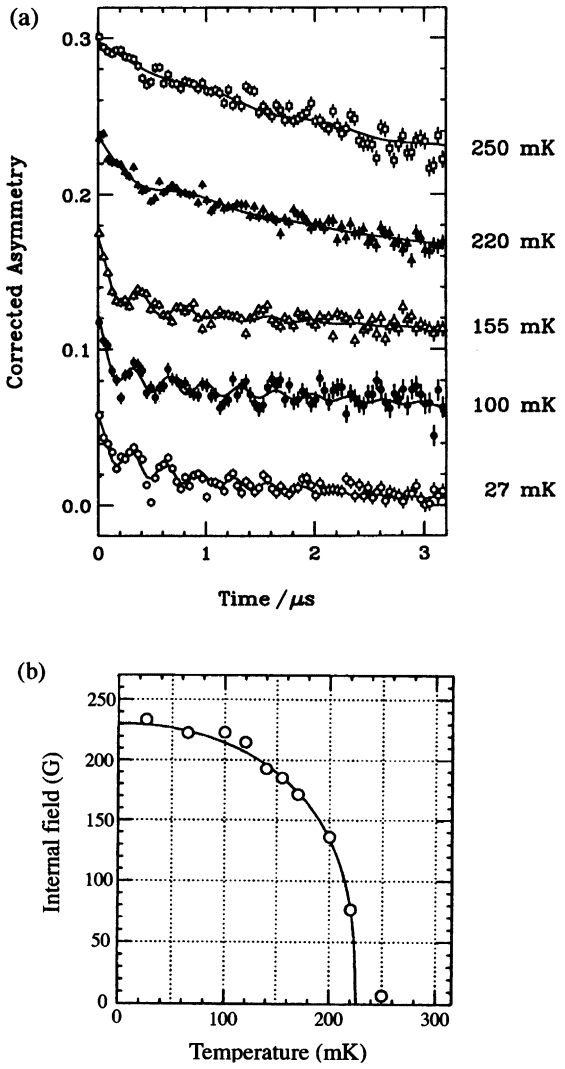

Fig. 1. (a) ZF-μSR time spectra of Biph-TEMPO. Solid curves are results of fitting based on rotation/relaxation functions. (b) Temperature dependence of the internal magnetic field at the muon site of Biph-TEMPO. Solid lines are best fit based on Eq. (1).

In the presence of an internal magnetic field at the muon site, B_{int}, the muon spin undergoes Larmor precession with a frequency $\nu_\mu = (\gamma_\mu/2\pi)B_{int}$, where $\gamma_\mu/2\pi$ is the muon gyromagnetic ratio, and the oscillation frequency can be reduced to an internal magnetic field. The temperature dependence of B_{int} is shown in Fig. 1(b). The results were fitted to

$$B_{int}(T) = B_{int}(0)[1 - (T/T_C)^{\alpha}]^{\beta}, \quad (1)$$

where α stands for the index of the spin wave theory and β is the critical exponent. The optimized parameters, together with those of Cl-, Ph-, and 4Py-TEMPOs, are listed in Table 1. T_C values were precisely determined to be 0.28, 0.22, and 0.17 K for Cl-, Biph-, and Ph-TEMPOs, respectively. The obtained values $\beta =$ 0.304, 0.356, and 0.362 are close to the theoretical value for three-dimensional Heisenberg ferromagnet.

For the antiferromagnet 4Py-TEMPO, rotation was also observed below the transition temperature T_N [11]. Although the results are preliminary the B_{int} of 4Py-TEMPO was estimated to be ≈ 110 G at 28 mK, which is almost half of the TEMPO-based ferromagnets, Cl-, Biph-, and Ph-TEMPOs.

4. Discussion

When a muon is injected into a specimen, electron capture can take place [5], and a Mu (muonium, μ^+e^-) attaches to a particular molecule. An electronic spin state of the muonated molecule is a singlet ($S = 0$) or a triplet ($S = 1$). If a bare muon μ^+ attaches to a radical group, the resulting electronic state is a doublet ($S = 1/2$). For $S \neq 0$, the hyperfine field at the muon site is expected to have a high frequency and is undetectable within the time resolution of the apparatus used in the present study. We can propose that the observed precession signal is due to singlet states, and the μ^+ experiences only inter-molecular hyperfine fields as drawn in Fig. 2(a). For nitronyl nitroxide radicals, Blundell and co-workers [6] previously suggested formation of a similar muonated singlet species. When μ^+ is trapped at an azomethine nitrogen, the distance between the radical center and μ^+ is ≈ 5 Å, and a hyperfine field at the muon site is so weak that an oscillation may be observable. The ab initio calculations of the hyperfine fields at the muon sites in the crystals of Ph-TEMPO [17,18] show that the smaller B_{int} (59 G) in Ph-TEMPO is likely to be due to μ^+ trapped at the azomethine nitrogen atom.

X-ray crystal structure analyses of these magnets revealed that the N–O radical groups are located on two-dimensional zig–zag planes [21,22]. The inter-

Table 1
Results of ZF-μSR study and X-ray crystal structure analysis for Cl-, Biph-, Ph-, and 4Py-TEMPO radicals

Aryl group	*p*-ClC_6H_4 ferromagnet	*p*-Biphenylyl ferromagnet	Phenyl ferromagnet	4-Pyridyl antiferromagnet
ZF-μSR				
T_C, T_N (K)	0.28	0.22	0.17	~0.07
Number of signals	1	1	2	1
$B_{int}(0)$ (G)	231.1 ± 0.8	230.5 ± 1.2	222.6 ± 0.8	~110
α	2.56 ± 0.05	2.12 ± 0.19	1.53 ± 0.05	
β	0.304 ± 0.001	0.356 ± 0.033	0.362 ± 0.007	
$B_{int}(0)$ (G)			59.2 ± 0.3	
α			5.48 ± 0.92	
β			0.437 ± 0.082	
X-ray analysis [a]				
Intra-sheet O···O (Å)	5.89	5.96	5.62	5.96
	5.94	6.09	6.14	6.77
Inter-sheet O···O (Å)	10.86	13.40	11.89	8.99
Sheet structure	Pleated	Pleated	Zig–zag	Pleated

[a] Refs. [21,22].

molecular O···O distances are summarized in Table 1. The inter-sheet O···O distances are 11–13 Å, which are almost twice the intra-sheet O···O distances. In particular, Cl- and Biph-TEMPO radicals have practically the same two-dimensional structure and only the inter-sheet distance is different [12,13]. The internal fields of both ferromagnets are 231 G. This finding supports that every Mu is trapped at a similar position, and also indicates that the internal field is mainly due to a sum of individual dipolar fields of neighboring N–O groups within a sheet. The lower T_C of Biph-TEMPO than that of Cl-TEMPO is reasonably attributed to the longer inter-sheet distance of Biph-TEMPO.

The crystal of Ph-TEMPO also possesses a two-dimensional N–O network [14], but the molecular packing is different from those of Cl- and Biph-TEMPOs. The N–O groups in Ph-TEMPO are arranged in a zig–zag fashion along two directions, whereas those in Cl- and Biph-TEMPOs are arranged parallel in one direction. Despite the structural difference, the larger B_{int} (223 G) of the two in Ph-TEMPO is comparable to those of Cl- and Biph-TEMPOs (231 G). This finding can be interpreted as follows. The muon site for the larger B_{int} has a similar situation to those of Cl- and Biph-TEMPOs as described in Fig. 2(a), giving comparable internal fields at the muon sites. Furthermore, the comparable B_{int} values were observed as a sum of the individual dipolar fields within a sheet, only when they are aligned in the same mutual direction with respect to the sheet structures.

The dependence of the hyperfine fields upon the direction of the ordered moments has been examined by calculation [17,18]. For Cl- and Biph-TEMPOs the hyperfine field exhibited a maximum in the [010] direction and the calculated value in this direction reproduced the experimental one. Similarly for Ph-TEMPO the [100] direction gave a maximum and showed an agreement with the experiment. The [010] direction for Cl- and Biph-TEMPOs and the [100] direction for Ph-TEMPO are nearly perpendicular to the two-dimensional sheet structures as shown in Fig. 2(b), being preferable for the three-dimensional ordering based on the inter-sheet dipolar interactions. Such dipolar interactions are also proposed for inorganic layered magnets by Drillon and co-workers [23].

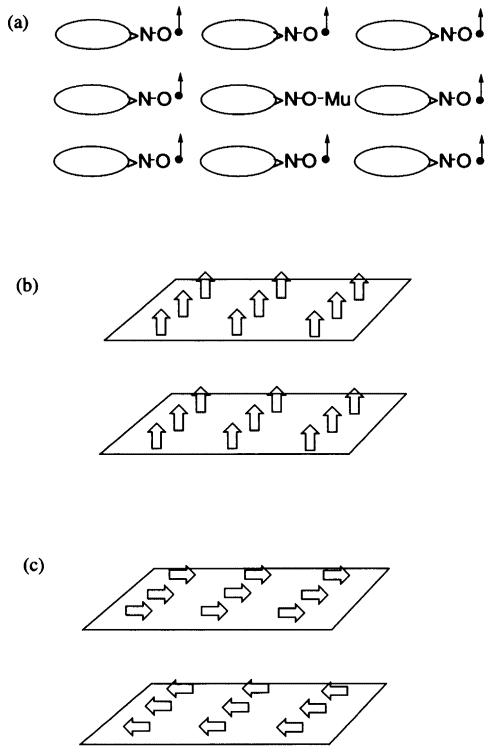

Fig. 2. (a) A model for implantation of a muon into nitroxide radical crystals. Mu is formed by an electron capture of μ^+. (b) A model for ferromagnetic ordering based on dipolar interaction between the two-dimensional ferromagnetic sheets. (c) A model for antiferromagnetic ordering based on dipolar interaction.

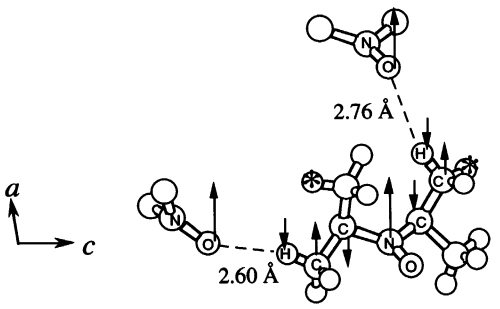

Fig. 3. Polarized spin densities along the contacting framework on a two-dimensional N–O network of Cl-TEMPO. Only selected portions are shown. Positively spin-polarized β-hydrogen atoms are indicated with asterisks.

In the case of antiferromagnets the internal field of 4Py-TEMPO was ≈ 110 G, which is much smaller than those of Cl-, Biph-, and Ph-TEMPOs. The ab initio calculation on the hyperfine field at the muon site for 4Py-TEMPO [17,18] exhibited a minimum in the [101] direction, assuming a two-dimensional ferromagnetic structure, and the calculated value is close to the observed one. The [101] direction is parallel to the two-dimensional sheet structure of the N–O groups, and consequently the dipolar interaction favors anti-parallel alignment between the sheets as shown in Fig. 2(c). The positive Weiss temperature of 4Py-TEMPO [9] is supposed to arise from the dominant two-dimensional ferromagnetic interaction. In conclusion, according to the inter-sheet dipolar mechanism proposed here, the ferro- and antiferromagnetism of the TEMPO-based magnets can be explained as ferro- and antiferromagnetic couplings, respectively, among the ferromagnetic two-dimensional sheets.

We have described the "β-hydrogen mechanism" for intra-sheet ferromagnetic exchange interactions [12,24], which is consistent with the present work. As the crystal structure analysis clarified, every N–O oxygen atom is located *always* near methyl- and/or methylene-hydrogen atoms at a β-position from an N–O group in the adjacent molecules. Negative spin densities are dominantly polarized at H_β atoms due to an intra-molecular spin-polarization schematically drawn as $ON(\uparrow)$–$C_\alpha(\downarrow)$–$C_\beta(\uparrow)$–$H_\beta(\downarrow)$. The solid-state NMR [25], solution ENDOR [26], and ab initio calculation results [25,27] of TEMPO radicals support these polarized spin densities, although the polarized neutron diffraction study of Cl-TEMPO does not agree with the calculation results [28]. Assuming negative spin density on a contacting H_β, an inter-molecular overlap between the H_β1s and the N–O π* orbitals induces positive spin density on the N–O group, thereby giving rise to a parallel spin alignment of N–O groups. Fig. 3 depicts the alternating spin density $ON(\uparrow) - C_\alpha(\downarrow) - C_\beta(\uparrow) - H_\beta(\downarrow)\cdots ON(\uparrow)$ along two exchange pathways within a sheet.

Detailed inspection of the molecular packing patterns may exploit an appropriate process for studying ferromagnetic materials based on crystal engineering techniques. Veciana and co-workers [29,30] reported a statistical analysis of the packing patterns from a large structural database of compounds containing nitronyl nitroxide radical units. After the spatial distribution of the $C_\beta - H_\beta\cdots ON$ contacts was analyzed, no correspondence could be found between the presence of intermolecular ferro- or antiferromagnetic interactions and the geometry of any of the contacts. This report seemingly rules out the "β-hydrogen mechanism". However, there are a few imperfect treatments in these statistical tests as follows. More delicate statistical tests may afford a clue to structure–magnetism relationship.

1. They are carried out on the data in which ferro- and antiferromagnetic interactions are simultaneously present, as already mentioned [30]. Actually, both interactions were reported to be observed and separately evaluated in a few TEMPO-based metamagnets [24,31]. The "ferromagnetic subset" contains contacts favoring antiferromagnetic coupling, and vice versa.
2. The most important point is that the sign of polarized spin density on H_β atoms generally depends on σ-skeletal conformation. It is well known that a hyperfine splitting constant (hfsc) of a γ-hydrogen atom in 1-propyl radical is exceptionally positive, i.e. polarized spin density is positive, when the C–C–C–H skeleton has a W-type conformation [32]. In TEMPO moieties there are two types of β-hydrogen atoms: positively and negatively spin-polarized. An hfsc of H_β in a limited region of the dihedral N–C–C–H angle is positive [33], as indicated with H* in Fig. 3. The positive spin density at H* is rationalized by a canonical structure drawn below:

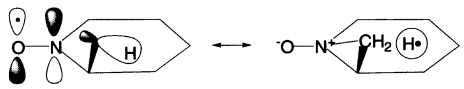

Ab initio calculation on TEMPO moieties reproduces the signs of polarized spin densities on methyl hydrogen atoms [25]. Inter-molecular contacts are ferromagnetic if the spin density on H atoms is negative and antiferromagnetic if it is positive. On the two-dimensional N–O networks of the TEMPO-based magnets, however, all of the contacting H_β atoms carry negative spin density, successfully explaining the ferromagnetic sheets of the TEMPO-magnets.
3. The "β-hydrogen mechanism" requires substantial inter-molecular overlap between H1s and N–O π* orbitals [7]. If a β-hydrogen atom is located on any nodal planes of the singly occupied molecular orbital of an adjacent molecule, ferromagnetic coupling cannot be expected. In fact, such a rare spatial arrangement was reported on a diphenyl nitroxide

derivative [34]. There are two nodal planes around an >N–O unit owing to the π* character. For a nitronyl nitroxide group another node is present at the central carbon atom of the ONCNO skeleton. Complicated situations in which H_β atoms are located on or off nodal planes can hardly be distinguished only by plots using two or three parameters.

5. Summary

We have measured ZF-μSR on three organic ferromagnets and one antiferromagnet. The three-dimensional ferromagnetic orderings have been observed for the ferromagnets, and the precise Curie temperatures have been determined. The precession frequencies ranging 220–230 G suggest that these ferromagnets possess similar muon-trapped sites and that the ferromagnetism is brought about by the primary two-dimensional magnetic ordering together with the inter-sheet dipolar interaction. The ''β-hydrogen mechanism'' previously proposed seems operative in the two-dimensional ferromagnetic sheets of TEMPO-based magnets.

Acknowledgements

This work was supported by Grants-in-Aid for Scientific Research on Priority Areas (730/11224204 and 297/12020219) from the Ministry of Education, Science, Sports and Culture, Japan.

References

[1] O. Kahn, (Ed.) Proceedings of the 6th International Conference on Molecule-Based Magnets. Mol. Cryst. Liq. Cryst. 334, 335 (1999).
[2] M. Kinoshita, P. Turek, M. Tamura, Y. Nozawa, D. Shiomi, Y. Nakazawa, M. Ishikawa, M. Takahashi, K. Awaga, T. Inabe, Y. Maruyama, Chem. Lett. (1991) 1225.
[3] L.P. Le, A. Keren, G.M. Luke, W.D. Wu, Y.J. Uemura, M. Tamura, M. Ishikawa, M. Kinoshita, Chem. Phys. Lett. 206 (1993) 405.
[4] S.J. Blundell, P.A. Pattenden, R.M. Valladares, F.L. Pratt, T. Sugano, W. Hayes, Solid State Commun. 92 (1994) 569.
[5] S.L. Blundell, P.A. Pattenden, F.L. Pratt, K.H. Chow, W. Hayes, T. Sugano, Hyperfine Int. 104 (1997) 251.
[6] S.J. Blundell, P.A. Pattenden, F.L. Pratt, R.M. Valladares, T. Sugano, W. Hayes, Europhys. Lett. 31 (1995) 573.
[7] T. Nogami, T. Ishida, M. Yasui, F. Iwasaki, N. Takeda, M. Ishikawa, T. Kawakami, K. Yamaguchi, Bull. Chem. Soc. Jpn 69 (1996) 1841.
[8] K. Togashi, R. Imachi, K. Tomioka, H. Tsuboi, T. Ishida, T. Nogami, N. Takeda, M. Ishikawa, Bull. Chem. Soc. Jpn 69 (1996) 2821.
[9] S. Ohira, T. Ishida, T. Nogami, I. Watanabe, F.L. Pratt, K. Nagamine, Physica B 289–290 (2000) 123.
[10] R. Imachi, T. Ishida, T. Nogami, S. Ohira, K. Nishiyama, K. Nagamine, Chem. Lett. (1997) 233.
[11] T. Ishida, S. Ohira, T. Ise, K. Nakayama, I. Watanabe, T. Nogami, K. Nagamine, Chem. Phys. Lett. 330 (2001) 110.
[12] T. Nogami, T. Ishida, H. Tsuboi, H. Yoshikawa, H. Yamamoto, M. Yasui, F. Iwasaki, H. Iwamura, N. Takeda, M. Ishikawa, Chem. Lett. (1995) 635.
[13] T. Ishida, H. Tsuboi, T. Nogami, H. Yoshikawa, M. Yasui, F. Iwasaki, H. Iwamura, N. Takeda, M. Ishikawa, Chem. Lett. (1994) 919.
[14] T. Nogami, K. Tomioka, T. Ishida, H. Yoshikawa, M. Yasui, F. Iwasaki, H. Iwamura, N. Takeda, M. Ishikawa, Chem. Lett. (1994) 29.
[15] Y. Miyazaki, T. Matsumoto, T. Ishida, T. Nogami, M. Sorai, Bul. Chem. Soc. Jpn 73 (2000) 67.
[16] T. Nogami, T. Ishida, M. Yasui, F. Iwasaki, H. Iwamura, N. Takeda, M. Ishikawa, Mol. Cryst. Liq. Cryst. 279 (1996) 97.
[17] T.M. Briere, J. Jeong, T.P. Das, S. Ohira, K. Nagamine, Physica B 289–290 (2000) 128.
[18] J. Jeong, T.M. Briere, N. Sahoo, T.P. Das, S. Ohira, K. Nishiyama, K. Nagamine, Physica B 289–290 (2000) 132.
[19] K. Tomioka, T. Ishida, T. Nogami, H. Iwamura, Chem. Lett. (1993) 625.
[20] K. Tomioka, S.-I. Mitsubori, T. Ishida, T. Nogami, H. Iwamura, Chem. Lett. (1993) 1239.
[21] F. Iwasaki, J.H. Yoshikawa, H. Yamamoto, E. Kan-nari, K. Takada, M. Yasui, T. Ishida, T. Nogami, Acta Crystallogr., Sect. B 55 (1999) 231.
[22] F. Iwasaki, J.H. Yoshikawa, H. Yamamoto, K. Takada, E. Kan-nari, M. Yasui, T. Ishida, T. Nogami, Acta Crystallogr., Sect. B 55 (1999) 1057.
[23] V. Laget, S. Rouba, P. Rabu, C. Hornick, M. Drillon, J. Magn. Magn. Mater. 154 (1996) L7.
[24] T. Ishida, K. Tomioka, T. Nogami, H. Yoshikawa, M. Yasui, F. Iwasaki, H. Iwamura, N. Takeda, M. Ishikawa, Chem. Phys. Lett. 247 (1995) 7.
[25] G. Maruta, S. Takeda, R. Imachi, T. Ishida, T. Nogami, K. Yamaguchi, J. Am. Chem. Soc. 121 (1999) 424.
[26] Y. Kotake, K. Kuwata, Chem. Lett. (1984) 83.
[27] B. Gillon, P. Becker, Y. Ellinger, Mol. Phys. 48 (1983) 763.
[28] Y. Pontillon, A. Grand, T. Ishida, E. Leliévre-Berna, T. Nogami, E. Ressouche, J. Schweizer, J. Mater. Chem. 10 (2000) 1539.
[29] M. Deumal, J. Cirujeda, J. Veciana, J.J. Novoa, Chem. Eur. J. 5 (1999) 1631.
[30] J. Veciana, J. Cirujeda, J.J. Novoa, M. Deumal, in: P.M. Lahti (Ed.), Magnetic Properties of Organic Materials, Marcel Dekker, New York, 1999, pp. 573–600.
[31] A. Benoit, J. Flouquet, B. Gillon, J. Schweizer, J. Magn. Magn. Mater. 31–34 (1983) 1115.
[32] Y. Ellinger, R. Subra, J. Chem. Phys. 62 (1975) 10.
[33] D. Ondercin, T. Sandreczki, R.W. Kreilick, J. Magn. Reson. 34 (1979) 151.
[34] M. Nakagawa, T. Ishida, M. Suzuki, D. Hashizume, M. Yasui, F. Iwasaki, T. Nogami, Chem. Phys. Lett. 302 (1999) 125.

PERGAMON

Polyhedron 20 (2001) 1551–1555

POLYHEDRON

www.elsevier.nl/locate/poly

Ferromagnetic $S = 1$ chain formed by a square Ni_2S_2 motif in $Ni(qt)_2$ (qt = quinoline-8-thiolate). Magnetic properties of related compounds

Takashi Miyake, Takayuki Ishida *, Daisuke Hashizume, Fujiko Iwasaki, Takashi Nogami

Department of Applied Physics and Chemistry, The University of Electro-Communications, Chofu, Tokyo 182-8585, Japan

Received 17 September 2000; accepted 9 November 2000

Abstract

ML_2 complexes [$M = Fe^{2+}$, Co^{2+}, Ni^{2+}, Cu^{2+}; L = quinolin-8-olate (q), quinoline-8-thiolate (qt)] were prepared and their magnetic properties were studied. X-ray crystal structure analysis of $Ni(qt)_2$ reveals that nickel(II) ions are arranged to form a one-dimensional structure with double thiolate bridges. Magnetic susceptibility measurements of $Ni(qt)_2$ indicate that the nickel $S = 1$ spins are ferromagnetically coupled within a chain. Other ML_2 showed antiferromagnetic interactions. Magnetic properties of molecular complexes of ML_2 with 7,7,8,8-tetracynanoquinodimethane (TCNQ) were also investigated. The crystal structure of $Ni(qt)_2$(TCNQ) was determined.

Keywords: Nickel(II) ion; Magnetic susceptibility; One-dimensional structure; Quinoline; TCNQ

1. Introduction

Recently there has been increased interest in the studies on molecule-based magnetic metals [1–4]. We examined the possibility of forming charge-transfer (CT) complexes of paramagnetic ML_2 [$M = Mn^{2+}$, Fe^{2+}, Co^{2+}, Ni^{2+}, Cu^{2+}; L = 8-quinolinolate (q), 8-quinolinethiolate (qt)], since $Cu(q)_2$ and $Pd(q)_2$ were reported to afford molecular complexes with 1,2,4,5-tetracyanobenzene (TCNB) [5]. Although their crystal structures have been determined, their physical properties and those of their related compounds have not been reported so far. ML_2 complexes were easily obtained by complexation of a metal dihalide with commercially available qH or qtH·HCl. Their magnetic and electron-donating properties were investigated. In the course of our study, we have found that $Ni(qt)_2$ has a nearly ideal one-dimensional magnetic structure due to a unique molecular assembly [6].

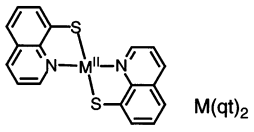

$M(qt)_2$

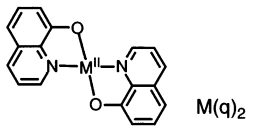

$M(q)_2$

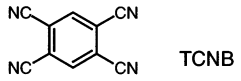

TCNB

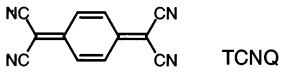

TCNQ

2. Experimental

Complexation with $NiCl_2·6H_2O$ and 2 equiv. of qtH·HCl in methanol gave $Ni(qt)_2$ as a dark brown powder (yield: 81%). Recrystallization of the product from benzonitrile gave black needle-like crystals (m.p. > 300°C). The elemental analysis (C,H,N) satisfied the formula $Ni(qt)_2$. $Fe(qt)_2$ and $Cu(qt)_2$ were prepared from $FeCl_2$ and $CuCl_2·2H_2O$, respectively, in place of $NiCl_2·6H_2O$, according to similar procedures. They were obtained as a black and a brown powder, respectively, and used directly for further analysis, since $Fe(qt)_2$ and $Cu(qt)_2$ are practically insoluble in benzo-

* Corresponding author. Tel.: +81-424-43-5490; fax: +81-424-43-5501.

E-mail address: ishi@pc.uec.ac.jp (T. Ishida).

0277-5387/01/$ - see front matter
PII: S0277-5387(01)00653-2

Table 1
Curie constants and Weiss temperatures of $M(q)_2$ and $M(qt)_2$ measured at 5000 Oe

	Compounds					
	$Fe(q)_2$	$Co(q)_2$	$Ni(q)_2$	$Cu(q)_2$	$Fe(qt)_2$	$Cu(qt)_2$
C (cm^3 K mol^{-1})	3.23	2.56	1.28	0.444	4.76	0.402
θ (K)	−0.76	−12	−19	−0.71	−0.85	−2.3

nitrile, chloroform, or *N*,*N*-dimethylformamide. $M(q)_2$ complexes (M = Fe, Co, Ni) were obtained by using qH and the corresponding metal(II) chlorides in methanol in the presence of catalytic amount of aqueous HCl [7]. $M(q)_2$ (M = Fe, Co, Ni) were purified by recrystallization from chloroform, giving a black, a brown, and a light green powder, respectively. $Cu(q)_2$ was purchased from Tokyo Chemical Industry.

The molecular complex $Ni(qt)_2$ with 7,7,8,8-tetracynanoquinodimethane (TCNQ) was obtained by mixing benzonitrile solutions containing $Ni(qt)_2$ and TCNQ at approximately 80°C, followed by standing at room temperature for a month. Black platelet crystals were precipitated and they were used for crystal structure analysis and magnetic measurements. Molecular complexes of $M(q)_2$(TCNQ) (M = Co, Ni, Cu) were prepared in chloroform, giving a green powder, a dark green powder, and a black platelet crystalline product, respectively.

Elemental analysis (C,H,N) was done on a Fisons EA-1108 by the usual combustion method. Cyclic voltammetry was recorded on a BAS CV-50W in acetonitrile with Ag/Ag^+ as the reference electrode, Pt as the working and counter electrodes and $Bu_4N^+BF_4^-$ as supporting electrolyte.

X-ray diffraction data of $Ni(qt)_2$ and $Ni(qt)_2$(TCNQ) were collected with graphite monochromated Mo Kα and Cu Kα radiations, respectively, on a Raxis-Rapid IP diffractometer (Rigaku). The atomic positions were directly solved with SIR92 [8] and refined with teXsan [9] using all of the diffraction data.

Magnetic properties were measured on Quantum Design MPMS and PPMS systems equipped with 7 and 9 T magnets, respectively. The diamagnetic contribution of the sample itself was estimated from Pascal's constants.

3. Results and discussion

The magnetism of ML_2, except for $Ni(qt)_2$, simply obeyed the Curie–Weiss law. The Curie constants and Weiss temperatures are summarized in Table 1. The Weiss temperatures in Table 1 are negative, indicating the presence of antiferromagnetic interactions. On the other hand, Fig. 1(a) shows the temperature dependence of the product of magnetic susceptibility and temperature ($\chi_{mol}T$) for $Ni(qt)_2$, measured at 500 Oe [6]. With decreasing temperature, the $\chi_{mol}T$ value monotonically increased and reached 5.07 cm^3 K mol^{-1} at 1.8 K. Fig. 1(b) shows the magnetization curve measured at 2.0 K. The magnetization largely exceeded the Brillouin function of $S = 1$. Thus the presence of ferromagnetic interaction among the nickel(II) spins was confirmed. No magnetic phase transition could be found above 1.8 K.

The X-ray crystallographic analysis of $Ni(qt)_2$ [6] reveals a uniform one-dimensional molecular arrangement. As Fig. 2 shows every nickel(II) ion is located at an inversion center and is surrounded by two nitrogen and two sulfur atoms at *trans* equatorial positions with bond distances of 2.07 and 2.40 Å for Ni–N and Ni–S, respectively. Almost planar quinoline moieties are ar-

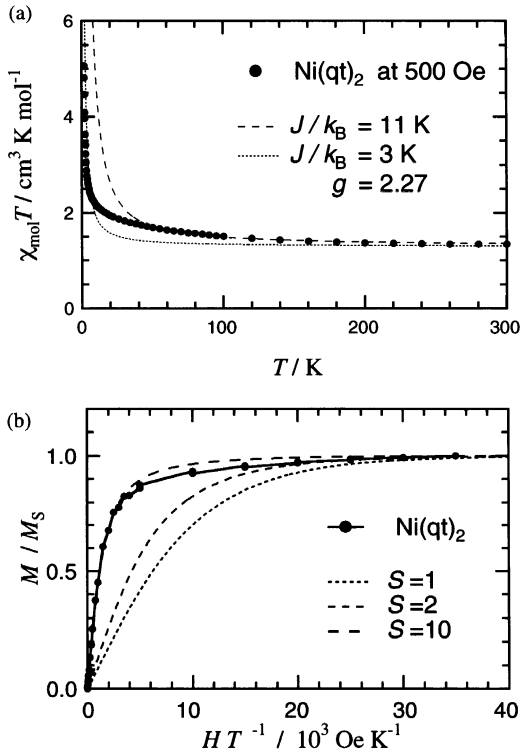

Fig. 1. (a) Temperature dependence of the product $\chi_{mol}T$ for $Ni(qt)_2$ measured at 500 Oe. The broken lines correspond to the calculated curves based on Fisher's equation with $J/k_B = 11$ and 3 K. (b) Magnetization curve of $Ni(qt)_2$ measured at 2.0 K. The Brillouin functions of $S = 1$, 2 and 10 are shown with broken lines.

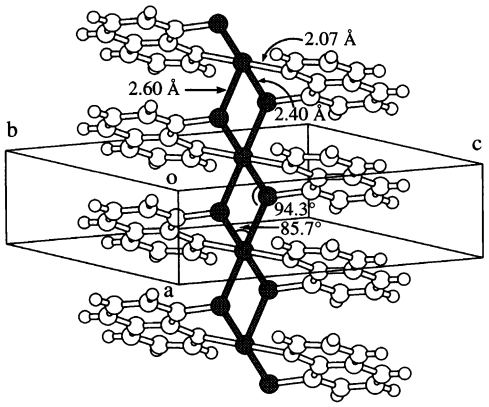

Fig. 2. One-dimensional structure of $Ni(qt)_2$. Ni and S atoms are shaded. Selected bond lengths and angles are shown.

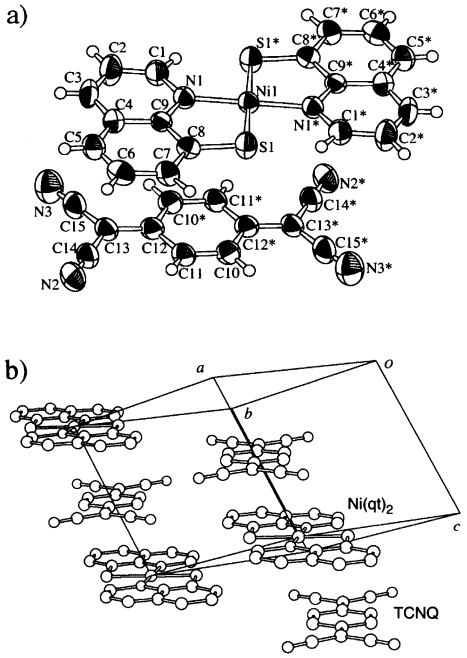

Fig. 3. (a) ORTEP drawing of $Ni(qt)_2(TCNQ)$ at the 50% probability level. Atomic numbering is also shown for non-hydrogen atoms. (b) Molecular arrangement of $Ni(qt)_2$ and TCNQ moieties in the crystal of $Ni(qt)_2(TCNQ)$.

ranged to construct a column along the *a* axis. The sulfur atom in a qt anion is deviated from the averaged quinoline plane toward a neighboring Ni ion, in which the axial coordination is found with a Ni–S distance of 2.60 Å. The angles of S–Ni–S and Ni–S–Ni are 85.6 and 94.4°, respectively. All of the Ni_2S_2 units are coplanar within a chain. The shortest inter-chain Ni···Ni distance is 9.85 Å, which is much longer than the shortest intra-chain distance (3.67 Å). There is no appreciable contact between chains. Therefore the crystal of $Ni(qt)_2$ has almost an ideal one-dimensional structure. The observed ferromagnetic interaction is due to the intra-chain interaction. We can estimate $J/k_B = +7 \pm 4$ K with $g = 2.27$ by fitting to an analytical expression for the magnetic susceptibility of an infinite chain derived by Fisher [10].

The Ni–S–Ni angle in $Ni(qt)_2$ is 94.3°, which is close to 90°. The magnetic d orbitals of the $S = 1$ nickel(II) ion are assigned to be $d_{x^2-y^2}$ and d_{z^2}. The geometry of the Ni_2S_2 unit favors a ferromagnetic superexchange drawn as: $d_{x^2-y^2} \| p_y \perp p_z \| d_{z^2}$. The J value is comparable to those of several oligonuclear nickel(II) complexes containing a cubane-like Ni_4O_4 core [11,12], in which the Ni–O–Ni angles were designed to be a right angle. Whereas several nickel(II) cluster complexes containing a square Ni_2S_2 core have been reported, they were diamagnetic in most cases [13,14]. Although uniform one-dimensional nickel(II) systems showing antiferromagnetic interaction have been extensively studied in connection with Haldane's conjecture [15], those showing a ferromagnetic interaction are rather limited in halogen- [16–18] and pseudohalogen-bridged [19,20] compounds. Thus, the complex $Ni(qt)_2$ is the first example of an $S = 1$ ferromagnetic chain consisting of a Ni_2S_2-type repeating motif.

We examined the electron-donating properties of ML_2 by means of cyclic voltammetry. The cyclic voltammograms of $Co(q)_2$, $Ni(q)_2$, $Cu(q)_2$, $Co(qt)_2$, and $Ni(qt)_2$ exhibited irreversible anodic peaks at 0.68, 0.67, 0.67, 0.51 and 0.28 V, respectively (in CH_3CN; reference electrode — Ag/Ag^+; scan rate — 100 mV s^{-1}). Their electron-donating abilities are confirmed. In particular, $Ni(qt)_2$ is a relatively strong donor, and this finding may be responsible for a different D/A ratio (D and A denote donor and acceptor molecules, respectively) in complexation with TCNQ as described below.

Molecular complexes of ML_2 with TCNQ were obtained in chloroform or benzonitrile. The elemental analysis revealed a D/A ratio of 1:2 for $Co(q)_2(TCNQ)_2$, $Ni(q)_2(TCNQ)_2$ and $Cu(q)_2(TCNQ)_2$. On the other hand, $Ni(qt)_2$ and TCNQ gave black polycrystals, whose D/A composition of 1:1 was determined by means of X-ray crystal structure analysis.

The crystal of $Ni(qt)_2(TCNQ)$ belongs to a triclinic space group $P\bar{1}$ and the cell parameters are $a =$ 8.7345(7), $b = 9.7142(6)$, $c = 8.0982(8)$ Å, $\alpha =$ 106.1392(2), $\beta = 100.058(3)$ and $\gamma = 76.333(3)°$. The molecular structure of $Ni(qt)_2(TCNQ)$ is shown in Fig. 3(a). The $Ni(qt)_2$ and TCNQ moieties are highly planar. The nickel(II) ion is surrounded by two sulfur and two nitrogen atoms at the *trans* equatorial sites with bond lengths of 2.175(1) and 1.913(4) Å, respectively, which are remarkably shorter than those of thiolate-bridged $Ni(qt)_2$ (Fig. 2). The molecular arrangement of $Ni(qt)_2$ and TCNQ moieties is shown in Fig. 3(b). The molecular planes of $Ni(qt)_2$ and TCNQ are parallel to each other in a mixed stack with a rather short inter-plane distance of approximately 3.35 Å.

Table 2
Curie constants and Weiss temperatures of $M(q)_2(TCNQ)_2$ measured at 5000 Oe

	Compounds		
	$Co(q)_2(TCNQ)_2$	$Ni(q)_2(TCNQ)_2$	$Cu(q)_2(TCNQ)_2$
C (cm^3 K mol^{-1})	2.53	1.60	0.547
θ (K)	−1.4	−13	−0.98

In order to estimate degree of CT, the detailed structure of the TCNQ moiety in $Ni(qt)_2(TCNQ)$ is stated briefly. The bond lengths of C12–C13, C10–C12*, C11–C12 and C10–C11 are 1.371(8), 1.446(8), 1.437(9) and 1.341(9) Å, respectively. These values are close to the corresponding values of neutral TCNQ [21] rather than $TCNQ^-$ [22]. Thus, it is concluded that $Ni(qt)_2(TCNQ)$ is a neutral π-complex, and the magnetic interaction between the nickel(II) ions is expected to be small due to an intervening TCNQ molecule.

The magnetic susceptibilities of $M(q)_2(TCNQ)_2$ ($M = Co^{2+}$, Ni^{2+}, Cu^{2+}) are found to obey the Curie–Weiss law. Dominant antiferromagnetic interactions were observed, as indicated by the negative Weiss temperatures (Table 2). Preliminary results on the magnetism of $Ni(qt)_2(TCNQ)$ also suggest the presence of a weak antiferromagnetic interaction.

McConnell proposed a model for ferromagnetic spin alignment using ionic CT salts [23]. In a normal mixed-stack of CT solids, intermolecular spin pairing is the result of the mixing of the ground state (D^+A^-) and a singlet back-CT state of a DA pair. McConnell applied this to a DA system where the neutral D (or A) is a triplet molecule, and proposed that if an ionic CT pair having a back-CT excitation to a neutral triplet state could be built, then the D^+A^- pair could also be a triplet, owing to mixing of the CT state with the neutral state. Triplet or higher multiplet donor molecules are required along this approach to CT-based ferromagnets. In the present study the degree of CT of $Ni(qt)_2(TCNQ)$ is not sufficient for realizing the McConnell model. Complexation with stronger acceptors such as F_4TCNQ is now under way.

4. Summary

The ferromagnetic interaction of $Ni(qt)_2$ has been clarified to be operative within a linear chain structure having a repeating motif of Ni_2S_2. Other complexes ML_2 obtained here showed antiferromagnetic interactions. Their TCNQ complexes [$Co(q)_2(TCNQ)_2$, $Ni(q)_2(TCNQ)_2$, $Cu(q)_2(TCNQ)_2$, and $Ni(qt)_2(TCNQ)$] were prepared.

5. Supplementary material

Crystallographic data (excluding structure factors) for the structures of $Ni(qt)_2$ and $Ni(qt)_2(TCNQ)$ have been deposited with the Cambridge Crystallographic Data Center, CCDC Nos 151618 and 151608, respectively. Copies of this information can be obtained free of charge on application to CCDC, 12 Union Road, Cambridge, CB2 1EZ, UK (fax: +44-1223-336033; e-mail: deposit@ccdc.cam.ac.uk or www: http://www.ccdc.cam.ac.uk).

Acknowledgements

This work was supported by Grants-in-Aid for Scientific Research (401/11136212, 730/11224204 and 297/12020219) from the Ministry of Education, Science, Sports and Culture, Japan.

References

[1] T. Otsuka, A. Kobayashi, Y. Miyamoto, J. Kiuchi, N. Wada, E. Ojima, H. Fujiwara, H. Kobayashi, Chem. Lett. (2000) 732.
[2] H. Kobayashi, A. Sato, H. Tanaka, A. Kobayashi, P. Cassoux, Coord. Chem. Rev. 190 (1999) 921.
[3] M. Clemente-Leon, E. Coronado, J.R. Galan-Mascaros, C.J Gómez-Garcia, C. Rovira, V.N. Laukhin, Synth. Met. 103 (1999) 2339.
[4] E. Coronado, J.R. Galán-Mascarós, C.J. Gómez-Garcia, V. Laukhin, Nature 408 (2000) 447.
[5] (a) P. Murray-Rust, J.D. Wright, J. Chem. Soc. (A) (1968) 247. (b) B. Kamenar, C.K. Prout, J.D. Wright, J. Chem. Soc. (A) (1966) 661.
[6] T. Miyake, T. Ishida, D. Hashizume, F. Iwasaki, T. Nogami, Chem. Lett. (2000) 952.
[7] A.S. Bailey, R.J.P. Williams, J.D. Wright, J. Chem. Soc. (1965) 2579.
[8] A. Altomare, M.C. Burla, M. Camalli, M. Cascarano, C. Giacovazzo, A. Guagliardi, G. Polidori, J. Appl. Crystallogr. 27 (1994) 435.
[9] Crystal Structure Analysis Package, Molecular Structure Corporation, 1985, 1999.
[10] M.E. Fisher, Am. J. Phys. 32 (1964) 343.
[11] J.A. Barnes, W.E. Hatfield, Inorg. Chem. 10 (1971) 2355.
[12] A. Escuer, M. Font-Bardía, S.B. Kumar, X. Solans, R. Vicente, Polyhedron 18 (1999) 909.
[13] G.R. Brubaker, J.C. Latta, D.C. Aquino, Inorg. Chem. 9 (1970) 2608.
[14] T.B. Rauchfuss, D.M. Roundhill, J. Am. Chem. Soc. 97 (1975) 3386.
[15] F.D.M. Haldane, Phys. Rev. Lett. 50 (1983) 1153.
[16] C. Dupas, J.-P. Renard, J. Chem. Phys. 61 (1974) 3871.
[17] F.W. Klaaijsen, Z. Dokoupil, W.J. Huiskamp, Physica 79B (1975) 547.
[18] W.E. Estes, R.R. Weller, W.E. Hatfield, Inorg. Chem. 19 (1980) 26.
[19] P. Chaudhuri, T. Weyhermuller, E. Bill, K. Wieghardt, Inorg. Chim. Acta 252 (1996) 195 (and references cited therein).

[20] A. Escuer, R. Vicente, M.S. El Fallah, X. Solans, M. Font-Bardía, J. Chem. Soc., Dalton Trans. (1996) 1013.
[21] R.E. Long, R.A Sparks, K.N. Trueblood, Acta Crystallogr. 18 (1965) 932.
[22] M. Konno, Y. Saito, Acta Crystallogr., Sect. B 30 (1974) 1294.
[23] H. McConnell, Proc. Robert A. Welch Found. Conf. Chem. Res. 11 (1967) 144.

PERGAMON

Polyhedron 20 (2001) 1557–1561

POLYHEDRON

www.elsevier.nl/locate/poly

Radical-copper hexanuclear arrays showing intermolecular ferromagnetic interactions

Junichi Omata, Takayuki Ishida *, Daisuke Hashizume, Fujiko Iwasaki, Takashi Nogami

Department of Applied Physics and Chemistry, The University of Electro-Communications, Chofu, Tokyo 182-8585, Japan

Received 17 September 2000; accepted 8 November 2000

Abstract

Hexanuclear arrays $[CuX_2{\cdot}(4PMNN)]_6$ (X = Br, Cl; 4PMNN = 4-pyrimidinyl nitronyl nitroxide) construct a perfect column perpendicular to the molecular plane and consequently a honeycomb-like channel structure is formed. The diameters of the channels are approximately 11.5 Å. The inner axial sites of the copper ions remain vacant and are thought to be available for further coordination. The host–guest complexes using $[CuCl_2{\cdot}(4PMNN)]_6$ were synthesized, and their ferromagnetic interactions enhanced by the guest inclusion. A possible supramolecular control of molecular magnetism is proposed.

Keywords: Ferromagnetic interaction; Supramolecule; Channel; Nitroxide; Ligand; Free radical

1. Introduction

Self-assembled discrete oligonuclear complexes with paramagnetic transition metal ions have fascinated chemists owing to their architectural beauty [1] as well as their mesoscopic physical properties [1,2]. We have reported the magnetism of pyrimidine-bridged transition metal complexes [3]. The pyrimidine–metal building block can form di- and trinuclear zero-dimensional [4], *cis*- and *trans*-zigzag one-dimensional [3], and chiral three-dimensional structures [5]. In the course of our study on the role of radical-substituted pyrimidine as ferro- and antiferromagnetic couplers across the μ-1,3-NCN bridges, we have found that discrete hexanuclear arrays $[CuX_2{\cdot}(4PMNN)]_6$ (**1**: X = Br, **2**: X = Cl; 4PMNN = 4-pyrimidinyl nitronyl nitroxide) predominantly exhibited ferromagnetic intermolecular interactions [6]. Host–guest complexation of these complexes was attempted because they have a large cavity with a diameter of approximately 11.5 Å and the inner vacant sites (an axial site of the copper ion) are thought to be available for further coordination of the guest molecules.

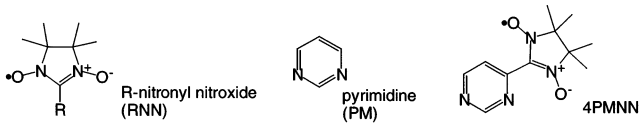

2. Experimental

Complexes **1** and **2** were synthesized as follows.[1] A methanol solution containing 4PMNN and $CuBr_2$ with a molar ratio of 1/1 was allowed to stand at room temperature for a week. Dark green needles of **1** were precipitated and collected on a filter. The resultant crystals are suitable for elemental analysis, X-ray dif-

* Corresponding author. Tel.: +81-424-43-5490; fax: +81-424-43-5501.

E-mail address: ishi@pc.uec.ac.jp (T. Ishida).

[1] Crystallographic data of the two complexes are given in Ref. [6]. Crystallographic data of $\mathbf{1}{\cdot}(0.3H_2O)_6$ are: $C_{11}H_{15}Br_2CuN_4O_2{\cdot}0.3H_2O$, trigonal, $R\bar{3}$, $a = b = 28.172(2)$, $c = 12.590(2)$ Å, $\gamma = 120°$, $V = 8653(2)$ Å^3, $Z = 18$, $D_{calc} = 1.605$ g cm^{-3}, $R = 0.058$ ($I > 2\sigma(I)$) for 4407 observed reflections. Crystallographic data of $\mathbf{2}{\cdot}(0.3H_2O)_6$ are: $C_{11}H_{15}Cl_2CuN_4O_2{\cdot}0.3H_2O$, trigonal, $R\bar{3}$, $a = b = 28.261(1)$, $c = 12.378(1)$ Å, $V = 8561(1)$ Å^3, $Z = 18$, $D_{calc} = 1.312$ g cm^{-3}, $R = 0.061$ ($I > 2\sigma(I)$) for 4363 observed reflections.

0277-5387/01/$ - see front matter
PII: S0277-5387(01)00654-4

fraction, and magnetic studies. Green needle crystals of **2** were prepared using $CuCl_2$ in place of $CuBr_2$.

Host–guest complexation was carried out by means of co-crystallization. The following procedure is typical. A methanol solution containing 4PMNN, $CuCl_2{\cdot}2H_2O$, and a guest material with a molar ratio 1:1:1 was allowed to stand for a week. The elemental analysis indicates that the products contain approximately 0.33 M of guest molecules. *Anal*. Found: C, 33.19; H, 4.12; N, 13.11. Calc. for **2**·(trimesic acid)$_{0.33}$·$(H_2O)_7$: C, 33.57; H, 4.57; N, 13.62%. Found: C, 34.45; H, 4.39; N, 13.55. Calc. for **2**·(terephthalaldehydic acid)$_{0.33}$·$(H_2O)_{10}$: C, 34.44; H, 4.46; N, 14.04%. Found: C, 34.90; H, 4.64; N, 13.55. Calc. for **2**·(isophthalic acid)$_{0.33}$·$(H_2O)_6$: C, 34.63; H, 4.40; N, 14.11%.

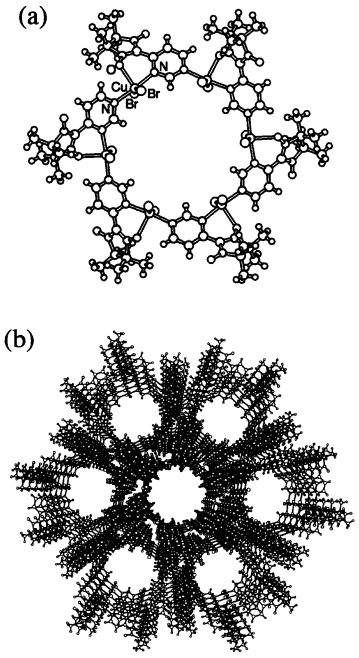

Fig. 1. (a) Molecular structure of **1**. (b) Molecular arrangement in the crystal of **1** viewed along the *c* axis.

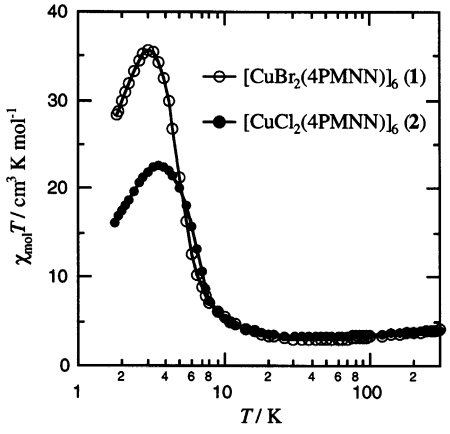

Fig. 2. Temperature dependence of the product of χ_{mol} and T for **1** and **2** measured at 500 Oe. The solid lines are shown as a guide to the eye.

X-ray diffraction data of **1** and **2** [6] were collected on a Raxis-Rapid IP diffractometer (Rigaku). The cell constants of the host–guest complexes were determined in a rhombohedral R space group using graphite monochromated Cu Kα radiation at ambient temperature. **2**·(trimesic acid)$_{0.33}$·$(H_2O)_7$: $a = 28.238(6)$, $b = 28.236(8)$, $c = 12.465(5)$ Å, $\alpha = 89.98(4)$, $\beta = 90.03(2)$, $\gamma = 120.01(2)°$. **2**·(terephthalaldehydic acid)$_{0.33}$·$(H_2O)_{10}$: $a = 28.2(3)$, $b = 28.2(3)$, $c = 12.5(3)$ Å, $\alpha = 90(2)$, $\beta = 90(1)$, $\gamma = 120(1)°$. **2**·(isophthalic acid)$_{0.33}$·$(H_2O)_6$: $a = 28.32(6)$, $b = 28.27(5)$, $c = 12.44(5)$ Å, $\alpha = 90.2(3)$, $\beta = 90.0(2)$, $\gamma = 120.0(2)°$. The relatively large experimental errors are due to the small size of the single crystals.

3. Results and discussion

We describe here the structure of **1** [6] since the crystals of **1** and **2** have an isostructure belonging to a space group trigonal $R\bar{3}$ (Fig. 1). One $CuBr_2$·(4PMNN) unit is crystallographically independent. A molecule consists of a cyclic head-to-tail hexamer of $CuBr_2$·(4PMNN), in which the pyrimidine (PM) rings work as μ-NCN bridges. The copper ion is pentacoordinated to form a square-pyramidal structure. Two bromide ions and two PM nitrogen atoms are bonded at the *trans*-equatorial positions. The atomic distances of Cu–Br are 2.40 Å and those of Cu–N, 2.02 and 2.03 Å. One oxygen atom in the nitronyl nitroxide (NN) group is coordinated at an axial position with the Cu–O distance of 2.22 Å. The formation of a wheel-like hexamer is rationalized in terms of crystal engineering: a PM ligand has two lone-pairs with a rigid angle of 120° and a metal ion has two coordination sites with an angle of 180°. Thus, the resultant array shapes a cavity with a nanosized diameter; the atomic distances of the opposing Cu···Cu are 11.50 and 11.57 Å for **1** and **2**, respectively.

As Fig. 1(b) shows, the hexanuclear arrays construct a column along the *c* axis and consequently a honeycomb-like channel structure is formed. The intracolumnar neighboring molecules are related by the *c*-translation. Note that the elemental analysis and X-ray diffraction study of **1** and **2** indicate that the channels are practically empty. Crystal solvents are supposed to be easily removed from the channel during the usual evacuation process prior to the analysis.

Magnetic properties were measured on a Quantum Design MPMS SQUID magnetometer in a temperature range 1.8–300 K. Fig. 2 shows the temperature dependence of the product of magnetic susceptibility and temperature ($\chi_{mol}T$) for **1** and **2** measured at 500 Oe. The spin-only $\chi_{mol}T$ value of a molecule having 12

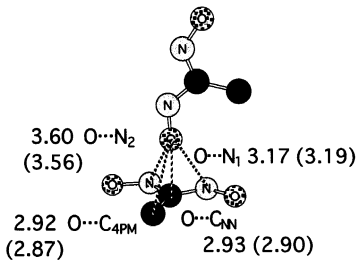

Fig. 3. Inter-columnar atomic contacts for the crystal of **1** are shown in Å with dotted lines. Those values for the crystal of **2** are shown in parentheses. The ONCNO moiety and the C_{4PM} atom of the pyrimidinyl 4-position are shown.

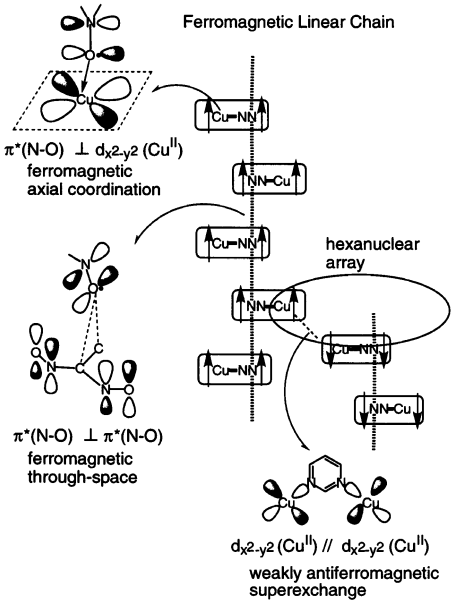

Fig. 4. Plausible magnetic structure.

paramagnetic $S = 1/2$ spins is 4.5 $cm^3\,K\,mol^{-1}$ assuming $g_{av} = 2.0$, in apparent agreement with the experimental values. However, an extrapolated value of $\chi_{mol}T$ at higher temperatures seems to be larger than 4.5 $cm^3\,K\,mol^{-1}$, suggesting that the interaction between the radical and the copper(II) is relatively large and ferromagnetic. With decreasing temperature the $\chi_{mol}T$ values gradually decreased but below approximately 40 K they started to increase. This 'ferrimagnetic-like' behavior showing a broad minimum demonstrates the simultaneous presence of ferro- and antiferromagnetic interactions. The $\chi_{mol}T$ values reached maxima of 35.6 and 22.6 $cm^3\,K\,mol^{-1}$ for **1** and **2**, respectively, and finally decreased again below approximately 3 K. The final decrease is more remarkable in measurements at larger applied fields (as exemplified by the $\chi_{mol}T$ vs. T plot for **2** at 5000 Oe in Fig. 5 vs. that at 500 Oe in Fig. 2), probably owing to a saturation effect. The maximum values correspond to spin-only values of approximately $S = 8$ for **1** and S of slightly larger than 6 for **2**. The ferromagnetic coupling should be attributed to intermolecular interactions.

As mentioned in Section 1, high-spin polynuclear compounds are of current interest in connection with single-molecule magnets [2]. Now we verify whether or not complexes **1** and **2** have a high-spin ground state. We can find a chelate structure in the repeating unit CuX_2·(4PMNN), in which the NN oxygen atom is axially coordinated to the copper ion. The orthogonality of Cu $3d_{x^2-y^2}$ and O $2p_z$ orbitals favors ferromagnetic interaction between the Cu and NN spins [7]. This geometry seems to afford the largest magnetic interaction in view of the short distance between the spins. We can also find that the PM bridges two copper ions. We have clarified the relationship between coordination structures and magnetic couplings in PM-bridged copper(II) complexes [3,8,9]. In the present case, every PM nitrogen atom is coordinated at an equatorial position and consequently the PM bridge should be an antiferromagnetic coupler. The magnetism is expected to show antiferromagnetic coupling among six triplet units and the experimental results above 40 K (Fig. 2) agree with this interpretation. The increase of $\chi_{mol}T$ below 40 K must be attributed to intermolecular ferromagnetic interactions.

As Fig. 3 shows relatively short van der Waals contacts can be pointed out between columns. The shortest distance is found between a terminal NN oxygen atom and a carbon atom of the PM 4-position in a neighboring molecule ($O\cdots C_{4PM}$). The second shortest distance is found between a terminal NN oxygen atom and a central NN carbon atom ($O\cdots C_{NN}$). The almost vertical spatial arrangement of two NN units gives a T-shaped configuration. We performed semi-empirical molecular orbital calculation of 4PMNN [10], confirming that the NN group has a node of the singly occupied molecular orbital (SOMO) at the central carbon atom, and that any atoms of the PM group do not have appreciable coefficients of the SOMO. The ($O\cdots C_{NN}$) contact gives rise to ferromagnetic coupling on the basis of McConnell's theory [11]. Similar situations were reported on lithium *p*-NN-substituted benzoate [12] and 1,2,4-triazole-3yl-NN [13]. Furthermore, Awaga [14] has proposed that a large SOMO–NHOMO overlap due to contact between an NN group and a substituent bonded to the central carbon atom is required for appreciable ferromagnetic interaction. Therefore, the first and second shortest inter-atomic contacts in the present study are both responsible for the observed ferromagnetic interaction. The geometry depicted in Fig. 3 successively repeats by a 3_1 screw symmetry along the *c* axis, i.e. perpendicular to the macrocyclic molecular plane, among the columns. A plausible magnetic structure is drawn in Fig. 4. The crystals of **1** and **2** are regarded as ferromagnetic chains accompanied by antiferromagnetic coupling among the chains.

These complexes have a rare structure: a ferromagnetic chain which grows along the tube-like cavity. The framework with a large cavity does not collapse without guests, which may also attract attention in connection with synthetic zeolites. In order to develop a possible supramolecular control of molecular magnetism, we attempted host–guest complexation of **1** and **2**. It can be pointed out that another axial site of the copper ion remains vacant and guest molecules having lone-pairs are acceptable inside. Symmetrical di-, tri- and hexasubstituted benzene derivatives, such as terephthalaldehyde, hexachlorobenzene, trimesic acid, are expected to be good candidates for guest molecules from computational modeling [15]; bond lengths of possible inner axial coordination range around 2 Å.

The specimens of host–guest complexes of **2** containing trimesic acid, terephthalaldehydic acid and isophthalic acid were prepared by a co-crystallization method, giving dark green fine polycrystals. The inclusion of the guest molecules was indicated by the elemental analysis as well as IR spectroscopy; additional signals were found around 1650 and 3400 cm^{-1}, which are ascribable to carboxyl groups. The elemental analysis suggests that the occupancies of the guest molecule are somewhat lower than unity (approximately 0.33). The X-ray crystal structure analysis revealed the presence of appreciable electron density within a channel but the atomic positions of the guest molecules could not be determined precisely. The cell constants of the host–guest complexes of **2** are very close to those of **2** itself, unequivocally indicating that the structure of the host cage is retained. Furthermore, the guest molecules reside within a channel and not in the exohedral clearance. The inter-columnar van der Waals contacts affording the ferromagnetic pathway proposed above are also retained.

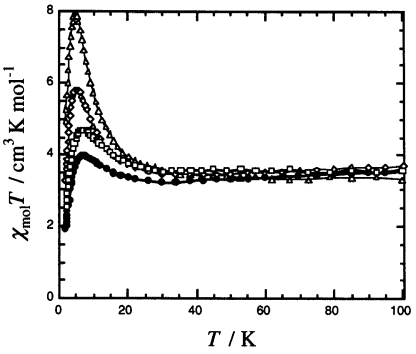

Fig. 5. Temperature dependence of the product of χ_{mol} and T measured at 5 kOe for **1** (filled circles) and host–guest complexes of **1** with terephthalaldehydic acid (triangles), trimesic acid (diamonds) and isophthalic acid (squares). The analysis is based on the formula weight of $[CuCl_2 \cdot (4PMNN)]_6$. The solid lines are shown as a guide to the eye.

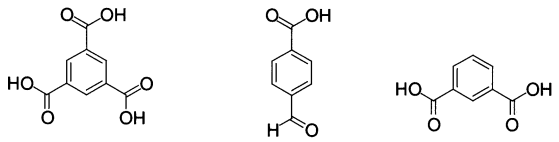

As Fig. 5 shows, the ferromagnetic behavior is much emphasized by the inclusion. With a decrease of temperature the $\chi_{mol}T$ value of the host–guest complexes of **2** increased more significantly than that of **2** itself. The similar magnetic behavior strongly indicates that they involve the same magnetic structure as that drawn in Fig. 4. The bulkiness of the guest molecules changes the inter-atomic distances among the columns (Fig. 3) and it is most likely that the oxygen atoms and contacting carbon atoms in the neighboring molecules get closer to each other. These results suggest that the molecular magnetism is tunable by such supramolecular techniques.

4. Summary

Discrete hexanuclear complexes **1** and **2** construct a perfect column perpendicular to the macrocyclic molecular plane. The diameters of the honeycomb-like channels are approximately 11.5 Å and the ferromagnetic one-dimensional structures are characterized along the column direction. Thus, we can regard these complexes as 'magnetic nanotubes'. The host–guest complexes are synthesized and the magnetic properties are tuned by the inclusion. The present work cultivates a new strategy of molecular magnetism; supramolecular control of molecular magnetism is proposed.

5. Supplementary material

Crystallographic data (excluding structure factors) for the structures of $\mathbf{1} \cdot (0.3H_2O)_6$ and $\mathbf{2} \cdot (0.3H_2O)_6$ have been deposited with the Cambridge Crystallographic Centre, CCDC nos. 151258 and 151259, respectively. Copies of this information can be obtained free of charge on application to CCDC, 12 Union Road, Cambridge CB2 1EZ, UK (fax: +44-122-336033; e-mail: deposit@ccdc.cam.ac.uk or www: http://www.ccdc.cam.ac.uk).

Acknowledgements

This work was supported by Grants-in-Aid for Scientific Research (730/11224204 and 297/12020219) from the Ministry of Education, Science, Sports and Culture, Japan.

References

[1] (a) K.L. Taft, S.J. Lippard, J. Am. Chem. Soc. 112 (1990) 9629. (b) G.L. Abbati, A. Cornia, A.C. Fabretti, A. Caneschi, D. Gatteschi, Inorg. Chem. 37 (1998) 1430. (c) A.J. Blake, C.M. Grant, S. Parsons, J.M. Rawson, E.P. Winpenny, J. Chem. Soc., Chem. Commun. (1994) 2363. (d) A. Caneschi, D. Gatteschi, J. Laugier, P. Rey, R. Sessoli, C. Zanchini, J. Am. Chem. Soc. 110 (1988) 2795. (e) D. Gatteschi, A. Caneschi, L. Pardi, R. Sessoli, Science 265 (1994) 1054.

[2] (a) J.R. Friedman, M.P. Sarachik, J. Tejada, R. Ziolo, Phys. Rev. Lett. 76 (1996) 3830. (b) L. Thomas, F. Lionti, R. Ballow, D. Gatteschi, R. Sessoli, B. Barbara, Nature 383 (1996) 145.

[3] (a) T. Ishida, T. Nogami, Recent Res. Dev. Pure Appl. Chem. 1 (1997) 1. (b) T. Ishida, K. Nakayama, M. Nakagawa, W. Sato, Y. Ishikawa, M. Yasui, F. Iwasaki, T. Nogami, Synth. Met. 85 (1997) 1655.

[4] M. Nakagawa, Y. Ishikawa, T. Kogane, T. Ishida, M. Yasui, F. Iwasaki, T. Nogami, Mol. Cryst. Liq. Cryst. 286 (1996) 29.

[5] N. Nakayama, T. Ishida, R. Takayama, D. Hashizume, M. Yasui, F. Iwasaki, T. Nogami, Chem. Lett. (1998) 497.

[6] J. Omata, T. Ishida, D. Hashizume, F. Iwasaki, T. Nogami, Inorg. Chem. (2000), in print.

[7] (a) A. Caneschi, D. Gatteschi, J. Laugier, P. Rey, J. Am. Chem. Soc. 109 (1987) 2191. (b) A. Caneschi, D. Gatteschi, P. Rey, R. Sessoli, Acc. Chem. Res. 22 (1989) 392.

[8] F. Mohri, K. Yoshizawa, T. Yamabe, T. Ishida, T. Nogami, Mol. Engng, 8 (1999) 357.

[9] M. Yasui, Y. Ishikawa, N. Akiyama, T. Ishida, T. Nogami, F. Iwasaki, Acta Crystallogr., Sect. B (2001), in print.

[10] J.J.P. Stewart, MOPAC ver. 6.0, QCPE #455.

[11] H.M. McConnell, J. Chem. Phys. 39 (1963) 1910.

[12] (a) K. Inoue, H. Iwamura, Chem. Phys. Lett. 207 (1995) 551. (b) T. Kawakami, A. Oda, W. Mori, K. Yamaguchi, K. Inoue, H. Iwamura, Mol. Cryst. Liq. Cryst. 279 (1996) 29.

[13] T. Kawakami, K. Yamaguchi, F. Matsuoka, Y. Yamashita, O. Kahn, Polyhedron 20 (2001), this issue.

[14] (a) K. Awaga, T. Inabe, Y. Maruyama, Chem. Phys. Lett. 190 (1992) 349. (b) K. Awaga, in: P.M. Lahti (Ed.), Magnetic Properties of Organic Materials, Marcel Dekker, New York, 1999, pp. 519–534 (chap. 25).

[15] Oxford Molecular Group, Molecular Mechanics Calculation on CAChe 3.9, 1996.

PERGAMON

Polyhedron 20 (2001) 1223–1227

POLYHEDRON

www.elsevier.nl/locate/poly

Anomalous magnetism in organic radical ferromagnets 4-arylmethyleneamino-2,2,6,6-tetramethylpiperidin-1-yloxyl just above T_C studied by the μSR method

S. Ohira [a,*], K. Nakayama [b], T. Ise [b], T. Ishida [b], T. Nogami [b], I. Watanabe [a], K. Nagamine [a,c]

[a] *Muon Science Laboratory, The Institute of Physical and Chemical Research (RIKEN), 2-1 Hirosawa, Wako, Saitama 351-0198, Japan*
[b] *Department of Applied Physics and Chemistry, The University of Electro-communications, 1-5-1 Chofugaoka, Chofu, Tokyo 182-8585, Japan*
[c] *Meson Science Laboratory, Institute of Materials Structure Science, High Energy Accelerator Research Organization (KEK-MSL), 1-1 Oho, Tsukuba, Ibaraki 305-0801, Japan*

Received 17 September 2000; accepted 4 December 2000

Abstract

The magnetic property of 4-arylmethyleneamino-TEMPO (TEMPO = 2,2,6,6-tetramethylpiperidin-1-yloxyl) just above the Curie temperature was studied by muon spin relaxation (μSR) method microscopically. In the longitudinal-field (LF) measurement, muon spin depolarization due to dynamical radical spin fluctuations was expected. However, we observed a random static internal magnetic field at the muon site down to T_C. A distribution width of the random internal magnetic field increased, as if induced by LF, with increasing LF, and was saturated eventually. This remarkable behavior appears below the temperature where the ac susceptibility starts to increase rapidly [Chem. Lett. (1995) 635; Chem. Lett. (1994) 919; Chem. Lett. (1994) 29].

We report the critical phenomena observed in the μSR studies on the TEMPO derivatives and discuss the relationship between the results and the magnetic structure in the ordered state.

Keywords: Organic radical ferromagnet; TEMPO; μSR; Critical phenomena

1. Introduction

Organic radical magnets containing a stable unpaired electron on a molecule have been developed and studied by various methods in recent years [1,4,5]. Most of the organic materials show a high low-dimensionality, and have attracted the attention of many physicists and chemists. Organic magnets having a 2,2,6,6-tetramethylpiperidin-1-yloxyl (TEMPO) group are known to show a strong two-dimensionality in their crystal structures. Each radical spin is localized at the N–O site on a molecule. It has been suggested that these systems show an intra-sheet ferromagnetic interaction originating from an intra- and inter-molecular spin-polarization mechanism [6]. The intra-sheet magnetic interactions are expected to be much stronger than the inter-sheet one because of the shorter O···O distances [7]. Although the distances are not directly related to the magnetic interaction because of the negligible exchange interactions in these systems, the inter-sheet correlation path should be more complicated. For 4-(*p*-chlorobenzylideneamino)-TEMPO (Cl-TEMPO), the ac susceptibility χ_{ac} starts to increase at around 0.4 K, whereas zero-field (ZF) muon spin relaxation (μSR) and specific heat measurements revealed 0.28 K as the three-dimensional (3D) ferromagnetic transition temperature, which corresponded to the temperature where χ_{ac} showed a peak [1,8,9]. The specific heat measurement also suggested a 2D magnetic interaction above T_C [9]. From these results, a crossover from 2D to 3D magnetic interaction is expected to be observed between the two temperatures.

The muon is a local probe whose behavior sensitively depends on the dynamical or static magnetic fields at its site, and is suitable for investigating low-dimensional

* Corresponding author. Fax: +81-48-4624648.
E-mail address: ohira@riken.go.jp (S. Ohira).

0277-5387/01/$ - see front matter
PII: S0277-5387(01)00597-6

systems. Therefore, μSR measurements are versatile tools for observing magnetic properties microscopically. Especially longitudinal-field (LF) μSR measurements are useful to investigate spin dynamics and to obtain an estimate of the internal field distribution and the frequency of fluctuating radical spins. In our previous LF μSR study on this radical, a random and static internal field was observed just above the phase transition temperature for the long-range magnetic ordering (= 0.28 K) [10]. In addition, we observed a muon spin rotation frequency, which increased as the temperature was lowered down to 0.3 K in a transverse-field (TF) μSR study [11]. Such anomalous behavior may be associated with the two-dimensionality of the system, because the temperature at which the anomaly appears is consistent with that for the rapid increase of χ_{ac}.

Other TEMPO derivatives, benzylideneamino-TEMPO (Ph-TEMPO) and 4-(*p*-phenylbenzylideneamino)-TEMPO (Biph-TEMPO) also show a χ_{ac} peak at 0.18 and 0.27 K, respectively [2,3]. And ZF μSR measurements for both systems showed ferromagnetic ordering below 0.17 and 0.22 K, respectively [12]. Thus the same behavior as observed in Cl-TEMPO is also expected in these two systems.

We carried out an additional LF μSR measurement on Cl-TEMPO, in order to understand this remarkable phenomenon in detail, and on the two other ferromagnetic TEMPO derivatives, Ph-TEMPO and Biph-TEMPO in order to investigate their critical behavior above T_C. In this paper, we discuss the magnetic structures in the TEMPO derivatives just above T_C systematically, based on the LF μSR results.

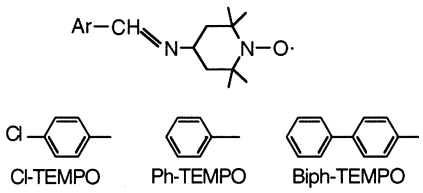

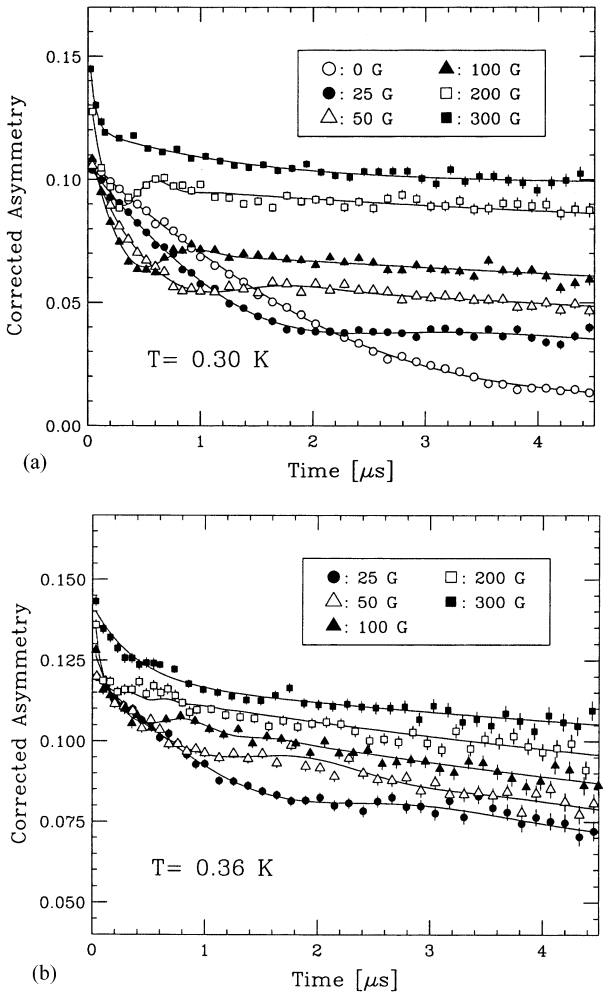

Fig. 1. LF μSR time spectra of Cl-TEMPO at: (a) 0.30 K; and (b) 0.36 K. The spectra below LF = 200 G are well fitted by the LF Kubo–Toyabe function which describes muon spin relaxation due to random static internal magnetic fields.

2. Experimental

The LF μSR measurement on Cl-TEMPO was carried out at the RIKEN-RAL Muon Facility in the UK by using a ^{3}He cryostat down to 0.3 K. The two other systems, Ph-TEMPO and Biph-TEMPO were measured at Meson Science Laboratory in the High Energy Accelerator Research Organization (KEK-MSL), using a top-loading ^{3}He-^{4}He dilution refrigerator. A pulsed surface muon beam with the momentum of 27 MeV c^{-1} was used. The muon spin is completely polarized along the direction of the momentum. Decay positrons, which are preferentially emitted from the muon along the muon spin direction, were detected by forward and backward counters. The asymmetry is described as $A(t) = [N_F(t) - \alpha N_B(t)]/[N_F(t) + \alpha N_B(t)]$, where N_F and N_B are the number of the decay positrons counted by the forward and backward counters, respectively, and α is a geometrical factor to set the baseline of $A(t)$ to be 0.

Single crystals of these systems are prepared, according to the method reported elsewhere [13,14]. Each sample was mounted on a silver plate and fixed on the sample holder of the cryostat. The muon was injected into the samples so that its initial spin polarization was perpendicular to the *a*-axis of Cl-TEMPO and Biph-TEMPO and perpendicular to the *bc* plane of Ph-TEMPO. An LF was applied parallel to the initial muon spin direction.

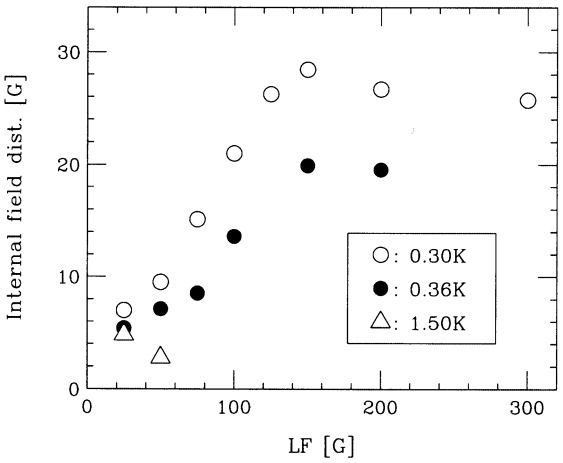

Fig. 2. LF dependence of the distribution width of the random static field of Cl-TEMPO at 0.30, 0.36 and 1.5 K.

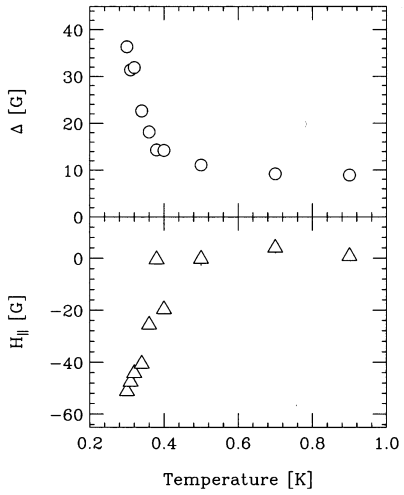

Fig. 3. Temperature dependences of the internal field distribution Δ and the parallel component to LF of internal field $H_{\parallel}$ in Cl-TEMPO under LF of 100 G. $H_{\parallel}$ is obtained by subtracting the applied LF value (= 100 G) from the fitting result of a parameter H_{LF}.

3. Results and discussion

Fig. 1 shows the LF μSR time spectra for Cl-TEMPO at 0.30 and 0.36 K. The time spectra below 200 G can be well reproduced by an LF Kubo–Toyabe function [15]. This indicates that a random static internal magnetic field appears at the muon site under LF of less than 200 G below 0.36 K, whereas a fluctuating magnetic field is expected to be observed just above T_C in conventional magnetic materials. The muon spin is almost repolarized under 300 G at 0.30 K. The time spectra below 200 G were fitted by Eq. (1)

$$A(t) = A_{KT}G_{KT}(\Delta,H_{LF},\nu,t) + A_{fast}\exp(-\lambda_{fast}t) + A_{slow}\exp(-\lambda_{slow}t), \quad (1)$$

where $A_{KT}G_{KT}(\Delta,H_{LF},\nu,t)$ is the dynamical Kubo–Toyabe function, which describes the muon spin depolarization caused by random fields under LF. Δ is the width of the internal magnetic field distribution at the muon site, H_{LF} the applied LF and ν the hopping rate of the muon and/or internal field, respectively.

A_{KT} was almost independent of LF up to about 100 G, though it is not shown here. ν decreased with increasing LF because the muon spin relaxation is suppressed by LF. The field distribution is conventionally independent of the applied field. However, in the case of this system, Δ increases with increasing LF, as if induced by the external field [10]. The LF dependences of the distribution of the random field, Δ, at 0.30, 0.36 and 1.5 K are shown in Fig. 2. The value of saturated Δ at 0.30 K is obviously larger than that of the nuclear dipole field, which is estimated to be about 4 G. Similar LF dependence to that at 0.30 K was also observed at 0.36 K, that is, Δ increased with increasing LF, and was saturated under LF of more than 150 G. The saturation of the internal field seems to follow the magnetization. However, the observed field is not due to aligned radical spins along the external field but *randomness*. At 1.5 K, the random static field component can be observed under below 50 G, and the muon spin is decoupled by LF higher than 100 G. The result has a remarkable feature. The saturated value of Δ decreases with increasing temperature away from T_C. This feature can be understood from the susceptibility and magnetization curves [1]. The finite Δ could be explained by a distribution of paramagnetic shifts for the various crystallites in the sample with different orientations of the *b*- and *c*-axes with respect to the applied field.

Such a field dependence is observed below around 0.4 K [10]. This is consistent with the temperature at which the rapid increase of χ_{ac} starts [1]. The temperature dependences of Δ and $H_{\parallel}$ are shown in Fig. 3. $H_{\parallel}$ is defined as follows. In the case where an isotropic internal magnetic field occurs under LF, the best fit for a spectrum should give almost the same value to the parameter H_{LF} as the applied LF value. On the other hand, if the center of the internal field distribution in the LF direction is shifted by the external field, the fitting result of H_{LF} will deviate from the applied LF value. We define this deviation as $H_{\parallel}$, which corresponds to the mean value of the internal field parallel to LF, and is obtained by subtracting the applied LF value from the fitting parameter H_{LF}. Both Δ and the magnitude of $H_{\parallel}$ show a rapid increase with decreasing temperature below around 0.4 K. We notice here that the longitudinal component of internal field $H_{\parallel}$, which is a little bit larger than Δ, exists opposite to the applied LF. Because the radical spins aligned along LF produce dipolar fields with opposite direction at the muon site, it is suggested that the parallel component of the radical spin occurs by being forced to cant by LF. Taking into account the clear oscillation observed in

the previous ZF μSR study [8], this magnetic state seems quite different from the 3D ferromagnetic ordered state.

A similar behavior was also observed in the other systems, Ph-TEMPO and Biph-TEMPO. The LF μSR time spectra are similar to those in Cl-TEMPO. Fig. 4 shows the LF dependence of the distribution width of the random static internal field in Ph-TEMPO at 0.20 K and in Biph-TEMPO at 0.30 and 0.40 K. These systems are suggested to show a ferromagnetic phase transition at 0.17 and 0.22 K, respectively, from our ZF SR studies [12]. For Biph-TEMPO, the saturation of the random field distribution was observed at 0.30 K, while the LF dependence was ambiguous at 0.40 K, at which χ_{ac} started to increase rapidly [2]. The reason why the saturated value of Δ is smaller than that in Cl-TEMPO at 0.30 K is expected to be smaller T/T_C value; in other words, the distribution width is expected to reflect the spin susceptibility. In the case of Ph-TEMPO, Δ increases under LF lower than 100 G with increasing LF, as well as the two other systems. It is unclear whether Δ is saturated under higher fields or not because the muon spins which make up the Kubo–Toyabe component are decoupled by an LF of 150 G. However, the situation of Ph-TEMPO at 0.20 K should be similar to Cl-TEMPO at 0.30 K. The Δ value observed under each LF in Ph-TEMPO at 0.20 K is close to that in Cl-TEMPO at 0.30 K.

Biph-TEMPO has a *pleated* N–O sheet structure quite similar to that of Cl-TEMPO, and the distance between the sheets is longer than that of Cl-TEMPO [7]. On the other hand, the N–O sheet of Ph-TEMPO exhibits a *zig–zag* structure [7]. This difference is expected to cause different inter-sheet magnetic correlation paths, not intra-sheet ones. In our studies, the three systems showed results similar to each other. It was evidenced that the difference in the N–O sheet structure is not reflected in the two-dimensionality of the systems.

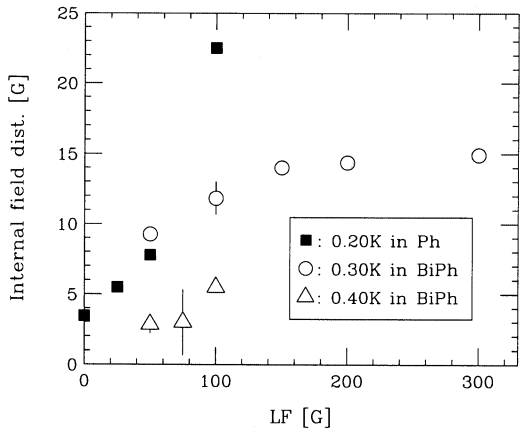

Fig. 4. LF dependence of the distribution width of the random field of Ph-TEMPO at 0.20 K and Biph-TEMPO at 0.30 and 0.40 K.

4. Conclusions

LF μSR measurements were carried out on Cl-, Ph- and Biph-TEMPOs, in order to study microscopically the critical phenomena in organic radical 2D systems. Muon spin depolarization due to a random static internal field was observed in each system above T_C. According to the analysis, the saturated values for the distribution widths of the random static field were about 30 G for Cl-TEMPO and 15 G for Biph-TEMPO at 0.30 K. These values are larger than that for the nuclear dipolar field, which is about 5 G. Therefore, it is expected that the remarkable behavior reflects the high two-dimensionality in the systems. The origin of the distribution widths is ascribed to the distributions of paramagnetic shifts in the fluctuation-suppressed systems, the distributions being associated with different crystallites in the sample.

No remarkable difference in the three investigated systems was observed in the LF μSR measurements. It was confirmed that the difference in the N–O sheet structure is not reflected in the two-dimensionality of the systems.

Acknowledgements

One of the authors (S.O.) is supported by the Special Postdoctoral Researchers Program at RIKEN.

References

[1] T. Nogami, T. Ishida, H. Tsuboi, H. Yoshikawa, H. Yamamoto, M. Yasui, F. Iwasaki, H. Iwamura, N. Takeda, M. Ishikawa, Chem. Lett. (1995) 635.
[2] T. Ishida, H. Tsuboi, T. Nogami, H. Yoshikawa, M. Yasui, F. Iwasaki, H. Iwamura, N. Takeda, M. Ishikawa, Chem. Lett. (1994) 919.
[3] T. Nogami, K. Tomioka, T. Ishida, H. Yoshikawa, M. Yasui, F. Iwasaki, H. Iwamura, N. Takeda, M. Ishikawa, Chem. Lett. (1994) 29.
[4] M. Kinoshita, P. Turek, M. Tamura, K. Nozawa, D. Shiomi, Y. Nakazawa, M. Ishikawa, M. Takahashi, K. Awaga, T. Inabe, Y. Maruyama, Chem. Lett. (1991) 1225.
[5] M. Tamura, Y. Nakazawa, D. Shiomi, K. Nozawa, Y. Hosokoshi, M. Ishikawa, M. Takahashi, M. Kinoshita, Chem. Phys. Lett. 186 (1991) 401.
[6] T. Nogami, T. Ishida, M. Yasui, F. Iwasaki, N. Takeda, M. Ishikawa, T. Kawakami, K. Yamaguchi, Bull. Chem. Soc. Jpn 69 (1996) 1841.
[7] M. Yasui, H. Yoshikawa, H. Yamamoto, T. Ishida, T. Nogami, F. Iwasaki, Mol. Cryst. Liq. Cryst. 279 (1996) 77.
[8] R. Imachi, T. Ishida, T. Nogami, S. Ohira, K. Nishiyama, K. Nagamine, Chem. Lett. (1997) 233.
[9] Y. Miyazaki, T. Matsumoto, T. Ishida, T. Nogami, M. Sorai, Bull. Chem. Soc. Jpn 73 (2000) 67.
[10] S. Ohira, I. Watanabe, K. Nakayama, T. Ishida, T. Nogami, K. Nagamine, Riken Rev. 20 (1999) 48.

[11] S. Ohira, T. Ishida, T. Nogami, I. Watanabe, K. Nagamine, Physica B 289–290 (2000) 123.
[12] (a) T. Ishida, S. Ohira, T. Ise, K. Nakayama, I. Watanabe, T. Nogami, K. Nagamine, Chem. Phys. Lett. 330 (2000) 10. (b) T. Ishida, S. Ohira, T. Ise, K. Nakayama, I. Watanabe, T. Nogami, K. Nagamine, this proceedings.
[13] K. Tomioka, T. Ishida, T. Nogami, H. Iwamura, Chem. Lett. (1993) 625.
[14] K. Tomioka, S.-i. Mitsubori, T. Ishida, T. Nogami, H. Iwamura, Chem. Lett. (1993) 1239.
[15] R.S. Hayano, Y.J. Uemura, J. Imazato, N. Nishida, T. Yamazaki, R. Kubo, Phys. Rev. B 20 (1979) 850.

ELSEVIER

www.elsevier.com/locate/ica
Inorganica Chimica Acta 329 (2002) 31–35

Inorganica Chimica Acta

Novel organic–inorganic molecular assembly: a copper(I) and copper(II) mixed-valent cluster with bromide bridges and paramagnetic ligands

Tomoo Katayama, Takayuki Ishida *, Takashi Nogami

Department of Applied Physics and Chemistry, The University of Electro-Communications, Chofu, Tokyo 182-8585, Japan

Received 9 July 2001; accepted 29 October 2001

Abstract

Complex $pbt_2Cu_8Br_{12}$ [pbt = pyridine-2,6-diylbis(methyleneamino-TEMPO)] was synthesized from $CuBr_2$ and a new ligand pbt, and characterized by means of X-ray crystal structure analysis and magnetic measurements. The centrosymmetric molecule consists of a Cu_6Br_{10} cluster sandwiched with two pbt·CuBr complexes. Detailed geometrical analysis and magnetic analysis reveal the presence of four copper(I) and four copper(II) ions in a molecule. Antiferromagnetic couplings observed can be attributed to the intermolecular radical···radical and intramolecular copper(II)···copper(II) interactions.

Keywords: Copper complexes; Bromocuprates; TEMPO; Magnetic properties; Crystal structures

1. Introduction

Discrete metal-cluster molecules with bridging ligands are of increasing interest for the development of molecule-based magnets [1], since the single-molecule magnets and super-high-spin molecules were discovered in μ-oxometalates [2] and μ-cyanometalates [3]. The oxomanganates showing a quantum tunneling effect consist of mixed-valent manganese(II) and (IV) ions [2]. We have found a novel μ-bromocuprate containing both copper(I) and (II) ions in the course of our studies on organic–inorganic hybrid magnets, while only copper(I) halides have been known to aggregate to give a variety of structures (cubane- [4], adamantane- [5], step-like structures [6], for instance). A few examples of one-dimensional copper(I)–copper(II) complexes with halide bridges were reported [7] and detailed investigation on the geometry around the copper ions afforded the information of the valency. We report here the molecular structure and magnetic properties of a hybrid cluster consisting of four copper(I) and four copper(II) ions, 12 bromide ions, and two ligands with two radical groups each.

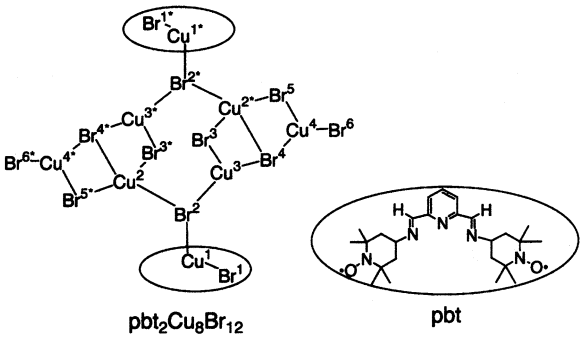

2. Experimental

2.1. Synthesis of pbt

The organic moiety, pyridine-2,6-diylbis(methyleneamino-TEMPO) (abbreviated as pbt hereafter), was easily prepared according to the method previously reported (TEMPO = 2,2,6,6-tetramethylpiperidin-1-

* Corresponding author. Tel.: +81-424-43 5490; fax: +81-424-43 5501.
E-mail address: ishi@pc.uec.ac.jp (T. Ishida).

0020-1693/02/$ - see front matter
PII: S0020-1693(01)00795-2

yloxyl) [8]. An ethanol solution (10 ml) containing 2,6-diformylpyridine (1.35 g, 1.0×10^{-2} mol) and 4-amino-TEMPO (3.98 g, 2.3×10^{-2} mol) was refluxed under N_2 for 12 h. After the solution was concentrated under reduced pressure, the resultant crystals of pbt were collected on a filter (yield: 68%, red needles, m.p. 203–205 °C from CH_2Cl_2/EtOH). ESR spectrum of pbt exhibited a 1:1:1 triplet pattern with $g = 2.0061$ and $a_N = 15.5$ G in benzene at room temperature (r.t.).

2.2. Synthesis of $pbt_2Cu_8Br_{12}$

A methanol solution (15 ml) containing pbt (80 mg, 1.8×10^{-4} mol) and 2.5 equiv. of $CuBr_2$ (100 mg, 4.5×10^{-4} mol) was allowed to stand at r.t. for 24 h, giving brown needles of $pbt_2Cu_8Br_{12}\cdot 2H_2O$ (45 mg, yield: 21% from pbt), which were suitable for X-ray diffraction and magnetic studies. *Anal.* Calc. for $C_{50}H_{82}Br_{12}Cu_8N_{10}O_6$: C, 25.9; N, 5.9; H, 3.6. Found: C, 25.8; N, 5.4; H, 3.7%. The elemental analysis agrees with the formula determined by X-ray crystal structure analysis.

2.3. X-ray crystal structure analysis

X-ray diffraction data of $pbt_2Cu_8Br_{12}\cdot 2H_2O$ were collected in a Rigaku R-axis IP diffractometer with a graphite-monochromated Mo Kα radiation at 100 K. Numerical absorption correction was applied. The structure was solved with the direct method in the SIR92 program [9] and the atomic coordinates and thermal displacement parameters (excluding coordinates and parameters of hydrogen atoms) were refined by a full-matrix least-squares method on the TEXSAN program [10]. All the unique reflection data were used. A significant residual electron density in the difference map was assigned to a water molecule and the refinement was much improved. Final residual densities were found near bromide anions. Hydrogen atoms in pbt were placed in calculated positions. Selected crystallographic data are summarized in Table 1.

2.4. Magnetic measurements

Magnetic susceptibilities were measured in a Quantum Design MPMS SQUID magnetometer at 5 kOe in a temperature range down to 1.8 K. The magnetic responses were corrected with diamagnetic blank data of the sample holder obtained separately. The diamagnetic contribution of sample itself was estimated from Pascal's constants.

3. Results and discussion

3.1. Molecular structures

As Fig. 1 shows, the centrosymmetric molecule consists of a Cu_6Br_{10} cluster sandwiched with two

Table 1
Crystal data and structure refinement parameters for $pbt_2Cu_8Br_{12}\cdot 2H_2O$

Empirical formula	$C_{50}H_{82}Br_{12}Cu_8N_{10}O_6$
Habit	brown needle
Dimension (mm)	$0.25 \times 0.10 \times 0.08$
λ (Å)	0.71069
T (K)	100
Crystal system	triclinic
Space group	$P\bar{1}$
Unit cell dimensions	
a (Å)	12.961(2)
b (Å)	16.545(3)
c (Å)	9.392(1)
α (°)	99.697(9)
β (°)	97.774(6)
γ (°)	71.761(6)
V (Å^3)	1878.2(6)
Z	1
D_{calc} (g cm^{-3})	2.110
μ (mm^{-1})	8.669
Observed reflections	23 530
Unique reflections	7494
R_{int}	0.062
Data/parameter ratio	19.26
$R(F)$ [a] ($I > 2.0\sigma(I)$)	0.0642
$R_w(F^2)$ [b] (all data)	0.1884
Goodness-of-fit	1.461

[a] $R = \Sigma||F_o| - |F_c||/\Sigma|F_o|$.
[b] $R_w = [\Sigma w(F_o^2 - F_c^2)^2/\Sigma w(F_c^2)^2]^{1/2}$.

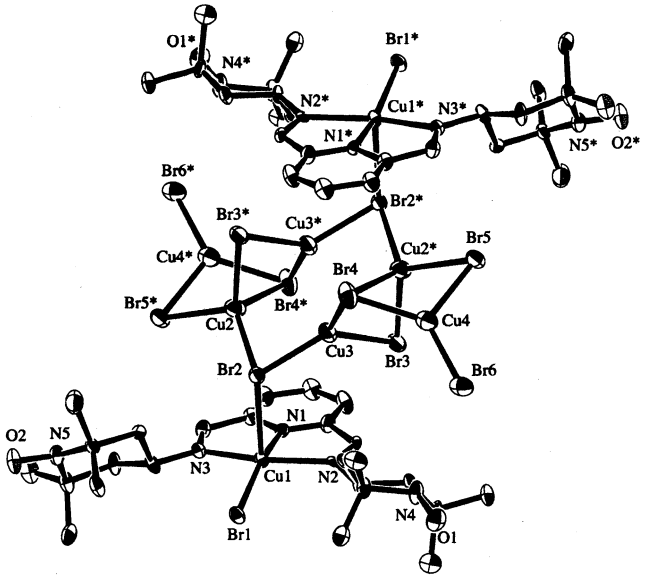

Fig. 1. Molecular structure of $pbt_2Cu_8Br_{12}$ with thermal ellipsoids at the 50% level. Crystal solvent molecules (H_2O) and hydrogen atoms are omitted for the sake of clarity. Selected atomic numbering is also shown. Asterisks denote a symmetry code of $1-x$, $1-y$, $2-z$.

Table 2
Selected bond lengths (Å) and bond angles (°) for $pbt_2Cu_8Br_{12}\cdot 2H_2O$

Bond lengths	
Br1–Cu1	2.334(1)
Br2–Cu1	2.780(2)
N1–Cu1	1.937(8)
N2–Cu1	2.091(7)
N3–Cu1	2.088(8)
Br2–Cu2	2.411(2)
Br3*–Cu2	2.446(2)
Br4*–Cu2	2.734(2)
Br5*–Cu2	2.470(2)
Br2–Cu3	2.373(2)
Br3–Cu3	2.381(2)
Br4–Cu3	2.452(2)
Br4–Cu4	2.383(2)
Br5–Cu4	2.433(2)
Br6–Cu4	2.337(2)
Cu2···Cu3*	2.764(2)
Cu2···Cu4*	2.691(2)
Cu3···Br3*	3.780(2)
Cu3···Br4*	4.031(2)
Bond angles	
Br1–Cu1–Br2	104.24(5)
Br1–Cu1–N1	162.4(2)
Br1–Cu1–N2	101.1(2)
Br1–Cu1–N3	99.0(2)
Br2–Cu1–N1	93.3(2)
Br2–Cu1–N2	90.8(2)
Br2–Cu1–N3	95.0(2)
N1–Cu1–N2	79.1(3)
N1–Cu1–N3	78.3(3)
N2–Cu1–N3	157.0(3)
Br2–Cu2–Br3*	112.28(7)
Br2–Cu2–Br4*	120.20(7)
Br2–Cu2–Br5*	113.52(6)
Br3*–Cu2–Br4*	98.72(6)
Br3*–Cu2–Br5*	112.80(7)
Br4*–Cu2–Br5*	97.89(6)
Br2–Cu3–Br3	128.90(7)
Br2–Cu3–Br4	117.64(6)
Br3–Cu3–Br4	109.03(6)
Br4–Cu4–Br5	109.33(7)
Br4–Cu4–Br6	130.51(7)
Br5–Cu4–Br6	119.50(7)

*, the symmetry operation code: $1-x$, $1-y$, $2-z$.

pbt·CuBr complexes. The coordination geometry of Cu1 is a tetragonal-pyramid. A tridentate pbt is coordinated at three equatorial positions of Cu1 and the π-conjugation moiety in pbt is highly planar. The geometrical parameters of the TEMPO moieties are normal [11]. The nitroxide groups do not act as ligands and consequently magnetically isolated within a molecule. Br1 and Br2 are coordinated at equatorial and axial positions with the bond lengths of 2.334(1) and 2.780(2) Å, respectively (Table 2).

We can find a Cu–Br alternating eight-membered ring in the center of the molecule. The coordination sphere of Cu2 can be regarded to be tetrahedral surrounded with four Br ions; the angles of Br2–Cu2–Br5*, Br2–Cu2–Br3*, and Br3*–Cu2–Br5* are 113.52(6), 112.28(7), and 112.80(7)°, respectively, clearly indicating the pyramidalization of Cu2 (the symmetry operation code of *: $1-x$, $1-y$, $2-z$). The Cu2–Br4* distance (2.734(2) Å) is longer than those of the Cu2–Br2, –Br3*, and –Br5* distances (2.41–2.47 Å). The two four-membered rings, Cu2–Br4*–Cu3*–Br3* and Cu2–Br4*–Cu4*–Br5*, form a butterfly arrangement.

On the other hand, Cu3 and Cu4 seem to have trigonal planar structures, suggested by the Br2–Cu3–Br3, Br2–Cu3–Br4, and Br3–Cu3–Br4 angles of 128.90(7), 117.64(6), and 109.03(6)°, respectively, and Br4–Cu4–Br5, Br4–Cu4–Br6, and Br5–Cu4–Br6 angles of 109.33(7), 130.51(7), and 119.50(7)°, respectively. The Cu–Br bond lengths around Cu3 and Cu4 range from 2.34 to 2.45 Å. The Cu3···Br3* and Cu3···Br4* distances are 3.780(2) and 4.031(2) Å, respectively, which are considerably longer than the bonded Cu–Br distances (see Table 2).

If we ignore the relatively long interatomic distances of Cu1–Br2 and Cu2–Br4*, the molecule can be divided into three portions, a cluster ion $[Cu_6Br_{10}]^{2-}$ and two $[pbt\cdot Cu^{II}Br]^{+}$ complex ions. The $[Cu_6Br_{10}]^{2-}$ ion can be regarded to have fused six-, eight-, and six-membered rings. Hu and Holt reported the structure of $[Cu^{I}_6Br_{10}]^{4-}$ with a similar centrosymmetric tricyclosystem [12]. We can assign the valence of each copper ion in $[Cu_6Br_{10}]^{2-}$ from structural comparison between the two Cu_6Br_{10} ions. Since no pyramidalization takes place in any copper atoms of the $[Cu^{I}_6Br_{10}]^{4-}$ ion [12], Cu3 and Cu4 in $pbt_2Cu_8Br_{12}$ are assigned to be usual three-coordinated copper(I) ions while Cu2 to be a tetrahedral copper(II) ion. Tetrahedral geometries with Jahn–Teller distortion are often found in $Cu^{II}Br_4^{2-}$ [13], which may be related to the local structure around Cu2. The tetragonal-pyramid structure of Cu1 also suggests a dicationic nature of Cu1. Thus, there are four copper(I) and four copper(II) ions in $pbt_2Cu_8Br_{12}$, which is consistent with the neutral molecule as a whole.

Relatively short metal–metal distances are also found in Cu2···Cu3* (2.764(2) Å) and Cu2···Cu4* (2.691(2) Å). However, these distances are longer than those of Cu(I)···Cu(I) in $[Cu_6Br_{10}]^{4-}$ [12], suggesting the presence of a Coulombic repulsion effect rather than any bonding character between copper ions in the present complex. Dancey et al. reported a direct Cu(I)–Cu(II) bond with the distance of 2.445(4) Å [14]. A delocalized mixed-valent Cu(1.5)–Cu(1.5) bond with the bond length of 2.5 Å was characterized for cytochrome *c* oxidase [15]. Therefore, the long distances of Cu2···Cu3* and Cu2···Cu4* in $pbt_2Cu_8Br_{12}$ suggest that there is no metal–metal bond in $pbt_2Cu_8Br_{12}$.

The coordination environment of Cu(II) in the pbt·CuBr moiety is quite different from those of Cu(I)

in the bromocuprate cluster, and accordingly this relation belongs to the class I system according to the Robin and Day criterion [16]. Although no direct Cu(I)···Cu(II) bond was observed in the bromocuprate cluster, possibility of electron delocalization through a bromide bridge is not wholly eliminated, since the elongation of the Cu2–Br4* bond implies that the coordination sphere of Cu2 is an intermediate between trigonal planar and tetragonal structures. The mixed-valency in the $[Cu_6Br_{10}]^{2-}$ moiety may be described as a class II system.

Fig. 2 shows the molecular arrangement of $pbt_2Cu_8Br_{12}$ in the crystal. There is only one centrosymmetric molecule in the triclinic cell. The pbt·CuBr moieties are located in a parallel and side-by-side manner. Intermolecular distances between nitroxide groups are relatively short, as indicated with dotted lines in Fig. 2. The O1···O2# distance is 4.37(1) Å (the symmetry code of #: $1+x$, y, $-1+z$).

3.2. Magnetic properties

We measured magnetic susceptibility of $pbt_2Cu_8Br_{12}\cdot 2H_2O$ at 5 kOe on a SQUID magnetometer. As Fig. 3 shows, the $\chi_{mol}T$ value at 300 K is 3.4 $cm^3\,K\,mol^{-1}$, supporting the presence of eight paramagnetic $S=1/2$ spins in a molecule. The Curie constant (C) and Weiss temperature (θ) were obtained to be 3.67 $cm^3\,K\,mol^{-1}$ and -24 K, respectively, from the Curie–Weiss equation [$\chi_{mol}=C/(T-\theta)$], but the fit is rather unsatisfactory. The decrease of $\chi_{mol}T$ in a low temperature region indicates that antiferromagnetic interactions are dominantly operative.

Intramolecular magnetic interaction of a TEMPO moiety seems negligible because of the long distances. Actually, the 1:1:1 triplet hyperfine structure was observed in the ESR spectrum of pbt, indicating that two nitroxide spins are magnetically isolated. On the other hand, a rather short intermolecular distance between

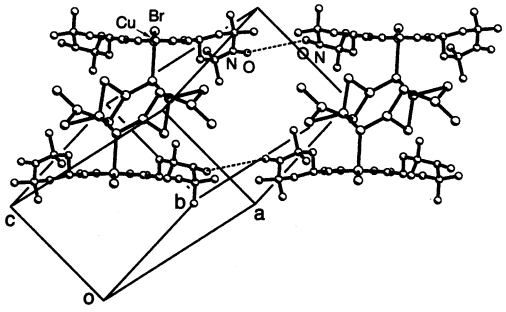

Fig. 2. Molecular arrangement of $pbt_2Cu_8Br_{12}$ in the crystal of $pbt_2Cu_8Br_{12}\cdot 2H_2O$. Hydrogen atoms are omitted for the sake of clarity. Relatively short intermolecular atomic distances between NO groups are shown with dotted lines.

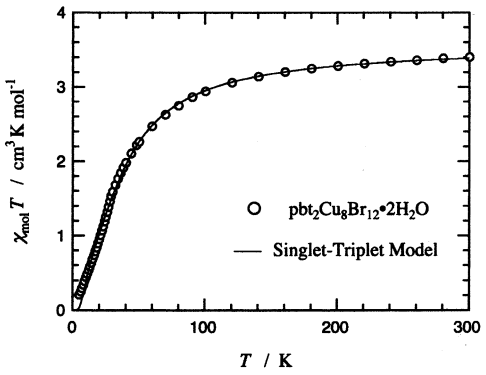

Fig. 3. Temperature dependence of the product of magnetic susceptibility and temperature ($\chi_{mol}T$) for $pbt_2Cu_8Br_{12}\cdot 2H_2O$. Best fit to the combined singlet–triplet model is shown with a solid line. For the equation and optimized parameters, see the text.

nitroxide groups is found. Two TEMPO radicals are regarded to form a dimer with antiferromagnetic coupling. In addition, magnetic interaction in $Cu1^{II}$–Br2–$Cu2^{II}$ should also be antiferromagnetic because the $\chi_{mol}T$ value approaches to zero with decreasing temperature. The magnetic data are fit to a combined equation from two singlet–triplet models [17]; one is defined between two nitroxide spins in an intermolecular fashion, and the other between two copper(II) spins within a molecule. We obtained $2J/k_B=-25.6\pm0.6$ K with $g=2.0$ (fixed) for organic spins and $2J/k_B=-85\pm2$ K with $g=2.35\pm0.01$ for copper(II) spins. The calculated curve is superposed in Fig. 3, and reproduces the experimental data well.

4. Conclusions

The novel organic–inorganic hybrid paramagnetic molecule, $pbt_2Cu_8Br_{12}$, has been prepared, which possess a mixed-valent $Cu^{I}_4Cu^{II}_4$ cluster bridged by bromide anions. We used $CuBr_2$ for the preparation of $pbt_2Cu_8Br_{12}\cdot 2H_2O$. The copper(I) ions in $pbt_2Cu_8Br_{12}$ are supposed to be formed by reduction of copper(II) ions with the TEMPO radicals, viewing from the redox potentials of TEMPO derivatives [18]. Among various TEMPO-mediated oxidation reactions Semmelhack et al. exploited a catalytic cycle of oxidation of alcohols involving a redox reaction of TEMPO and copper(II) as a key step [19]. In the present system an appreciable part of pbt works as a reducing agent in the complexation step, being responsible for the low yield of $pbt_2Cu_8Br_{12}\cdot 2H_2O$. The crystal structure analysis revealed the nano-sized self-assemblage of an organic–inorganic–organic sandwich-type hybrid. This work may cultivate a new architecture for molecule-based magnetic materials using polybromometalate frameworks.

5. Supplementary material

Crystallographic data for the structural analysis have been deposited with the Cambridge Crystallographic Data Centre, CCDC No. 159479 for $pbt_2Cu_8Br_{12}\cdot 2H_2O$. Copies of this information may be obtained free of charge from The Director, CCDC, 12 Union Road, Cambridge, CB2 1EZ, UK (fax: +44-1223-336-033; e-mail: deposit@ccdc.cam.ac.uk or www: http://www.ccdc.cam.ac.uk).

Acknowledgements

This work was partially supported by Grants-in-Aid for Scientific Research on Priority Areas of 'Molecular Conductors and Magnets' (No. 730/11224204) and Scientific Research (C) (No. 13640575) from the Ministry of Education, Culture, Sports, Science and Technology, Japan.

References

[1] D. Gatteschi, A. Caneschi, L. Pardi, R. Sessoli, Science 265 (1994) 1054.
[2] J. Yoo, E.K. Brechin, A. Yamaguchi, M. Nakano, J.C. Huffman, A.L. Maniero, L.C. Brunel, K. Awaga, H. Ishimoto, G. Christou, D.N. Hendrickson, Inorg. Chem. 39 (2000) 3615 (and references therein).
[3] (a) Z.-J. Zhong, H. Seino, Y. Mizobe, M. Hidai, A. Fujishima, S.-i. Ohkoshi, K. Hashimoto, J. Am. Chem. Soc. 122 (2000) 2952;
(b) J. Larionova, M. Gross, M. Pilkington, H. Andres, H. Stoeckli-Evans, H.U. Gudel, S. Decurtins, Angew. Chem., Int. Ed. Engl. 39 (2000) 1605.
[4] (a) J.C. Dyason, P.C. Healy, J. Chem. Soc., Dalton Trans. (1985) 831;
(b) H. Oshio, T. Ito, ACS Symp. Ser. 644 (1996) 266.
[5] S. Andersson, S. Jagner, Acta Chem. Scand., Part A 40 (1986) 210.
[6] A. Camus, G. Nardin, L. Randaccio, Inorg. Chim. Acta 12 (1975) 23.
[7] (a) R.D. Willett, Inorg. Chem. 26 (1987) 3423;
(b) B. Scott, R. Willet, L. Porter, J. Williams, Inorg. Chem. 31 (1992) 2483.
[8] (a) T. Nogami, T. Ishida, M. Yasui, F. Iwasaki, N. Takeda, M. Ishikawa, T. Kawakami, K. Yamaguchi, Bull. Chem. Soc. Jpn. 69 (1996) 1841;
(b) K. Togashi, R. Imachi, K. Tomioka, H. Tsuboi, T. Ishida, T. Nogami, N. Takeda, M. Ishikawa, Bull. Chem. Soc. Jpn. 69 (1996) 2821.
[9] A. Altomare, M.C. Burla, M. Camalli, M. Cascarano, C. Giacovazzo, A. Guagliardi, G. Polidori, J. Appl. Crystallogr. 27 (1994) 435.
[10] Single Crystal Structure Analysis Software Version 1.10, Molecular Structure Corporation, 3200 Research Forest Drive, The Woodlands, TX 77381, USA.
[11] (a) F. Iwasaki, J.H. Yoshikawa, H. Yamamoto, E. Kan-nari, K. Takada, M. Yasui, T. Ishida, T. Nogami, Acta Crystallogr., Sect. B 55 (1999) 231;
(b) F. Iwasaki, J.H. Yoshikawa, H. Yamamoto, K. Takada, E. Kan-nari, M. Yasui, T. Ishida, T. Nogami, Acta Crystallogr., Sect. B 55 (1999) 1057.
[12] G. Hu, E.M. Holt, Acta Crystallogr., Sect. C 50 (1994) 1890.
[13] K. Waizumi, H. Masuda, H. Einaga, N. Fukushima, Chem. Lett. (1993) 1145 (and references therein).
[14] K.P. Dancey, P.A. Tasker, R. Price, W.E. Hatfield, D. Brower, J. Chem. Soc., Chem. Commun. (1980) 1248.
[15] N.J. Blackburn, S. de Vries, M.E. Barr, R.P. Houser, W.B. Tolman, D. Sanders, J.A. Fee, J. Am. Chem. Soc. 119 (1997) 6135.
[16] M.B. Robin, P. Day, Adv. Inorg. Chem. Radiochem. 10 (1967) 248.
[17] B. Bleaney, K.D. Bowers, Proc. R. Soc. Lond., Ser. A 214 (1952) 451.
[18] J.R. Fish, S.G. Swarts, M.D. Sevilla, T. Malinski, J. Phys. Chem. 92 (1988) 3745.
[19] (a) M.F. Semmelhack, C.R. Schmidt, D.A. Cortés, C.S. Chou, J. Am. Chem. Soc. 106 (1984) 3374;
(b) B. Betzemeier, M. Cavazzini, S. Quici, P. Knochel, Tetrahedron Lett. 41 (2000) 4343.

Low-Temperature Heat Capacity and One-Dimensional Ferromagnetic Behavior of the Organic Free Radical 4-Benzylideneamino-2,2,6,6-tetramethylpiperidin-1-oxyl (BATMP)[#]

Takeshi Sakakibara,[†] Yuji Miyazaki,[†] Takayuki Ishida,[§] Takashi Nogami,[§] and Michio Sorai*,[†]

Research Center for Molecular Thermodynamics, Graduate School of Science, Osaka University, Toyonaka, Osaka 560-0043, Japan, and Department of Applied Physics and Chemistry, The University of Electro-Communications, Chofugaoka, Chofu, Tokyo 182-8585, Japan

Received: March 6, 2002

Heat capacities of the organic free radical ferromagnet 4-benzylideneamino-2,2,6,6-tetramethylpiperidin-1-oxyl (BATMP) crystal were measured in the temperature range between 0.1 and 300 K by adiabatic calorimetry. A ferromagnetic phase transition was found at $T_C = 0.19$ K, and a broad heat-capacity anomaly was found arising from the short-range ordering above T_C characteristic of low-dimensional magnetic spin systems. The enthalpy and entropy gains due to both the magnetic phase transition and the heat-capacity anomaly were evaluated to be $\Delta H = 3.86$ J mol^{-1} and $\Delta S = 5.64$ J K^{-1} mol^{-1}, respectively. The value of the experimental magnetic entropy agrees well with the theoretical value R ln 2 (5.76 J K^{-1} mol^{-1}) expected for a spin quantum number $S = {}^1/_2$ spin system (R is the gas constant). The magnetic heat capacity hump due to the short-range order was well accounted for in terms of an $S = {}^1/_2$ one-dimensional ferromagnetic Heisenberg model with the intrachain exchange interaction $J/k_B = 0.95$ K (k_B is Boltzmann's constant). This fact suggests that BATMP crystal is a one-dimensional ferromagnet above T_C. The spin wave analysis of the magnetic heat capacities below T_C revealed that BATMP crystal is in a three-dimensional ferromagnetic state below T_C and the averaged interchain exchange interaction is $J'/k_B = 0.026$ K.

1. Introduction

Development and research on purely organic ferromagnets have been one of the subjects attracting many organic and physical chemists and chemical physicists,[1−7] because one can easily design a variety of molecular and crystal structures in comparison to ordinary magnets such as metals and metal oxides. Furthermore, because most organic magnetic molecules indicate very small magnetic anisotropy, they can be regarded as ideal Heisenberg spin systems, which lead to interesting quantum spin systems. Despite tiny magnetic anisotropy, most organic magnetic crystals exhibit low-dimensional magnetic properties owing to structural anisotropy of constituent molecules.

A class of organic free radicals with 2,2,6,6-tetramethylpiperidin-1-oxyl (TEMPO for short) are typical organic magnets. TEMPO radicals are known to manifest a variety of magnetism by changing the substituent group of TEMPO. Up to now, many TEMPO derivatives have been synthesized and investigated.[8−10]

The TEMPO radical treated here, 4-benzylideneamino-2,2,6,6-tetramethylpiperidin-1-oxyl (abbreviated as BATMP and illustrated in Figure 1), is one of the ferromagnetic TEMPO derivatives. Magnetic measurements of the polycrystalline sample[10c,10d,10f] revealed that BATMP crystal has a positive paramagnetic Curie temperature ($\theta = 0.7$ K) and exhibits a ferromagnetic phase transition at $T_C = 0.18$ K below which a magnetic hysteresis occurs. On the basis of the magnetic susceptibilities above T_C,[10c] the intermolecular exchange interaction parameter was estimated to be $J/k_B = 0.87$ K by the spin quantum number $S = {}^1/_2$ Heisenberg linear chain model and $J/k_B = 2.2$ K by the singlet−triplet model, where k_B denotes Boltzmann's constant. Zero-field muon spin rotation/relaxation/resonance (μSR)[11] indicated that BATMP crystal is a three-dimensional Heisenberg ferromagnet below $T_C = 0.17$ K. X-ray structural analysis and theoretical calculation[10d,12] predicted that BATMP crystal would have a two-dimensional ferromagnetic structure parallel to the *bc* plane.

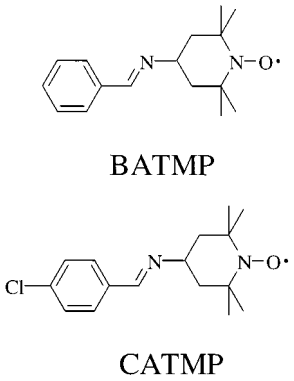

Figure 1. Molecular structure of BATMP and CATMP.

Heat capacity measurement as well as magnetic measurement is a useful tool to investigate magnetic substances. From heat capacities of magnetic materials, one can elucidate the precise magnetic phase transition temperature, spin−spin interaction, magnetic dimensionality, and type of magnetism. Our research group has so far revealed interesting magnetisms of some TEMPO derivative crystals by adiabatic calorimetry.[9a,9b,9d,13,14] The aim of the present work is to elucidate the magnetic properties of the BATMP crystal similar to 4-(4-chlorobenzyli-

[#] Contribution No. 63 from the Research Center for Molecular Thermodynamics.

* To whom correspondence should be addressed. Tel: +81-6-6850-5523. Fax: +81-6-6850-5526. E-mail: sorai@chem.sci.osaka-u.ac.jp.

[†] Osaka University.

[§] The University of Electro-Communications.

10.1021/jp020634n CCC: $22.00
Published on Web 06/05/2002

deneamino)-2,2,6,6-tetramethylpiperidin-1-oxyl (CATMP for short).[10f,10g,15]

2. Experimental Section

Synthesis and purification of BATMP crystal were performed according to the reported method.[10a,10b] The result of elemental analysis of the obtained crystal agreed well with the theoretical values. Calcd for BATMP ($C_{16}H_{23}N_2O$): C, 74.09; H, 8.94; N, 10.80. Found: C, 73.94; H, 8.97; N, 10.79.

In the low-temperature region between 0.1 and 10 K, a very-low-temperature adiabatic calorimeter with a ^{3}He/^{4}He dilution refrigerator[16] was employed, while from 5 to 300 K, an adiabatic microcalorimeter[17] was used. For the very-low-temperature adiabatic calorimeter, 1.254 09 g of the polycrystalline sample was formed into a pellet with a 2 cm diameter and ~2 mm thickness. The pellet was loaded in a gold-plated copper holder with direct thermal contact. For the adiabatic microcalorimeter, 1.341 45 g of the polycrystalline sample was loaded into a gold-plated copper container together with helium gas at ambient pressure to aid thermal equilibration. The true sample masses were derived from buoyancy correction with the sample density, 1.127 g cm^{-3}.[10d]

3. Results and Discussion

A. Heat Capacity. Molar heat capacities at constant pressure, C_p, of BATMP crystal are listed in Table 1 and plotted against temperature, T, in Figure 2. A distinct heat capacity peak due to the ferromagnetic phase transition was observed at $T_C = 0.19$ K, which coincides well with $T_C = 0.18$ K by the magnetic susceptibility measurement[10d,10f] and $T_C = 0.17$ K by the μSR measurement.[11] Furthermore, a heat capacity hump was found in the temperature region centered around 1 K. This thermal anomaly can be regarded as a short-range ordering effect of spins characteristic of low-dimensional magnets.

B. Determination of Lattice and Magnetic Heat Capacities. In general, heat capacities of magnetic substances consist of lattice heat capacities and magnetic heat capacities. We estimated the magnetic heat capacities of BATMP crystal by determining the lattice heat capacity curve and then by subtracting it from the total heat capacities. The observed heat capacities above the magnetic transition temperature can be expressed by the sum of the lattice heat capacities, C_p(lattice), and the magnetic heat capacities due to the short-range order, C_p(short-range). At low temperatures, C_p(lattice) can be approximated by a temperature polynomial with cubic and higher odd powers, while C_p(short-range) may be expressed by a term proportional to T^{-2}.[18] Hence, the total heat capacities, C_p, are given by

$$C_p = C_p(\text{lattice}) + C_p(\text{short-range}) = \sum_{i=1}^{n} c_i T^{2i+1} + c_{n+1} T^{-2} \quad (1)$$

In the present study, we could fit quite well the heat capacity data from 3 to 10 K to eq 1 with $n = 3$: $c_1 = 5.134 \times 10^{-3}$ J K^{-4} mol^{-1}, $c_2 = 2.482 \times 10^{-5}$ J K^{-6} mol^{-1}, $c_3 = -2.391 \times 10^{-7}$ J K^{-8} mol^{-1}, and $c_4 = 3.407$ J K mol^{-1}. The obtained lattice heat capacity curve is shown in Figure 2a by a solid curve.

The excess heat capacities, ΔC_p, arising from the magnetic effect were evaluated by subtraction of the lattice heat capacity from the observed one. Figure 3 shows the plot of ΔC_p against T.

C. Magnetic Enthalpy and Entropy. The magnetic enthalpy and entropy were estimated to be $\Delta H = 3.86$ J mol^{-1} and $\Delta S = 5.64$ J K^{-1} mol^{-1} by integration of the following heat capacities with respect to T and ln T, respectively: (i) spin wave heat capacity below 0.1 K, which will be described later, (ii) the observed magnetic heat capacities between 0.1 and 6.5 K, and (iii) the T^{-2} term in eq 1 from 6.5 K to infinite temperature. This magnetic entropy agrees well with the expected value R ln 2 (5.76 J K^{-1} mol^{-1}) for the magnetic systems with $S = {}^1/_2$ spins, where R is the gas constant. This fact reveals that the present sample really consists of pure organic radical molecules with $S = {}^1/_2$ electron spins.

D. Magnetic Properties. Above T_C, the heat capacity exhibits a remarkable hump centered around 1 K arising from the short-range order of spins characteristic of low-dimensional magnetic systems. In the previous calorimetric study[14] for CATMP crystal having a two-dimensional layer structure,[10g] we revealed that the observed heat capacity anomaly due to the short-range order is reproduced well by the $S = {}^1/_2$ two-dimensional ferromagnetic Heisenberg model of square lattice with the intralayer exchange interaction, $J/k_B = 0.42$ K, where the spin Hamiltonian $H = -2JS_iS_j$ is adopted. Because BATMP crystal has been reported to possess a two-dimensional layer structure[10d] similar to CATMP crystal, one may expect that BATMP crystal would have a two-dimensional magnetic structure. In reality, however, we obtained the result that the magnetic heat capacities between 1 and 5 K are reproduced well by the $S = {}^1/_2$ one-dimensional ferromagnetic Heisenberg model[19] with the intrachain exchange interaction $J/k_B = 0.95$ K rather than by a two-dimensional ferromagnetic Heisenberg model of square lattice. The Padé approximation was used to fit the magnetic heat capacities to the model. The theoretical heat capacity curve thus estimated is drawn in Figure 3 by a solid curve. The present intrachain exchange interaction agrees well with $J/k_B = 0.87$ K estimated by the magnetic susceptibility measurement.[10c]

Next, we discuss the temperature dependence of the magnetic heat capacity below T_C. Magnetic heat capacities of magnetic substances at very low temperatures are generally approximated by the spin wave theory. The heat capacity due to the spin wave (magnon) excitation is proportional to $T^{d/n}$,[20] where d stands for the dimensionality of the magnetic lattice and n is defined as the exponent in the dispersion relation: $n = 1$ for antiferromagnets and $n = 2$ for ferromagnets. To elucidate the nature of the magnetic ordering structure below T_C, we first fitted the following equation to four points of the magnetic heat capacity data at the lowest measurement temperatures:

$$\Delta C_p = aT^{\alpha} \quad (2)$$

The power index α of T was thus estimated to be 1.69. This value is close to ${}^3/_2$, indicating that BATMP crystal is a three-dimensional ferromagnet below T_C. Therefore, we once more fitted eq 2 with $\alpha = {}^3/_2$ to the same data points to yield $a = 51.5$ J K$^{-5/2}$ mol^{-1}. The spin wave heat capacity thus determined is represented in Figure 3 by a broken curve.

Finally, to estimate the value of the interchain exchange interaction, we compared eq 2 with the estimated parameters with the following spin wave heat capacity in three-dimensional ferromagnets possessing nonequivalent spin−spin interaction paths:[13,14]

$$C_{SW} = \frac{5R\zeta({}^5/_2)\Gamma({}^5/_2)}{16\pi^2 S^{3/2}}\left(\frac{k_B{}^3}{2J_1J_2J_3}\right)^{1/2} T^{3/2} \quad (3)$$

where J_1, J_2, and J_3 are the positive exchange interaction parameters for three directions, ζ is Riemann's zeta function,

TABLE 1: Molar Heat Capacities of BATMP Crystal (M = 295.37 g mol^{-1})[a]

T, K	C_p, J K^{-1} mol^{-1}	T, K	C_p, J K^{-1} mol^{-1}	T, K	C_p, J K^{-1} mol^{-1}	T, K	C_p, J K^{-1} mol^{-1}	T, K	C_p, J K^{-1} mol^{-1}
series 1		0.473	1.318	4.335	0.6327	143.27	189.2	10.79	6.557
0.154	2.229	0.504	1.261	4.758	0.7388	145.30	191.5	11.48	7.594
0.163	2.331	0.550	1.241	5.214	0.8883	147.33	193.6	12.20	8.785
0.173	2.930	0.614	1.200	5.609	1.175	149.36	195.9	12.89	9.952
0.186	3.599	0.681	1.183	6.092	1.471	151.89	198.8	13.56	10.83
0.201	2.785	0.755	1.157	6.515	1.681	154.91	202.1	14.23	12.12
0.212	2.416	0.835	1.143	6.919	2.049	157.93	205.3	14.94	13.61
0.233	2.222			7.497	2.589	160.95	208.6	15.64	14.66
0.261	1.864	series 6		8.185	3.278	163.97	212.0	16.39	16.03
0.290	1.667	0.185	3.504	8.923	4.138	167.00	215.3	17.15	17.36
0.321	1.533	0.196	2.848	9.723	4.910	170.02	218.5	17.93	18.94
0.353	1.495	0.209	2.689			173.05	221.6	18.71	20.56
0.395	1.378	0.225	2.226	series 9		176.07	225.0	19.51	22.12
0.452	1.286	0.240	2.118	1.173	1.030	179.09	228.4	20.35	23.42
0.517	1.254	0.258	1.939	1.327	0.9567	182.12	231.6	21.25	25.35
0.585	1.205	0.274	1.813	1.510	0.8912	185.15	234.8	22.22	27.30
0.660	1.171	0.292	1.722	1.702	0.8231	188.17	238.0	23.26	29.16
0.735	1.160	0.312	1.655	1.921	0.7643	191.20	241.4	24.49	31.44
0.818	1.130	0.334	1.536	2.164	0.6814	194.23	244.7	25.84	34.02
0.909	1.098	0.361	1.467	2.460	0.5934	197.25	247.8	27.20	36.37
1.002	1.086	0.394	1.389	2.750	0.5334	200.28	251.2	28.58	38.88
1.139	1.031	0.427	1.342	3.072	0.5099	203.31	254.4	29.96	41.51
1.274	0.9746	0.463	1.303	3.389	0.5103	206.34	257.5	31.38	43.51
1.442	0.9156	0.500	1.256	3.734	0.5301	209.37	260.9	32.79	46.04
1.662	0.8096			4.103	0.5906	212.40	264.1	34.20	48.57
1.882	0.7352	series 7		4.507	0.6616	215.43	267.0	35.62	50.70
		0.169	2.867	4.940	0.7968	218.45	270.1	37.05	52.95
series 2		0.178	3.247	5.408	0.9670	221.48	273.5	38.48	55.34
0.254	1.816	0.188	3.279	5.891	1.219	224.51	276.9	39.92	57.56
0.285	1.778	0.199	2.881	6.428	1.573	227.53	280.2	41.37	60.19
0.317	1.629	0.214	2.581	7.045	2.013	230.56	283.3	42.82	62.12
0.352	1.511	0.231	2.249	7.713	2.595	233.59	286.6	44.28	64.22
0.389	1.445	0.248	1.928	8.434	3.325	236.61	289.8	45.74	66.54
0.426	1.350	0.274	1.825	9.214	4.225	239.64	292.9	47.20	68.26
0.463	1.283	0.310	1.644	10.06	4.980	242.66	296.1	48.67	70.35
0.501	1.251	0.351	1.513			245.69	299.6	50.14	72.69
0.541	1.256	0.395	1.402	series 10		248.71	303.2	51.85	75.02
0.602	1.184	0.443	1.323	80.81	113.6	251.74	306.2	53.78	77.92
0.678	1.174	0.495	1.265	82.74	115.8	254.76	309.5	55.71	80.66
		0.534	1.274	84.74	118.4	257.79	313.0	57.66	83.27
series 3		0.586	1.198	86.74	121.2	260.81	316.4	59.60	85.87
0.147	2.023	0.651	1.172	88.74	123.8	263.83	319.9	61.56	88.55
0.164	2.508	0.719	1.155	90.74	126.3	266.86	323.2	63.52	91.04
0.179	3.226	0.772	1.135	92.75	128.9	269.88	326.2	65.48	93.78
0.188	3.128	0.845	1.125	94.76	131.5	272.90	329.6	67.44	96.48
0.196	3.084	0.947	1.090	96.76	133.9	275.90	333.9	69.41	98.69
0.211	2.516	1.056	1.052	98.77	136.6	278.89	337.6	71.38	101.4
0.223	2.331	1.171	1.020	100.79	139.4	281.89	341.0	73.36	103.9
0.241	2.094	1.308	0.9616	102.80	141.8	284.88	344.6	75.33	106.5
0.290	1.752	1.470	0.8934	104.81	144.4	287.88	348.0	77.31	109.1
0.343	1.508	1.647	0.8127	106.83	147.0	290.87	351.6	79.30	111.8
		1.921	0.7075	108.85	149.4	293.87	354.8	81.28	114.3
series 4				110.86	151.9	296.86	357.9	83.26	117.0
0.227	2.329	series 8		112.88	154.3	299.86	362.1	85.25	119.8
0.248	1.967	0.954	1.123	114.90	156.5			87.24	122.3
0.272	1.787	1.100	1.074	116.93	159.0	series 11		89.23	125.0
0.297	1.620	1.241	1.014	118.95	161.4	5.475	1.040	91.23	127.5
		1.395	0.9724	120.97	163.9	5.649	1.195	93.22	130.1
series 5		1.572	0.8807	122.99	166.4	5.901	1.315	95.21	132.6
0.243	2.000	1.723	0.8126	125.02	168.5	6.244	1.474	97.21	135.4
0.265	1.870	1.884	0.7653	127.04	170.7	6.622	1.649	99.21	137.6
0.289	1.698	2.083	0.6868	129.07	173.1	7.056	2.062		
0.313	1.639	2.338	0.6104	131.10	175.3	7.518	2.566		
0.336	1.547	2.624	0.5720	133.12	177.5	8.010	3.057		
0.361	1.489	2.923	0.5192	135.15	179.9	8.496	3.526		
0.387	1.463	3.238	0.5079	137.18	182.2	8.982	4.073		
0.416	1.377	3.572	0.5182	139.21	184.5	9.518	4.817		
0.444	1.317	3.940	0.5574	141.24	186.8	10.12	5.587		

[a] Data in series 1−9 and series 10 and 11 were collected by use of different adiabatic calorimeters.

Γ is Euler's gamma function, and S is the spin quantum number. In this case, $J_1 = J = 0.95k_B$ K, $J_2 = J_3 = J'$, which is an averaged interchain exchange interaction, and $S = {}^1/_2$. As a result, comparison of eq 2 with eq 3 yielded $J'/k_B = 0.026$ K.

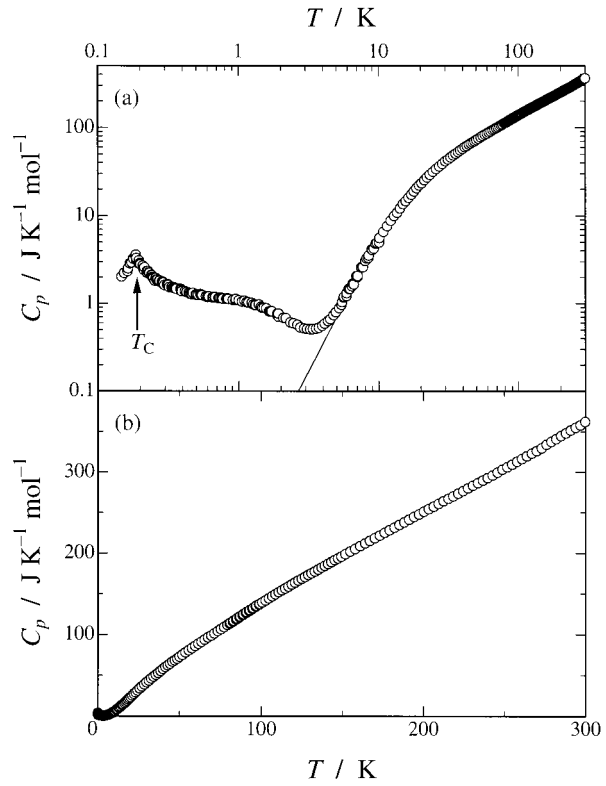

Figure 2. Molar heat capacities of BATMP crystal on (a) logarithmic and (b) normal scales. Solid curve indicates estimated lattice heat capacity.

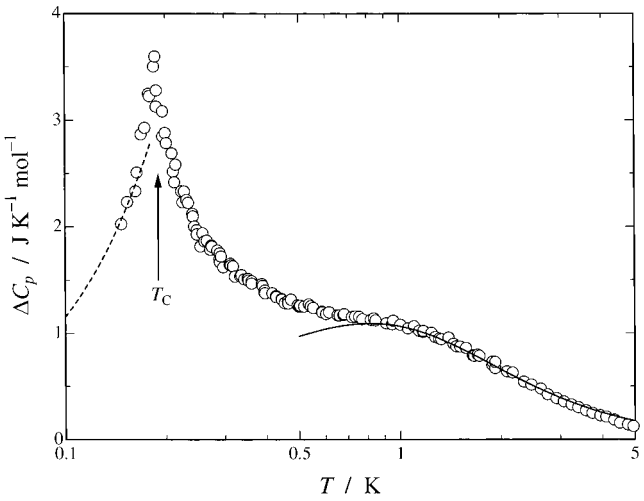

Figure 3. Magnetic heat capacities of BATMP crystal. Solid curve indicates the heat capacity calculated from high-temperature series expansion for $S = {}^1/_2$ one-dimensional ferromagnetic Heisenberg model with $J/k_B = 0.95$ K. Broken curve shows the heat capacity derived from spin wave theory for three-dimensional ferromagnets.

For a possible mechanism of the ferromagnetic interaction working between the N−O radicals of adjacent TEMPO moieties in some TEMPO radical crystals, Nogami et al.[10g,12] proposed the β-hydrogen mechanism that a positive spin on the N−O radical induces negative spins on the β-hydrogen atoms due to an intramolecular spin polarization, such as ON(↑)−C_α(↓)−C_β(↑)−H_β(↓), inducing a positive spin on the N−O sites of the adjacent molecules in turn. They expected two-dimensional magnetic network structures for four ferromagnetic TEMPO derivative crystals Ar−CH=N−TEMPO (Ar = phenyl, 4-(methylthio)phenyl, 4-chlorophenyl, and 4-biphenylyl) on the basis of the distance between the N−O radicals of the adjacent molecules by the X-ray structural analyses.[10d,10e,10g,10j,12] Actually, we revealed that CATMP (Ar = 4-chlorophenyl) crystal exhibits two-dimensional ferromagnetism above T_C by the heat capacity experiment.[14] In the present case, however, we elucidate that BATMP crystal is characterized not by two-dimensional but by one-dimensional magnets. A few possible reasons for that are considered. One is that the magnitude of the exchange interaction between the N−O radicals of the adjacent TEMPO moieties decreases rapidly as the distance between the N−O radicals increases. In CATMP crystal, the O···O distances along the *a* and *c* axes are 5.91 and 5.95 Å, respectively,[10g] which are substantially equal within ∼0.7%. On the other hand, in BATMP crystal, the O···O distances along the *b* and *c* axes are 6.15 and 5.62 Å, respectively,[10d] the difference of which is as large as 9%. In A_2CuX_4 and $A'CuX_4$ compounds (A, A′ are mono- and divalent nonmagnetic cations; X is a halide anion), actually, the magnitude of the exchange interaction between the CuX_4^{2-} ions decreases exponentially as the X···X distance increases.[21] Another possibility is that the paths of the exchange interaction for both crystals are different because of the difference of the crystal structure. CATMP crystal possesses a parallel arrangement of the N−O groups along the *a* axis and a zigzag arrangement of the N−O groups along the *c* axis in the two-dimensional sheet,[10g] whereas BATMP crystal has only a zigzag arrangement of the N−O groups along the *b* and *c* axes.[10d] The difference of the arrangement of the N−O group for both crystals causes the different intermolecular atomic contacts and consequently different magnitudes of exchange interaction on the basis of the β-hydrogen mechanism. In fact, distances of O···H(axial methyl) and O···H(equatorial methyl) are the shortest in the *c* and *a* axis directions, respectively, within a sheet arrangement of BATMP. On the other hand, distances of O···H(methylene) and O···H(equatorial methyl) are shortest in the *b* and *c* axis directions, respectively, for CATMP. The experimental results suggest that one of the two intrasheet exchange interactions in BATMP is negligible above T_C, while both intrasheet interactions are appreciable above T_C for CATMP.

From comparison between eqs 2 and 3, we could estimate the averaged interchain exchange interaction $J'/k_B = 0.026$ K. Because of the difference between the O···O distances along the *a* and *b* axes (11.89 and 6.15 Å, respectively), however, the interchain exchange interactions along the *a* and *b* axes would be rather different. In the case of CATMP crystal, the interchain exchange interaction along the *c* axis was estimated to be $J'/k_B = 0.024$ K,[14] which corresponds to the exchange interaction working between the N−O radicals with the O···O distance of 10.86 Å.[10g] Therefore, the exchange interaction along the *a* axis for BATMP crystal is expected to be smaller than that along the *c* axis for CATMP crystal.

4. Conclusions

Heat capacities of the organic ferromagnet BATMP radical crystal were measured from 0.1 to 300 K by adiabatic calorimetry. A heat capacity peak due to a ferromagnetic phase transition was observed at $T_C = 0.19$ K. Above T_C, a heat capacity hump was also found, which arises from the short-range order of the spins characteristic of low-dimensional magnetic materials. The magnetic enthalpy and entropy were evaluated to be $\Delta H = 3.86$ J mol^{-1} and $\Delta S = 5.64$ J K^{-1} mol^{-1}, respectively. The experimental magnetic entropy is in good agreement with the expected value R ln 2 (5.76 J K^{-1} mol^{-1}) for $S = {}^1/_2$ spin systems. Contrary to the prediction that the BATMP crystal possesses a similar two-dimensional crystal

structure[10d] to that in CATMP crystal,[10g] BATMP crystal exhibits one-dimensional ferromagnetism above T_C. The magnetic heat capacity hump due to the short-range order was reproduced well by the $S = {}^1/_2$ one-dimensional ferromagnetic Heisenberg model with the intrachain exchange interaction $J/k_B = 0.95$ K. The spin wave analysis of the magnetic heat capacities below T_C revealed that the BATMP crystal orders into a three-dimensional ferromagnetic state below T_C and has the averaged interchain exchange interaction $J'/k_B = 0.026$ K.

In this work, we showed that a slight difference of the crystal structures in TEMPO derivative radicals affects their magnetism dramatically. If we measure the heat capacities of 4-(4-methylthiobenzylideneamino)-TEMPO[10j] and 4-(4-phenylbenzylideneamino)-TEMPO[10e] radical crystals, which are isomorphous to the BATMP crystal[10d] and CATMP crystal,[10g] respectively, we would gain a useful clue to elucidate the mechanism of their magnetic dimensionality more clearly.

References and Notes

(1) *Magnetic Molecular Materials*; Gatteschi, D., Kahn, O., Miller, J. S., Palacio, F., Eds.; NATO ASI Series E; Kluwer Academic Publishers: Dordrecht, 1991; Vol. 198.

(2) Kahn, O. *Molecular Magnetism*; Wiley-VCH: New York, 1993.

(3) *Magnetism: A Supramolecular Function*; Kahn, O., Ed.; NATO ASI Series C; Kluwer Academic Publishers: Dordrecht, 1996; Vol. 484.

(4) *Molecular Magnetism: From Molecular Assemblies to the Devices*; Coronado, E., Delhaès, P., Gatteschi, D., Miller, J. S., Eds.; NATO ASI Series E; Kluwer Academic Publishers: Dordrecht, 1996; Vol. 321.

(5) *Molecule-Based Magnetic Materials: Theory, Techniques, and Applications*; Turnbull, M. M., Sugimoto, T., Thompson, L. K., Eds.; ACS Symposium Series 644; American Chemical Society: Washington, DC, 1996.

(6) *Magnetic Properties of Organic Materials*; Lahti, P. M., Ed.; Marcel Dekker: New York, 1999.

(7) *Molecular Magnetism: New Magnetic Materials*; Ito, K., Kinoshita, M., Eds.; Kodansha & Gordon and Breach Science Publishers: Tokyo & Amsterdam, 2000.

(8) Bordeaux, P. D.; Lajzerowicz, J. *Acta Crystallogr. B* **1977**, *33*, 1837.

(9) (a) Sugimoto, H.; Aota, H.; Harada, A.; Morishima, Y.; Kamachi, M.; Mori, W.; Kishita, M.; Ohmae, N.; Nakano, M.; Sorai, M. *Chem. Lett.* **1991**, 2095. (b) Kamachi, M.; Sugimoto, H.; Kajiwara, A.; Harada, A.; Morishima, Y.; Mori, W.; Ohmae, N.; Nakano, M.; Sorai, M.; Kobayashi, T.; Amaya, K. *Mol. Cryst. Liq. Cryst.* **1993**, *232*, 53. (c) Kajiwara, A.; Sugimoto, H.; Kamachi, M. *Bull. Chem. Soc. Jpn.* **1994**, *67*, 2373. (d) Kajiwara, A.; Mori, W.; Sorai, M.; Yamaguchi, K.; Kamachi, M. *Mol. Cryst. Liq. Cryst.* **1995**, *272*, 67.

(10) (a) Ishida, T.; Tomioka, K.; Nogami, T.; Iwamura, H.; Yamaguchi, K.; Mori, W.; Shirota, Y. *Mol. Cryst. Liq. Cryst.* **1993**, *232*, 99. (b) Tomioka, K.; Ishida, T.; Nogami, T.; Iwamura, H. *Chem. Lett.* **1993**, 625. (c) Tomioka, K.; Mitsubori, S.; Ishida, T.; Nogami, T.; Iwamura, H. *Chem. Lett.* **1993**, 1239. (d) Nogami, T.; Tomioka, K.; Ishida, T.; Yoshikawa, H.; Yasui, M.; Iwasaki, F.; Iwamura, H.; Takeda, N.; Ishikawa, M. *Chem. Lett.* **1994**, 29. (e) Ishida, T.; Tsuboi, H.; Nogami, T.; Yoshikawa, H.; Yasui, M.; Iwasaki, F.; Iwamura, H.; Takeda, N.; Ishikawa, M. *Chem. Lett.* **1994**, 919. (f) Nogami, T.; Ishida, T.; Yoshikawa, H.; Yasui, M.; Iwasaki, F.; Iwamura, H.; Takeda, N.; Ishikawa, M. *Synth. Met.* **1995**, *71*, 1813. (g) Nogami, T.; Ishida, T.; Tsuboi, H.; Yoshikawa, H.; Yamamoto, H.; Yasui, M.; Iwasaki, F.; Iwamura, H.; Takeda, N.; Ishikawa, M. *Chem. Lett.* **1995**, 635. (h) Ishida, T.; Tomioka, K.; Nogami, T.; Yoshikawa, H.; Yasui, M.; Iwasaki, F.; Takeda, N.; Ishikawa, M. *Chem. Phys. Lett.* **1995**, *247*, 7. (i) Yasui, M.; Yoshikawa, H.; Yamamoto, H.; Ishida, T.; Nogami, T.; Iwasaki, F. *Mol. Cryst. Liq. Cryst.* **1996**, *279*, 77. (j) Nogami, T.; Ishida, T.; Yasui, M.; Iwasaki, F.; Iwamura, H.; Takeda, N.; Ishikawa, M. *Mol. Cryst. Liq. Cryst.* **1996**, *279*, 97. (k) Togashi, K.; Imachi, R.; Tomioka, K.; Tsuboi, H.; Ishida, T.; Nogami, T.; Takeda, N.; Ishikawa, M. *Bull. Chem. Soc. Jpn.* **1996**, *69*, 2821. (l) Nogami, T.; Imachi, R.; Ishida, T.; Takeda, N.; Ishikawa, M. *Mol. Cryst. Liq. Cryst.* **1997**, *305*, 211. (m) Iwasaki, F.; Yoshikawa, J. H.; Yamamoto, H.; Kan-nari, E.; Takada, K.; Yasui, M.; Ishida, T.; Nogami, T. *Acta Crystallogr. B* **1999**, *55*, 231. (n) Iwasaki, F.; Yoshikawa, J. H.; Yamamoto, H.; Takada, K.; Kan-nari, E.; Yasui, M.; Ishida, T.; Nogami, T. *Acta Crystallogr. B* **1999**, *55*, 1057.

(11) Ishida, T.; Ohira, S.; Ise, T.; Nakayama, K.; Watanabe, I.; Nogami, T.; Nagamine, K. *Chem. Phys. Lett.* **2000**, *330*, 110.

(12) Nogami, T.; Ishida, T.; Yasui, M.; Iwasaki, F.; Takeda, N.; Ishikawa, M.; Kawakami, T.; Yamaguchi, K. *Bull. Chem. Soc. Jpn.* **1996**, *69*, 1841.

(13) Ohmae, N.; Kajiwara, A.; Miyazaki, Y.; Kamachi, M.; Sorai, M. *Thermochim. Acta* **1995**, *267*, 435.

(14) Miyazaki, Y.; Matsumoto, T.; Ishida, T.; Nogami, T.; Sorai, M. *Bull. Chem. Soc. Jpn.* **2000**, *73*, 67.

(15) Imachi, R.; Ishida, T.; Nogami, T.; Ohira, S.; Nishiyama, K.; Nagamine, K. *Chem. Lett.* **1997**, 233.

(16) Murakawa, S.; Wakamatsu, T.; Nakano, M.; Sorai, M.; Suga, H. *J. Chem. Thermodyn.* **1987**, *19*, 1275.

(17) Kume, Y.; Miyazaki, Y.; Matsuo, T.; Suga, H. *J. Phys. Chem. Solids* **1992**, *53*, 1297.

(18) Blöte, H. M. J. *Physica B* **1975**, *79*, 427.

(19) de Neef, T.; Kuipers, A. J. M.; Kopinga, K. *J. Phys. A* **1974**, *7*, L171.

(20) de Jongh, L. J.; Miedema, A. R. *Adv. Phys.* **1974**, *23*, 1.

(21) Willett, R. D.; Place, H.; Middleton, M. *J. Am. Chem. Soc.* **1988**, *110*, 8639.

DALTON
FULL PAPER

Antiferromagnetic coupling of transition metal spins across pyrimidine and pyrazine bridges in dinuclear manganese(II), cobalt(II), nickel(II) and copper(II) 1,1,1,5,5,5-hexafluoropentane-2,4-dionate complexes

Takayuki Ishida,*[a] Takashi Kawakami,[b] Shin-ichi Mitsubori,[a] Takashi Nogami,[a] Kizashi Yamaguchi[b] and Hiizu Iwamura[c]

[a] Department of Applied Physics and Chemistry, The University of Electro-Communications, Chofu, Tokyo 182-8585, Japan. E-mail: ishi@pc.uec.ac.jp
[b] Department of Chemistry, Graduate School of Science, Osaka University, Osaka 560-0043, Japan
[c] The University of the Air, Wakaba, Mihama-ku, Chiba 261-8586, Japan

Received 14th March 2002, Accepted 10th June 2002
First published as an Advance Article on the web 11th July 2002

Dinuclear manganese(II), cobalt(II), nickel(II), and copper(II) complexes bridged by pyrimidine and pyrazine derivatives, L[M(hfac)$_2$]$_2$ [L = 4,6-di(2-pyridyl)pyrimidine (DPPM), 2,3-di(2-pyridyl)pyrazine (DPPZ); M = Mn, Co, Ni, Cu; hfac = 1,1,1,5,5,5-hexafluoropentane-2,4-dionate], were synthesized and their magnetic properties were studied. Antiferromagnetic couplings across the pyrimidine ring were observed for the DPPM complexes with the exchange parameters, $2J/k_B$, of −0.40, −3.1, −9.1 and −46 K for M = Mn, Co, Ni and Cu, respectively. The pyrimidine nitrogen atoms are coordinated at the axial position of each metal ion for M = Mn, Co and Ni, and coordinated equatorially for M = Cu. The DPPZ complexes also exhibited antiferromagnetic interactions, which are weaker than those of the DPPM complexes. Crystal structure analysis indicated that the molecular structures of the four DPPZ complexes are essentially the same in spite of various space groups. Ab initio unrestricted Hartree-Fock calculations on DPPM[Cu(hfac)$_2$]$_2$ predicting a positive effective exchange integral (J) are inconsistent with the experiments, because of overestimation of the role of π-type spin-polarization in DPPM. The J value from the density functional UB3LYP calculations is close to the experimentally determined value, which arises from a σ-type exchange pathway across the pyrimidine ring.

Introduction

Control of magnetic interactions in polynuclear complexes is a key technique for building molecule-based magnets.[1] High-spin organic molecules (**A** and its analogs with spin sources of radicals, carbenes, or nitrenes) are accessible when nonbonding molecular orbitals are present due to π-topological symmetry of the alternant hydrocarbon skeletons.[2] Mataga proposed honeycomb-like high-spin polyradicals and Iwamura modified a model using carbenes (**B**).[3] These model compounds are very attractive but idealistic from the synthetic point of view. Substitution of m-phenylene and carbene groups with pyrimidine and transition metal ions, respectively, would make a reaction path more realizable.[4] However, application of the strategy of organic high-spin molecules to transition-metal complexes is not sufficiently understood, and the complexes used for this approach are rare.[4–9] There has been no systematic research on the role of pyrimidine or pyrazine as magnetic couplers before our study.[4]

We have reported the pyrimidine(PM)-bridged dioxovanadium(IV) complex, PM[VO(hfac)$_2$]$_2$ (hfac = 1,1,1,5,5,5-hexafluoropentane-2,4-dionate), with a ground triplet state (**C**).[10,11] The dπ character of vanadium(IV) spins is supposed to be crucial for ferromagnetic coupling.[11] The oxovanadium oxygen atom can work as a cap which occupies an axial position and accordingly facilitates exclusive preparation of dinuclear compounds using bis(hfac) metal salts. We designed another type of PM-bridged complex L[M(hfac)$_2$]$_2$ as a dinuclear prototype, in which two 2-pyridyl groups are introduced at the 4- and 6-positions on PM as a cap. Thus, target compounds have two (bpy)M(hfac)$_2$-type coordination structures (bpy denotes 2,2′-bipyridyl) which are connected by the 1,3-μ-PM ligand, and the octahedral coordination sites of each metal ion are occupied with N_2O_4 atoms from three bidentate ligands.

We preliminarily reported the antiferromagnetic interactions of these dinuclear Mn, Co, Ni and Cu complexes with L = 4,6-di(2-pyridyl)pyrimidine (DPPM)[4] (for the molecular structures, see below). In this article, we describe the X-ray crystal structures of the DPPM-bridged complexes and discuss a mechanism of antiferromagnetic exchange coupling across the PM bridges. We also compare their molecular structures and magnetic properties with those of the corresponding pyrazine (PZ) derivatives L[M(hfac)$_2$]$_2$ [L = 2,3-di(2-pyridyl)pyrazine) (DPPZ)]. The complexes investigated in the present work are abbreviated as **DPPM–M** and **DPPZ–M** hereafter, in which **M** denotes the hfac salts of divalent transition metal ions (Mn, Co, Ni and Cu).

In addition to the experimental studies, our theoretical treatments enable us to investigate magnetic properties and gain insight into exchange mechanisms. Ab initio unrestricted Hartree-Fock (UHF) and density functional (DFT) calculations were carried out for the **DPPM–Cu** molecule. The calculation includes all of the atoms and the atomic positions determined by the X-ray diffraction study. Disagreement between two calculations will be discussed.

DOI: 10.1039/b202635j

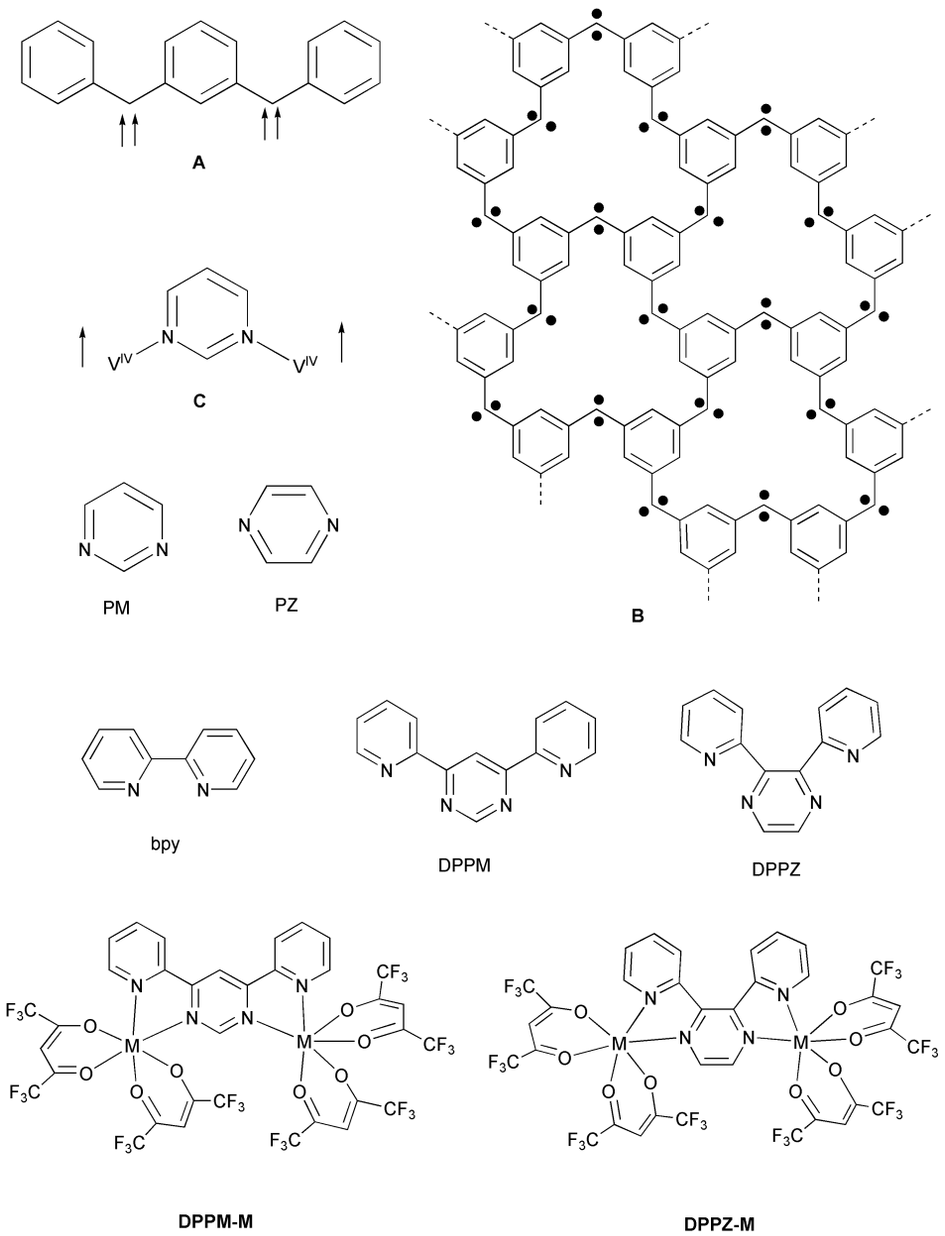

Experimental

Materials

The hfac salts of Mn^{II}, Co^{II}, Ni^{II} and Cu^{II} were purchased from Tokyo Chemical Industry. The DPPZ ligand was purchased from Aldrich. They were used without further purification. The DPPM ligand was prepared according to the literature method.[12] Typical procedures of the preparation of **DPPM–** and **DPPZ–M** are as follows.

A chloroform solution (5 mL) containing the bridging ligand (23 mg, 0.1 mmol) was added to a solution of $M(hfac)_2$ (ca. 0.1 g, 0.2 mmol) in a 4 : 1 chloroform–methanol mixed solvent (5 mL). After refluxing for 1 h, the mixture was concentrated to ca. 5 mL by a rotary evaporator. The crude product of the complex was crystallized after standing at room temperature and collected on a filter. For the preparation of **DPPM–Mn**, chloroform and diethyl ether were used as a solvent. For the preparation of **DPPM–Cu**, chloroform was used as a solvent, and the complexation was conducted at room temperature because the green microcrystalline product appeared immediately after mixing two chloroform solutions. The specimens suitable for elemental analysis, X-ray crystallographic analysis, and magnetic study were purified by repeated recrystallization.

Table 1 summarizes the yields, crystallization solvents, elemental analysis for the complexes obtained here. The elemental analysis and X-ray diffraction study indicate that the **DPPM–M** crystals contain a half mole of benzene as a crystal solvent.[13] Two types of the crystals of **DPPZ–Mn** were found, benzene-solvated and non-solvated forms. The former gave a good single crystal, which was suitable for X-ray crystallographic analysis.

X-Ray crystallographic analysis

Diffraction data were collected on a Rigaku R-axis RAPID diffractometer with graphite monochromated Mo-Kα radiation ($\lambda = 0.71069$ Å) at 100 K, unless otherwise noted. The data were collected at 220 and 190 K for **DPPZ–Ni** and **–Cu**, respectively, because micro cracks occurred on cooling down to lower temperatures. The structures were directly solved by a heavy-atom Patterson method in the teXsan program package.[14] Numerical absorption correction was used. All of the hydrogen atoms could be found in difference Fourier maps, and the parameters of the hydrogen atoms were included in the refinement. The thermal displacement parameters were refined anisotropically for non-hydrogen atoms and isotropically for hydrogen atoms. Full-matrix least-squares methods were applied using all of the unique diffraction data.

Table 1 Yields, melting points, and elemental analyses of **DPPM–** and **DPPZ–M** (M = Mn, Co, Ni and Cu)

Compound	Yield (%)[a]	Mp/°C	Recryst. solv.	Anal.[b] C (%)	H (%)	N (%)
DPPM–Mn·0.5C_6H_6	36[c]	263(dec)	C_6H_6–CH_3OH	35.45 (36.69)	1.33 (1.41)	4.26 (4.63)
DPPM–Co·0.5C_6H_6	18	288(dec)	C_6H_6–CH_3OH	35.93 (36.45)	1.46 (1.41)	4.94 (4.60)
DPPM–Ni·0.5C_6H_6	76	305(dec)	C_6H_6–CH_3OH–CH_3COCH_3	36.29 (36.46)	1.62 (1.41)	5.01 (4.60)
DPPM–Cu·0.5C_6H_6	20[d]	217(dec)	C_6H_6–CH_3OH	35.57 (36.17)	1.41 (1.40)	4.63 (4.56)
DPPZ–Mn	53	159–161	$CHCl_3$–n-C_6H_{14}	33.22 (34.83)	1.34 (1.20)	4.19 (4.78)
DPPZ–Co	60	221–223	$CHCl_3$–n-C_6H_{14}	34.56 (34.60)	1.35 (1.20)	5.00 (4.75)
DPPZ–Ni	66	253–254	$CHCl_3$–CH_3OH	34.63 (34.61)	1.33 (1.20)	5.04 (4.75)
DPPZ–Cu	21	80–83	CH_2Cl_2–n-C_6H_{14}	34.25 (34.33)	1.37 (1.19)	4.83 (4.71)

[a] All the complexations were carried out in a refluxing chloroform–methanol mixed solvent for 1 h, unless otherwise noted. [b] Calculated values in parentheses. [c] In chloroform–diethyl ether. [d] In chloroform at room temperature.

There are two conformations for each trifluoromethyl group as indicated by electron densities in difference Fourier maps and by elongated thermal ellipsoids of fluorine atoms even at 100 K. Disorder models were applied for trifluoromethyl groups belonging to C20 and C24 in **DPPM–Mn**, C25, and C34 in **DPPZ–Ni**, and C19, C25, and C34 in **DPPZ–Cu**, which appreciably improved the refinement. Tables 2 and 3 summarize the selected crystallographic data of **DPPM–** and **DPPZ–M**, respectively.

CCDC reference numbers 180719–180726.

See http://www.rsc.org/suppdata/dt/b2/b202635j/ for crystallographic data in CIF or other electronic format.

Magnetic measurements

Magnetic susceptibilities were measured on a Quantum Design MPMS SQUID magnetometer at 0.5 T in a temperature range down to 1.8 K. The magnetic responses were corrected with diamagnetic blank data of the sample holder obtained separately. The diamagnetic contribution of the sample itself was estimated from Pascal's constants.

Molecular orbital calculations

Molecular orbital calculations were employed using unrestricted Hartree-Fock (UHF) and unrestricted density functional (DFT) UBLYP (Becke–Lee–Yang–Parr) methods in the Gaussian98 program packages.[15] UB2LYP (half-and-half) and UB3LYP[16] methods were also used for hybrid methods between HF and DFT. The basis set (3333/33/3) and diffuse and polarized functions were applied for Cu and 4–31G for the other atoms. In this expression '3' means that three primitive Gaussian-type functions are used for one constructed function. Here, four s-type, two p-type, and one d-type functions are considered, which are applied to the electron configuration of the Cu atom, i.e., (1s, 2s, 3s, 4s), (2p, 3p), and (3d). The atomic positions were available from the X-ray crystallographic analysis.

Results

Structures of DPPM– and DPPZ–M

The crystal structures of **DPPM–M** (M = Mn, Co, Ni and Cu) are isomorphous and the molecular structure and atomic numbering of **DPPM–Co** are shown in Fig. 1(a). The atoms of **DPPM–Mn**, **Ni** and **Cu** are similarly numbered. Selected

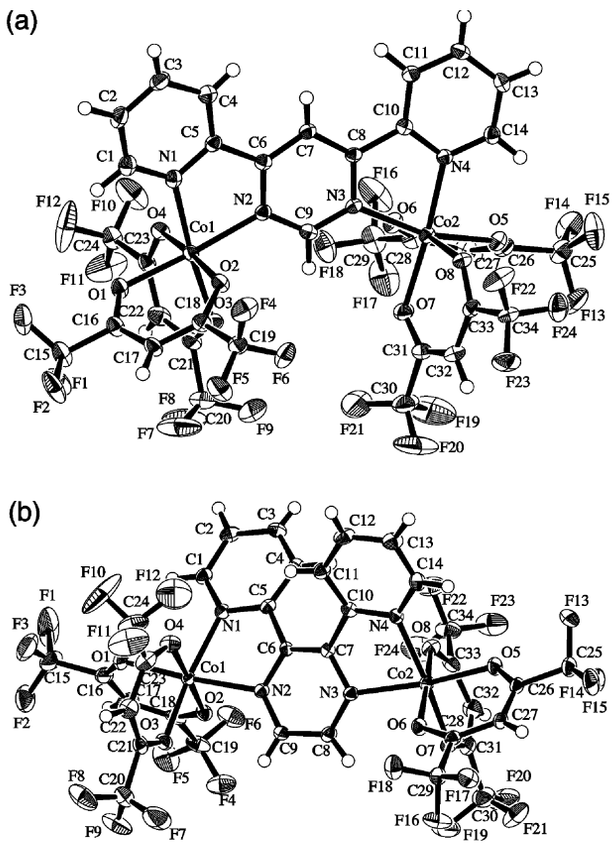

Fig. 1 Ortep drawings of **DPPM–Co** (a) and **DPPZ–Co** (b) with thermal ellipsoids at the 50% probability level. Atomic numberings are also shown.

bond distances and angles of **DPPM–M** are listed in Table 4. Although the two metal ions M1 and M2 are crystallographically independent, the coordination spheres of M1 and M2 are similar to each other; the molecule has a pseudo-C_2 symmetry with respect to the C7–C9 axis. The crystal consists of a racemate of Δ–Δ and Λ–Λ enantiomers, which are related by an inversion symmetry in the $P\bar{1}$ space group. The DPPM moieties are almost planar as indicated by small torsion angles (< 4°) around the C5–C6 and C8–C10 bonds.

Several intermolecular F ··· F contacts are found, but these contacts can hardly afford any appreciable magnetic exchange pathways. Furthermore, benzene molecules reside in the middle

Table 2 Crystallographic data for **DPPM–M**·0.5C_6H_6 (M = Mn, Co, Ni and Cu)

M	Mn	Co	Ni	Cu
Formula	$C_{37}H_{17}N_4O_8F_{24}Mn_2$	$C_{37}H_{17}N_4O_8F_{24}Co_2$	$C_{37}H_{17}N_4O_8F_{24}Ni_2$	$C_{37}H_{17}N_4O_8F_{24}Cu_2$
Habit	Orange needles	Red needles	Green needles	Green needles
Dimensions/mm	0.4 × 0.12 × 0.12	0.43 × 0.18 × 0.15	0.65 × 0.40 × 0.15	0.25 × 0.20 × 0.08
T/K	100	100	100	100
Crystal system	Triclinic	Triclinic	Triclinic	Triclinic
Space group	$P\bar{1}$	$P\bar{1}$	$P\bar{1}$	$P\bar{1}$
a/Å	14.012(3)	13.8200(5)	13.943(2)	13.649(2)
b/Å	15.195(4)	15.0112(7)	15.060(2)	15.335(2)
c/Å	11.832(2)	11.7748(6)	11.682(2)	11.875(1)
α/° [a]	96.148(10)	95.758(1)	95.441(7)	95.023(6)
β/° [a]	88.615(5)	89.758(1)	91.207(7)	99.372(4)
γ/° [a]	113.49(1)	114.153(2)	114.168(3)	111.435(2)
V/Å^3	2296.5(8)	2215.8(2)	2223.1(5)	2253.3(4)
Z	2	2	2	2
D_{calc}/g cm^{-3}	1.752	1.827	1.821	1.811
Unique data for refinement	9865	9757	9655	9617
μ(Mo-Kα)/mm^{-1}	0.701	0.906	1.003	1.098
R (F) [b] (I > 2σ(I))	0.0578	0.0462	0.0539	0.0621
$R_w(F^2)$ [c] (all data)	0.163	0.147	0.169	0.180
G.O.F.	1.43	1.47	1.46	1.39

[a] The cell parameters are transformed for the sake of comparison. These angles are conventionally taken to be α = 96.148(10), β = 91.385(5), γ = 66.51(1)° for M = Mn and α = 95.758(1), β = 90.242(1), γ = 65.847(2)° for M = Co. [b] $R = \Sigma||F_o| - |F_c||/\Sigma|F_o|$. [c] $R_w = [\Sigma w(F_o^2 - F_c^2)^2/\Sigma w(F_o^2)^2]^{1/2}$.

Table 3 Crystallographic data for **DPPZ–M**·(solvent) (M = Mn, Co, Ni and Cu)

M	Mn	Co	Ni	Cu
Formula	$C_{40}H_{20}N_4O_8F_{24}Mn_2$	$C_{34}H_{14}N_4O_8F_{24}Co_2$	$C_{34}H_{14}N_4O_8F_{24}Ni_2$	$C_{34}H_{14}N_4O_8F_{24}Cu_2$
Habit	Orange platelets	Red blocks	Blue blocks	Green blocks
Dimensions/mm	0.35 × 0.35 × 0.10	0.50 × 0.35 × 0.15	0.35 × 0.15 × 0.15	0.26 × 0.23 × 0.10
T/K	100	100	220	190
Crystal system	Triclinic	Monoclinic	Monoclinic	Monoclinic
Space group	$P\bar{1}$	$P2_1/n$	$P2_1/c$	$P2_1/c$
a/Å	13.180(2)	13.1827(4)	13.6123(7)	13.9013(5)
b/Å	14.202(2)	13.0002(4)	19.486(1)	18.4749(6)
c/Å	13.163(1)	24.7946(8)	16.861(1)	17.4447(6)
α/°	100.171(2)	90	90	90
β/°	94.470(6)	98.895(1)	98.962(4)	99.128(1)
γ/°	72.635(3)	90	90	90
V/Å^3	2313.9(5)	4198.1(2)	4417.7(5)	4423.5(3)
Z	2	4	4	4
D_{calc}/g cm^{-3}	1.795	1.867	1.774	1.786
Unique data for refinement	9718	9518	8574	9146
μ(Mo-Kα)/mm^{-1}	0.699	0.952	1.006	1.115
R (F) [a] (I > 2σ(I))	0.0538	0.0544	0.0618	0.0481
$R_w(F^2)$ [b] (all data)	0.174	0.155	0.197	0.145
G.O.F.	1.47	1.45	0.999	0.973

[a] $R = \Sigma||F_o| - |F_c||/\Sigma|F_o|$. [b] $R_w = [\Sigma w(F_o^2 - F_c^2)^2/\Sigma w(F_o^2)^2]^{1/2}$.

of two molecules of **DPPM–M** as a crystal solvent, and π-electron systems of bridging ligands are considerably separated from a neighboring molecule. Thus, each molecule should be magnetically isolated.

We focus our attention on detailed geometries around the metal ions and especially around M1–N2 and M2–N3 bonds which provide the main exchange pathway. The M–N bond lengths decrease in the order of M = Mn, Co, Ni and Cu (Table 4). The M–N distances are much longer than M–O distances in **DPPM–Mn** and **–Co**, indicating that the pyrimidine N2 and N3 atoms are coordinated at axial positions. Since the M1–N2 and M2–N3 distances are only slightly longer than other bonds for **DPPM–Ni**, the geometrical assignment of the Mn and Co complexes may hold for the Ni complex. On the other hand, the M1–O2 and M1–O4 distances are longer than those of M1–O1, –O3, –N1, and –N2 for **DPPM–Cu**, indicating that the nitrogen atoms are equatorially coordinated.

The crystals of **DPPZ–M** (M = Mn, Co, Ni and Cu) have various space groups, but the molecular structures are essentially identical to each other. The molecular structure and atomic numbering of **DPPZ–Co** are shown in Fig. 1(b). The atoms in the Mn, Ni, and Cu complexes are similarly numbered. Selected bond distances and angles of **DPPZ–M** are listed in Table 5. Owing to the steric hindrance, the DPPZ moieties are largely twisted by angles of 17–39° around the C5–C6 and C7–C10 bonds. Each molecule has a Δ–Δ or Λ–Λ conformation, and the enantiomers are related by an inversion symmetry in the centrosymmetric space groups.

Similarly to the DPPM complexes, the pyrazine nitrogen atoms (N2 and N3) are coordinated from the axial directions for **DPPZ–Mn**, **–Co**, and **–Ni** (Table 5). As described in the Experimental section, the crystals of **DPPZ–Ni** and **–Cu** lost their transparency on cooling below ca. 220 and 190 K, respectively, strongly suggesting that a structural phase transition took place. Actually, the cell constants at 100 K are somewhat different from those at 220 and 190 K.[17]

Magnetic properties

Fig. 2 shows the temperature dependence of the $\chi_{mol}T$ product per molecule for **DPPM–M**. The $\chi_{mol}T$ values at 300 K indicate that each metal ion has a high-spin state. The $\chi_{mol}T$ values

Table 4 Selected bond lengths (Å) and angles (°) for **DPPM–M**·$0.5C_6H_6$ (M = Mn, Co, Ni and Cu)

M	Mn	Co	Ni	Cu
M1–O1	2.161(2)	2.074(2)	2.048(2)	1.933(2)
M1–O2	2.179(2)	2.068(2)	2.045(2)	2.250(3)
M1–O3	2.157(3)	2.049(2)	2.034(3)	1.966(3)
M1–O4	2.138(2)	2.046(2)	2.029(2)	2.414(3)
M1–N1	2.243(3)	2.106(2)	2.063(3)	2.001(3)
M1–N2	2.272(3)	2.121(2)	2.079(3)	2.001(3)
M2–O5	2.132(3)	2.044(2)	2.027(2)	2.020(3)
M2–O6	2.154(2)	2.053(2)	2.027(2)	2.326(3)
M2–O7	2.129(3)	2.051(2)	2.027(2)	1.938(3)
M2–O8	2.195(2)	2.087(2)	2.061(2)	2.211(3)
M2–N3	2.297(3)	2.136(2)	2.096(3)	2.035(3)
M2–N4	2.253(3)	2.109(2)	2.067(3)	1.989(3)
O1–M1–O2	83.56(9)	87.40(8)	89.24(9)	87.37(10)
O3–M1–O4	82.11(10)	87.21(8)	89.55(10)	83.1(1)
N1–M1–N2	72.9(1)	77.20(9)	79.3(1)	80.7(1)
O5–M2–O6	83.33(9)	87.76(8)	89.89(9)	81.9(1)
O7–M2–O8	82.92(9)	86.88(8)	88.69(9)	87.1(1)
N3–M2–N4	72.2(1)	76.61(8)	78.8(1)	80.6(1)
N1–C5–C6–N2	−.0(4)	−2.9(3)	−1.6(4)	−0.5(4)
N3–C8–C10–N4	−4.1(4)	−1.8(3)	0.3(4)	−4.0(4)

Table 5 Selected bond lengths (Å) and angles (°) for **DPPZ–M** (M = Mn, Co, Ni and Cu)

M	Mn	Co	Ni	Cu
M1–O1	2.106(2)	2.052(3)	2.030(4)	1.967(2)
M1–O2	2.163(2)	2.042(3)	2.017(3)	2.224(2)
M1–O3	2.121(2)	2.070(3)	2.036(4)	1.976(3)
M1–O4	2.197(2)	2.067(3)	2.026(4)	2.217(2)
M1–N1	2.227(3)	2.105(3)	2.051(4)	1.998(3)
M1–N2	2.280(3)	2.132(3)	2.070(4)	2.031(3)
M2–O5	2.121(2)	2.026(3)	2.014(3)	2.169(2)
M2–O6	2.155(2)	2.052(3)	2.014(3)	1.960(2)
M2–O7	2.135(2)	2.056(3)	2.024(4)	1.967(2)
M2–O8	2.151(2)	2.078(3)	2.026(4)	1.960(2)
M2–N3	2.284(3)	2.134(3)	2.136(4)	2.455(3)
M2–N4	2.242(3)	2.112(3)	2.076(4)	2.037(3)
O1–M1–O2	82.21(9)	88.9(1)	90.8(1)	87.95(9)
O3–M1–O4	81.11(9)	86.6(1)	88.7(2)	85.6(1)
N1–M1–N2	72.43(10)	77.2(1)	79.2(2)	80.1(1)
O5–M2–O6	83.10(9)	88.9(1)	90.8(1)	89.25(8)
O7–M2–O8	82.90(9)	86.0(1)	89.6(1)	90.62(10)
N3–M2–N4	72.04(10)	77.0(1)	78.5(2)	74.87(10)
N1–C5–C6–N2	25.7(4)	18.3(4)	23.3(6)	16.8(4)
N3–C7–C10–N4	19.4(4)	23.1(4)	28.2(6)	38.8(4)

dominantly decrease with decreasing temperature for all of the complexes investigated here, clearly indicating that the spins of the metal ions are antiferromagnetically coupled; namely, the dinuclear molecules have a low-spin ground state. Since the X-ray crystal structure analysis indicates that no appreciable interatomic contacts were found among the molecules, the magnetic interaction should be attributed to the intramolecular coupling.

We analyzed these data by the dinuclear models as expressed by eqn. 1, on the basis of the conventional van Vleck equation for Heisenberg spins.[1,18] The spin Hamiltonian is defined by $H = -2JS_i \cdot S_j$.

$$\chi_{mol} = \frac{2Ng^2\mu_B^2}{k_B T} \frac{e^{-2x} + 5Ae^{-6x} + 14Be^{-12x} + 30Ce^{-20x} + 55De^{-30x}}{1 + 3e^{-2x} + 5Ae^{-6x} + 7Be^{-12x} + 9Ce^{-20x} + 11De^{-30x}} \quad (1)$$

where $x = -J/k_BT$.

The parameters A–D should be set as follows. A = B = C = D = 0 for S = 1/2 (M = Cu(II)); A = 1 and B = C = D = 0 for S = 1 (M = Ni(II)); A = B = 1 and C = D = 0 for S = 3/2 (M = Co(II)); A = B = C = D = 1 for S = 5/2 (M = Mn(II)).

We have to take into account the contribution of angular momentum for the cobalt(II) (d^7) complexes and the van Vleck treatment may give approximate results. Indeed, the $\chi_{mol}T$ vs. T plots of **DPPM–** and **DPPZ–Co** show somewhat anomalous behavior, which cannot be explained by spin–spin coupling alone. On the other hand, manganese(II) (d^5), nickel(II) (d^8), and copper(II) (d^9) complexes usually have negligible contribution of angular momentum, and obey the Heisenberg–van Vleck model.

The optimized parameters are listed in Table 6, and theoretical curves with these parameters are superposed in Fig. 2. The negative J values imply that the two metal spins are antiferromagnetically correlated. A significantly large antiferromagnetic interaction ($2J/k_B = -46$ K) was observed for **DPPM–Cu**, where the singlet–triplet energy gap corresponds to 2J. In sharp contrast to m-phenylene-bridged diradicals and dicarbenes (**A**) having a high-spin ground state, the present work unequivocally demonstrates that **DPPM–Cu**

Table 6 Best fit parameters for **DPPM–** and **DPPZ–M** (M = Mn, Co, Ni and Cu)

Compound	g	$2J(k_B^{-1})$/K
DPPM–Mn·$0.5C_6H_6$	2.07	−0.40
DPPM–Co·$0.5C_6H_6$	~2.69	~−3.1
DPPM–Ni·$0.5C_6H_6$	2.30	−9.1
DPPM–Cu·$0.5C_6H_6$	2.29	−46
DPPZ–Mn	2.00	−0.34
DPPZ–Mn·C_6H_6	2.00	−0.40
DPPZ–Co	~2.6	[a]
DPPZ–Ni	2.19	−1.19
DPPZ–Cu	2.12	<0.1

[a] The data did not obey the Heisenberg–van Vleck equation.

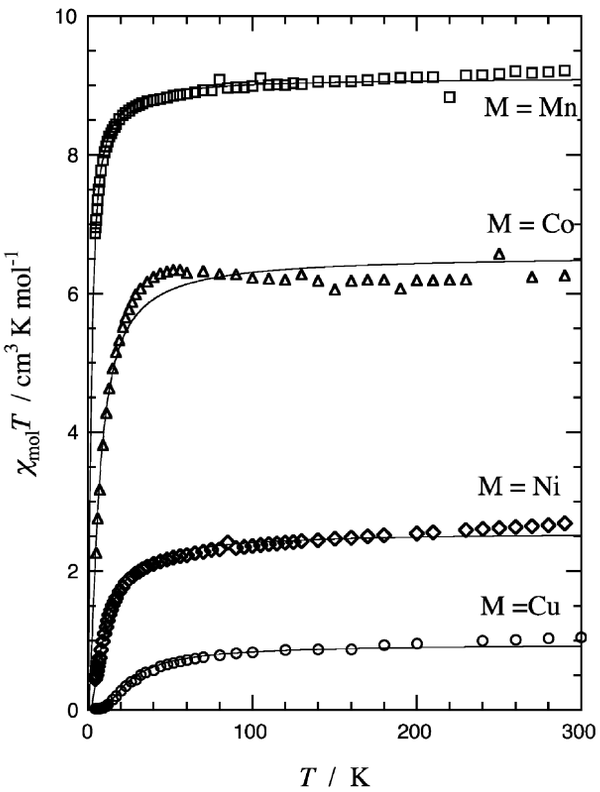

Fig. 2 Temperature dependence of the product $\chi_{mol}T$ for **DPPM–Mn**, **Co**, **Ni** and **Cu**. The solid lines represent the fits to the equation based on the dinuclear model.

has a singlet ground state. Antiferromagnetic couplings have also been reported in other PM-bridged copper(II) complexes.[19–21]

The $\chi_{mol}T$ vs. T plots for **DPPM–Mn** and **–Ni** also fit well to the dinuclear model equations, as indicated by the calculated curves (Fig. 2). Antiferromagnetic couplings are observed regardless of the different coordination basal planes in **DPPM–Mn**, **Co**, **Ni** and **Cu**. In the case of **DPPM–Co**, the $\chi_{mol}T$ value increases on cooling, reaches to a broad maximum, and finally decreases. The increase of $\chi_{mol}T$ may be attributed to the contribution of angular momentum of the cobalt spins. A similar broad maximum is observed in the measurements on **DPPZ–Co** (see below). These broad maxima seem to result from the same origin but a sharp decrease at low temperature was observed only for **DPPM–Co**. The negative J value of **DPPM–Co** was estimated, considering the final decrease to be important.

Magnetic measurements on the **DPPZ–M** series may afford a good comparison of the role of exchange couplers in the isomeric pyrimidine and pyrazine bridges. Fig. 3 shows the

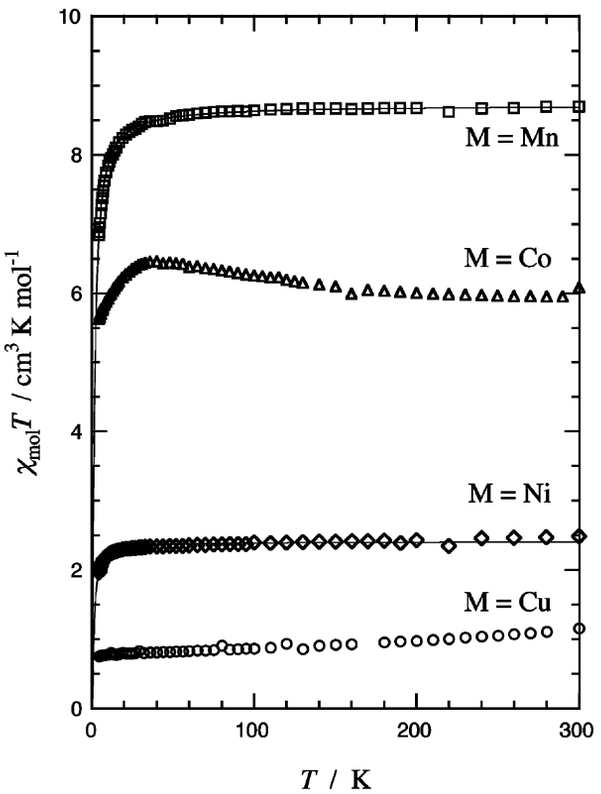

Fig. 3 Temperature dependence of the product $\chi_{mol}T$ for **DPPZ–Mn**, **Co**, **Ni** and **Cu**. The solid lines represent the fits to the equation based on the dinuclear model.

temperature dependence of the $\chi_{mol}T$ values for the DPPZ-bridged complexes. We obtained two forms of the crystals of **DPPZ–Mn** with and without solvated benzene molecules. Their magnetic properties were essentially identical to each other and the optimized parameters of **DPPZ–Mn**·C_6H_6 are also listed in Table 6. This supports the magnetic interactions obtained here being ascribed as intramolecular in nature.

The parameter of magnetic interaction in **DPPZ–Co** could not be determined, but from the comparison of the decreases of $\chi_{mol}T$ in the low temperature region in **DPPM–** and **DPPZ–Co** we can assume that **DPPZ–Co** has a smaller |J| than **DPPM–Co**. The exchange parameter for **DPPZ–Ni** was determined by the theoretical fit. The complex **DPPZ–Cu** has practically no interaction.[17] The absolute J values of **DPPZ–Co**, **–Ni**, and **–Cu** are smaller than those of the corresponding DPPM complexes. On the other hand, **DPPM–** and **DPPZ–Mn** have comparable J values.

Table 7 Effective exchange integrals (J_{ab}) and spin densities calculated from ab initio UHF and DFT (UB2LYP, UB3LYP and UBLYP) methods for **DPPM–Cu**

Method	UHF	UB2LYP	UB3LYP	UBLYP
$J_{ab}(X)$[a]/cm^{-1}	144.9	−6.9	−16.7	−66.1
$J_{ab}(AP–X)$[a]/cm^{-1}	120.2	−6.9	−16.6	−64.0
Spin densities for the most stable spin state[b]				
Cu1	0.896	0.700	0.515	0.406
N2	0.338	0.049	0.055	0.052
C9	−0.348	0.002	0.001	0.001
N3	0.350	−0.061	−0.068	−0.066
Cu2	0.893	−0.699	−0.519	−0.414
N1	0.176	0.088	0.091	0.086
O1	0.018	0.058	0.106	0.124
O2	0.002	0.005	0.011	0.010
O3	0.032	0.096	0.155	0.168
O4	−0.005	0.003	0.014	0.031

[a] $J_{ab}(X)$ and $J_{ab}(AP–X)$ are effective exchange integrals without and with spin projection, respectively. [b] High- and low-spin states for UHF and DFT calculations, respectively.

We should briefly report on magnetic properties of mononuclear complexes. We also prepared the complexes (bpy)-M(hfac)$_2$ (M = Mn, Co, Ni and Cu; abbreviated as **BPY–M**). The temperature dependence of the magnetic susceptibility for **BPY–Mn** and **–Cu** simply obey the Curie law (C = 4.38 and 0.436 cm^3 K mol^{-1}, respectively). A negligible Weiss temperature was obtained for **BPY–Ni** from the Curie–Weiss equation (C = 1.20 cm^3 K mol^{-1} and θ = −0.1 K). These findings support intermolecular interactions being neglected when bulky hfac ligands prevent intermolecular contacts, and also the temperature dependence observed for **DPPM–** and **DPPZ–M** can be attributed to the spin–spin interaction and not to any contribution of mononuclear origin (e.g., zero-field splitting). Since **BPY–Co** does not obey the Curie–Weiss law, it seems difficult to determine precisely the exchange parameters for **DPPM–** and **DPPZ–Co**.

Molecular orbital calculations

We employed ab initio unrestricted Hartree-Fock (UHF) calculations and density functional (DFT) UBLYP, UB2LYP and UB3LYP calculations for evaluation of the exchange parameter J and spin distribution on the ligand in **DPPM–Cu**. Table 7 shows the J_{ab} values obtained by the above computational methods. Here, $J_{ab}(X)$ and $J_{ab}(AP–X)$ imply effective exchange integrals without and with spin projection to reduce spin contamination, respectively. The following conclusions are extracted from Table 7:

(1) The UHF method gave a positive J_{ab} value and large ferromagnetic interaction is expected between two Cu atoms. The UHF calculation is inconsistent with the experimental results. (2) The J_{ab} values calculated by UB3LYP are −16.6 cm^{-1} for **DPPM–Cu**. This value corresponds to $2J/k_B$ = −46.3 K, which is very close to the experimental value (Table 6). (3) All of the DFT methods give negative J_{ab} values and the absolute values increase in the order UB2LYP < UB3LYP < UBLYP. The difference between $J_{ab}(X)$ and $J_{ab}(AP–X)$ values is very small and accordingly the spin contamination is small. (4) The nitrogen atoms (N1 and N2) carry positive spin densities for all calculation methods. (5) The UHF calculation gave large spin densities on the PM ring.

DFT methods have been shown to give good agreement with spin densities derived from polarized neutron diffraction[22] and NMR[23] experiments and also to give good estimates of magnetic interactions.[24] In the present study, the DFT UB3LYP calculations reproduced well the experimental magnetic interactions in **DPPM–Cu**. Fig. 4(b) and 4(c) illustrate the spin densities for the ground states calculated by UHF (high-spin) and

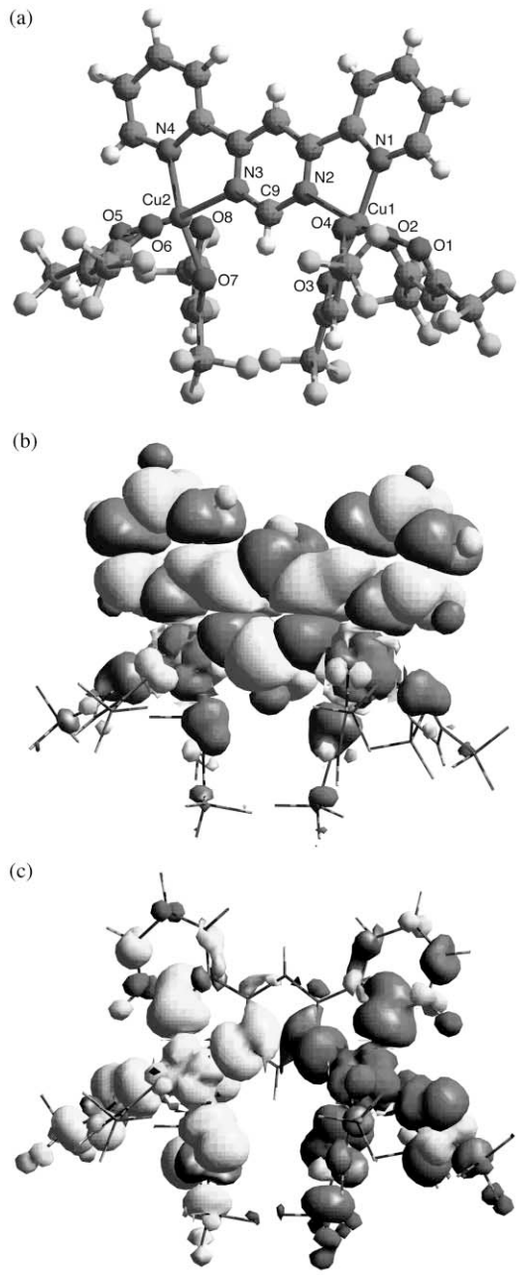

Fig. 4 Calculated spin density distribution at the most stable spin state of **DPPM–Cu** with the surface threshold level of 0.001. (a) Structure of the calculated molecule. (b) Calculation by the ab initio UHF method. (c) Calculation by the UB3LYP method. For details of the calculations, see the text.

UB3LYP (low-spin), respectively. The regions of up (alpha) and down (beta) densities are shown in dark and light gray colors, respectively, and the cut-o threshold is set to be 0.001. Fig. 4(a) depicts the skeleton of the molecule. The total spin densities condensed on each atom are also listed in Table 7.

Discussion

We have reported that the PM- and PZ-bridged dinuclear oxovanadium complexes exhibit intramolecular ferro- and antiferromagnetic interactions, respectively,[11] being in good agreement with the spin-polarization mechanism as in organic compounds. The electron configuration of vanadium() is d^1 (t_{2g}^1) which aords a π-type symmetry around a metal–ligand bond and the $d\pi$–$p\pi$ orbital overlap between the metal and coordinated atoms is essential for realization of ferromagnetic interaction.[11] In the present study, however, both PM and PZ bridges play the role of antiferromagnetic coupler. The d electron configuration, especially $d\sigma$ (e_g) spins which Mn^{II}, Co^{II}, Ni^{II} and Cu^{II} ions possess in the present complexes, seems to be crucial for the magnetic interaction.

The coordination geometry (axial or equatorial) is also very important, as suggested by the following instance. Two types of polymeric copper() nitrate complexes have been reported: ferromagnetic $[PM_2{\cdot}Cu(NO_3)_2]_n$ and antiferromagnetic $[PM{\cdot}Cu(NO_3)_2{\cdot}(H_2O)_2]_n$.[19] The former has axial coordination at one nitrogen atom of PM and equatorial coordination at the other (axial–equatorial, see Scheme 1). An equatorial–equatorial

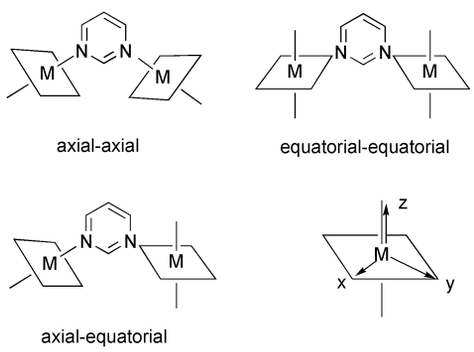

Scheme 1 Classification of coordination geometry for dinuclear pyrimidine complexes and definition of local x,y,z coordinates around a metal ion.

coordination was found in the latter complex. The extended Hückel molecular orbital calculation analysis suggests that the $d\sigma$–$n\sigma$ orbital overlaps between copper $d_{x^2-y^2}$ and nitrogen n orbitals on both sides are related to an antiferromagnetic superexchange coupling across the PM ring.[25] The PM nitrogen atoms in **DPPM–Cu** are coordinated at the equatorial sites and the antiferromagnetic J value is comparable to those of the polynuclear complexes reported previously.[19,20] Compounds **DPPM–Mn**, **–Co**, and **–Ni** have axial–axial coordination geometries, and there are $d\sigma$–$n\sigma$ orbital overlaps between d_{z^2} and nitrogen n orbitals on both sides.

Antiferromagnetic couplings in PM_2CoX_2 (X = Cl and Br)[26] and $PM{\cdot}Co[N(CN)_2]_2$[27] were also reported, but the coordination geometries are dierent; the PM nitrogen atoms are coordinated at axial positions in $PM{\cdot}Co[N(CN)_2]_2$ but at equatorial positions in PM_2CoX_2. The magnetic d_{z^2} and $d_{x^2-y^2}$ orbitals, both of which the high-spin (S = 3/2) cobalt ions usually possess, are available for $d\sigma$–$n\sigma$ orbital overlap. As a consequence, the cobalt spins are antiferromagnetically correlated regardless of the coordination sites. Furthermore, for the isostructral nickel() derivatives, PM_2NiCl_2[28] and $PM{\cdot}Ni[N(CN)_2]_2$,[29] antiferromagnetic couplings observed can be interpreted likewise in terms of $d\sigma$–$n\sigma$-type orbital overlap. In view of a number of the experimental results obtained up to now, $d\sigma$–$n\sigma$ orbital overlap on both sides of PM is concluded to favor antiferromagnetic coupling.

We performed ab initio and DFT molecular orbital calculations and found that the DFT results reproduced well the experimental results. Let us consider the shape of spin density distribution by graphical representation in order to explain and understand the conclusions described in the Results section. From Fig. 4 and Table 7, we find that Cu1 and coordinated nitrogen atoms (N1 and N2) carry spin densities with the same sign for all calculation methods. These spin structures can be interpreted in terms of the spin delocalization eect.[30] The spin delocalization eect in the Cu–N bond illustrates a resonance between Cu(↑)–N(↑↓) and Cu(↑↓)–N(↑) based on a ligand-to-metal charge transfer model, giving rise to the positive spin density on N. This situation shows a sharp contrast to those of organic high-spin materials bridged by m-phenylenes,[2] in which the spin density alternates throughout the π-conjugated hydrocarbon networks. It should be noted that the high-spin

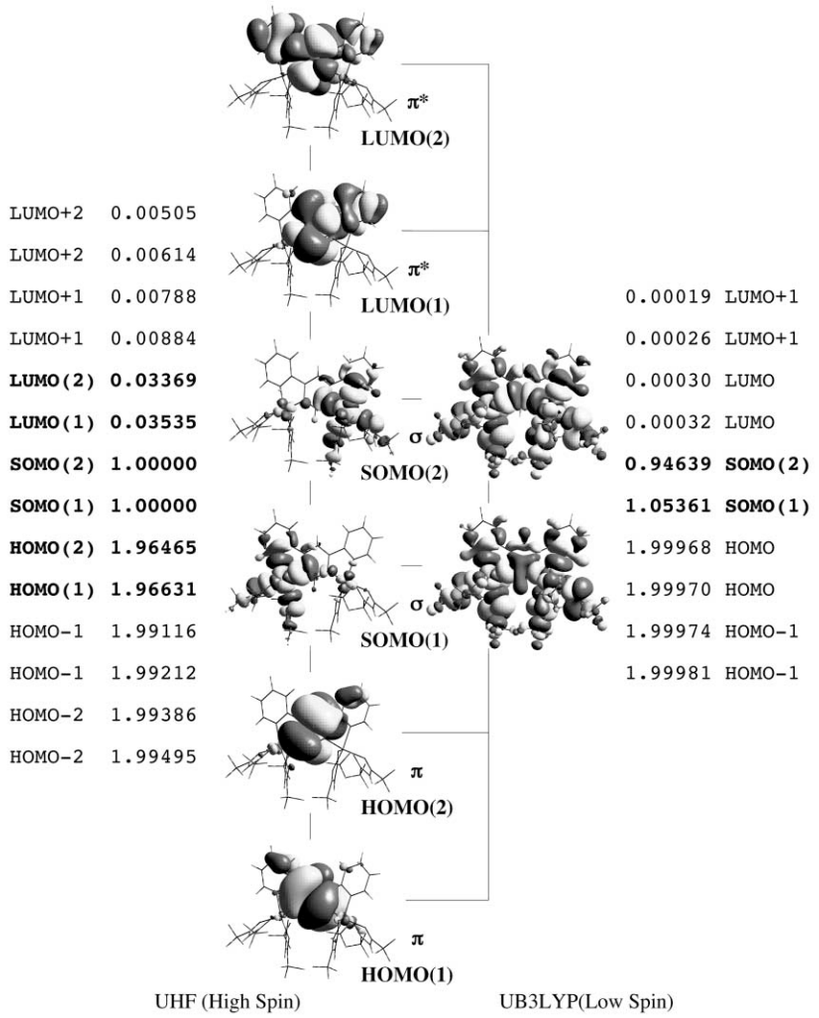

Fig. 5 Natural orbital coefficients and surfaces calculated by the UHF (left) and UB3LYP (right) methods for **DPPM–Cu**. Bold-faced natural orbitals appreciably contribute to the configuration interaction. For details of the calculations, see the text.

bisoxovanadium complex (**B**) showed a spin alternation in the V–PM–V skeleton, i.e., the nitrogen atom carries a negative spin density[11] like the organic high-spin materials.

We also find that the UHF method gives much larger spin densities on the atoms of the ligand than the UB2LYP, UB3LYP and UBLYP methods. Furthermore, alternating spin densities on the PM ring are induced in the high-spin solution by UHF, whereas only nitrogen atoms (N2 and N3 in the PM bridge and N1 and N4 in the 2-pyridyl groups) in the ligand possess appreciable spin densities in the UB3LYP result.

Natural orbital[31] analysis for the **DPPM–Cu** molecules was carried out in order to study the contribution of frontier orbitals to the configuration interaction. The natural orbital coefficients for each orbital (highest-occupied molecular orbital (HOMO), singly-occupied molecular orbital (SOMO), lowest-unoccupied molecular orbital (LUMO) etc.) and their graphical representations for UHF (high-spin) and UB3LYP (low-spin) results are summarized in Fig. 5. The occupation numbers for SOMO(1) and SOMO(2) are close to unity and one electron occupies each orbital for both UHF and UB3LYP results. The lobes of these SOMOs spread not only over Cu atoms but also over their coordinated atoms through σ-bonds. In the case of UHF treatment two SOMOs and four other orbitals (HOMOs and LUMOs) must be taken into account in describing the configuration interaction, because the coefficients differ considerably from 2 or 0. The latter orbitals are localized on PM and possess a π-orbital nature. A π-pathway along N2–C9–N3 seems feasible for the magnetic interaction (Fig. 6(a)).

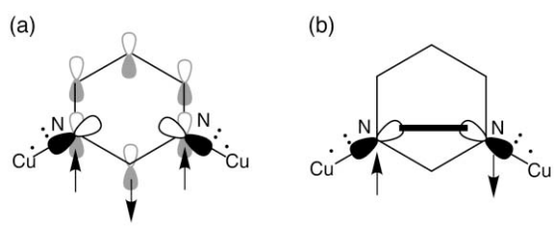

Fig. 6 Magnetic interaction paths. (a) Spin-polarization mechanism via π-bonds in the UHF calculation. The phase of $2p_z$ atomic orbitals are arbitrary. (b) Direct σ-type N ··· N interaction for the UB3LYP calculation. The lobes are drawn for the SOMO(1) case (Fig. 5).

On the other hand, only two SOMOs are essential to the configuration interaction for the UB3LYP solution. The two SOMOs have σ character. As the lobes of the SOMOs of UB3LYP show, a σ-pathway along Cu1–N2–N3–Cu2 can be proposed for the through-bond exchange mechanism (Fig. 6(b)). A similar direct N–N interaction has previously been proposed for the extended Hückel analysis of the PM-bridged copper(II) nitrate complex.[25] Therefore, the disagreement between the J_{ab} values obtained from the UHF and DFT calculations arises from overestimation of the π-type spin-polarization in the UHF treatment. As stated in the Introduction, the strategy realizing organic high-spin carbenes and radicals is based on π-spin-polarization,[2] and this strategy can not be applied for the present complex system.

Given that π-type spin-polarization effects should be negligible, we can propose a simplified rule which predicts the

role of magnetic couplers, using the Anderson–Goodenough–Kanamori theorem on the M_1–X–M_2 system.[32–34] When there is an appreciable orbital overlap between a magnetic orbital ϕ_1 on M_1 and an atomic orbital χ on X and at the same time there is also an overlap between χ and a magnetic orbital ϕ_2 on M_2, the spins of M_1 and M_2 are antiferromagnetically coupled. In the present complexes, the antiferromagnetic coupling is rationalized by assuming that χ is a molecular orbital of PM. The PM has local molecular orbitals consisting of $n_A + n_B$ and $n_A - n_B$, where n_A and n_B denote the lone pair of each nitrogen atom in PM, and no orthogonality is expected from the M_1–PM–M_2 system. Thus, the PM bridges work as antiferromagnetic couplers. This rule can also be applied to the PZ-bridged systems. Since the PZ has molecular orbitals $n_A + n_B$ and $n_A - n_B$ as well, the PZ bridge works as an antiferromagnetic coupler. In short, $\phi_1(d_{z^2})$ // χ // $\phi_2(d_{z^2})$ and $\phi_1(d_{x^2-y^2})$ // χ // $\phi_2(d_{x^2-y^2})$ bring about antiferromagnetic couplings for the axial–axial and equatorial–equatorial coordination geometries, respectively, where "//" denotes the presence of an orbital overlap. Only in the geometrically rare case of $\phi_1(d_{x^2-y^2}) \perp \chi$ // $\phi_2(d_{x^2-y^2})$ for axial–equatorial coordination of some copper complexes, where "$\perp$" denotes the absence of any orbital overlap, does the PM bridge work as a ferromagnetic coupler.

The manganese(II) and cobalt(II) ions simultaneously have dπ and dσ spins. A detailed computational analysis of the simplest Mn–PM–Mn molecule with hypothetical hydride ligands has been reported recently.[30] The magnetic interaction is more complex because many kinds of magnetic interactions are present. As described above, after a positive spin density is polarized at the coordinated nitrogen atom, π- and σ-pathways may be operative which bring about ferro- and antiferromagnetic couplings, respectively. A σ-type spin-polarization pathway is also possible along the Mn–N–C–N–Mn bonded skeleton (not along the Mn–N ··· N–Mn shortcut), which may contribute as a ferromagnetic coupling term. When a negative spin polarization is assumed at the nitrogen atom using dπ spins as in the bisoxovanadium case,[11] possible ferromagnetic coupling contributes to the total interaction. In addition, symmetrical orthogonality suggests that the magnetic interaction of dπ–PM–dσ combination would be ferromagnetic, as clearly demonstrated for the bimetallic VO–Cu complexes.[35,36] Actually, the UB2LYP and UB3LYP calculations and UBLYP calculation on the hypothetical Mn–PM–Mn gave opposite solutions of J owing to a delicate balance.[30] The experimental results on **DPPM–** and **DPPZ–Mn** indicate that the antiferromagnetic contributions slightly surpass the ferromagnetic ones.

We found that the order of the absolute values of J for **DPPM–M** was J(Mn) < J(Co) < J(Ni) < J(Cu). The structural difference such as bond lengths of M1–N1 and M2–N3 should be taken into consideration. The observed order of J is consistent with the order of the M–N bond lengths (Table 4); shorter bond lengths bring about stronger interaction in general. We can propose another possible explanation, since typical dσ(d^9)–PMσ–dσ(d^9) and dπ(d^1)–PMπ–dπ(d^1) exchange pathways were clarified for **DPPM–Cu** and PM[VO(hfac)$_2$]$_2$,[11] respectively; the interaction in **DPPM–M** may be approximately explained by the balance between two major contributions from σ and π pathways. The observed magnetic interaction parameter J is expressed by the mean of the individual interactions J(i–j) between each unpaired electron (i) on one metal ion and each unpaired electron (j) on another metal ion.[37] Whereas the J(e_g–e_g) terms are antiferromagnetic as shown by **DPPM–Cu**, the J(t_{2g}–e_g) terms are ferromagnetic owing to orthogonality and the J(t_{2g}–t_{2g}) are also possibly ferromagnetic as clarified by PM[VO(hfac)$_2$]$_2$.[11] Taking the dinuclear Mn(II) complexes for example, only four terms are antiferromagnetic out of the total 25 terms. It is conceivable that the J values of **DPPM–M** positively shift with an increase of the number of magnetic t_{2g} orbitals.

Conclusion

We have clarified that both PM and PZ work as antiferromagnetic couplers in the dinuclear Mn^{II}, Co^{II}, Ni^{II} and Cu^{II} complexes and that the origin of the antiferromagnetic coupling is a superexchange through σ-bonds. For high-spin organic molecules using m-phenylene linkages the synthesis is laborious and perfect chemical transformation is difficult as the number of spins increases,[38] while pyrimidine-bridged transition-metal complexes have some advantages due to the nature of self-assembly. The present work suggests that metal ions with only dπ spins are potentially good candidates for developing pyrimidine-bridged magnets along this strategy.

Acknowledgements

This work was supported by Grant-in-Aid for Scientific Research on Priority Areas of "Molecular Conductors and Magnets" (No. 730/11224204) and by Grant-in-Aid for Scientific Research (No. 13640575) from the Ministry of Education, Culture, Sports, Science and Technology, Japan.

References and notes

1 O. Kahn, Molecular Magnetism, VCH, New York, 1993.
2 H. Iwamura, Adv. Phys. Org. Chem., 1990, **26**, 179; A. Rajca, Chem. Rev., 1994, **94**, 871; J. C. Longuet-Higgins, J. Chem. Phys., 1950, **18**, 265; J. A. Crayston, J. N. Devine and J. C. Walton, Tetrahedron, 2000, **56**, 7829.
3 N. Mataga, Theor. Chim. Acta, 1967, **10**, 372; K. Matsuda, N. Nakamura, K. Takahashi, K. Inoue, N. Koga and H. Iwamura, J. Am. Chem. Soc., 1995, **117**, 5550.
4 T. Ishida, S.-i Mitsubori, T. Nogami and H. Iwamura, Mol. Cryst. Liq. Cryst., 1993, **233**, 345.
5 T. Ishida and T. Nogami, Recent Res. Dev. Pure Appl. Chem., 1997, **1**, 1; T. Ishida, S.-i. Mitsubori, T. Nogami, Y. Ishikawa, M. Yasui, F. Iwasaki, H. Iwamura, N. Takeda and M. Ishikawa, Synth. Met., 1995, **71**, 1791.
6 L. C. Francesconi, D. R. Corbin, A. W. Clauss, D. N. Hendrickson and G. D. Stucky, Inorg. Chem., 1981, **20**, 2078.
7 V. A. Ung, S. M. Couchman, J. C. Jeffery, J. A. McCleverty, M. D. Ward, F. Totti and D. Gatteschi, Inorg. Chem., 1999, **38**, 365.
8 H. Oshio and H. Ichida, J. Phys. Chem., 1995, **99**, 3294; H. Oshio, J. Chem. Soc., Chem. Commun., 1991, 240.
9 F. Lloret, G. De Munno, M. Julve, J. Cano, R. Ruiz and A. Caneschi, Angew. Chem., Int. Ed., 1998, **37**, 135.
10 S.-i. Mitsubori, T. Ishida, T. Nogami and H. Iwamura, Chem. Lett., 1994, 285; S.-I. Mitsubori, T. Ishida, T. Nogami, H. Iwamura, N. Takeda and M. Ishikawa, Chem. Lett., 1994, 685.
11 T. Ishida, S.-i. Mitsubori, T. Nogami, N. Takeda, M. Ishikawa and H. Iwamura, Inorg. Chem., 2001, **40**, 7059.
12 J. J. Lafferty and F. H. Case, J. Org. Chem., 1967, **32**, 1591.
13 The composition formula of the **DPPM–M** crystals in ref. 4 should be corrected to **DPPM–M**·0.5C_6H_6.
14 teXsan: crystal structure analysis package, Molecular Structure Corp., The Woodlands, TX, 1985, 1999.
15 Gaussian98, M. J. Frisch, G. W. Trucks, H. B. Schlegel, G. E. Scuseria, M. A. Robb, J. R. Cheeseman, V. G. Zakrzewski, J. A. Montgomery, Jr., R. E. Stratmann, J. C. Burant, S. Dapprich, J. M. Millam, A. D. Daniels, K. N. Kudin, M. C. Strain, O. Farkas, J. Tomasi, V. Barone, M. Cossi, R. Cammi, B. Mennucci, C. Pomelli, C. Adamo, S. Clifford, J. Ochterski, G. A. Petersson, P. Y. Ayala, Q. Cui, K. Morokuma, D. K. Malick, A. D. Rabuck, K. Raghavachari, J. B. Foresman, J. Cioslowski, J. V. Ortiz, A. G. Baboul, B. B. Stefanov, G. Liu, A. Liashenko, P. Piskorz, I. Komaromi, R. Gomperts, R. L. Martin, D. J. Fox, T. Keith, M. A. Al-Laham, C. Y. Peng, A. Nanayakkara, C. Gonzalez, M. Challacombe, P. M. W. Gill, B. G. Johnson, W. Chen, M. W. Wong, J. L. Andres, M. Head-Gordon, E. S. Replogle and J. A. Pople, Gaussian, Inc., Pittsburgh, PA, 1998.
16 A. D. Becke, J. Chem. Phys., 1993, **98**, 5648; A. D. Becke, Phys. Rev. A, 1988, **38**, 3098; C. Lee, W. Yang and R. G. Parr, Phys. Rev. B, 1988, **37**, 785.
17 Preliminary analysis of bond lengths of the low temperature phase of **DPPZ–Cu** measured at 100 K indicates that N2 and N3 are coordinated at the axial positions. The Cu1–N2 distance [2.175(8) Å] was longer than any other distances around Cu1 and the Cu2–N3

distance [2.360(7) Å] was also longer than any other distances around Cu2 at 100 K. No interaction between two Cu ions is rationalized by this structure. Selected crystallographic data are as follows: $C_{34}H_{14}N_4O_8F_{24}Cu_2$, T = 100 K, $P2_1/c$, a = 15.280(7), b = 17.349(6), c = 16.094(4) Å, β = 91.61(3)°, Z = 4, R = 0.0853 ($I > 2\sigma(I)$).
18 W. Wojciechowski, Inorg. Chim. Acta, 1967, **1**, 319.
19 M. Yasui, Y. Ishikawa, N. Akiyama, T. Ishida, T. Nogami and F. Iwasaki, Acta Crystallogr., Sect. B, 2001, **57**, 288; R. Feyerherm, S. Abens, D. Günther, T. Ishida, M. Meissner, M. Meschke, T. Nogami and M. Steiner, J. Phys.: Condens. Matter, 2000, **12**, 8495.
20 T. Ezuhara, K. Endo, K. Matsuda and Y. Aoyama, New J. Chem., 2000, **24**, 609.
21 J. Omata, T. Ishida, D. Hashizume, F. Iwasaki and T. Nogami, Inorg. Chem., 2001, **40**, 3954.
22 Y. Pontillon, A. Grand, T. Ishida, E. Lelièvre-Berna, T. Nogami, E. Ressouche and J. Schweizer, J. Mater. Chem., 2000, **10**, 1539.
23 G. Maruta, S. Takeda, R. Imachi, T. Ishida, T. Nogami and K. Yamaguchi, J. Am. Chem. Soc., 1999, **121**, 424.
24 V. A. Reznikov, I. V. Ovcharenko, N. V. Pervukhina, V. N. Ikorskii, A. Grand and V. I. Ovcharenko, Chem. Commun., 1999, 539; Y. Takano, Y. Kitagawa, T. Onishi, Y. Yoshioka, K. Yamaguchi, N. Koga and H. Iwamura, J. Am. Chem. Soc., 2002, **124**, 450.
25 F. Mohri, K. Yoshizawa, T. Yamabe, T. Ishida and T. Nogami, Mol. Eng., 1999, **8**, 357.
26 K. Nakayama, T. Ishida, R. Takayama, D. Hashizume, M. Yasui, F. Iwasaki and T. Nogami, Chem. Lett., 1998, 497.
27 T. Kusaka, T. Ishida, D. Hashizume, F. Iwasaki and T. Nogami, Chem. Lett., 2000, 1146.
28 K. Zusai, T. Kusaka, T. Ishida, R. Feryerherm, M. Steiner and T. Nogami, Mol. Cryst. Liq. Cryst., 2000, **343**, 127.
29 T. Kusaka, T. Ishida, D. Hashizume, F. Iwasaki and T. Nogami, Mol. Cryst. Liq. Cryst., 2002, **376**, 463.
30 Y. Takano, T. Onishi, Y. Kitagawa, T. Soda, Y. Yoshioka and K. Yamaguchi, Int. J. Quantum Chem., 2000, **80**, 681.
31 K. Yamaguchi, M. Okamura, K. Takeda and S. Yamanaka, Int. J. Quantum Chem., Quantum Chem. Symp., 1993, **27**, 501.
32 P. W. Anderson, Phys. Rev., 1959, **115**, 2.
33 J. B. Goodenough, Phys. Rev., 1955, **100**, 564.
34 J. Kanamori, J. Phys. Chem. Solids, 1959, **10**, 87.
35 N. Torihara, H. Okawa and S. Kida, Chem. Lett., 1978, 1269.
36 O. Kahn, J. Galy, Y. Journaux, J. Jaud and I. Morgenstern-Badarau, J. Am. Chem. Soc., 1982, **104**, 2165.
37 M. Ohba, H. Tamaki, N. Matsumoto and H. Okawa, Inorg. Chem., 1993, **32**, 5385.
38 S. Rajca and A. Rajca, J. Solid State Chem., 2001, **159**, 460; K. Matsuda, N. Nakamura, K. Inoue, N. Koga and H. Iwamura, Bull. Chem. Soc. Jpn., 1996, **69**, 1483.

Pergamon

Tetrahedron Letters 43 (2002) 5521–5524

TETRAHEDRON LETTERS

Convenient synthesis and host–guest compounds of 9,9′(10*H*,10′*H*)-spirobiacridines

Motohiro Ooishi, Makoto Seino, Ron Imachi, Takayuki Ishida* and Takashi Nogami*

Department of Applied Physics and Chemistry, The University of Electro-Communications, Chofu, Tokyo 182-8585, Japan

Received 22 April 2002; revised 6 June 2002; accepted 14 June 2002

Abstract—9,9′(10*H*,10′*H*)-Spirobiacridine and its 2-methoxy derivative were prepared from the corresponding diphenylamines and acridone in three steps. A nearly D_{2d} molecular skeleton of the spiro compounds was confirmed by X-ray crystallographic analysis. The spirobiacridines can work as a new class of host compounds owing to their ability to form nearly rectangular hydrophobic cages in the crystal.

Spiro-compounds involving orthogonally fused π-conjugated moieties are supposed to have potential utility for molecular electronic devices,[1] and spirobifluorene[2] and spiro-fused thiophene systems[3] are proposed for action as a transistor source-drain channel. The orthogonal arrangement of two π-conjugated portions also attracts much attention in magnetochemistry[4] as well as physical organic chemistry, especially in connection with spiro-conjugation.[5,6] We have developed a convenient synthetic route to 9,9′(10*H*,10′*H*)-spirobiacridine (**1**) and its 2-methoxy derivative (**2**). Weber and coworkers proposed that crystals of spiro-compounds gave a high percentage of free volume into which small guest molecules might be enclosed, owing to their bulky and rigid molecular geometry.[7] However, there are quite a few reports on clathration using spiro-compounds.[7–9] In the course of our study on the crystal structure analysis of **1** and **2**, we have found that **2** afforded a variety of solvated crystalline compounds.

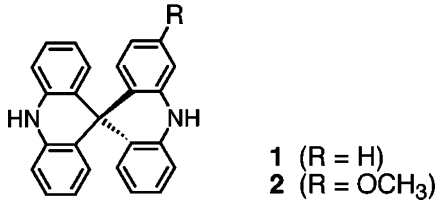

1 (R = H)
2 (R = OCH_3)

Compound **1** was prepared in three steps from the starting materials, diphenylamine (**3**) and acridone (**4**), as follows:

(i) The NH group in **3** was easily protected with a *t*-butoxycarbonyl group (BOC), giving BOC-**3** (for the structural formula, see Scheme 1). The BOC group facilitates directed *ortho*-metallation in BOC-**3**.[10]

(ii) The NH group in **4** was protected with a conventional 2-methoxyethoxymethyl group (MEM) by use of NaH followed by MEM-Cl in *N*,*N*-dimethylformamide to give MEM-**4**[11] (for the structural formula, see Scheme 1).

(iii) A one-pot procedure was developed for addition reaction of MEM-**4** with an *ortho*-lithiated compound from BOC-**3** and the acid-catalyzed intramolecular Friedel–Crafts reaction of the resultant carbinol[12] followed by acid-catalyzed cleavage of the BOC and MEM groups, giving the final product (**1**) (Scheme 1).

The following procedure is typical for the third step described above. To a tetrahydrofuran (THF) solution (10 mL) containing BOC-**3** (1.27 g, 4.71 mmol) and *N*,*N*,*N*′,*N*′-tetramethylethylenediamine (TEMDA; 0.80 mL, 5.3 mmol), a hexane solution of *t*-BuLi (1.48 mol/L, 3.50 mL, 5.2 mmol) was added with a syringe at −78°C. After being stirred for 2 h, a THF solution (25 mL) of MEM-**4** (1.41 g, 4.98 mmol) was added to the mixture at −78°C. The reaction vessel was gradually warmed to room temperature over 2 h. The solution was acidified with diluted HCl (0.5 mol/L, 5.0 mL) and stirred at room temperature overnight. The reaction mixture was further acidified with diluted HCl (0.5 mol/L, 10 mL) and again stirred for 1 day. After aqueous K_2CO_3 was added until the mixture was neutralized, CH_2Cl_2 was added. The organic layer was

Keywords: spiro compounds; lithiation; acridines; X-ray crystal structures; host compounds.

* Corresponding authors. Tel.: +81-424-43-5490; fax: +81-424-43-5501; e-mail: ishi@pc.uec.ac.jp

0040-4039/02/$ - see front matter
PII: S0040-4039(02)01165-6

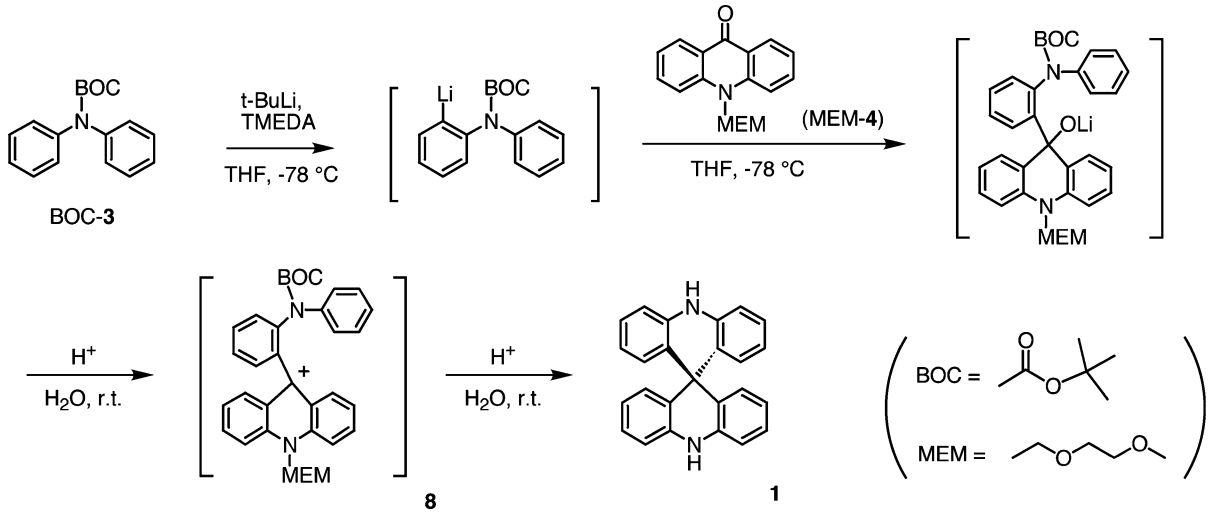

Scheme 1. Synthetic route to spirobiacridine.

separated, washed with water, dried over $MgSO_4$, and concentrated under reduced pressure. The residue was purified by passing a short column (silica gel, eluted with 1:1 hexane/CH_2Cl_2) and recrystallization from hexane/CH_2Cl_2 gave pure **1** (mp>300°C)[13] (0.847 g, 2.45 mmol). The isolated yield was 52% from BOC-**3**.

Daltrozzo and co-workers reported the synthesis of **1** in 7% yield from the same starting materials **3** and **4** under harsh conditions (260°C in an autoclave).[13] The present method considerably improves the yield, and the reaction can be easily conducted under ambient pressure in ordinary apparatus. They also reported the synthesis of **5** from **6** by applying the Grignard reaction with *N*-methylacridone.[14] However, *o*-halogenated diphenylamines are required and the synthetic labor increases accordingly, compared with the present preparation.

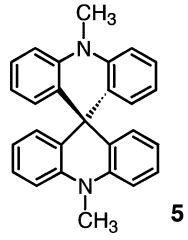

5

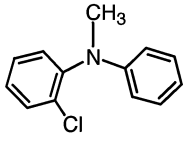

6

Note that only 9-(2-phenylaminophenyl)acridine (**7**)[15] was obtained as the final product when we used BOC-**4** in place of MEM-**4**. A trityl-type cation (**8**) is assumed to be a key intermediate. This finding suggests that aromatization of **8** competes with the desired Friedel–Crafts reaction. The retardation of the N-C(MEM) cleavage compared to the N-C(BOC) cleavage plays a crucial role in this reaction.

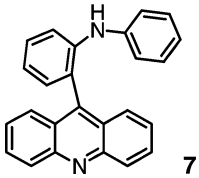

7

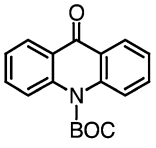

BOC-**4**

A methoxy-substituted derivative could also be prepared in a similar manner to that of **1**. After a BOC group was introduced to 3-methoxydiphenylamine (**9**), the resultant BOC-**9** was coupled with MEM-**4** to give a new compound 2-methoxyspirobiacirdine (**2**), which was purified by means of HPLC (Japan Analytical Industry, JAIGEL 1H+1H, eluted with $CHCl_3$). The isolated yield was 23% from BOC-**9**. The spectroscopic data of **2** satisfy the molecular structure,[16] which was finally confirmed by X-ray crystallographic analysis (see below).

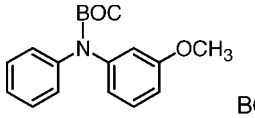

BOC-**9**

We have to state possible positions of directed lithiation in BOC-**9**, since **2** was obtained as an unexpected major isomer. Detailed analyses of ^1H NMR and mass spectra for the deuterated products after D_2O-quenching experiments reveal that the lithiation preferentially takes place at the 2 position (**A**); deuterated BOC-**9** showed a considerably lowered signal at 6.78 ppm ascribable to the proton of the 2 position and practically no ^1H–^1H coupling related to H2 in the 1D and 2D ^1H NMR measurements. This finding is explained by the stabilization with both neighboring BOC and CH_3O groups in **A**. However, the structure of main product **2** indicates that the 6 and 2′ positions are lithiated (**B** and **C**, respectively). There seems to be an equilibrium among **A**–**C**, and **A** hardly reacts with MEM-**4** because of the steric congestion while **B** and **C** are consumed and supplied from **A** via the equilibrium.

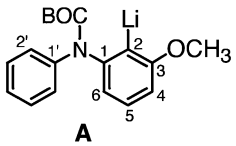

A

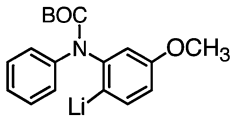

B

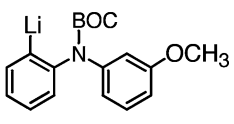

C

We confirmed the molecular structures of **1** and **2** by means of X-ray crystallographic analysis.[17] Two acridine planes in **1** are perpendicular to each other as demonstrated by the dihedral angle between the two averaged planes of 90.53(3)° (each least-square averaged plane was defined with the C and N atoms in a diphenylamine moiety). No appreciable pyramidalization is found at the nitrogen atoms. The molecule has a pseudo-D_{2d} structure although two acridine moieties are crystallographically independent. As Fig. 1 shows, **2** has essentially the same structure as that of **1** except for the additional methoxy group. The orthogonal arrangement between two acridine planes was indicated similarly by the dihedral angle of 90.20(3)° between them.

The spirobiacridines can work as a new class of a host compound. The rigid molecular structure of **2** is likely to form nearly rectangular hydrophobic cages in the crystal, where the solvent molecules can be incorporated. In fact, solvated crystals were obtained by crystallization in all cases investigated here. Binary compounds **2**·$(CH_2Cl_2)_2$ and **2**·$(CHCl_3)_2$ and a ternary compound **2**·CH_2Cl_2·C_6H_6 (Fig. 2) were obtained from the corresponding solutions, whose compositions were determined by X-ray crystallographic analysis.[17] A few appreciable van der Waals contacts could be found between the guest molecules and **2**. The nearest interatomic distance is 3.366(3) Å [Cl(1)···C(16)] between **2** and CH_2Cl_2, which is shorter than the sum of the van der Waals radii.[18] For the crystals of **2**·$(CH_2Cl_2)_2$ and **2**·$(CHCl_3)_2$, the chlorine atoms of the solvent molecules have contact likewise with the skeletal carbon atoms in **2**; the shortest Cl···C distances are 3.482(2) and 3.260(6) Å for **2**·$(CH_2Cl_2)_2$ and **2**·$(CHCl_3)_2$, respectively.

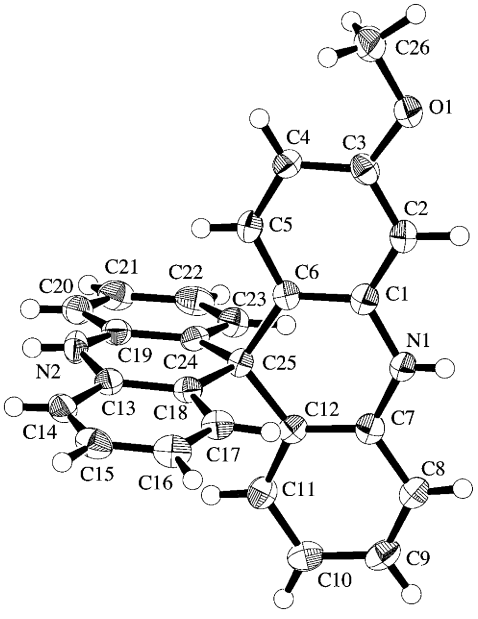

Figure 1. Molecular structure of **2** in the crystal of **2**·$(CH_2Cl_2)_2$ with thermal ellipsoids at the 50% level. Selected bond lengths (Å) and angles (°): C6–C25 1.532(3), C12–C25 1.535(3), C18–C25 1.532(3), C24–C25 1.530(3), C6–C25–C12 110.7(2), C18–C25–C24 110.8(2).

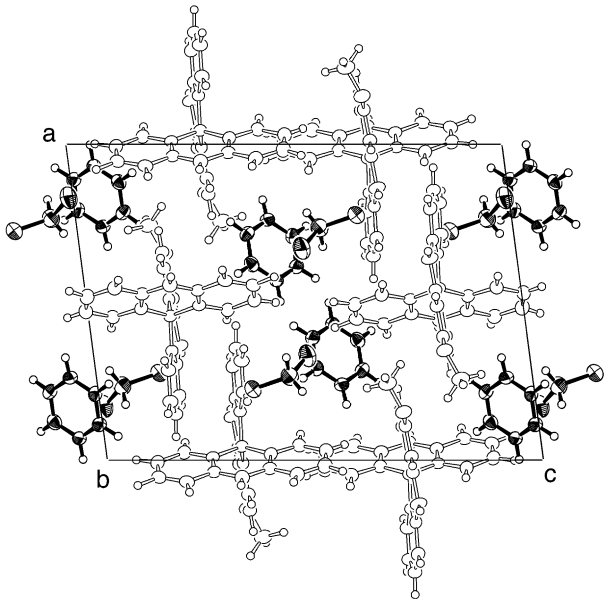

Figure 2. Crystal structure of **2**·CH_2Cl_2·C_6H_6 with thermal ellipsoids at the 50% level. The guest molecules CH_2Cl_2 and C_6H_6 are shaded.

Although **2** has two NH groups, there are no hydrogen bonds in the above solvated crystals, which is in sharp contrast to the hydrogen-bonded host–guest compounds involving 9,9′-spirobifluorene-2,2′-dicarboxylic acid[7] for example. The host–guest interactions in the solvated crystalline compounds of **2** originate in hydrophobic interaction and van der Waals contacts.

In summary, we have reported here a convenient synthesis of **1** and **2** from the corresponding diphenylamines and acridone in three steps. Novel host–guest compounds have been characterized. Conducting and/or magnetic materials derived from spiro-conjugation systems are of great interest as described above, and the present work suggests that these physical properties based on intermolecular interactions may be tuned and controlled by formation of host–guest complexes. Synthesis of nitroxide radicals from **1** and **2** according to established methods[19] is now underway.[20]

Acknowledgements

This work was supported by a Grant-in-Aid for Scientific Research on Priority Areas of ''Molecular Conductors and Magnets'' (No. 730/11224204) and by a Grant-in-Aid for Scientific Research (No. 13640575) from the Ministry of Education, Culture, Sports, Science, and Technology, Japan.

References

1. Joachim, C.; Gimzewski, J. K.; Aviram, A. *Nature* **2000**, *408*, 541.
2. (a) Tour, J. M.; Wu, R.; Schumm, J. S. *J. Am. Chem. Soc.* **1990**, *112*, 5662; (b) Wu, R.; Schumm, J. S.; Pearson, D. L.; Tour, J. M. *J. Org. Chem.* **1996**, *61*, 6906.
3. Aviram, A. *J. Am. Chem. Soc.* **1988**, *110*, 5687.
4. (a) Chiarelli, R.; Novak, M. A.; Rassat, A.; Tholence, J. L. *Nature* **1993**, *363*, 147; (b) Dupeyre, R. M.; Rassat, A.; Ronzaud, J. *J. Am. Chem. Soc.* **1974**, *96*, 6559.
5. (a) Haddon, R. C.; Chichester, S. V.; Marshall, J. H. *Tetrahedron Lett.* **1986**, *42*, 6293; (b) Chi, X.; Itkis, M. E.; Kirschbaum, K.; Pinkerton, A. A.; Oakley, R. T.; Cordes, A. W.; Haddon, R. C. *J. Am. Chem. Soc.* **2001**, *123*, 4041.
6. Frank, N. L.; Rodolphe, C.; Sutter, J.-P.; Daro, N.; Kahn, O.; Coulon, C.; Green, M. T.; Golhen, S.; Ouahab, L. *J. Am. Chem. Soc.* **2000**, *122*, 2053.
7. Czugler, M.; Stezowski, J. J.; Weber, E. *J. Chem. Soc., Chem. Commun.* **1983**, 154.
8. Krieger, C.; Diederich, F. *Chem. Ber.* **1985**, *118*, 3620.
9. Lustenberger, P.; Martinborough, E.; Denti, T. M.; Diederich, F. *J. Chem. Soc., Perkin Trans. 2* **1998**, 747.
10. MacNeil, S. L.; Gray, M.; Briggs, L. E.; Li, J. J.; Snieckus, V. *Synlett* **1998**, 419.
11. Zeng, Z.; Zimmerman, S. C. *Tetrahedron Lett.* **1988**, *29*, 5123.
12. Berti, C.; Colonna, M.; Greci, L.; Marchertti, L. *Gazz. Chim. Ital.* **1978**, *108*, 659.
13. Tritschler, W.; Sturm, E.; Kiesele, H.; Daltrozzo, E. *Chem. Ber.* **1984**, *117*, 2703.
14. Sturm, E.; Kiesele, H.; Daltrozzo, E. *Chem. Ber.* **1978**, *111*, 227.
15. Mp 122–123°C. ^{1}H NMR (270 MHz, $CDCl_3$): δ 5.1 (1H, bs), 6.85–6.94 (2H, m), 7.07–7.25 (4H, m), 7.41–7.55 (4H, m), 7.71–7.79 (4H, m), 8.22 (2H, d, $J=8.7$ Hz). ^{13}C NMR (125 MHz, $CDCl_3$): δ 116.1, 119.7, 120.3, 122.0, 123.8, 125.4, 126.2, 126.4, 129.2, 129.6, 129.8, 130.3, 131.8, 142.1, 142.2, 143.8, 149.0. MS (EI, 70 eV) m/z 346 (M^+), 269, 77.
16. ^{1}H NMR (500 MHz, $CDCl_3$): δ 3.73 (3H, s), 6.21 (2H, brs), 6.24 (1H, d, $J=2$ Hz), 6.28 (1H, dd, $J=2$, 9 Hz), 6.66–6.70 (6H, m), 6.84 (1H, d, $J=9$ Hz), 6.93–6.96 (3H, m), 6.98–7.01 (3H, m). ^{13}C NMR (125 MHz, $CDCl_3$): δ 46.6, 55.1, 97.8, 107.2, 113.11, 113.13, 120.8, 120.9, 123.8, 126.9, 130.7, 130.9, 132.2, 132.3, 133.3, 135.6, 135.7, 136.6, 158.5. Two signals accidentally overlap at 126.9 ppm, as suggested by the relative signal intensity. MS (EI, 70 eV) m/z 376 (M^+), 360, 345. The mp could not be determined because of liberation of crystal solvent molecules.
17. Data were collected on a Rigaku RAPID IP diffractometer using graphite-monochromated CuKα radiation ($\lambda=$ 1.54184 Å) at 100 K. All of the atoms including hydrogens could be found in difference Fourier maps. The atomic coordinates and thermal displacement parameters were refined anisotropically for non-hydrogen atoms and isotropically for hydrogen atoms using all the reflection data of $2\theta<136°$. Selected crystallographic data: **1**, $C_{25}H_{18}N_2$, monoclinic, $C2/c$, $a=17.576(1)$, $b=$ 11.7483(8), $c=18.449(2)$ Å, $\beta=115.730$ (3)°, $V=$ 3431.9(4) Å^3, $Z=8$, $D_{calc}=1.341$ g cm^{-3}, R ($I>2\sigma(I)$) $=0.0550$, R_w (all data) $=0.1346$ for 3043 observed reflections. **2**·$(CH_2Cl_2)_2$, $C_{28}H_{24}Cl_4N_2O$, monoclinic, $P2_1/c$, $a=15.332(1)$, $b=9.9600(7)$, $c=16.605(1)$ Å, $\beta=95.671(2)°$, $V=2523.3(3)$ Å^3, $Z=4$, $D_{calcd}=1.438$ g cm^{-3}, R ($I>2\sigma(I)$) $=0.0545$, R_w (all data) $=0.1437$ for 4590 observed reflections. **2**·$(CHCl_3)_2$, $C_{28}H_{22}Cl_6N_2O$, orthorhombic, $Pca2_1$, $a=19.8734(8)$, $b=13.1781(5)$, $c=$ 10.5520(4) Å, $V=2763.5(3)$ Å^3, $Z=4$, $D_{calc}=1.479$ g cm^{-3}, R ($I>2\sigma(I)$) $=0.0693$, R_w (all data) $=0.2093$ for 2650 observed reflections. **2**·CH_2Cl_2·C_6H_6, $C_{33}H_{26}Cl_2N_2O$, monoclinic, $P2_1/n$, $a=13.9196(6)$, $b=$ 10.2311(5), $c=19.0260(9)$ Å, $V=2686.4(2)$ Å^3, $Z=4$, $D_{calcd}=1.329$ g cm^{-3}, R ($I>2\sigma(I)$) $=0.0661$, R_w (all data) $=0.1720$ for 4706 observed reflections. One chlorine atom in **2**·$(CHCl_3)_2$ was analyzed to be disordered into two positions. Crystallographic data (excluding structure factors) for **1**, **2**·$(CH_2Cl_2)_2$, **2**·$(CHCl_3)_2$, and **2**·CH_2Cl_2·C_6H_6 have been deposited with the Cambridge Crystallographic Data Centre as supplementary publication nos. CCDC 184259–184262.
18. Bondi, A. *J. Phys. Chem.* **1964**, *68*, 441.
19. (a) Imachi, R.; Ishida, T.; Suzuki, M.; Yasui, M.; Iwasaki, F.; Nogami, T. *Chem. Lett.* **1997**, 743; (b) Nakagawa, M.; Ishida, T.; Suzuki, M.; Hashizume, D.; Yasui, M.; Iwasaki, F.; Nogami, T. *Chem. Phys. Lett.* **1999**, *302*, 125; (c) Seino, M.; Akui, Y.; Ishida, T.; Nogami, T. *Synth. Met.*, in press.
20. A nitroxide radical (**10**) prepared from **1** was found to possess ability to construct host–guest complexes. The crystal structure of **10** precipitated from CH_2Cl_2 was preliminarily characterized to be **10**·$(CH_2Cl_2)_2$ in a monoclinic $C2/c$ space group by means of X-ray crystallographic analysis.

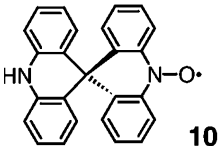

10

Metal-Azide-Pyrimidine Complexes $M(N_3)_2(pm)$ with a Three-Dimensional Network Showing Weak Ferromagnetism for M = Mn and Fe and Antiferromagnetism for M = Co and Ni

Yoshitaka Doi, Takayuki Ishida,* and Takashi Nogami*

Department of Applied Physics and Chemistry, The University of Electro-Communications, Chofu, Tokyo 182-8585

(Received June 7, 2002)

Antiferromagnetic phase transitions of $M(N_3)_2(pm)$ were observed at 51, 39, 41, and 46 K for M = Mn, Fe, Co, and Ni, respectively; here pm denotes pyrimidine. Single-crystal X-ray crystallographic analysis for M = Mn, Fe, and Co and powder X-ray diffraction measurements for M = Ni revealed that they were isomorphous. The N_3 and pm moieties contribute μ-1,3-bridged two-dimensional and μ-1,3-bridged one-dimensional structures, respectively, thus forming a three-dimensional framework. Antiferromagnetic couplings through the bridging ligands are consistent with superexchange mechanisms based on the coordination geometry determined. Small spin canting was observed below the transition temperature for M = Mn and Fe. The cant angles are estimated to be 0.06 and 0.13°, respectively, from the spontaneous magnetization at 10 K.

There have been numerous reports on infinite metal-organic polymeric frameworks involving N-donor bridging ligands.[1] We have reported the magnetism of pyrimidine(pm)-bridged transition metal complexes in connection with the high-spin *m*-phenylene-bridged poly-carbenes and -radicals.[2] The role of pm as magnetic couplers has been clarified to depend on the magnetic orbitals on the metal ions and the coordination geometries.[3] Various magnets have also been reported that contain d-transition metal ions and polycyano-anion bridges such as $N(CN)_2^-$.[4,5] Ternary systems are of increasing interest, and the peculiar crystal structures have been reported for $Mn[N(CN)_2]_2(pz)$[6] and $Cu[N(CN)_2]_2(pz)$,[7] where pz denotes pyrazine. We preliminarily reported the crystal structure and magnetic phase transition of $M^{II}[N(CN)_2]_2(pm)(solvent)$ (M = Fe,[8] Co,[8] Ni[9]) containing both $N(CN)_2^-$ and pm bridges. Their magnetic phase transition temperatures were generally low,[8,9] mainly because of the effective low dimensionality; the $N(CN)_2$ bridge works only as a μ-1,5-bridge that mediates much weaker magnetic exchange interaction than the μ-1,3-pm bridge. A copper(II) derivative $Cu[N(CN)_2]_2(pm)(CH_3CN)$ whose crystal structure was quite similar to those of $M[N(CN)_2]_2(pm)(solvent)$ (M = Fe, Co, Ni) was also synthesized, but it does not undergo any magnetic phase transition down to 2 K.[10] We turned our attention to shorter bridging anions. The azido-bridges are generally observed as end-on (μ-1,1) and end-to-end (μ-1,3) coordination modes, and their role as magnetic couplers have widely been investigated.[11,12] We prepared transition metal complexes, $M(N_3)_2(pm)$, with three-dimensional networks of transition metal ions containing both μ-1,3-azide and μ-1,3-pm bridges (the structural formula is shown in Chart 1; **1**, **2**, **3**, and **4** for M = Mn, Fe, Co, and Ni, respectively). We will describe here the crystal structures and magnetic properties of **1**–**4**. Escuer and co-workers have independently studied the crystal structure and magnetic property of **1**.[13] Our results on **1** are essentially the same as theirs. We will discuss here the comparison of the magnetic properties of **1** with those of **2**–**4**.

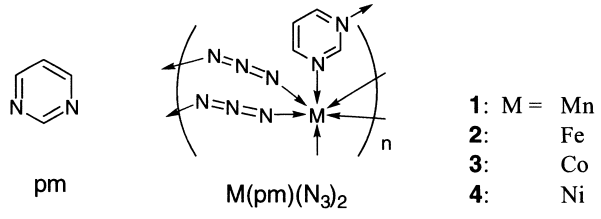

Chart 1.

Experimental

Caution. Azide derivatives are potentially explosive. Only a small amount of material should be prepared, and it should be handled with caution.

Materials. The following synthetic procedure is typical. An aqueous solution (1 cm^3) containing pm (79.9 mg, 1.00 mmol) and NaN_3 (130.2 mg, 2.00 mmol) was added to an aqueous solution (1 cm^3) of $MnCl_2{\cdot}4H_2O$ (198.5 mg, 1.00 mmol). The mixture was allowed to stand for several days to give colorless single crystals of $Mn(N_3)_2(pm)$ (**1**) suitable for X-ray diffraction study. Similar procedures using $FeCl_2{\cdot}4H_2O$ and $CoCl_2{\cdot}6H_2O$ in place of $MnCl_2{\cdot}4H_2O$ gave yellow and purple crystals of **2** and **3**, respectively. Preparation using $NiCl_2{\cdot}6H_2O$ gave light green fine powder of $Ni(N_3)_2(pm)$ (**4**). Elemental analyses (C, H, N) of **1**–**4** on a Fisons EA-1108 by a usual combustion method supported the formula of $M(N_3)_2(pm)$. Anal. Calcd. for $C_4H_4N_8Mn$ (**1**): C, 21.93; H, 1.84; N, 51.15%. Found: C, 21.53; H, 1.93; N, 50.56%. Calcd. for $C_4H_4N_8Fe$ (**2**): C, 21.84; H, 1.83; N, 50.94%. Found: C, 22.11; H, 1.67; N, 50.39%. Calcd. for $C_4H_4N_8Co$ (**3**): C, 21.54; H, 1.81; N, 50.23%. Found: C, 21.53; H, 1.78; N, 49.93%. Calcd. for $C_4H_4N_8Ni$ (**4**): C, 21.56; H, 1.81; N, 50.29%. Found: C, 21.52; H,

1.96; N, 49.92%.

X-ray Crystallographic Analysis. Diffraction data of single crystals of **1**–**3** were collected on a Rigaku R-axis RAPID diffractometer with graphite monochromated Mo $K\alpha$ radiation (λ = 0.71069 Å) at 90 or 100 K. The structures were directly solved by a heavy-atom Patterson method in the teXsan program package.[14] Numerical absorption correction was used. All of the hydrogen atoms could be found in difference Fourier maps, and the parameters of the hydrogen atoms were included in the refinement. The thermal displacement parameters were refined anisotropically for non-hydrogen atoms and isotropically for hydrogen atoms. Full-matrix least-squares methods were applied using all of the unique diffraction data. Crystallographic data have been deposited as Document No. 75044 at the Office of the Editor of Bull. Chem. Soc. Jpn. and also deposited with the CCDC (the reference numbers are 186730–186732 for **1**–**3**). Powder pattern data of **4** were recorded on a Rigaku RAD-B diffractometer with graphite monochromated Cu $K\alpha$ radiation (λ = 1.5418 Å) at 300 K. Refined cell constants were calculated on the Rietan2000 program[15] using all data in a range of $10° < 2\theta < 60°$.

Magnetic Measurements. Dc and ac magnetic susceptibilities of polycrystalline samples of **1**–**4** were measured on Quantum Design MPMS SQUID and PPMS magnetometers equipped with 7 and 9 T coils, respectively, in a temperature range down to 1.8 K. The magnetic responses were corrected with diamagnetic blank data of the sample holder obtained separately. The diamagnetic contribution of the sample itself was estimated from Pascal's constant. Ac magnetic susceptibilities were measured on a PPMS ac/dc magnetometer. An ac magnetic field (amplitude: 10 Oe, frequency: 100, 1000, and 10000 Hz) was applied to polycrystalline samples.

Results

X-ray Crystal Structure Analysis. Table 1 summarizes the X-ray crystallographic data for **1**–**3**. The crystals of **1**–**3** are practically identical, belonging to a space group monoclinic *C*2/*m*. Figure 1 shows the crystal structure of **2**. There is only one M ion in a crystallographically independent unit. Each octahedral M ion resides at an inversion center and is coordinated by four azide N atoms and two pm N atoms (Fig. 1(a)). The M ion and two N_3^- ions construct a two-dimensional network parallel to the *ac*-plane (Fig. 1(b)); an almost square lattice is formed by a repeating macrocyclic $[MN_3]_4$ motif. Selected bond lengths for **1**–**3** are listed in Table 2. In the coordination sphere of **1**–**3**, the bond length of M1–N1(pm nitrogen) is longer than those of other M1–N bonds, indicating that the pm nitrogen atoms are located at the axial positions. The pm molecules bridge inter-sheet M ions (Fig. 1(c)), and they construct a *trans* zigzag chain along the *b*-axis. In short, the N_3 and pm moieties contribute μ-1,3-bridged two-dimensional and μ-1,3-bridged one-dimensional structures, respectively, thus forming a three-dimensional framework. The pm plane is located in a nearly gauche manner with respect to the equatorial M–N bonds, as indicated by the dihedral angles of ca. 30° around C1–N1–M1–N2 (Table 2).

The intra-sheet M···M separations are 5.6–5.9 Å across the μ-1,3-azide bridges. The M···M separations of 6.0–6.1 Å across the pm bridge are slightly longer than those across the azide bridge. Since the $d_{x^2-y^2}$ and d_{z^2} are magnetic orbitals in high-spin manganese(II), iron(II), cobalt(II), and nickel(II) ions viewing from the electon configuration $(t_{2g})^n(e_g)^2$, both pm and azide bridges afford appreciable magnetic exchange pathways. The σ-type orbital overlap between the d_z^2 and nitrogen lone pair gives rise to antiferromagnetic superexchange coupling between two d_z^2 spins for pm-bridged complexes.[3] In the present complexes, the pm bridges can work as an antiferromagnetic coupler. Due to the strong directionality of the pm lone-pairs, the elongated octahedral axes of neighboring Mn ions are canted by 109.6(1)°. Within a two-dimensional Mn-azide network, the octahedral axes of neighboring Mn ions are also canted by the same angle. Similar structural arguments hold also for **2** and **3**.

Unfortunately, **4** was obtained only as a fine powder form. We measured the X-ray powder diffraction of **4**. The experimental and simulation results are summarized in Fig. 2. The

Table 1. Crystallographic Parameters of $M(N_3)_2(pm)$ (M = Mn, Fe, Co)

M	Mn	Fe	Co
Formula	$C_4H_4N_8Mn$	$C_4H_4N_8Fe$	$C_4H_4N_8Co$
Habit	Colorless needle	Orange needle	Pink needle
Crystal system	Monoclinic	Monoclinic	Monoclinic
Space group	*C*2/*m*	*C*2/*m*	*C*2/*m*
a / Å	11.325(2)	11.312(1)	11.197(1)
b / Å	12.278(3)	12.0984(8)	11.956(1)
c / Å	7.624(2)	7.5450(7)	7.5049(8)
β / °	129.88(1)	130.837(3)	130.645(3)
V / Å^3	813.5(3)	781.2(1)	762.3(2)
Z	4	4	4
d_{calc} / g cm^{-3}	1.789	1.870	1.943
T / K	90.	100.	100.
λ / Å	0.7107	0.7107	0.7107
μ / mm^{-1}	1.586	1.891	2.213
Reflections	888	901	902
$R(F^2)$ ($I > 2\sigma(I)$)	0.0469	0.0289	0.0324
$Rw(F)$ (all data)	0.1518	0.0880	0.0932
G.O.F.	1.333	1.117	1.499

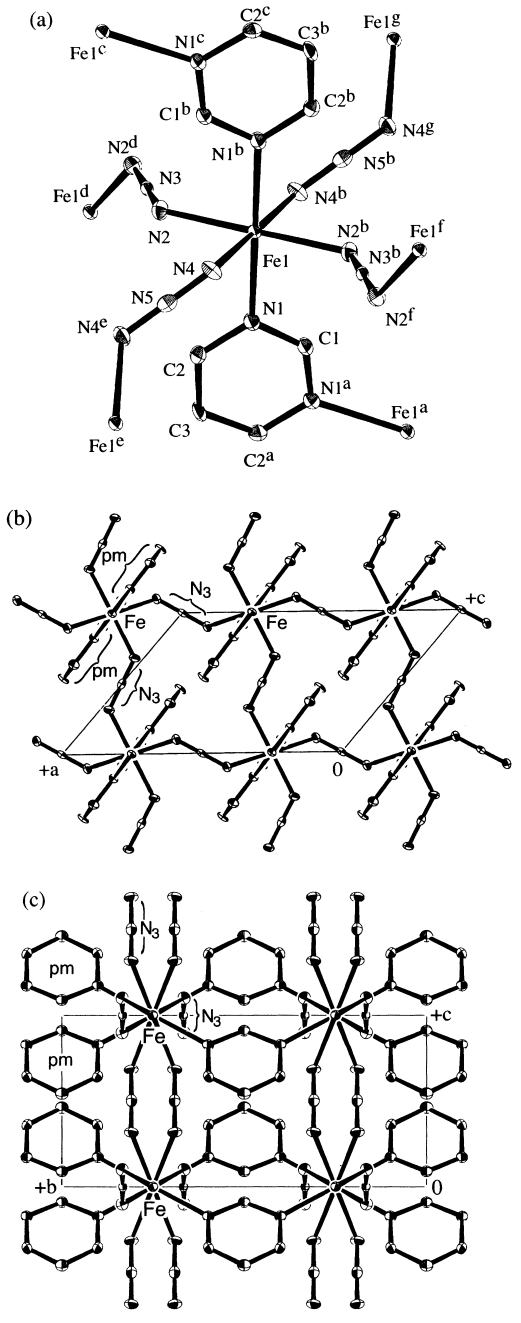

16

Fig. 1. Crystal structure of $Fe(N_3)_2(pm)$ (**2**). Hydrogen atoms are omitted for the sake of clarity. (a) Ortep drawing at the 50% probability level with atom labeling scheme. Symmetry codes: a: $x, -y, z$; b: $-x + 3/2, -y + 1/2, -z$; c: $-x + 3/2, y + 1/2, -z$; d: $-x + 1, y, -z$; e: $-x + 2, y, 1 - z$; f: $x + 1/2, -y + 1/2, z$; g: $x - 1/2, -y + 1/2, z - 1$. (b) Packing diagram viewed along the *b* axis. (c) Viewed along the *a* axis.

Table 2. Selected Bond Lengths, Angles, and Interatomic Distances of $M(N_3)_2(pm)$ (M = Mn, Fe, Co)[a)]

M	Mn	Fe	Co
M1–N1	2.283(3)	2.212(2)	2.165(2)
M1–N2	2.198(3)	2.153(2)	2.123(2)
M1–N4	2.219(3)	2.139(2)	2.125(2)
N1–M1–N2	90.1(1)	90.31(8)	90.56(6)
N1–M1–N4	91.4(1)	92.66(9)	92.60(7)
N2–M1–N4	92.7(1)	91.87(9)	92.05(7)
M1–N2–N3	124.0(2)	126.4(2)	125.6(1)
M1–N4–N5	124.2(2)	124.0(2)	124.1(1)
C1–N1–M1–N2	150.2(4)	149.7(3)	149.8(2)
C1–N1–M1–N4	−122.5(4)	−122.2(3)	−122.3(2)
$M1\cdots M1^{a}$	6.139(2)	6.0492(4)	5.9780(7)
$M1\cdots M1^{d}$	5.663(1)	5.6561(5)	5.5987(7)
$M1\cdots M1^{e}$	5.9010(1)	5.7539(1)	5.7385(1)

a) Symmetry codes: *a*: $x, -y, z$; *d*: $-x + 1, y, -z$; e: $-x + 2, y, 1-z$.

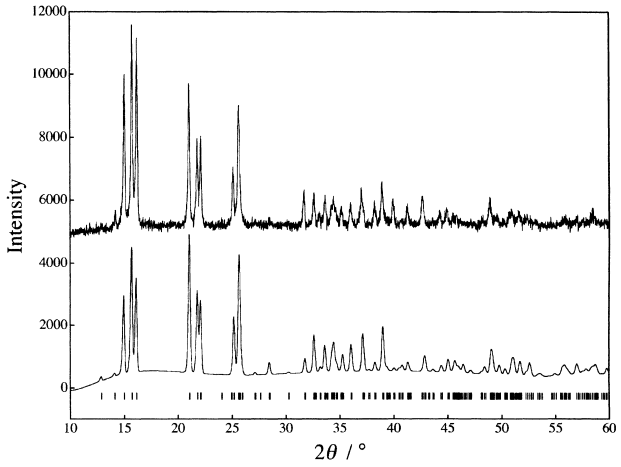

Fig. 2. Experimental (top) and simulated (bottom) profiles of powder X-ray diffraction pattern of $Ni(N_3)_2(pm)$ (**4**). Diffraction positions are indicated by ticks. Optimized cell parameters are: $a = 11.07(1)$, $b = 11.812(6)$, $c = 7.40(1)$ Å, and $\beta = 130.42(6)°$.

profile of **4** is consistent with the cell parameters of $a = 11.07(1)$, $b = 11.812(6)$, $c = 7.40(1)$ Å, $\beta = 130.42(6)°$, and $V = 737(1)$ Å^3, assuming a monoclinic $C2/m$ space group and $Z = 4$. These values are very close to those of **1**–**3** (Table 1). Since the simulation well reproduced the experimental profile, we can safely assume that the crystal structure of **4** is isostructural with those of **1**–**3**. From detailed comparison of the cell lengths and volume, an obvious trend of shrinkage of the cell can be found in the order of M = Mn, Fe, Co, and Ni. The covalent radii of metal ions are responsible for the shrinkage, as indicated by the difference of the M–N bond lengths (Table 2).

Magnetic Properties. Figure 3 shows the temperature dependence of MT/H for **1**–**4** measured at 5 kOe. As a decrease of temperature, the MT/H value ($\chi_{mol}T$ value in a paramagnetic phase) decreased down to ca. 50 K in all cases, indicating the presence of dominant antiferromagnetic coupling among the metal spins.

A best fit of the magnetic susceptibility data of **1** above 200 K to the Curie–Weiss equation [$\chi_{mol} = C/(T - \theta)$] gave $C =$

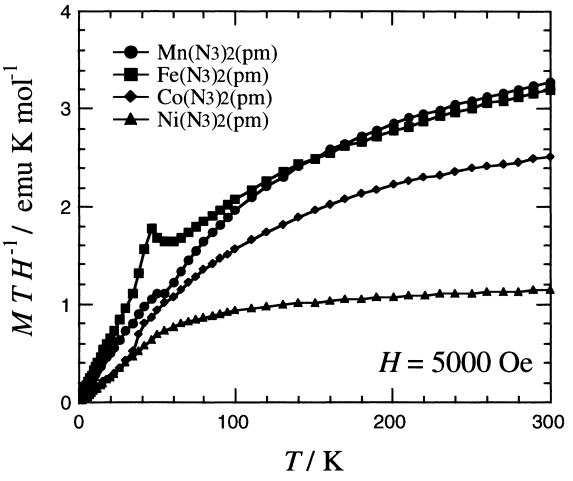

Fig. 3. Temperature dependence of *MT*/*H* for $M(N_3)_2(pm)$ (M = Mn, Fe, Co, and Ni) measured at 5 kOe.

4.56 cm^3 K mol^{-1} and $\theta = -119$ K for **1**. The Landé *g* factor of **1** was derived to be 2.04 for the above Curie constant (*C*) with $S = 5/2$. This g value is somewhat large but very close to that of isomeric $Mn(N_3)_2(pz)$ ($g = 2.03$).[16] The negative Weiss temperature (θ) value clearly indicates the presence of antiferromagnetic interaction among the Mn^{II} spins. A similar analysis for **2** gave $C = 4.62$ cm^3 K mol^{-1} and $\theta = -134$ K. The *g* factor was 2.48 with $S = 2$. The *MT*/*H* values of **1** and **2** do not show monotonic temperature dependence; there is a peak at about 45 K for **1** and a small dip is found at about 55 K for **2**. The size of these anomalies depended on the magnitude of the applied magnetic field. The field-cooled measurements at a small field will be described later.

On the other hand, the *MT*/*H* values of **3** and **4** exhibited monotonic temperature dependence. The Curie and Weiss constants obtained from the data above 200 K are: $C = 3.38$ cm^3 K mol^{-1} and $\theta = -104$ K for **3** and $C = 1.33$ cm^3 K mol^{-1} and $\theta = -49$ K for **4**. The *g* values of metal ions in **3** and **4** are 2.69 and 2.30, respectively. From a close look at the *MT*/*H* curve of **3**, a sharp drop can be found around 35 K, and the *M* vs *T* plot of **3** gave a sharp λ-type maximum at about 42 K (not shown). Similarly, the *M* vs *T* plot of **4** also shows a maximum at about 44 K. These findings suggest that the antiferromagnetic orderings take place around these temperatures.

We measured field-cooled magnetizations, remnant magnetizations, and zero-field-cooled magnetizations of **1**–**4**. The temperature dependence of the field-cooled magnetization at 5 Oe showed clear upsurges at about 51 and 40 K for **1** and **2**, respectively (Fig. 4(a)). After the applied field was removed, the remnant magnetizations disappeared at the same temperatures. The remnant magnetization was observed below the transition temperature in spite of the negative Weiss temperature, indicating that the specimen is a canted antiferromagnet (weak ferromagnet). To determine the magnetic phase transition temperatures more precisely, we performed ac magnetic susceptibility (χ_{ac}) measurements for **1**–**4**. As Fig. 4(b) shows, the real part of the ac magnetic susceptibility (χ_{ac}') exhibited

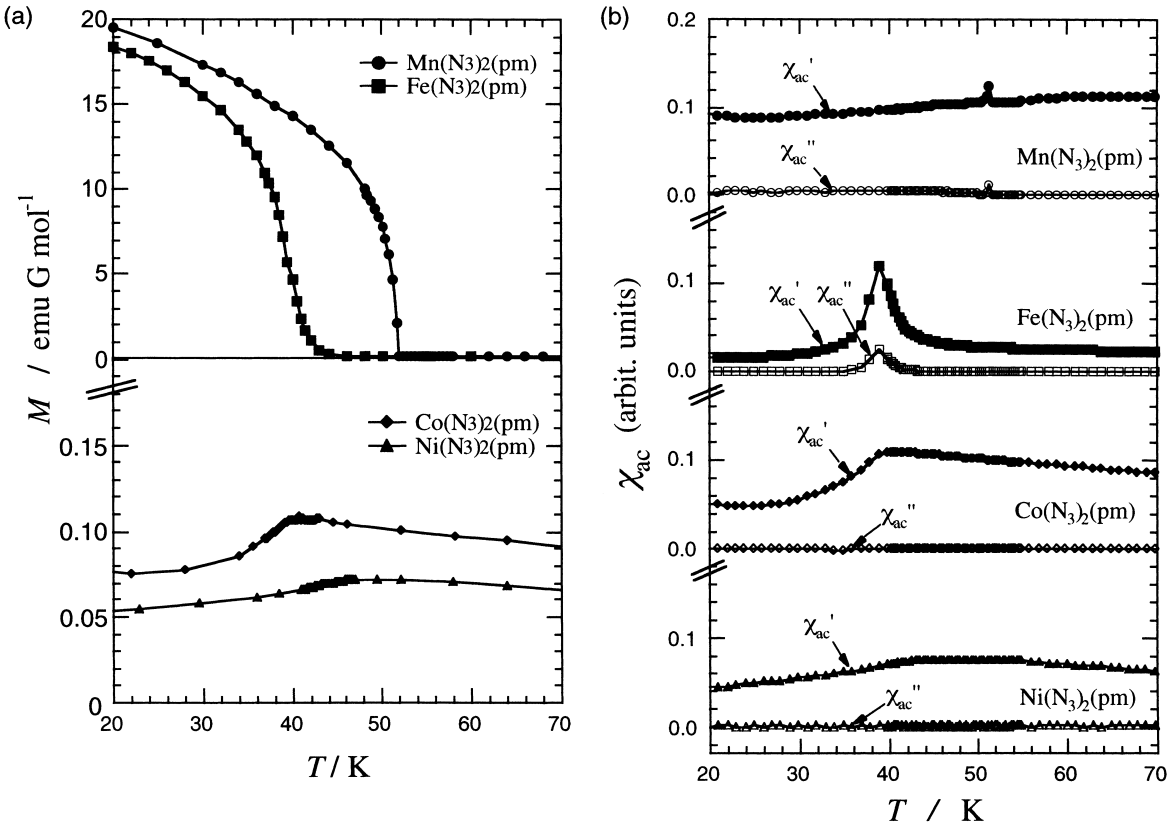

Fig. 4. (a) Field-cooled magnetization of $M(N_3)_2(pm)$ (M = Mn, Fe, Co, and Ni) measured at 5 Oe. (b) Ac susceptibility (χ_{ac}' and χ_{ac}'') of $M(N_3)_2(pm)$ (M = Mn, Fe, Co, and Ni) at an ac magnetic field of 10 Oe with a frequency of 1 kHz.

peaks at 51 and 39 K for **1** and **2**, respectively, supporting the occurrence of magnetic phase transition. Furthermore, the imaginary part of the ac susceptibility (χ_{ac}'') also showed peaks at the same temperatures. No frequency dependence was observed for ν = 100, 1000, and 10000 Hz, indicating that the materials have no spin-glass or superparamagnetic property. On the other hand, the χ_{ac}' of **3** shows an abrupt drop at 41 K on cooling, indicating that **3** is an antiferromagnet below 41 K. Similarly, the χ_{ac}' of **4** shows a decrease on cooling below 46 K. The rather broad peak seems to be caused by the poor crystallinity of **4** compared with those of **1**–**3**. The similarity of these magnetic properties of **3** and **4** is rationalized by taking the isomorphism into consideration. In sharp contrast to the case of **1** and **2**, the χ_{ac}'' of **3** and **4** exhibited no anomaly around the magnetic phase transition temperature, which suggests that the magnetic ground states of **1** and **2** are different from those of **3** and **4**.

In order to clarify the nature of magnetism below the transition temperature, we measured *M*–*H* curves for **1**–**4**. Figure 5(a) shows the magnetization curve of **1** measured at 10 K. The magnetization varied linearly up to 70 kOe, owing to strong antiferromagnetic interaction. This finding is compatible with the dominant antiferromagnetic behavior of **1** observed in the *MT*/*H* vs *T* plot (Fig. 3). However, we can find a small hysteresis loop in a low field region. The spontaneous magnetization extrapolated to $H \rightarrow 0$ Oe was found to be 30 erg Oe^{-1} mol^{-1} and the coercive field was 250 Oe (the inset of Fig. 5(a)). This magnetic behavior of **3** is typical of a weak ferromagnet (canted antiferromagnet). The cant angle was estimated to be 0.06° from $\sin^{-1}(M_{sp}/M_{sat})$ where M_{sp} and M_{sat} imply the spontaneous magnetization and saturation magnetization, respectively. A calculated M_{sat}, $N_A g \mu_B S$, was used in the above estimation because the magnetization did not saturate up to the highest applied field in our measurements.

Similarly, the *M*–*H* curve of **2** showed a basically antiferromagnetic nature with a hysteresis loop (Fig. 5(b)). The spontaneous magnetization was 60 erg Oe^{-1} mol^{-1} and the coercive force was 1200 Oe. The cant angle was estimated to be 0.13°.

On the other hand, the *M*–*H* curves of **3** and **4** indicate that they are genuine antiferromagnets. Figures 5(c) and 5(d) show that the magnetization varied almost linearly up to 90 kOe. In spite of the ambiguous broad peaks in the FCM and χ_{ac}' measurements of **4**, the *M*–*H* curve of **4** supports the occurrence of an antiferromagnetic phase transition. The curvature of the *M* vs. *H* plot (Fig. 5(d)) was convex downward on increasing an applied field, indicating a possible spin–flop transition on applying a further field. This curvature depends very little on temperature. Actually, the *M*–*H* curve of **4** measured at 2 K was essentially the same as that at 10 K; no obvious spin-flop transition was observed up to H = 90 kOe even at 2 K.

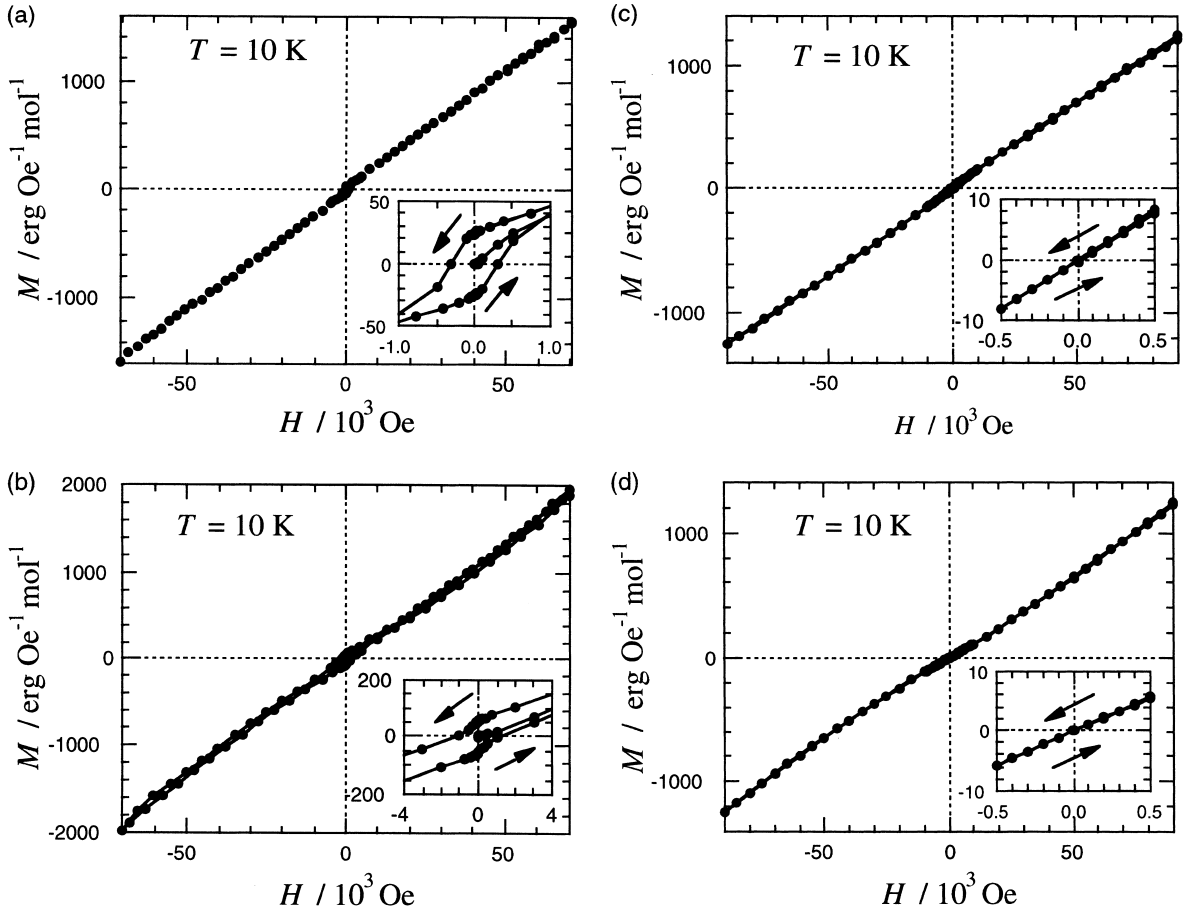

Fig. 5. *M*–*H* curves of $M(N_3)_2$(pm) (a, b, c, and d for M = Mn, Fe, Co, and Ni, respectively) measured at 10 K. Insets show a magnification of a low field region.

The downward curvature is responsible for the abrupt decrease in the *MT*/*H* vs *T* plot, which is characteristic of antiferromagnets. The canted antiferromagnets, **1** and **2**, exhibited a peak or dip of the *MT*/*H* values on cooling (Fig. 3), the origin of which is supposed as follows. The presence of spontaneous magnetization gives rise to an increase of the *MT*/*H* value while the downward curvature leads to a decrease of the *MT*/*H* values. The peak or dip is observed as a results of a balance of the two opposite effects. In fact, the anomalies of **1** and **2** in the *MT*/*H* vs *T* plot depend on the applied field as described above.

Discussion

The structural comparison between $M(N_3)_2(pm)$ and $M[N(CN)_2]_2(pm)$[8,9] indicates that the following features are common in spite of different crystal systems: 1) M^{II} and two anions construct a two-dimensional network. 2) Pm molecules bridge inter-sheet M^{II}, forming a pm-M *trans* zigzag chain. 3) Crystallographically asymmetric units contain only one metal ion. 4) Each octahedral M^{II} ion resides at an inversion center and is coordinated by four anion N atoms at the equatorial sites and by two pm N atoms at the axial sites. As Fig. 6 shows, similar networks of the crystal structures suggest that the mechanisms of canted antiferromagnetisms of $M(N_3)_2(pm)$ (M = Mn, Fe) and $M[N(CN)_2]_2(pm)$ (M = Fe, Co) are related to each other. Only the pm bridge in $M[N(CN)_2]_2(pm)$ brings about a main magnetic exchange pathway because the metal···metal distances across the $N(CN)_2$ bridge are rather long (ca. 9 Å).[8] On the other hand, both pm and N_3 bridges work as appreciable exchange couplers for $M(N_3)_2(pm)$ with the metal···metal distances of ca. 6 Å in three directions (Table 2). Namely, the latter has an ideal three-dimensional character but the former has a nearly one-dimensional character. A superexchange mechanism tells us that two d_z^2 spins should be antiferromagnetically correlated through the pm bridge.[3,8] The end-on-end azide bridges usually work as antiferromagnetic couplers.[11,12] Therefore, dominant antiferromagnetic orderings take place for both $M(N_3)_2(pm)$ and $M[N(CN)_2]_2(pm)$, but the transition temperatures are quite different (39 K vs 3.2 K[8] for M = Fe; 41 K vs 1.8 K[8] for M = Co; 46 K vs 8.3 K[9] for M = Ni). These findings can be regarded as a successful result in pursuing high-T_c (or T_N) materials by choosing smaller anions.

We demonstrated that **4** was an antiferromagnet, suggesting that the end-to-end N_3 bridge play the role of an antiferromagnetic coupler. Monfort and co-workers reported that a two-dimensional material containing nickel(II) and azide formed a ferromagnetic sheet, in which the end-to-end N_3 bridge works as a ferromagnetic coupler.[17] It has generally been found that end-to-end azide coordination gives rise to antiferromagnetic coupling whilst end-on coordination results in ferromagnetic coupling between nickel(II) and copper(II) ions.[11,12] Our result on **4** is normal and a possible reason for the difference of magnetic roles seems to originate from geometries such as torsion angles around M–N_3–M as well as bond angles around M–N–N. The crystal structure of **4** could not be determined and is only assumed to be isostructural with **1**–**3**. The following instance affords some valuable information. Do and co-workers reported ferromagnetic couplings in one-dimensional systems containing end-to-end azide-bridges.[18] The M–N_3–M torsion angles in their complex are 71.6 and 75.7° for M = Co and Ni, respectively. On the other hand, the Co–N_3–Co torsion angle of **3** was 108.5°, which does not lead to incidental orthogonality and consequently two cobalt ions are antiferromagnetically correlated. The Co–N–N bond angles for both complexes, which are another important geometrical parameter for magnetic coupling, fall into the usually observed range of 120–140°. Thus, the Co–N_3–Co torsion angle is more important for the magnetic coupling than the Co–N–N angles.

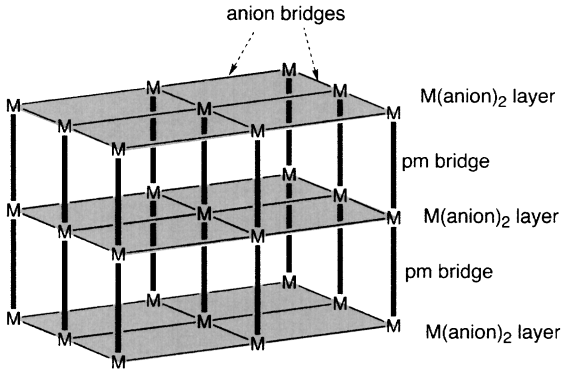

Fig. 6. Schematic drawing of the crystal structure of $M(X)_2(pm)$ (M = Mn^{2+}, Fe^{2+}, Co^{2+}, Ni^{2+}; X = N_3^-, $N(CN)_2^-$).

A canting angle for **1** of 0.06° was estimated from the small spontaneous magnetization (30 erg Oe^{-1} mol^{-1}). The canted antiferromagnetisms have often been found in three-dimensionally bridged transition-metal complexes, such as $M[N(CN)_2]_2$.[19] The Dzyaloshinsky–Moriya[20] mechanism was supposed for the canted antiferromagnetism of **1** in spite of the centrosymmetric crystal structure.[19] According to this interpretation, the small cant angle in **1** is reasonable because the cant angle is proportional to spin-orbit coupling, i.e., to the deviation of the g factor from 2.0023. The magnetic measurements revealed the *g* factor of **1** is 2.04. On the other hand, the cant angle of **2** is estimated to be 0.13°, which is considerably larger than that of the Mn complex. The large deviation of the *g* factor from 2.0023 was indicated by the observed *g* factor of 2.49, which is responsible for the large cant angle.

Cortés et al.[21] and Miller et al.[22] independently reported that the three-dimensional manganese(II) array of $Mn(N_3)_2$(4,4′-bipyridyl) showed weak ferromagnetism. The origin of the weak ferromagnetism was proposed to be due to the presence of an antisymmetric term in the Mn···Mn interaction in spite of *g* equaling 2.00 because it crystallized in an acentric space group.[22] However, there is an only one metal ion in a crystallographically independent unit of $M(N_3)_2(pm)$ and the crystal inversion center resides at the metal ion site. A possible explanation for the antisymmetric exchange mechanism is a structural modulation which leads to a lower crystal symmetry involving slightly different metal sites.

The weak-ferromagnetic behavior is intrinsic and reproducible, as supported by the parallel work on **1** done by Escuer et al.[13] They also found a weak-ferromagnetic ordering below 50 K and a very weak (0.003 $N_A\mu_B$) remnant magnetization at 2 K. Although the *M*–*H* curve was not shown,[13] this remnant value is supposed to be consistent with M_{sp} in the present study, because the estimation of M_{sp} by extrapolation is usually

larger than the observed remnant magnetization. They suggested that the spin canting originated from the large dihedral angle between the Mn-azide planes of neighbouring units. We have to add a comment on the geometry of the inter-plane Mn–pm–Mn zig-zag array. The large dihedral angles are found at neighboring units in all three directions, and all of the Mn···Mn distances are comparable due to μ-1,3-bridges in every neighboring unit. Therefore, the spin canting may originate from the large dihedral angles across the pm bridges as well as across the azide bridges.

Although the crystal structures of the present series are isomorphous, **1** and **2** are canted antiferromagnets but **3** and **4** are antiferromagnets. Unexpectedly, **1** containing manganese(II) ions is a canted antiferromagnet whereas **3** containing cobalt(II) ions is an antiferromagnet. The cobalt(II) ion usually has a large single-ion magnetic anisotropy and a large deviation of g from 2.0023, which might favor canted magnetic structures. Actually, the series of $M^{II}[N(CN)_2]_2(pm)$ (M = Fe, Co, Ni) were characterized as canted antiferromagnets.[8,9] In the series of $MCl_2(pm)_2$, the iron(II) and cobalt(II) derivatives were canted antiferromagnets[23] but the nickel(II) one was a normal antiferromagnet.[24] The present result indicates that various magnetic ground states are influenced not only by single ion anisotropy. Detailed structural differences of the coordination structure and the magnetic orbitals among the electron configurations of d^5, d^6, d^7, and d^8 should also be taken into account together with the crystal structure modulation as described above. More curious results were reported for the $M[N(CN)_2]_2$ series: canted antiferromagnets were obtained for M = Mn and Fe, but ferromagnetic orderings were observed for M = Co and Ni.[5] The origin of these various magnetic behaviors has not been clarified sufficiently and further investigation is required.

In summary, the basically antiferromagnetic structures were characterized for all of the complexes investigated here, being consistent with dominant antiferromagnetic couplings both across the pm and azide bridges. The presence or absence of spin canting is found to depend on the metal ion species; the manganese(II) and iron(II) derivatives are weak ferromagnets and the cobalt(II) and nickel(II) ones are antiferromagnets.

We acknowledge Dr. Masanori Yasui and Prof. Fujiko Iwasaki, The University of Electro-Communications, for their kind assistance in the X-ray powder diffraction analysis. This work was supported by a Grant-in-Aid for Scientific Research on Priority Areas of "Molecular Conductors and Magnets" (No. 730/11224204) and by a Grant-in-Aid for Scientific Research (No. 13640575), both from the Ministry of Education, Culture, Sports, Science and Technology.

References

1 P. J. Stang and B. Olenyuk, *Acc. Chem. Res.*, **30**, 502 (1997); O. M. Yaghi, H. Li, C. Davis, D. Richardson, and T. L. Groy, *Acc. Chem. Res.*, **31**, 474 (1998); M. Eddaoudi, D. B. Moler, H. Li, B. Chem, T. M. Reineke, M. O'Keeffe, and O. M. Yaghi, *Acc. Chem. Res.*, **34**, 319 (2001); S. Kitagawa and M. Kondo, *Bull. Chem. Soc. Jpn.*, **71**, 1739 (1998).

2 T. Ishida and T. Nogami, *Recent Res. Devel. Pure Appl. Chem.*, **1**, 1 (1997).

3 T. Ishida, S.-i. Mitsubori, T. Nogami, N. Takeda, M. Ishikawa, and H. Iwamura, *Inorg. Chem.*, **40**, 7059 (2001); T. Ishida, T. Kawakami, S.-i. Mitsubori, T. Nogami, K. Yamaguchi, and H. Iwamura, *J. Chem. Soc., Dalton Trans.*, **2002**, 3177.

4 S. R. Batten, P. Jensen, B. Moubaraki, K. S. Murray, and R. Robson, *Chem. Commun.*, **1998**, 439; M. Kurmoo and C. J. Kepert, *New J. Chem.*, **22**, 1515 (1998); J. L. Manson, C. R. Kmety, Q. Z. Huang, J. W. Lynn, G. M. Bendele, S. Pagola, P. W. Stephens, L. M. Liable-Sands, A. L. Rheingold, A. J. Epstein, and J. S. Miller, *Chem. Mater.*, **10**, 2552 (1998); J. L. Manson, C. R. Kmety, A. J. Epstein, and J. S. Miller, *Inorg. Chem.*, **38**, 2552 (1999).

5 J. S. Miller and J. L. Manson, *Acc. Chem. Res.*, **34**, 563 (2001).

6 J. L. Manson, C. D. Incarvito, A. L. Rheingold, and J. S. Miller, *J. Chem. Soc., Dalton Trans.*, **1998**, 3705; J. L. Manson, Q.-z. Huang, J. W. Lynn, H.-J. Koo, M.-H. Whangbo, R. Bateman, T. Otsuka, N. Wada, D. N. Argyriou, and J. S. Miller, *J. Am. Chem. Soc.*, **123**, 162 (2001).

7 P. Jensen, S. R. Batten, G. R. Fallon, D. C. R. Hockless, B. Moubaraki, K. S. Murray, and R. Robson, *J. Solid State Chem.*, **145**, 387 (1999).

8 T. Kusaka, T. Ishida, D. Hashizume, F. Iwasaki, and T. Nogami, *Chem. Lett.*, **2000**, 1146; T. Kusaka, T. Ishida, and T. Nogami, *Mol. Cryst. Liq. Cryst.*, **379**, 259 (2002).

9 T. Kusaka, T. Ishida, D. Hashizume, F. Iwasaki, and T. Nogami, *Mol. Cryst. Liq. Cryst.*, **376**, 463 (2002).

10 I. Riggio, G. A. van Albada, D. D. Ellis, A. L. Spek, J. Reedijk, *Inorg. Chim. Acta*, **313**, 120 (2001).

11 E. Ruiz, J. Cano, S. Alvarez, and P. Alemany, *J. Am. Chem. Soc.*, **120**, 11122 (1998); P. Chaudhuri, T. Weyhermüller, E. Bill, and K. Wieghardt, *Inorg. Chim. Acta*, **252**, 195 (1996).

12 O. Kahn, "Molecular Magnetism", VCH, New York (1993), Chap. 6.

13 A. Escuer, R. Vicente, F. A. Mautner, M. A. S. Goher, and M. A. M. Abu-Youssef, *Chem. Commun.*, **2002**, 64.

14 "teXsan: crystal structure analysis package," Molecular Structure Corp., The Woodlands, TX (1985, 1999).

15 "Rietan2000": F. Izumi and T. Ikeda, *Mater. Sci. Forum*, **321-324**, 198 (2000).

16 J. L. Manson, A. M. Arif, and J. S. Miller, *Chem. Commun.*, **1999**, 1479.

17 M. Monfort, I. Resino, J. Ribas, and H. Stoeckli-Evans, *Angew. Chem., Int. Ed. Engl.*, **39**, 191 (2000).

18 C. S. Hong, J.-e. Koo, S.-K. Son, Y. S. Lee, Y.-S. Kim, and Y. Do, *Chem. Eur. J.*, **7**, 4243 (2001).

19 S. R. Batten, P. Jensen, C. J. Kepert, M. Kurmoo, B. Moubaraki, K. S. Murray, and D. J. Price, *J. Chem. Soc., Dalton Trans.*, **1999**, 2987.

20 I. Dzyaloshinsky, *J. Phys. Chem. Solids*, **4**, 241 (1958); T. Moriya, *Phys. Rev.*, **120**, 91 (1960).

21 S. Martín, M. G. Barandika, L. Lezama, J. L. Pizarro, Z. E. Serna, J. I. R. de Larramendi, M. I. Arriortua, T. Rojo, and R. Cortés, *Inorg. Chem.*, **40**, 4209 (2001).

22 S. Han, J. L. Manson, J. Kim, and J. S. Miller, *Inorg. Chem.*, **39**, 4182 (2000).

23 K. Nakayama, T. Ishida, R. Takayama, D. Hashizume, M. Yasui, F. Iwasaki, and T. Nogami, *Chem. Lett.*, **1998**, 497.

24 K. Zusai, T. Kusaka, T. Ishida, R. Feyerherm, M. Steiner, and T. Nogami, *Mol. Cryst. Liq. Cryst.*, **343**, 127 (2000).

Crystal Structures and Magnetic Properties of Copper(II) Hexafluoroacetylacetonate Complexes with hnn and hin and Manganese(II) Hexafluoroacetylacetonate Complex with hin (hnn = 4,4,5,5-Tetramethylimidazolin-1-oxyl 3-Oxide; hin = 4,4,5,5-Tetramethylimidazolin-1-oxyl)

Tomoaki Ise, Takayuki Ishida,* and Takashi Nogami*

Department of Applied Physics and Chemistry, The University of Electro-Communications, Chofu, Tokyo 182-8585

(Received June 14, 2002)

We report here the structures and magnetic properties of hnn and hin complexes with copper(II) and manganese(II) hexafluoroacetylacetonates, [{Cu(hfac)$_2$(H$_2$O)}$_2$(μ-hnn)] (**1**), [Cu(hfac)$_2$(hin)$_2$] (**2**), and [Mn(hfac)$_2$(hin)$_2$] (**3**). X-ray crystallographic analysis of **1** revealed that **1** was a dinuclear complex containing an hnn bridge. Magnetic measurements of **1** indicate the presence of intramolecular ferromagnetic coupling between copper and radical spins. The data were analyzed as a metal-radical-metal three-spin system, giving $2J/k = +16.2$ K ($H = -2J(S_1S_2 + S_2S_3)$). The ferromagnetic interaction can be explained in terms of the axial coordination of the hnn nitrogen to Cu(II). Complexes **2** and **3** were revealed to be isomorphous mononuclear complexes possessing two hin ligands. Although the molecules have a radical-metal-radical system, the magnetic data of **3** could not be analysed only with intramolecular interactions. Strong intermolecular antiferromagnetic interactions ($2|J|/k \gg 300$ K) were suggested among the hin ligands because the interatomic O···N distances (2.41–2.51 Å) were shorter than the sum of the van der Waals radii for **2** and **3**. These strong interactions are successfully introduced to metal-radical hybrid systems owing to the choice of small ligands, although the complexes do not possess polymeric networks.

There have been a number of hybrid-complexes which have flexible functionality of organic materials and strong magnetic interactions between metal ions and radicals.[1] The design of magnetic materials with a high bulk ferromagnetic or ferrimagnetic transition temperature, T_c, is one of the main challenges in this field. T_c is well known to be strongly dependent on the magnitude of the exchange interaction between the spin sources.[2] We assume that the choice of small ligands and anions is crucial in order to bestow strong exchange interaction on magnetic materials. We chose 4,4,5,5-tetramethylimidazolin-1-oxyl 3-oxide (hnn) and 4,4,5,5-tetramethylimidazolin-1-oxyl (hin) as ligands (Chart 1). These are the smallest derivatives in the nitronylnitroxide and iminonitroxide families.[3] These radicals can bridge paramagnetic metal ions through the O–N–C–N–O or O–N–C–N π-electron systems. Although the isolation of hin was claimed to be difficult because of its instability,[3] complexation affords a chance to purify and characterize hin compounds. Stabilization by complex formation is widely utilized for preparation of compounds of low-valent main group elements.[4] We have reported a practically diamagnetic hin complex, [CdCl$_2$(hin)$_4$], owing to extraordinarily strong intermolecular antiferromagnetic coupling.[5] We report here the X-ray crystal structures and magnetic properties of the hnn and hin complexes with paramagnetic [Cu(hfac)$_2$] (hfac = 1,1,1,5,5,5-hexafluoropentane-2,4-dionate). We also report structures and magnetic properties of the isomorphous hin complex with Mn(hfac)$_2$ in order to elucidate magnetic exchange pathways.

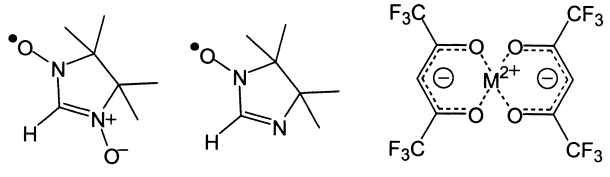

Chart 1.

Experimental

Materials. 4,4,5,5-Tetramethylimidazolin-1-oxyl 3-Oxide (hnn) was prepared according to the procedure previously reported.[3] 4,4,5,5-Tetramethylimidazolin-1-oxyl (hin) was prepared according to the literature method[3] with a slight modification.

4,4,5,5-Tetramethylimidazolin-1-oxyl (hin): Solutions of hnn (1.0 g, 6.4 mmol) in CH_2Cl_2 (5 mL) was added to a suspension of $NaNO_2$ (1.1 g, 16 mmol) in CH_2Cl_2 (30 mL) and CH_3CO_2H (3.5 mL, 61 mmol). The reaction mixture was stirred for 5 min to give a bright orange solution. After filtration and neutralization with aqueous $NaHCO_3$, the organic layer was washed with water, and the aqueous phase was extracted with CH_2Cl_2 (100 mL). The combined organic phase was dried over $MgSO_4$. The solution was concentrated and chromatographed over a short column (silica gel). Elution with a solution of CH_2Cl_2/diethyl

ether (4/1 in volume) followed by removal of the solvent in vacuo gave a pure orange product of 680 mg (75%).

[{Cu(hfac)$_2$(H$_2$O)}$_2$(μ-hnn)] (1): Solutions of hnn (100 mg, 0.64 mmol) in CH_2Cl_2 (7.0 mL) and of Cu(hfac)$_2$ (302 mg, 0.64 mmol) in CH_2Cl_2 (2.0 mL) were mixed, the combined solution was allowed to stand in a cool and dark place for 2 days, and dark-red crystals of **1** were precipitated.

[Cu(hfac)$_2$(hin)$_2$] (2): Solutions of hin (200 mg, 1.42 mmol) in dry diethyl ether (0.8 mL) and of Cu(hfac)$_2$ (339 mg, 0.71 mmol) in dry diethyl ether (0.5 mL) were mixed, the combined solution was allowed to stand in a cool and dark place for 1 day, and dark-brown crystals of **2** were precipitated.

[Mn(hfac)$_2$(hin)$_2$] (3): Solutions of hin (100 mg, 0.71 mmol) in dry diethyl ether (0.2 mL) and of dehydrated Mn(hfac)$_2$ (333 mg, 0.71 mmol) in dry ether (0.2 mL) were mixed, the combined solution was allowed to stand in a cool and dark place for one day, and dark-brown crystals of **3** were precipitated.

The isolated hnn, [{Cu(hfac)$_2$(H$_2$O)}$_2$(μ-hnn)], [Cu(hfac)$_2$-(hin)$_2$] and [Mn(hfac)$_2$(hin)$_2$] could be stored at -20 °C for several months, but isolated hin completely decomposed upon standing overnight at room temperature.

Elemental analysis (C, H, N) of these complexes on a Fisons EA-1108 by a usual combustion method revealed that the metal/radical ratios are 2/1, 1/2, and 1/2 for **1**, **2**, and **3**, respectively. Anal. Calcd. for $C_{27}H_{21}N_2O_{12}F_{24}Cu_2$ (**1**): C, 28.27; H, 1.84; N, 2.43%. Found: C, 28.45; H, 1.95; N, 2.85%. Calcd. for $C_{24}H_{28}N_4O_6F_{12}Cu_1$ (**2**): C, 37.73; H, 3.27; N, 7.13%. Found: C, 37.93; H, 3.71; N, 7.37%. Calcd. for $C_{24}H_{28}N_4O_6F_{12}Mn_1$ (**3**): C, 38.36; H, 3.76; N, 7.46%. Found: C, 38.66; H, 3.57; N, 7.59%.

X-ray Crystallographic Analysis. X-ray diffraction data were collected on a Rigaku Raxis-Rapid IP diffractometer with graphite monochromated Mo $K\alpha$ radiation (λ = 0.71069 Å) at 90.2 or 153 K. The structures were directly solved by a heavy-atom Patterson method in the teXsan program package.[6] Numerical absorption correction was used. Full-matrix least-squares methods were applied using all of the unique diffraction data.[7] A trifluoromethyl group C(11) of **1** was solved to be disordered into two conformations with a 1/1 population, leading to a considerable improvement in the refinement for **1**. The thermal displacement parameters of non-hydrogen atoms were anisotropically refined, but the positional and isotropic thermal parameters of hydrogen atoms were not refined. For **2** and **3**, all of the trifluoromethyl groups were solved in a disordered model. All of the hydrogen atoms could be found in difference Fourier maps, and the parameters of the hydrogen atoms were included in the refinement. The R_1 value of **3** was 0.081 because of the large thermal anisotropy of fluorine atoms, although other atoms could be satisfactorily refined.

Magnetic Measurements. Magnetic susceptibility was measured on a Quantum Design MPMS SQUID magnetometer equipped with a 7 T coil in a temperature range down to 1.8 K. The magnetic responses were corrected with diamagnetic blank data of the sample holder, obtained separately. The diamagnetic contribution of the sample itself was estimated from Pascal's constant.

Results and Discussion

X-ray Crystal Structure Analysis. Table 1 summarizes the X-ray crystallographic data for [{Cu(hfac)$_2$(H$_2$O)}$_2$(μ-hnn)] (**1**), [Cu(hfac)$_2$(hin)$_2$] (**2**), and [Mn(hfac)$_2$(hin)$_2$] (**3**). Figure 1 shows the molecular structure of **1**, which reveals a dinuclear complex involving an hnn bridge. One Cu(hfac)$_2$·H$_2$O and a half of hnn are crystallographically independent. The central hnn ligand is sandwitched by two copper ions, forming a linear three-spin system. The copper ions are coordinated by four oxygens of two hfac ligands occupying the equatorial positions. One oxygen of hnn and H$_2$O are coordinated at the axial position. Selected bond distances and angles are given in Table 2. The octahedra of both copper centers are severely distorted with the axial Cu(1)–O(5) and Cu(1)–O(6) bonds much longer than the equatorial ones: 2.46(2) and 2.25(8) Å vs 1.94(9), 1.93(4), 1.94(2) and 1.96(1) Å. An axial site of Cu is capped by oxygen atom of H$_2$O, which prevents the formation of a polymeric network in the crystal. This complex is expected to show intramolecular ferromagnetic interaction, i.e., the molecule has a ground quartet state, because this coordination type is essentially the same as that of [Cu(hfac)$_2$NN–Me] (NN–Me = 2,4,4,5,5–pentamethylimidazoline-1-oxyl 3-oxide), which shows ferromagnetic interaction between the Cu ion and radical spin.[8] This ferromagnetic interaction can be explained in terms of orbital orthogonality between the copper $3d_{x^2-y^2}$ and the nitrogen $2p_z$ orbitals, since the

Table 1. Selected X-ray Crystallographic Data of **1**, **2** and **3**

Compound	**1**	**2**	**3**
Formula	$C_{27}H_{21}N_2O_{12}F_{24}Cu_2$	$C_{24}H_{28}N_4O_6F_{12}Cu$	$C_{24}H_{28}N_4O_6F_{12}Mn$
Mol wt	1148.52	760.03	751.42
Crystal system	Orthombic	Triclinic	Triclinic
Space group	*Fdd*2	$P\bar{1}$	$P\bar{1}$
a/Å	35.607(7)	11.088(1)	10.985(5)
b/Å	13.173(9)	16.871(5)	17.153(3)
c/Å	17.094(1)	10.061(1)	9.778(3)
α/ degree		105.50(1)	105.18(5)
β/ degree		111.66(4)	110.59(4)
γ/ degree		72.14(8)	75.21(7)
V/Å^3	8018.66(4)	1634.25(5)	1637.29(6)
Z	8	2	2
D_{calc}/ g cm^{-3}	1.90	1.54	1.52
T/K	90.2	90.2	153
$R(I > 2\sigma(I))$	0.038	0.051	0.081

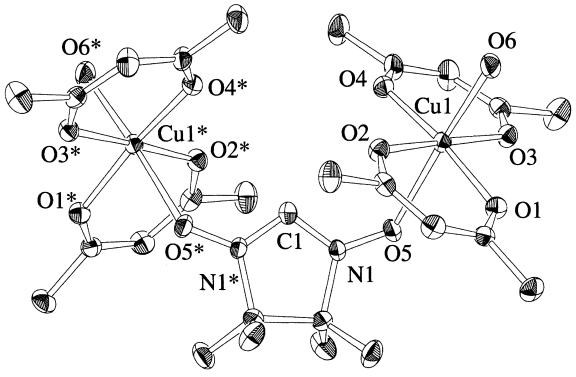

Fig. 1. ORTEP view of [{Cu(hfac)$_2$(H$_2$O)}$_2$(μ-hnn)] at the 50% probability level. The fluorine and hydrogen atoms are omitted for the sake of clarity. Symmetry opetration code for* is $-x + 3/2, -y + 1/2, z$.

Table 2. Selected Bond Distances (Å) and Angles (Degree) for [{Cu(hfac)$_2$(H$_2$O)}$_2$(μ-hnn)] (**1**)

Cu(1)–O(1)	1.949(2)	Cu(1)–O(4)	1.961(2)
Cu(1)–O(2)	1.934(2)	Cu(1)–O(5)	2.462(2)
Cu(1)–O(3)	1.940(2)	Cu(1)–O(6)	2.258(2)
N(1)–C(1)	1.323(7)	O(5)–N(1)	1.285(3)
O(1)–Cu(1)–O(2)	92.84(9)	O(1)–Cu(1)–O(3)	85.36(9)
O(1)–Cu(1)–O(4)	170.6(1)	O(1)–Cu(1)–O(5)	85.70(8)
O(1)–Cu(1)–O(6)	90.72(9)	O(2)–Cu(1)–O(3)	178.20(9)
O(2)–Cu(1)–O(4)	89.14(9)	O(2)–Cu(1)–O(5)	90.05(8)
O(2)–Cu(1)–O(6)	88.98(9)	O(3)–Cu(1)–O(4)	92.65(9)
O(3)–Cu(1)–O(5)	90.97(9)	O(3)–Cu(1)–O(6)	90.97(9)
O(4)–Cu(1)–O(5)	85.11(8)	O(4)–Cu(1)–O(6)	98.51(9)
O(5)–Cu(1)–O(6)	176.24(9)		

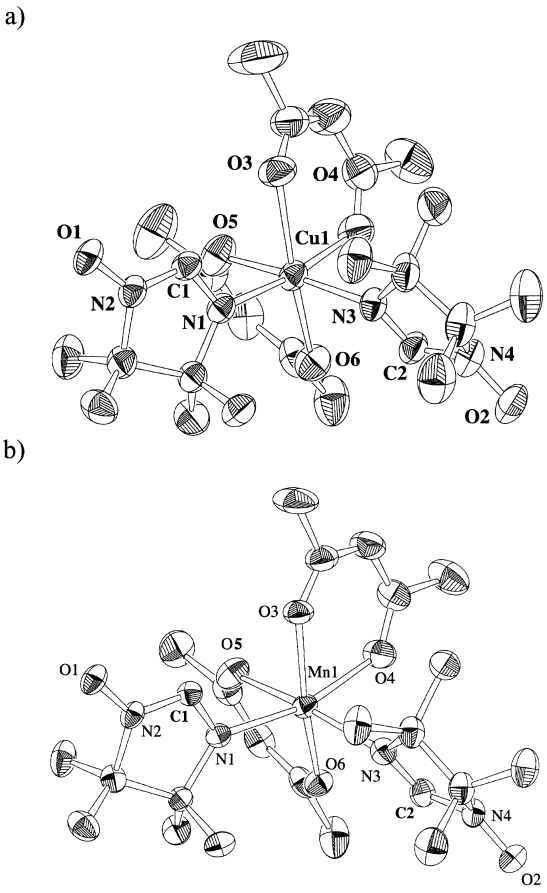

Fig. 2. ORTEP drawings of [Cu(hfac)$_2$(hin)$_2$] (a) and [Mn(hfac)$_2$(hin)$_2$] (b) at the 50% probability level. The fluorine and hydrogen atoms are omitted for the sake of clarity.

nitroxide oxygen atom is coordinated at an axial site of the copper ion.

Figure 2(a) shows that **2** is a mononuclear complex. The copper atoms are octahedrally coordinated by two oxygens of two hfac ligands and two nitrogens of hin. The interatomic bond distances of N(1)–C(1), N(2)–C(1) and O(1)–N(2) are close to the corresponding distances in other iminonitroxide radical derivatives.[9] Two oxygens of two hfac ligands are coordinated at the axial position. Selected bond distances and angles are given in Table 3 (M = Cu). The imino nitrogen atom coordinates to the Cu ion, whereas the nitroxide oxygen atom remains uncoordinated in spite of the potential coordination ability of nitroxide oxygen atoms. The strong coordination ability of the imino nitrogen atoms can be understood in view of the steric congestion around imino nitrogen and nitroxide oxygen atoms. This complex is expected to show intramolecular antiferromagnetic interaction because the hin nitrogen atom coordinates to an equatorial site of the Cu ion, in contrast to the hnn oxygen atoms occupying axial positions of the Cu ion in **1**.

In order to compare the structures and magnetic properties of other metal derivatives, we also prepared complexes consisting of hin and Mn(hfac)$_2$. Figure 2(b) shows that **3** is a mononuclear complex which an isomorphous structure of **2**. Selected bond distances and angles are given in Table 3 (M = Mn). The molecular arrangements of **2** and **3** are also quite similar.

Compounds **2** and **3** do not form any polymeric network in the crystals. However, as Fig. 3 shows, short intermolecular distances of 2.45(2) Å (O(1)···N(2*)) and 2.50(6) Å (O(2)···N(4#)) were found in **2**, and 2.41(3) Å (O(1)···N(2*)) and 2.42(1) Å (O(2)···N(4#)) in **3**, where* and # denote symmetry operation codes of $1-x, 1-y, 1-z$ and $-x, -y, -z$, respectively. These distances are much shorter than the sum of the van der Waals radii of oxygen and nitrogen (3.07 Å).[10] We assumed that hin groups formed an intermolecular dimer of nitroxide groups. The intermolecular magnetic interactions in **2** and **3** are expected to be antiferromagnetic because of the orbital overlap between adjacent magnetic orbitals.

Magnetic Properties. Magnetic susceptibility χ_m of **1** was measured in the temperature range 1.8–100 K, and the plot of $\chi_m T$ vs temperature is shown in Fig. 4. At 100 K, the $\chi_m T$ value for **1** is 1.3 cm^3 mol^{-1} K. Upon cooling, $\chi_m T$ increased to the maximum value (1.92 cm^3 mol^{-1} K) at 5 K, and then decreased. This magnetic behavior indicates that intramolecular ferromagnetic interaction is operative for **1**, together with a slight intermolecular antiferromagnetic interaction. We attempted to fit the result of the magnetic measurements by using the linear three spins system of $S = 1/2$ model given by Eq. 1,[11] based on the spin Hamiltonian $H = -2J(S_1 \cdot S_2 + S_2 \cdot S_3)$ with a Weiss constant θ, where all symbols have their usual

Table 3. Selected Bond Distances (Å) and Angles (Degree) for $[M(hfac)_2(hin)_2]$

	M = Cu	M = Mn
M(1)–O(3)	2.262(2)	2.148(2)
M(1)–O(4)	2.001(2)	2.174(2)
M(1)–O(5)	2.004(2)	2.177(2)
M(1)–O(6)	2.349(2)	2.163(2)
M(1)–N(1)	2.036(2)	2.224(3)
M(1)–N(3)	2.032(2)	2.208(3)
N(1)–C(1)	1.276(4)	1.279(3)
N(2)–C(1)	1.369(4)	1.375(3)
O(1)–N(2)	1.267(3)	1.264(3)
N(3)–C(2)	1.284(4)	1.283(3)
N(4)–C(2)	1.384(4)	1.374(3)
O(2)–N(4)	1.271(4)	1.259(3)
O(3)–M(1)–O(4)	84.05(8)	81.29(7)
O(3)–M(1)–O(5)	85.52(8)	89.62(8)
O(3)–M(1)–O(6)	159.49(8)	163.28(8)
O(3)–M(1)–N(1)	89.19(8)	86.72(8)
O(3)–M(1)–N(3)	100.85(8)	99.51(8)
O(4)–M(1)–O(5)	89.92(9)	89.03(8)
O(4)–M(1)–O(6)	79.09(8)	84.47(7)
O(4)–M(1)–N(1)	171.77(8)	166.45(8)
O(4)–M(1)–N(3)	87.18(9)	88.47(8)
O(5)–M(1)–O(6)	82.90(8)	81.40(7)
O(5)–M(1)–N(1)	84.87(8)	84.59(8)
O(5)–M(1)–N(3)	172.67(8)	170.05(8)
O(6)–M(1)–N(1)	106.50(8)	106.29(8)
O(6)–M(1)–N(3)	89.95(8)	88.78(7)
N(1)–M(1)–N(3)	98.74(8)	99.77(8)

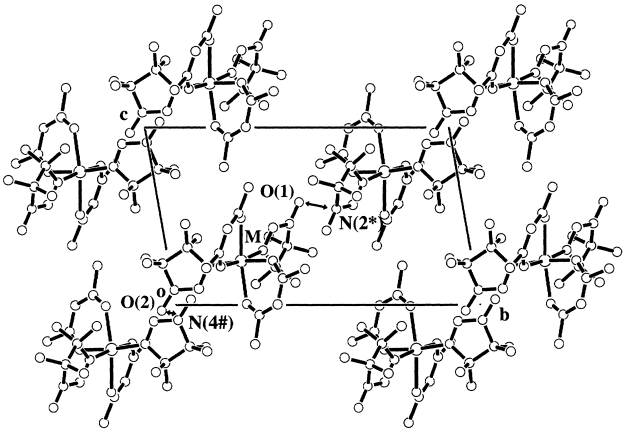

Fig. 3. Intermolecular short distances in the crystals of $[M(hfac)_2(hin)_2]$. Selected interatomic distances are: $d(O(1)\cdots N(2^*))$ = 2.45(2) and $d(O(2)\cdots N(4\#))$ = 2.50(6) Å for M = Cu. $d(O(1)\cdots N(2^*))$ = 2.41(3) and $d(O(2)\cdots N(4\#))$ = 2.42(1) Å for M = Mn. Symmetry operation codes : *: $1-x, 1-y, 1-z$; #: $-x, -y, -z$.

meaning. The exchange parameter J is the spin-spin coupling constant between Cu ions and radical. The best fit parameters of g, $2J/k$, and θ values are 2.068, +16.2 K, and −0.2 K respectively. The $2J/k$ value for **1** is slightly smaller than that for $[Cu(hfac)_2NN–Me]$ (+18.5 K).[8]

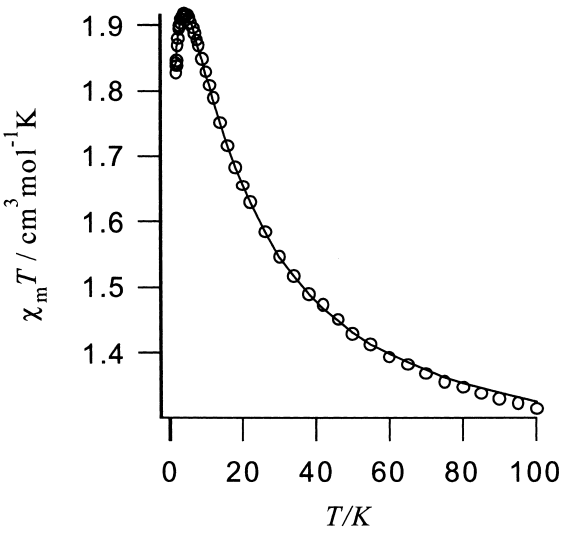

Fig. 4. Temperature dependence of the product $\chi_m T$ of $[\{Cu(hfac)_2(H_2O)\}_2(\mu\text{-hnn})]$ (○). Solid line corresponds to the theoretical curve, parameters of which are given in the text.

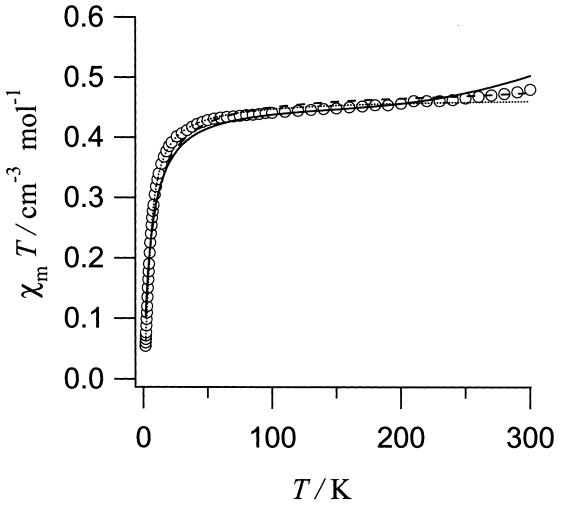

Fig. 5. Temperature dependence of the product $\chi_m T$ of $[Cu(hfac)_2(hin)_2]$ (○), compared with the theoretical curves based on Eq. 1 (—), Eq. 2 (- - -) and Eq. 4 (···), respectively.

$$\chi = \frac{Ng^2\mu_B{}^2}{4k(T-\theta)} \frac{10 + \exp(-J/kT) + \exp(-3J/kT)}{2 + \exp(-J/kT) + \exp(-3J/kT)} \quad (1)$$

The plot of $\chi_m T$ vs temperature of **2** is shown in Fig. 5. At room temperature, the $\chi_m T$ value, 0.48 cm^3 mol^{-1} K, is lower than the expected value of three S = 1/2 spin (1.125 cm^3 mol^{-1} K). This result indicates that a large intra- or intermolecular antiferromagnetic interaction is operative in **2** at this temperature. The above structural analysis of **2** showed that hin moieties formed a dimer. In this case, there are two conceivable models. One is a doublet/quartet model with a Weiss constant (Eq. 1),[11] on the basis of three-spin systems which is similar to the case of **1**. We assume here that the exchange in-

teraction between Cu-hin is larger than that between the through-space hin···hin dimer. The best fit parameters of g, $2J/k$, and θ values are 2.23, −425 K, and −5.9 K, respectively.

The other model is a combined singlet/triplet + doublet model with a Weiss constant (Eq. 2). We assume that the exchange interaction within the hin···hin dimer is larger than that of Cu-hin and that the second term of Eq. 2 implies a Curie spin from the copper ion ($S = 1/2$). The exchange parameter J is the spin-spin coupling constant between radical dimers, and θ is among Cu ions. The best fit parameters of the g, $2J/k$, and θ values are 2.26, −998 K, and −6.7 K, respectively.

$$\chi = \frac{2Ng^2\mu_B{}^2}{kT}\frac{1}{3+\exp(-2J/kT)} + \frac{Ng^2\mu_B{}^2S(S+1)}{3k(T-\theta)} \quad (2)$$

For further discussion about exchange pathways in the crystal of **2**, especially which model described above is more reliable, the following experimental results give valuable information. We prepared the manganese derivative (**3**) according to the same synthetic procedure as that of **2** and revealed that the molecular and crystal structures of **3** were essentially the same as those of **2**. We analyzed magnetic data of **3** based on the same magnetic coupling model with different spin quantum number of the metal ion. The plot of χ_mT vs temperature of **3** is shown in Fig. 6. At room temperature, the χ_mT value, 4.41 cm^3 mol^{-1} K, is lower than the expected value of the sum of two $S = 1/2$ and one $S = 5/2$ spins (5.125 cm^3 mol^{-1} K). This result indicates that a large intra- or intermolecular antiferromagnetic interaction is operative in **3** at this temperature, like the case of **2**. On cooling, the χ_mT value decreases and reaches a plateau (about 4.3 cm^3 mol^{-1} K) in a temperature range 250–140 K. This plateau is consistent with a paramagnetic Mn ion (4.375 cm^3 mol^{-1} K). The above structural analysis of **3** showed that hin moieties formed a dimer. Thus, we can propose that very strong antiferromagnetic interactions operate in an hin dimer in the crystal at this temperature range, and that the magnetic moments of hin are completely canceled. We attempted to fit the result of the magnetic measurements by using a combined dimer model given by Eq. 2 with $S = 5/2$. The exchange parameter J is the spin–spin coupling constants between radical dimer, θ is between Mn ions. The best fit parameters of the g, $2J/k$, and θ values are 2.04, −3840 K, and −6.2 K, respectively. Because of a slight temperature dependence of χ_mT up to 300 K, the estimated J value does not have sufficient accuracy, but we can conclude that $J/k \gg 300$ K.

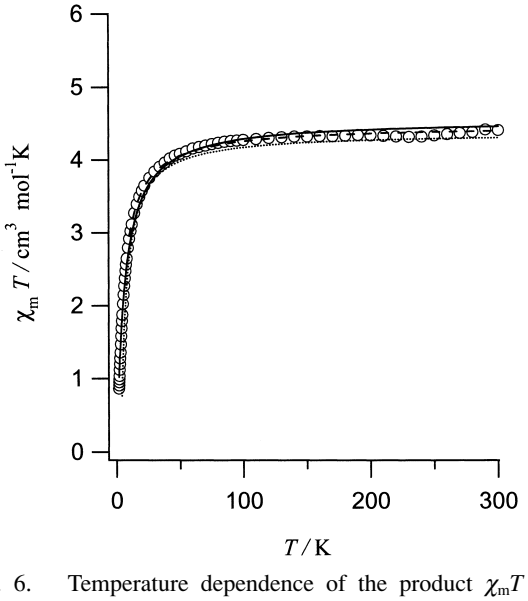

Fig. 6. Temperature dependence of the product χ_mT of [Mn(hfac)$_2$(hin)$_2$] (○), compared with the theoretical curves based on Eq. 2 (—), Eq. 3 (- - -) and Eq. 5 (···), respectively.

On the other hand, assuming that the magnitude of intramolecular interaction is larger than that of intermolecular interaction, antiferromagnetic interaction between an Mn ion ($S = 5/2$) and two hin ($S = 1/2$) must be operative. We attempted to fit the result of the magnetic measurements by using a linear-arrayed model of $S = 1/2$, 5/2, and 1/2 given by Eq. 3.[12]

$$\chi = \frac{Ng^2\mu_B{}^2}{12(T-\theta)}\frac{30\exp A + 105\exp B + 252\exp C + 105}{2\exp A + 3\exp B + 4\exp C + 3} \quad (3)$$

$$A = \frac{-7J}{kT},\ B = \frac{-2J}{kT},\ \text{and}\ C = \frac{5J}{kT}.$$

The exchange parameter J is ascribable to the spin-spin coupling constants between Mn ion and radicals, and θ is among molecules. The best fit parameters of g, $2J/k$, and θ values are 3.09, −994 K, and −5.1 K, respectively. This g value is not acceptable for Mn ions, and consequently this model should be abandoned.

Therefore, it seems reasonable to conclude that the magnitude of intermolecular through-space interaction is larger than that of intramolecular through-bond interaction in the case of **2** and **3**. Furthermore, the intermolecular interactions are much larger than 300 K. These results indicate that the hin ligands can be useful for achieving the strong intermolecular exchange interaction.

Assuming that both **2** and **3** can be regarded as chains of the Cu and Mn ions, respectively, with intervening hin pairs, we attempted to fit the result of the magnetic measurements of **2** and **3** by using chain models of $S = 1/2$ given by Eq. 4[13] and $S = 5/2$ given by Eq. 5,[14] based on the spin Hamiltonian $H = -2J\,\Sigma S_i \cdot S_{i+1}$, respectively. The calculated curves are superposed in Figs. 5 and 6. The exchange parameter J is ascribable to the spin-spin coupling constant between the metal ions in the chain. The best fit parameters of g and $2J/k$ are 2.23 and −13 K for **2** and 2.00 and −1.6 K for **3**, respectively. These chain models are good fits for both cases of **2** and **3**. This result indicates that the magnitude of the antiferromagnetic interaction is as large as a chemical bond, and that the hin pair plays a role of an antiferromagnetic coupler.

$$\chi = \frac{Ng^2\mu_B{}^2}{k}\frac{0.25 + 0.074975x + 0.075235x^2}{1.0 + 0.9913x + 0.172135x^2 + 0.757825x^3} \qquad x = \frac{|J|}{2kT} \quad (4)$$

$$\chi = \frac{35Ng^2\mu_B{}^2}{12k}\frac{1+u}{1-u} \qquad u = \coth\left[\frac{35J}{8kT}\right] - \left[\frac{8kT}{35J}\right] \quad (5)$$

We have demonstrated the preparation and full characterization of [{Cu(hfac)$_2$(H$_2$O)}$_2$(μ-hnn)] and [Cu(hfac)$_2$(hin)$_2$]. The different exchange interactions of **1** and **2** are due to different coordination geometries of ligand molecules to Cu ion. This result indicates that the choice of a small ligand is effective to bestow strong exchange interaction. Recently Gateschi and co-workers reported that polymeric metal hexafluoroacetylacetonate-nitronylnitroxide systems were potentially good candidates for single-molecule magnets.[15] Complexes **1**, **2**, and **3** can be regarded as prototypes of possible polymeric forms when possible intrachain ferro- or ferrimagnetic coupling take place rather than antiferromagnetic hin···hin coupling. Preparation of polymeric complexes using hin and hnn with other large anisotropically metal ions such as Co(II) ions is currently underway.

This work was supported by Grants-in-Aid for Scientific Research on Priority Areas (No. 730/11224204 and 401/11136212) from the Ministry of Education, Culture, Sports, Science and Technology.

References

1 A. Caneschi, D. Gatteschi, and R. Sessoli, *Acc. Chem. Res.*, **22**, 392 (1989); A. Caneschi, D. Gatteschi, and P. Rey, *Prog. Inorg. Chem.*, **39**, 331 (1991).

2 O. Kahn, "Molecular Magnetism", VHC, New York (1993).

3 E. F. Ullman, L. Call, and J. H. Osiecki, *J. Org. Chem.*, **35**, 3623 (1970).

4 For example, W. E. Buhro, A. T. Patton, C. E. Strouse, and J. A. Gladysz, *J. Am. Chem. Soc.*, **105**, 1056 (1983).

5 T. Ise, T. Ishida, and T. Nogami, *Mol. Cryst. Liq. Cryst.*, **379**, 147 (2002).

6 "*teXsan*: crystal structure analysis package," Molecular Structure Corp., The Woodland, TX (1985, 1999).

7 The CIF data for the three crystals are deposited as Document No. 75052 at the Office of the Editor of Bull. Chem. Soc. Jpn. Crystallographic data have been deposited at the CCDC, 12 Union Road, Cambridge CBZ IEZ, UK and copies can be obtained on request, free of charge, by quoting the publication and the deposition numbers 187504–187506 for **1**–**3**.

8 A. Caneschi, D. Gatteschi, J. Laugier, and P. Rey, *J. Am. Chem. Soc.*, **109**, 2191 (1987).

9 For example, H. Oshio, T. Watanabe, A. Ohto, T. Ito, and H. Masuda, *Inorg. Chem*, **35**, 472 (1996).

10 A. Bondi, *J. Phys. Chem.*, **68**, 441 (1964).

11 N. Tyutyulkov and C. S. Karabunarliev, *Int. J. Quantum Chem*, **29**, 1325 (1986).

12 M. Kitano, Y. Ishimaru, K. Inoue, N. Koga, and H. Iwamura, *Inorg. Chem*, **33**, 6012 (1994).

13 J. C. Bonner and M. E. Fisher, *Phys. Rev. A*, **135**, 640 (1964).

14 M. E. Fisher, *Am. J. Phys.*, **32**, 343 (1964).

15 A. Caneschi, D. Gatteschi, N. Lalioti, C. Sangregorio, R. Sessoli, G. Venturi, A. Vindigni, A. Rettori, M. G. Pini, and M. A. Novak, *Angew. Chem,. Int, Ed.*, **40**, 1760 (2001).

Mol. Cryst. Liq. Cryst., Vol. 376, pp. 455-462

1058-725X/02 $12.00+.00

Radical-Copper Macrocycles and Related Compounds

JUNICHI OMATA, TAKAYUKI ISHIDA, DAISUKE HASHIZUME, FUJIKO IWASAKI and TAKASHI NOGAMI

Department of Applied Physics and Chemistry, The University of Electro-Communications, Chofu, Tokyo 182-8585, Japan

4-Pyrimidinyl nitronyl nitroxide (4PMNN) was synthesized and characterized, and four 4PMNN-metal(II) chloride complexes were investigated. Hexanuclear macrocyclic $[CuCl_2•(4PMNN)]_6$ shows intermolecular ferromagnetic interaction. $MnCl_2•(4PMNN)$ exhibits antiferromagnetic interaction. Mononuclear $CoCl_2•(4PMNN)_2$ shows ferrimagnetic phase transition at ca. 3 K. $NiCl_2•(4PMNN)_2$ are practically diamagnetic below 100 K.

Keywords: X-ray diffraction, magnetic phase transition, pyrimidine, radical, nitronyl nitroxide

INTRODUCTION

The metal-radical approach has been successful to design ferrimagnetic compounds that show magnetic order at low temperatures [1]. We have reported the magnetism of pyrimidine-bridged transition metal complexes [2,3,4] in connection with the organic high-spin *m*-phenylene-bridged poly-carbenes and -radicals [5]. In the course of our study on the role of radical-substituted pyrimidine as ferro- and antiferromagnetic couplers across the μ-1,3-NCN bridges, we have found that hexanuclear arrays $[(4PMNN)•CuX_2]_6$ (**1**: X = Br, **2**: X = Cl; 4PMNN = 4-pyrimidinyl nitronyl nitroxide) exhibited ferromagnetic intermolecular interactions [6]. We report here the magnetic properties

of 4PMNN-MCl_2 complexes (M = Mn, Co, Ni) together with that of the 4PMNN ligand itself.

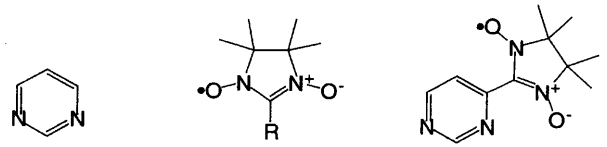

pyrimidine (PM) | R-nitronyl nitroxide (RNN) | 4PMNN

EXPERIMENTAL

4-pyrimidinecarboxaldehyde was prepared according to the method previously reported [7] by using *N,N*-dimethylformamide diethyl acetal and pyruvic aldehyde dimethyl acetal as starting materials. The formyl group was converted to a nitronyl nitroxide group by Ullman's method [8], giving blue plates of 4PMNN in 76% yield from the aldehyde (mp. 128-131 °C, recrystallized from ether-hexane). Anal. Found: C, 56.64; H, 6.48; N, 23.63%. Calc.: C, 56.16; H, 6.43; 23.82%. MS (EI, 70 eV) *m/z* 236 (68%, MH^+), 106 (100%). ESR (benzene, room temperature) g = 2.0065, a_N = 7.1 G (quintet).

The typical procedure of complexation is as follows. A methanol solution (10 ml) containing 34 mg of 4PMNN and 35 mg of $CuBr_2$ was allowed to stand at room temperature for a week. Dark green needles (18 mg) of $CuCl_2•(4PMNN)$ were precipitated and collected on a filter, which are suitable for magnetic studies. The composition was determined by means of elemental analysis (C, H, N).

X-Ray diffraction data were collected on a Rigaku Raxis-Rapid IP diffractometer with monochromated Mo$K\alpha$ and Cu$K\alpha$ radiations. Structures were solved by direct methods and the atomic positions were refined by full-matrix least-squares methods using all of the reflections. Magnetic properties were measured on Quantum Design MPMS SQUID and PPMS ac/dc magnetometers equipped with 7 and 9 T superconducting magnets, respectively. Diamagnetic contribution of the sample itself was estimated from Pascal's constants.

RESULTS AND DISCUSSION

4PMNN

X-Ray crystal structure analysis of 4PMNN [9] indicates that there are 8 molecules in a unit cell, only two molecules of which are shown in Figure 1 for the sake of clarity. The dotted lines represent intermolecular contacts within the sum of the van der Waals radii; 3.23 Å for O···C_{6PM} and 3.29 Å for O···N_{1PM}.

Figure 2 shows the temperature dependences of the product $\chi_{mol}T$ and $1/\chi_{mol}$. The $\chi_{mol}T$ value at 100 K was 0.38 cm^3 K mol^{-1}, clearly indicating the purity of the specimen. The Weiss temperature was -1.6 K. Semi-empirical UHF/PM3 calculation [10] on 4PMNN with the determined atomic coordinates suggests that spin polarization takes place along the conjugated skeleton, and the spin density of C_{6PM} is slightly positive. According to the McConnell theory [11], the O···C_{6PM} contact gives rise to intermolecular antiferromagnetic interaction.

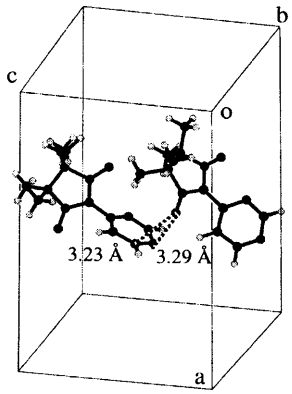

FIGURE 1 Crystal structure of 4PMNN.

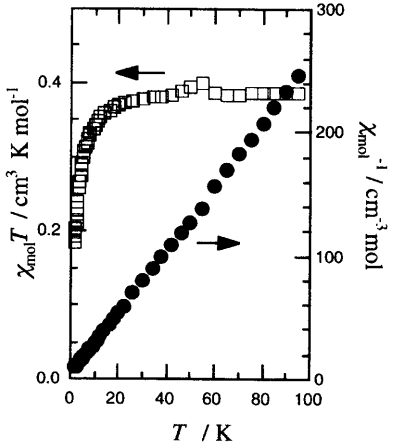

FIGURE 2 Temperature dependences of $\chi_{mol}T$ and $1/\chi_{mol}$ for 4PMNN.

MCl_2•(4PMNN)

There are two types of ligand/metal ratios (1:1 and 2:1) found in complexes obtained from 4PMNN and metal(II) chlorides. Elemental analysis revealed that the complexes obtained from 4PMNN with $MnCl_2$ and $CuCl_2$ has a ligand/metal ratio of 1:1. Figure 3 shows temperature dependence of $\chi_{mol}T$ for $MnCl_2$•(4PMNN) and $CuCl_2$•(4PMNN) measured at 5 kOe. The $\chi_{mol}T$ value of the former monotonically decreases with a decrease of temperature and almost obeys the Curie-Weiss law with the constants of 3.59 cm^3 K mol^{-1} and -14 K. On the other hand, the $\chi_{mol}T$ value of $CuCl_2$•(4PMNN) increases with a decrease of temperature, and below 8 K the $\chi_{mol}T$ value decreases.

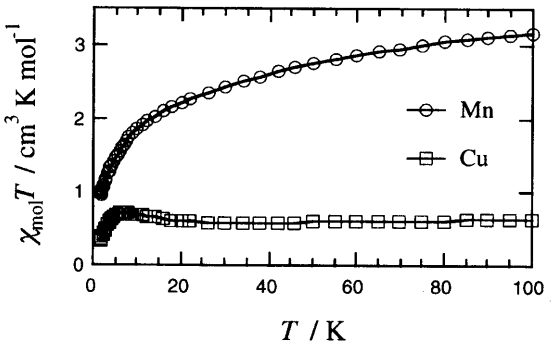

FIGURE 3 Temperature dependence of $\chi_{mol}T$ for $MnCl_2$•(4PMNN) and $CuCl_2$•(4PMNN) measured at 5 kOe. The solid lines are shown for a guide to the eye.

The crystal structure of $CuCl_2$•(4PMNN) was determined (Figure 4); the molecule consists of a head-to-tail hexamer and the hexamers construct a one-dimensional columnar structure [6]. The magnetic behavior is explained by competitive intramolecular antiferromagnetic interaction and intermolecular ferromagnetic interaction [6]. This compound did not show any magnetic phase transition down to 1.8 K. Possible supramolecular control of the magnetism is proposed by means of the guest-molecule inclusion into the cavity of $CuCl_2$•(4PMNN) [12].

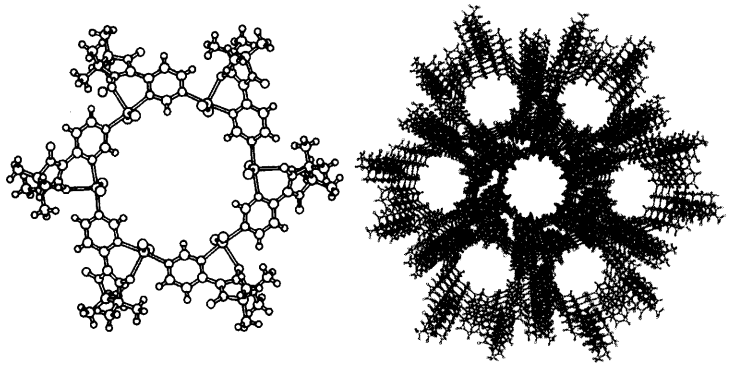

FIGURE 4 Molecular (left) and crystal structures (right) of hexameric $CuCl_2$•(4PMNN).

MCl_2•(4PMNN)$_2$

Elemental analysis revealed that the complexes obtained from 4PMNN with $CoCl_2$ and $NiCl_2$ had a ligand/metal ratio of 2:1. Figure 5 shows temperature dependence of $\chi_{mol}T$ for $CoCl_2$•(4PMNN)$_2$ and $NiCl_2$•(4PMNN)$_2$ measured at 5 kOe. The $\chi_{mol}T$ value of $NiCl_2$•(4PMNN)$_2$ was small and constant just like a diamagnetic compound, owing to fairy large antiferromagnetic interaction. There are two possible explanations: when a nickel(II) ion has a low spin state (S_{Ni} = 0), two 4PMNN moieties are antiferromagnetically coupled each other. It is more likely that each 4PMNN moiety correlates antiferromagnetically with a high-spin nickel(II). Crystal structure analysis of $NiCl_2$•(4PMNN)$_2$ is now underway.

On the other hand, a decrease of $\chi_{mol}T$ was found in lowering temperature for $CoCl_2$•(4PMNN)$_2$ (Figure 5). This behavior can be attributed to antiferromagnetic interaction, although the effects of the orbital angular momentum in cobalt(II) ions can not be eliminated at this stage. The $\chi_{mol}T$ value at 100 K indicates that the presence of three S = 1/2 spins, i.e., the cobalt(II) ion has a low spin state. A clear anomaly is found below 5 K and the $\chi_{mol}T$ curve has a peak at ca. 3 K. Figure 6 shows the magnetization curve of $CoCl_2$•(4PMNN)$_2$ measured at 1.8 K,

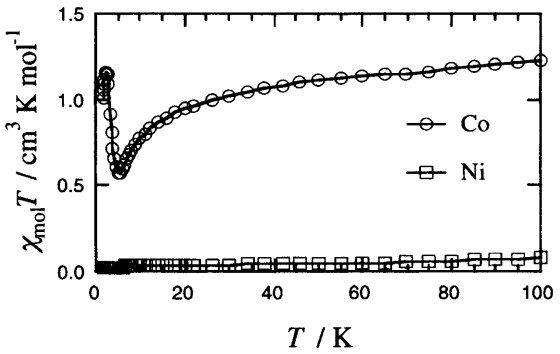

FIGURE 5 Temperature dependence of $\chi_{mol}T$ for $CoCl_2$•(4PMNN)$_2$ and $NiCl_2$•(4PMNN)$_2$ measured at 5 kOe. The solid lines are shown for a guide to the eye.

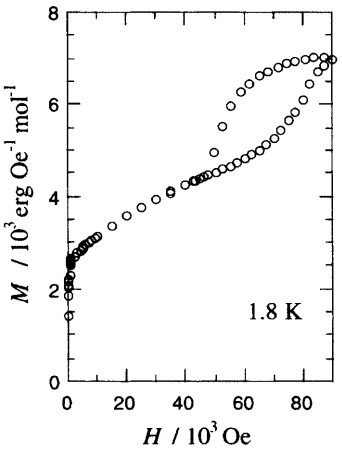

FIGURE 6 Magnetization curve of $CoCl_2$•(4PMNN)$_2$ measured at 1.8 K.

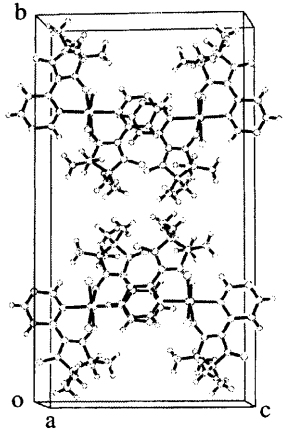

FIGURE 7 Crystal structure of $CoCl_2$•(4PMNN)$_2$.

which exhibits a spontaneous magnetization of 2.6 x 10^3 erg Oe^{-1} mol^{-1}. With an increase of the applied field, the magnetization increased and reached to ca. 5.0 x 10^3 erg Oe^{-1} mol^{-1} around 65 kOe, which is close to the theoretical saturation value of S_{total} = 1/2. Therefore antiferromagnetic coupling is present in the three spin system. The magnetization started again to increase at ca. 65 kOe, which seems to be ferri- to ferromagnetic transition. Hysteresis behavior found in a high field region supports the ferromagnetic phase in this region.

The X-ray crystal structure analysis of $CoCl_2$•$(4PMNN)_2$ revealed that the complex consists of discrete mononuclear molecules; the N_{3PM} atom contribute a six-membered chelate but the N_{1PM} atom does not work as an N-donor (Figure 7) [13]. Intermolecular atomic contacts were found between the nitronyl nitroxide oxygen and methyl hydrogen atoms. Assuming that negative spin densities are polarized on methyl hydrogen atoms, the through-space interaction is ferromagnetic. A possible spin polarization is superposed to selected moieties of two adjacent molecules in Figure 8.

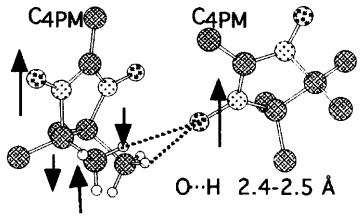

FIGURE 8 Intermolecular ferromagnetic exchange mechanism.

Similar magnetic interactions are reported on TEMPO-based ferromagnetic materials [14]. The magnetic ground state of $CoCl_2$•$(4PMNN)_2$ is schematically drawn as: $[\uparrow_{NN} - \downarrow_{Co} - \uparrow_{NN}] \cdots [\uparrow_{NN} - \downarrow_{Co} - \uparrow_{NN}] \cdots$, where "···" denotes intermolecular H···O interaction. These contacts are found in two directions parallel to the *ac*-plane.

SUMMARY

As the crystal structure analysis of $CuCl_2$•(4PMNN) and $CoCl_2$•$(4PMNN)_2$ clarified, they do not have polymeric structures. The intermolecular interactions are found to be ferromagnetic and the mechanisms are proposed based on the geometry of intermolecular van der Waals contacts. The mechanisms for purely organic ferromagnetic materials can be applied to molecular crystals of metal-radical complexes because the organic moieties in the periphery of the complex serve interactive sites between molecules.

Acknowledgments

This work was supported by Grants-in-Aid for Scientific Research on Priority Areas (Nos. 730/11224204 and 297/12020219) from the Ministry of Education, Science, Sports and Culture, Japan.

References

[1] A. Caneschi, D. Gatteschi, P. Rey, and R. Sessoli, *Acc. Chem. Res*, **22**, 392 (1989) ; K. Inoue, T. Hayamizu, H. Iwamura, D. Hashizume, and Y. Ohashi, Y. *J. Am. Chem. Soc.*, **118**, 1803 (1996).

[2] T. Ishida and T. Nogami, *Recent Res. Devel. Pure Appl. Chem.*, **1**, 1 (1997); T. Ishida, K. Nakayama, M. Nakagawa, W. Sato, Y. Ishikawa, M. Yasui, F. Iwasaki, and T. Nogami, *Synth. Met.*, **85**, 1655 (1997).

[3] K. Nakayama, T. Ishida, R. Takayama, D. Hashizume, M. Yasui, F. Iwasaki, and T. Nogami, *Chem. Lett.*, **1998**, 497; K. Zusai, T. Kusaka, T. Ishida, R. Feyerherm, M. Steiner, and T. Nogami, *Mol. Cryst. Liq. Cryst.*, **343**, 127 (2000).

[4] T. Kusaka, T. Ishida, D. Hashizume, F. Iwasaki, and T. Nogami, *Chem. Lett.*, **2000**, 1146.

[5] H. Iwamura, *Adv. Phys. Org. Chem.*, **26**, 179 (1990).

[6] J. Omata, T. Ishida, D. Hashizume, F. Iwasaki, and T. Nogami, *Inorg. Chem.*, in press.

[7] H. Bredereck, R. Sell, and F. Effenberger, *Chem. Ber.*, **97**, 3406 (1964).

[8] E. F. Ullman, J. H. Osiecki, and R. Darcy, *J. Am. Chem. Soc.*, **94**, 7049 (1972).

[9] Crystallographic data for 4PMNN: orthorhombic, *Pbca*, a = 16.4071(7), b = 13.2968(6), c = 10.8253(5) Å, V = 2361.7(2) $Å^3$, Z = 8, D_{calc} = 1.32 g/cm^3, R = 0.056, R_w = 0.078 for 2163 reflections.

[10] J. J. P. Stewart, MOPAC ver 6.0, *QCPE* #455.

[11] H. M. McConnell, *J. Chem. Phys.*, **39**, 1910 (1963).

[12] J. Omata, T. Ishida, D. Hashizume, F. Iwasaki, and T. Nogami, *Polyhedron*, in press.

[13] Crystallographic data for $CoCl_2$•$(4PMNN)_2$: orthorhombic, *Pnna*, a = 7.493(4), b = 28.04(1), c = 14.963(8) Å, V = 3143(5) $Å^3$, Z = 4, D_{calc} = 1.27 g/cm^3, R = 0.13 ($I > 2\sigma(I)$) for 2715 reflections.

[14] T. Ishida, K. Tomioka, T. Nogami, H. Yoshikawa, M. Yasui, F. Iwasaki, H. Iwamura, N. Takeda, and M. Ishikawa, *Chem. Phys. Lett.*, **247**, 7 (1995); T. Nogami, T. Ishida, M. Yasui, F. Iwasaki, N. Takeda, M. Ishikawa, T. Kawakami, and K. Yamaguchi, *Bull. Chem. Soc. Jpn.*, **69**, 1841 (1996).

Mol. Cryst. Liq. Cryst., Vol. 376, pp. 463-468

1058-725X/02 $12.00+.00

Magnetic Phase Transition of FE^{II}, CO^{II} and NI^{II} Complexes Bridged by Pyrimidine and Dicyanamide

TAKAHARU KUSAKA, TAKAYUKI ISHIDA, DAISUKE HASHIZUME, FUJIKO IWASAKI and TAKASHI NOGAMI

Department of Applied Physics and Chemistry, The University of Electro-Communications, Chofu, Tokyo 182-8585, Japan

X-Ray diffraction study reveals that complexes $M^{II}[N(CN)_2]_2$-(pyrimidine) (M = Fe, Co, Ni) have an isomorphous 3-D network, in which $N(CN)_2^-$ and pyrimidine contribute μ-1,5-bridged 2-D and μ-1,3-bridged 1-D structures, respectively. Magnetic measurements indicate that the Fe, Co, and Ni complexes behave as weak ferromagnets below the transition temperatures of 3.2, 1.8, and 8.3 K, respectively.

Keywords: weak ferromagnet, canted antiferromagnet, X-ray diffraction, magnetic phase transition

INTRODUCTION

Magnetism of transition-metal complexes with a 3-dimensional network is of current interest for developing high T_C magnets. Various magnets have been reported containing polycyano-anion bridges such as $C(CN)_3^-$ [1] and $N(CN)_2^-$ anions [2]. We have reported the magnetism of pyrimidine-bridged transition metal complexes [3,4,5]. Ternary systems are also intensively studied and the peculiar crystal and magnetic structures of $Mn[N(CN)_2]_2(pz)$ [6] have been reported for an instance. Very recently we reported the crystal structure and magnetic phase transition of $M^{II}[N(CN)_2]_2(pm)$ [M = Fe (**1**), Co (**2**); pm = pyrimidine] containing both μ-1,5-$N(CN)_2^-$ and μ-1,3-pm bridges [5]. We report here the crystal structure and magnetic properties of a nickel(II)

analogue, $Ni[N(CN)_2]_2(pm)$ (**3**). In contrast to antiferromagnetism of $Mn[N(CN)_2]_2(pz)$ containing similar μ-1,5-$N(CN)_2^-$ bridges [6], **1** - **3** show spontaneous magnetization below their transition temperature.

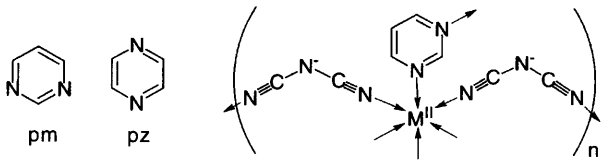

1: M = Fe, **2**: M = Co, **3**: M = Ni

EXPERIMENTAL

An EtOH-H_2O solution containing pm and $NaN(CN)_2$ with a 1/2 molar ratio was added to an aqueous solution of $FeCl_2 \cdot 4H_2O$ which was equimolar of pm. The mixture was allowed to stand for several days to give yellow single crystals of **1**. Similar procedures using $CoCl_2 \cdot 6H_2O$ and $NiCl_2 \cdot 6H_2O$ in place of $FeCl_2 \cdot 4H_2O$ gave red and blue crystals of **2** and **3**, respectively. Elemental analyses (C, H, N) of **1** - **3** on a Fisons EA-1108 by a usual combustion method revealed that the crystals contained 0.5-1.0 molar of EtOH as a crystal solvent.

X-Ray diffraction data were collected on a Rigaku Raxis-Rapid IP diffractometer with monochromated Mo$K\alpha$ and Cu$K\alpha$ radiations. Structures were solved by direct methods and the atomic positions were refined by full-matrix least-squares methods using all of the reflections. Magnetic properties were measured on Quantum Design MPMS SQUID and PPMS ac/dc magnetometers.

RESULTS AND DISCUSSION

X-Ray crystal structure analysis

Table 1 summarizes the X-ray crystallographic data for **1** - **3**. The crystals of **1** - **3** are isomorphous, belonging to a space group orthorhombic *Pnma*. Figure 1 shows the crystal structure of **3**. Following features are common to **1** - **3**: 1) M^{II} and two $N(CN)_2^-$ ions construct two-dimensional network parallel to the *ac*-plane. 2) Pm molecules bridge inter-sheet M^{II} ions along the *b*-axis, forming a pm-M *trans* zigzag chain. 3) Crystallographically independent units contain

one metal ion. 4) Each octahedral M^{II} ion resides at an inversion center and is coordinated by four nitrile N atoms at the equatorial sites [7] and by two pm N atoms at the axial sites [8]. 5) The $N(CN)_2^-$ moiety was disordered into two positions. The amide nitrogen atom does not act as an N-donor. 6) The M···M separation across the pm bridge is shorter than that across the $N(CN)_2^-$ bridge. The pm bridge may afford a principal magnetic exchange pathway. 7) Crystal solvent molecules are disordered with the occupancy smaller than unity.

TABLE 1 Selected X-ray crystallographic data of **1** - **3**.

compound	**1**	**2**	**3**
Formula	$FeC_8N_8{\bullet}C_2H_5OH$	$CoC_8N_8{\bullet}C_2H_5OH$	$NiC_8N_8{\bullet}H_2O$
Space group	*Pnma*	*Pnma*	*Pnma*
a / Å	12.917(1)	12.8586(4)	12.676(2)
b / Å	12.0440(6)	11.9268(4)	11.898(1)
c / Å	9.2575(8)	9.2126(2)	9.297(2)
V / Å^3	1440.2(2)	1412.86(7)	1402.0(3)
Z	4	4	4
D_{calc} / g cm^{-3}	1.449	1.491	1.283
T / K	100	100	296
R ($I > 2\sigma(I)$)	0.059	0.067	0.046
Reflections	1663	1699	1344
Reference	[5]	[5]	this work

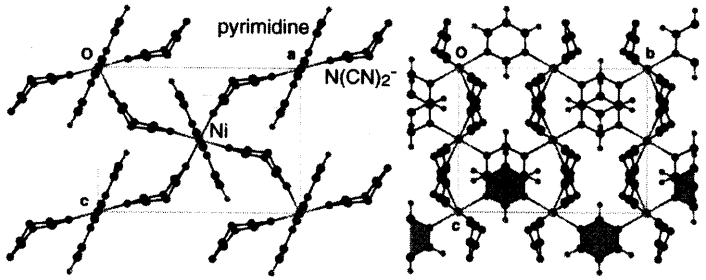

FIGURE 1 Crystal structure of $Ni[N(CN)_2]_2(pm)$ (**3**), viewed along the *b* (left) and *a* axes (right). Disordered solvent molecules are omitted for the sake of clarity. A one-dimensional Ni-pm chain is shaded.

Magnetic properties

Figure 2 shows the temperature dependence of the product of magnetic susceptibility and temperature ($\chi_{mol}T$) for **1** - **3** together with those of $Mn[N(CN)_2]_2(pm)$ and $Cu[N(CN)_2]_2(pm)_{0.75}$ measured at 5 kOe. Although the decreases in $\chi_{mol}T$ with a decrease of temperature are partly attributed to effects of the orbital angular momentum in metal ions, dominant antiferromagnetic interactions are assumed for all of the complexes, because the following magneto-structure relationship can be pointed out. In the crystals of **1** - **3**, every pm nitrogen atom is coordinated at an equatorial position, where a magnetic $d_{x^2-y^2}$ orbital of a high-spin Fe^{II}, Co^{II}, or Ni^{II} ion overlaps with a nitrogen lone pair. Their high-spin states are confirmed by the $\chi_{mol}T$ values at 100 K. Thus, the role of an antiferromagnetic coupler is rationalized in terms of the superexchange mechanism similarly to the case of the pm-bridged copper(II) complexes [9]. Small peaks are found for **1** - **3** in Figure 2. We focus discussion on the magnetism of **3** here, since the detailed magnetic studies on **1** and **2** have been described elsewhere [5].

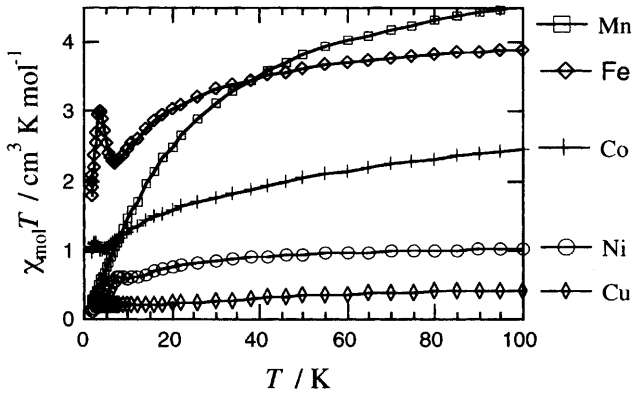

FIGURE 2 Temperature dependence of $\chi_{mol}T$ for $M[N(CN)_2]_2(pm)$ complexes measured at 5 kOe.

In order to clarify the occurrence of magnetic phase transition of **3** around the peaking temperature of $\chi_{mol}T$ (8 K), field-cooled

magnetization (FCM), remnant magnetization (RM), and zero-field-cooled magnetization (ZFCM) were measured (Figure 3(a)). The FCM measured at an applied field of 5 Oe started to diverge at 8.5 K. The RM decreased and disappeared at 8.3 K, which we define as a transition temperature. The ZFCM, measured on heating at an applied field of 5 Oe, showed a maximum at 8.2 K and coincided with FCM above 8.2 K. Figure 3(b) shows the magnetization curve of **3** measured at 4 K. The magnetization varied linearly up to 70 kOe, owing to strong antiferromagnetic interaction. This finding is compatible with the dominant antiferromagnetic behavior of **3** observed in the $\chi_{mol}T$ vs T plot (Figure 2). However, the spontaneous magnetization extrapolated to $H \rightarrow 0$ Oe was found to be 70 erg Oe^{-1} mol^{-1} (the inset of Figure 3(b)).

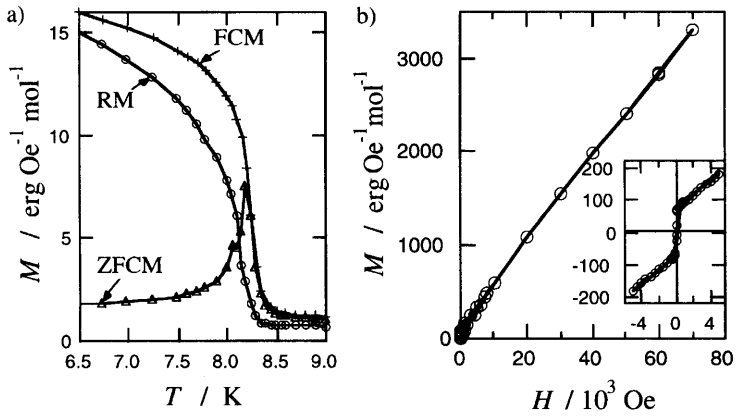

FIGURE 3 (a) Field-cooled magnetization (FCM, 5 Oe), remnant magnetization (RM), and zero-field-cooled magnetization (ZFCM, 5 Oe) for $Ni[N(CN)_2]_2(pm)$ (**3**). (b) Magnetization curve of **3** measured at 4 K. An M-H loop near $H = 0$ Oe is magnified in the inset. The solid lines are shown as a guide to the eye.

The magnetic behavior of **3** is typical of a weak ferromagnet (canted antiferromagnet). Thus, the isomorphous series of **1** - **3** were all

proved to be weak ferromagnets. The spontaneous magnetization of **1** and **2** are 5.8×10^3 and 2.5×10^3 erg Oe^{-1} mol^{-1} at 2.0 and 1.8 K, respectively [5], which are much larger than that of **3** at 4 K in spite of practically the same crystal structure. The transition temperatures (T_N's) of **1** - **3** were 3.2, 1.8 [5], and 8.3 K, respectively. We have recently reported that another isomorphous series of $MCl_2 \cdot (pm)_2$, whose T_N's are 6.1, 4.4, and 16 K for M = Fe, Co, and Ni, respectively [4]. Interestingly, the dependence of T_N upon metal ion species is parallel to each other. Furthermore, the transition temperatures of $M[N(CN)_2]_2$ (M = Fe: T_N = 18.5 K [2b]; M = Co: T_C = 9.2 K [2c]; M = Ni: T_C = 20.6 K [2c]) show a similar tendency of the metal ion dependence.

References

[1] S. R. Batten, B. F. Hoskins, B. Moubaraki, K. S. Murray, and R. Robson, *J. Chem. Soc., Dalton Trans.*, **1999**, 2977; H. Hoshino, K. Iida, T. Kawamoto, and T. Mori, *Inorg. Chem.*, **38**, 4229 (1999); J. L. Manson, C. Campana, and J. S. Miller, *Chem. Commun.*, **1998**, 251.

[2] a) S. R. Batten, P. Jensen, B. Moubaraki, K. S. Murray, and R. Robson, *Chem. Commun.*, **1998**, 439. b) M. Kurmoo and C. J. Kepert, *New J. Chem.*, **22**, 1515 (1998). c) J. L. Manson, C. R. Kmety, Q. Z. Huang, J. W. Lynn, G. M. Bendele, S. Pagola, P. W. Stephens, L. M. Liable-Sands, A. L. Rheingold, A. J. Epstein, and J. S. Miller, *Chem. Mater.*, **10**, 2552 (1998). d) J. L. Manson, C. R. Kmety, A. J. Epstein, and J. S. Miller, *Inorg. Chem.*, **38**, 2552 (1999).

[3] T. Ishida and T. Nogami, *Recent Res. Devel. Pure Appl. Chem.*, **1**, 1 (1997); T. Ishida, K. Nakayama, M. Nakagawa, W. Sato, Y. Ishikawa, M. Yasui, F. Iwasaki, and T. Nogami, *Synth. Met.*, **85**, 1655 (1997).

[4] K. Nakayama, T. Ishida, R. Takayama, D. Hashizume, M. Yasui, F. Iwasaki, and T. Nogami, *Chem. Lett.*, **1998**, 497; K. Zusai, T. Kusaka, T. Ishida, R. Feyerherm, M. Steiner, and T. Nogami, *Mol. Cryst. Liq. Cryst.*, **343**, 127 (2000).

[5] T. Kusaka, T. Ishida, D. Hashizume, F. Iwasaki, and T. Nogami, *Chem. Lett.*, **2000**, 1146.

[6] J. L. Manson, C. D. Incarvito, A. L. Rheingold, and J. S. Miller, *J. Chem. Soc., Dalton Trans.*, **1998**, 3705.

[7] The interatomic distances between M and N(nitrile): **1**, 2.138(4), 2.142(4) Å; **2**, 2.103(4), 2.105(4) Å; **3**, 2.060(3), 2.061(2) Å.

[8] The interatomic distances between M and N(pyrimidine): **1**, 2.202(4) Å; **2**, 2.154(4) Å; **3**, 2.113(3) Å.

[9] F. Mohri, K. Yoshizawa, T. Yamabe, T. Ishida, and T. Nogami, *Mol. Engineer.*, **8**, 357 (1999); M. Yasui, Y. Ishikawa, N. Akiyama, T. Ishida, T. Nogami, and F. Iwasaki, *Acta Cryst. B*. in press.

Mol. Cryst. Liq. Cryst., Vol. 379, pp. 259-264

1058-725X/02 $12.00 + .00
DOI: 10.1080/10587250290090570

Solvated Magnets of $Fe[N(CN)_2]_2$(pyrimidine): Transition Phenomena Tuned by Guests

TAKAHARU KUSAKA, TAKAYUKI ISHIDA
and TAKASHI NOGAMI

Department of Applied Physics and Chemistry, The University of Electro-Communications, Chofu, Tokyo 182-8585, Japan

Low-temperature magnets derived from $Fe[N(CN)_2]_2$(pyrimidine) have guest molecules incorporated in the clearance of the 3-D framework. The ac and dc magnetic susceptibility measurements reveal that the temperature of magnetic phase transition (T_N) depends on the guest molecules. They are characterized as weak ferromagnets below T_N. The compound containing uncoordinated pyrimidine molecules as a guest showed the highest T_N of 5.6 K in this family.

Keywords: host-guest compound; weak ferromagnet; X-ray diffraction; magnetic phase transition

INTRODUCTION

Magnetism of transition-metal complexes with 3-dimensional networks is of current interest for developing high T_C magnets[1]. Self-assembled complexes also attract attention for porous materials affording potential application in many areas (gas absorption for instance)[2]. Porous magnets enable us to examine possible control of the magnetism by means of supramolecular techniques[3]. Recently we reported the crystal structure and magnetic phase transition of

$M^{II}[N(CN)_2]_2$(pm) (M = Fe[4], Co[4], Ni[5]; pm = pyrimidine) containing both μ-1,5-$N(CN)_2^-$ and μ-1,3-pm bridges. The specimen prepared from an ethanol solution was revealed to contain ethanol molecules as a guest[4]. Magnetic measurements indicate that the Fe complex behaves as a weak ferromagnet below the transition temperature (T_N) of 3.2 K[4]. We report here the solvent-effect on the magnetic properties of solvated magnets of $Fe[N(CN)_2]_2$(pm) since preparation from various solvents gave isomorphous compounds with only slight structural modification.

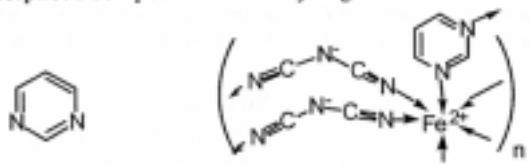

pm $Fe[N(CN)]_2$(pm)

EXPERIMENTAL

The following synthetic procedure is typical. An aqueous solution containing pm and $NaN(CN)_2$ with a 1/1 molar ratio was added to an aqueous solution of a half molar amount of $FeCl_2 \cdot 4H_2O$. The mixture was allowed to stand for several days to give yellow single crystals (**1**). The polycrystalline samples of **2**, **3**, and **4** were prepared similarly from EtOH-H_2O (1/2), PrOH-H_2O (1/4), and BuOH-H_2O (1/15) mixed solutions, respectively, by using the pm/$NaN(CN)_2$/$FeCl_2$ ratio of 1/2/1. Elemental analysis (C, H, N), X-ray crystallographic analysis, and magnetic measurements of these compounds were done immediately after the isolation on a filter. The elemental analysis revealed that the composition formulae were $Fe[N(CN)_2]_2$(pm)$(guest)_n$, where $(guest)_n$ = $(pm)_1$, $(EtOH)_1$, $(PrOH)_1$, and $(BuOH)_{0.5}$ for **1** - **4**, respectively.

X-Ray diffraction data were collected on a Rigaku Raxis-Rapid IP diffractometer with monochromated Mo*K*a radiation. Structures were solved by direct methods and the atomic positions were refined by full-matrix least-squares methods using all of the reflections.

Magnetic properties were measured on Quantum Design MPMS SQUID and PPMS ac/dc magnetometers. Diamagnetic contribution of

the sample itself was estimated from Pascal's constant.

RESULTS AND DISCUSSION

X-Ray Crystal Structure Analysis

The crystals of **1** - **4** are isomorphous, belonging to a space group orthorhombic *Pnma*. Figure 1 shows the crystal structure of **1**. The guest molecule in **1** was characterized to be an uncoordinated pm. The hydrogen atoms in the guest pm were experimentally determined; the orientation of the six-membered ring shows no disorder. There is only one Fe ion in an asymmetric unit. Each octahedral Fe ion resides at an inversion center and is coordinated by four nitrile N atoms at the equatorial sites and by two pm N atoms at the axial sites. The Fe and two $N(CN)_2^-$ ions construct a two-dimensional network parallel to the *ac*-plane. The pm molecules bridge inter-sheet Fe ions along the *b*-axis. The $N(CN)_2^-$ and pm moieties contribute μ-1,5-bridged 2-D and μ-1,3-bridged 1-D structures, respectively, forming a 3-D framework.

The $Fe[N(CN)_2]_2$(pm) skeletons are essentially the same among **1** - **4**, except for the small change of the cell lengths (Table 1) and the presence of disorder of the $N(CN)_2^-$ positions in **2** - **4**. The crystal structure of **2** was published elsewhere[4]. The solvent molecules in **2** - **4** were found in difference Fourier maps but their positional and thermal displacement parameters could not be completely determined owing to disorder.

FIGURE 1 Stereo-view of the crystal structure of **1**.

TABLE 1 Selected crystallographic parameters of **1** - **4**.[a]

Compound	**1**	**2**	**3**	**4**
Guest	pyrimidine	ethanol[b]	propanol[b]	1/2 butanol[b]
a / Å	13.0061(5)	12.9378(7)	12.597(5)	12.9486(7)
b / Å	12.3550(4)	12.0279(6)	12.001(6)	12.2052(6)
c / Å	9.2235(4)	9.2456(4)	9.461(4)	9.4499(6)
V / Å^3	1482.1(1)	1438.8(1)	1430(1)	1493.5(2)
D_{calc} / g cm^{-3}	1.560	1.450	1.523	1.584

[a] Measured at 90 K. The space groups are orthorhombic *Pnma* and $Z = 4$. [b] Determined by elemental analysis (C, H, N).

Magnetic Properties

We measured field-cooled magnetization, remnant magnetization, and zero-field-cooled magnetization of **1** - **4**. The temperature dependence of the field-cooled magnetization at 5 Oe showed clear upsurges at about 5.6, 3.7, 4.6, and 3.6 K for **1** - **4**, respectively, and, after the applied field was removed, the remnant magnetizations were disappeared at the same temperatures. As Figure 2 shows, the ac magnetic susceptibility (χ_{ac}') measurements (100 Hz) exhibited peaks at 5.6, 3.3, 4.4, and 3.6 K, respectively, supporting the occurrence of magnetic phase transition.

Although the μ-1,3 pm bridge is supposed to work as a major exchange coupler in veiw of the Fe···Fe distances[4], we could find no relation between the transition temperatures and the *b* lengths. The transition temperature may be ruled also by secondary exchange couplings in the 3-dimensional network. Furthermore, the magnetic interaction is susceptible to the local geometry such as bond angles around Fe ions. Accordingly it is difficult to find relationship between the cell constants and transition temperatures. The magnetic ordering seems to be affected by crystallographic disorders, since **1** has no disorder of $N(CN)_2^-$ or of guest molecules and showed the highest transition temperature in spite of the relatively large cell volume.

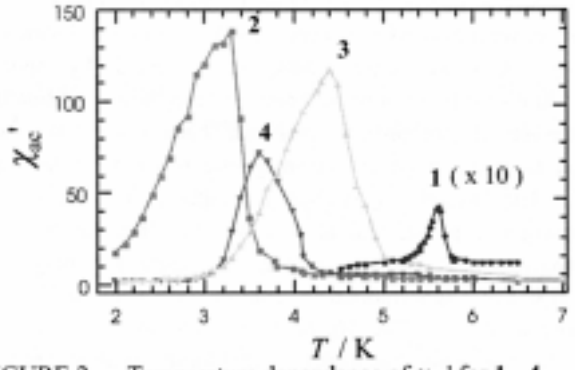

FIGURE 2 Temperature dependence of χ_{ac}' for **1** - **4**.

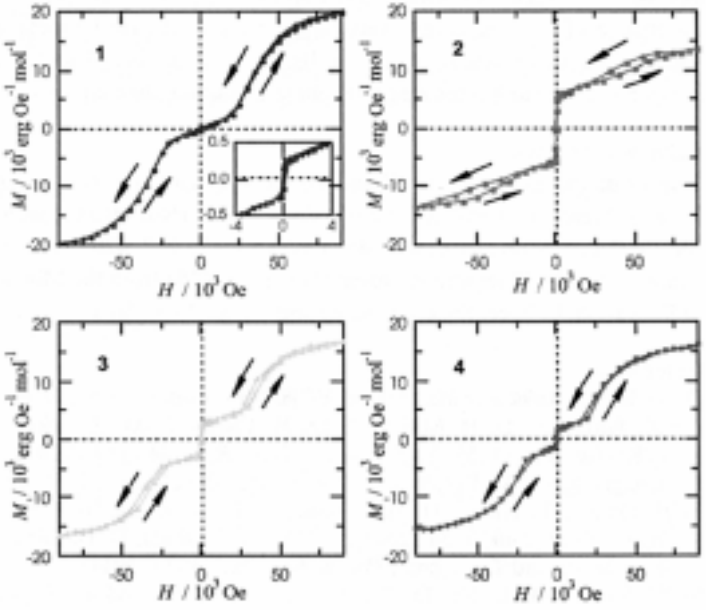

FIGURE 3 Hysteresis curves of **1** - **4** measured at 2.0 K. The solid lines are shown for a guide to the eye.

In order to clarify the nature of magnetism below the transition temperature, we measured *M-H* curves for **1** - **4**. Figure 3 shows that **1** - **4** behave as weak ferromagnets, as indicated by spontaneous magnetizations (M_S) in a low field region. Stepwise saturation behavior was observed, the origin of which has been proposed as spin-flip transition from a canted antiferromagnetic phase to a ferromagnetic phase[4]. The smaller M_S implies a smaller cant angle in a canted antiferromagnetic phase, and after a possible spin-flip transition the saturation magnetization should be larger in a canted ferromagentic phase. This interpretation is supported by comparison of the *M-H* curve of **1** with those of **2** - **4**. The M_S of **1** was the smallest and the strong antiferromagnetic nature seems responsible for the small χ_{ac}' peak of **1**.

In conclusion, we found that the molecular guests were incorporated in the clearance of the $Fe[N(CN)_2]_2(pm)$ skeleton. The T_N change of ca. 2 K is relatively large in the liquid He temperature region. The deformation of unit cells as well as the disorder of components may affect the magnetic phase transition phenomena.

Acknowledgments

This work was supported by Grants-in-Aid for Scientific Research on Priority Areas of "Metal-Assembled Complexes" (No. 401/11136212) and "Molecular Conductors and Magnets" (No. 730/11224204) and by a Grant-in-Aid for Scientific Research (No. 13640575) from the Ministry of Education, Culture, Sports, Science and Technology, Japan.

References

[1.]O. Kahn, *Molecular Magnetism*, VCH, New York (1993).

[2.]M. Eddaoudi, D. B. Moler, H. Li, B. Chem, T. M. Reineke, M. O'Keeffe, and O. M. Yaghi, *Acc. Chem. Res.*, **34**, 319 (2001); S. Kitagawa, and M. Kondo, *Bull. Chem. Soc. Jpn.*, **71**, 1739 (1998).

[3.]J. Omata, T. Ishida, D. Hashizume, F. Iwasaki, and T. Nogami, *Inorg. Chem.*, **40**, 3954 (2001); J. Omata, T. Ishida, D. Hashizume, F. Iwasaki, and T. Nogami, *Polyhedron*, **20**, 1557 (2001).

[4.]T. Kusaka, T. Ishida, D. Hashizume, F. Iwasaki, and T. Nogami, *Chem. Lett.*, **2000**, 1146.

[5.]T. Kusaka, T. Ishida, D. Hashizume, F. Iwasaki, and T. Nogami, *Mol. Cryst. Liq. Cryst.*, in press.

Mol. Cryst. Liq. Cryst., Vol. 379, pp. 147-152

1058-725X/02 $12.00+.00
DOI: 10.1080/10587250290090390

First Isolation and Characterization of an HIN Complex, $CdCl_2(HIN)_4$ (HIN = 4,4,5,5-Tetramethylimidazolin-1-oxyl)

TOMOAKI ISE, TAKAYUKI ISHIDA and TAKASHI NOGAMI

Department of Applied Physics and Chemistry, The University of Electro-Communications, Chofu, Tokyo 182-8585, Japan

We report here for the first time the X-ray crystal structure and magnetic properties of an HIN complex, $CdCl_2(HIN)_4$, showing very strong antiferromagnetic interaction. X-ray crystal structure analysis reveals that intermolecular O···N distance (2.33 and 2.42 Å) are considerably short.

Keywords: X-ray diffraction, diamagnetic metal, unstable organic radicals, metal-radical complex

INTRODUCTION

The metal-radical approach is a promising strategy for molecule-based magnetic materials[1]. The imino- and nitronylnitroxide radical derivatives have been known as available ligands for magnetic materials and a large number of complexes have been developed as ferro- or ferrimagnets[2]. We assume that the choice of small ligands and anions is crucial in order to bestow strong magnetic interaction and raise magnetic phase transition temperatures in the metal-radical approach. We chose α-hydroiminonitroxide (HIN) as a ligand, which is the smallest derivative in the imino- and nitronylnitroxide family.

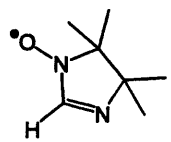

HIN

Although the isolation of HIN was

claimed to be difficult because of its instability[3], complexation affords a chance to purify and characterize HIN compounds. Stabilization based on complex formation is widely utilized for preparation of low-valent main group element compounds[4]. We report here for the first time the X-ray crystal structure and magnetic properties of an HIN complex, $CdCl_2(HIN)_4$. Extraordinary strong magnetic interaction was observed as expected from the small size of the ligand.

EXPERIMENTAL

4,4,5,5-Tetramethylimidazolin-1-oxyl (HIN) was prepared according to the procedure previously reported[3]. Solutions of HIN (100 mg, 0.71 mmol) in H_2O (1.5 ml) and of $CdCl_2 \cdot 2.5H_2O$ (162 mg, 0.71 mmol) in H_2O (0.5 ml) were mixed, the combined solution was allowed to stand in a cool and dark place for 2 h, and orange crystals of $CdCl_2(HIN)_4$ were precipitated. Elemental analysis (C, H, N) of this complex on a Fisons EA-1108 by a usual combustion method revealed that the metal/ligand ratio is 1:4. X-Ray diffraction data were collected on a Rigaku Raxis-Rapid IP diffractometer with monochromated Mo$K\alpha$ radiation. Structure was solved by direct methods and refined using all of the reflections. Magnetic susceptibility was measured on a Quantum Design MPMS SQUID magnetometer.

RESULTS AND DISCUSSION

X-Ray Crystal Structure Analysis

Table 1 summarizes the X-ray crystallographic data for $CdCl_2(HIN)_4$. Figure 1 shows that $CdCl_2(HIN)_4$ is a mononuclear complex. There are two crystallographically independent HIN units in a molecule. The imino nitrogen atoms N(1) and N(3) are coordinated to the Cd ion whereas the nitroxide oxygen atoms O(1) and O(2) remain

uncoordinated. The strong coordination ability of the imino nitrogen atoms can be understood in view of the steric congestion around imino nitrogen and nitroxide oxygen atoms.

This complex does not form any covalent network in the crystal. However, as Figure 2 shows, considerably short intermolecular distances of 2.33(2) and 2.41(8) Å are found between O(1)···N(2*) and O(2)···N(4*), respectively. These distances are much shorter than the sum of the van der Waals radii of oxygen and nitrogen (3.07 Å)[5]. We assumed that HIN groups formed a dimer by contacting nitroxide groups in an intermolecular fashion.

TABLE 1 Selected X-ray crystallographic data of $CdCl_2(HIN)_4$.

Formula	$CdCl_2(C_7H_{13}N_2O)_4$
Space group	$P\bar{1}$
a/ Å	10.417(4)
b/ Å	10.591(1)
c/ Å	9.455(8)
α/ degrees	105.78(6)
β/ degrees	103.25(2)
γ/ degrees	115.56(2)
V/ Å^3	830.3(1)
Z	1
D_{calc}/ g cm^{-3}	1.50
T/K	100
$R(I>2\sigma(I))$	0.025

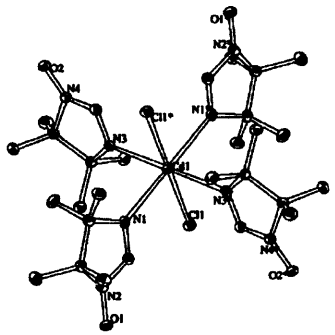

FIGURE 1 Molecular structure of $CdCl_2(HIN)_4$. Methyl hydrogen atoms are omitted for clarity.

Magnetic properties

Temperature dependences of the molar magnetic susceptibility χ_m and the product $\chi_m T$ are shown in Figure 3. Since some metal complexes with organic paramagnetic ligands and diamagnetic metals have been reported to show magnetic interactions through the diamagnetic metal

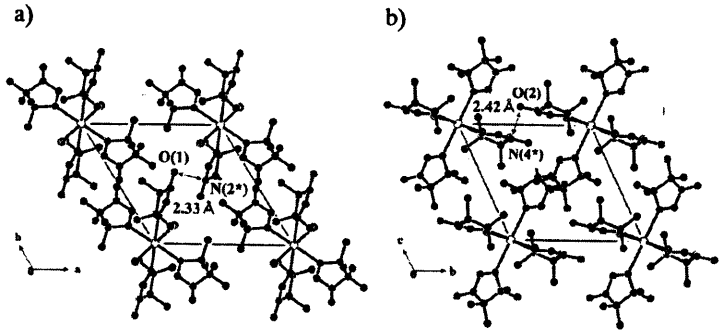

FIGURE 2 Molecular arrangement in the crystal of $CdCl_2(HIN)_4$. Short intermolecular contacts are indicated. a) Viewed along the *c* axis. b) Viewed along the *a* axis.

ion[6], the present complex also attracts attention to intra- and intermolecular magnetic interactions. The $\chi_m T$ value at 300 K was 0.04 emu K mol^{-1} while the calculated value of a paramagnetic four-spin system is 1.5 emu K mol^{-1}. The $\chi_m T$ value hardly changes on lowering the temperature. The above structural analysis of $CdCl_2(HIN)_4$ clarified that every two HIN moieties formed a dimer. In this complex, there are two possible pathways of magnetic interactions; one is intramolecular interaction through the Cd ion and the other intermolecular interaction through the nitroxide contacts. We assume that the latter is stronger than the former viewing from considerably short intermolecular contacts.

There are two crystallographically independent dimers in a unit cell. We attempted to fit the result of the magnetic measurements by using a combined dimer model given by eq 1, based on the spin Hamiltonian $H = -2J_1 S_1 \cdot S_2 - 2J_2 S_3 \cdot S_4$, where all symbols have their usual meaning. The symbol α in eq1 means the ratio of S=1/2 paramagnetic impurity contained. The exchange parameters J_1 and J_2 are the spin-spin coupling constants between O(2)···N(4) and O(1)···

N(2), respectively. The estimated values of $|J_1/k|$ and $|J_2/k|$ are larger than 700 K, and paramagnetic impurity component is about 2%.

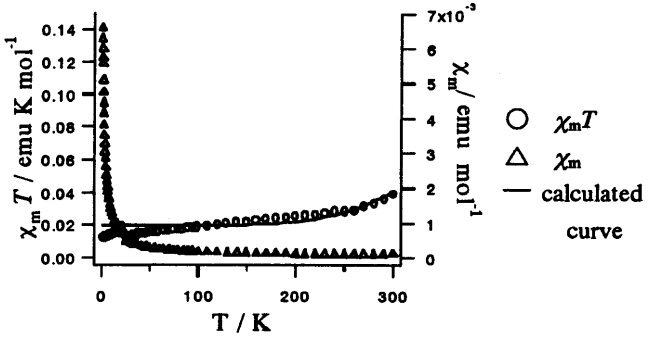

FIGURE 3 Temperature dependence of the molar magnetic susceptibility χ_m and the product $\chi_m T$ of $CdCl_2(HIN)_4$.

$$\chi = (1-\alpha)\left[\frac{2Ng^2\mu_B^2}{kT}\frac{1}{3+\exp(-2J_1/kT)} + \frac{2Ng^2\mu_B^2}{kT}\frac{1}{3+\exp(-2J_2/kT)}\right] + 2\alpha\frac{N^2g^2\mu_B^2}{3kT} \quad (1)$$

These results show that $CdCl_2(HIN)_4$ is practically diamagnetic below 300 K, and contains a small amount of monomeric impurities.

The α-4,4,5,5-tetramethylimidazolin-1-oxyl-3-oxide (α-HNN)[3] has been known as the smallest nitronylnitroxide radical. The α-HNN forms a dimer structure in the crystal, and exhibits large intermolecular antiferromagnetic interaction (J/k= -22 K) due to the close spacing between the ONCNO moieties[7]. The shortest intermolecular atomic distance between the ONCNO groups is 3.376(3) Å[7], whereas we can find much shorter distances (2.33(2) and 2.41(8) Å) in $CdCl_2(HIN)_4$. Therefore, the magnetic interaction of $CdCl_2(HIN)_4$ is reasonably attributed to intermolecular interaction.

This result indicates that the HIN ligands can be used for achieving the strong intermolecular exchange interaction.

CONCLUSION

We have demonstrated the preparation and full characterization of $CdCl_2(HIN)_4$. Considerably strong antiferromagnetic coupling ($|J/k|$>700K) was observed and assigned to intermolecular interactions.

Acknowledgments

This work was supported by Grants-in-Aid for Scientific Research on Priority Areas (Nos. 730/11224204 and 401/11136212) from the Ministry of Education, Science, Sports and Culture, Japan

References

[1.]A. Caneschi, D. Gatteschi and R. Sessoli, *Acc. Chem. Res.*, **22**, 392(1989); A. Caneschi, D. Gatteschi and P. Rey, *Prog. Inorg. Chem.*, **39**, 331(1991).

[2.]A. Caneschi, D. Gatteschi, J. P. Renard, P. Rey and R. Sessoli, *Inorg. Chem.*, **28**, 3314(1989); A. Caneschi, D. Gatteschi, J. P. Renard, P. Rey and R. Sessoli, *Inorg. Chem.*, **28**, 1976(1989); A. Caneschi, D. Gatteschi, J. P. Renard, P. Rey and R. Sessoli, *J. Am. Chem. Soc.*, **111**, 785(1989).

[3.]E. F. Ullman, L. Call, and J. H. Osiecki, *J. Org. Chem.*, **35**, 3623(1970).

[4.]For example, W. E. Buhro, A.T. Patton, C.E. Strouse, and J. A. Gladysz, *J. Am. Chem. Soc.*, **105**, 1056(1983).

[5.]A. Bondi, *J. Phys. Chem.*, **68**, 441(1964).

[6.]H. Oshio, T. Watanabe, A. Ohta, T. Ito, and U. Nagashima, *Angew. Chem., Int. Ed. Engl.*, **33**, 670(1994); C. J. Lee, H. H. Wei, G. H. Lee, and Y. Wang, *Inorg. Chem. Commun*, **3**, 690(2000).

[7.]Y. Hosokoshi, M. Tamura, K. Nozawa, S. Suzuki, H. Sawa, R. Kato, and M. Kinoshita, *Mol. Cryst. Liq. Cryst.*, **271**, 115(1995).

Nitronyl Nitroxide Substituted Aniline *o*-APNN with a Three-dimensional Hydrogen Bond Network Showing Ferromagnetic Interaction

Kentaro Doi, Takayuki Ishida,* and Takashi Nogami
Department of Applied Physics and Chemistry, The University of Electro-Communications, Chofu, Tokyo 182-8585

(Received March 27, 2003; CL-030254)

o-Aminophenyl nitronyl nitroxide (*o*-APNN) was prepared as the first aniline-substituted nitronyl nitroxide. X-Ray crystallographic analysis reveals a 3-D hydrogen bonded network due to the branching nature of $-NH_2$. Magnetic measurements indicate the presence of ferromagnetic interaction.

Hydrogen bonds play an important role in crystal engineering[1] and have been much argued in connection with the ability of propagating ferromagnetic interaction in organic magnetic materials.[2] Phenols **1**–**5** (for the chemical formulas, see below) carrying the nitronyl nitroxide group (abbreviated as NN hereafter) have been reported to exhibit intermolecular ferromagnetic interaction.[3–8] Among them, **2** and **3** which possess a hydroxyl group at the *ortho* position become genuine organic ferromagnets below ca. 0.5 K.[4,5] On the other hand, there is no report on the corresponding anilines carrying NN because undesired side-reactions take place according to a conventional synthetic procedure exploited by Ullman.[9] Namely, the amino group can not coexist with precursory aromatic aldehydes because of formation of imines.[10] Furthermore, the anilines are supposed to be oxidation-sensitive and accordingly unstable like the catechol-substituted nitronyl nitroxide.[7] We report here the preparation and magnetic properties of the first NN-substituted aniline, *o*-APNN.

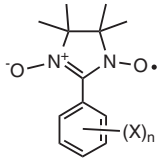

$(X)_n$ = 4-OH (**1**)
2,5-$(OH)_2$ (**2**)
2-OH (**3**)
3,5-$(OH)_2$ (**4**)
3,4-$(OH)_2$ (**5**)
2-NH_2 (*o*-APNN)

The amino group was introduced after the diazaacetal cyclization of the aldehyde group (Scheme 1). Precursor **6** was prepared from *o*-nitrobenzaldehyde according to Ullman's method.[9,11] A methanol solution (65 ml) containing **6** (1.50 g; 5.30 mmol) and an aqueous solution (10 ml) of NH_4Cl (1.68 g; 31.8 mmol) were combined, and zinc (5.50 g; 84.6 mmol) was added to the mixture in small portions at room temperature for 3 h. After the mixture was stirred for 2 d, the solid was removed by filtration. Concentration of the filtrate gave a yellow solid (1.31 g) containing **7** which was used without purification. The above product (1.31 g) was suspended to 500 ml of water, an aqueous solution (ca. 10 ml) of $NaIO_4$ (1.12 g; 5.30 mmol) was added dropwise, and the resultant brown mixture was stirred at room temperature for 30 min. The organic compounds were extracted with chloroform and separated by passing a short column of silica gel with 1/1 ethyl acetate–hexane as an eluent. A purple fraction was collected and concentrated under reduced pressure. Recrystallization from CH_2Cl_2–CH_3OH gave blue blocks of *o*-APNN (271 mg; 1.08 mmol) in 20% yield from **6**, mp. 160–162 °C. Fortunately, *o*-APNN can be handled under air in the crystalline form and in solutions. The ESR spectrum (X-band, benzene, room temperature) of *o*-APNN showed a 1:2:3:2:1 quintet with $a_N = 7.5$ G at $g = 2.0065$, which is typical of NN radicals.

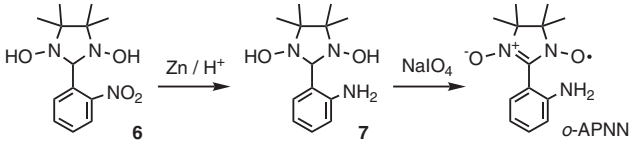

Scheme 1. Synthetic route to *o*-APNN.

X-Ray diffraction data of *o*-APNN were collected at 100 K.[12] Figure 1(a) shows the molecular structure of *o*-APNN. The dihedral angle between the benzene ring and O–N–C–N–O fragment is 47.88(5)°. Some hydrogen atoms are located very close to the NN oxygen atoms with the O···H distances of 2.1–2.5 Å. An intramolecular hydrogen bond is found in N1-H1···O1 with the N1···O1 distance of 2.895(2) Å. Figure 1(b) shows the molecular packing in the crystal of *o*-APNN. Owing to the geometry of $-NH_2$ group, branched intermolecular hydrogen bonds are found between the amino protons and neighboring NN oxygen atoms. H1 intervenes between N1 and $O2^{\#}$ which are separated by 3.171(2) Å. Accordingly, O1 and $O2^{\#}$ can interact through the bending O1···H1···$O2^{\#}$ system. H2 also participates in a hydrogen bond N1–H2···O1* which is nearly linear with the N1···O1* distance of 2.989(2) Å. Two superexchange-like interactions can be proposed along O1···H1–N1–H2···O1* and $O2^{\#}$···H1–N1–H2···O1*, and intramolecular spin-polarization effect along O1–N2–C7–C6–C1–N1–H1 and –H2 should be taken into consideration. These hydrogen bonds successively repeat along the cell axes with 2_1 screw symmetries due to the space group $P2_12_12_1$. Thus, the crystal has a chiral three-dimensional hydrogen bonded network. Relatively short O···H_{methyl} distances are also found between O2 and $H11^{\#}$ (2.54(3) Å) and between O1 and $H8^{\ddagger}$ (2.96(3) Å).[13]

Magnetic susceptibility of *o*-APNN was measured on a SQUID magnetometer in a temperature range 1.8–100 K. As Fig. 2 shows, the magnetic susceptibility of *o*-APNN obeyed the Curie-Weiss law ($\chi_{mol} = C/(T-\theta)$) with $C = 0.375\ cm^3\ K\ mol^{-1}$ and $\theta = +0.74$ K. The *M*-*H* curve measured at 1.8 K exhibited paramagnetic behavior, and the data fell close to the theoretical Brillouin function of $S = 3/2$. These findings indicate that the ferromagnetic interaction is operative in the crystal of *o*-APNN.

From the previous reports on phenols **2**[4] and **3**,[5] the hydroxyl group at the *ortho* position seems to be crucial in crystal packing and structural dimensionality, and the mechanistic investigation on the exchange interaction in **2** led to the spin po-

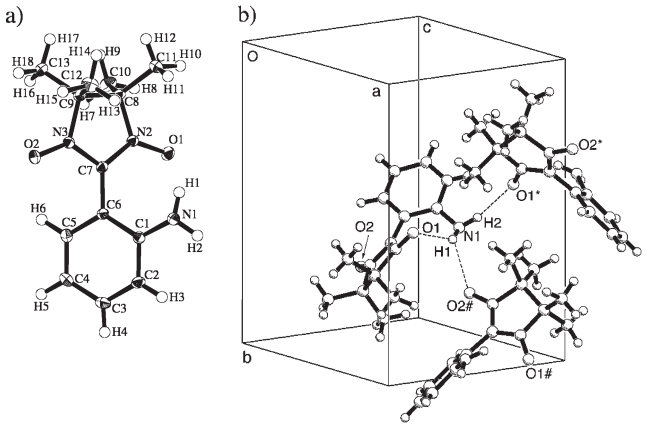

Figure 1. (a) Ortep drawing of *o*-APNN with thermal ellipsoids at the 50% level. The size of hydrogen atoms is arbitrary. (b) Molecular arrangement in the crystal of *o*-APNN. Hydrogen bonds are denoted with dotted lines. Symmetry operation codes for # and * are $1/2 + x$, $1/2 - y$, $2 - z$ and $1/2 - x$, $-y$, $1/2 + z$, respectively.

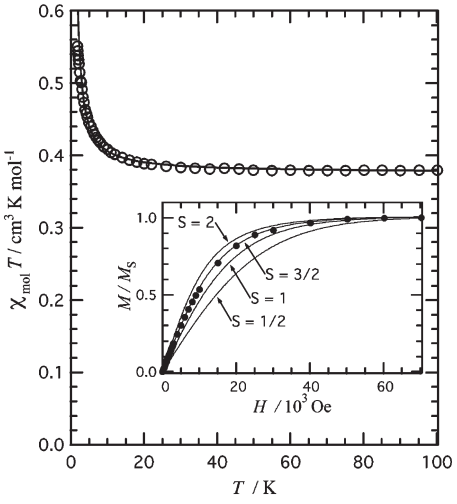

Figure 2. Temperature dependence of $\chi_{mol}T$ and $\chi_{mol}{}^{-1}$ for *o*-APNN. The solid line represents the Curie-Weiss analysis. Inset shows the *M*-*H* curve measured at 1.8 K. The solid lines correspond to the Brillouin functions of $S = 1/2 - 2$.

larization scheme through the hydrogen bonds described as $O_{NN}(\uparrow)\cdots H(\downarrow)\cdots O_{NN}(\uparrow)$.[4] Furthermore, the solid-state ^1H and ^2H NMR results on **3** revealed the negative spin density on the hydroxyl hydrogen atom.[8] In the present study, although we have no experimental evidence of the spin density on the amino hydrogen atoms, we can propose that H1 is negatively spin polarized in the same way as **2**, and that the intermolecular ferromagnetic interaction can be explained as $O1(\uparrow)\cdots H1(\downarrow)\cdots O2^{\#}(\uparrow)$ owing to the O–H bonding nature. Intramolecular spin polarization also gives negative spin density on H1 and H2, assuming that the nitrogen in *o*-APNN works similarly to the oxygen in **3**.[8] Thus, the hydrogen bonds between $O1\cdots O1^*$ and $O2^{\#}\cdots O1^*$ through the amino group can promote ferromagnetic exchange interactions. However, their interactions may be weaker than that of $O1\cdots H1\cdots O2^{\#}$ because of the longer distances. The present discussion does not exclude other possible ferromagnetic exchange pathways such as the β-hydrogen mechanism.[2b]

In summary, we have synthesized *o*-APNN as an NN-substituted aniline for the first time and constructed the three-dimensional hydrogen bond network due to the branching character of $-NH_2$, where the hydrogen bonds provide ferromagnetic exchange pathways. The *ortho* position has a geometrical advantage for the hydrogen bonds, and this work may afford a clue to crystal and molecular designs for organic ferromagnetic crystals.

References and Notes

1 M. C. Etter, *Acc. Chem. Res.*, **23**, 120 (1990); J.-M. Lehn, M. Mascal, A. DeCian, and J. Fischer, *J. Chem. Soc., Perkin Trans. 2*, **1992**, 461; G. R. Desiraju, *Acc. Chem. Res.*, **35**, 565 (2002).

2 a) G. Maruta, S. Takeda, R. Imachi, T. Ishida, T. Nogami, and K. Yamaguchi, *J. Am. Chem. Soc.*, **121**, 424 (1999). b) T. Nogami, T. Ishida, M. Yasui, F. Iwasaki, N. Takeda, M. Ishikawa, T. Kawakami, and K. Yamaguchi, *Bull. Chem. Soc. Jpn.*, **69**, 1841 (1996). c) N. Yoshioka, M. Irisawa, Y. Mochizuki, T. Kato, H. Inoue, and S. Ohba, *Chem. Lett.*, **1997**, 251. d) D. Papoutsakis, J. P. Kirby, J. E. Jackson, and D. G. Nocera, *Chem.—Eur. J.*, **5**, 1474 (1999). e) Y. Pontillon, T. Akita, A. Grand, K. Kobayashi, E. Lelievre-Berna, J. Pecaut, E. Ressouche, and J. Schweizer, *J. Am. Chem. Soc.*, **121**, 10126 (1999). f) J. R. Ferrer, P. M. Lahti, C. George, P. Oliete, M. Julier, and F. Palacio, *Chem. Mater.*, **13**, 2447 (2001).

3 E. Hernandez, M. Mas, M. E. Molis, C. Rovira, and J. Veciana, *Angew. Chem., Int. Ed. Engl.*, **32**, 882 (1993).

4 T. Sugawara, M. M. Matsushita, A. Izuoka, N. Wada, N. Takeda, and M. Ishikawa, *J. Chem. Soc., Chem. Commun.*, **1994**, 1723; M. M. Matsushita, A. Izuoka, T. Sugawara, T. Kobayashi, N. Wada, N. Takeda, and M. Ishikawa, *J. Am. Chem. Soc.*, **119**, 4369 (1997).

5 J. Cirujeda, M. Mas, E. Molins, F. L. Panthou, J. Laugier, J. G. Park, C. Paulsen, P. Rey, C. Rovira, and J. Veciana, *J. Chem. Soc., Chem. Commun.*, **1995**, 709.

6 J. L. Garcia-Munoz, J. Cirujeda, J. Veciana, and S. F. J. Cox, *Chem. Phys. Lett.*, **293**, 160 (1998).

7 J. Cirujeda, L. E. Ochando, J. M. Amigo, C. Rovira, J. Rius, and J. Veciana, *Angew. Chem., Int. Ed. Engl.*, **34**, 55 (1995).

8 H. Heise, F. H. Kölen, F. Mota, J. J. Novoa, and J. Veciana, *J. Am. Chem. Soc.*, **121**, 9659 (1999).

9 E. F. Ullman, J. H. Osiecki, and R. Darcy, *J. Am. Chem. Soc.*, **94**, 7049 (1972).

10 L. A. Bigelow and H. Eatough, *Org. Synth.*, Coll. Vol. **I**, 80 (1941).

11 O. Shimomura, K. Abe, and M. Hirota, *J. Chem. Soc., Parkin Trans. 2*, **1988**, 795.

12 Crystallographic data for *o*-APNN: $C_{13}H_{18}N_3O_2$, orthorhombic, $P2_12_12_1$, $a = 10.7178(4)$, $b = 12.9588(4)$, $c = 9.0698(4)$ Å, $V = 1259.7(1)$ Å^3, $Z = 4$, $D_{calcd} = 1.309\,g\,cm^{-3}$, $\mu(Mo\,K\alpha) = 0.09\,mm^{-1}$, $R = 0.042$ ($I > 2.0\sigma(I)$), $R_w = 0.104$ (all data) for 2107 unique reflections. All of the hydrogen atoms could be found in difference Fourier maps, and their coordinates and isotropic temperature factors were included in the refinement.

13 The symmetry operation code of ‡ is $1/2 - x$, $-y$, $-1/2 + z$.

Published on the web (Advance View) May 27, 2003; DOI 10.1246/cl.2003.544

Available online at www.sciencedirect.com
SCIENCE DIRECT®
Inorganic Chemistry Communications 6 (2003) 1122–1125
INORGANIC CHEMISTRY COMMUNICATIONS
www.elsevier.com/locate/inoche

Metamagnetic behavior of $[Ni(4ImNNH)_2(NO_3)_2]$ having a ground high-spin state (4ImNNH = 4-imidazolyl nitronyl nitroxide)

Chigusa Aoki, Takayuki Ishida *, Takashi Nogami

Department of Applied Physics and Chemistry, The University of Electro-Communications, Chofugaoka 1-5-1, Chofu, Tokyo 182-8585, Japan

Received 10 May 2003; accepted 28 May 2003
Published online: 5 July 2003

Abstract

A new chelating radical ligand 4ImNNH (2-(4-imidazolyl)-4,4,5,5-tetramethylimidazolin-1-yloxyl 3-oxide) was prepared, and complexation with nickel(II) nitrate gave $[Ni(4ImNNH)_2(NO_3)_2]$ as a discrete mononuclear complex. Magnetic measurements revealed that $[Ni(4ImNNH)_2(NO_3)_2]$ had a ground high-spin state ($S_{total} = 2$) and exhibited metamagnetic behavior below 3.4 K.

Keywords: Nickel(II); Free radical; Ferromagnetic interaction; Hydrogen bond

1. Introduction

The nitronyl nitroxide (NN) family has been widely utilized in constructing ferri- and ferromagnetic networks with dimensionality because of their bidentate nature suitable for bridge formation [1]. In addition, intermolecular ferromagnetic couplings are often observed in NN radical crystals [2], and it holds also for the metal–radical materials possessing the NN group as a peripheral substituent [3]. Rey and co-workers [4] exploited the imidazolate anion having the NN group at the 2-position, i.e., 2ImNN, and reported that the two-dimensional networking solids containing 2ImNN showed bulk ferrimagnetic behavior. We designed a new radical ligand, 4ImNNH (4-imidazolyl nitronyl nitroxide) and found that $[Ni(4ImNNH)_2(NO_3)_2]$ (**1**) showed both intra- and intermolecular ferromagnetic interactions and underwent a magnetic phase transition in spite of a mononuclear form.

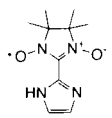

2ImNNH

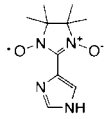

4ImNNH

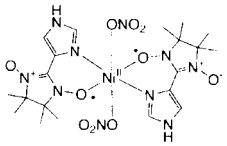

1

2. Experimental

2.1. Materials

The 4ImNNH ligand was prepared according to Ullman's method [5] by using 4-formylimidazole as a starting material. An ethanol solution (2.5 ml) of $Ni(NO_3)_2 \cdot 6H_2O$ (30.2 mg; 0.104 mmol) and 4ImNNH (44.8 mg; 0.201 mmol) was allowed to stand in a refrigerator for a week. The resultant black polycrystals of **1** were collected on a filter and washed with a small amount of water, which are suitable for X-ray crystal structure and magnetic studies. The yield of **1** was 59.7 mg (94%). The elemental analysis (C, H, N) of **1** on a Fisons EA-1108 by a usual combustion method supported the formula of $C_{20}H_{30}N_{10}NiO_{10}$.

2.2. Instruments

X-ray diffraction data of **1** were collected on a Rigaku R-axis RAPID diffractometer with graphite monochro-

* Corresponding author. Tel.: +81424435490; fax: +81424435501.
E-mail address: ishi@pc.uec.ac.jp (T. Ishida).

1387-7003/$ - see front matter © 2003 Elsevier Science B.V. All rights reserved.
doi:10.1016/S1387-7003(03)00204-1

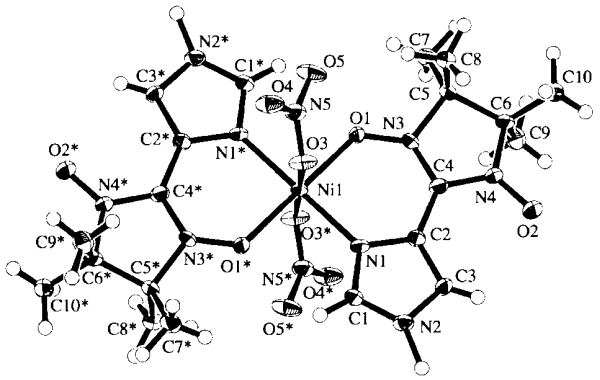

Fig. 1. Ortep drawing of the molecular structure of $[Ni(4ImNNH)_2(NO_3)_2]$ (**1**) at the 50% probability level. Atomic numbering is also shown. The symmetry operation code for * is $1-x$, $1-y$, $1-z$.

mated Mo Kα radiation ($\lambda = 0.71069$ A) at 100 K. Selected crystallographic data for **1**: $C_{20}H_{30}N_{10}NiO_{10}$, monoclinic $P2_1/a$, $a = 13.3490(9)$, $b = 10.9253(7)$, $c = 13.297(1)$ A, $\beta = 43.384(2)°$, $V = 1332.1(2)$ A^3, $Z = 2$, $d_{calc} = 1.569$ g cm $^{-3}$, μ(Mo Kα) = 0.802 mm $^{-1}$, $R(F) = 0.062(I > 2.0\sigma(I))$, $R_w(F^2) = 0.165$ (all data) for 2815 unique reflections.

Magnetic properties of **1** were measured on a Quantum Design MPMS SQUID magnetometer equipped with a 7 T coil in a temperature range 1.8–300 K. The magnetic responses were corrected with diamagnetic blank data of the sample holder obtained separately. The diamagnetic contribution of the sample itself was estimated from Pascal's constants.

3. Results

Fig. 1 shows the molecular structure of **1**. A half of molecule is crystallographically independent; the octahedral Ni ion resides at an inversion center. The Ni ion is coordinated by two NN oxygen atoms and two imidazole nitrogen atoms from the equatorial positions. The axial positions are occupied by nitrate oxygen atoms with a slight elongation of ca. 0.1 A. The six-membered chelate rings are highly planar as indicated by the Ni1–O1–N3–C4 torsion angle of 6.3(4)°, which seems the most important for intramolecular magnetic coupling. The crystallographic analysis on the Cu^{II} analogue ($[Cu(4ImNNH)_2(NO_3)_2]$) showed a more distorted structure of six-membered chelate rings (15.6(4)° for the Cu1–O1–N3–C4 torsion angle) [6].

Intermolecular hydrogen bonds are found in the crystal of **1**. Fig. 2 shows the molecular arrangement of **1**. The N–H group in the imidazole ring plays a key role; this H atom is located considerably close to nitrate O atoms in a neighboring molecule with the O3···H3# and O4···H3# distances of 2.15(9) and 1.67(8) A. A very short C–H···O contact is also found between H1 and O2# (2.36(4) A), which is shorter than the sum of the van der Waals radii (2.7 A). There are two strands, H-donor/acceptor and H-acceptor/donor combinations, in each neighboring pair. This geometry successively repeats along the $a + b$ and $a - b$ directions, and accordingly they form a two-dimensional H-bonding network parallel to the ab plane. Interatomic Ni···Ni distances are 7.27 and 8.62 A within a sheet and 11.05 A between the sheets.

Fig. 3 shows the temperature dependence of the $\chi_{mol}T$ value for **1** measured at 5 kOe. The $\chi_{mol}T$ value increases

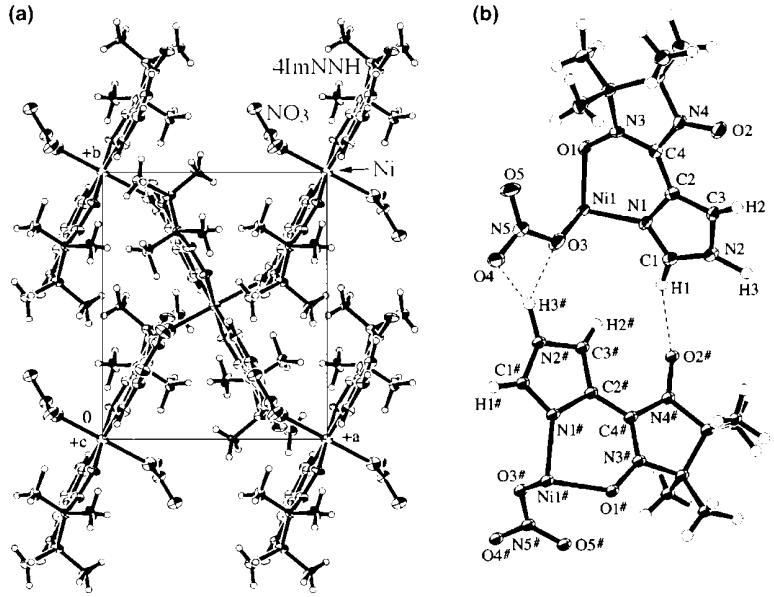

Fig. 2. (a) Molecular arrangement in the crystal of $[Ni(4ImNNH)_2(NO_3)_2]$ (**1**) viewed along the c-axis. (b) Nearest neighboring half molecules of **1**. Intermolecular hydrogen bonds are shown with dotted lines. The symmetry operation code for # is $3/2 - x$, $y - 1/2$, $-z + 1$.

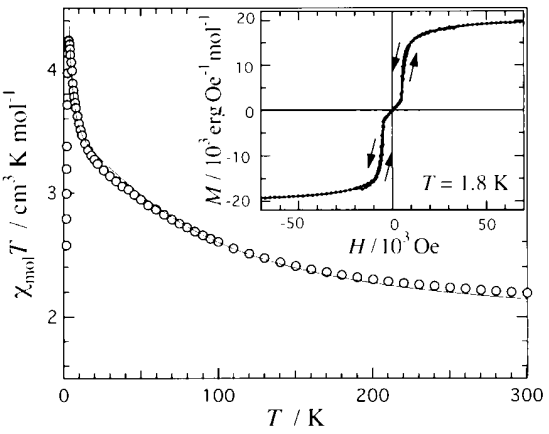

Fig. 3. Temperature dependence of $\chi_{mol}T$ for $[Ni(4ImNNH)_2(NO_3)_2]$ (1) measured at 5 kOe. A solid line represents the calculated curve. For details, see the text. Inset shows the M–H curve of 1 measured at 1.8 K.

with decreasing temperature. The observed $\chi_{mol}T$ value around a bend at 14 K is 3.3 cm^3 K mol^{-1}, which is slightly larger than the spin-only value 3.0 cm^3 K mol^{-1} for $S_{total} = 2$. A sharp increase below 14 K is due to intermolecular ferromagnetic interaction. Therefore, both intra- and intermolecular magnetic couplings are ferromagnetic. The molecular structures of 1 is regarded as a linear radical–metal–radical triad system, and the $\chi_{mol}T$ values are quantitatively analyzed according to the spin Hamiltonian $H = -2J(S_{NN1} \cdot S_{Ni} + S_{Ni} \cdot S_{NN2})$ based on the molecular symmetry. The van Vleck treatment gave the following expression, where a Weiss temperature is introduced for intermolecular magnetic interaction.

$$\chi_{mol} = \frac{2N_A g^2 \mu_B}{k(T-\theta)} \times \frac{\exp(-2J/kT) + 1 + 5\exp(2J/kT)}{\exp(-4J/kT) + 3\exp(-2J/kT) + 3 + 5\exp(2J/kT)}.$$

The optimized parameters are: $g = 2.06(1)$, $2J/k_B = +85(3)$ K and $\theta = +1.04(3)$ K. The calculated curves are superposed on the data points in Fig. 3. The fitting is satisfactory above 4 K, and the spin–spin coupling model is reliable. An abrupt drop was observed at 4 K, suggesting that magnetic phase transition takes place near the peaking temperature.

In order to elucidate the magnetic ground state of 1, we measured the M–H curve at 1.8 K. As the inset of Fig. 3 shows, the ground state is antiferromagnetic and a metamagnetic transition occurs near 0.55 T with a very small hysteresis during the metamagnetic transition. Metamagnetism implies the simultaneous presence of ferro- and antiferromagnetic interactions. The saturation magnetization was ca. 2.0×10^4 erg Oe^{-1} mol^{-1} at 7 T, being in good agreement with the ground $S_{total} = 2$ species where all spins are ferromagnetically correlated. The transition temperature (T_N) was determined to be 3.4 K from a sharp peak in the field-cooled magnetization measurements at 5 Oe.

4. Discussion

Antiferromagnetic interactions in Ni^{II}–radical systems were usually obtained from six-membered chelate rings using the 2-pyridyl NN ligand for example [7], because of a severe non-planar distortion to lose the orthogonality between the magnetic Ni dσ and NN π^* orbitals. Actually ferromagnetic interactions were observed only in a few Ni^{II} and Cu^{II} complexes having five-membered chelate rings [8]. In contrast to the literature results, 1 having six-membered chelate rings showed intramolecular ferromagnetic interaction. As the X-ray diffraction study of 1 reveals, the chelate ring is highly planar, owing to the advantage of the imidazole ring used. Namely, the angles of C4–C2–N1 and C2–N1–Ni1 are larger than those in the pyridine analogues [7,9] so that the bent chelate structure is spread to recover a plane. Preliminary results on the magnetic properties of $[Cu(4ImNNH)_2(NO_3)_2]$ revealed that the intramolecular couplings were antiferromagnetic [6], probably because of the non-planar distortion in the chelate rings.

As the X-ray crystallographic analysis revealed, the H-bond contacts are found in two directions, $a + b$ and $a - b$, forming a two-dimensional network due to the symmetry (Fig. 2). In the NN···imidazole contact, the spin-polarization mechanism may be operative. A superexchange-like interaction through Ni(1)–imidazole···NN should also be taken into account. The magnetic interaction through the nitrate···imidazole contact seems to be small, because the contacting atoms carry only polarized spin densities. The temperature dependence of χ_{mol} for 1 reveals two main ferromagnetic exchange couplings ascribable to intra- and intermolecular interactions. The metamagnetic behavior indicates that there is a secondary weak intermolecular interaction which is antiferromagnetic, while the major intermolecular interaction is ferromagnetic. Since the ground antiferromagnetic structure can be described as inter-sheet antiferromagnetic coupling among ferromagnetically correlated sheets, the H-bonding two-dimensional network is assumed to be ferromagnetic. The present complex may afford a clue to molecular and crystal designs for hydrogen bonded solids showing ferromagnetic interaction.

Acknowledgements

This work was supported by a Grant-in-Aid for Scientific Research on Priority Areas of "Molecular

Conductors and Magnets" (No. 730/11224204) and by a Grant-in-Aid for Scientific Research (No. 13640575), both from the Ministry of Education, Culture, Sports, Science and Technology, Japan.

References

[1] A. Caneschi, D. Gatteschi, P. Rey, R. Sessoli, Acc. Chem. Res. 22 (1989) 392.

[2] M. Kinoshita, P. Turek, M. Tamura, Y. Nozawa, D. Shiomi, Y. Nakazawa, M. Ishikawa, M. Takahashi, K. Awaga, T. Inabe, Y. Maruyama, Chem. Lett. (1991) 1225;
T. Sugawara, M.M. Matsushita, A. Izuoka, N. Wada, N. Takeda, M. Ishikawa, J. Chem. Soc. Chem. Commun. (1994) 1723.

[3] J. Omata, T. Ishida, D. Hashizume, F. Iwasaki, T. Nogami, Inorg. Chem. 40 (2001) 3954;
J. Omata, T. Ishida, D. Hashizume, F. Iwasaki, T. Nogami, Mol. Cryst. Liq. Cryst. 376 (2002) 455.

[4] K. Fegy, D. Luneau, T. Ohm, C. Paulsen, P. Rey, Angew. Chem. Int. Ed. Engl. 37 (1998) 1270;
K. Fegy, N. Sanz, D. Luneau, E. Belorizky, P. Rey, Inorg. Chem. 37 (1998) 4518;
K. Fegy, D. Luneau, E. Belorizky, M. Novac, J.-L. Tholence, C. Paulsen, T. Ohm, P. Rey, Inorg. Chem. 37 (1998) 4524.

[5] E.F. Ullman, J.H. Osiecki, D.G.B. Boocock, R. Darcy, J. Am. Chem. Soc. 94 (1972) 7049.

[6] C. Aoki, T. Ishida, T. Nogami, in preparation.

[7] C. Benelli, A. Dei, D. Gatteschi, L. Pardi, Inorg. Chem. 27 (1988) 2831;
N. Yoshioka, M. Irisawa, M. Abe, T. Aoki, N. Aizawa, H. Inoue, Mol. Cryst. Liq. Cryst. 306 (1997) 397.

[8] D. Luneau, P. Rey, J. Laugier, P. Fries, A. Caneschi, D. Gatteschi, R. Sessoli, J. Am. Chem. Soc. 113 (1991) 1245;
D. Luneau, P. Rey, J. Laugier, E. Belorizky, A. Conge, Inorg. Chem. 31 (1992) 3578;
Y. Yamamoto, T. Suzuki, S. Kaizaki, J. Chem. Soc. Dalton Trans. (2001) 2943.

[9] G.R. Lewis, A.J. Blake, Acta Crystallogr. C 58 (2002) m398.

Available online at www.sciencedirect.com
SCIENCE DIRECT®
Chemical Physics Letters 378 (2003) 337–342
CHEMICAL PHYSICS LETTERS
www.elsevier.com/locate/cplett

Rectangular tetragadolinium complex ion with a ground $S = 27/2$ state containing bis(dimethylglyoximato)copper(II) as a ferrimagnetic exchange coupler

Yasuko Kobayashi, Sohei Ueki, Takayuki Ishida *, Takashi Nogami

Department of Applied Physics and Chemistry, The University of Electro-Communications, Chofu, Tokyo 182-8585, Japan

Received 4 July 2003; in final form 12 July 2003
Published online: 26 August 2003

Abstract

Pentanuclear $[Cu(dmg)_2\{Gd(hfac)_2\}_4(AcO)_4](Ph_4P)_2$ (**1**) (dmg = dimethylglyoximate dianion; hfac = 1,1,1,5,5,5-hexafluoropentane-2,4-dionate) containing a central copper(II) and four peripheral gadolinium(III) ions was prepared and the crystal structure was determined by X-ray diffraction. Magnetic measurements on **1** revealed high ground spin multiplicity, as expected regardless of the sign of magnetic Cu···Gd coupling through N–O bridges. The ground state was suggested to be $S_{total} = 27/2$ with the exchange parameter $2J/k_B = -2.9(2)$ K between the Gd and Cu ions. The antiferromagnetic coupling is operative owing to the largely distorted Gd–O–N–Cu bridges.

1. Introduction

Discrete oligonuclear complexes with bridging ligands are of increasing interest for development of molecule-based magnets since single-molecule magnets [1,2] were discovered in μ-oxometallates [3] and μ-cyanometallates [4]. However, no chemical modification of the bridges has yet been made on oxo- and cyano-bridges. To exploit adjustable and short brigding ligands, we planned to utilize oximate coordination compounds to template synthesis of oligonuclear complexes, where the N–O groups can bridge in heterometallic systems [5]. Recently, single-chain magnets have been developed in manganese(III)–nickel(II) coordination polymers using the N–O bridge of pyridine-2-aldoximate [6]. We applied bis(dimethylglyoximato)metal(II) ($[M^{II}(Hdmg)_2]$) to preparation of d–f bimetallic ferro- or ferrimagnetic materials (see Scheme 1).

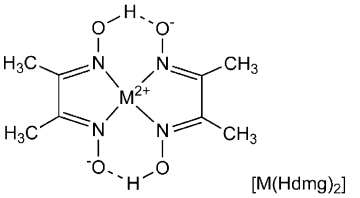

Scheme 1.

* Corresponding author. Fax: +81-424-43-5501.
E-mail address: ishi@pc.uec.ac.jp (T. Ishida).

0009-2614/$ - see front matter © 2003 Elsevier B.V. All rights reserved.
doi:10.1016/S0009-2614(03)01323-X

2. Experimental

After deprotonation of $[Cu(Hdmg)_2]$ in basic media, the resultant anionic oxygen atoms were planned to be trapped with lanthanide hexafluoroacetylacetonate, $Ln(hfac)_3$ [7]. The following procedure was typical. $[Cu(Hdmg)_2]$ (22.1 mg; 0.075 mmol) was dissolved in ethanol (1.25 ml) containing KOH (8.4 mg; 0.15 mmol), and it was combined with an ethanolic solution (1 ml) containing $Gd(OAc)_3 \cdot 4H_2O$ (41.1 mg; 0.1 mmol) and $Gd(hfac)_3 \cdot 2H_2O$ (163.4 mg; 0.2 mmol) at room temperature. After tetraphenylphosphonium chloride (57.1 mg; 0.15 mmol) in ethanol (0.5 ml) was added to the above mixture, slight colorless impurities were removed by filtration. Reddish brown plates of $[Cu(dmg)_2\{Gd(hfac)_2\}_4(AcO)_4](Ph_4P)_2$ (**1**), precipitated from the clear filtrate at room temperature for one day, were suitable for X-ray and magnetic studies. The yield was 49%. An elemental analysis supported the chemical formula and deprotonation of Hdmg was confirmed by means of detailed IR spectroscopic analysis; no absorption band due to OH group was found in comparison with the spectra of $[Cu(Hdmg)_2]$-derived compounds [5,8–10].

Similar synthetic procedures using Nd and La salts as starting materials in place of the Gd salts gave $[Cu(dmg)_2\{Ln(hfac)_2\}_4(AcO)_4](Ph_4P)_2$ (Ln = Nd (**2**), La (**3**)). Water was used as a solvent for $La(OAc)_3 \cdot 1.5H_2O$ because of its low solubility in ethanol. The IR spectra of **2** and **3** were practically identical with that of **1**.

Diffraction data of single crystals of **1** and **2** were collected on a Rigaku R-axis RAPID diffractometer with graphite monochromated MoKα radiation ($k = 0.71069$ Å) at 100 K. The structures were solved by direct methods and expanded using Fourier techniques in the teXsan program package [11]. Numerical absorption correction was used. The thermal displacement parameters were refined anisotropically for non-hydrogen atoms and isotropically for hydrogen atoms. Full-matrix least-squares methods were applied using all of the unique reflection data. Selected crystallographic data are: **1**: $C_{104}H_{72}CuF_{48}Gd_4N_4O_{28}P_2$, $M = 3492.14$, monoclinic, $P2_1/n$, $a = 19.2094(6)$, $b = 14.1094(4)$, $c = 22.7613(8)$ Å, $b = 100.766(1)°$, $V = 6060.5(3)$ Å^3, $Z = 2$, $d_{calc} = 1.914$ g cm^{-3}, $l = 2.51$ mm^{-1}, $R(I > 2r(I)) = 0.053$, R_w (all data) = 0.168 for 14054 unique reflections ($2h_{max} = 56.6°$). **2**: $C_{104}H_{72}CuF_{48}N_4Nd_4O_{28}P_2$, $M = 3440.10$, monoclinic, $P2_1/n$, $a = 19.2669(8)$, $b = 14.1111(8)$, $c = 22.691(1)$ Å, $b = 101.227(2)°$, $V = 6051.0(5)$Å^3, $Z = 2$, $d_{calc} = 1.888$ g cm^{-3}, $l = 2.03$ mm^{-1}, $R(I > 2r(I)) = 0.059$, R_w (all data) = 0.177 for 12286 unique reflections ($2h_{max} = 53.0°$). CCDC reference numbers are 205989 and 205990 for **1** and **2**, respectively.

Dc magnetic susceptibilities of randomly oriented polycrystalline samples of **1–3** were measured on a Quantum Design MPMS SQUID magnetometer equipped with a 7 T coil in a temperature range 1.8–300 K. The magnetic responses were corrected with diamagnetic blank data of the sample holder measured separately. The diamagnetic contribution of the sample itself was estimated from Pascal's constants.

ESR spectra of **1** were recorded on a Bruker ESP300E X-band (9.7 GHz) spectrometer. The spectrum of **1** exhibited a broad single transition line at $g = 2.03$ with a peak-to-peak line width of 1400 G.

3. Results and discussion

The single-crystal X-ray diffraction analysis revealed that **1** and **2** were isomorphous. Fig. 1 shows the structure of $[Cu(dmg)_2\{Gd(hfac)_2\}_4(AcO)_4]^{2-}$. The central copper ion resides at the crystallographic inversion center. There are two crystallographically independent $Gd(hfac)_2$ groups: one is octa- and the other nona-coordinate. Owing to the symmetry the five metal ions are located on one plane. The peripheral Gd ions form an almost rectangular array, and the basal plane of the central Cu ion is strictly perpendicular to the rectangle. Each oximato oxygen atom is nearly planar trivalent and reasonably assigned to be monoanionic, which is supported by the IR analysis, and accordingly the nominal charges of Cu and Gd are concluded to be 2+ and 3+, respectively.

The $[Cu(dmg)_2]^{2-}$ ion is surrounded by four $Gd(hfac)_2^+$ ions with the oximato NO^- groups,

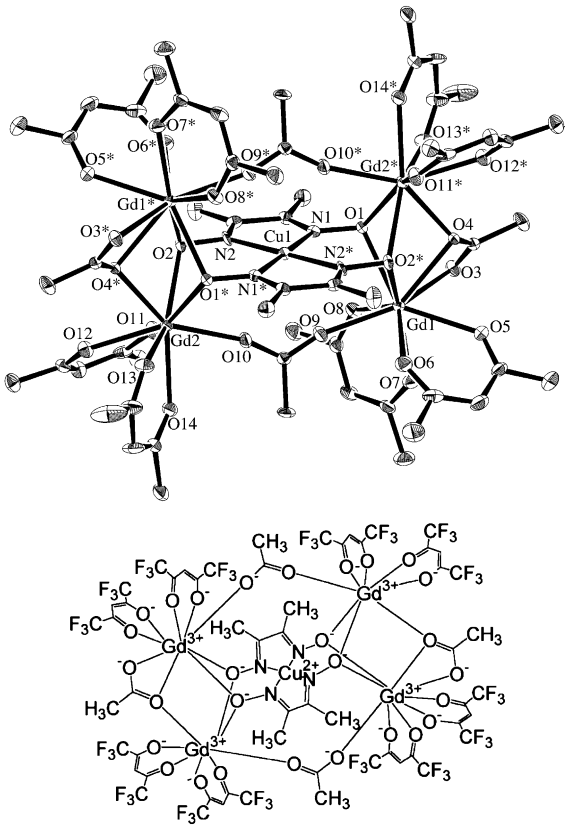

Fig. 1. An ORTEP drawing of the $[Cu(dmg)_2\{Gd(hfac)_2\}_4(AcO)_4]^{2-}$ moiety in the crystal of **1** with the thermal ellipsoids at the 50 % level (top). The H and F atoms are omitted for clarity. The symmetry operation code for * is $-x, 1-y, 1-z$.

which may afford magnetic exchange pathways. The Gd1–O1, Gd1–O2*, Gd2–O1*, and Gd2–O2 distances are 2.453(4), 2.468(4), 2.406(3), and 2.406(4) Å, respectively. Other Gd–O distances are ranged from 2.31 to 2.49 Å. The interatomic Cu1···Gd1 and ···Gd2 distances are 3.8183(3) and 3.8538(2) Å, respectively. For the shorter edge of the rectangular Gd array, the oximato oxygen atoms doubly bridge two Gd ions, and they show a butterfly-like structure in the Gd_2O_2 moiety. An acetate oxygen atom also bridges Gd1 and Gd2* ions. The interatomic Gd1···Gd2* distance is 3.7138(3) Å. For the longer edge, an acetate anion bridges Gd1 and Gd2 in a μ-1,3 manner. The Gd1···Gd2 distance is 6.7135(4) Å.

The ground spin quantum number may be large regardless of the sign of magnetic coupling between the Cu^{II} and Gd^{III} ions, assuming that the Cu···Gd couplings are dominant compared with the Gd···Gd couplings. Actually, magnetic measurements on the polycrystalline sample of **1** at 500 Oe showed that the $\nu_{mol}T$ product increased at lower temperature (Fig. 2). This finding indicates the presence of ferro- or ferrimagnetic coupling which can be attributed to intramolecular interaction because the bulky hfac ligands and Ph_4P^+ ions separate the Gd_4Cu_1 cores.

Since the angular momentum contribution of Gd^{III} ($S_{Gd} = 7/2$) and Cu^{II} ($S_{Cu} = 1/2$) ions is negligible, the theoretical high-temperature limit of the spin-only $\nu_{mol}T$ value should be 31.9 cm^3 K mol^{-1}. The experimental value at 100 K, 30.5 cm^3 K mol^{-1}, is slightly smaller than this theoretical value. Unfortunately, we could not reach the $\nu_{mol}T$ plateau defined by the ground spin state by lowering temperature, but we can estimate the ground state of **1** as follows from the experimental $\nu_{mol}T$ value of 81.3 cm^3 K mol^{-1} at 1.8 K. The $\nu_{mol}T$

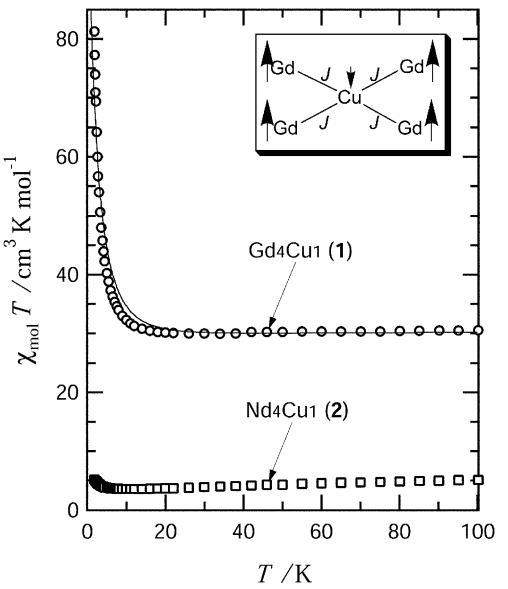

Fig. 2. Temperature dependence of $\nu_{mol}T$ for $[Cu(dmg)_2\{Ln(hfac)_2\}_4(AcO)_4](Ph_4P)_2$ (Ln = Gd (**1**) and Nd (**2**)). The solid line represents a theoretical fit. See text for the equation and parameters. The inset shows the exchange coupling model for the Gd_4Cu_1 core.

value for $S_{total} = 22/2$ expected from ferromagnetically correlated three Gd^{III} and one Cu^{II} ions should be 66.0 cm^3 K mol^{-1} and the experimental value much exceeds the calculated one, indicating that more than three Gd ions are ferromagnetically correlated. Taking the molecular symmetry into consideration, we can safely assume that all of the Gd spins are aligned parallel. A very slight decrease in the $v_{mol}T$ value of **1** can be found on cooling from 100 to about 20 K, suggesting that ferrimagnetic coupling takes place in **1**. Thus, the Cu spin is assumed to be aligned antiparallel with respect to the four Gd spins at the ground state. The data above 40 K were analyzed with the Curie–Weiss equation $[v_{mol} = C/(T - h)]$, giving $C = 30.77(3)$ cm^3 K mol^{-1} and $h = -0.9(1)$ K. The apparent negative h implies antiferromagnetic coupling, and a more quantitative analysis of the exchange parameter (J) will be discussed below.

There have been many reports on ferromagnetic couplings between Gd^{III} and Cu^{II} spins [12–15], and we have to pay attention in particular to oximato-bridged Gd^{III} and Cu^{II} systems showing ferro- and antiferromagnetic interactions depending on the coordination geometry [16,17]. Costes et al. [16,17] have proposed that bent structures in the Gd–O–N–Cu bridges favor antiferromagnetic interaction. In the present complex, antiferromagnetic coupling may occur owing to the largely distorted Gd–O–N–Cu bridges as indicated by the torsion angles: 58.8(3),)54.5(4), 51.7(4), and)54.7(4)° for Gd1–O1–N1–Cu1, Gd1–O2*–N2*–Cu1, Gd2*–O1–N1–Cu1, and Gd2*–O2*–N2*–Cu1, respectively. Interactions across the acetate bridges between Gd···Gd seem to be small, and even through efficient monoatomic bridges couplings between Gd ions are reported to be as small as $2J/k_B = -0.06$ K [18,19] and)0.3 K [20]. An exceptionally ferromagnetic example was recently reported for oxo-bridged Gd···Gd interactions but the magnetic coupling is also weak ($2J/k_B = +0.052$ K) [21]. To simplify a model, interactions between Gd ions are neglected and all of the Gd···Cu relations are assumed to be uniform (the inset of Fig. 2). The susceptibility data were analyzed according to the Heisenberg spin Hamiltonian $H = -2J(S_1 \cdot S_2 + S_1 \cdot S_3 + S_1 \cdot S_4 + S_1 \cdot S_5)$, where suffix 1 denotes Cu spin and suffixes 2–5 denote Gd spins. We obtained the following expression of the molar magnetic susceptibility:

$$v_{mol} = p\frac{Ng^2b^2}{3k_BT}\frac{A}{B}, \quad (1)$$

where A and B are functions of J/k_B (see Appendix A).

The X-band ESR spectrum on the randomly oriented polycrystalline sample of **1** showed a single signal centered at $g = 2.03$ at room temperature. The observed g value is rationalized by the average from the g values of copper(II) and gadolinium(III) ions. We fixed the g value at 2.03 and introduced a purity factor (p) into Eq. (1). The best fit gave $2J/k_B = -2.9(2)$ K and $p = 0.93(2)$. The calculated curve is superimposed in Fig. 2. Another solution with $2J/k_B = +2.4(2)$ K (ferromagnetic) and $p = 0.86(3)$ gave an inferior fit, indicating that the antiferromagnetic coupling is more likely.

The magnetization curve measured at 1.8 K (Fig. 3) showed paramagnetic behavior and the experimental data largely exceed the calculated value based on a case with non-interacting four $S = 7/2$ and one $S = 1/2$ spins. The apparent spin quantum number was ≈10 and the data points are located below the theoretical $S_{total} = 27/2$ line. As

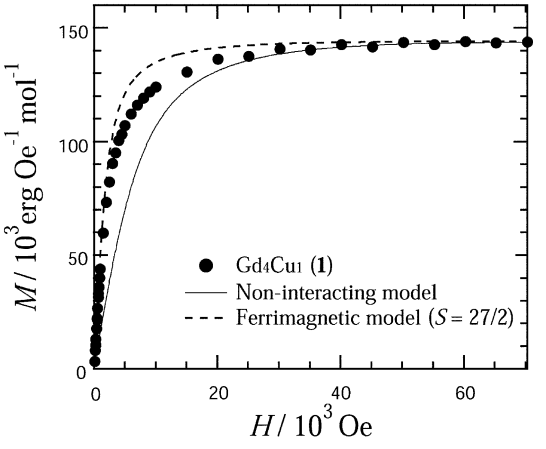

Fig. 3. The M–H curve measured at 1.8 K for **1**. The solid line represents a case with non-interacting four $S = 7/2$ and one $S = 1/2$ spins. The dotted line is a Brillouin function of $S_{total} = 27/2$.

the $v_{mol}T$ vs T plot (Fig. 2) shows, the magnetization at 1.8 K contains contributions from thermally populated spin states above the ground state, and the experimental data seem to fall between the theoretical value of the ground state and the non-interacting limit. The saturated magnetization at 7 T was 1.44×10^4 erg Oe^{-1} mol^{-1}, which corresponds to 94% of the calculated value, 1.53×10^4 erg Oe^{-1} mol^{-1} with $S_{total} = 27/2$ and $g = 2.03$. This percentage agrees with the results of the $v_{mol}T$ vs T plot, supporting the conclusion of the ferrimagnetic coupling in the Gd_4Cu_1 system.

The temperature dependence of $v_{mol}T$ for **2** (Fig. 2) shows that the $v_{mol}T$ value gradually decreases with decreasing temperature, reaches a minimum 3.57 cm^3 K mol^{-1} around 9 K, and turns to increase rapidly to 5.25 cm^3 K mol^{-1} at 1.8 K. The final increase may be attributed to the ferrimagnetic coupling between Nd^{III} and Cu^{II} spins. The experimental $v_{mol}T$ value at 300 K, 6.70 cm^3 K mol^{-1}, agreed with the calculated value of 6.92 cm^3 K mol^{-1} for non-interacting four Nd^{III} and one Cu^{II} ions. The magnetic measurements on **3** revealed that only one $S_{Cu} = 1/2$ spin was present without any appreciable interaction ($v_{mol}T = 0.401$ cm^3 K mol^{-1} at 1.8 K), being consistent with the valences of the La^{III} and Cu^{II} ions.

4. Summary

We have reported the structural and magnetic characterization of **1** and related compounds. The bis(dimethylglyoximato)copper(II) dianion works not only as a template in synthesis but also as an exchange coupler in magnetic interaction. The ground S_{total} number is considerably large because of the components appropriately chosen; the copper(II) and gadolinium(III) ions carry the smallest and largest spins, respectively, among the available d and f metal ions. Although ferromagnetic couplings between copper(II) and gadolinium(III) ions have often been observed and reported [12–15], the present complex has antiferromagnetic coupling, affording the ferrimagnetic ground state of $S_{total} = 27/2$. The rectangular configuration of four gadolinium or other lanthanide ions can be regarded as a novel building block for molecule-based magnetic materials.

Acknowledgements

The authors thank Dr. Masafumi Tamura (RIKEN) for valuable comments on magnetic properties of lanthanide ions. This work has been supported by a Grant-in-Aid for Scientific Research (No. 13640575) from the Ministry of Education, Culture, Sports, Science and Technology, Japan.

Appendix A

Assuming that the spin–spin exchange coupling model can be drawn as the inset of Fig. 2, we obtained the Heisenberg spin Hamiltonian $H = -2J(S_1 \cdot S_2 + S_1 \cdot S_3 + S_1 \cdot S_4 + S_1 \cdot S_5)$ and the following expression of the molar magnetic susceptibility, by application of Kambe's vector coupling method [22] and the van Vleck equation:

$$v_{mol} = \frac{Ng^2b^2}{3k_BT}\frac{A}{B}$$

with

$$\begin{aligned} A = \frac{1}{4}\Bigg\{ & 26970 + 21924\exp\left(-\frac{29J}{k_BT}\right) \\ & + 65772\exp\left(-\frac{J}{k_BT}\right) + 52650\exp\left(-\frac{28J}{k_BT}\right) \\ & + 105300\exp\left(-\frac{2J}{k_BT}\right) + 82800\exp\left(-\frac{27J}{k_BT}\right) \\ & + 138000\exp\left(-\frac{3J}{k_BT}\right) + 106260\exp\left(-\frac{26J}{k_BT}\right) \\ & + 159390\exp\left(-\frac{4J}{k_BT}\right) + 119700\exp\left(-\frac{25J}{k_BT}\right) \\ & + 167580\exp\left(-\frac{5J}{k_BT}\right) + 122094\exp\left(-\frac{24J}{k_BT}\right) \\ & + 162792\exp\left(-\frac{6J}{k_BT}\right) + 114240\exp\left(-\frac{23J}{k_BT}\right) \\ & + 146880\exp\left(-\frac{7J}{k_BT}\right) + 98280\exp\left(-\frac{22J}{k_BT}\right) \end{aligned}$$

$$+ 111930\exp\left(-\frac{8J}{k_BT}\right) + 70356\exp\left(-\frac{21J}{k_BT}\right) + 73788\exp\left(-\frac{9J}{k_BT}\right) + 42570\exp\left(-\frac{20J}{k_BT}\right) + 41580\exp\left(-\frac{10J}{k_BT}\right) + 21168\exp\left(-\frac{19J}{k_BT}\right) + 19152\exp\left(-\frac{11J}{k_BT}\right) + 7980\exp\left(-\frac{18J}{k_BT}\right) + 6510\exp\left(-\frac{12J}{k_BT}\right) + 1860\exp\left(-\frac{17J}{k_BT}\right) + 1260\exp\left(-\frac{13J}{k_BT}\right) + 126\exp\left(-\frac{16J}{k_BT}\right) + 48\exp\left(-\frac{14J}{k_BT}\right)\Bigg\}$$

and

$$B = 30 + 28\exp\left(-\frac{29J}{k_BT}\right) + 84\exp\left(-\frac{J}{k_BT}\right) + 78\exp\left(-\frac{28J}{k_BT}\right) + 156\exp\left(-\frac{2J}{k_BT}\right) + 144\exp\left(-\frac{27J}{k_BT}\right) + 240\exp\left(-\frac{3J}{k_BT}\right) + 220\exp\left(-\frac{26J}{k_BT}\right) + 330\exp\left(-\frac{4J}{k_BT}\right) + 300\exp\left(-\frac{25J}{k_BT}\right) + 420\exp\left(-\frac{5J}{k_BT}\right) + 378\exp\left(-\frac{24J}{k_BT}\right) + 504\exp\left(-\frac{6J}{k_BT}\right) + 448\exp\left(-\frac{23J}{k_BT}\right) + 576\exp\left(-\frac{7J}{k_BT}\right) + 504\exp\left(-\frac{22J}{k_BT}\right) + 574\exp\left(-\frac{8J}{k_BT}\right) + 492\exp\left(-\frac{21J}{k_BT}\right) + 516\exp\left(-\frac{9J}{k_BT}\right) + 430\exp\left(-\frac{20J}{k_BT}\right) + 420\exp\left(-\frac{10J}{k_BT}\right) + 336\exp\left(-\frac{19J}{k_BT}\right) + 304\exp\left(-\frac{11J}{k_BT}\right) + 228\exp\left(-\frac{18J}{k_BT}\right) + 186\exp\left(-\frac{12J}{k_BT}\right) + 124\exp\left(-\frac{17J}{k_BT}\right) + 84\exp\left(-\frac{13J}{k_BT}\right) + 42\exp\left(-\frac{16J}{k_BT}\right) + 16\exp\left(-\frac{14J}{k_BT}\right).$$

References

[1] D. Gatteschi, A. Caneschi, L. Pardi, R. Sessoli, Science 265 (1994) 1054.
[2] G. Christou, D. Gatteschi, D.N. Hendrickson, R. Sessoli, MRS Bull. 25 (2000) 66.
[3] J. Yoo, E.K. Brechin, A. Yamaguchi, M. Nakano, J.C. Huffman, A.L. Maniero, L.C. Brunel, K. Awaga, H. Ishimoto, G. Christou, D.N. Hendrickson, Inorg. Chem. 39 (2000) 3615.
[4] J.J. Sokol, A.G. Hee, J.R. Long, J. Am. Chem. Soc. 124 (2002) 7656.
[5] F. Lloret, R. Ruiz, B. Cervera, I. Castro, M. Julve, J. Faus, J.A. Real, F. Sapiña, Y. Journaux, J.C. Colin, M. Verdaguer, J. Chem. Soc., Chem. Commun. (1994) 2615.
[6] R. Clérac, H. Miyasaka, M. Yamashita, C. Coulon, J. Am. Chem. Soc. 124 (2002) 12837.
[7] M.F. Richardson, W.F. Wagner, D.E. Sands, J. Inorg. Nucl. Chem. 30 (1968) 1275.
[8] R. Ruiz, J. Sanz, B. Cervera, F. Lloret, M. Julve, C. Bois, J. Faus, M.C. Muñoz, J. Chem. Soc., Dalton Trans. (1993) 1623.
[9] A.G. Sharpe, D.B. Wakefield, J. Chem. Soc. (1957) 281.
[10] F. Lloret, R. Ruiz, M. Julve, J. Faus, Y. Journaux, I. Castro, M. Verdaguer, Chem. Mater. 4 (1992) 1150.
[11] TeXsan, Single Crystal Structure Analysis Software, ver. 1.10, Molecular Structure Corp., The Woodlands, TX, USA and Rigaku Co. Ltd., Tokyo, Japan, 1999.
[12] A. Bencini, C. Benelli, A. Caneschi, R.L. Carlin, A. Dei, D. Gatteschi, J. Am. Chem. Soc. 107 (1985) 8128.
[13] N. Matsumoto, M. Sakamoto, H. Tamaki, H. Okawa, S. Kida, Chem. Lett. (1990) 853.
[14] A.J. Blake, P.E.Y. Milne, P. Thornton, R.E.P. Winpenny, Angew. Chem. Int. Ed. Engl. 30 (1991) 1139.
[15] O. Guillow, P. Bergerat, O. Kahn, E. Bakalbassis, K. Boubekeur, P. Batail, M. Guillot, Inorg. Chem. 31 (1992) 110.
[16] J.-P. Costes, F. Dahan, A. Dupuis, J.-P. Laurent, Inorg. Chem. 39 (2000) 169.
[17] J.-P. Costes, F. Dahan, A. Dupuis, Inorg. Chem. 39 (2000) 5994.
[18] S. Liu, L. Gelmini, S.J. Rettig, R.C. Thompson, C. Orvig, J. Am. Chem. Soc. 114 (1992) 6081.
[19] J.-P. Costes, F. Dahan, A. Dupuis, S. Lagrave, J.-P. Laurent, Inorg. Chem. 37 (1998) 153.
[20] J.-P. Costes, F. Dahan, F. Nicodème, Inorg. Chem. 40 (2001) 5285.
[21] J.-P. Costes, J.-M.C. Juan, F. Dahan, F. Nicodème, J. Chem. Soc., Dalton Trans. (2003) 1272.
[22] K. Kambe, J. Phys. Soc. Jpn. 5 (1950) 48.

Inorg. Chem. **2003**, *42*, 6106–6113

Ferro- and Ferrimagnetic Chains of hin-Bridged Copper(II) and Manganese(II) and hnn-Bridged Manganese(II) Complexes (hin = 4,4,5,5-Tetramethylimidazolin-1-oxyl; hnn = 4,4,5,5-Tetramethylimidazolin-1-oxyl 3-Oxide)

Tomoaki Ise,[†] Takayuki Ishida,* Daisuke Hashizume,[‡] Fujiko Iwasaki, and Takashi Nogami

Department of Applied Physics and Chemistry, The University of Electro-Communications, Chofu, Tokyo 182-8585, Japan

Received April 14, 2003

We have exploited potential utility of 4,4,5,5-tetramethylimidazolin-1-oxyl (hin) and 4,4,5,5-tetramethylimidazolin-1-oxyl 3-oxide (hnn) as μ-1,4 and μ-1,5 bridging ligands, respectively, carrying an unpaired electron in development of metal–radical hybrid magnets. X-ray diffraction measurements of $[Cu(hfac)_2hin]$ (**1**), $[Mn(hfac)_2hin]$ (**2**), and $[Mn(hfac)_2hnn]$ (**3**) revealed one-dimensional metal–radical alternating chain structures, where hfac denotes 1,1,1,5,5,5-hexafluoropentane-2,4-dionate. Magnetic measurements of **1** indicate the presence of intrachain ferromagnetic coupling between copper and radical spins. The magnetic exchange parameter was estimated as $2J/k = 56.8$ K based on an $S = {}^1/_2$ equally spaced ferromagnetic chain model ($H = -2J\sum S_i \cdot S_{i+1}$). This ferromagnetic interaction can be explained in terms of the axial coordination of the hin nitrogen or oxygen to Cu^{II}. The $\chi_m T$ value of **2** and **3** increased on cooling, and the magnetic data could be analyzed by Seiden's ferrimagnetic chain model, giving $2J/k = -325$ and -740 K, respectively. The antiferromagnetic interaction of **2** and **3** can be attributed to orbital overlap between the manganese and the oxygen or nitrogen magnetic orbitals. The exchange interactions between Cu–hin and Mn–hnn are larger than those of typical Cu– and Mn–nitronyl nitroxide complexes, indicating that the choice of small ligands is a promising strategy to bestow strong exchange interaction. Compound **3** became a ferrimagnet below 4.4 K, owing to ferromagnetic coupling among the ferrimagnetic chains.

Introduction

The design and synthesis of molecule-based magnetic materials is one of the major subjects of materials science. There have been ample examples of alternating one-dimensional complexes containing nitronyl nitroxide radicals (Chart 1) and metal hfac salts[1] in pursuit of metal−radical hybrid magnets (hfac denotes 1,1,1,5,5,5-hexafluoropentane-2,4-dionate). The ferro- and ferrimagnetic couplings within the chain structure have been well characterized, depending on the symmetry of d-magnetic orbitals on the metal ions and also on the mutual geometry of the ligating oxygen atoms and metal ions (equatorial/axial positions of the metal ions, trans/cis zigzag structures of the chains, etc.). The imino nitroxide radicals are also well-known[2] and the imino nitrogen atom is potentially available for coordination to metal ions.[3] However, there has been no report on one- or higher-dimensional complexes containing imino nitroxide bridges.

Chart 1. Structural Formulas

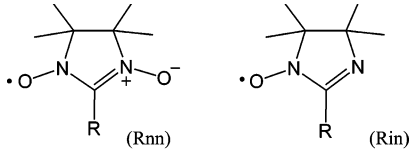

nitronyl nitroxide imino nitroxide

* Corresponding author. Phone: +81-424-43-5490. Fax: +81-424-43-5501. E-mail address: ishi@pc.uec.ac.jp.

[†] Present address: Department of Materials Science, Graduate School of Science, Osaka City University, Sumiyoshi-ku, Osaka 558-8585, Japan.

[‡] Present address: Molecular Characterization Division, The Institute of Physical and Chemical Research (RIKEN), Hirosawa, Wako 351-0198, Japan.

(1) Caneschi, A.; Gatteschi, D.; R. Sessoli, R. *Acc. Chem. Res.* **1989**, *22*, 392. Caneschi, A.; Gatteschi, D.; Rey, P. *Prog. Inorg. Chem.* **1991**, *39*, 33. Caneschi, A.; Gatteschi, D.; Renard, J. P.; Rey, P.; Sessoli, R. *Inorg. Chem.* **1989**, *28*, 1976. Caneschi, A.; Gatteschi, D.; Renard, J. P.; Rey, P.; Sessoli, R. *J. Am. Chem. Soc.* **1989**, *111*, 785.

(2) Ullman, E. F.; Call, L.; Osiecki, J. H. *J. Org. Chem.* **1970**, *35*, 3623.

10.1021/ic034392x CCC: $25.00
Published on Web 08/23/2003

We assume that the choice of small ligands and anions is crucial in order to bestow strong exchange interaction on magnetic materials. Furthermore, imino nitroxides can serve as a μ-1,4 bridge, which is shorter than nitronyl nitroxides widely used as a μ-1,5 bridge. We chose 4,4,5,5-tetramethylimidazolin-1-oxyl (hin) and 4,4,5,5-tetramethylimidazolin-1-oxyl 3-oxide (hnn) (R = H in Chart 1) as the smallest ligands in the imino and nitronyl nitroxide families.[2] Although the isolation of hin was claimed to be difficult because of its instability,[2] complexation affords a chance to purify and characterize hin compounds. Actually, $[CdCl_2(hin)_4]$ was characterized as the first hin complex.[4] We also reported two mononuclear complexes, $[M(hfac)_2(hin)_2]$ (M = Cu, Mn),[5] in which the imino nitrogen atom is coordinated to the metal ion, whereas the nitroxide oxygen atom remains uncoordinated. We report here the crystal structure and magnetic properties of $[M(hfac)_2hin]$ (M = Cu (**1**), Mn(**2**)) and $[Mn(hfac)_2hnn]$ (**3**) as one-dimensional complexes. These hin compounds are the first examples which possess ferro- or ferrimagnetic infinite chain structures containing imino nitroxide bridges.

Experimental Section

Materials. 4,4,5,5-Tetramethylimidazolin-1-oxyl (hin) was prepared according to the literature method[2] with a slight modification.[5]

$[Cu(hfac)_2hin]$ (1). After the solutions of hin (100 mg, 0.71 mmol) in dry ether (3 mL) and of dehydrated $Cu(hfac)_2$ (1.0 g, 2.1 mmol) in dry ether (3 mL) were mixed, the combined solution was allowed to stand in a cool and dark place for 1 day, and dark-brown crystals of **1** were precipitated. $[Mn(hfac)_2hin]$ (**2**) was synthesized in a similar manner. Unfortunately, **2** was obtained only as a fine polycrystalline form. When the molar ratio of starting materials was 1/1, we obtained only mononuclear complexes $[M(hfac)_2(hin)_2]$.[5]

$[Mn(hfac)_2hnn]$ (3). Solutions of dehydrated $Mn(hfac)_2$ (300 mg, 0.64 mmol) in a mixed solvent of dry *n*-heptane (70 mL) and ether (5 mL) and of hnn (100 mg, 0.64 mmol) in dry CH_2Cl_2 (10 mL) were combined, then the solution was allowed to stand in a cool and dark place for 1 day, and dark-purple crystals of $[Mn(hfac)_2hnn]$ were precipitated.

Elemental analysis (C, H, N) of these complexes on a Fisons EA-1108 by a usual combustion method revealed that the metal/radical ratios were 1/1 for **1**−**3**. Anal. Calcd for $C_{17}H_{15}N_2O_5F_{12}Cu_1$ (**1**): C, 32.99; H, 2.44; N, 4.53. Found: C, 32.37; H, 1.87; N, 4.62. Calcd for $C_{17}H_{15}N_2O_5F_{12}Mn_1$ (**2**): C, 33.46; H, 2.48; N, 4.59. Found: C, 33.61; H, 2.55; N, 4.09. Calcd for $C_{17}H_{15}N_2O_6F_{12}Mn_1$ (**3**): C, 32.64; H, 2.41; N, 4.47. Found: C, 31.98; H, 2.78; N, 4.69.

X-ray Crystallographic Analysis. Single-crystal diffraction data of **1** and **3** were collected on a Rigaku Raxis-Rapid diffractometer with graphite-monochromated Mo Kα radiation at 93 and 100 K, respectively. Numerical absorption correction was used. Full-matrix least-squares methods were applied using all of the unique diffraction data. The structure of **1** was solved by a direct method (SIR97[6]) and refined by a full-matrix least-squares method with the SHELXL97[7] program. Anisotropic temperature factors were applied for non-hydrogen atoms except for C6 and C7. Since C6 and C7 are very close to symmetry relatives in a disordered model, application of anisotropic temperature factors for the atoms brings about large parameter interaction and leads to unrealistic structures. Hydrogen atoms were refined by use of the riding model. The structure of **3** was directly solved by a heavy-atom Patterson method in the teXsan program package.[8] The thermal displacement parameters of all non-hydrogen atoms were refined anisotropically, and those of hydrogen atoms were done isotropically. A conformationally disordered model for the C34 trifluoromethyl group was applied to improve the refinement, and the optimized occupancy ratio was 0.68/0.32. Selected crystallographic data of **1** and **3** are listed in Table 1.[9]

Table 1. Selected X-ray Crystallographic Data of $[Cu(hfac)_2hin]$ (**1**) and $[Mn(hfac)_2hnn]$ (**3**)

compound	$[Cu(hfac)_2hin]$ (**1**)	$[Mn(hfac)_2hnn]$ (**3**)
formula	$C_{17}H_{15}N_2O_5F_{12}Cu_1$	$C_{17}H_{15}N_2O_6F_{12}Mn_1$
fw	618.84	626.23
crystal system	orthorhombic	monoclinic
space group	*Pbcn*	$P2_1/a$
a/Å	16.859(1)	17.8592(9)
b/Å	10.835(6)	12.4360(5)
c/Å	12.830(1)	21.702(1)
β/deg	90	103.486(1)
V/Å^3	2343.7(3)	4687.1(4)
Z	4	8
D_{calc}/g cm^{-3}	1.75	1.77
T/K	93	100
$R(I > 2\sigma(I))^a$	0.046	0.068
R_w (all data)^b	0.108	0.200

^{a} $R = \sum(||F_o| - |F_c||)/\sum|F_o|$. ^{b} $R_w = [\sum w(|F_o| - |F_c|)^2/\sum w|F_c|^2]^{1/2}$.

Magnetic measurements. Magnetic properties of polycrystalline specimens were measured on a Quantum Design MPMS SQUID magnetometer equipped with a 7 T coil in a temperature range down to 1.8 K. The magnetic responses were corrected with diamagnetic blank data of the sample holder obtained separately. The diamagnetic contribution of the sample itself was estimated from Pascal's constants. Ac magnetic susceptibility was measured on a Quantum Design PPMS ac/dc magnetometer in a temperature range down to 2.0 K.

Results

Crystal Structures. Figure 1a shows a repeating unit of **1**, and a half of the unit is crystallographically independent. The hin ligand lies close to the 2-fold axis at (0, y, $^1/_4$) and displays a 2-fold disorder about that axis. One of the disordered parts having a Cu−N2 bond is omitted in Figure 1a, but Cu−O3 and Cu−N2 bonds are completely disordered with the 50% occupancy each at every Cu axial position. The Cu atom is located on a crystallographic inversion center

(3) Luneau, D.; Rey, P.; Laugier, J.; Fries, P.; Caneschi, A.; Gatteschi, D.; Sessoli, R. *J. Am. Chem. Soc.* **1991**, *113*, 1245. Oshio, H.; Watanabe, T.; Ohto, A.; Ito, T.; Masuda, H. *Inorg. Chem.* **1996**, *35*, 472. Cogne, A.; Laugier, J.; Luneau, D.; Rey, P. *Inorg. Chem.* **2000**, *39*, 5510. Yamamoto, Y.; Suzuki, T.; Kaizaki, S. *J. Chem. Soc., Dalton Trans.* **2001**, 2943. Tsukuda, T.; Suzuki, T.; Kaizaki, S. *J. Chem. Soc., Dalton Trans.* **2002**, 1721. Ichimura, T.; Doi, K.; Mitsuhashi, C.; Ishida, T.; Nogami, T. *Polyhydron* **2003**, *22*, 2557.

(4) Ise, T.; Ishida, T.; Nogami, T. *Mol. Cryst. Liq. Cryst.* **2002**, *379*, 147.

(5) Ise, T.; Ishida, T.; Nogami, T. *Bull. Chem. Soc. Jpn.* **2002**, *75*, 2468.

(6) Altomare, A.; Burla, M. C.; Camalli, M.; Cascarano, G.; Giacovazzo, C.; Guagliardi, A.; Moliterni, A. G. G.; Polidori, G.; Spagna, R. *J. Appl. Crystallogr.* **1999**, *32*, 115.

(7) Sheldrick, G. M. *SHELXL97*; University of Göttingen: Göttingen, Germany, 1997.

(8) *teXsan: crystal structure analysis package*; Molecular Structure Corp.: The Woodlands, TX, 1985, 1999.

(9) The structural parameters and magnetic exchange parameters of **1** and **2** in this article are more refined and accordingly more reliable than those preliminarily reported. Ise, T.; Ishida, T.; Nogami, T. *Synth. Met.* **2003**, *137*, 1281.

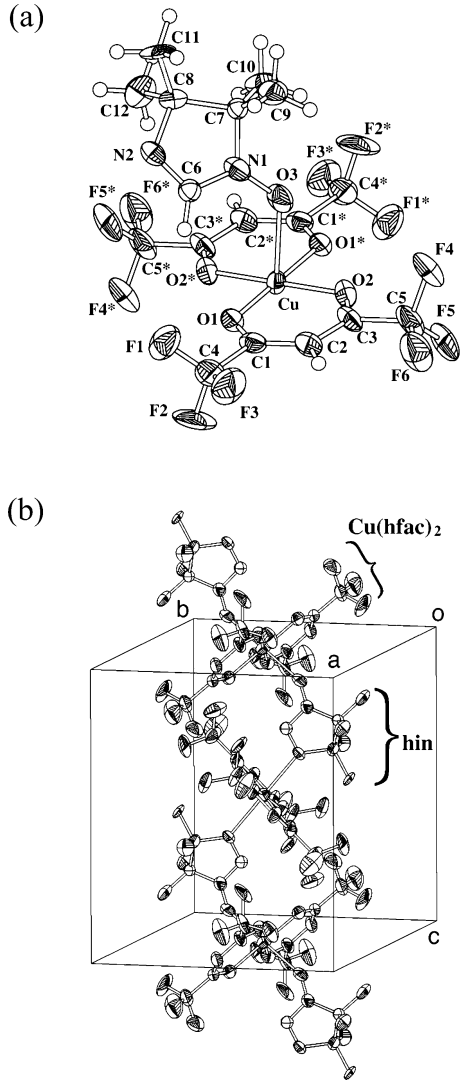

Figure 1. (a) ORTEP view of a repeating unit of [Cu(hfac)$_2$hin] (**1**) at the 50% probability level. Only one of two disordered hin configurations is shown. Symmetry operation code for asterisk (*) is $-x$, $-y$, $-z$. (b) Chain structure of **1**. Hydrogen atoms are omitted for the sake of clarity.

Table 2. Selected Bond Distances (Å) and Angles (deg) for [Cu(hfac)$_2$hin] (**1**)

Cu−O1	1.974(2)	Cu−O2	1.938(2)
Cu−O3	2.286(5)	Cu−N2	2.405(7)
C6−N1	1.371(7)	C6−N2	1.274(8)
N1−O3	1.280(7)		
O1−Cu−O2	92.07(9)	O1−Cu−O3	85.10(1)
O2−Cu−O3	98.48(1)	N1−O3−Cu	124.8(5)

at (0, 0, 0). Those symmetry operations generate a one-dimensional structure, in which the hin ligands bind the Cu atoms, and the resultant repeating motifs of hin−Cu(hfac)$_2$ are arranged in a trans zigzag manner as shown in Figure 1b.

Table 2 summarizes selected bond distances and angles for **1**. The octahedra of both copper centers are severely distorted with the axial Cu−O3 and Cu−N2 bonds much longer than the equatorial ones: 2.286(5) and 2.405(7) Å vs 1.974(2) and 1.938(2) Å. The bond length of Cu−O3 is slightly shorter than the typical distances of Cu−O in other nitronyl nitroxide radical complexes.[1] The hin plane is located

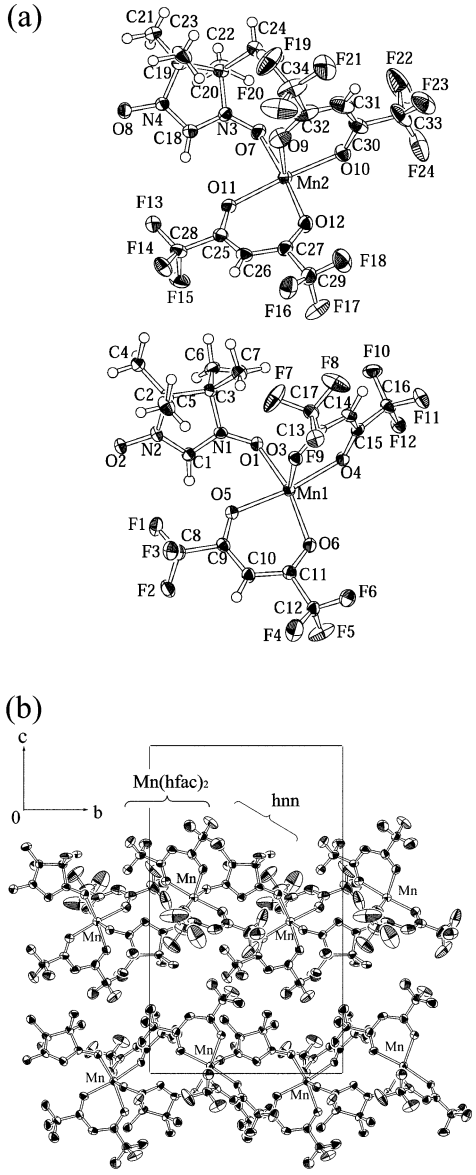

Figure 2. (a) ORTEP view of two independent repeating units of [Mn(hfac)$_2$hnn] (**3**) at the 50% probability level. Only major conformation is shown for a disordered trifluoromethyl group (C34F19F20F21). (b) Chain structures of **3**. Hydrogen atoms are omitted for the sake of clarity.

on a staggered position with respect to the equatorial Cu−O bonds, as indicated by the torsion angle O1−Cu−O3−N1 of 119.5°. The axial O3 and N2 atoms are deviated by only about 10° from the normal to the basal coordination plane. This geometry brings about almost orthogonal arrangement of the magnetic copper $3d_{x^2-y^2}$ orbital and the hin oxygen or nitrogen $2p_z$ orbital. The dihedral angle between two neighboring Cu basal planes is 88.2° in a chain.

Since **2** did not afford single crystals suitable for the X-ray crystal structure analysis, we can report only the cell constants of **2**. The *a*, *b*, and *c* lengths are 15.69(7), 11.65(4), and 13.6(2) Å, respectively, in an orthorhombic crystal system at 296 K. The same crystal system and similar *a*, *b*, and *c* lengths found in **1** and **2** strongly suggest that they are isomorphous.

Figure 2a shows the repeating units of **3**. There are two crystallographically independent hnn−Mn(hfac)$_2$ moieties in

Table 3. Selected Bond Distances (Å) and Angles (deg) for [Mn(hfac)$_2$hnn] (**3**)[a]

Mn1−O1	2.149(2)	Mn2−O7	2.145(3)
Mn1−O2#	2.149(3)	Mn2−O8§	2.142(3)
Mn1−O3	2.149(3)	Mn2−O9	2.147(4)
Mn1−O4	2.150(3)	Mn2−O10	2.122(3)
Mn1−O5	2.152(3)	Mn2−O11	2.151(3)
Mn1−O6	2.164(3)	Mn2−O12	2.163(3)
O1−Mn1−O2#	86.4(1)	O7−Mn2−O8§	87.9(1)
O1−Mn1−O3	95.1(1)	O7−Mn2−O9	87.3(1)
O1−Mn1−O4	88.03(9)	O7−Mn2−O10	93.5(1)
O1−Mn1−O5	85.25(9)	O7−Mn2−O11	91.0(1)
O1−Mn1−O6	165.8(1)	O7−Mn2−O12	173.1(1)
O2#−Mn1−O3	168.1(1)	O8§−Mn2−O9	170.1(1)
O2#−Mn1−O4	85.7(1)	O8§−Mn2−O10	87.8(1)
O2#−Mn1−O5	99.0(1)	O8§−Mn2−O11	91.6(1)
O2#−Mn1−O6	87.2(1)	O8§−Mn2−O12	95.5(1)
O3−Mn1−O4	82.6(1)	O9−Mn2−O10	83.9(1)
O3−Mn1−O5	92.9(1)	O9−Mn2−O11	97.1(1)
O3−Mn1−O6	93.8(1)	O9−Mn2−O12	90.2(1)
O4−Mn1−O5	171.5(1)	O10−Mn2−O11	175.4(1)
O4−Mn1−O6	104.09(9)	O10−Mn2−O12	92.4(1)
O5−Mn1−O6	83.28(9)	O11−Mn2−O12	83.2(1)

[a] Symmetry operation codes: #, $^3/_2 - x$, $-^1/_2 + y$, $1 - z$; §, $^3/_2 - x$, $-^1/_2 + y$, $2 - z$.

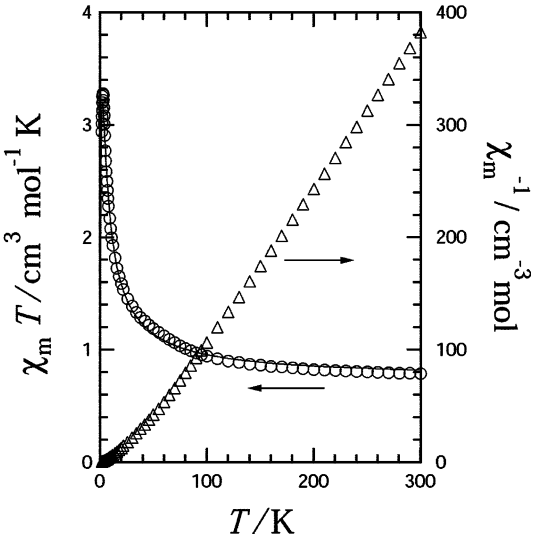

Figure 3. Temperature dependence of the product $\chi_m T$ (○) and χ_m^{-1} (△) measured at 5000 Oe for [Cu(hfac)$_2$hin] (**1**). A solid line represents the theoretical curve based on an $S = ^1/_2$ ferromagnetic chain model.

a unit cell of **3**, but they are practically identical. Each Mn^{II} ion is hexacoordinated by four oxygen atoms of two hfac molecules and by two oxygen atoms of two different hnn radicals. The bond lengths of Mn−O(hnn) are 2.149(2) and 2.149(3) Å for one motif and 2.145(3) and 2.142(3) Å for another. Since the octahedral Mn^{II} ion has a d-electron configuration of $(t_{2g})^3(e_g)^2$, orbital overlaps between the magnetic orbitals of Mn dπ and hnn π^* should be substantial, giving antiferromagnetic interaction. Table 3 summarizes selected bond distances and angles of **3**. Figure 2b shows the linear cis chains of **3**; two hnn oxygen atoms are coordinated in a cis configuration with the O(hnn)−Mn−O(hnn) angles of 86.4(1)° and 87.9(1)°. There are two independent chains running along the *b* axis, which are arrayed alternatively.

Magnetic Properties. The temperature dependence of $\chi_m T$ and χ_m^{-1} measured at 5000 Oe for **1** is shown in Figure 3.

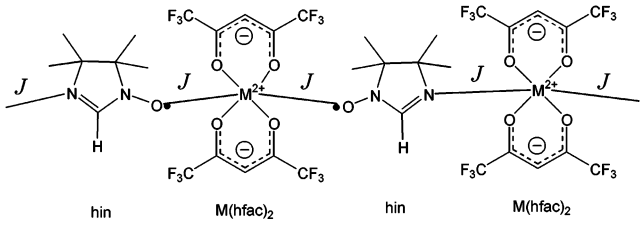

Figure 4. The schematic view of the chain structure of [M(hfac)$_2$hin]. The exchange interaction *J* is defined as an averaged value of M−O and M−N interactions.

The $\chi_m T$ value of **1** is 0.78 cm^3 mol^{-1} K at 300 K, which is slightly larger than the calculated value of 0.75 cm^3 mol^{-1} K for a noncoupled system ($g = 2.0$). A positive Weiss temperature was obtained for **1** from the Curie−Weiss equation $\chi = C/(T - \theta)$ with $C = 0.732$ cm^3 mol^{-1} K and $\theta = 21.9$ K. This finding implies that ferromagnetic interaction is dominant in **1**. Upon cooling, the $\chi_m T$ values increased to a maximum value of 3.28 cm^3 mol^{-1} K at 2.8 K and then decreased. The maximum value is much larger than those of $S = 1$ (1.0 cm^3 mol^{-1} K) due to an expected high-spin repeating unit for **1**, indicating that the ferromagnetic interaction is operative infinitely along the chain structure. The magnetic couplings through Cu−O and Cu−N bonds are expected to be different. However, because of the highly disordered hin orientations, the magnetic exchange coupling in **1** can be described with an averaged parameter *J* (Figure 4).

The experimental data were analyzed by using an $S = ^1/_2$ ferromagnetic chain model[10] (eq 1) for **1** with the Hamiltonian $H = -2J\sum S_i \cdot S_{i+1}$, where all symbols have their usual meaning.

$$\chi = \frac{Ng^2\mu_B{}^2}{4kT}\left[\frac{A}{B}\right]^{2/3} \tag{1}$$

where

$$A = 1.0 + 5.7979916y + 16.902653y^2 + 29.376885y^3 + 29.832959y^4 + 14.036918y^5$$

$$B = 1.0 + 2.7979916y + 7.0086780y^2 + 8.653644y^3 + 4.5743114y^4$$

and

$$y = J/2kT$$

A molecular field correction has been considered in the mean-field approximation with zj' as the magnetic interaction between chains.[11]

$$\chi_m = \frac{\chi}{1 - \chi(2zj'/Ng^2\mu_B{}^2)}$$

The following best fit parameters for **1** were obtained: $2J/k = +56.8$ K, $2zj'/k = -0.91$ K, and $g = 2.00$. The calculated

(10) Baker, G. A.; Rushbrooke, G. S. J.; Gillbert, H. E. *Phys. Rev.* **1964**, *135A*, 1272.
(11) Myers, B. E.; Berger, L.; Friedberg, S. A. *J. Appl. Phys.* **1968**, *40*, 1149.

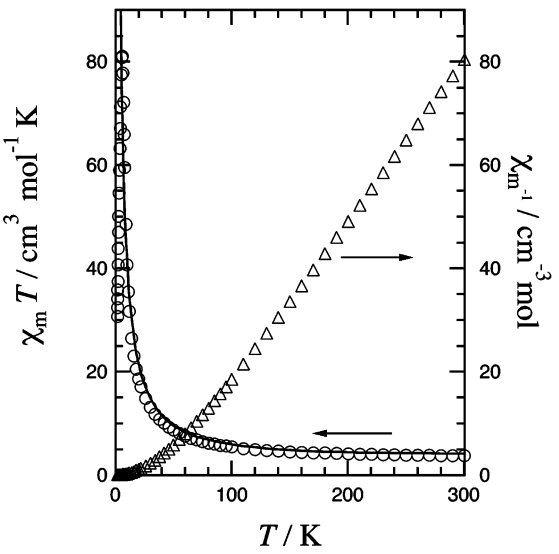

Figure 5. Temperature dependence of the product $\chi_m T$ (O) and χ_m^{-1} (△) measured at 500 Oe for [Mn(hfac)$_2$hin] (**2**). Solid line represents the theoretical curve based on the Seiden ferrimagnetic chain model.

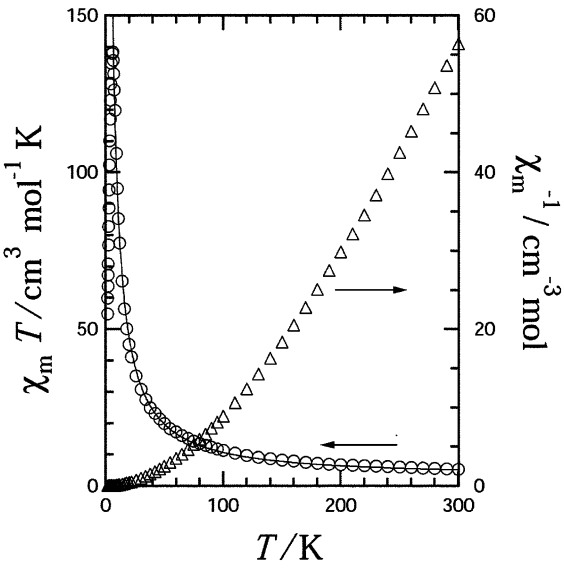

Figure 6. Temperature dependence of the product $\chi_m T$ (○) and χ_m^{-1} (△) measured at 500 Oe for [Mn(hfac)$_2$hnn] (**3**). Solid line represents the theoretical curve based on the Seiden ferrimagnetic chain model.

curve is superimposed in Figure 3. The final drop of the $\chi_m T$ value below 2.8 K is attributed also to a saturation effect of magnetization, and j' was somewhat overestimated. The $2J/k$ value for **1** is larger than that for [Cu(hfac)$_2$menn] (+36.9 K, menn = 2,4,4,5,5-pentamethylimidazoline-1-oxyl 3-oxide),[12] which shows ferromagnetic interaction between the Cu ion and radical spin. This result suggests that the hin ligands can be useful for achieving the strong exchange interaction.

The temperature dependences of $\chi_m T$ and χ_m^{-1} measured at 500 Oe for manganese(II) complexes **2** and **3** are shown in Figures 5 and 6, respectively. The $\chi_m T$ value of **2** at 300 K (3.73 cm^3 mol^{-1} K) is smaller than the calculated value of 4.75 cm^3 mol^{-1} K for a noncoupled system. This finding indicates that ferrimagnetic interaction is operative in **2**. On the other hand, the $\chi_m T$ value of **3** at 300 K (5.3 cm^3 mol^{-1} K) is larger than that of a noncoupled system. Only from this result we cannot tell whether the interaction of **3** is ferromagnetic or ferrimagnetic, but a quantitative analysis based on a ferromagnetic model gave unsatisfactory results. We assume that a broad minimum characteristic of ferrimagnetic systems appears at ca. 300 K for **2** and at a temperature much higher than 300 K for **3**.

Upon cooling, the $\chi_m T$ values increased to a maximum value 81.0 cm^3 mol^{-1} K at 6 K for **2** and 139 cm^3 mol^{-1} K at 6 K for **3** and then decreased. The maximum values are much larger than that of $S = 2$ (3.0 cm^3 mol^{-1} K) due to an antiferromagnetically correlated unit for **2** and **3**. This magnetic behavior indicates that ferrimagnetic interaction is operative infinitely along the chain structures. We analyzed the experimental data according to Seiden's ferrimagnetic chain model[13] (eq 2). Here, the definition of δ and Λ as a function of JS/kT is described in the literature.[13,14] In the case of **3**, an averaged parameter J is applied though there are two independent chains. The small letter s and capital letter S refer to the spin of $^1/_2$ (hin) and spin of $^5/_2$ (Mn^{II}), respectively. A purity factor α was introduced, and the g-value was fixed to be 2.00. The best fit parameter is $2J/k$ = −325 K for **2** and −740 K for **3**. The estimated purities are 90% for **2** and 100% for **3**, suggesting the presence of solvent or decomposed diamagnetic impurity in the specimen of **2**.

$$\chi_m = \alpha\frac{N\mu_B^2}{3kT}\left[g_s^2S^2\left(\frac{S+1}{S}+\frac{2\delta}{1-\delta}\right)-4g_Sg_s\Lambda sS\frac{1}{1-\delta}+ g_s^2\left(s(s+1)+2\Lambda^2s^2\frac{1}{1-\delta}\right)\right] \quad (2)$$

The $M-H$ curves of **1** and **2** measured at 1.8 K are shown in Figure 7. The saturation magnetizations of 11000 and 21000 erg Oe^{-1} mol^{-1} for **1** and **2**, respectively, correspond to the values of $S = 1$ and $S = 2$ with $g = 2$, supporting the presence of strong ferro- and antiferromagnetic couplings between metal and radical spins, respectively. Furthermore, the experimental data exceeded the theoretical Brillouin functions, and the ferro- and ferrimagnetic chain structures

(12) Caneschi, A.; Gatteschi, D.; Laugier, J.; Rey, P. *J. Am. Chem. Soc.* **1987**, *109*, 2191. Cabello, C. I.; Caneschi, A.; Carlin, R. L.; Gatteschi, D.; Rey, P.; Sessoli, R. *Inorg. Chem.* **1990**, *29*, 2582.

(13) Seiden, J. *J. Phys. (Paris) Lett.* **1983**, *44*, L947.

(14)
$$\gamma = -JS/2kT$$
$$a_0 = 4\left[\gamma^{-1}\sinh\gamma-\gamma^{-2}\cosh\gamma+\gamma^{-2}\right]$$
$$a_1 = 12\left[\left(\gamma^{-1}+12\gamma^{-3}\right)\sinh\gamma-\left(5\gamma^{-2}+12\gamma^{-4}\right)\cosh\gamma-\gamma^{-2}+12\gamma^{-4}\right]$$
$$b_0 = \gamma^{-1}\left(\cosh\gamma-1\right)$$
$$b_1 = 3\left[\left(\gamma^{-1}+4\gamma^{-3}\right)\cosh\gamma-4\gamma^{-2}\sinh\gamma+\gamma^{-1}-4\gamma^{-3}\right]$$
$$\delta = \frac{a_1}{3a_0},\quad \Lambda = 2\left[\frac{b_1}{3a_0}+\frac{b_0}{a_0}\right]$$

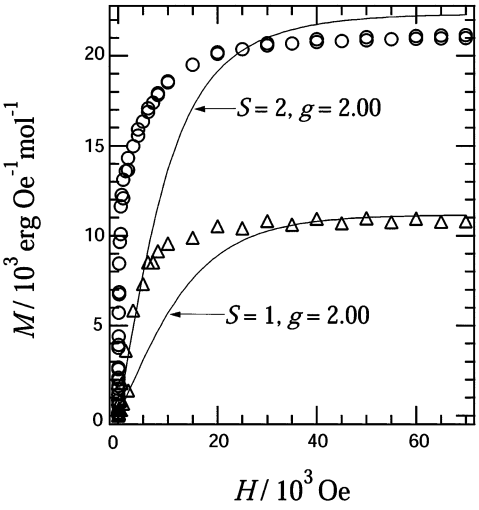

Figure 7. Field dependence of the magnetization of [Cu(hfac)$_2$hin] (**1**; △) and [Mn(hfac)$_2$hin] (**2**; ○) measured at 1.8 K. Solid lines correspond to the theoretical Brillouin functions of $S = 1$ and 2.

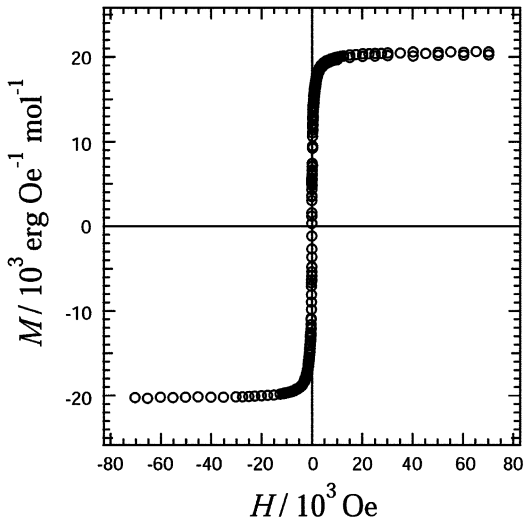

Figure 8. Field dependence of the magnetization of [Mn(hfac)$_2$hnn] (**3**) measured at 1.8 K.

are confirmed for **1** and **2**, respectively. In the case of **2**, the saturation magnetization is slightly smaller than the theoretical value of $S = 2$ and $g = 2$ (22300 erg Oe^{-1} mol^{-1}). The purity was estimated to be 94%, in accordance with the result of the temperature dependence of $\chi_m T$. No bulk magnetic ordering was observed down to 1.8 K. This paramagnetic behavior is rationalized by the one-dimensional character of **1** and **2**.

The $M-H$ curves of **3** measured at 1.8 K are shown in Figure 8. The saturation magnetizations of 21000 erg Oe^{-1} mol^{-1} correspond to the values of $S = 2$ with $g = 2.0$, supporting the antiferromagnetic couplings between Mn^{II} and radical spins like **2**. The magnetization curve of **3** measured at 1.8 K shows a very small hysteresis behavior with the coercive field of ca. 30 Oe. This finding indicates that bulk magnetic ordering took place above 1.8 K. In order to determine the magnetic phase transition temperature (T_N), we measured field-cooled magnetization, remnant magnetization, and zero-field-cooled magnetization for **3** (Figure 9a). The T_N was defined to be 4.4 K where the RM disappeared

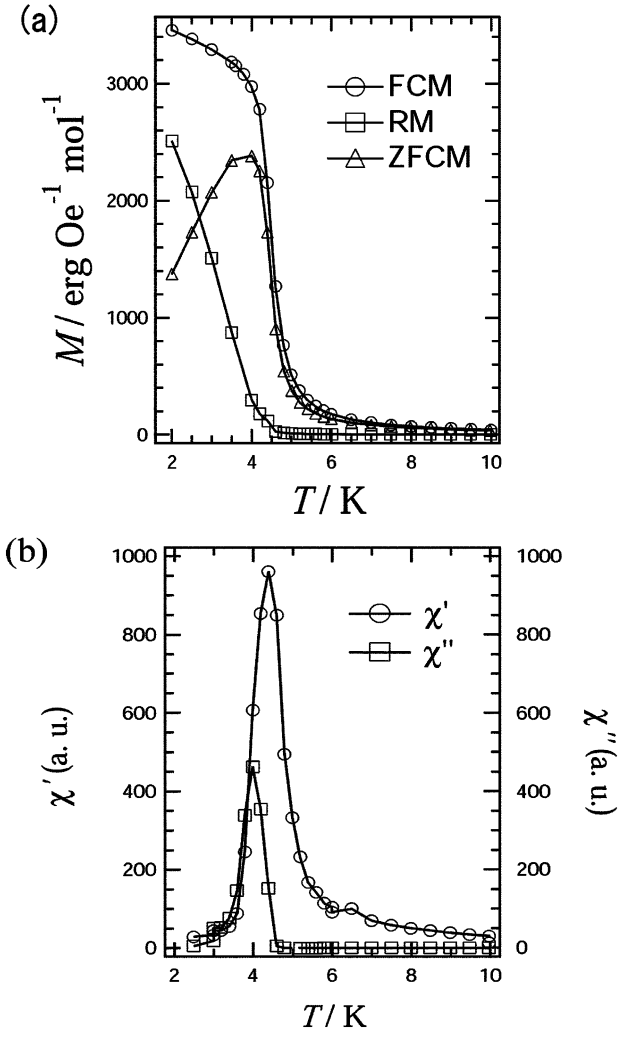

Figure 9. (a) Field-cooled magnetization (FCM), remnant magnetization (RM), and zero-field-cooled magnetization (ZFCM) of [Mn(hfac)$_2$hnn] (**3**) measured at 5, 0, and 5 Oe, respectively. (b) Temperature dependence of the in-phase (χ') and out-of-phase (χ'') components of the ac susceptibility of **3** (ac magnetic field: amplitude, 5 Oe; frequency, 10000 Hz). Solid lines are drawn as a guide to the eye.

completely on warming. The alternating current (ac) magnetic susceptibility of **3** was measured in the ac field amplitude of 5 Oe oscillating at 10000 Hz in a temperature range 10−2 K (Figure 9b). The peak of the real component (χ') at 4.4 K is noticeable. This behavior implies that the long-range magnetic ordering occurs at $T_N = 4.4$ K. We observed no frequency dependence of the real or imaginary part of the ac susceptibility for **3**.

Discussion

We have described the crystal structure of **1**, which is the first example of an infinite chain complex containing the hin bridge. The ferromagnetic interaction of **1** can be explained in terms of orbital orthogonality between the copper $3d_{x^2-y^2}$ and the oxygen or nitrogen $2p_z$ orbitals, as often discussed in Cu(hfac)$_2$ nitronyl nitroxide complexes.[12] On the other hand, the antiferromagnetic interaction of **2** and **3** can be attributed to orbital overlap between the manganese $3d_{xz}$ and $3d_{yz}$ and the oxygen or nitrogen $2p_z$ orbitals, like

$Mn(hfac)_2$ nitronyl nitroxide complexes.[15] Such ferro- and antiferromagnetic couplings have been widely observed in metal−oxygen coordination bonds in nitronyl nitroxide complexes. In the present study, a similar argument can also be applied to the coordinating metal−nitrogen bonds in the hin complexes.

Interestingly, the magnetic exchange couplings between metal and hin spins in **1** ($2J/k = +56.8$ K) are larger than those of the corresponding nitronyl nitroxide derivatives ([$Cu(hfac)_2$Rnn]: $2J/k = +36.9$ and $+30.8$ K (R = methyl and isopropyl, respectively)).[12] Strong interaction can be expected in less bulky systems in general, and the present results are ascribable especially to the choice of the smallest ligands in the nitronyl nitroxide and imino nitroxide families. For more detailed discussion, we have to think of several features based on geometrical and electronic structures of **1**. The bond distances of Cu−N2 and Cu−O3 are comparable to or slightly shorter than the typical values of Cu−O for nitronyl nitroxide complexes (e.g.: [$Cu(hfac)_2$Rnn], 2.341(6) and 2.431(5) Å for R = methyl,[12] 2.407(6) and 2.446(8) Å for R = isopropyl;[12] [$\{Cu(hfac)_2(H_2O)\}_2(\mu$-hnn)],[5] 2.462(2) Å). However, the slight difference of the bond lengths alone can hardly account for the large exchange interaction of **1**.

As McConnell has pointed out, the exchange coupling is proportional to the spin densities on the interacting atoms ($H^{AB} = -S^A \cdot S^B \sum J_{ij} \rho_i^A \rho_j^B$),[16] and accordingly the higher spin densities on the terminal atoms (N and O) of the ONCN group than those of the ONCNO group may afford stronger exchange interactions. We have no experimental evidence of the spin distribution in hin and hnn. The spin distributions in hin and hnn can be estimated by means of semiempirical calculation methods. We carried out UHF/PM3[17] calculations using the geometries determined by the X-ray crystallographic analysis; the atomic coordinates of hnn and hin were available from the hnn moiety in [$\{Cu(hfac)_2(H_2O)\}_2(\mu$-hnn)][5] and the hin moiety in [$Cu(hfac)_2$hin]. The calculated spin densities are $\rho(O) = 0.323$ for hnn and $\rho(O) = 0.429$ and $\rho(N_{terminal}) = 0.376$ for hin. The higher spin densities in hin are responsible for the stronger ferromagnetic interactions in comparison to those of the hnn complexes.

In the case of manganese(II) complexes, the magnitude of the exchange interaction of **2** ($2J/k = -325$ K) is comparable to those of other nitronyl nitroxide derivatives ([$Mn(hfac)_2$Rnn]: $2J/k = -471$, -371, -310, and -297 K (R = isopropyl, ethyl, methyl, and phenyl, respectively)).[15] However, the exchange interaction of **2** is much weaker than that of **3** ($2J/k = -740$ K) probably because of stronger chemical affinity of Mn−O than that of Mn−N. Indeed the bond lengths between manganese and nitroxide oxygen are shorter than those of manganese and imino nitroxide nitrogen. Unfortunately we could not determine the crystal structure of **2**, and we compare the bond lengths between **3** and a prototype compound [$Mn(hfac)_2(hin)_2$];[5] 2.139(4), 2.142(4), 2.129(4), and 2.139(4) Å for the Mn−O(hnn) bonds vs 2.208(3) and 2.224(3) Å for the Mn−N(hin) bonds. The shorter Mn(II)−O bond lengths bring about the stronger exchange interactions between Mn(II) and radical spins. Therefore, the advantage of the higher spin density at the $N_{terminal}$ atom in hin is canceled out by the long Mn−N bond in **3**.

Nevertheless, we can stress that hnn is a promising ligand for development of strongly correlated ferrimagnetic systems, as demonstrated by the considerably large intrachain interaction in [$Mn(hfac)_2$hnn] (**3**). The hin ligand is also a good candidate for constructing copper(II)-based magnetic systems such as [$Cu(hfac)_2$hin] (**1**), although it seems to be less useful in constructing manganese(II)-based magnetic systems.

The mechanism of the three-dimensional magnetic order of **3** can be understood similarly to the system of [$Mn(hfac)_2$Rnn] (R = isopropyl, *n*-propyl, and ethyl) reported by Gatteschi.[15] The T_N for **3** (4.6 K) is lower, while the magnitude of exchange interaction of **3** ($2J/k = -740$ K) is much stronger than those of other nitronyl nitroxide derivatives ([$Mn(hfac)_2$Rnn]: $T_N = 8.1$ and 8.6 K; $2J/k = -371$ and -361 K (R = ethyl and *n*-propyl, respectively)). Reasons for the low T_N of **3** are not clear so far. The transition temperatures generally depend not only on the intrachain interaction but also on the interchain ones. Owing to the smaller substituent in **3** than those in [$Mn(hfac)_2$Rnn] derivatives, the interchain Mn···Mn distances in **3** are shorter than those in the latter; 8.35−11.3 Å for **3** and 8.89−12.11 Å for [$Mn(hfac)_2$Rnn] (R = ethyl and *n*-propyl). We can hardly explain that the longer interchain distances bring about the higher T_N, but only point out the similar distance dependence of the transition temperatures of layered magnets reported by Drillon, Awaga, and their co-workers.[18] They proposed the through-space dipolar interaction between the layers to interpret the unexpected finding of the high T_N related with the large spacing. Preliminary results of the magnetic measurements on a single crystal of **3** suggest that the easy magnetization axis lies along the chain direction. In this situation antiparallel alignment of the classical magnetic moments is preferable, and the shorter distance between the chains is unfavorable for parallel moment alignment, presumably giving the lower T_N.

Summary

We have demonstrated the one-dimensional magnetic properties of [$Cu(hfac)_2$hin] and [$Mn(hfac)_2$hin]. They are the first examples of the hin−metal complexes with one-dimensional magnetic structures. Relatively strong magnetic couplings, especially in the copper(II) complex, were found in the hin complexes compared with the conventional Rnn

(15) Caneschi, A.; Gatteschi, D.; Renard, J. P.; Rey, P.; Sessoli, R. *Inorg. Chem.* **1989**, *28*, 3314. Caneschi, A.; Gatteschi, D.; Lalioti, N.; Sangregorio, C.; Sessoli, R. *J. Chem. Soc., Dalton Trans.* **2000**, 3907. Caneschi, A.; Gatteschi, D.; Rey, P.; Sessoli, R. *Inorg. Chem.* **1988**, *27*, 1756.
(16) McConnell, H. M. *J. Chem. Phys.* **1963**, *39*, 1910.
(17) Stewart, J. J. P. *MOPAC 97*; Fujitsu Ltd: Tokyo, Japan, 1997.
(18) Rabu, R.; Rouba, S.; Laget, V.; Hornic, C.; Drillon, M. *Chem. Commun.* **1996**, 1107. Laget, V.; Rouba, S.; Hornic, C.; Drillon, M. *J. Magn. Magn. Mater.* **1996**, *154*, L7. Laget, V.; Hornic, C.; Rabu, P.; Drillon, M.; Ziessel, R. *Cood. Chem. Rev.* **1998**, *178−180*, 1533. Fujita, W.; Awaga, K. *Inorg. Chem.* **1996**, *35*, 1915. Fujita, W.; Awaga, K. *J. Am. Chem. Soc.* **1997**, *119*, 4563. Girtu, M. A.; Wynn, C. M.; Fujita, W.; Awaga, K.; Epstein, A. J. *Phys. Rev. B* **1998**, *57*, 11058. Hornick, C.; Rabu, P.; Drillon, M. *Polyhedron* **2000**, *19*, 259.

complexes. Furthermore, we also found that, even when the hnn is available, it can be useful in pursuit of strongly correlated magnetic materials using manganese(II) ions.

Recently Gatteschi and co-workers reported that polymeric $M(hfac)_2$−nitronyl nitroxide systems were potentially good candidates for single-molecule magnets.[19] Slow magnetic relaxation in one-dimensional magnets requires the condition that the ratio of the intrachain interaction over the interchain interaction must be high.[19] The stronger intrachain interactions across the hin bridge than those across nitronyl nitroxide bridges may satisfy this requirement. Preparation of polymeric complexes using hin with other metal ions having large single-ion anisotropy such as cobalt(II) ions in place of copper(II) and manganese(II) is currently underway.

Acknowledgment. This work was supported by Grants-in-Aid for Scientific Research on Priority Areas (No. 730/11224204 and 401/11136212) from the Ministry of Education, Culture, Sports, Science and Technology, Japan.

Supporting Information Available: Crystallographic data (excluding structure factors) for the structures of **1** and **3** in CIF format. This material is available free of charge via the Internet at http://pubs.acs.org.

IC034392X

(19) Caneschi, A.; Gatteschi, D.; Lalioti, N.; Sangregorio, C.; Sessoli, R.; Venturi, G.; Vindigni, A.; Rettori, A.; Pini, M. G.; Novak, M. A. *Angew. Chem., Int. Ed.* **2001**, *40*, 1760

A Self-assembled Helix from 4,6-Dimethylpyrimidine and Copper(II) Bromide

Takayuki Ishida,* Liming Yang, and Takashi Nogami
Department of Applied Physics and Chemistry, The University of Electro-Communications, Chofu, Tokyo 182-8585

(Received July 10, 2003; CL-030625)

A 1:1 polymeric complex of 4,6-dimethlpyrimidine and $CuBr_2$ was spontaneously resolved to afford a 6_1 helix. Steric effects seem to play an important role for constructing a helical structure. Magnetic measurements showed a uniform $S = 1/2$ 1-D behavior. A dinuclear complex is also obtained as a precursor to the polymeric complex.

Various self-assembled structures have been developed from pyrimidines and transition metal ions, such as di- and trinuclear complexes,[1] hexagons,[2] *cis*-[3] and *trans*-zigzag chains,[4–6] and 3-D networks.[7] Lehn and co-workers exploited supramolecular approaches to helicates using oligo-bipyridines.[8] Oligo-terpyridines and -phenanthrolines have also been utilized for various helicates.[9] Peng et al.[10] and Cotton et al.[11] reported the metal wires supported by helical oligo-dipyridylamido ligands. We will report here a chiral crystal containing a 6_1 helical structure consisting of simple 4,6-dimethlpyrimidine (DMPM) and copper(II) bromide; namely, a helicate was prepared without support from pre-organization of ligands.

An ethanol solution (3 mL) containing DMPM (46 mg; 0.42 mmol) was slowly added to an ethanol solution containing $CuBr_2$ (92 mg; 0.41 mmol), and the combined solution was allowed to stand in a refrigerator for a day. Black hexagonal prisms of $[DMPM{\cdot}CuBr_2{\cdot}(C_2H_5OH)_x]_n$ (**1**) were precipitated. They were collected on a filter and washed with a small amount of ethanol. The yield was 66 mg (0.20 mmol; 48%). The crystals were subjected to structural and magnetic studies without further purification. Anal. Calcd.: C, 8.26; N, 22.43; H, 2.67% for **1** with $x = 0.17$. Found: C, 8.19; N, 22.98; H, 2.59%. The elemental analysis indicated that the products contained some solvent, depending on the degree of evacuation. A similar procedure using methanol as a solvent gave green blocks of a dinuclear complex $[DMPM_3{\cdot}(CuBr_2)_2{\cdot}(CH_3OH)_2]$ (**2**). In some case both types of compounds were precipitated at a time, and the crystals could be separated manually based on the different shapes and colors under a microscope.

Diffraction data of a single crystal of **1** were collected on a Rigaku R-axis RAPID diffractometer with graphite monochromated Mo Kα radiation ($\lambda = 0.71069$ Å) at 90 K.[12] The space group was hexagonal $P6_122$. A half portion of DMPM and $CuBr_2$ was crystallographically independent and $Z = 12$. The molecular structure was expanded according to the symmetry, giving a helical structure (Figure 1).

The space group of **1** is chiral, and there is no enanthiomeric helix in a crystal. Thus, spontaneous resolution took place during the crystallization, though the starting materials DMPM and $CuBr_2$ are achiral.

The dc magnetic susceptibility of the randomly oriented polycrystalline sample of **1** was measured on a Quantum Design MPMS SQUID magnetometer at 5 kOe over a temperature range 1.8–300 K. As Figure 2 shows, the molar magnetic susceptibility

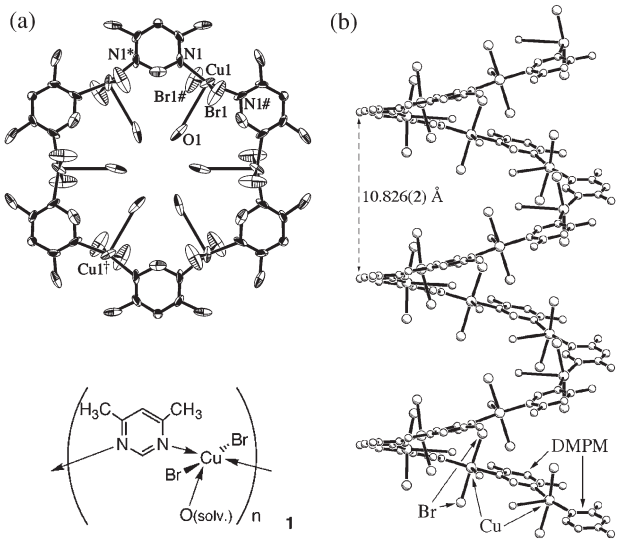

Figure 1. Crystal structure of $[DMPM{\cdot}CuBr_2{\cdot}(C_2H_5OH)_x]_n$ (**1**; $x = 1$). (a) ORTEP drawing as a top view with thermal ellipsoids at the 50% probability level. Hydrogen atoms are omitted. A structural formula is also shown. Only oxygen atoms are drawn for the solvent molecules.[12] Selected interatomic distances and angles are: Cu1–Br1, 2.346(2); Cu1–O1, 3.10(2); Cu1–N1, 2.02(1) Å; Br1–Cu1–Br1#, 168.6(2); N1–Cu1–N1#, 163.1(7); Br1–Cu1–O1, 84.3(1); Br1–Cu1–N1, 91.1(4); Br1–Cu1–N1#, 90.5(4); O1–Cu1–N1, 98.5(3)°; Cu1···Cu1†, 12.04 Å. Symmetry operation codes for *, #, and † are $(-y, -x, -7/6 - z)$, $(x - y, -y, -1 - z)$, and $(-x, -y, 1/2 + z)$, respectively. (b) A side view. Three pitches are shown in an infinite helix.

of **1** was reproduced with a combined expression of a Bonner–Fisher term[13] and a small contribution of a Curie spin. The best optimized parameters were: $g = 2.16(1)$ and $2J/k_B = -56.7(3)$ K, where the spin Hamiltonian is defined as $H = -2JS_1 \cdot S_2$. This finding indicates that the copper spins are arranged in a 1-D array with equally spacing, being consistent with the crystal structure determined. The Curie term ($C_{Curie} = 0.014\,cm^3K\,mol^{-1}$) corresponds to 3.2% of the total copper(II) spins, which is ascribable to lattice defects or other origins (e.g. staggered fields caused by the canting *g*-tensors of neighboring Cu ions).[5]

In **1**, pyrimidine nitrogen atoms were coordinated at the equatorial positions. The σ-type orbital overlaps between copper $d_{x^2-y^2}$ and nitrogen n orbitals on both sides bring about an antiferromagnetic superexchange through the pyrimidine molecular orbitals.[3,4,14]

Steric effects seem to play an important role in forming hexagons vs zigzag chains, as previously pointed out on the crystal engineering of isophthalic acids.[15] Actually, the methyl groups in DMPM are needed for the preparation of **1**, as indicated by the following results: Complexation of unsubstituted pyrimidine

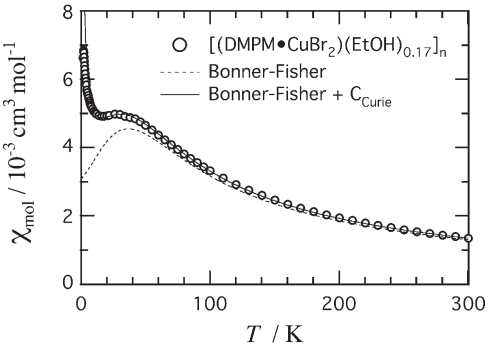

Figure 2. Temperature dependence of the molar magnetic susceptibility χ_{mol} for $[DMPM{\cdot}CuBr_2{\cdot}(C_2H_5OH)_{0.17}]_n$ (**1**). Solid and dotted lines represent calculated curves. For details, see the text.

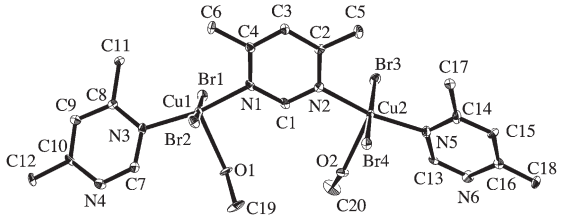

Figure 3. ORTEP drawing of $[DMPM_2{\cdot}(CuBr_2)_2{\cdot}(CH_3OH)_2]$ (**2**) with thermal ellipsoids at the 50% probability level. H atoms are omitted.

(PM) and $CuBr_2$ gave only unidentified solids, and the PM-bridged copper(II) nitrate and 1,1,1,5,5,5-hexafluoropentane-2,4,-dionate complexes have been characterized as zigzag chains.[3–6] We also have to pay attention to solvated molecules in coordination compounds.[16] To clarify driving forces of the helix formation preferable to planar cyclization, we analyzed the molecular structure of **2**[17] (Figure 3), which can be regarded as a precursor of **1**.

Each copper(II) ion in **2** possesses a methanol molecule as an axial ligand. Owing to the steric repulsion, the copper ions can not accept another axial ligand, and the *anti* configuration is favored with respect to methanol and two methyl groups (O1–C19 and C6; O1–C19 and C11). Accordingly, the two methyl groups are located in the same hemisphere of the copper surroundings, giving rise to a bent $(DMPM)_3(CuBr_2)_2$ backbone. This geometry also forces two neighboring methanol ligands close to each other (see C19 and C20), and they have to steer to opposite directions. The neighboring copper basal planes are twisted. A possible mechanism for the helix formation of **1** is as follows. Ethanol molecules are once coordinated to copper(II) ions, and a bent and twisted DMPM–$CuBr_2$ backbone is formed like **2**. After the helical polymerization, the ethanol ligands easily escape from the axial positions because of the less ligating nature than that of methanol. In fact, the X-ray crystal structure of freshly prepared **1** was solved to be a helix in a trigonal $P3_121$ space group at 90 K. Although the final R factors were rather unsatisfactory ($R = 0.083$ [$I > 2\sigma(I)$]), the electron density peaks due to the solvent could be observed more sharply than the analysis on evacuated samples.

We thank Dr. D. Hashizume and Prof. F. Iwasaki for kind assistance in the X-ray crystal structure analysis.

References and Notes

1 T. Kogane, K. Kobayashi, M. Ishii, R. Hirota, and M. Nakahara, *J. Chem. Soc., Dalton Trans.*, **1994**, 13; M. Nakagawa, Y. Ishikawa, T. Kogane, T. Ishida, M. Yasui, F. Iwasaki, and T. Nogami, *Mol. Cryst. Liq. Cryst.*, **286**, 29 (1996).
2 J. Omata, T. Ishida, D. Hashizume, F. Iwasaki, and T. Nogami, *Inorg. Chem.*, **40**, 3954 (2001); L. C. Tabares, J. A. R. Navarro, and J. M. Salas, *J. Am. Chem. Soc.*, **123**, 383 (2001).
3 M. Yasui, Y. Ishikawa, N. Akiyama, T. Ishida, T. Nogami, and F. Iwasaki, *Acta Crystallogr., Sect. B*, **57**, 288 (2001); T. Ishida, K. Nakayama, M. Nakagawa, W. Sato, Y. Ishikawa, M. Yasui, F. Iwasaki, and T. Nogami, *Synth. Met.*, **85**, 1655 (1997).
4 F. Mohri, K. Yoshizawa, T. Yamabe, T. Ishida, and T. Nogami, *Mol. Eng.*, **8**, 357 (1999).
5 R. Feyerherm, S. Abens, D. Günther, T. Ishida, M. Meissner, M. Meschke, T. Nogami, and M. Steiner, *J. Phys.: Condens. Matter*, **12**, 8495 (2000); R. Feyerherm, T. Ishida, T. Nogami, and M. Steiner, *Mol. Cryst. Liq. Cryst.*, **335**, 235 (1999).
6 T. Ezuhara, K. Endo, K. Matsuda, and Y. Aoyama, *New J. Chem.*, **24**, 609 (2000).
7 K. Nakayama, T. Ishida, R. Takayama, D. Hashizume, M. Yasui, F. Iwasaki, and T. Nogami, *Chem. Lett.*, **1998**, 497; K. Zusai, T. Kusaka, T. Ishida, R. Feyerherm, M. Steiner, and T. Nogami, *Mol. Cryst. Liq. Cryst.*, **343**, 127 (2000); S. W. Keller, *Angew. Chem., Int. Ed.*, **36**, 247 (1997); H. Cai, H.-M. Hu, W.-Z. Chen, H.-G. Zhu, and X.-Z. You, *Chem. Lett.*, **1999**, 221.
8 R. Kämer, J.-M. Lehn, and A. Marquis-Rigault, *Proc. Natl. Acad. Sci. U.S.A.*, **90**, 5394 (1993); B. Hasenknopf, J.-M. Lehn, B. O. Kneisel, G. Baum, and D. Fenske, *Angew. Chem., Int. Ed.*, **35**, 1838 (1996).
9 C. Piguet, G. Bernardinelli, and G. Hopfgartner, *Chem. Rev.*, **97**, 2005 (1997).
10 S.-M. Peng, C.-C. Wang, Y.-L. Jang, Y.-H. Chen, F.-Y. Li, C.-Y. Mou, and M.-K. Leung, *J. Magn. Magn. Mater.*, **209**, 80 (2000).
11 F. A. Cotton, L. M. Daniels, T. Lu, C. A. Murillo, and X. Wang, *J. Chem. Soc., Dalton Trans.*, **1999**, 517.
12 Selected crystallographic data for **1**: $C_3H_4Br_1Cu_{0.5}N_1O_{0.5}$, hexagonal $P6_122$, $a = 14.162(3)$, $c = 10.826(2)$ Å, $V = 1880.4(7)$ Å^3, $Z = 12$, $D_{calc} = 1.852\,g\,cm^{-3}$, μ(Mo Kα) = $8.10\,mm^{-1}$, $R = 0.058$ ($I > 2.0\sigma(I)$), $R_w = 0.147$ (all data), $T = 90$ K for 749 unique reflections. An appreciable electron density was found at an axial position of Cu1, and tentatively assigned as an oxygen atom. However, the ethanol skeleton could not be determined owing to disorder.
13 J. C. Bonner and M. E. Fisher, *Phys. Rev. A*, **135**, 640 (1964).
14 T. Ishida, T. Kawakami, S.-i. Mitsubori, T. Nogami, K. Yamaguchi, and H. Iwamura, *J. Chem. Soc., Dalton Trans.*, **2002**, 3177.
15 J. Yang, J.-L. Marendaz, S. J. Geib, and A. D. Hamilton, *Tetrahedron Lett.*, **35**, 3665 (1994).
16 H. Abourahma, B. Moulton, V. Kravtsov, and M. J. Zaworotko, *J. Am. Chem. Soc.*, **124**, 9990 (2002).
17 Selected crystallographic data for **2**: $C_{20}H_{32}Br_4Cu_2N_6O_2$, monoclinic Cc, $a = 10.187(1)$, $b = 53.072(5)$, $c = 7.1953(8)$ Å, $\beta = 134.797(4)^\circ$, $V = 2760.5(5)$ Å^3, $Z = 4$, $D_{calc} = 2.01\,g\,cm^{-3}$, μ(Mo Kα) = $7.38\,mm^{-1}$, $R = 0.040$ ($I > 2.0\sigma(I)$), $R_w = 0.117$ (all data), $T = 90$ K for 3607 unique reflections.

Published on the web (Advance View) October 6, 2003; DOI 10.1246/cl.2003.1018

Inorg. Chem. **2003**, *42*, 7616–7625

Molecular Metamagnet [Ni(4ImNNH)$_2$(NO$_3$)$_2$] (4ImNNH = 4-Imidazolyl Nitronyl Nitroxide) and the Related Compounds Showing Supramolecular H-Bonding Interactions

Chigusa Aoki, Takayuki Ishida,* and Takashi Nogami

Department of Applied Physics and Chemistry, The University of Electro-Communications, Chofu, Tokyo 182-8585, Japan

Received July 30, 2003

A new chelating radical ligand 4ImNNH (2-(4-imidazolyl)-4,4,5,5-tetramethylimidazolin-1-oxyl 3-oxide) was prepared, and complexation with divalent transition metal salts gave complexes, [M(4ImNNH)$_2$X$_2$], which showed intermolecular ferromagnetic interaction in high probability (7 out of 10 paramagnetic compounds investigated here). The nitrate complexes (X = NO$_3$; M = Mn (**1**), Co (**2**), Ni (**3**), Cu (**4**)) crystallize isomorphously in monoclinic space group $P2_1/a$. The equatorial positions are occupied with two 4ImNNH chelates and the nitrate oxygen atoms are located at the axial positions. Magnetic measurements revealed that the intramolecular exchange couplings in **1**, **2**, and **4** were antiferromagnetic, while that in **3** was ferromagnetic with $2J/k_B = +85$ K, where the spin Hamiltonian is defined as $H = -2J(S_1 \cdot S_2 + S_2 \cdot S_3)$ based on the molecular structures determined as the linear radical–metal–radical triads. The intramolecular ferromagnetic interaction in **3** is interpreted in terms of orthogonality between the radical π^* and metal dσ orbitals. Compounds **1**–**3** exhibited intermolecular ferromagnetic interaction ascribable to a two-dimensional hydrogen bond network parallel to the crystallographic *ab* plane. Complex **3** became an antiferromagnet below 3.4 K and exhibited a metamagnetic transition on applying a magnetic field of 5.5 kOe at 1.8 K. The complexes prepared from metal halides, [M(4ImNNH)$_2$X$_2$] (X = Cl, Br; M = Mn, Co, Ni, Cu), showed intramolecular antiferromagnetic interactions, which are successfully analyzed based on the radical–metal–radical system. The crystal structures determined here on **1**–**4**, [Mn(4ImNNH)$_2$Cl$_2$], and [Cu(4ImNNH)$_2$Br$_2$] always have intermolecular hydrogen bonds of H(imidazole)···X(axial ligand)–M, where X = NO$_3$, Cl, Br. This interaction seems to play an important role in molecular packing and presumably also in magnetic coupling.

Introduction

Polymeric complex formation containing transition metal ions and bridging radical ligands is supposed as an important strategy for constructing ferri- and ferromagnetic networks with dimensionality.[1−3] The nitronyl nitroxide (4,4,5,5-tetramethylimidazolin-1-oxyl 3-oxide; abbreviated as NN hereafter) family has been widely utilized because of their bidentate nature suitable for bridge formation[1] (Chart 1). In addition, intermolecular ferromagnetic couplings are often observed in NN radical crystals,[4−8] and it holds also for the metal−radical materials possessing the NN group as a peripheral substituent.[9] The role of hydrogen (H) bonds has been discussed in connection with ferromagentic exchange

* Author to whom correspondence should be addressed. E-mail: ishi@pc.uec.ac.jp.

(1) Caneschi, A.; Gatteschi, D.; Rey, P.; Sessoli, R. *Acc. Chem. Res.* **1989**, *22*, 392.
(2) Inoue, K.; Hayamizu, T.; Iwamura, H.; Hashizume, D.; Ohashi, Y. *J. Am. Chem. Soc.* **1996**, *118*, 1803. Stumpf, H. O.; Ouahab, L.; Pei, Y.; Grandjean, D.; Kahn, O. *Science* **1993**, *261*, 447. Ise, T.; Ishida, T.; Hashizume, D.; Iwasaki, F.; Nogami, T. *Inorg. Chem.* **2003**, *42*, 6106.
(3) Miller, J. S.; Epstein, A. J. *Angew. Chem., Int. Ed. Engl.* **1994**, *33*, 385. Fujita, W.; Awaga, K.; Takahashi, M.; Takeda, M.; Yamazaki, T. *Chem. Phys. Lett.* **2002**, *362*, 97.
(4) Kinoshita, M.; Turek, P.; Tamura, M.; Nozawa, Y.; Shiomi, D.; Nakazawa, Y.; Ishikawa, M.; Takahashi, M.; Awaga, K.; Inabe, T.; Maruyama, Y. *Chem. Lett.* **1991**, 1225.
(5) Sugawara, T.; Matsushita, M. M.; Izuoka, A.; Wada, N.; Takeda, N.; Ishikawa, M. *J. Chem. Soc., Chem. Commun.* **1994**, 1723. Matsushita, M. M.; Izuoka, A.; Sugawara, T.; Kobayashi, T.; Wada, N.; Takeda, N.; Ishikawa, M. *J. Am. Chem. Soc.* **1997**, *119*, 4369.
(6) Cirujeda, J.; Mas, M.; Molins, E.; Panthou, F. L.; Laugier, J.; Park, J. G.; Paulsen, C.; Rey, P.; Rovira, C.; Veciana, J. *J. Chem. Soc., Chem. Commun.* **1995**, 709. Cirujeda, J.; Ochando, L. E.; Amigo, J. M.; Rovira, C.; Rius, J.; Veciana, J. *Angew. Chem., Int. Ed. Engl.* **1995**, *34*, 55. Hernandez, E.; Mas, M.; Molis, M. E.; Rovira, C.; Veciana, J. *Angew. Chem., Int. Ed. Engl.* **1993**, *32*, 882.
(7) Yoshioka, N.; Irisawa, M.; Mochizuki, Y.; Kato, T.; Inoue, H.; Ohba, S. *Chem. Lett.* **1997**, 251.
(8) Doi, K.; Ishida, T.; Nogami, T. *Chem. Lett.* **2003**, 544.

10.1021/ic0349048 CCC: $25.00
Published on Web 10/16/2003

Chart 1

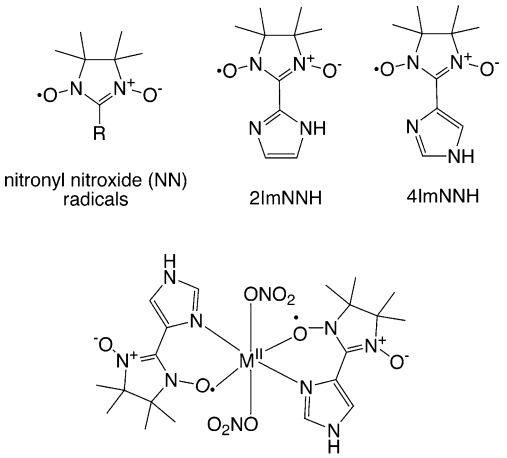

pathways.[5−8] Rey and co-workers reported the anionizable radical ligand, 2ImNNH (2-imidazolyl NN; ImH denotes imidazole), which was applied to the formation of two-dimensional magnetic materials as the anionic form.[10] We designed an isomeric radical ligand, 4ImNNH (4-imidazolyl NN), which affords networking directions different from those of 2ImNNH. Actually, the direction of H-bonds from the 4-imidazolyl NH group is quite important for the present study.

We have studied the crystal structures and magnetic properties of [M(4ImNNH)$_2$(NO$_3$)$_2$] (M = Mn (**1**), Co (**2**), Ni (**3**), Cu (**4**)) and preliminarily reported the intramolecular ferromagnetic coupling in **3** between nickel(II) and radical spins.[11] There have been ample examples of ferrimagnets[1,2] according to the metal−radical approach.[1] However, the magnets based on genuine ferromagnetic coupling are rare.[12] In addition to the issue on the intramolecular interaction, **3** also showed intermolecular ferromagnetic interaction.[11] To investigate the intermolecular magneto-structure relationship as well as intramolecular one, we prepared chloride and bromide series [M(4ImNNH)$_2$X$_2$] (M = Mn, Co, Ni, Cu (**5**−**8** for X = Cl; **9**−**12** for X = Br)) and found that seven compounds exhibited intermolecular ferromagnetic interaction. We will report here the structural and magnetic characterization of **1**−**12**.

Experimental Section

Materials. The NN-substituted ligand 4ImNNH was prepared according to Ullman's method[13] by using 4-formylimidazole as a starting material. The precursor bishydroxyimidazoline was obtained in 27% yield from 4-formylimidazole, and the treatment with $NaIO_4$ in water gave 4ImNNH as dark blue polycrystals in 37% yield from the bishydroxyimidazoline, mp 154−160 °C (CH_2Cl_2-hexane). The ESR spectrum measured on a Bruker ESP300E supports the presence of the nitronyl nitroxide group. The spectrum shows a 1:2:3:2:1 quintet pattern with $g = 2.0066$ and $a_N = 7.59$ G in toluene at room temperature.

The following complexation procedure is typical. An ethanol solution (2.5 mL) containing $Ni(NO_3)_2 \cdot 6H_2O$ (30.2 mg, 0.104 mmol) and 4ImNNH (44.8 mg, 0.201 mmol) was allowed to stand in a refrigerator for a week. The resultant black crystals of **3** were collected on a filter and washed with a small amount of water, which are suitable for X-ray crystal structure and magnetic studies. The yield of **3** was 59.7 mg (94%). Similarly, other complexes were obtained in good yields (typically about 90% for X = NO_3, 80% for X = Cl, and about 60% for X = Br), using the corresponding metal salts as starting materials. For preparation of single crystals of **4**, methanol was used as a solvent because only poorly resolved crystals were obtained from ethanol. Elemental analyses (C, H, N) on a Fisons EA-1108 by a usual combustion method supported the formulas of [M(4ImNNH)$_2$X$_2$] in the 0.3% range.

X-ray Crystallography. Diffraction data of single crystals of 4ImNNH, **1**−**4**, **5**, and **12** were collected on a Rigaku R-axis RAPID diffractometer with graphite monochromated Mo Kα radiation ($\lambda = 0.71069$ Å) at 90 K for 4ImNNH and 100 K for the coordination compounds. The structures were directly solved by a heavy-atom Patterson method or the SIR program[14] in the teXsan program package.[15] Numerical absorption correction was used. All of the hydrogen atoms could be found in difference Fourier maps, and the parameters of the hydrogen atoms were included in the refinement. The thermal displacement parameters were refined anisotropically for non-hydrogen atoms and isotropically for hydrogen atoms. Full-matrix least-squares methods were applied using all of the unique reflection data. Crystal data are summarized in Table 1 and selected structural parameters in Tables 2 and 3.

Magnetic Measurements. dc magnetic susceptibilities of randomly oriented polycrystalline samples of 4ImNNH and **1**−**12** were measured on a Quantum Design MPMS SQUID magnetometer equipped with a 7 T coil in a temperature range 1.8−300 K. The magnetic responses were corrected with diamagnetic blank data of the sample holder measured separately. The diamagnetic contribution of the sample itself was estimated from Pascal's constants.

Results

Characterization of 4ImNNH. The molecular structure of 4ImNNH was determined by X-ray crystallographic analysis (see Supporting Information, Figure S1). Since the hydrogen atoms could be found experimentally, we determined the exact form of 4ImNNH because the imidazole ring in 4ImNNH possesses tautomeric isomerism. The 4ImNNH molecule was proved to possess a 1*H*-form in the crystal, as indicated by imino N1 and amino N2 nitrogen atoms in Figure 1. In contrast to our expectation, the imidazole N−H proton does not form an intramolecular chelate. Instead, it participates in a branching H-bond in an

(9) Omata, J.; Ishida, T.; Hashizume, D.; Iwasaki, F.; Nogami, T. *Inorg. Chem.* **2001**, *40*, 3954. Omata, J.; Ishida, T.; Hashizume, D.; Iwasaki, F.; Nogami, T. *Mol. Cryst. Liq. Cryst.* **2002**, *376*, 455.
(10) Fegy, K.; Luneau, D.; Ohm, T.; Paulsen, C.; Rey, P. *Angew. Chem., Int. Ed.* **1998**, *37*, 1270. Fegy, K.; Sanz, N.; Luneau, D.; Belorizky, E.; Rey, P. *Inorg. Chem.* **1998**, *37*, 4518. Fegy, K.; Luneau, D.; Belorizky, E.; Novac, M.; Tholence, J.-L.; Paulsen, C.; Ohm, T.; Rey, P. *Inorg. Chem.* **1998**, *37*, 4524.
(11) Aoki, C.; Ishida, T.; Nogami, T. *Inorg. Chem. Commun.* **2003**, *6*, 1122.
(12) Miller, J. S.; Epstein, A. J.; Reiff, W. M. *Acc. Chem. Res.* **1988**, *21*, 114.
(13) Ullman, E. F.; Osiecki, J. H.; Boocock, D. G. B.; Darcy, R. *J. Am. Chem. Soc.* **1972**, *94*, 7049.
(14) Altomare, A.; Burla, M. C.; Camalli, M.; Cascarano, G.; Giacovazzo, C.; Guagliardi, A.; Moliterni, A. G. G.; Polidori, G.; Spagna, R. *J. Appl. Crystallogr.* **1999**, *32*, 115.
(15) TeXsan, Single-Crystal Structure Analysis Software, ver. 1.10, Molecular Structure Corp., The Woodlands, TX, and Rigaku Co. Ltd., Akishima, Tokyo, Japan, 1999.

Table 1. Crystallographic Data for 4ImNNH, $[M(4ImNNH)_2(NO_3)_2]$ (M = Mn (**1**), Co (**2**), Ni (**3**), Cu (**4**)), $[Mn(4ImNNH)_2Cl_2]$ (**5**), and $[Cu(4ImNNH)_2Br_2]$ (**12**)

compds	4ImNNH	**1**	**2**	**3**	**4**	**5**	**12**
formula	$C_{10}H_{15}N_4O_2$	$C_{20}H_{30}N_{10}O_{10}Mn_1$	$C_{20}H_{30}N_{10}O_{10}Co_1$	$C_{20}H_{30}N_{10}O_{10}Ni_1$	$C_{20}H_{30}N_{10}O_{10}Cu_1$	$C_{20}H_{30}Cl_2N_8O_4Mn_1$	$C_{20}H_{30}Br_2N_8O_4Cu_1$
habit	black platelet	black block	black block	black block	black block	black platelet	black platelet
dimension (mm^3)	0.5 × 0.5 × 0.1	0.8 × 0.5 × 0.2	0.4 × 0.2 × 0.1	0.3 × 0.3 × 0.1	0.4 × 0.35 × 0.08	0.3 × 0.3 × 0.08	0.4 × 0.3 × 0.08
T/K	90	100	100	100	100	100	100
cryst syst	tetragonal	monoclinic	monoclinic	monoclinic	monoclinic	triclinic	monoclinic
space group	$I4_1/a$	$P2_1/a$	$P2_1/a$	$P2_1/a$	$P2_1/a$	$P\bar{1}$	$P2/c$
a (Å)	20.7966(9)	13.3749(9)	13.3545(2)	13.3490(9)	12.7794(7)	7.5167(9)	17.603(2)
b (Å)	20.7966(9)	11.0529(9)	10.8843(3)	10.9253(7)	11.1557(7)	8.917(1)	7.4777(7)
c (Å)	10.6931(5)	13.3455(7)	13.3566(5)	13.297(1)	13.191(1)	9.743(2)	17.582(2)
α (deg)	90	90	90	90	90	76.161(4)	90
β (deg)	90	43.615(2)	43.306(1)	43.384(2)	44.373(2)	85.579(3)	35.096(4)
α (deg)	90	90	90	90	90	87.805(5)	90
V ($Å^3$)	4624.7(3)	1360.9(2)	1331.62(7)	1332.1(2)	1315.2(2)	632.1(1)	1330.6(3)
Z	16	2	2	2	2	1	2
D_{calc} ($g\ cm^{-3}$)	1.282	1.526	1.570	1.569	1.601	1.503	1.672
unique data for refinement	2656	3087	3032	2815	2803	2487	2893
μ (Mo Kα) (mm^{-1})	0.093	0.557	0.718	0.802	0.905	0.777	3.874
$R(F)^a$ ($I > 2\sigma(I)$)	0.0402	0.0546	0.0671	0.0624	0.0633	0.0531	0.0673
$R_w(F^2)^b$ (all data)	0.0874	0.1388	0.1797	0.1659	0.2061	0.1466	0.1913

[a] $R = \sum||F_o| - |F_c||/\sum|F_o|$. [b] $R_w = [\sum w(F_o^2 - F_c^2)^2/\sum w(F_o^2)^2]^{1/2}$.

Table 2. Selected Bond Lengths (Å), Bond Angles (deg), and Dihedral Angles (deg) for $[M(4ImNNH)_2(NO_3)_2]$ (M = Mn (**1**), Co (**2**), Ni (**3**), Cu (**4**))

M	Mn	Co	Ni	Cu
M1−O1	2.132(1)	2.035(2)	2.038(2)	1.986(3)
M1−N1	2.167(2)	2.063(3)	2.020(3)	1.948(3)
M1−O3	2.240(1)	2.159(2)	2.129(2)	2.473(2)
O1−N3	1.293(2)	1.304(3)	1.302(3)	1.302(4)
O2−N4	1.276(2)	1.273(3)	1.271(4)	1.278(4)
N1−C2	1.389(3)	1.393(4)	1.384(4)	1.396(4)
N3−C4	1.350(3)	1.328(4)	1.331(4)	1.328(5)
N4−C4	1.355(3)	1.358(4)	1.361(4)	1.351(4)
C2−C4	1.438(3)	1.437(4)	1.436(5)	1.438(5)
O1−M1−O3	94.77(5)	94.04(7)	95.37(9)	92.50(9)
O1−M1−N1	85.11(6)	89.26(9)	89.4(1)	88.1(1)
O3−M1−N1	88.15(6)	87.38(8)	89.4(1)	90.0(1)
M1−O1−N3	127.8(1)	126.1(2)	125.6(2)	124.7(2)
M1−O3−N5	120.4(1)	121.9(2)	123.8(2)	115.2(2)
M1−N1−C2	126.9(1)	126.1(2)	126.4(2)	126.7(3)
O3−M1−O1−N3	68.6(1)	72.7(2)	83.2(2)	77.1(2)
O3−M1−N1−C2	−84.3(1)	−87.4(2)	−93.6(2)	−88.5(2)
M1−O1−N3−C4	18.6(2)	15.7(3)	6.3(4)	15.6(4)
M1−N1−C2−C4	−1.3(2)	1.1(3)	3.0(4)	3.6(4)
N1−C2−C4−N3	−7.3(3)	−5.8(4)	−5.5(5)	−5.7(5)

intermolecular manner; the intermolecular $H3_{ImH}\cdots O1_{NN}'$ and $H3_{ImH}\cdots N1_{ImH}'$ distances are 2.24(1) and 2.06(1) Å, respectively, which are much shorter than the sum of the van der Waals radii (2.7 Å),[16] where the symmetry operation code for ′ is $^3/_4 - y, -^3/_4 + x, ^1/_4 + z$. This finding suggests the potential ability of acidic H3 to form H-bonds when 4ImNNH is incorporated in coordination compounds. The strongly directive nature of the branching H-bond near a right angle leads to a 4_1 helix structure in an $I4_1/a$ space group. The purity of 4ImNNH was confirmed by the Curie−Weiss analysis ($\chi_{mol} = C/(T - \theta)$) of the magnetic susceptibility, giving $C = 0.370\ cm^3\ K\ mol^{-1}$ ($0.375\ cm^3\ K\ mol^{-1}$ in theory) with $\theta = -0.52$ K.

(16) Bondi, A. *J. Phys. Chem.* **1964**, *68*, 441.

Table 3. Intermolecular Atomic Distances (Å) for $[M(4ImNNH)_2(NO_3)_2]$ (M = Mn (**1**), Co (**2**), Ni (**3**), Cu (**4**))[a]

M	Mn	Co	Ni	Cu
C1···O2#	2.986(3)	2.948(4)	2.939(4)	2.948(5)
N2···O2#	3.382(3)	3.291(3)	3.245(4)	3.281(4)
H1···O2#	2.38(2)	2.41(3)	2.36(4)	2.45(5)
H3···O2#	3.15(3)	3.13(4)	3.32(9)	3.12(5)
O3···C3#	3.287(3)	3.311(4)	3.239(4)	3.186(5)
O3···N2#	3.093(3)	3.146(4)	3.103(4)	3.067(4)
O3···H2#	2.85(3)	2.86(4)	2.72(4)	2.58(4)
O3···H3#	2.54(3)	2.49(4)	2.15(9)	2.45(5)
O4···N2#	2.823(2)	2.797(3)	2.801(4)	2.741(4)
O4···H3#	2.00(3)	1.93(4)	1.67(8)	1.68(6)

[a] Symmetry operation code for # is $^3/_2 - x, -^1/_2 + y, -z + 1$.

X-ray Crystal Structure Analysis of $[M(4ImNNH)_2X_2]$. Table 1 shows the cell parameters of **1**−**4**. Their crystal structures are practically identical, belonging to a monoclinic space group $P2_1/a$. Figure 2a shows the molecular structure of **1** (for those of **2**−**4**, see Figure S2, Supporting Information). Half of the molecule is crystallographically independent; the octahedral M ion resides at an inversion center. The metal ion is coordinated by two NN oxygen atoms and two imidazole nitrogen atoms from the equatorial positions. The axial positions are occupied by nitrate oxygen atoms. Table 2 summarizes the selected bond lengths and angles. The octahedrons are elongated by ca. 0.1 Å for **1**−**3** and 0.5 Å for **4**. The axial directions are slightly deviated from the normal of the equatorial plane, as indicated by the O1−M1−O3 and O3−M1−N1 angles ranging from 94.04(7) to 95.37(9)° and 87.38(8) to 89.4(1)°, respectively,

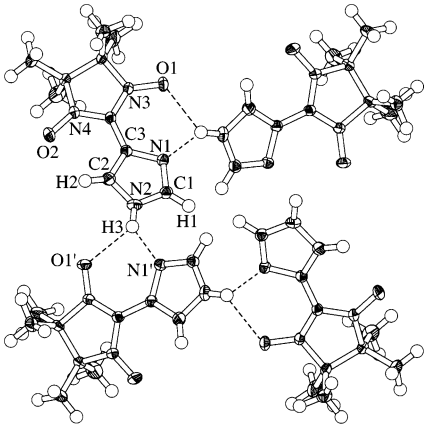

Figure 1. Ortep drawing of four 4ImNNH molecules at the 50% probability level. They form a 4_1 helix along the *c* axis. Intermolecular hydrogen bonds are indicated with dotted lines. The distances are 2.24(1) Å for $H3_{ImH}\cdots O1_{NN}'$ and 2.06(1) Å for $H3_{ImH}\cdots N1_{ImH}'$. The symmetry operation code for ′ is $^3/_4 - y$, $-^3/_4 + x$, $^1/_4 + z$.

for **1**−**3**. For **4**, these angles were nearly orthogonal (92.50(9) and 90.0(1)°, respectively).

The six-membered chelate rings are slightly deviated from an ideal plane, as indicated by the torsion angle around M1−O1−N3−C4, M1−N1−C2−C4, and N1−C2−C4−N3. Interestingly, the torsion angle around M1−O1−N3−C4 drastically decreases in the order of Mn, Co, and Ni, which seems to be related to the bond lengths of M−O and M−N and also to the deformation from an ideal octahedron. The shorter bond lengths bring about smaller and less distorted six-membered rings, and accordingly the chelate ring in **3** is highly planar with negligible torsion. On the other hand, the torsion angle around M1−O1−N3−C4 in **4** is much larger than that in **3**. The steric congestion of the chelate ring may increase possibly because of too short equatorial M−O and M−N bonds. The torsion around M1−O1−N3−C4 is most important for magnetic coupling between the M spin and the NN radical spin, especially for M = Ni and Cu, from the viewpoint of the overlap between two magnetic orbitals (see below).

Intermolecular H-bonds are found in the crystals of **1**−**4**. Figure 2b shows the molecular arrangement of **1**. The NH group in the imidazole ring plays a key role: this hydrogen atom (H3) is located considerably close to nitrate oxygen atoms in a neighboring molecule as indicated by d_1 ($O4_{nitrate}\cdots H3_{ImH}$#) and d_2 ($O3_{nitrate}\cdots H3_{ImH}$#) in Figure 2b and also slightly close to a nitroxide oxygen atom with the $H3_{ImH}\cdots O2_{NN}$# distance of 3.15(3) Å (the symmetry operation code for # is $^3/_2 - x$, $y - {}^1/_2$, $-z + 1$). In the latter geometry a very short C−H···O contact is also found between H1 and $O2_{NN}$# (d_3 in Figure 2b), which is shorter than the sum of the van der Waals radii (2.7 Å).[16] As Figure 2b shows, there are two strands between the H-donor/acceptor and H-acceptor/donor sites in each neighboring pair. This geometry successively repeats along the $a + b$ and $a - b$ directions, owing to the symmetry, and accordingly they form a two-dimensional H-bond network parallel to the *ab* plane (Figure 2c). A detailed description on the structure of **3** has been reported elsewhere.[11] The multiple and self-

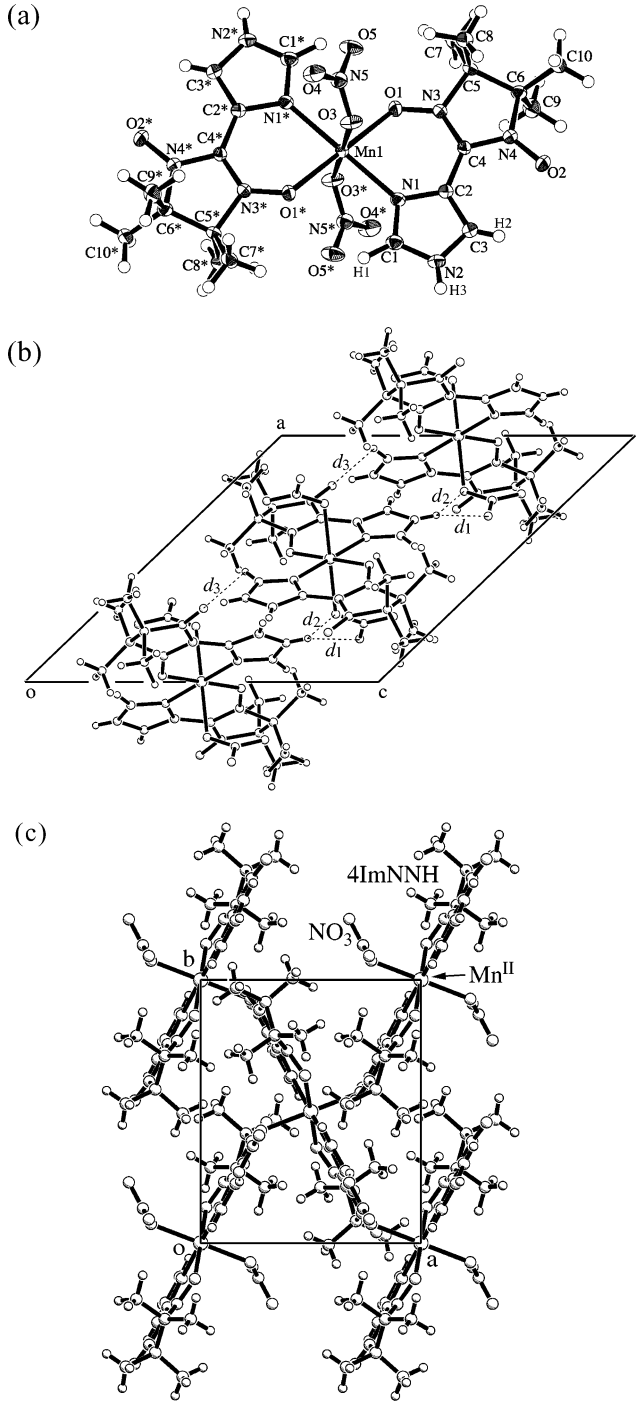

Figure 2. (a) Ortep drawing of the molecular structure of [Mn(4ImNNH)$_2$(NO$_3$)$_2$] (**1**) at the 50% probability level. Atomic numbering is also shown. The symmetry operation code for * is $1 - x$, $1 - y$, $1 - z$. (b) Molecular arrangement in the crystal of **1** viewed along the *b* axis. Intermolecular hydrogen bonds are indicated with dotted lines. The distances are as follows: d_1($O4_{nitrate}\cdots H3_{ImH}$#) = 2.00(3) Å; d_2($O3_{nitrate}\cdots H3_{ImH}$#) = 2.54(3) Å; d_3($H1_{ImH}\cdots O2_{NN}$#) = 2.38(2) Å, where the symmetry operation code for # is $^3/_2 - x$, $-{}^1/_2 + y$, $1 - z$. (c) Molecular arrangement in the crystal of **1** viewed along the *c* axis.

complementary H-bonds stabilize the side-by-side molecular arrangement,[17] and therefore **1**−**4** are assumed to afford isomorphous crystals. The interatomic distances are summarized in Table 3.

(17) For example, Zeng, H.; Yang, X.; Brown, A. L.; Martinovic, S.; Smith, R. D.; Gong, B. *Chem. Commun.* **2003**, 1556.

Table 4. Selected Bond Lengths (Å), Bond Angles (deg), and Dihedral Angles (deg) for $[Mn(4ImNNH)_2Cl_2]$ (**5**) and $[Cu(4ImNNH)_2Br_2]$ (**12**)

compound	**5** (M = Mn, X = Cl)	**12** (M = Cu, X = Br)
M1−O1	2.168(2)	2.032(3)
M1−N1	2.193(2)	1.934(4)
M1−X1	2.5425(6)	3.0058(5)
O1−N3	1.300(3)	1.302(5)
O2−N4	1.281(3)	1.275(6)
N1−C2	1.314(4)	1.376(6)
N3−C4	1.343(4)	1.336(7)
N4−C4	1.355(4)	1.344(6)
C2−C4	1.428(4)	1.426(6)
O1−M1−X1	92.46(5)	96.98(9)
O1−M1−N1	82.81(8)	89.7(2)
X1−M1−N1	89.50(6)	88.67(9)
M1−O1−N3	118.0(2)	119.4(3)
M1−N1−C2	123.1(2)	124.2(3)
X1−M1−O1−N3	136.0(2)	127.2(3)
X1−M1−N1−C2	−123.9(2)	−122.0(4)
M1−O1−N3−C4	−44.2(3)	−34.4(6)
M1−N1−C2−C4	9.4(3)	5.7(6)
N1−C2−C4−N3	14.6(4)	13.0(7)

We also prepared $[M(4ImNNH)_2X_2]$ complexes from metal chlorides and bromides to search for ferromagnetic systems. Elemental analysis clarified the stoicheometry of all of the complexes as $[M(4ImNNH)_2X_2]$. Only two of them could afford good crystals suitable for X-ray crystallographic analysis. The molecular structures of $[Mn(4ImNNH)_2Cl_2]$ (**5**) (Figure S3a, Supporting Information) is similar to those of **1**−**4** except for the axial ligands; the metal ion resides at the crystal inversion center and two 4ImNNH ligands occupy at the equatorial positions. Selected geometrical parameters are listed in Table 4. Although **1** and **5** possess different molecular packing, as indicated by the crystal systems and space groups ($P2_1/a$ and $P\bar{1}$ for **1** and **5**, respectively), intermolecular H-bonding is also formed in $Cl1\cdots H3_{ImH}{}^{\dagger}$ for **5** (Figure 3a), like $H_{ImH}\cdots O_{nitrate}$ in **1**. The $Cl1\cdots H3_{ImH}{}^{\dagger}$ distance was 2.16(4) Å, which is much shorter than the sum of the van der Waals radii (2.95 Å).[16] The nearest neighboring molecules of **5** are related by the *a*-axis translation and connected with two H-bonds of a H-donor/acceptor and H-acceptor/donor pair. The double H···Cl H-bonds successively repeat along the *a* axis, thus constructing a H-bonding ladder structure.

X-ray crystal structure analysis on $[Cu(4ImNNH)_2Br_2]$ (**12**) was also successful. The molecular structure of **12** (Figure S3, Supporting Information) is similar to that of **5** expected for the axial ligand. Owing to the elongated distortion from an octahedron and to the large covalent radius of Br, the Cu−Br bond length of 3.0058(5) Å is extremely long (Table 4), leading to a different molecular packing and space group ($P2/c$) compared with **5** and the nitrate compounds. The important torsion angle around M1−O1−N3−C4 in **12** is much larger than those in **3** and **4**. Despite the different space group, a similar intermolecular H-bond could also be found in the crystal of **12** (Figure 3b). The $Br1\cdots H3_{ImH}{}^{\ddagger}$ distance (2.41(6) Å) is much shorter than the sum of the van der Waals radii (3.05 Å).[16] The nearest neighboring molecules of **12** are related to the *b*-axis translation. The H···Br H-bonds repeat along the *b* axis, giving a H-bond ladder structure like **5**.

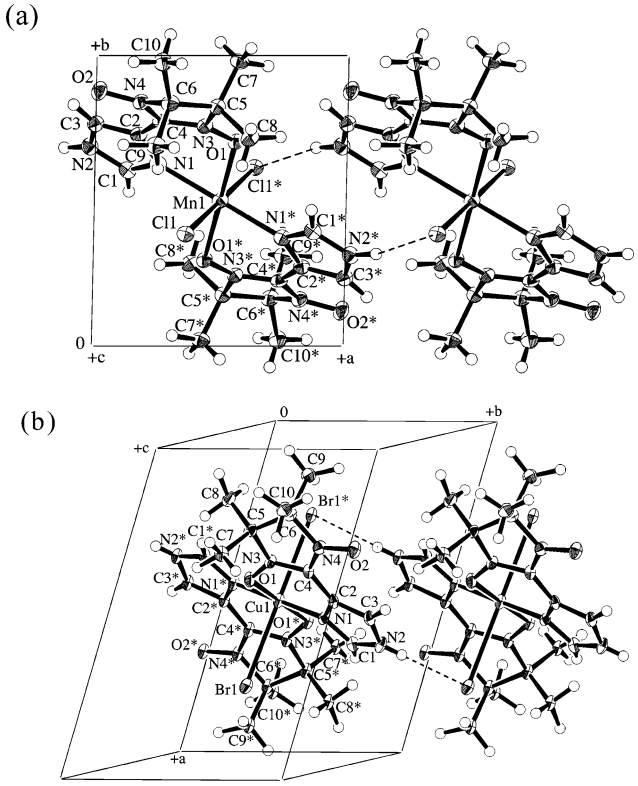

Figure 3. (a) Molecular arrangement in the crystals of **5** viewed along the *c* axis. Intermolecular hydrogen bonds are indicated with dotted lines. The distance is $d(Cl1\cdots H3_{ImH}{}^{\dagger}) = 2.16(4)$ Å. The symmetry operation codes for * and † are $1-x, 1-y, 1-z$ and $-1+x, y, z$, respectively. (b) Molecular arrangement in the crystals of **12**. Intermolecular hydrogen bonds are indicated with dotted lines. The distance is $d(Br1\cdots H3_{ImH}{}^{\ddagger}) = 2.41(5)$ Å. The symmetry operation codes for * and ‡ are $1-x, 1-y, 1-z$ and $x, 1+y, z$, respectively.

The cystal structures determined here on the $[M(4ImNNH)_2X_2]$-type complexes always have the intermolecular H-bonds of H(imidazole)···X(axial ligand)−M, regardless of the various space groups. The two-dimensional networks are found in the nitrate complexes (**1**−**4**) and the one-dimensional ladder in the halide complexes (**5** and **12**).

Magnetic Properties of $[M(4ImNNH)_2X_2]$. Figure 4a shows the temperature dependence of the $\chi_{mol}T$ values for **1**−**4** measured at 5 kOe. The $\chi_{mol}T$ value of **1** decreases with decreasing temperature down to ca. 20 K, indicating the presence of antiferromagnetic coupling. The observed $\chi_{mol}T$ value of 3.16 cm^3 K mol^{-1} at 300 K is much smaller than the theoretical spin-only value of 5.1 cm^3 K mol^{-1}. The plateau around 30 K has 1.80 cm^3 K mol^{-1}, which corresponds to the spin-only value 1.88 cm^3 K mol^{-1} with $S_{total} = {}^3/_2$. Thus, the decrease of $\chi_{mol}T$ can be ascribed to considerably strong intramolecular antiferromagnetic (ferrimagnetic) coupling through the direct manganese−radical bonds. Below 20 K, the $\chi_{mol}T$ value of **1** turns to increase on cooling. This behavior is ascribed to intermolecular ferromagnetic interaction.

The $\chi_{mol}T$ value for **2** behaves similar to that of **1**. With decreasing temperature the $\chi_{mol}T$ value of **2** once decreases and increases very slightly below 4 K, indicating intermolecular ferromagnetic coupling among the ferrimagnetically correlated radical−cobat(II)−radical molecules with $S_{total} =$

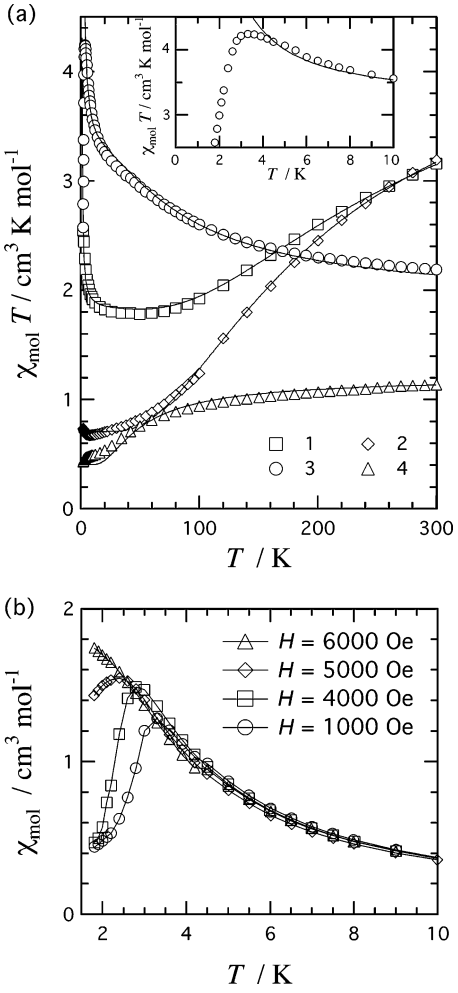

Figure 4. (a) Temperature dependence of the $\chi_{mol}T$ values for [M(4ImNNH)$_2$(NO$_3$)$_2$] (M = Mn (**1**), Co (**2**), Ni (**3**), Cu(**4**)) measured at 5 kOe. Solid lines represent the calculated values. For the equations and parameters, see the text and Table 5. Inset: magnification of a low-temperature region for **3**. (b) Temperature dependence of χ_{mol} (or M/H in an ordered state) for **3** measured at 1, 4, 5, and 6 kOe. Solid lines are shown for a guide to the eye.

$^1/_2$. We have to take into account the contribution of angular momentum for the cobalt(II) complex and the van Vleck treatment may give only approximate results, while manganese(II), nickel(II), and copper(II) ions usually have negligible contribution of angular momentum. However, the optimized result well-reproduced the experimental data (the solid lines in Figure 4a), which supports the belief that the temperature dependence of the $\chi_{mol}T$ value is reasonably ascribed mainly to the magnetic exchange coupling. The $\chi_{mol}T$ value for **4** shows monotonic decrease, suggesting that intramolecular magnetic coupling is antiferromagnetic. The $\chi_{mol}T$ value around 10 K agrees with $S_{total} = {}^1/_2$.

On the other hand, the $\chi_{mol}T$ value of **3** increases with decreasing temperature. The observed $\chi_{mol}T$ value around a bend at 14 K is 3.3 cm^3 K mol^{-1}, which is slightly larger than the spin-only value 3.0 cm^3 K mol^{-1} for $S_{total} = 2$. The secondary sharp increase below 14 K is due to intermolecular ferromagnetic interaction. Therefore, both intra- and intermolecular magnetic couplings are ferromagnetic. An abrupt drop was observed at 4 K, suggesting that magnetic phase transition takes place near the peaking temperature. We measured the field dependence of the peaking behavior of **3** (Figure 4b). The χ_{mol} peaks were found at 3.3, 2.8, and 2.4 K when the external fields of 1, 4, and 5 kOe were applied, respectively, and finally the peak vanished at 6 kOe. This finding suggests that the ground state of **3** is antiferromagnetic, despite the presence of both ferromagnetic intra- and intermolecular interactions.

The molecular structures of **1**−**4** are regarded as a linear radical−metal−radical triad system, and the $\chi_{mol}T$ values are quantitatively analyzed according to the spin exchange Hamiltonian $H = -2J(S_1 \cdot S_2 + S_2 \cdot S_3)$ based on the molecular symmetry; the suffixes 1 and 3 denote NN and 2 denotes metal spins. The van Vleck treatment gave the following expressions (eqs 1−4)[18] for **1**−**4**, respectively. The Weiss temperature is introduced for intermolecular magnetic interaction. The optimized parameters are summarized in Table 5. The calculated curves are superposed on the data points in Figure 4a, and the fittings are satisfactory. This fact supports the reliability of the spin−spin coupling model, although there is possibility of the presence of zero-field splitting or other origins of single ions for **1**−**3**.

$$\chi_{mol} = \frac{N_A g^2 \mu_B}{4k(T-\theta)} \frac{10\exp(-7J/kT) + 35\exp(-2J/kT) + 35 + 84\exp(5J/kT)}{2\exp(-7J/kT) + 3\exp(-2J/kT) + 3 + 4\exp(5J/kT)} \quad (1)$$

$$\chi_{mol} = \frac{N_A g^2 \mu_B}{4k(T-\theta)} \frac{\exp(-5J/kT) + 10\exp(-2J/kT) + 10 + 35\exp(3J/kT)}{\exp(-5J/kT) + 2\exp(-2J/kT) + 2 + 3\exp(3J/kT)} \quad (2)$$

$$\chi_{mol} = \frac{2N_A g^2 \mu_B}{k(T-\theta)} \frac{\exp(-2J/kT) + 1 + 5\exp(2J/kT)}{\exp(-4J/kT) + 3\exp(-2J/kT) + 3 + 5\exp(2J/kT)} \quad (3)$$

$$\chi_{mol} = \frac{N_A g^2 \mu_B}{2k(T-\theta)} \frac{\exp(-2J/kT) + 1 + 10\exp(J/kT)}{2\exp(-2J/kT) + 2 + 4\exp(J/kT)} \quad (4)$$

The intermolecular ferromagnetic interaction was finally confirmed by the $M-H$ curves (magnetization curves as a function of applied magnetic field). Figure 5 shows the $M-H$ curves of **1** measured at 1.8 and 3.5 K. The observed magnetization at 3.5 K rapidly increased over the theoretical Brillouin function of $S_{total} = {}^3/_2$ and the saturation was more significant at 1.8 K, clearly indicating the presence of intermolecular ferromagnetic interaction. Unfortunately, compound **1** did not undergo any magnetic phase transition down to 1.8 K. Note that the saturation magnetization of 1.52×10^4 erg Oe^{-1} mol^{-1} at 70 kOe corresponds to the antiferromagnetically correlated radical−metal−radical system of $S_{total} = {}^3/_2$, in sharp contrast to that of **3** owing to the intramolecular ferromagnetic correlation (see below).

(18) Gruber, S. J.; Harris, C. M.; Sinn, E. *J. Chem. Phys.* **1968**, *49*, 2183.

Table 5. Optimized Parameters g, J/k_B, and θ of $[M(4ImNNH)_2X_2]$ (M = Mn, Co, Ni, Cu; X = NO_3, Cl, Br)[a]

X	M	g	$2Jk_B^{-1}$/K	θ/K
NO_3	Mn (**1**)	1.96(1)	−140(3)	0.58(2)
	Co (**2**)	2.75(1)	−155(2)	0[b,c]
	Ni (**3**)	2.06(1)	85(3)	1.04(3)
	Cu (**4**)	2.08(1)	−58(4)	0[b]
Cl	Mn (**5**)	2.01(1)	−175(2)	0.52(1)
	Co (**6**)	2.69(2)	−270(4)	0.11(6)
	Ni (**7**)	2.22(1)	−201(2)	0[b]
	Cu (**8**)	2.11(1)	−247(7)	−2.7(2)
Br	Mn (**9**)	1.95(1)	−156(2)	0.24(1)
	Co (**10**)	2.57(1)	−238(2)	0[b]
	Ni (**11**)	2.28(4)	−165(2)	0[b]
	Cu (**12**)	2.05(1)	−372(5)	1.69(7)

[a] The Heisenberg spin Hamiltonian is defined as $H = -2J(S_1 \cdot S_2 + S_2 \cdot S_3)$. [b] The Weiss temperature is not included in the parameter optimization.[c] A very small positive θ is assumed.

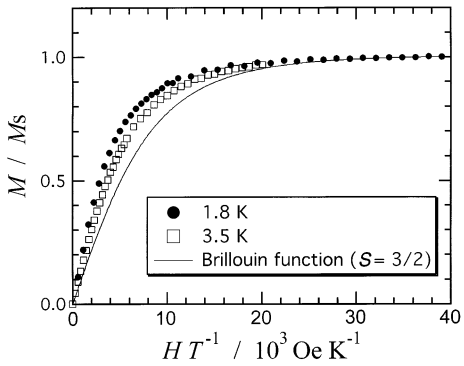

Figure 5. $M-H$ curves of $[Mn(4ImNNH)_2(NO_3)_2]$ (**1**) measured at 1.8 and 3.5 K. A solid line represents the theoretical Brillouin function of $S = {}^3/_2$.

To elucidate the magnetic ground state of **3**, we measured the $M-H$ curve of **3** at 1.8 K. As Figure 6a shows, the ground state is antiferromagnetic and a metamagnetic transition occurs near 5.5 kOe with a very small hysteresis during the metamagnetic transition. The critical field determined here is consistent with the disappearance of the χ_{mol} peak on applying the field as shown in Figure 4b. The metamagnetism implies the simultaneous presence of intermolecular ferro- and antiferromagnetic interactions. The temperature dependence of χ_{mol} for **3** reveals two main ferromagnetic exchange couplings ascribable to intra- and intermolecular interactions. This finding indicates that an additional weak antiferromagnetic interaction is operative in the crystal of **3**. The saturation magnetization was ca. 2.0×10^4 erg Oe^{-1} mol^{-1}, in good agreement with the ground $S_{total} = 2$ species where all spins are ferromagnetically correlated. The transition temperature (T_N) was determined by means of the field-cooled magnetization measurements at 5 Oe (Figure 6b). A sharp peak was found at 3.4 K, which we define as the magnetic phase transition temperature.

The magnetic susceptibilities of **5**−**12** were measured (Figure 7) and analyzed using eqs 1−4. The optimized parameters are summarized in Table 5, which clearly shows that all of them exhibited intramolecular antiferomagnetic coupling and that four complexes (**5**, **6**, **9**, and **12**) exhibited intermolecular ferromagnetic coupling. The calculated curves reproduce well the experimental data, supporting the proposed molecular structure of radical−metal−radical systems.

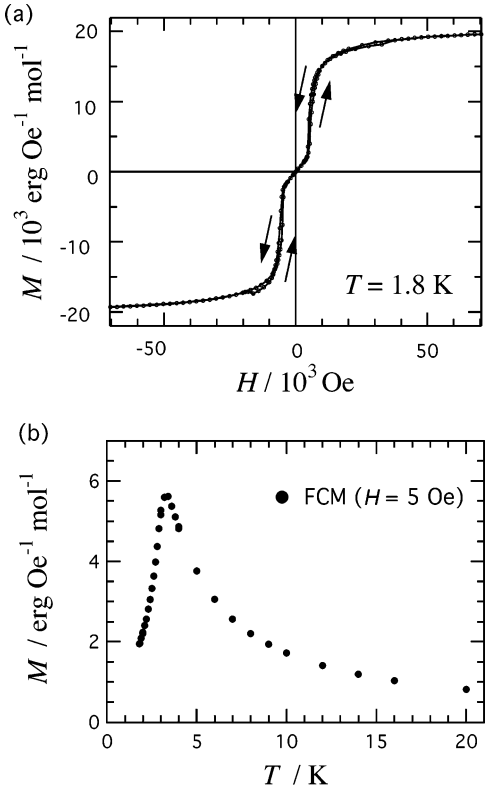

Figure 6. (a) $M-H$ curve of $[Ni(4ImNNH)_2(NO_3)_2]$ (**3**) measured at 1.8 K. Solid lines are drawn for a guide to the eye. (b) Field-cooled magnetization of **3** measured at 5 Oe.

Their field-cooled magnetization measurements revealed that they underwent no magnetic phase transition above 1.8 K.

Discussion

Intramolecular Ferromagnetic Coupling. The electron configurations of the high-spin Mn^{II} and Co^{II} ions are $(t_{2g})^3(e_g)^2$ and $(t_{2g})^5(e_g)^2$, respectively, and therefore the intramolecular antiferromagnetic couplings between the magnetic t_{2g} spins and the nitroxide π^* spin are explained in terms of the $d\pi-p\pi$ orbital overlap, which dominantly contributes to the total magnetic interaction observed, compared with minor $d\sigma-p\pi$ contribution. On the other hand, Ni^{II} and Cu^{II} ions have only e_g spins, that is, $d\sigma$ spins, and the magnetic coupling may be ferromagnetic depending largely on the coordination geometry.

When TEMPO and PROXYL radicals are available, the magnetic interactions between copper(II) and equatorially coordinated nitroxide radicals are usually observed to be antiferromagnetic[19] (TEMPO = 2,2,6,6-tetramethylpiperidin-1-yloxyl, PROXYL = 2,2,4,4-tetramethylpyrrolidin-1-yloxyl). However, Luneau and co-workers reported pioneering works on the ferromagnetic interaction between metal and radical spins in $[M(hfac)_2(2PyIN)]$ (M = Ni, Cu; hfac = 1,1,1,5,5,5-hexafluoropentane-2,4-dionate) where IN denotes the imino nitroxide radical (Chart 2).[20] It has been established that the ferromagnetic coupling is caused by the strict

(19) Dickman, M. H.; Doedens, R. J. *Inorg. Chem.* **1981**, *20*, 2677. Porter, L. C.; Dickmann, M. H.; Doedens, R. J. *Inorg. Chem.* **1983**, *22*, 1962. Porter, L. C.; Doedens, R. J. *Inorg. Chem.* **1985**, *24*, 1006. Lim, Y. Y.; Drago, R. S. *Inorg. Chem.* **1972**, *11*, 1334.

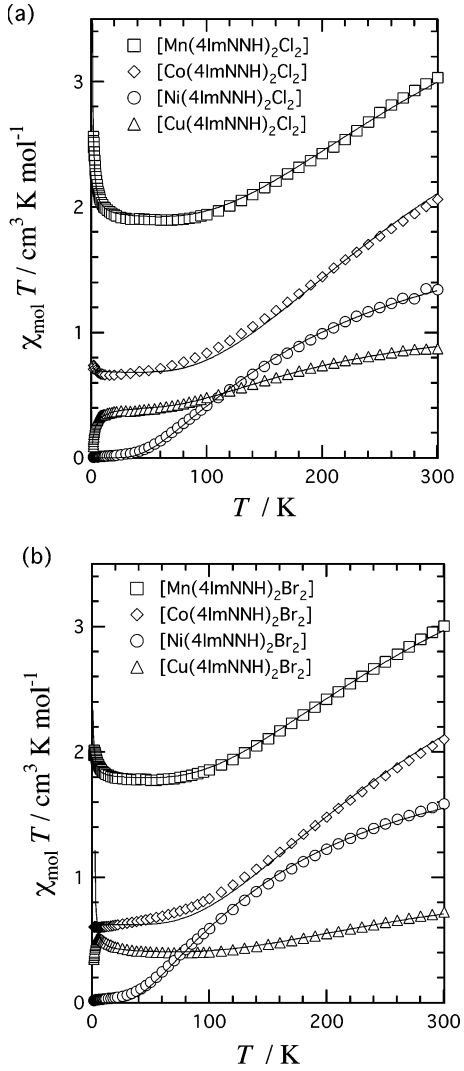

Figure 7. Temperature dependence of the $\chi_{mol}T$ values for [M(4ImNNH)$_2$X$_2$] (M = Mn, Co, Ni, Cu; X = Cl (a), Br (b)) measured at 5 kOe. Solid lines represent the calculated values. For the equations and parameters, see the text and Table 5.

Chart 2

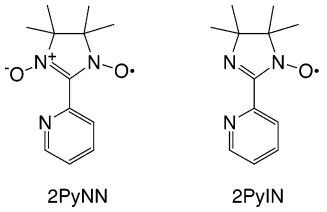

orthogonality between the metal dσ and radical π* spins as described in Figure 8a when radical chelate ligands, such as 2PyIN[20] and *o*-semiquinones,[21] are coordinated at the equatorial positions. Kaizaki and co-workers also supported the above mechanism from the study on [NiCl$_2$(2PyIN)$_2$].[22] The highly planar five-membered chelate ring plays a very important role in the ferromagnetic interactions. On the other hand, in the case of the corresponding 2PyNN derivative, the intramolecular coupling in [Cu(ClO$_4$)$_2$(2PyNN)] was antiferromagnetic.[23] The reason arises from a severe nonplanar distortion[24] to lose the orthogonality (Figure 8b) like the TEMPO and PROXYL cases.[19] Therefore, in contrast to the literature results, **3** having six-membered chelate rings showed exceptionally intramolecular ferromagnetic interaction. As the X-ray diffraction study of **3** reveals, the chelate ring is highly planar, owing to the advantage of the imidazole ring used. Namely, the imidazole ring is less bulky than the pyridine ring so that the bent chelate structure can be spread to recover a plane.

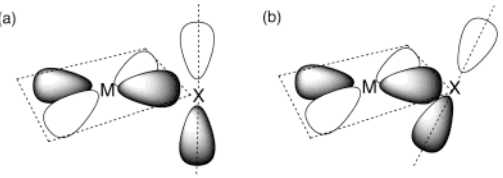

Figure 8. Schematic drawings of mutual geometries between magnetic dσ(metal) and pπ*(O in nitronyl nitroxide, N in imino nitroxide) orbitals for nickel(II) and copper(II) complexes coordinated by nitronyl nitoxide or imino nitroxide from equatorial positions. (a) A strictly orthogonal case. (b) An overlapped case.

The considerably large ferromagnetic interactions were found in the semiquinone complexes containing copper(II) ($2J/hc = 220$ cm^{-1}) and nickel(II) ($2J/hc > 400$ cm^{-1}).[21] In the 2PyIN complexes, fairly large ferromagnetic interactions were observed as well; $2J/hc > 300$ cm^{-1} for the copper(II) complex and 94 cm^{-1} for the nickel(II) one.[7] The magnetic couplings due to the direct equatorial coordination of the radical center are usually very large, but the present value of **3** is only moderate (85(3) K corresponds to 60(2) cm^{-1}). Antiferromagnetic contribution due to orbital overlap seems to cancel out partly the large ferromagnetic coupling. In view of the fact that there has been found only one case showing intramolecular ferromagnetic interaction among six dσ complexes [M(4ImNNH)$_2$X$_2$] (M = Ni, Cu; X = NO$_3$, Cl, Br), the present dσ complexes seem to lie on the border between the orthogonal and overlapped cases (Figure 8) in connection with nonplanar distortion of the chlate rings.

Complexes **4** and **12** having copper ions showed intramolecular antiferromagnetic interactions and the magnitude of the magnetic coupling in **12** ($2J/k_B = -372(5)$ K) is much larger than that of **4** (−58(4) K; Table 5). The antiferromagnetic contribution is supposed to increase with an increase of the M1−O1−N3−C4 torsion angle. The larger Cu1−O1−N3−C4 torsion (−34.4(6)°) in **12** is responsible for the larger negative *J* value in comparison with the case of **4** (Tables 2 and 4).

Intermolecular Ferromagnetic Coupling. We have clearly demonstrated that **3** is a metamagnet below 3.4 K. The measurements of temperature dependence of χ_{mol} revealed

(20) Luneau, D.; Rey, P.; Laugier, J.; Fries, P.; Caneschi, A.; Gatteschi, D.; Sessoli, R. *J. Am. Chem. Soc.* **1991**, *113*, 1245. Luneau, D.; Rey, P.; Laugier, J.; Belorizky, E.; Conge, A. *Inorg. Chem.* **1992**, *31*, 3578.
(21) Kahn, O.; Prins, R.; Reedijk, J.; Thompson, J. S. *Inorg. Chem.* **1987**, *26*, 3557. Benelli, C.; Dei. A.; Gatteschi, D.; Pardi, L. *Inorg. Chem.* **1988**, *27*, 2831.
(22) Yamamoto, Y.; Suzuki, T.; Kaizaki, S. *J. Chem. Soc., Dalton Trans.* **2001**, 1566.
(23) Yoshioka, N.; Irisawa, M.; Abe, M.; Aoki, T.; Aizawa, N.; Inoue, H. *Mol. Cryst. Liq. Cryst.* **1997**, *306*, 397.
(24) Luneau, D.; Risoan, G.; Rey, P.; Grand, A.; Caneschi, A.; Gatteschi, D.; Laugier, J. *Inorg. Chem.* **1993**, *32*, 5616. Lewis, G. R.; Blake, A. J. *Acta Crystallogr. C*, **2002**, *58*, m398.

the presence of ferromagnetic intra- and intermolecular interactions. We assume that there is a secondary weak intermolecular interaction which would be antiferromagnetic, while the major intermolecular interaction is ferromagnetic. The metamagnetic structure may be described as interchain antiferromagnetic coupling among ferromagnetically correlated chains[25,26] or as intersheet antiferromagnetic coupling among ferromagnetically correlated sheets.[27,28] As the X-ray crystallographic analysis revealed, the H-bonds are found in two directions, $a + b$ and $a - b$, forming a two-dimensional network (Figure 2b). We have to think that the interaction of the sheet structure parallel to the *ab* plane (J_{ab}) is ferromagnetic and that the intersheet interaction (J_c) is antiferromagnetic. The J_c is very small and origins of J_c can hardly be discussed, but mechanisms of J_{ab} are worth being discussed based on the structure determined.

The spin-polarization mechanism[29] may be operative in pathways through the contacts O2···H1# and O2···H3#, namely, N3#(↑)−C4#(↓)−C2#(↑)−C3#(↓)−N2#(↑)−H3#(↓)···O2(↑) or N3#(↑)−C4#(↓)−C2#(↑)−N1#(↓)−C1#(↑)−H1#(↓)···O2(↑). However, it has not been established whether the spin polarization originally developed on alternant hydrocarbons can be applied to heteroaromatic and five-membered imidazole rings, although the magnetic couplings through thiophene,[30] pyridine,[31] and phenol[5] groups were interpreted in terms of the spin polarization. A superexchange interaction along Ni−imidazole···O2# is also taken into consideration. Another possible explanation is as follows. The singly occupied molecular orbital (SOMO) is highly localized at the N−O group in NN compounds while the next highest occupied molecular orbital (NHOMO) is delocalized over the whole molecule, as confirmed by the UHF/PM3 calculation[32] using the determined geometry from the ligand portion in **3**. Awaga and co-workers proposed[33] that the ferromagnetic intermolecular exchange interaction in *β*-*p*-nitrophenyl NN was brought about from the conditions that intermolecular SOMO−SOMO overlap was negligible while SOMO−NHOMO overlap was substantial, which requires accordingly the proximity between the NN group and the *p*-nitrophenyl group in an adjacent molecule. This interpretation seems to hold for the present complexes (**1**−**4**). The NN group and imidazole ring are located closely and connected with the H-bonds, while the NN groups are apart from each other, thus leading to ferromagnetic coupling between the NN spins. It should be noted that these geometries can be realized by the H-bonds between the axial ligand and the imidazole NH proton in a side-by-side and head-to-tail manner.

The shortest interatomic distance is found between nitrate oxygen and imidazole hydrogen atoms. In contrast to the NN···imidazole contacts described above, the magnetic interaction through the nitrate···imidazole contacts seems to be very small because the contacting atoms carry only polarized spin density, which is supposed to be very small. McConnell proposed that the magnetic coupling is proportional to the product of the spin densities at contacting atoms ($H_{AB} = -S_A \cdot S_B \Sigma J_{ij} \rho_i^A \rho_j^B$).[34] Nevertheless, the H-bond character in the nitrate···imidazole contacts plays an important role in the molecular packing viewing from the extremely short interatomic distance.

The double H-bonds described as [−M−X(axial ligand)···H_{ImH}−]$_2$ for **5** and **12** (Figure 3) forms a macrocyclic structure which contains two imidazole rings. These imidazole rings are arranged in a parallel manner, owing to the symmetry. A mechanism for magnetic interaction in aromatic radicals was proposed by McConnell[34] and experimentally verified using a paracyclophane skeleton and a pancake-type aromatic dimer.[35] A through-space $\pi-\pi$ interaction between the imidazole rings may bring about magnetic interactions.

We found the intermolecular ferromagnetic interaction in the series of [M(4ImNNH)$_2$X$_2$] (M = Mn, Co, Ni, Cu; X = NO_3, Cl, Br) with high probability (7 cases out of 10 excluding **7** and **11** because of the diamagnetic ground states), as evidenced by the $\chi_{mol}T$ increase from the plateau defined by the ground state. The H-bonds in **1**−**4** are concluded to afford ferromagnetic couplings and those in **5**−**12** may also provide ferromagnetic exchange pathways. Crystal designs involving H-bonds seem very important for the development of molecule-based magnetic materials.

Summary

A new radical chelating ligand 4ImNNH and new complexes **1**−**12** were prepared. Magnetic measurements revealed that the NN and nickel(II) spins in **3** were ferromagnetically correlated with $2J/k_B = 85$ K. Furthermore, **3** underwent a magnetic phase transition to become an antiferromagnet below 3.4 K and also exhibited a metamagnetic transition on applying a magnetic field of 5.5 kOe at 1.8 K. The two-dimensional ferromagnetic network is assumed, which is accompanied by two-strand H-bonds at

(25) Miller, J. S.; Zhang, J. H.; Reiff, W. M.; Dixon, D. A.; Preston, L. D.; Reis, A. H., Jr.; Gebert, E.; Extine, M.; Troup, J.; Epstein, A. J.; Ward, M. D. *J. Phys. Chem.* **1987**, *91*, 4344. Reiff, W. M.; Wong, H.; Foner, S.; Frankel, R. B.; Long, G. J. *J. Chem. Phys.* **1978**, *68*, 4781.

(26) Ishida, T.; Tomioka, K.; Nogami, T.; Yoshikawa, H.; Yasui, M.; Iwasaki, F.; Iwamura, H.; Takeda, N.; Ishikawa, M. *Chem. Phys. Lett.* **1995**, *247*, 7.

(27) Rabu, P.; Rueff, J. M.; Huang, Z. L.; Angelov, S.; Souletie, J.; Drillon, M. *Polyhedron* **2001**, *20*, 1677. Sekine, T.; Okuno, T.; Awaga, K. *Inorg. Chem.* **1998**, *37*, 2129. Monfort, M.; Resino, I.; Ribas, J.; Stoeckli-Evans, H. *Angew. Chem., Int. Ed.* **2000**, *39*, 191. Usuki, N.; Ohba, M.; Okawa, H. *Bull. Chem. Soc. Jpn.* **2002**, *75*, 1693.

(28) Benoit, A.; Flouquet, J.; Gillon, B.; Schweizer, J. *J. Magn. Magn. Mater.* **1983**, *31*−*34*, 1115. Ishida, T.; Ohira, S.; Watanabe, I.; Nogami, T.; Nagamine, K. *Polyhedron* **2001**, *20*, 1551.

(29) Iwamura, H. *Adv. Phys. Org. Chem.* **1990**, *26*, 179. Rajca, A. *Chem. Rev.* **1994**, *94*, 871. Longuet-Higgins, J. C. *J. Chem. Phys.* **1950**, *18*, 265. Crayston, J. A.; Devine, J. N.; Walton, J. C. *Tetrahedron* **2000**, *56*, 7829.

(30) Akita, T.; Mazaki, Y.; Kobayashi, K.; Koga, N.; Iwamura, H. *J. Org. Chem.* **1995**, *60*, 2092.

(31) Kumada, H.; Sakane, A.; Koga, N.; Iwamura, H. *J. Chem. Soc., Dalton, Trans.* **2000**, 911. Kitano, M.; Ishimaru, Y.; Inoue, K.; Koga, N.; Iwamura, H. *Inorg. Chem.* **1994**, *33*, 6012. Ishimaru, Y.; Kitano, M.; Kumada, H.; Koga, N.; Iwamura, H. *Inorg. Chem.* **1998**, *37*, 2273.

(32) Stewart, J. J. P. MOPAC ver 6.0, *QCPE* #455.

(33) Awaga, K.; Inabe, T.; Maruyama, Y. *Chem. Phys. Lett.* **1992**, *190*, 349. Awaga, K. In *Magnetic Properties of Organic Materials*; Lahti, P. M., Ed.; Marcel Dekker: New York, 1999; Chapter 25, pp 519−534.

(34) McConnell, *J. Chem. Phys.* **1963**, *39*, 1910.

(35) Izuoka, A.; Murata, S.; Sugawara, T.; Iwamura, H. *J. Am. Chem. Soc.* **1985**, *107*, 1786. Imachi, R.; Ishida, T.; Suzuki, M.; Yasui, M.; Iwasaki, F.; Nogami, T. *Chem. Lett.* **1997**, 743.

the NN···imidazole contact and at the nitrate···imidazole contacts. Although both intra- and intermolecular magnetic exchange couplings are dominantly ferromagnetic for **3**, the magnetic ground state is concluded to be antiferromagnetic owing to antiferromagnetic coupling ascribable to the weak intersheet interaction. There are two categories of molecular-based magnets: ferrimagnets and ferromagnets. Rey and coworkers reported the ferrimagnets containing two-dimensional networks by use of the 2ImNN anion and manganese(II) ion.[10] We can propose a strategy toward *ferro*magnets containing an anionic 4ImNN and nickel(II) cation via the deprotonation process from **3** and, even when the 2ImNN anion or copper(II) ion is available, ferromagnets can also be expected because the chelate six-membered ring may favor a planar structure by using less bulky imidazole groups. Furthermore, the deprotonation will give rise to higher dimensionality due to the imidazolate bridges and magnetically dense systems because of the purge of bulky anions, probably leading to high ordering temperatures. Preparation of polymeric [M(4ImNN)$_2$] (M = Ni, Cu) solids as genuine ferromagnetic molecular materials is now underway.

Acknowledgment. This work was supported by a Grant-in-Aid for Scientific Research on Priority Areas of "Molecular Conductors and Magnets" (No. 730/11224204) and by a Grant-in-Aid for Scientific Research (No. 13640575), both from the Ministry of Education, Culture, Sports, Science and Technology, Japan.

Supporting Information Available: Crystallographic information files and ortep drawings of new compounds, 4ImNNH, **1**−**4**, **5**, and **12** and supplementary Figures S1−S3. This material is available free of charge via the Internet at http://pubs.acs.org.

IC0349048

ELSEVIER

Synthetic Metals 133–134 (2003) 581–583

SYNTHETIC METALS

www.elsevier.com/locate/synmet

Magnetic properties of 9,9-disubstituted 9,10-dihydroacridine-10-yloxyls☆

M. Seino, Y. Akui, T. Ishida*, T. Nogami

Department of Applied Physics and Chemistry, University of Electro-Communications, Chofu, Tokyo 182-8585, Japan

Abstract

Ferromagnetic intermolecular interactions were observed for 9-R-9-(pentadeuteriophenyl)-9,10-dihydroacridine-10-yloxyls (R = *n*-$C_{12}H_{25}$, *n*-$C_{13}H_{27}$). Superexchange-like interaction across the 9-phenyl ring is proposed, as illustrated by acridinoxyl ∥ phenyl ⊥ acridinoxyl, where the symbols ∥ and ⊥ denote the presence and absence of orbital overlaps, respectively.

Keywords: Free radicals; Nitroxides; Aminoxyls; Acridine; Ferromagnetic interaction

1. Introduction

We have reported organic ferro- and metamagnets possessing a TEMPO radical group [1], which exhibit magnetic phase transitions at or below 0.3 K. The sterically bulky substituents such as four methyl groups in a TEMPO moiety make the N–O radical centers apart, and the spin densities on aliphatic substituents are generally small. For developing high-T_c organic magnets, we turn our attention to π-conjugated radicals. Among them, all of the homologues of **1** were revealed to possess positive Weiss temperatures [2]. Radical BTAO (**2**, $R^1 = R^2 = p$-tolyl) forms a ferromagnetic pancake-type dimer [3], and DPAO (**2**, $R^1 = R^2 = n$-C_3H_7) also shows intermolecular ferromagnetic interaction [4]. In the course of our study on the magnetic properties of **2**, we have found another unique molecular arrangement of C_nPhAO-d_5 (**2**, $R^1 = n$-C_nH_{2n+1}, $R^2 = C_6D_5$) showing intermolecular ferromagnetic interaction. Deuteriums were introduced for study of high-resolution solid-state MAS ^{2}H NMR [5].

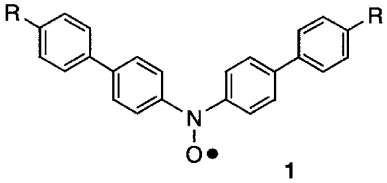

1

R = *n*-C_nH_{2n+1}
n = 0,1,2,...,7,10

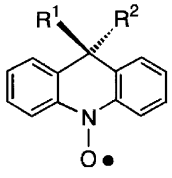

2

BTAO $R^1 = R^2 = p$-$CH_3C_6H_4$

DPAO $R^1 = R^2 = n$-C_3H_7

C_nPhAO-d_5 $R^1 = n$-C_nH_{2n+1}, $R^2 = C_6D_5$

2. Results and discussion

Fig. 1 shows the molecular structures of C_{12}- and C_{13}PhAO-d_5. The dihydroacridine moiety including the nitroxide oxygen atom is highly planar. The 9-phenyl ring is almost perpendicular to the acridine plane (the dihedral angles of 87.32(4) and 88.19(5)° for C_{12}- and C_{13}PhAO-d_5, respectively).

Fig. 2 shows the molecular arrangement of C_{12}PhAO-d_5. The crystals of C_{12}- and C_{13}PhAO-d_5 are isomorphous. Two molecules are related by inversion symmetry and the acridine planes are arranged in parallel. The phenyl substituents are also almost parallel in another direction. The alkyl groups are folded in the clearance of the rigid grid formed by acridine planes and phenyl groups. A sharp bend of the alkyl group takes place at the fifth carbon atom (C24), probably owing to accommodation of the crystal packing.

Since the spin distribution is considerably large on the acridine plane [3,4], we have to pay attention to intermolecular atomic contacts among the acridine skeletons in order to examine magnetic exchange pathways. Fig. 2(b) shows the shortest intermolecular contact in the crystals of C_{12}PhAO-d_5. The distances are 2.49(2) and 2.51(2) Å for

☆ Yamada Conference LVI, The Fourth International Symposium on Crystalline Organic Metals, Superconductors and Ferromagnets, ISCOM 2001—Abstract Number G16Mon.

* Corresponding author. Tel.: +81-424-43-5490; fax: +81-424-43-5483.
E-mail address: ishi@pc.uec.ac.jp (T. Ishida).

0379-6779/02/$ – see front matter © 2002 Elsevier Science B.V. All rights reserved.
PII: S0379-6779(02)00353-3

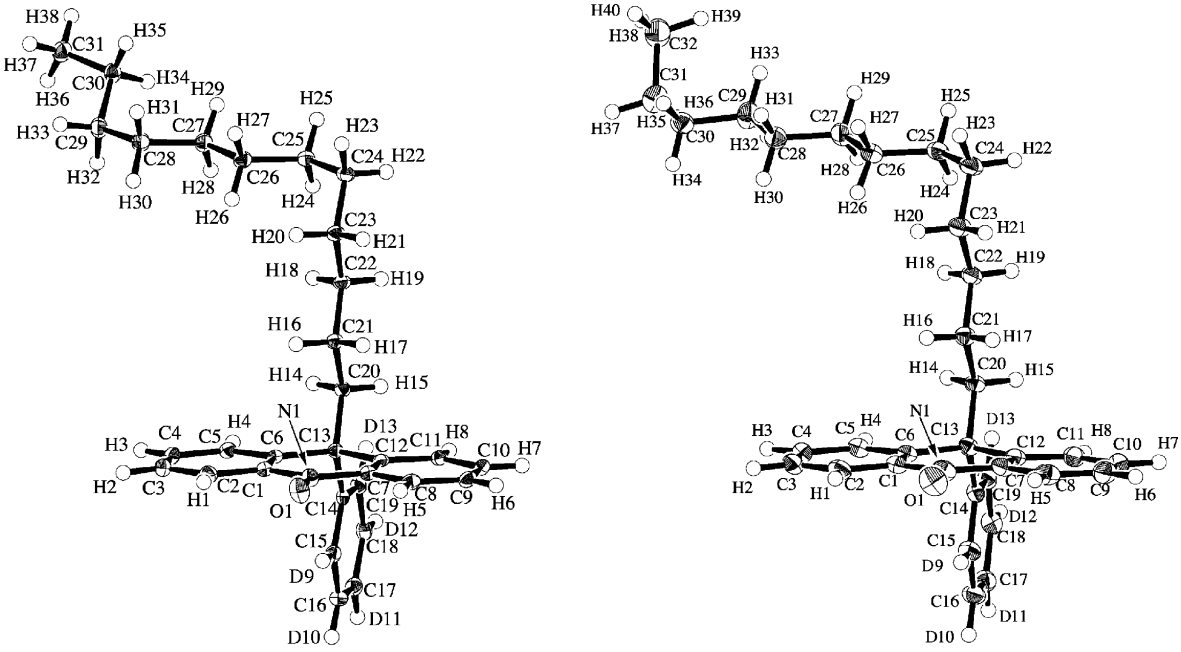

Fig. 1. Molecular structures of C_{12}PhAO-d_5 (left) and C_{13}PhAO-d_5 (right).

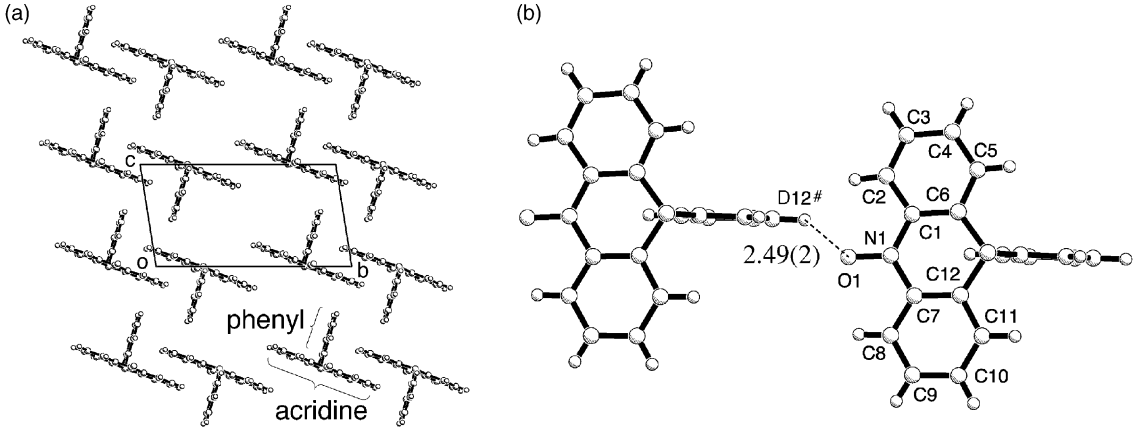

Fig. 2. Molecular arrangement (a) and the shortest intermolecular distance (b) in the crystal of C_{12}PhAO-d_5. The *n*-$C_{12}H_{25}$ groups are omitted for the sake of clarity.

$O1 \cdots D12^{\#}$ in C_{12}- and C_{13}PhAO-d_5, respectively. The D12 atom belongs to the *m*-position of the phenyl group.

We measured the temperature dependence of the molar magnetic susceptibilities (χ_{mol}) for C_{12}- and C_{13}PhAO-d_5. As Fig. 3 shows, intermolecular ferromagnetic interactions were observed for both compounds. The Weiss temperatures (θ's) of C_{12}- and C_{13}PhAO-d_5 were determined to be +0.95 and +0.36 K, respectively, from fitting to the Curie–Weiss equation, $\chi_{mol} = C/(T - \theta)$.

We can propose superexchange-like interaction across the 9-phenyl ring from the close intermolecular contacts. The $O1 \cdots D12^{\#}$ distance is considerably short, and spin densities are polarized at the $D12^{\#}$ atom and consequently at all atoms of the phenyl group. According to the Kanamori–Goodenough rule on the M_1–X–M_2 system for dinuclear transition–metal complexes [6,7], when there is an appreciable orbital overlap between a magnetic orbital ϕ_1 on M_1

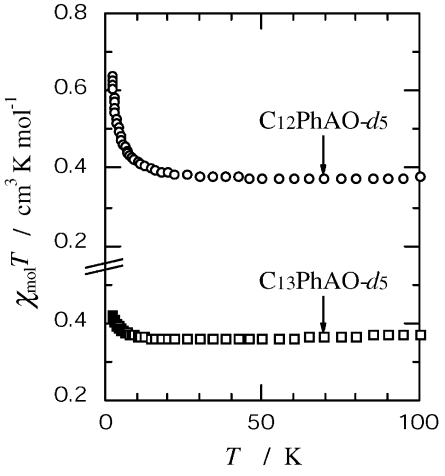

Fig. 3. Temperature dependence of the product $\chi_{mol}T$ for C_{12}PhAO-d_5 (top) and C_{13}PhAO-d_5 (bottom).

and an atomic orbital χ on *X*, and at the same time χ and a magnetic orbital ϕ_2 on M_2 are orthogonal, the spins of M_1 and M_2 are ferromagnetically coupled. In the present compounds, the ferromagnetic coupling is rationalized by assuming that X is a diamagnetic benzene bridging two organic free radicals, M_1 and M_2, and that χ is a molecular orbital of the benzene moiety. Therefore, superexchange-like interaction across the 9-phenyl ring is illustrated as acridinoxyl $\|$ phenyl $\perp$ acridinoxyl, where the symbols $\|$ and $\perp$ denote the presence and absence of inter- and intramolecular orbital overlaps, respectively. Studies of possible polarized spin densities on the 9-phenyl ring by means of solid-state ^{2}H NMR are now underway.

References

[1] T. Nogami, T. Ishida, M. Yasui, F. Iwasaki, N. Takeda, M. Ishikawa, T. Kawakami, K. Yamaguchi, Bull. Chem. Soc. Jpn. 69 (1996) 1841.
[2] T. Ishida, M. Nakagawa, R. Imachi, Y. Akui, S.-Y. Masaoka, M. Suzuki, D. Hashizume, M. Yasui, F. Iwasaki, T. Nogami, Mol. Cryst. Liq. Cryst. 334 (1999) 89.
[3] R. Imachi, T. Ishida, M. Suzuki, M. Yasui, F. Iwasaki, T. Nogami, Chem. Lett. (1997) 743.
[4] M. Nakagawa, T. Ishida, M. Suzuki, D. Hashizume, M. Yasui, F. Iwasaki, T. Nogami, Chem. Phys. Lett. 302 (1999) 125.
[5] G. Maruta, S. Takeda, R. Imachi, T. Ishida, T. Nogami, K. Yamaguchi, J. Am. Chem. Soc. 121 (1999) 424.
[6] J. Kanamori, J. Phys. Chem. Solids 10 (1959) 87.
[7] J.B. Goodenough, Phys. Rev. 100 (1955) 564.

ELSEVIER

Synthetic Metals 133–134 (2003) 611–613

SYNTHETIC METALS

www.elsevier.com/locate/synmet

Hybrid magnetic solids of radical-substituted heteroaromatic compounds with metal halides☆

T. Matsuyama, Y. Iwata, T. Ishida*, T. Nogami

Department of Applied Physics and Chemistry, The University of Electro-Communications, Chofu, Tokyo 182-8585, Japan

Abstract

Complexes of manganese(II), cobalt(II), nickel(II), and copper(II) chlorides with 5-pyrimidinyl nitronyl nitroxide (5PMNN) and pyrazinyl nitronyl nitroxide (PZNN) were synthesized. Ni- and $CoCl_2$·$(5PMNN)_2$ showed magnetic phase transitions at 5.8 and 2.3 K, respectively, and spin–flip behavior below the transition temperatures. X-ray crystal structure analyses revealed that Mn- and $CoCl_2$·$(PZNN)_2$ were mononuclear.

Keywords: Free radicals; Nitronyl nitroxide; Pyrimidine; Pyrazine; Magnetic phase transition

1. Introduction

We have reported the magnetic properties of pyrimidine-bridged transition metal complexes [1–3]. Rey and co-workers [4] reported a pioneering work on metal-radical materials of $Cu(hfac)_2$ complexes with radical-substituted heteroaromatic bridges, 5-pyrimidinyl nitronyl nitroxide (5PMNN) and pyrazinyl nitronyl nitroxide (PZNN). Okada and co-workers [5] also reported tri- and mononuclear $Cu(hfac)_2$ complexes containing 5PMNN. Small counter anions such as halide anions are preferable for developing magnetically dense systems, compared with the hfac anion. Thus, we designed networking hybrid solids of transition-metal halides with bridging ligands shown below. The complexes of copper(II) and cobalt(II) halides with 4PMNN have been reported recently [6,7].

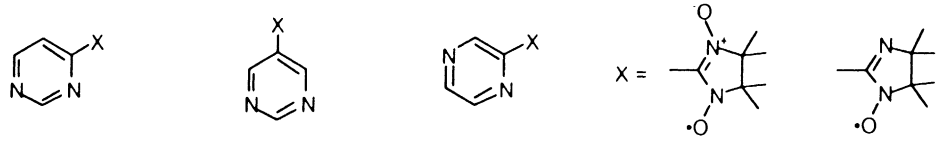

4PMNN, 4PMIN 5PMNN, 5PMIN PZNN, PZIN

2. Results and discussion

2.1. Complexes of 5PMNN

We measured the temperature dependence of the molar magnetic susceptibility (χ_{mol}) for MCl_2·$(5PMNN)_n$ (M = Mn, Co, Ni, Cu) (Fig. 1). Antiferromagnetic interactions were observed for $MnCl_2$·(5PMNN) and $CuCl_2$·$(5PMNN)_2$. On the other hand, ferromagnetic interaction was dominant for $NiCl_2$·$(5PMNN)_2$. The $\chi_{mol}T$ value at 100 K exceeds the calculated spin-only value and the maximum value at 6.5 K also exceeds the spin-only value of 3.0 cm^3 K mol^{-1} for a possible high-spin molecule.

The $\chi_{mol}T$ value of $CoCl_2$·$(5PMNN)_2$ once decreases but turns to increase around 20 K. After a maximum at 4.0 K the $\chi_{mol}T$ value decreases again. This behavior cannot be attributed only to spin–spin coupling because the magnetic properties of cobalt(II) complexes are usually affected by angular moment contribution. However, the sharp cusp indicates that a magnetic phase transition takes place around the peaking temperature.

Fig. 2(a) shows the field-cooled magnetization (FCM) of $NiCl_2$·$(5PMNN)_2$ measured at 3 Oe. A peak was found at

☆ Yamada Conference LVI, the Fourth International Symposium on Crystalline Organic Metals, Superconductors and Ferromagnets, ISCOM 2001—Abstract Number G25Mon.

* Corresponding author. Tel.: +81-424-43-5490; fax: +81-424-43-5483.
E-mail address: ishi@pc.uec.ac.jp (T. Ishida).

0379-6779/02/$ – see front matter
PII: S0379-6779(02)00360-0

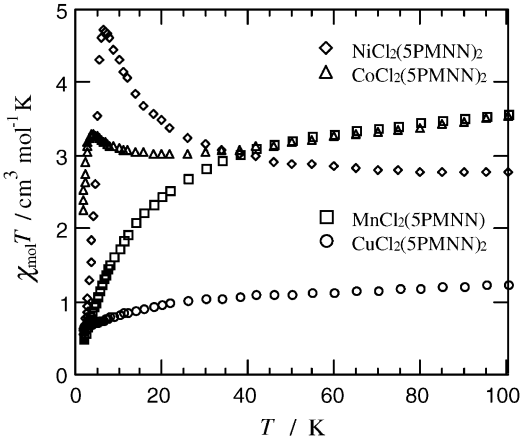

Fig. 1. Temperature dependence of $\chi_{mol}T$ of $MCl_2{\cdot}(5PMNN)_n$ (M = Mn, Co, Ni, Cu) measured at 5 kOe.

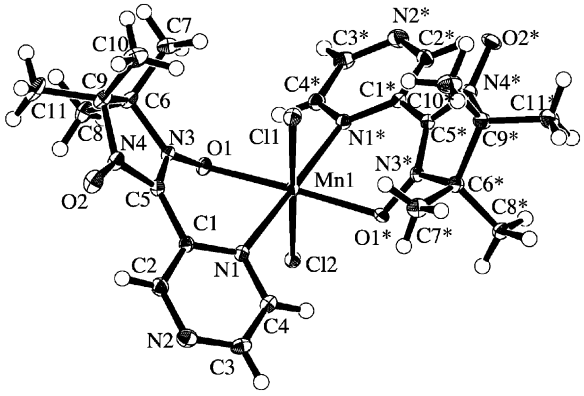

Fig. 3. ORTEP drawing of $MnCl_2{\cdot}(PZNN)_2$ with thermal ellipsoids at the 50% level.

5.8 K. As the temperature decreases, the magnetization increases not so sharply above T_c and significantly decreases below T_c, suggesting that the ground magnetic phase below T_c is antiferromagnetic. The FCM of $CoCl_2{\cdot}(5PMNN)_2$ diverges below 2.4 K and the RM completely disappears above 2.3 K (Fig. 2(b)). Although the remnant magnetization (RM) is observed, the temperature dependence of $\chi_{mol}T$ indicates that $CoCl_2{\cdot}(5PMNN)_2$ is not a ferromagnet.

The magnetization of $NiCl_2{\cdot}(5PMNN)_2$ at 70 kOe reaches ca. 2×10^4 cm^3 G mol^{-1} (Fig. 2(c)). This value is consistent with the four-spin system. An S-shaped magnetization curve was traced in both directions of applying and removing magnetic fields. Thus, this compound is characterized as a metamagnet with a spin–flip transition. The critical field is ca. 10 kOe. The antiferromagnetic nature at the ground state is consistent with the results of the FCM measurements. The *M–H* curve of $CoCl_2{\cdot}(5PMNN)_2$ exhibits a similar feature (not shown); a small S-shaped curve in a low field region is observed. However, this compound cannot be simply regarded as a metamagnet because residual spins are expected in it where antiferromagnetic interactions are dominant. Structures which afford ferrimagnetic RM below T_c should be taken into consideration. Although crystal structures of Ni- and $CoCl_2{\cdot}(5PMNN)_2$ could not be determined, the ligand 5PMNN is potentially tetradentate and these solids are likely to have magnetic networks.

2.2. Complexes of PZNN

Fig. 3 shows the molecular structure of $MnCl_2{\cdot}(PZNN)_2$. A half of it is crystallographically independent. The chlorine atoms are coordinated at the axial positions. Whereas N1 in the pyrazine ring and O1 in the nitronyl nitroxide group occupy the equatorial positions, N2 and O2 remain uncoordinated. Accordingly, the crystal consists of discrete mononuclear molecules. $CoCl_2{\cdot}(PZNN)_2$ is isostructural with $MnCl_2{\cdot}(PZNN)_2$.

Magnetic susceptibility measurements indicate the presence of considerably large antiferromagnetic interactions for the two compounds; the $\chi_{mol}T$ values below 100 K are much smaller than the calculated spin-only values. The interactions were ascribable to intramolecular antiferromagnetic coupling of the metal spin and radical spins through the M–O bonds.

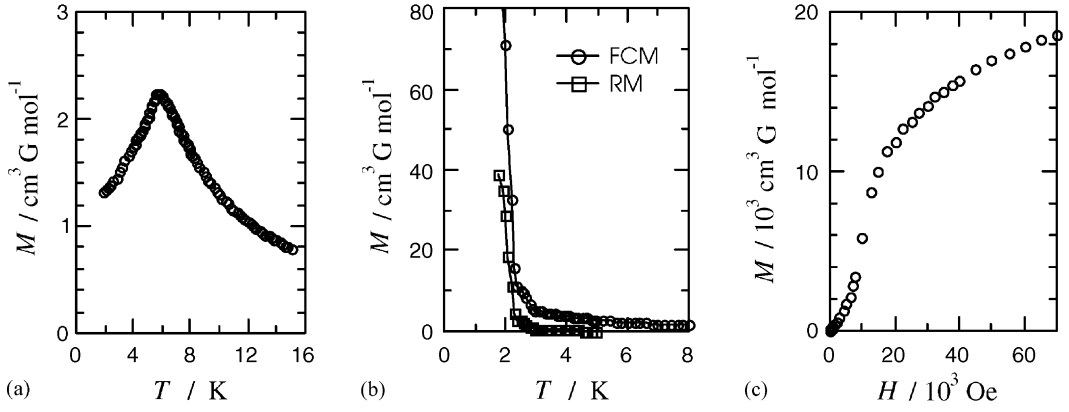

Fig. 2. (a) FCM of $NiCl_2{\cdot}(5PMNN)_2$. (b) FCM and RM of $CoCl_2{\cdot}(5PMNN)_2$. Solid lines are drawn for a guide to the eye. (c) *M–H* curve of $NiCl_2{\cdot}(5PMNN)_2$ at 3 K.

References

[1] T. Ishida, K. Nakayama, M. Nakagawa, W. Sato, Y. Ishikawa, M. Yasui, F. Iwasaki, T. Nogami, Synth. Met. 85 (1997) 1655.
[2] T. Ishida, T. Nogami, Recent Res. Dev. Pure Appl. Chem. 1 (1997) 1.
[3] T. Ishida, S.-I. Mitsubori, T. Nogami, N. Takeda, M. Ishikawa, H. Iwamura, Inorg. Chem. 40 (2001) 7059.
[4] K. Fegy, K.E. Vostrikova, D. Luneau, P. Rey, Mol. Cryst. Liq. Cryst. 305 (1997) 69.
[5] H. Mori, O. Nagao, M. Kozaki, D. Shiomi, K. Sato, T. Takui, K. Okada, Polyhedron 20 (2001) 1663.
[6] J. Omata, T. Ishida, D. Hashizume, F. Iwasaki, T. Nogami, Inorg. Chem. 40 (2001) 3954.
[7] J. Omata, T. Ishida, D. Hashizume, F. Iwasaki, T. Nogami, Mol. Cryst. Liq. Cryst. 376 (2002) 455.

ELSEVIER

Synthetic Metals 133–134 (2003) 577–579

SYNTHETIC METALS

www.elsevier.com/locate/synmet

Low temperature deuterium NMR studies on magnetism of TEMPO derivatives☆

G. Maruta[a,*], S. Takeda[a], M. Ooishi[b], R. Imachi[b], T. Ishida[b], T. Nogami[b]

[a]*Department of Chemistry, Graduate School of Science, Hokkaido University, Sapporo, Hokkaido 060-0810, Japan*
[b]*Department of Applied Physics and Chemistry, The University of Electro-Communications, Chofu, Tokyo 182-8585, Japan*

Abstract

We measured deuterium NMR of three TEMPO (2,2,6,6-tetramethylpiperidin-1-yloxyl) derivatives, 4-hydroxy-d_1-TEMPO, 4-hydroxyimino-d_1-TEMPO and Cl–C_6D_4–CD=N-TEMPO down to 2 K to investigate the magnetic local structure around the selectively deuterated sites. Hyperfine coupling constants (HFCCs) determined from the spectra are in good agreement with the results of our previous experiments at higher temperatures. We found: (i) each deuterium, which forms a hydrogen bond with the nitroxide group in the crystalline phases of 4-hydroxy- and 4-hydroxyimino-TEMPO has a large negative HFCC; (ii) electron spin density on Cl–C_6D_4-group in Cl–C_6D_4–CD=N-TEMPO crystal remains small in magnitude at 4.2 K.

Keywords: ^{2}H-NMR; Organic magnetism; TEMPO derivatives; Spin density; Contact shift

1. Introduction

An intermolecular magnetic interaction in a molecule-based magnet is the direct interaction between singly occupied molecular orbitals (SOMO) or one of the indirect interactions via spin polarized molecular orbitals [1]. The shape and mutual orientation of SOMO, which can be precisely determined by polarized neutron diffraction (PND) [2] are crucial for the direct interaction. On the other hand, atomic spin densities of hydrogen atoms in close contact with the radical group of the neighboring molecule are clue to the indirect interaction. In a previous paper, we demonstrated that deuterium magic angle spinning NMR (^{2}H-MAS NMR) has many advantages for measuring the spin density of selected hydrogen atom in a molecular crystal [1]. High speed MAS technique, however, is difficult at cryogenic temperature. In this paper, we report validity of static ^{2}H-NMR to determine the hyperfine coupling constant (HFCC) of a selected hydrogen atom at cryogenic temperatures.

2. Experiment

Preparations of 4-hydroxyimino-d_1-TEMPO (OXTMP-d_1) and Cl–C_6D_4–CD=N-TEMPO (CLTMP-d_5) are described in Refs. [1,3], respectively. The hydrogen bond of 4-hydroxy-d_1-TEMPO (TEMPOL-d_1) was deuterated in a similar manner to OXTMP-d_1. ^{2}H-NMR was measured for ca. 20 mg of polycrystalline specimens with Bruker DSX300 equipped with a laboratory-made cryostat between 2 and 300 K. A series of echo signal was measured between 45 and 47 MHz at a magnetic field of 7 T, with 50–200 kHz step to cover the whole signal. The spectra shown in Fig. 1 is the envelop of the echo signals. ^{2}H-MAS NMR of TEMPOL-d_1 and CLTMP-d_5 are measured by the same procedure described in Ref. [1].

3. Results and discussion

^{2}H-NMR spectrum of paramagnetic polycrystalline specimen has a structure due to electric quadruple interaction and magnetic dipolar interaction between deuteron and electron [4]. The dipolar interaction is proportional to the magnetic susceptibility of the sample though the quadruple interaction is independent of temperature. Moreover, the frequency of the center of gravity of the spectrum is proportional to both the HFCC of the deuteron and the

☆ Yamada Conference LVI, The Fourth International Symposium on Crystalline Organic Metals, Superconductors and Ferromagnets, ISCOM 2001—Abstract Number G15Wed.

* Corresponding author. Tel.: +81-11-706-3504; fax: +81-11-706-4841.
E-mail address: maruta@sci.hokudai.ac.jp (G. Maruta).

0379-6779/02/$ – see front matter © 2002 Published by Elsevier Science B.V.
PII: S0379-6779(02)00352-1

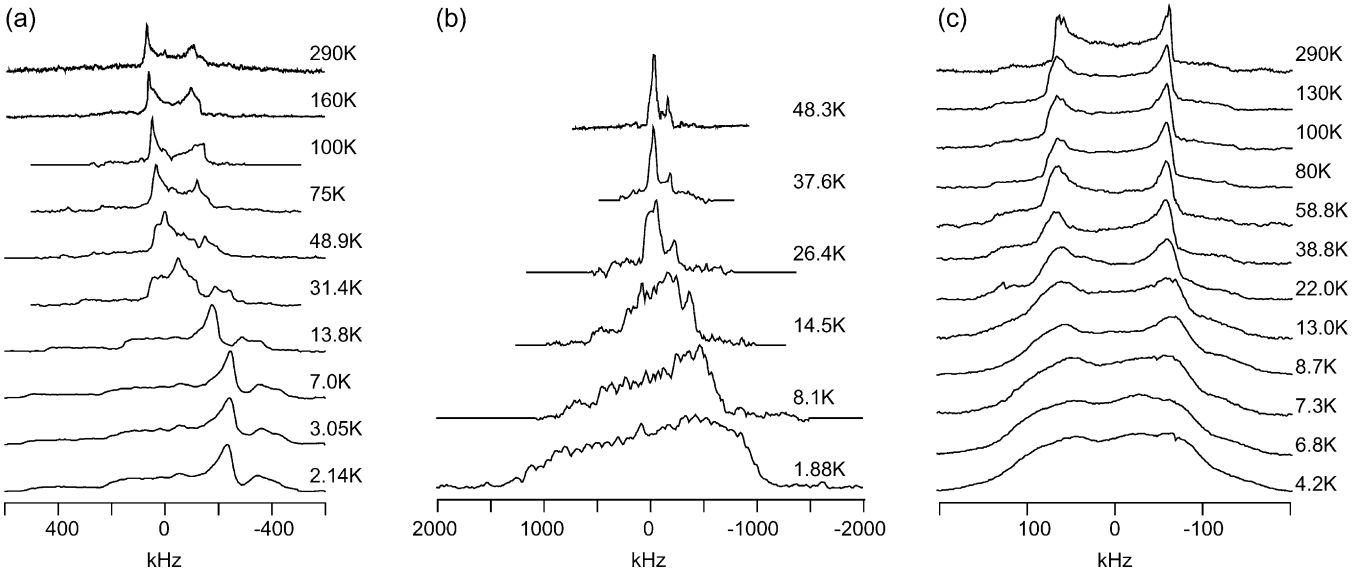

Fig. 1. ^{2}H-NMR spectra of (a) TEMPOL-d_1, (b) OXTMP-d_1 and (c) CLTMP-d_5.

Table 1
Experimentally determined HFCCs (MHz) of the deuterons of TEMPO derivatives

Material	^{2}H-NMR	^{2}H-MAS NMR[a]	Deduced from other experiments
TEMPOL-d_1	−0.55	−0.58	−1.14 ± 0.22[b]
OXTMP-d_1	−0.5	−0.45[c]	
CLTMP-d_5	<0.10[d]	<0.02[d]	−0.2, 0.1, 0.1, −0.2, −0.6[e]

[a] Determined above 180 K.
[b] ^{1}H-NMR at 4.2 K [5]. Converted from proton's HFCC using $A_F(^2H) = A_F(^1H) \times (\gamma_D/\gamma_H)$, provided that isotope effect is negligible.
[c] Ref. [1].
[d] Upper limit of the absolute value.
[e] PND at 1.5 K [2]. The HFCCs are estimated from the atomic spin densities of the corresponding carbon atoms using McConnel relation.

susceptibility. Hence, we can determine microscopic susceptibility and electron spin density at the selected hydrogen atom simultaneously.

Fig. 1(a) shows representative spectra of TEMPOL-d_1. Parameters of the quadruple interaction were determined to be $e^2qQ/h = 228$ kHz, $\eta = 0.1$, which are typical values for OD···O hydrogen bonded system, from the spectra above 30 K. The HFCC and Weiss temperature of −0.55 MHz and -5 ± 3 K, respectively, were deduced from the spectra above 15 K. Temperature dependence of the spectrum for OXTMP-d_1 (Fig. 1(b)) was analyzed in a similar method. The obtained HFCCs listed in Table 1 are in good agreement with those determined by ^{2}H-MAS NMR, indicating that spin density on the hydrogen atom is independent of temperature. As noted in Refs. [1,5], these large negative HFCCs of the hydrogen atoms are due to the hydrogen bond with the nitroxide group in the crystalline phases. DFT calculation on a single molecule model without hydrogen bond indicated that negative and positive small spin densities are induced on the hydrogen atoms in OXTMP and TEMPOL molecules, respectively, by intramolecular spin polarization effect. Thus, ferromagnetic interaction via the hydrogen bond in OXTMP can be interpreted in terms of the in-phase overlap between inter- and intramolecular spin polarization. On the other hand, the opposite sign between the two polarization effects, or out-of-phase overlap, in TEMPOL explains antiferromagnetic interaction in this crystal. Hydrogen bond can be ferromagnetic or antiferromagnetic coupler, depending on the molecular structure.

Cl–C_6H_4–CH=N-group is believed to be an interlayer magnetic coupler in a pseudo-two-dimensional ferromagnet, CLTMP [6]. Fig. 1(c) shows that the Fermi contact shifts of the deuterium of this group are much smaller than those of the above two TEMPOs, indicating the small spin density of the group. MAS NMR at high temperatures also implied small but finite spin density distribution. This result is in contradiction to both spin density distribution determined by PND and DFT calculation [2]. The interlayer magnetic interaction in CLTMP as well as its spin density distribution remains an open question.

Acknowledgements

This research was supported by The Mitsubishi Foundation. Helpful collaborations by Dr. T. Kawakami and Mr. Y. Nagayama are also acknowledged.

References

[1] G. Maruta, S. Takeda, R. Imachi, T. Ishida, T. Nogami, K. Yamaguchi, J. Am. Chem. Soc. 121 (1999) 424.
[2] Y. Pontillon, A. Grand, T. Ishida, E. Lelièvre-Berna, T. Nogami, E. Ressouche, J. Schweizer, J. Mater. Chem. 10 (2000) 1539.

[3] R. Imachi, T. Ishida, M. Yasui, F. Iwasaki, N. Takeda, M. Ishikawa, Synth. Met. 85 (1997) 1743.
[4] T.-H. Lin, J.A. DiNatale, R.R. Vold, J. Am. Chem. Soc. 116 (1994) 2133.
[5] D. Ondercin, T. Sandreczki, R.W. Kreilick, J. Mag. Reson. 34 (1979) 151.
[6] T. Nogami, T. Ishida, M. Yasui, F. Iwasaki, N. Takeda, M. Ishikawa, T. Kawakami, K. Yamaguchi, Bull. Chem. Soc. Jpn. 69 (1996) 1841.

ELSEVIER

Synthetic Metals 137 (2003) 1281–1282

SYNTHETIC METALS

www.elsevier.com/locate/synmet

Hydroiminonitroxide Complexes with Metal Hexafluoroacetylacetonates

Tomoaki Ise, Takayuki Ishida, and Takashi Nogami

Department of Applied Physics and Chemistry, The University of Electro-Communications, Chofugaoka, Chofu, Tokyo 182-8585, Japan

Received 2 July 2002; accepted 20 October 2002

Abstract

Hybrid metal-radical magnetic solids, $Cu(hfac)_2 \cdot$ HIN (**1**) and $Mn(hfac)_2 \cdot$ HIN (**2**) were synthesized, where HIN denotes 4,4,5,5-tetramethylimidazolin-1-oxyl. X-ray diffraction measurements of **1** and **2** showed 1-dimensional metal-radical alternating chain structures. Magnetic data of **1** and **2** could be analyzed by 1-D ferro- and ferrimagnetic chain models, respectively.

keywords: Magnetic measurements

Introduction

Iminonitroxide and nitronylnitroxide radical derivatives have been utilized for magnetic materials, and a large number of complexes have been developed as ferro- or ferrimagnets[1]. Recently Gateschi and co-workers reported that polymeric metal hexafluoroacetylacetonate-nitronylnitroxide systems were potentially good candidates for single-molecule magnets[2]. We assume that the choice of small ligands and anions is crucial in order to bestow strong exchange interaction on magnetic materials. We chose 4,4,5,5-tetramethylimidazolin-1-oxyl (HIN) as the smallest ligand in the iminonitroxide family[3]. We obtained mononuclear complexes, $Cu(hfac)_2(HIN)_2$ and $Mn(hfac)_2(HIN)_2$[4], which have considerably strong intermolecular antiferromagnetic interactions ($2J/k >> 300$ K) among the HIN ligands (hfac = 1,1,1,5,5,5-hexafluoropentane-2,4-dionate). In these complexes, the imino nitrogen atom coordinates to the metal ion, whereas the nitroxide oxygen atom remains uncoordinated. We attempted to construct polymeric networks for achieving ferro- or ferrimagnetic materials. We obtained two novel complexes by changing the molar ratios of the starting materials used. The metal/ligand ratios of these complexes are found to be 1/1 by elemental analysis, which is expected for 1-dimensial 1/1 polymer structures of **1** and **2** (Chart 1).

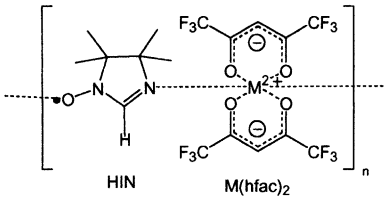

Chart 1. The structural formula of **1** (M = Cu) and **2** (M = Mn).

Experimental

$Cu(hfac)_2 \cdot$ HIN (1) : Solutions of HIN[3,4] (100 mg, 0.71 mmol) in dry diethyl ether (3 ml) and of dehydrated $Cu(hfac)_2$ (1.0 g, 2.1 mmol) in dry diethyl ether (3 ml) were mixed, the combined solution was allowed to stand in a cool and dark place for 1 day, and dark-brown crystals of **1** were precipitated. $Mn(hfac)_2 \cdot$ HIN (**2**) was synthesized in a similar manner. Unfortunately, **2** was obtained only as a powder form.

Elemental analysis (C, H, N) of these complexes on a Fisons EA-1108 by a usual combustion method revealed that the metal/radical ratios were 1/1 for **1** and **2**. Anal. Calc. for $C_{17}H_{15}N_2O_5F_{12}Cu_1$ (**1**): C, 32.99; H, 2.44; N, 4.53 %. Found: C, 34.65; H, 2.39; N, 4.62 %. Calc. for $C_{17}H_{15}N_2O_5F_{12}Mn_1$ (**2**): C, 33.46; H, 2.48; N, 4.59 %. Found: C, 33.61; H, 2.55; N, 4.09 %. X-Ray diffraction data of **1** were collected on a Rigaku Raxis-Rapid IP diffractometer with monochromated Mo$K\alpha$ radiation at 90 K. The cell parameters of **2** were obtained by X-ray powder diffraction. Magnetic susceptibility was measured on a Quantum Design MPMS SQUID magnetometer in a temperature range of 1.8 - 300 K at 5000 Oe.

Results and discussion

Table 1 summarizes selected X-ray crystallographic data for **1** and **2**. The cell parameters of **1** and **2** are similar to each other, and they seems to be isomorphous. Crystal structure of **1** was found to be a 1-dimensional *trans* straight chain consisting of $[Cu(hfac)_2 \cdot HIN]_n$. The distance between neighboring two Cu ions is 6.42 Å, which is considerably shorter than the corresponding distance in $Cu(hfac)_2$MeNN (7.96 Å; MeNN = 2,4,4,5,5-

doi:10.1016/S0379-6779(02)01140-2

HIN ligand is sandwitched by two Cu ions.

The plots of $\chi_m T$ vs T of **1** and **2** are shown in Fig. 1. At 300 K, the $\chi_m T$ value of **1** is 0.78 $cm^3 mol^{-1}K$, which is slightly larger than the calculated value of 0.75 $cm^3 mol^{-1}K$ for a noncoupled system. On the other hand, the $\chi_m T$ of **2** at 300 K is 3.46 $cm^3 mol^{-1}K$ which is smaller than the calculated value of 4.75 $cm^3 mol^{-1}K$ for a noncoupled system. These findings indicate that ferro- and antiferromagnetic interactions are operative in **1** and **2**, respectively. Upon cooling, the $\chi_m T$ values increased to a maximum value 3.28 $cm^3 mol^{-1}$ K at 2.8 K for **1** and 22.9 $cm^3 mol^{-1}$ K at 12 K for **2**, and then decreased. These maximum values are larger than those of $S = 1$ due to an expected high-spin repeating unit (1.0 $cm^3 mol^{-1}$ K) for **1** and $S = 2$ due to an antiferromagnetically correlated unit (3.0 $cm^3 mol^{-1}$ K) for **2**. These magnetic behaviors indicate that the ferro- and antiferromagnetic interactions are operative infinitely along the chain structures for **1** and **2**, respectively. A satisfactory fit of the experimental data was made by using an $S = 1/2$ ferromagnetic chain model[6] for **1** and a Seiden ferrimagnetic chain model[7] for **2** with the Hamiltonian $H = -2J\sum S_i S_{i+1}$. The best fit parameters are : $g = 1.977$, $2J/k = +59$ K and $\theta = -0.89$ K for **1** ; $g = 2.22$, $2J/k = -173$ K for **2**, respectively.

The field dependence of the magnetization showed no bulk magnetic ordering above 1.8 K (Fig. 2). The saturation magnetizations of 11000 and 21000 erg $Oe^{-1}mol^{-1}$ for **1** and **2**, respectively, correspond to $S = 1$ and $S = 2$ with $g = 2$, supporting the ferro- and antiferromagnetic couplings between metal and radical spins, respectively. Furthermore, the experimental data exceeded the theoretical Brillouin functions, and the ferro- and ferrimagnetic chain structures are confirmed for **1** and **2**, respectively.

The ferromagnetic interaction of **1** can be explained in terms of orbital orthogonality between the copper $3d_{x2-y2}$ and the oxygen or nitrogen $2p_z$ orbitals, as seen in $Cu(hfac)_2$ nitronyl nitroxide complexes[5]. The antiferromagnetic interaction of **2** can be attributed to orbital overlap between the manganese $3d(t_{2g})$ and the oxygen or nitrogen $2p_z$ orbitals, like $Mn(hfac)_2$ nitronyl nitroxide complexes[8].

Table 1. The cell parameters of **1** and **2**.

Compound	1	2
Crystal system	Orthorhombic	Orthorhombic
Space group	*Pbcn*	
a/ Å	16.864(3)	15.313
b/ Å	10.836(1)	11.350
c/ Å	12.841(6)	13.302

Acknowledgments

This work was supported by a Grant-in-Aid for Scientific Research on Priority Areas (No. 730/11224204) and by a the Ministry of Education, Culture, Sports, Science and Technology, Japan

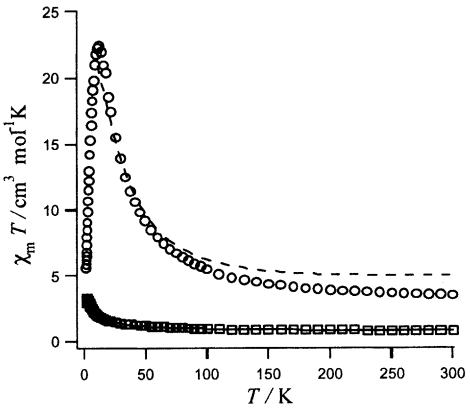

Figure 1. Temperature dependence of the product $\chi_m T$ of $Cu(hfac)_2(HIN)$ (□) and $Mn(hfac)_2(HIN)$ (○) measured at 5 kOe. Solid and broken lines correspond to the theoretical curves based on $S = 1/2$ 1-D ferromagnetic chain model and the Seiden ferrimagnetic chain model, respectively.

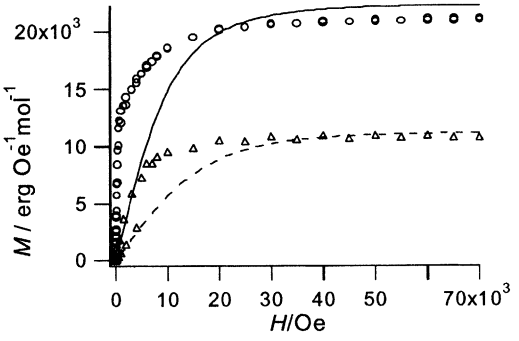

Figure 2. Field dependence of the magnetization of $Cu(hfac)_2(HIN)$ (□) and $Mn(hfac)_2(HIN)$ (○) measured at 1.8 K. Solid and broken lines correspond to theoretical Brillouin functions with $S = 2$ and $S = 1$, respectively.

References

[1] A. Caneschi, D. Gatteschi and R. Sessoli, *Acc. Chem. Res.*, **22**, 392(1989); A. Caneschi, D. Gatteschi and P. Rey, *Prog. Inorg. Chem.*, **39**, 331(1991).

[2] A. Caneschi, D. Gatteschi, N. Lalioti, C. Sangregorio, R. Sessoli, G. Venturi, A. Vindigni, A. Rettori, M. G. Pini, and M. A. Novak, *Angew. Chem. Int. Ed.*, **40**, 1760(2001).

[3] E. F. Ullman, L. Call, and J. H. Osiecki, *J. Org. Chem.*, **35**, 3623(1970).

[4] T. Ise, T. Ishida, and T. Nogami, *Bull. Chem. Soc. Jpn*, in press.

[5] A. Caneschi, D. Gatteschi, J.Laugier, and P.Rey, *J. Am. Chem. Soc.*, **109**, 2191(1987); C. I. Cabello, A. Caneschi, R. L. Carlin, D. Gatteschi, P. Rey, and R. Sessoli, *Inorg. Chem.*, **29**, 2582(1990).

[6] G. A. Baker, G. S. J. Rushbrooke, H. E. Gillbert, *Phys. Rev.* **135A**, 1272(1964).

[7] M. Verdaguer, A. Gleize, J.P. Renard, J. Seiden, *Phys. Rev,* **B 29**, 5144(1984).

[8] A. Caneschi, D. Gatteschi, J. P. Renard, P. Rey, and R. Sessoli, *Inorg. Chem.*, **28**, 3314(1989); A. Caneschi, D. Gatteschi, N. Lalioti, C. Sangregorio, and R. Sessoli, *J. Chem. Soc., Dalton Trans.*, 3907(2000).

Available online at www.sciencedirect.com
SCIENCE DIRECT®
PERGAMON
Polyhedron 22 (2003) 2133–2138
POLYHEDRON
www.elsevier.com/locate/poly

Host–guest chemistry of radical-copper wheels. A supramolecular control of magnetic exchange coupling

Takayuki Ishida *, Junichi Omata, Takashi Nogami

Department of Applied Physics and Chemistry, The University of Electro-Communications, Chofu, Tokyo 182-8585, Japan

Received 6 October 2002; accepted 11 January 2003

Abstract

The crystal of the hexanuclear wheel-shaped complex, $[CuCl_2\cdot(4PMNN)]_6$ (**1**), has a channel structure in a direction perpendicular to the molecular plane (4PMNN = 4-pyrimidinyl nitronyl nitroxide). Excess LiCl, NaCl, or KCl added to a methanol solution of **1** yielded the corresponding guest-included compounds, $(LiCl)_6$@**1**, $(NaCl)_2$@**1**, and $(KCl)_2$@**1**. The inclusion of the guests was confirmed by means of elemental analysis and X-ray diffraction study. The crystallographic *c* length and the cell volume were slightly shrunk by the guest inclusion. The ferromagnetic interaction, which is ascribed to intermolecular contacts between the nitronyl nitroxide groups, was remarkably enhanced almost in proportion to the cell shrinkage. Similar enhancement was observed for the host–guest complexes from the bromide analogue $[CuBr_2\cdot(4PMNN)]_6$. The crystallization in the presence of water gave $(H_2O)_n$@**1**. In addition to enhancement of the ferromagnetic interaction of $(H_2O)_n$@**1**, we found that the ferromagnetic interaction decreased back to a level of that of the empty **1** after removal of H_2O by evacuation.

Keywords: Ferromagnetic interaction; Supramolecule; Channel; Nitroxide; Ligand; Free radical

1. Introduction

Self-assembled discrete oligonuclear complexes with paramagnetic transition metal-ions have fascinated chemists owing to their architectural beauty as well as their mesoscopic physical properties [1]. Supramolecular techniques such as host–guest complex formation have been applied to fine-tune molecule-based magnetic materials [2]. In the course of our study on the role of radical-substituted pyrimidine (PM) as ferro- and antiferromagnetic couplers, we have found that discrete hexanuclear arrays $[CuX_2\cdot(4PMNN)]_6$ (**1**: X = Cl; **2**: X = Br; 4PMNN = 4-pyrimidinyl nitronyl nitroxide) exhibited ferromagnetic intermolecular interactions [3]. The crystals of **1** and **2** have a channel structure in a direction perpendicular to the molecular plane (Fig. 1) [3,4], and we named them 'magnetic nanotubes' [4] since the channel has a diameter of 11.5 Å defined with the opposing Cu···Cu distance. The crystal structure analysis of **1** and **2** suggests that the inner axial sites of the copper(II) ion are partially hydrated with the occupancy of the water molecule as small as 0.3 [3]. Host–guest complexation of these porous complexes was attempted because the vacant sites are assumed to be available for further coordination from guest molecules.

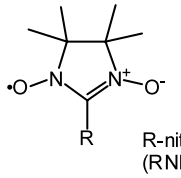

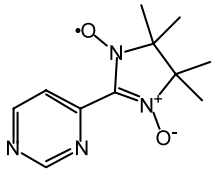

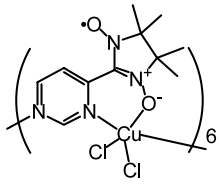

1

While conventional host compounds such as crown ethers possess lone-pairs inside as metal-ion binding

* Corresponding author. Tel.: +81-424-43-5490; fax: +81-424-43-5501.
E-mail address: ishi@pc.uec.ac.jp (T. Ishida).

0277-5387/03/$ - see front matter © 2003 Elsevier Science Ltd. All rights reserved.
doi:10.1016/S0277-5387(03)00206-7

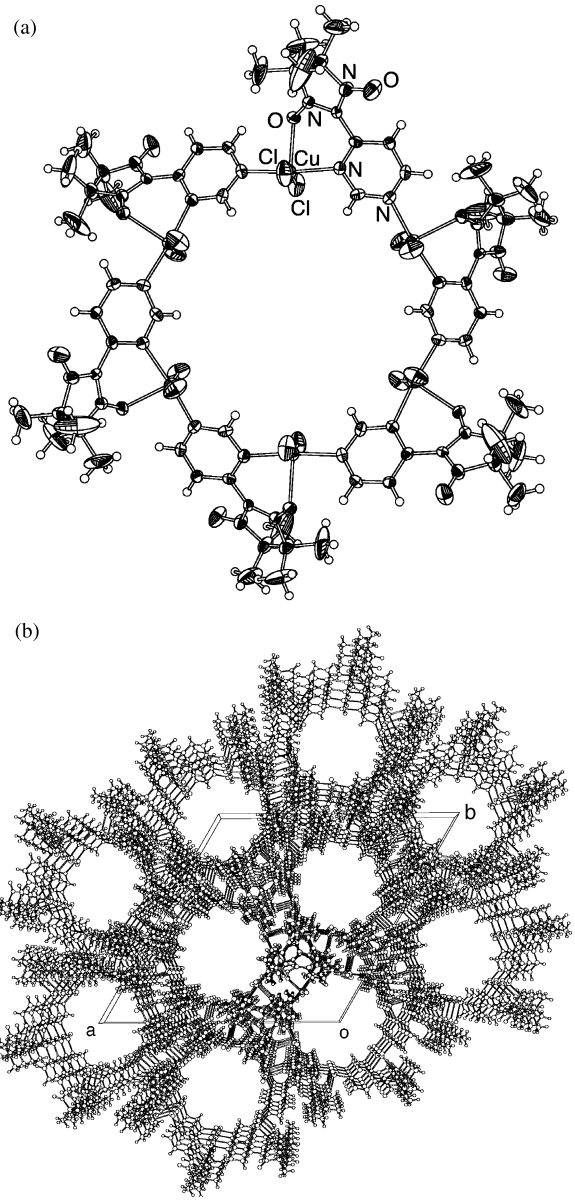

Fig. 1. (a) Molecular structure of **1**. (b) Molecular arrangement in the crystal of **1** viewed along the *c* axis.

sites, **1** and **2** conversely have lone-pair accepting sites inside. Thus, amines, acids, and halides are candidates for guest molecules in the present study. Actually, some organic molecules such as 1,3,5-tricarboxylbenzene were found to be incorporated in **1** [4]. We will report here new host–guest complexes of **1** with alkali-metal chlorides, namely, $(MCl)_n$@**1**. Very interestingly, they showed remarkable enhancement of the ferromagnetic interaction compared with that of **1** itself. In addition to the enhancement, we also found that reduction of the ferromagnetic interaction in the hydrated complex, $(H_2O)_n$@**1**, after removal of water by evacuation.

2. Experiments

Complex **1** as an almost empty specimen was synthesized according to the reported method [3]. Host–guest complexation was carried out by means of co-crystallization. The following procedure is typical. A homogenous methanol solution (12 ml) containing 4PMNN (42.1 mg, 0.18 mmol), $CuCl_2\cdot 2H_2O$ (32.7 mg, 0.19 mmol), and a guest material LiCl (35.7 mg, 0.85 mmol) was allowed to stand at room temperature for 2 days. Black needles were precipitated from the above mixture and collected on a filter. In the case of hydration, to a clear methanol solution (8 ml) containing 4PMNN (33.0 mg, 0.14 mmol) and $CuCl_2\cdot 2H_2O$ (23.1 mg, 0.14 mmol) was added water (0.5 ml), and black needles were precipitated and collected.

The dehydration experiment of $(H_2O)_n$@**1** was carried out as follows. After the magnetic susceptibility of freshly prepared $(H_2O)_n$@**1** was measured in a usual capsule-type holder, the capsule was picked up out of a magnetometer probe, opened carefully, and subjected to evacuation in a vacuum desiccator with an oil rotary pump for 2 days. The capsule was capped again and the magnetic properties of the sample in the same capsule were measured under the same conditions as the first measurement.

Elemental analyses (C, H, N) were done on a Fisons EA-1108 by a usual combustion method. X-Ray diffraction data were collected on a Raxis-Rapid IP diffractometer (Rigaku). The cell constants of the host–guest complexes were determined using graphite monochromated Cu Kα radiation at 298 ± 2 K. Magnetic susceptibilities of randomly oriented polycrystalline samples were measured on a Quantum Design MPMS SQUID magnetometer equipped with a 7 T coil in a temperature range 1.8–300 K. The magnetic responses were corrected with diamagnetic blank data of the sample holder obtained separately. The diamagnetic contribution of the sample itself was estimated from Pascal's constants.

3. Results

Co-crystallization methods afforded polycrystalline samples of $(MCl)_n$@**1**, which apparently has the same

Table 1
Elemental analysis of $(MCl)_n$@**1** and **1**

	C	N	H (%)
$(LiCl)_6(4PMNN\cdot CuCl_2)_6$	31.50 (32.06)	13.41 (13.60)	2.27 (3.67)
$(NaCl)_2(4PMNN\cdot CuCl_2)_6$	33.69 (33.94)	13.72 (14.39)	4.77 (3.89)
$(KCl)_2(4PMNN\cdot CuCl_2)_6$	33.70 (33.48)	13.72 (14.20)	4.77 (3.83)
$(4PMNN\cdot CuCl_2)_6$	36.19 (35.74)	14.79 (15.15)	4.39 (4.09)

Calculated values are written in parenthesis.

crystal habit as that of the empty complex (**1**). Table 1 summarizes the results of elemental analysis on $(MCl)_n$@**1** and **1**. This analysis clearly demonstrates the presence of guest molecules in the co-crystallized specimens from comparison with that of **1**, and suggests the following formula, $(LiCl)_6$@**1**, $(NaCl)_2$@**1**, and $(KCl)_2$@**1**. To clarify whether the guest molecules are located in an endohedral or exohedral position of the macrocyclic structure, X-ray crystallographic analysis was carried out on single crystals. The specimens belong to a rhombohedral crystal system with cell constants similar to those of **1**. Although the analysis of $(MCl)_n$@**1** revealed the presence of appreciable electron densities within a tube, especially in the inner axial site of the copper(II) ions, the atomic positions of the guest molecules could not be determined precisely owing to disorder. We can report only the cell constants of these complexes (Table 2). The cell constants were varied beyond the standard deviations as the guest molecules are incorporated but the cell dimensions were not so expanded as expected from the complex formation. These findings indicate that the molecular structure of the host (**1**) is retained and that the guest molecules are incorporated within a tube; thus, these complexes are expressed as $(guest)_n$@**1**. In the case of the hydrated complex the water molecules seems to escape readily [3] because the elemental analysis of $(H_2O)_n$@**1** showed poor reproducibility.

The magnetic properties of $(MCl)_n$@**1**, $(H_2O)_n$@**1**, and **1** were measured on a SQUID magnetometer under the same conditions. Fig. 2(a) summarizes the temperature dependences of the product of the molar magnetic susceptibility (χ_{mol}) and T for them. The peak formation of the $\chi_{mol}T$ value around 7 K for **1** is ascribed both to the *intermolecular ferromagnetic* and intramolecular antiferromagnetic interactions [3,4]. Upon cooling from 100 K, the $\chi_{mol}T$ values of the host–guest complexes of **1** increased more significantly and reached a higher maximum than that of **1** itself. The similarity of their magnetic behavior strongly indicates that the same magnetic coupling mechanism is involved and that structural perturbation from the original host (**1**) lead to the enhancement of the ferromagnetic coupling.

Fig. 2(b) shows the preliminary results on the bromide analogue. Complexation of 4PMNN and $CuBr_2$ gave the corresponding macrocyclic compound (**2**), and

Table 2
Cell constants of $(MCl)_n$@**1**, $(H_2O)_n$@**1**, and **1**

	a (Å)	c (Å)	V (Å^3)
$(LiCl)_6$@**1**	28.122(3)	12.415(3)	8502(2)
$(NaCl)_2$@**1**	28.247(2)	12.254(2)	8467(2)
$(KCl)_2$@**1**	28.1(1)	12.39(7)	8517(51)
1	28.261(2)	12.378(1)	8561(1)

$\alpha = \beta = 90°$, $\gamma = 120°$, $a = b$.

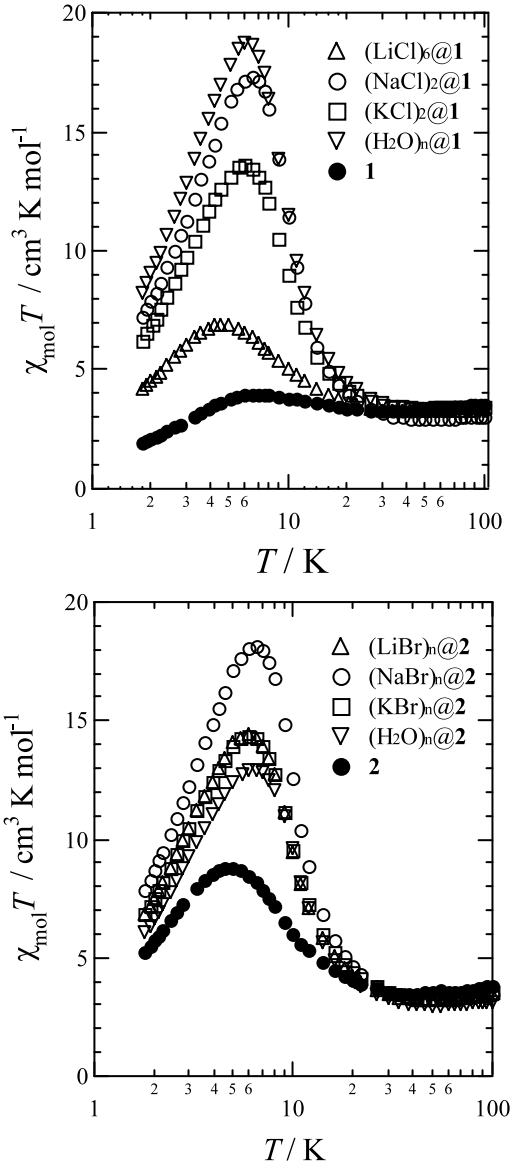

Fig. 2. Temperature dependence of the product of χ_{mol} and T measured at 5000 Oe for $(MCl)_n$@**1**, $(H_2O)_n$@**1**, and **1** (a) and $(MCl)_n$@**2**, $(H_2O)_n$@**2**, and **2** (b).

host–guest compounds are similarly prepared according to the co-crystallization method, affording $(MBr)_n$@**2** and $(H_2O)_n$@**2**. The magnetic susceptibility measurements under the same conditions as those of the chloride analogues also showed enhancement of the ferromagnetic coupling.

In order to exploit reversible control of magnetic couplings, we examined water molecules as a guest. Fig. 3 shows the temperature dependences of $\chi_{mol}T$ values for $(H_2O)_n$@**1** before and after evacuation. Before evacuation, with a decrease of temperature the $\chi_{mol}T$ value of $(H_2O)_n$@**1** increased more significantly than that of **1** itself just like $(MCl)_n$@**1**. After evacuation, the $\chi_{mol}T$ value was almost coincident with that of **1**. The change is quite drastic as indicated with an arrow in Fig.

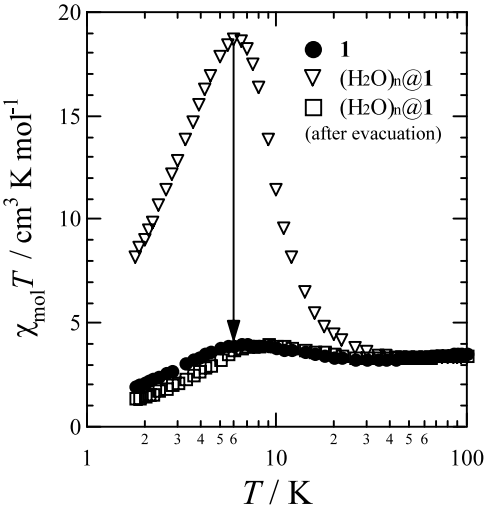

Fig. 3. Temperature dependence of the product of χ_{mol} and T of freshly prepared $(H_2O)_n$@**1** and evacuated $(H_2O)_n$@**1** together with that of **1** measured at 5000 Oe.

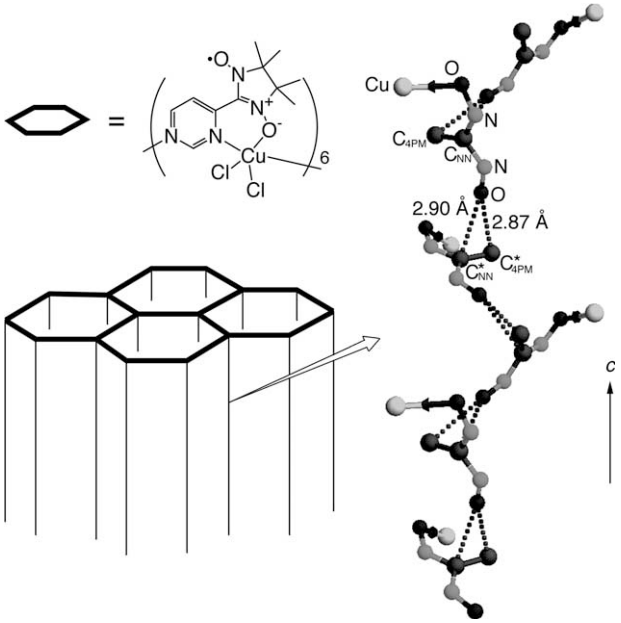

Fig. 4. (Left) Schematic drawing of the tube-like cavity in the crystal of **1**. (Right) Linear array of nitronyl nitroxide groups with a T-shaped configuration along the c-axis. Six ONC(–C)NO–Cu moieties are drawn. Interatomic distances within the sum of the van der Waals radii are shown with dotted lines. Symmetry operation code for * is $-y+2/3$, $x-y+1/3$, $z+1/3$.

3. This finding supports that the molecular and crystal structures of the host (**1**) are preserved during the evacuation process and the enhancement of the ferromagnetic coupling is caused by the guest inclusion. We further attempted to repeat the enhancement of the magnetic coupling by moisture adsorption. After the specimen was allowed to stand in a humid atmosphere its magnetic susceptibility was measured under the same conditions. However, such an enhancement could not be observed probably because of failure of water adsorption.

4. Discussion

We briefly review the magnetic coupling mechanisms in the crystal of **1** [3,4] in order to discuss the origin of the enhancement of ferromagnetic interaction. We can find a chelate structure in the repeating unit $CuCl_2\cdot$(4PMNN), in which the nitronyl notroxide (NN) oxygen atom is axially coordinated to the copper ion. The orthogonality of Cu $3d_{x^2-y^2}$ and O $2p_z$ orbitals favors ferromagnetic interaction between the Cu and NN spins [5]. We can also find that the PM bridges two copper ions. We have clarified the relationship between coordination structures and magnetic couplings in PM-bridged copper(II) complexes [6–9]. In the present case, every PM nitrogen atom is coordinated at an equatorial position and consequently the PM bridge should be an antiferromagnetic coupler. Furthermore, relatively short van der Waals contacts between columns can be pointed out, as shown with dotted lines in Fig. 4. The shortest distance is found between a terminal NN oxygen atom and a carbon atom of the PM 4-position in a neighboring molecule ($O\cdots C_{4PM}$). The second shortest distance is found between a terminal NN oxygen atom and a central NN carbon atom ($O\cdots C_{NN}$). Almost vertical spatial arrangement of two NN units gives a T-shaped configuration. This contact brings about ferromagnetic coupling on the basis of McConnell's theory [10–12]. The geometry depicted in Fig. 4 infinitely repeats by a 3_1 screw symmetry along the c axis, i.e., perpendicular to the macrocyclic molecular plane, among the columns. Detailed analysis suggests that intermolecular ferromagnetic interaction competes with intramolecular antiferromagnetic interaction and that the increasing behavior of the $\chi_{mol}T$ values on cooling from 100 to 7 K can be ascribed to the intermolecular interaction between the local $S=1$ units of the strongly correlated Cu and NN spins [3].

Now we will discuss what structural deformation affects the ferromagnetic coupling. We found a few correlations between the magnetic properties and cell parameters, as shown in Fig. 5(a) and (b). The cell volume (V) varied from 8561 to 8467 Å^3 and the $\chi_{mol}T$ maximum varied from 4 to 17 cm^3 K mol^{-1}. Obviously the sample with a smaller cell volume shows stronger ferromagnetic interaction. Fig. 5(a) shows the $\chi_{mol}T$ maximum vs. V plot for the complexes in the present study and also summarize the $\chi_{mol}T$ maximum values for the complexes containing organic guest molecules which have been previously reported [4]. In order to elucidate which axis is responsible for the variation of the cell volume, we plotted the $\chi_{mol}T$ maximum values against the a ($=b$) and c axes, and found a correlation

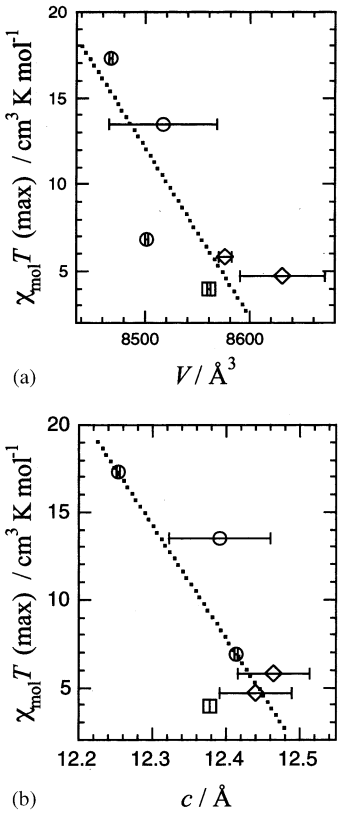

Fig. 5. Correlations between the $\chi_{mol}T$ maximum value and the cell volume (V) (a) and between the $\chi_{mol}T$ maximum value and the c length (b) for the host–guest compounds of **1**. Guest molecules are MCl (M = Li, Na, K) (circles), organic compounds [4] (diamonds), and none (squares). Dotted lines are shown for a guide to the eye.

with the c axis (Fig. 5(b)). The sample with a shorter c axis exhibits stronger ferromagnetic interaction, whilst the a axis is insensitive to the guest inclusion. This finding is rationalized by the fact that the rigid macrocyclic structure parallel to the ab plane is composed of covalent bonds. On the other hand, the column direction along the c axis can accommodate the cell shrinkage due to the guest inclusion, because the molecular stack was dominantly made with van der Waals interaction.

The guest inclusion causes to shrink the cell but not each molecule. The enhancement of the ferromagnetic interaction after the guest inclusion supports that the ferromagnetic interaction originates in the van der Waals contacts as depicted in Fig. 4. Therefore, we believe that shorter O···C distances in the T-shape arrangement of the radical moieties cause stronger ferromagnetic interaction. The shrinkage of the cell suggests the presence of attractive interaction in the host–guest system; in particular, the shortening of the c length may be interpreted in terms of guest–guest attractive interaction. There seem to be Coulombic interaction and hydrogen-bond interaction in $(MCl)_n$@**1** and $(H_2O)_n$@**1**, respectively, in the tube-like cavity along the c axis.

The guest inclusion accompanys not only shortening intermolecular contacts but also other possible geometrical deformation and electronic structural modification of the host, especially distortion of the magnetic orbital of the copper ion. Several factors are responsible for the variation of the magnetic behavior, and accordingly more detailed structural evidence could improve the understanding of the magneto-structure relationship.

5. Summary

Discrete hexanuclear complexes **1** and **2** construct a perfect column perpendicular to the macrocyclic molecular plane. The nano-scaled honeycomb-like channels are available for the host–guest complexes, and actually the magnetic properties are tuned by the inclusion. The present work can be regarded as an example of porous organic–inorganic hybrid solids utilized for chemically switchable magnetic materials.

Acknowledgements

This work was supported by a Grant-in-Aid for Scientific Research on Priority Areas of 'Molecular Conductors and Magnets' (No. 730/11224204) and by a Grant-in-Aid for Scientific Research (No. 13640575), both from the Ministry of Education, Culture, Sports, Science and Technology, Japan.

References

[1] (a) J.R. Friedman, M.P. Sarachik, J. Tejada, R. Ziolo, Phys. Rev. Lett. 76 (1996) 3830;
(b) L. Thomas, F. Lionti, R. Ballow, D. Gatteschi, R. Sessoli, B. Barbara, Nature 383 (1996) 145;
(c) W. Wernsdorfer, N. Allega-Alcalde, D.N. Hendrickson, G. Christou, Nature 416 (2002) 406.

[2] (a) Kusaka, T. Ishida, T. Nogami, Mol. Cryst. Liq. Cryst. 379 (2002) 259;
(b) K. Awaga, E. Coronado, M. Drillon, MRS Bull. (2000) 52;
(c) A. Rujiwatra, C.J. Kepert, J.B. Claridge, M.J. Rosseinsky, H. Kumagai, M. Kurmoo, J. Am. Chem. Soc. 123 (2001) 10584;
(d) S. Decurtins, R. Pellaux, G. Antorrena, F. Palacio, Coord. Chem. Rev. 190–192 (1999) 841;
(e) A. Cornia, M. Affronte, A.G.M. Jansen, G.L. Abbati, D. Gatteschi, Angew. Chem., Int. Ed. Engl. 38 (1999) 2264;
(f) A. Cornia, A. Caneschi, P. Dapporto, A.C. Fabretti, D. Gatteschi, W. Malavasi, C. Sangregorio, R. Sessoli, Angew. Chem., Int. Ed. Eng. 38 (1999) 1780;
(g) M. Nakano, A. Nakahama, S. Okuno, G.-E. Matsubayashi, W. Mori, M. Katada, Mol. Cryst. Liq. Cryst. 376 (2002) 399;
(h) C. Rancurel, N. Daro, O.B. Borobia, E. Herdtweck, J.-P. Sutter, Eur. J. Org. Chem. (2003) 167.

[3] J. Omata, T. Ishida, D. Hashizume, F. Iwasaki, T. Nogami, Inorg. Chem. 40 (2001) 3954.
[4] J. Omata, T. Ishida, D. Hashizume, F. Iwasaki, T. Nogami, Polyhedron 20 (2001) 1557.
[5] (a) A. Caneschi, D. Gatteschi, J. Laugier, P. Rey, J. Am. Chem. Soc. 109 (1987) 2191;
(b) A. Caneschi, D. Gatteschi, P. Rey, R. Sessoli, Acc. Chem. Res. 22 (1989) 392.
[6] T. Ishida, T. Kawakami, S.-I. Mitsubori, T. Nogami, K. Yamaguchi, H. Iwamura, J. Chem. Soc., Dalton Trans. (2002) 3177.
[7] (a) M. Yasui, Y. Ishikawa, N. Akiyama, T. Ishida, T. Nogami, F. Iwasaki, Acta Crystallogr., Sect. B 57 (2001) 288;
(b) F. Mohri, K. Yoshizawa, T. Yamabe, T. Ishida, T. Nogami, Mol. Eng. 8 (1999) 357;
(c) R. Feyerherm, S. Abens, D. Günther, T. Ishida, M. Meissner, M. Meschke, T. Nogami, M. Steiner, J. Phys.: Condens. Mat. 12 (2000) 8495.
[8] (a) T. Ishida, T. Nogami, Recent Res. Dev. Pure Appl. Chem. 1 (1997) 1;
(b) T. Ishida, K. Nakayama, M. Nakagawa, W. Sato, Y. Ishikawa, M. Yasui, F. Iwasaki, T. Nogami, Synthetic Met. 85 (1997) 1655.
[9] T. Ezuhara, K. Endo, K. Matsuda, Y. Aoyama, New J. Chem. 24 (2000) 609.
[10] H.M. McConnell, J. Chem. Phys. 39 (1963) 1910.
[11] (a) K. Inoue, H. Iwamura, Chem. Phys. Lett. 207 (1995) 551;
(b) T. Kawakami, A. Oda, W. Mori, K. Yamaguchi, K. Inoue, H. Iwamura, Mol. Cryst. Liq. Cryst. 279 (1996) 29.
[12] T. Kawakami, Y. Kitagawa, F. Matsuoka, Y. Yamashita, K. Yamaguchi, Polyhedron 20 (2001) 1235.

Available online at www.sciencedirect.com
SCIENCE DIRECT®
PERGAMON
Polyhedron 22 (2003) 2557–2564
POLYHEDRON
www.elsevier.com/locate/poly

meta-Phenylene-bridged bis(imino nitroxide) biradicals as potential high-spin ligands

Takayuki Ichimura, Kentaro Doi, Chiemi Mitsuhashi, Takayuki Ishida *, Takashi Nogami

Department of Applied Physics and Chemistry, The University of Electro-Communications, Chofu, Tokyo 182-8585, Japan

Received 7 October 2002; accepted 14 January 2003

Abstract

Frozen-solution ESR spectra of 4-hydroxy-1,3-phenylenebis(imino nitroxide) (**1**) and 2-hydroxy-5-methyl-1,3-phenylenebis(imino nitroxide) (**2**) in toluene showed fine structures due to the triplet states (imino nitroxide stands for 2-substituted 4,4,5,5-tetramethylimidazolin-3-yloxyl). The temperature dependence of the $\Delta m_s = \pm 2$ signal intensity for **1** followed the Curie law, suggesting that **1** has a ground triplet state. On the other hand, the triplet signal intensity of **2** did not obey the Curie law. The intramolecular magnetic coupling seems to depend on the twist angle between the imino nitroxide group and benzene ring. Complexation with $Cu(CH_3CO_2)_2 \cdot H_2O$ in ethanol gave a mononuclear complex, $Cu(\mathbf{L}^1)_2$, where $\mathbf{L}^1$ is the anionic form derived from **1**. The X-ray diffraction study of $Cu(\mathbf{L}^1)_2$ revealed that the central copper(II) ion had a twisted square plane; the dihedral angle between two chelating O–Cu–N planes was 45°. The magnetic measurements of $Cu(\mathbf{L}^1)_2$ indicated the presence of intramolecular ferromagnetic interaction, which is ascribed mainly to a ground quartet formation at the directly bonded radical–copper–radical moiety with $J_{radical-copper}/k_B = +132 \pm 5$ K, where the Heisenberg spin Hamiltonian is defined as $H = -2JS_iS_j$.

Keywords: Ferromagnetic interaction; Nitroxide; Ligand; Free radical; ESR

1. Introduction

Polymeric complex formation containing transition metal ions and bridging radical ligands [1], especially high-spin oligoradical ligands [2], is supposed as an important strategy for constructing three-dimensional ferri- and ferromagnetic networks. In some case, large counter anions such as 1,1,1,5,5,5-hexafluoropentane-2,4-dionate (hfac) seem to be a hindrance against constructing strongly exchange-coupled systems [3], though the hfac salts facilitate the complex formation owing to the enhanced Lewis acidity of the metal ion. We will report here the synthesis and magnetic properties of 4-hydroxy-1,3-phenylenebis(imino nitroxide) (**1**) and 2-hydroxy-5-methyl-1,3-phenylenebis(imino nitroxide) (**2**) in order to exploit new high-spin (triplet) ligands, where imino nitroxide denotes 2-substituted 4,4,5,5-tetramethylimidazolin-3-yloxyl. The parent bis(imino nitroxide) (**3**) has recently been clarified to possess a ground triplet state by means of ESR and magnetic susceptibility measurements [4]. There have also been reports on the corresponding bis(nitronyl nitroxide) radicals (nitronyl nitroxide stands for 2-substituted 4,4,5,5-tetramethylimidazolin-3-yloxyl-1-oxide) which reveals that the *meta*-phenylene spacer basically play a role of a ferromagnetic coupler [4–7], being consistent with the π-topological symmetry or spin-polarization scheme [8]. On the other hand, reports on the ground spin states of bis(imino nitroxides) are rare [4] and to our knowledge those of **1** and **2** are unknown so far. The central carbon atom in the nitronyl nitroxide ONCNO group has a node of the singly occupied molecular orbital (SOMO) because of the symmetry. The unsymmetric imino nitroxide ONCN group has a SOMO coefficient at the carbon atom, and the role of *m*-phenylene spacers may be modulated accordingly.

* Corresponding author. Tel.: +81-424-43-5490; fax: +81-424-43-5501.
E-mail address: ishi@pc.uec.ac.jp (T. Ishida).

0277-5387/03/$ - see front matter
doi:10.1016/S0277-5387(03)00299-7

Ligands $\mathbf{L}^1$ and $\mathbf{L}^2$ are planned to be derived from deprotonation of **1** and **2**. They are thought to possess the following advantages in pursuing high-T_C or T_N metal–radical magnets: (1) Chelation effect stabilizes coordination without hfac anions. (2) Anionic ligands $\mathbf{L}^1$ and $\mathbf{L}^2$ purge diamagnetic counter anions, which insulate magnetic networks. (3) Oligo-radicals have potential ability of forming three-dimensional networking structures owing to a multi-dentate character. We will also report here the crystal structure and magnetic properties of a mononuclear complex, $Cu(\mathbf{L}^1)_2$, as a prototype for possible polymeric metal–radical hybrid solids.

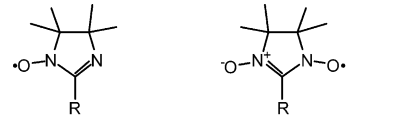

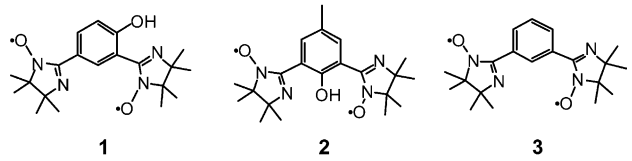

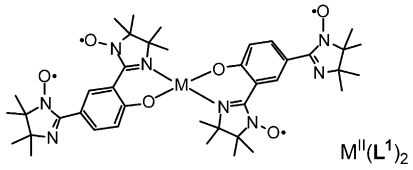

2. Experimental

2.1. Materials

We prepared bis(nitronyl nitroxides) as precursors of **1**–**3** according to Ullman et al.'s method [9]. Condensation reaction of the corresponding diformylphenols with 2,3-bis(hydroxylamino)-2,3-dimethylbutane followed by oxidation with sodium metaperiodate gave bis(nitronyl nitroxide) biradicals. The resultant biradicals were deoxygenated with nitrous acid [10]. Treatment of the bis(nitronyl nitroxides) with sodium nitrite and acetic acid in dichloromethane afforded the corresponding bis(imino nitroxide) biradicals. The specimens suitable for ESR, magnetic measurements, and X-ray diffraction study were purified by passing a short column (silica gel eluted with 1/1 ethyl acetate–hexane) followed by repeated recrystallization from dichloromethane–hexane. Compound **1**: m.p. 119 °C (dec.), ESR (benzene, room temperature) $g = 2.0062$, $a_N = 4.4$, 2.2 G. A broad dipolar signal overlapped the hyperfine structure. Compound **2**: m.p. 161–163 °C, ESR (benzene, room temperature) $g = 2.0062$, $a_N = 4.36$, 2.16 G. The observed hyperfine structure was well reproduced as a strongly exchanged "quintet of quintet" pattern. Compound **3** was satisfactorily analyzed with the literature data [4].

The following complexation procedure is typical. A methanol solution (1.3 ml) containing **1** (37 mg, 0.10 mmol) was added to a methanol solution (1.7 ml) containing $Cu(CH_3CO_2)_2 \cdot H_2O$ (10 mg, 0.05 mmol), and the combined solution was allowed to stand in a refrigerator overnight. Complex $Cu(\mathbf{L}^1)_2$ was precipitated as black needles. Anal. Calc. for $C_{40}H_{54}N_8O_6Cu$ ($Cu(\mathbf{L}^1)_2$): C, 59.57; H, 6.75; N, 13.90. Found: C, 59.59; H, 6.63; N, 13.58%.

2.2. Instruments

X-ray diffraction data of single crystals were collected on a Rigaku R-axis RAPID diffractometer with graphite monochromated Mo Kα ($\lambda = 0.71069$ Å) radiation for **1** and Cu Kα ($\lambda = 1.5418$ Å) radiation for $Cu(\mathbf{L}^1)_2$ at 100 K. The structures were solved by direct methods and expanded using Fourier techniques in the TEXSAN program package [11]. Numerical absorption correction was used. The thermal displacement parameters were refined anisotropically for non-hydrogen atoms. Hydrogen atoms were located at the calculated positions for $Cu(\mathbf{L}^1)_2$ and a disordered portion in **3**. Full-matrix least-squares methods were applied using all of the unique diffraction data.

ESR spectra were recorded on a Brucker ESP300E X-band (9.7 GHz) spectrometer equipped with an Oxford cryostat for low-temperature measurements. Saturation effects were carefully removed from the spectra by lowering the microwave power. Simulated spectra for the frozen and liquid solutions were calculated in the WINEPR SIMFONIA program [12].

Magnetic susceptibilities of polycrystalline samples were measured on a Quantum Design MPMS SQUID magnetometer equipped with a 7 T coil in a temperature range 1.8–300 K. The magnetic responses were corrected with diamagnetic blank data of the sample holder obtained separately. The diamagnetic contribution of the sample itself was estimated from Pascal's constants.

3. Results and discussion

3.1. Molecular and crystal structures

The molecular and crystal structures of **1** are shown in Fig. 1. Selected crystallographic parameters are listed in Table 1. The crystal structure was solved in an orthorhombic *Pbca* space group. All of the hydrogen atoms were experimentally found. The molecules are

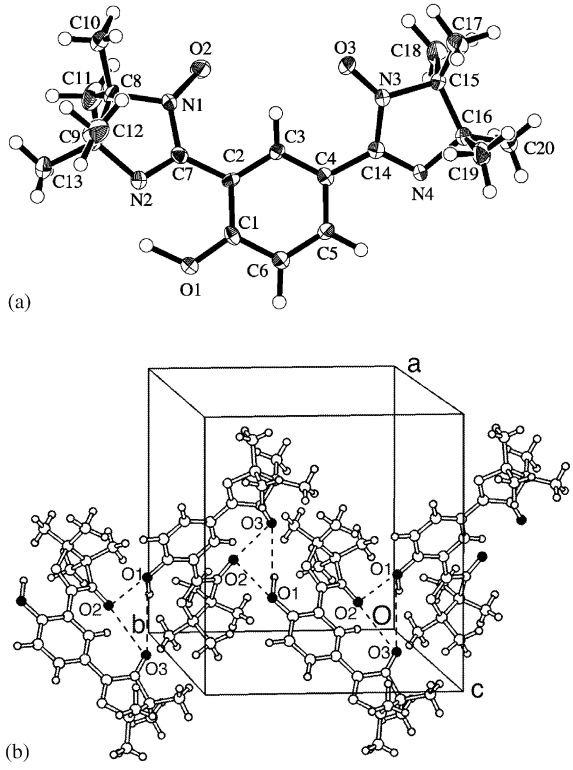

Fig. 1. (a) Ortep drawing of **1** with thermal ellipsoids at the 50% level for non-hydrogen atoms. (b) Molecular arrangements in the crystal of **1**. The oxygen atoms are darkened. The interatomic distances of O1···O2# and O1···O3# are 3.276(3) Å and 3.746(4) Å, respectively, where the symmetry operation code of # is $-x+3/2$, $y-1/2$, z.

Table 1
Crystallographic parameters of **1** and Cu($\mathbf{L}^1$)$_2$

Compounds	**1**	Cu($\mathbf{L}^1$)$_2$
Empirical formula	$C_{20}H_{28}N_4O_3$	$C_{40}H_{54}N_8O_6Cu_1(H_2O)_2$
Habit	red block	black block
Crystal system	orthorhombic	monoclinic
Space group	*Pbca*	$P2_1/c$
a (Å)	13.0055(4)	12.630(3)
b (Å)	12.1683(4)	14.160(4)
c (Å)	24.954(1)	24.700(6)
β (°)	90.	93.645(6)
V (Å^3)	3949.1(4)	4408(1)
Z	8	4
D_{calc} (g cm^{-3})	1.253	1.215
λ (Å)	0.71069	1.5418
T (K)	100	100
Reflections	3547	3457
$R(F^2)$ ($I > 2\sigma(I)$)	0.0989	0.0688
$R_w(F)$ (all data)	0.196	0.164

almost planer with respect to the π-conjugation system, as indicated by the dihedral angles between imidazoline and benzene rings (23.1(1)° and 8.0(1)° for the imino nitroxide groups at the 2- and 4-positions, respectively). An intramolecular hydrogen bond is found among the O1–H···N2 moiety, forming an almost planar six-membered ring.

As Fig. 1(b) shows, the intermolecular short contacts were found between hydroxyl oxygen and imino nitroxide oxygen atoms within 3.3 Å. Hydrogen bonding is an important factor for the crystal engineering and is also proposed to provide a magnetic coupling pathway [13–15]. A linear molecular arrangement of the molecule of **1** can be found along the b-axis with the O1–H···O2 and O1–H···O3 hydrogen bonds. Magnetic measurements of the crystal of **1** (see below) suggest that the intermolecular magnetic interactions through the hydrogen bonds (Fig. 1(b)) might be antiferromagnetic.

Unfortunately, **2** did not afford good crystals for the X-ray diffraction study. The crystal structure of **3** was satisfactorily analyzed and reproduced the results previously reported [4]. We collected the diffraction data at 100 K and intermolecular short contacts are precisely determined to be 3.30 and 3.33 Å for O···N and O···O at the nearest NO groups (Fig. 2), which are close to the sum of the van der Waals radii (ca. 3 Å). Consequently we can propose that the crystal of **3** consists of an antiferromagnetically correlated dimer.

In the course of our attempts to prepare transition metal ion complexes containing $\mathbf{L}^1$ and $\mathbf{L}^2$, Cu($\mathbf{L}^1$)$_2$ was obtained as single crystals, while Co($\mathbf{L}^1$)$_2$, Ni($\mathbf{L}^1$)$_2$, and Zn($\mathbf{L}^1$)$_2$ only as fine powder forms. Fig. 3 shows the molecular structure of Cu($\mathbf{L}^1$)$_2$. Selected crystallographic parameters are listed in Table 1 and important geometrical parameters are in Table 2. Complex Cu($\mathbf{L}^1$)$_2$ is mononuclear; outer imino nitroxide groups are free from metal coordination and no meaningful interatomic contacts were found among molecules. The thermal displacement factors of methyl groups were somewhat large even at 100 K, probably due to the presence of conformational isomers. However, disorder models did not improve the R factor.

The copper ion has an intermediate geometry between a square-planar structure and a tetrahedral one. Two chelating planes are canted each other, forming a dihedral angle of 45° between two planes of O1–Cu1–N2 and O4–Cu1–N6. Kahn, Luneau, and their coworkers clearly demonstrated that the orthogonal ar-

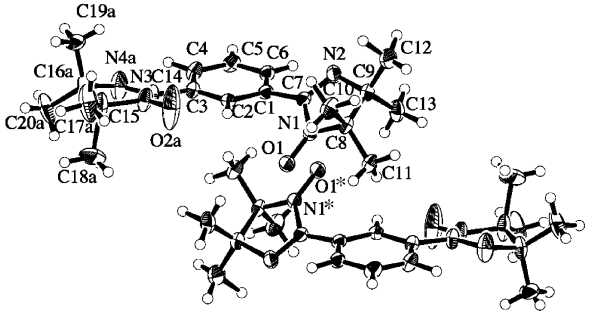

Fig. 2. Ortep drawing of two neighboring molecules of **3** with thermal ellipsoids at the 50% level. Only a major conformation is drawn. Interatomic distances are: O1···N1*, 3.302(3) Å; O1···O1*, 3.327(5) Å. The symmetry operation code for * is $-x+1$, $-y$, $-z+1$.

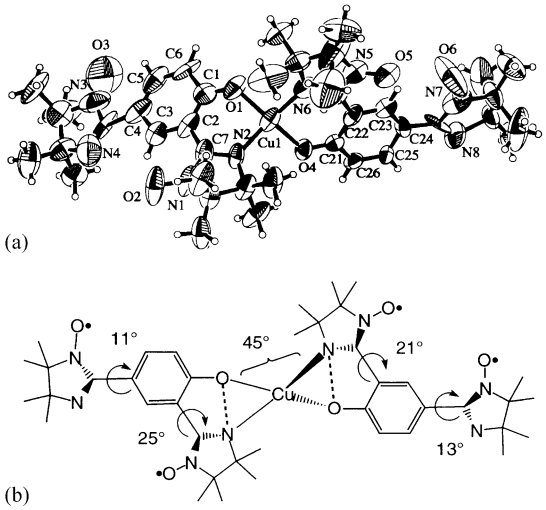

Fig. 3. (a) Ortep drawing of Cu($\mathbf{L}^1$)$_2$ with thermal ellipsoids at the 30% level. (b) Selected dihedral angles.

Table 2
Selected bond lengths (Å) and angles (°) in Cu($\mathbf{L}^1$)$_2$

Bond lengths	
Cu(1)–O(1)	1.905(5)
Cu(1)–O(4)	1.874(5)
Cu(1)–N(2)	1.980(8)
Cu(1)–N(5)	2.015(8)
O(1)–C(1)	1.30(1)
O(2)–N(1)	1.28(1)
O(3)–N(3)	1.20(2)
N(2)–C(7)	1.29(1)
O(4)–C(21)	1.27(1)
O(5)–N(5)	1.293(9)
N(5)–C(27)	1.40(1)
O(6)–N(7)	1.32(2)
Bond angles	
O(1)–Cu(1)–O(4)	148.3(3)
O(1)–Cu(1)–N(2)	92.0(3)
O(1)–Cu(1)–N(6)	99.0(3)
O(4)–Cu(1)–N(2)	94.3(3)
O(4)–Cu(1)–N(6)	92.1(3)
N(2)–Cu(1)–N(6)	147.5(3)
Cu(1)–O(1)–C(1)	127.3(7)
Cu(1)–N(2)–C(7)	121.9(7)
Cu(1)–O(4)–C(21)	128.3(6)
Cu(1)–N(6)–C(27)	122.6(8)
N(6)–C(27)–C(22)	124(1)
N(2)–C(7)–C(2)	126(1)

rangement between two magnetic orbitals, an organic π-spin and an inorganic dσ-spin, led to ferromagnetic coupling in radical–metal compounds such as the high-spin *o*-semiquinone–copper(II) complex [16] and 2-pyridyl imino nitroxide complexes containing copper(II) and nickel(II) ions [17]. In the present study, assuming that the imino nitrogen atom carrying a radical π-spin is directly bonded to the copper(II) ion at the equatorial position where the $d_{x^2-y^2}$ magnetic orbital resides, we can expect ferromagnetic coupling between the π and d spins and consequently a local high-spin ($S = 3/2$) in the radical–copper–radical moiety.

Each $\mathbf{L}^1$ moiety has a less coplanar π-conjugation system than those of **1**. The dihedral angles are shown in Fig. 3(b). Furthermore, the directions of the unsymmetrical ONCN groups are different between **1** and $\mathbf{L}^1$; the ONCN groups of **1** are arranged in a head-to-head manner, i.e., two oxygen atoms were closely located (Fig. 1(a)), whereas the ONCN groups are in a head-to-tail manner for one biradical portion of Cu($\mathbf{L}^1$)$_2$.

3.2. ESR spectra

We measured frozen-solution ESR spectra of **1**–**3** in toluene. Fig. 4 shows fine structures for **1** and **2**. The spectrum of **1** clearly exhibits six transition lines together with a central doublet signal as an impurity. The width between the most outer signals corresponds to a zero-field splitting parameter $|2D'|$ and the distance between the dipoles was calculated to be 5.1 Å from $|D'| = 204$ G. The X-ray crystallographic analysis revealed that two imino nitroxide oxygen atoms were closely located with the O2···O3 distance of 3.944 (4) Å. Viewing from spin delocalization on the ONCN π-system, the distance between the spins is better estimated from that of C···C than that of O···O. The C7···C14 distance is 5.028 (5) Å, which is very close to the value

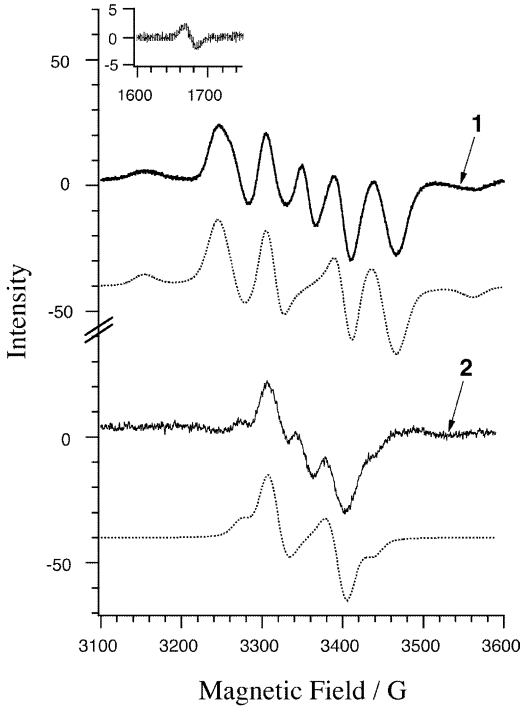

Fig. 4. Frozen solution ESR of **1** (10.8 K) and **2** (11.2 K) in toluene. The $\Delta m_s = \pm 2$ transition signal in a half-field region for **1** is shown in the inset. Simulated spectra were shown with dotted lines. For the optimized parameters, see the text.

calculated above. Another parameter $|E'|$ was estimated to be small (ca. <5 G) which could not be precisely determined, because the spectrum consists of two fine structures, probably due to the presence of another molecular conformation. The $|D'|$ value of the second conformer was 94 G, which is close to that of **3** (92 G in toluene; 90 G in xylene-dichloromethane [4]). The approximate dipole–dipole distance is calculated to be 6.8 Å, which is ascribable to a conformer with two NO groups apart by flipping the imino nitroxide ring by about 180°. The simulated spectrum of **1** in Fig. 4 was drawn as the sum of two components.

A forbidden ($\Delta m_s = \pm 2$ transition) signal was found near a half field (1670 G) for **1**, as shown in the inset of Fig. 4. The temperature dependence of the $\Delta m_s = \pm 2$ signal obeys the Curie law, $I_{ESR} = C/T$, where C is an arbitrary constant (Fig. 5). The ground spin multiplicity of **1** is suggested to be triplet. Turek and coworkers [4] reported that the parent bis(imino nitroxide) (**3**) also had a triplet ground state. These results are consistent with the general rule that the *m*-phenylenes serve as robust ferromagnetic couplers [8]. However, it is not completely eliminated that the singlet and triplet states are almost degenerate. Actually, the singlet–triplet gap of **3** was estimated as small as $J/k_B = 10 \pm 5$ K [4], and the phenolic hyroxyl group tends to reduce the ferromagnetic J values compared with a non-substituted biradical [7].

On the other hand, no forbidden signal was observed in the ESR spectra of **2**. The zero-field splitting parameters are: $|D'| = 82$ G and $|E'| < 5$ G. The $|D'|$ value is smaller than those of **1** and **3**, suggesting the spins in **2** are rather localized at the two imino nitroxide groups. Although the crystallographic analysis of **2** was unsuccessful, we suppose that the π-conjugation system of **2** is not a coplanar owing to the steric congestion at neighboring two imino nitroxide and a hydroxyl groups.

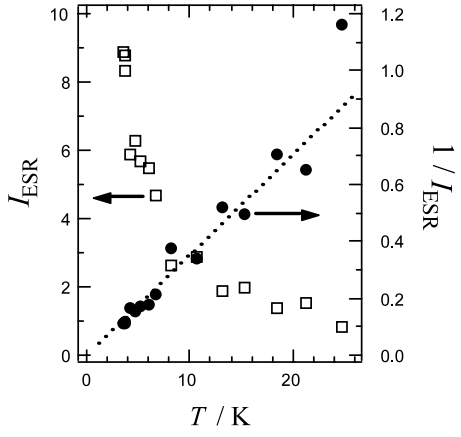

Fig. 5. Temperature dependence of I_{ESR} (left axis) and $1/I_{ESR}$ (right axis) for **1**. The ESR signal intensity (I_{ESR}) was defined by the peak height of the signal integral due to the $\Delta m_s = \pm 2$ transition. A dotted line is shown for a guide to the eye.

We examined the temperature dependence of the signal intensity of the triplet fine structure, and found that the intensity of the signal at 3320 G did not obey the Curie law. Assuming that the imino nitroxide and benzene rings in **2** are not conjugated practically, violation of the general rule is conceivable. Steric effects are known to give rise to stabilization of the singlet state for some *m*-phenylene-bridged bis(*t*-butyl nitroxide) radicals [18]. Such conformational effects may also hold for bis(imino nitroxide) radicals, as suggested from the computational analysis [4,19].

3.3. Magnetic properties

The results of the magnetic measurements on the polycrystalline samples of **1**–**3** are shown in Fig. 6. For all compounds, the products of the molar magnetic susceptibility (χ_{mol}) and T decrease on lowering temperature. The theoretical $\chi_{mol}T$ value of the high-temperature limit is 0.75 cm^3 K mol^{-1} and agrees well the experimental values at 300 K.

A stepwise behavior was found for **3**, which reproduces the result recently reported [4]. Analysis of the data on **3** may afford a valuable information. Intra- and intermolecular exchange coupling parameters, J_{intra} and J_{inter}, are defined as illustrated in Fig. 7, since the X-ray crystallographic analysis suggested the dimer formation in the crystal of **3** (Fig. 2). The best fit to the four-spin model [20] gave $J_{intra}/k_B = +20 \pm 1$ K and $J_{inter}/k_B = -88 \pm 3$ K, where the Heisenberg spin Hamiltonian is defined as $H = -2JS_iS_j$. A calculated curve is satisfactorily superposed to the experimental data as shown in Fig. 6, and the present result is essentially the same as the reported one [4]. It is noteworthy that the intermolecular antiferromagnetic coupling is much larger than the intramolecular ferromagnetic one and that the

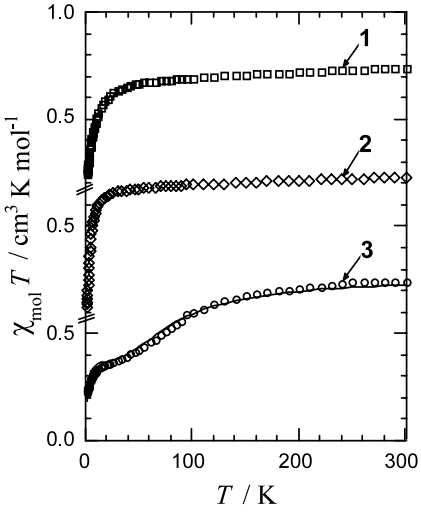

Fig. 6. Temperature dependence of the product of χ_{mol} and T measured at 5 kOe for **1**–**3**. The solid line represents a theoretical fit for **3** based on a dimeric four-spin system. For details, see the text.

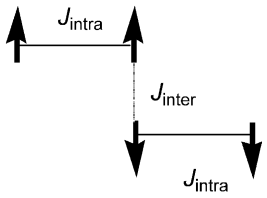

Fig. 7. Four-spin model proposed for **3** based on the X-ray crystallographic analysis.

latter is buried in the former, giving only the $\chi_{mol}T$ decrease on cooling.

The featureless decreases of $\chi_{mol}T$ of **1** and **2** leave no reliable analysis based on appropriate spin–spin coupling models. Apparent Weiss temperatures (θ) are determined to be -4.3 and -2.6 K for **1** and **2**, respectively, from the Curie–Weiss analysis ($\chi_{mol} = C/(T-\theta)$). No ferromagnetic behavior could be found in Fig. 6, but we can more cautiously conclude that the ferro- or antiferromagnetic interaction across the *m*-phenylene bridge should be smaller than the order of θ, if any, because antiferromagnetic intermolecular interactions may bury the intramolecular ferromagnetic interactions, as suggested from the results of **3**.

Magnetic susceptibility measurements on Cu($\mathbf{L}^1$)$_2$ revealed the role of *m*-phenylene bridge in $\mathbf{L}^1$ as magnetic couplers; the $\mathbf{L}^1$ has a nominal anionic charge which may bring about a magnetic role different from that of **1**. Fig. 8 shows the temperature dependence of the $\chi_{mol}T$ value of Cu($\mathbf{L}^1$)$_2$. With a decrease of temperature, the $\chi_{mol}T$ value once increased, reached a maximum of 2.65 cm^3 K mol^{-1} around 30 K, and then decreased. Although the increase of $\chi_{mol}T$ indicates the presence of ferromagnetic interaction, the experimental value was much smaller than the value of 4.38 cm^3 K mol^{-1} expected for a possible highest $S = 5/2$ state. The maximum value corresponds to a theoretical value of

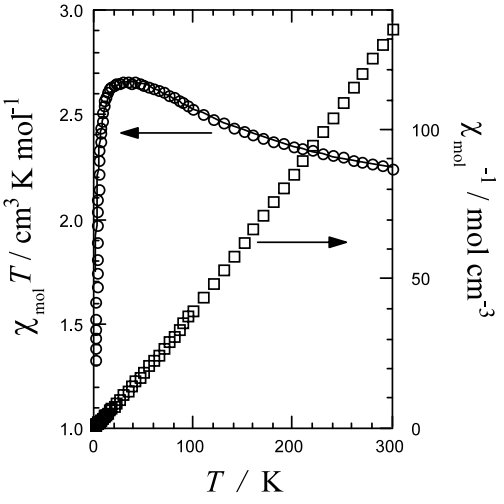

Fig. 8. Temperature dependence of the product of χ_{mol} and T measured at 5 kOe for Cu($\mathbf{L}^1$)$_2$. The solid line represents a theoretical fit. For details, see the text.

2.63 cm^3 K mol^{-1} expected for the sum of paramagnetic spins of two $S = 1/2$ and one $S = 3/2$ in a whole molecule. Thus, the increase of $\chi_{mol}T$ observed on cooling from 300 to 30 K can be ascribed mainly to the ferromagnetic coupling at the central radical–copper–radical moiety. This interpretation is rationalized by the fact that the magnetic coupling at directly bonded radical–copper system is considerably large. Actually, the high-spin *o*-semiquinone–copper(II) complex have a ferromagnetic coupling with $J/k_B = 160$ K [16], and the 2-pyridyl imino nitroxide–copper(II) complex with $J/k_B > 210$ K [17]. Very recently, Okada and Kaizaki independently studied the magnetic properties of **4** [21], which can be regarded as a model compound of the central portion of Cu($\mathbf{L}^1$)$_2$. According to their preliminary reports, **4** has a ground quartet state with ferromagnetic interaction of the order of 10^2 K.

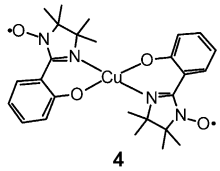

4

We analyzed the magnetic data on Cu($\mathbf{L}^1$)$_2$ using the following equation derived from the spin–pin Hamiltonian $H = -2J(S_1S_2 + S_2S_3)$ based on the model illustrated in Fig. 9:

$$\chi_{mol}T = \frac{N_A\beta^2 g^2}{2k_B} \times \left[1 + \frac{\exp(-2J/k_BT) + 1 + 10\exp(J/k_BT)}{2\exp(-2J/k_BT) + 2 + 4\exp(J/k_BT)}\right] \times \frac{T}{T-\theta}$$

Here, J is defined as a coupling parameter for both sides of the radical–copper interactions since the molecule is almost symmetrical. Possible magnetic couplings across the *m*-phenylene bridges as well as intermolecular couplings are confined to a Weiss mean field parameter θ. The parameters were optimized as $J/k_B = 132 \pm 5$ K, $\theta = -1.0 \pm 0.2$ K, and $g = 2.06 \pm 0.01$, and the calculated curve is superposed in Fig. 8. The data are satisfactorily fit, indicating that the model proposed is reliable. In spite of the distorted six-membered chelate ring and twisted two chelate rings, considerably large ferromagnetic coupling takes place between the radical and copper(II) spins. The ferro- or antiferromagnetic interaction across the *m*-phenylene

Fig. 9. A model containing a three-spin system plus two doublets proposed for Cu($\mathbf{L}^1$)$_2$ based on the X-ray crystallographic analysis.

bridge should be smaller than the order of θ. Therefore, we can conclude that the *m*-phenylene bridges work as not so strong ferromagnetic couplers in $\mathbf{L}^1$.

4. Summary

Although ESR is a versatile technique for determination of the spin-multiplicity of the molecule, we usually have to attention to the difference between molecular structures especially conformational isomerism in solid states and in solutions. The frozen-solution ESR results on **1** suggest that the ground state of **1** is triplet, whereas the solid-state magnetic susceptibility results on **1** and $Cu(\mathbf{L}^1)_2$ revealed that the *m*-phenylene bridges hardly worked as ferromagnetic couplers. This discrepancy may originate in conformational isomerism due to the steric effects of adjacent substituents as well as in electronic perturbation also due to the effects of substituents, such as hydroxyl and anionic phenolate groups. Taking all the results obtained here into consideration, *m*-phenylene-bridged bis(imino nitroxide) biradicals are not so good candidates in pursuit of high-spin ligands in contrast to our initial expectation, because the ferromagnetic interaction across the *m*-phenylene is a few kelvins at the most. However, we have clarified that the chelate structure of copper(II) *o*-imino nitroxide-substituted phenolates is available as a potential high-spin building block with considerably large ferromagnetic exchange coupling in the development of metal–radical hybrid magnets.

5. Supplementary material

Crystallographic data for the structural analysis(excluding structure factors) have been deposited with the Cambridge Crystallographic Data Centre, CCDC Nos. 194642 and 194643 for the compounds **1** and $Cu(\mathbf{L}^1)_2$, respectively. Copies of this information may be obtained free of charge from The Director, CCDC, 12 Union Road, Cambridge CB21 EZ, UK (fax: +44-1223-336033, e-mail: deposit@ccdc.cam.ac.uk or www: http://www.ccdc.cam.ac.uk).

Acknowledgements

This work was supported by a Grant-in-Aid for Scientific Research on Priority Areas of "Molecular Conductors and Magnets" (No. 730/11224204) and by a Grant-in-Aid for Scientific Research (No. 13640575), both from the Ministry of Education, Culture, Sports, Science and Technology, Japan.

References

[1] (a) A. Caneschi, D. Gatteschi, P. Rey, R. Sessoli, Acc. Chem. Res. 22 (1989) 392;
(b) H.O. Stumpf, L. Ouahab, Y. Pei, D. Grandjean, O. Kahn, Science 261 (1993) 447;
(c) J.S. Miller, A.J. Epstein, Angew. Chem., Int. Ed. Engl. 33 (1994) 385;
(d) W. Fujita, K. Awaga, M. Takahashi, M. Takeda, T. Yamazaki, Chem. Phys. Lett. 362 (2002) 97.
[2] (a) K. Inoue, T. Hayamizu, H. Iwamura, D. Hashizume, Y. Ohashi, J. Am. Chem. Soc. 118 (1996) 1803;
(b) H. Iwamura, K. Inoue, T. Hayamizu, Pure Appl. Chem. 68 (1996) 243.
[3] A. Caneschi, P. Chiesi, L. David, F. Ferraro, D. Gatteschi, R. Sessoli, Inorg. Chem. 32 (1993) 1445.
[4] L. Catala, J. Le Moigne, N. Kyritsakas, P. Rey, J.J. Novoa, P. Turek, Chem. Eur. J. 7 (2001) 2466.
[5] (a) A. Izuoka, M. Fukuda, T. Sugawara, Mol. Cryst. Liq. Cryst. 232 (1993) 103;
(b) A. Izuoka, R. Kumai, T. Sugawara, Adv. Mater. 7 (1995) 672;
(c) D. Shiomi, M. Tamura, H. Sawa, R. Kato, M. Kinoshita, J. Phys. Soc. Jpn. 62 (1993) 289.
[6] D. Shiomi, M. Nishizawa, K. Kamiyama, S. Hase, T. Kanaya, K. Sato, T. Takui, Synth. Met. 121 (2001) 1810.
[7] (a) S. Hase, D. Shiomi, K. Sato, T. Takui, Polyhedron 20 (2001) 1403;
(b) S. Hase, D. Shiomi, K. Sato, T. Takui, J. Mater. Chem. 11 (2001) 756.
[8] (a) H. Iwamura, Adv. Phys. Org. Chem. 26 (1990) 179;
(b) J. Veciana, H. Iwamura, MRS Bull. 25 (2000) 41;
(c) A. Rajca, Chem. Rev. 94 (1994) 871;
(d) J.A. Crayston, J.N. Devine, J.C. Walton, Tetrahedron 56 (2000) 7829.
[9] E.F. Ullman, J.H. Osiecki, D.G.B. Boocock, R. Darcy, J. Am. Chem. Soc. 94 (1972) 7049.
[10] E.F. Ullman, L. Call, J.H. Osiecki, J. Org. Chem. 35 (1970) 3623.
[11] TEXSAN: Crystal Structure Analysis Package, Molecular Structure Corp., The Woodlands, TX, 1985, 1999.
[12] Brucker WINEPR SIMFONIA, 1.25, shareware version, Brucker Analytical Instruments, Rheinstetten, Germany, 1996.
[13] (a) T. Sugawara, M.M. Matsushita, A. Izuoka, N. Wada, N. Takeda, M. Ishikawa, J. Chem. Soc., Chem. Commun. (1994) 1723;
(b) M.M. Matsushita, A. Izuoka, T. Sugawara, T. Kobayashi, N. Wada, N. Takeda, M. Ishikawa, J. Am. Chem. Soc. 119 (1997) 4369;
(c) J. Cirujeda, M. Mas, E. Molins, F.L. de Panthou, J. Laugier, J.G. Park, C. Paulsen, P. Rey, C. Rovira, J. Veciana, J. Chem. Soc., Chem. Commun. (1995) 709;
(d) E. Hernandez, M. Mas, E. Molins, C. Rovira, J. Veciana, Angew. Chem., Int. Ed. Engl. 32 (1993) 882.
[14] K. Doi, T. Ishida, T. Nogami, Chem. Lett. (2003), in press.
[15] F.M. Romero, R. Ziessel, M. Bonnet, Yl. Pontillon, E. Ressouche, J. Schweizer, B. Delley, A. Grand, C. Paulsen, J. Am. Chem. Soc. 122 (2000) 1298.
[16] O. Kahn, R. Prinz, J. Reedijk, J.S. Thompson, Inorg. Chem. 26 (1987) 3561.
[17] (a) D. Luneau, P. Rey, J. Laugier, P. Fries, A. Caneschi, D. Gatteschi, R. Sessoli, J. Am. Chem. Soc. 113 (1991) 1245;
(b) D. Luneau, P. Rety, J. Laugier, E. Belorizky, A. Congne, Inorg. Chem. 31 (1992) 3578.
[18] (a) F. Kanno, K. Inoue, N. Koga, H. Iwamura, J. Am. Chem. Soc. 115 (1993) 847;

(b) J. Fujita, M. Tanaka, H. Suemune, N. Koga, K. Matsuda, H. Iwamura, J. Am. Chem. Soc. 118 (1996) 9347;
(c) W.T. Borden, H. Iwamura, J.A. Berson, Acc. Chem. Res. 27 (1994) 109.

[19] (a) S. Fang, M.-S. Lee, D.A. Hrovat, W.T. Borden, J. Am. Chem. Soc. 117 (1995) 6727;
(b) P. Wautelet, L. Catala, A. Bieber, P. Turek, J.-J. Andre, Polyhedron 20 (2001) 1571.

[20] A. Escuer, S.B. Kumar, M. Font-Bardia, X. Solans, R. Vicente, Inorg. Chim. Acta 286 (1999) 62.

[21] (a) K. Tanaka, M. Kozaki, D. Shiomi, K. Sato, T. Takui, K. Okada, Abstract Book of the 81st Japan Chemical Society Spring Meeting (2002) 1249;
(b) H. Kanda, Y. Narumi, Y. Hosokoshi, T. Suzuki, S. Sawata, S. Kawata, K. Kindo, K. Inoue, S. Kaizaki, Abstract Book of the 81st Japan Chemical Society Spring Meeting (2002) 487.

Available online at www.sciencedirect.com
SCIENCE DIRECT®
ELSEVIER
Physica B 329–333 (2003) 1006–1007
PHYSICA B
www.elsevier.com/locate/physb

Effect of staggered field in $S = \frac{1}{2}$ antiferromagnetic chain: copper pyrimidine

Takayuki Asano[a,*], Daisuke Nomura[a], Yuji Inagaki[a], Yoshitami Ajiro[a], Hiroyuki Nojiri[b], Yasuo Narumi[c], Koichi Kindo[c], Takayuki Ishida[d], Takashi Nogami[d]

[a] *Department of Physics, Kyushu University, Fukuoka 812-8581, Japan*
[b] *Department of Physics, Okayama University, Okayama 700-8530, Japan*
[c] *KYOKUGEN, Osaka University, Toyonaka, Osaka 560-8531, Japan*
[d] *Department of Applied Physics and Chemistry, University of Electro-Communications, Chofu, Tokyo 182-8585, Japan*

Abstract

We report electron spin resonance (ESR) and magnetization measurements of the $S = \frac{1}{2}$ antiferromagnetic Heisenberg chain, Cu pyrimidine, $[PM \cdot Cu(NO_3)_2 \cdot (H_2O)_2]_n$ (PM = pyrimidine). The effect of staggered fields due to both the alternating g-tensor and the Dzyaloshinskii–Moriya interaction is clearly observed for the ESR line width and magnetization.

Keywords: Quantum spin; Field-induced gap; Cu pyrimidine; ESR

An $S = \frac{1}{2}$ antiferromagnetic Heisenberg chain (AFHC) has received considerable attention for its remarkable quantum effect. Here, we are interested in the quantum AFHC system with the transverse staggered field, for which rich physics is involved in relation to the exactly solvable model of quantum sine-Gordon (SG) chain. Cu benzoate is the first example which represents the model system subjected to an effective transverse staggered field arising in proportion to the applied external field, due to the alternating g-tensor and Dzyaloshinskii–Moriya (DM) interaction. In good agreement with the theoretical prediction based on field theoretical approaches [1], it has been shown experimentally by neutron scattering, specific heat [2], and electron spin resonance (ESR) measurements [3] that Cu benzoate exhibits the field-induced energy gap in the SG excitation spectrum as a function of external magnetic fields, $E_g(H) \propto H^{2/3}$. It is particularly important to provide other examples of real substances in order to inquire whether the observed behaviors are specific only to Cu benzoate or generic to the quantum system with the transverse staggered field.

Quite recently, Feyerherm et al. [4] have discovered another candidate, Cu pyrimidine, $[PM \cdot Cu(NO_3)_2 \cdot (H_2O)_2]_n$ (PM = pyrimidine) with $J/k_B = 36$ K which has the crystallographically feature very similar to that of Cu benzoate. Indeed, they revealed the angle-dependent field-induced gap as a function of the external magnetic field by specific heat measurements and determined that the largest staggered field and, hence, the largest energy gap are induced for the field direction along the c''-axis in the ac-plane from the analysis of angular dependent susceptibility. The main purpose of the present work is to clarify experimentally the effect of the transverse staggered field on the ESR line width and magnetization of Cu pyrimidine.

Fig. 1(a) shows the temperature dependence of line width ΔH_{pp}, defined as a peak-to-peak of ESR field-derivative signal at X-band. It is remarkable that the temperature dependence is drastically different between two field directions parallel and perpendicular to the c''-axis in the ac-plane. For $H \| c''$, the line width shows a divergent broadening proportional to T^{-2} at lower temperatures. In contrast, for $H \| a''$, which is

*Corresponding author.
E-mail address: asa6scp@mbox.nc.kyushu-u.ac.jp (T. Asano).

0921-4526/03/$ - see front matter
doi:10.1016/S0921-4526(02)02187-7

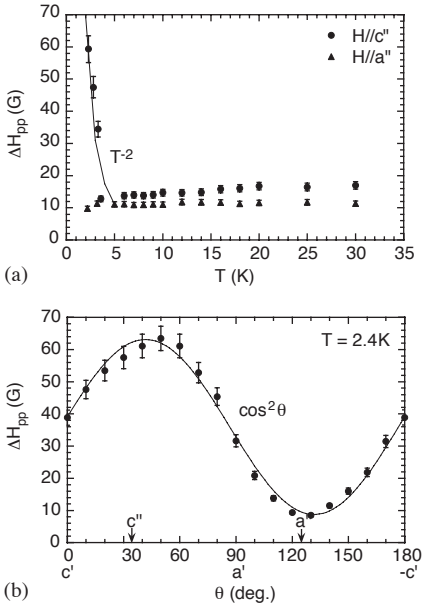

Fig. 1. (a) Temperature dependence of line width for $H\|c''$ and $H\|a''$. (b) Angular dependence of line width at 2.4 K in ac-plane on Cu pyrimidine.

perpendicular to the c''-axis and corresponds to the direction which we expect to be practically free from the effect of staggered field, the line width shows no broadening with decreasing temperature. A divergent broadening is often observed as the temperature approaches to the three-dimensional ordering. However, the present case is highly unusual in view of that there is a specific direction for which we observe no broadening. As shown in Fig. 1(b), the line width at the lowest temperature of 2.4 K changes quite systematically as a function of the field direction in the ac-plane and the angular dependence of the divergent contribution is well described by $\cos^2\theta$-law. According to the theory by Oshikawa and Affleck [1], the line width for the AFHC with the staggered field is expected to show a divergent broadening as $\Delta H_{pp} \propto (h/T)^2$ in the temperature range $T \ll J/k_B$ where h is the effective staggered field. This prediction is in good agreement with our observation both in the temperature dependence and the angular dependence of the divergent contribution because h is naturally expected to be proportional to $H\cos\theta$. It is interesting to note that almost the same angular dependence is observed for the divergent contribution of magnetic susceptibility due to the effect of the staggered field as reported in Ref. [4]. Also, it is interesting to note that the c''-axis does not coincide with any principal axes of alternating g-tensor, indicating the coexistence of the DM-interaction. The detailed analysis for the temperature and angular dependencies of the line width is discussed in Ref. [5].

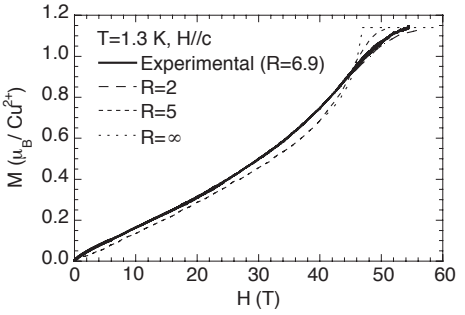

Fig. 2. Magnetization process of Cu pyrimidine for $H\|c$ at 1.3 K.

Fig. 2 shows the magnetization process at 1.3 K for $H\|c$ up to 54 T. It is estimated that the saturation field is about 47 T($= 2J/g\mu_B$) using $J/k_B = 36$ K and $g = 2.28$. The dashed lines are the theoretical curves for AFHC with no staggered field at zero and finite temperatures by Inawashiro and Katsura [6] and do not agree with the experimental data. The most striking difference is that the experimental curve show a monotonic change and no singular behavior at the saturation field. It is evident that this is not due to the effect of finite temperature as seen from the comparison with the calculation and, more confidently, from the experimental fact that the data at 4.2 K is almost the same though the $R = J/4k_BT$ factor increases three times at 1.3 K. It is natural to ascribe this discrepancy to the effect of staggered field since the sharp transition at the saturation field is expected to be obscured in the presence of conjugate field to the antiferromagnetic staggered magnetization. In fact, a recent calculation for AFHC with staggered field [7] explains no singular behavior at the saturation field as well as an initial sharp increment near zero field in agreement with our observation.

In conclusion, we have clearly observed the effect of the staggered fields due to both the alternating g-tensor and the Dzyaloshinskii–Moriya interaction on the ESR line width and magnetization of the recently discovered compound, Cu pyrimidine.

Acknowledgements

This work was partly supported by a Grant-in-Aid for Scientific Research from the Ministry of Education, Culture, Sports, Science and Technology of Japan.

References

[1] M. Oshikawa, I. Affleck, Phys. Rev. Lett. 79 (1997) 2883.
[2] D.C. Dender, et al., Phys. Rev. Lett. 79 (1997) 1750.
[3] T. Asano, et al., Phys. Rev. Lett. 84 (2000) 5880.
[4] R. Feyerherm, et al., J. Phys.: Condens. Matter 12 (2000) 1.
[5] T. Asano, et al., in preparation.
[6] S. Inawashiro, S. Katsura, Phys. Rev. 140 (1965) A892.
[7] N. Shibata, K. Ueda, J. Phys. Soc. Japan 70 (2001) 3690.

FULL PAPER

Dalton
www.rsc.org/dalton

Supramolecular triangular and linear arrays of metal–radical solids using pyrazolato-silver(I) motifs

Susumu Yamada, Takayuki Ishida * and Takashi Nogami
Department of Applied Physics and Chemistry, The University of Electro-Communications, Chofu, Tokyo 182-8585, Japan. E-mail: ishi@pc.uec.ac.jp; Fax: 81 424 43 5501; Tel: 81 424 43 5490

Received 6th October 2003, Accepted 30th January 2004
First published as an Advance Article on the web 12th February 2004

New chelating radical ligands pzNNH, pzINH, and pzbisINH (3-pyrazolyl nitronyl nitroxide, 3-pyrazolyl imino nitroxide, and pyrazole-3,5-diyl bis(imino nitroxide), respectively) were prepared. Complexation of these ligands with Ag^+ gave $[Ag(pzNN)]_n$, $[Ag(pzIN)]_6$, and $[Ag(pzbisIN)]_n$ containing the corresponding anionic forms of the ligands. From the X-ray crystal structure analysis, $[Ag(pzIN)]_6$ was characterized as a dimer of almost planar triangular moieties where the pyrazolate worked as a bridge, and metal–metal bonds brought about dimerization of triangles. $[Ag(pzbisIN)]_n$ was characterized as a uniform zigzag chain consisting of pyrazolate bridges and Ag ions with a *cis*-N_{pz}–Ag–N_{pz} coordination structure. Antiferromagnetic interactions observed could be analyzed based on the structures determined for both compounds. Ferromagnetic coupling was observed in $[Ag(pzNN)]_n$, and a polymeric structure was assumed although the crystal structure could not be determined. Novel supramolecular architectures using pyrazolate-substituted imino nitroxides have been developed, using the unique coordinative versatility of the pyrazolate derivatives.

Introduction

The nitronyl nitroxide (abbreviated as NN hereafter; Scheme 1) family has been the most widely utilized in constructing ferri- and ferromagnetic networks with one- to three-dimensionality.[1] The imino nitroxide (IN) derivatives have also been available for such purpose.[2] Various chelate compounds have been reported using 2-azaaromatic rings as R in Scheme 1, such as 2-pyridyl,[3] pyrazinyl,[4] 4-pyrimidinyl,[5] 2-imidazolyl,[6] 4-imidazolyl[7] *etc*., and the magnetic properties have been investigated in their metal–radical hybrid solids.[3–7] The ability of planar chelate formation for the INs has been reported to be superior to that for the corresponding NNs owing to the steric effects, as clarified for the coordination compounds containing 2-pyridyl groups.[3] Whereas 4-pyrazolyl NN derivatives are known,[8] no 3-pyrazolyl derivative has been reported so far to the best of our knowledge.

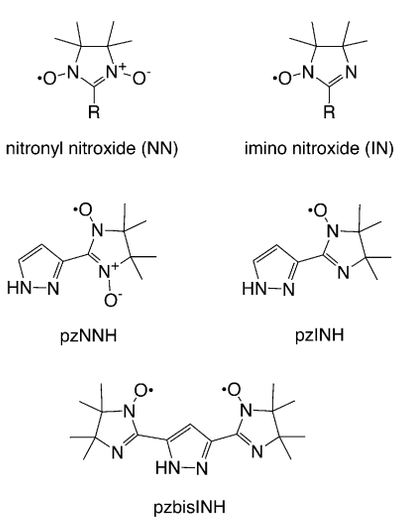

Scheme 1 Structural formulas

Pyrazolate anions and group 11 metal ions are known to form unique supramolecular assembly.[9] Monica and co-workers have reported copper(I) and silver(I) pyrazolates showing polymorphic crystals, triangular $[M(pz)]_3$ and linear $[M(pz)]_n$ (pz = pyrazolate).[10] Triangular gold(I) derivatives have also been reported and investigated in connection with aurophilic attractions (Au ··· Au interactions).[11,12] Metal–metal interactions for copper(I) and silver(I) ions have often been found in trinuclear $[M(pz)]_3$-type compounds.[10,13,14] Although such interactions have been used for supramolecular assembly in development for discotic liquid crystals[15] and dendron-aggregated materials,[16] there is no report on self-organization of pyrazole-substituted radical–metal solids toward hybrid magnetic materials. Herein we report self-assembled magnetic solids from silver(I) and new radical chelating ligands, 3-pyrazolyl nitronyl nitroxide (pzNNH), 3-pyrazolyl imino nitroxide (pzINH), and pyrazole-3,5-diyl bis(imino nitroxide) (pzbisINH). Since the Ag(I) ion is diamagnetic, the magnetism of the present compounds is attributed to the organic radical moieties.

Experimental

Materials

The precursory pzNNH (3-pyrazolyl nitronyl nitroxide) was prepared according to Ullman's method[17] from 3-formylpyrazole (Merck). After the introduction of the NN group, treatment of pzNNH with nitrous acid (generated from $NaNO_2$ and acetic acid)[18] gave pzINH. Although the preparation of 3,5-diformylpyrazole was described elsewhere,[19] we prepared 3,5-diformylpyrazole from methyl dimethoxyactate and pyruvic aldehyde dimethyl acetal *via* 3,5-bis(dimethoxymethyl)pyrazole according to the general methods for the preparations of 1,3-diketones and pyrazoles.[20] The IN groups in pzbisINH were directly introduced by oxidation of bis(monohydroxyimidazolidinyl)pyrazole obtained from spontaneous dehydration of bis(dihydroxyimidazolinyl)pyrazole under thermally harsh conditions.[21] The mps of pzNNH, pzINH, and pzbisINH were 127–129, 155–157, and 218–220 °C, respectively. The elemental analysis (C, H, N) of the radicals on a Fisons EA-1108 by a usual combustion method supported their chemical composition. Anal. Calcd for $C_{10}H_{15}N_4O_2$ (pzNNH): C, 53.80; H, 6.77; N, 27.03%. Found: C, 53.66; H, 6.78; N, 27.05%. Calcd for $C_{10}H_{15}N_4O$ (pzINH): C, 57.95; H, 7.30; N, 25.10%. Found: C,

DOI: 10.1039/b312406a

57.79; H, 7.37; N, 25.44%. Calcd for $C_{17}H_{26}N_6O_2$ (pzbisINH): C, 58.94; H, 7.56; N, 24.26%. Found: C, 58.56; H, 7.55; N, 24.08%. The EPR spectra measured on a Bruker ESP 300E (benzene, room temperature) were consistent with their molecular structures. The simulated spectra on the SimFonia program[22] satisfactorily reproduced the observed spectra with a_N = 7.56 (× 2) and g = 2.0064 for pzNNH, a_N = 9.05, 4.50 and g = 2.0058 for pzINH, and a_N = 4.52 (× 2), 2.14 (× 2) G and g = 2.0059 for pzbisINH. The IR spectra (KBr pellet) were measured on a HORIBA FT-IR 720. Absorption bands were found at 3286, 3170, 3114, 1300, 1098, and 922 cm^{-1} for pzNNH, 3150, 3048, 1369, 1290, and 781 cm^{-1} for pzINH, and 3156, 2977, 1559, 1375, and 1318 cm^{-1} for pzbisINH. Finally, the molecular structures of pzINH and pzbisINH were confirmed by means of X-ray crystallographic analysis.[23]

The following complexation procedure is typical. An acetonitrile solution (15 ml) containing $AgClO_4$ (20 mg; 0.097 mmol) and pzINH was combined with 1,8-diazabicyclo[5.4.0]-7-undecene (15 mg; 0.099 mmol) and the resultant mixture was allowed to stand at −20°C for 30 days. Red platelet crystals (11.09 mg; 0.035 mmol) of $[Ag(pzIN)]_6$ precipitated were collected on a filter and washed with a small amount of acetonitrile. The yield was 37%. The crystals were suitable for X-ray diffraction and magnetic studies without further purification. The elemental analysis (C, H, N) supported the formula with the 1/1 metal/ligand ratio. Anal. Calcd for $C_{10}H_{14}AgN_4O$: C, 38.24; H, 4.49; N, 17.84%. Found: C, 38.09; H, 4.48; N, 17.65%. IR (KBr): 2981, 2932, 1647, 1363, and 1319 cm^{-1}.

Red block crystals of $[Ag(pzbisIN)]_n$ were prepared in a manner similar to that of $[Ag(pzIN)]_6$ by using pzbisINH in place of pzINH. The yield was 60%. Anal. Calcd for $C_{17}H_{25}AgN_6O_2$: C, 45.04; H, 5.56; N, 23.80%. Found: C, 44.98; H, 5.54; N, 23.59%. IR (KBr): 2975, 2928, 1349, 1176, and 777 cm^{-1}.

Blue mica-like thin plates of $[Ag(pzNN)]_n$ were prepared in a manner similar to that of $[Ag(pzIN)]_6$ by using pzNNH and methanol as a solvent. The yield was 60%. Anal. Calcd for $C_{10}H_{14}AgN_4O_2$: C, 35.86; H, 4.06; N, 16.75%. Found: C, 36.38; H, 4.27; N, 16.97%. IR (KBr): 2977, 2931, 1587, 1369, and 1319 cm^{-1}.

X-ray crystallographic analysis

X-Ray diffraction data of $[Ag(pzIN)]_6$ and $[Ag(pzbisIN)]_n$ were collected on a Rigaku *R*-axis RAPID diffractometer with graphite monochromated Mo Kα radiation (λ = 0.71069 Å) at 90 K. The structures were directly solved by a heavy-atom Patterson method and expanded using Fourier techniques in the teXsan program package.[24] Numerical absorption correction was used. The thermal displacement parameters of non-hydrogen atoms were refined anisotropically. Full-matrix least-squares methods were applied using all of the unique reflection data. Hydrogen atoms were located at calculated positions. Selected crystallographic data are summarized in Table 1.

CCDC reference numbers 220151 and 220152.

See http://www.rsc.org/suppdata/dt/b3/b312406a/ for crystallographic data in CIF or other electronic format.

Magnetic measurements

Magnetic properties of $[Ag(pzIN)]_6$, $[Ag(pzbisIN)]_n$ and $[Ag(pzNN)]_n$ were measured on a Quantum Design MPMS SQUID magnetometer equipped with a 7 T coil in a temperature range 1.8–300 K. The magnetic responses were corrected with diamagnetic blank data of the sample holder measured separately. The diamagnetic contribution of the sample itself was estimated from Pascal's constants.

Table 1 Selected crystallographic data for $[Ag(pzIN)]_6$ and $[Ag(pzbisIN)]_n$

Compounds	$[Ag(pzIN)]_6$	$[Ag(pzbisIN)]_n$
Formula	$C_{10}H_{14}AgN_4O$	$C_{17}H_{25}AgN_6O_2$
Habit	Red platelet	Red block
Dimension/mm^3	0.4 × 0.3 × 0.02	0.2 × 0.2 × 0.1
T/K	90	90
Crystal system	Monoclinic	Orthorhombic
Space group	$P2_1/a$	$P2_12_12_1$
a/Å	14.1412(7)	6.9851(4)
b/Å	18.504(1)	12.5908(7)
c/Å	15.1158(8)	22.479(2)
β/°	115.497(3)	90
V/Å^3	3570.1(3)	1977.0(2)
Z	12	4
D_{calc}/g cm^{-3}	1.753	1.523
Unique data	6963	2415
μ(Mo Kα)/mm^{-1}	1.674	1.040
$R(F)^a(I > 2\sigma(I))$	0.0699	0.0462
$R_w(F^2)^b$ (all data)	0.1706	0.1275

^{a} $R = \Sigma\,||F_o| - |F_c||/\Sigma\,|F_o|$. ^{b} $R_w = [\Sigma\, w(F_o^2 - F_c^2)^2\,/\Sigma\, w(F_o^2)^2]^{1/2}$.

Table 2 Interatomic distances (Å) and angles (degrees) for $[Ag(pzIN)]_6$[a]

Ag1–N1	2.061(6)	N1–Ag1–N3	72.0(2)
Ag1–N3	2.620(6)	N1–Ag1–N6	166.7(2)
Ag1–N6	2.086(6)	N3–Ag1–N6	113.7(2)
Ag2–N5	2.097(5)	N5–Ag2–N7	68.6(2)
Ag2–N7	2.810(6)	N5–Ag2–N10	164.5(2)
Ag2–N10	2.113(6)	N7–Ag2–N10	122.0(2)
Ag3–N2	2.105(6)	N2–Ag3–N9	163.2(2)
Ag3–N9	2.124(6)	N2–Ag3–N11	116.9(2)
Ag3–N11	2.605(6)	N9–Ag3–N11	71.8(2)
N1–N2	1.379(8)	Ag1–N1–N2	130.8(4)
N1–C3	1.390(8)	Ag3–N2–N1	116.9(4)
C3–C4	1.47(1)	Ag2–N5–N6	126.3(4)
N3–C4	1.280(9)	Ag1–N6–N5	122.0(4)
N5–N6	1.354(7)	Ag3–N9–N10	130.3(4)
N5–C13	1.367(9)	Ag2–N10–N9	120.8(4)
C13–C14	1.444(9)	Ag3′–Ag1–N1	93.2(2)
N7–C14	1.270(8)	Ag3′–Ag1–N3	124.7(1)
N9–N10	1.373(8)	Ag3′–Ag1–N6	92.9(2)
N9–C23	1.348(8)	Ag1 –Ag3–N2	121.9(2)
C23–C24	1.45(1)	Ag1′–Ag3–N9	73.1(2)
N11–C24	1.288(9)	Ag1′–Ag3–N11	77.1(1)

[a] The symmetry operation code for ′ is $-x, -y, -z$.

Results and discussion

Crystal structures

Fig. 1(a) shows a half of the molecule of $[Ag(pzIN)]_6$ as an asymmetric unit. Three Ag cations and three pzIN anions form a cyclic trimer in a head-to-tail manner. The silver(I) ions are T-shaped tricoordinate but basically linear dicoordinate with pyrazolate nitrogen atoms at *trans* positions. The $Ag–N_{IN}$ interactions seem weak as indicated by longer interatomic distances (2.61–2.82 Å) than the $Ag–N_{pz}$ bonds (2.06–2.12 Å). Selected interatomic distances and bond angles are summarized in Table 2. This trinuclear and Ag_3N_6 macrocyclic structure is quite similar to those for $[M(pz)]_3$ and its derivatives (M = Cu, Ag, Au),[10–14] especially to that of $[M(3\text{-}(2\text{-pyridyl})pyrazolate)]_3$ (M = Cu, Ag)[13] involving the five-membered chelate structures. The pyrazole ring and IN imidazoline ring are almost coplanar in each pzIN ligand (the torsion angles around N1–C3–C4–N4, N5–C13–C14–N7, and N9–C23–C24–N11 are 10.2(6), −2(1), and −10(1)°, respectively), suggesting that attractive interactions between Ag ions and IN nitrogen atoms are appreciable, giving five-membered chelate structures. The strong and short $Ag–N_{pz}$ bonds may be interpreted in terms of dπ(Ag)–π*(pz) interaction like the Cu(I) case,[26] as evidenced by the relatively

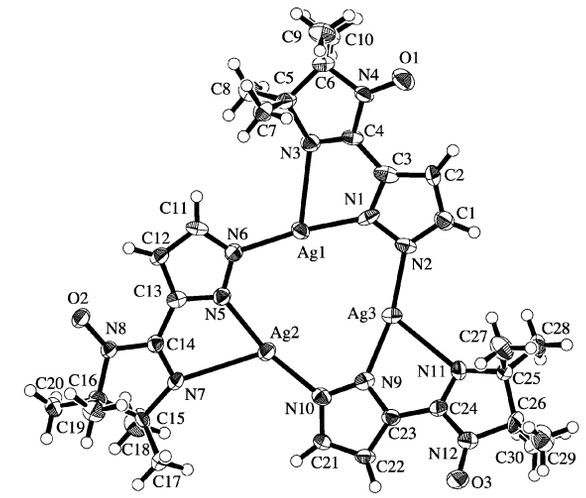

(a)

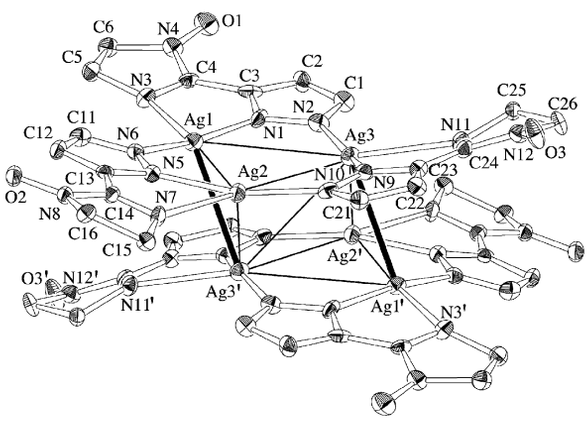

(b)

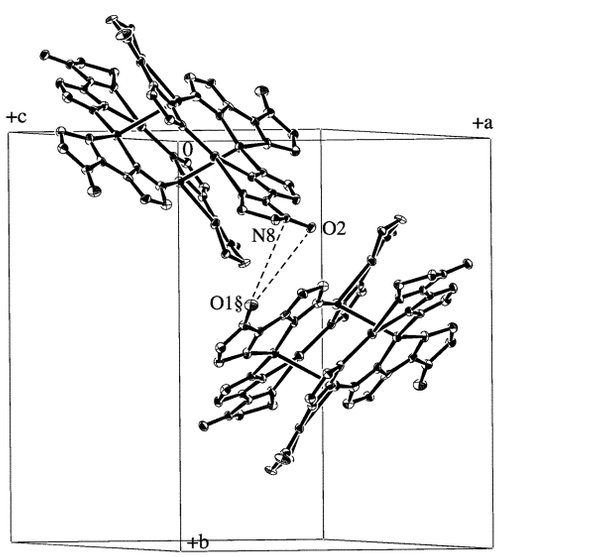

(c)

Fig. 1 (a) Ortep drawing of an asymmetric trinuclear unit in $[Ag(pzIN)]_6$ at the 50% probability level. Atomic numbering is also shown. (b) Molecular structure of $[Ag(pzIN)]_6$ where two trinuclear units are connected with metal–metal bonds (filled bonds). H atoms and methyl groups are omitted for clarity. Solid lines denotes Ag ··· Ag interactions. The symmetry operation code for ′ is $-x$, $-y$, $-z$. (c) Molecular arrangement in the crystal of $[Ag(pzIN)]_6$. H atoms and methyl groups are omitted for clarity. Dotted lines denote the intermolecular N8 ··· O1§ and O2 ··· O1§ distances of 4.218(8) and 4.443(8) Å, respectively. The symmetry operation code for § is $-1/2-x$, $1/2+y$, $-z$.

Table 3 Interatomic Ag–Ag distances (Å) and Ag–Ag–Ag angles (degrees) for $[Ag(pzIN)]_6$[a]

Ag1–Ag2	3.7080(7)	Ag3–Ag1– Ag2	62.74(1)
Ag1–Ag3	3.6935(8)	Ag1–Ag2– Ag3	58.45(1)
Ag1–Ag3′	3.1792(8)	Ag1–Ag3– Ag2	58.81(1)
Ag2–Ag3	3.8530(8)	Ag3′–Ag1– Ag2	62.53(2)
Ag2–Ag3′	3.6027(8)	Ag3–Ag1–Ag3′	64.78(2)
Ag3–Ag3′	3.707(1)	Ag1–Ag3–Ag1′	115.22(2)
		Ag1′–Ag3–Ag2	87.97(2)

[a] The symmetry operation code for ′ is $-x$, $-y$, $-z$.

long pz N–N bonds (1.379(8), 1.354(7), and 1.373(8) Å *vs.* 1.342(2) Å in pzINH[23] and 1.334 Å in $(pzH)_3$[27]).

Considerably short Ag ··· Ag distances are found between neighboring triangles related with the inversion symmetry; the shortest Ag ··· Ag distance is 3.1792(8) Å for Ag1–Ag3′ (the symmetry operation code for ′ is $-x$, $-y$, $-z$) as shown in Fig. 1(b). This distance is significantly shorter than the sum of the van der Waals radii (3.44 Å).[25] Ag1 and Ag3 ions are pyramidalized from the corresponding AgN_3 coordination planes toward the counter part of a dimer. Only two of the Ag ions (Ag1 and Ag3) in each trimer are involved in the Ag–Ag bonds and the third Ag ion (Ag2) is positioned near the pz ring at the opposite end of the inversion-related trimer unit. Dimerizations of the trimeric silver(I)-pyrazolate systems were similarly recognized in $[Ag(pz)]_3$, $[Ag(3\text{-pyridylpyrazolate})]_3$, and $[Ag(3,5\text{-bis}(i\text{-propylthiomethyl})pyrazolate)]_3$ with the Ag–Ag bond lengths of 3.431(4), 3.227(2), and 3.041(1) Å, respectively,[10,13,28] whereas non-interacting trinuclear molecules have also been reported for $[Ag(3,5\text{-diphenylpyrazolate})]_3$.[14]

We can point out two distorted Ag_4 tetrahedral skeletons of Ag1–Ag2–Ag3–Ag3′ and Ag1′–Ag2′–Ag3′–Ag3 with the interatomic distances of 3.69–3.85 Å. Selected interatomic Ag ··· Ag distances and angles are listed in Table 3. Ag2 is slightly pyramidalized toward Ag3′, suggesting that the Ag2 ··· Ag3′ interaction is substantial and attractive, although these distances are larger than the sum of the van der Waals radii (except for Ag1–Ag3′ as a metal–metal bond). The two tetrahedrons are fused with the Ag3–Ag3′ edge. Therefore, the molecule can be regarded also as the Ag_6^{6+} cluster surrounded by six pzIN radical anions. A similar edge-sharing bitetrahedron skeleton was reported for Au_6^{6+} in $[Au(3,5\text{-diphenylpyrazolate})]_6$.[12,14] The related Cu(I) complex containing weak Cu(I) ··· Cu(I) interactions is also known.[27]

The radical–radical distances are larger than 8 Å within a triangular array (Fig. 1(a)) and the magnetic interaction through IN–pz–Ag–IN seems very weak, but the inter-triangle radical–radical distances within a hexanuclear molecule are much shorter than those in a triangle; the interatomic distances are: O3 ··· N3′, 5.091(9); N12 ··· N3′, 4.852(9); N11 ··· N3′, 4.753(8) Å (Fig. 1(b)).

The IN oxygen atoms (O1, O2, and O3) in $[Ag(pzIN)]_6$ do not participate in coordination. The intramolecular spin–spin exchange interaction seems weak because of the long distance between them, but intermolecular through-space spin–spin interaction may take place because the peripheral IN oxygen atoms are closely located to neighboring molecules. Actually, as shown in Fig. 1(c), the intermolecular distances of N8 ··· O1§ and O2 ··· O1§ are 4.218(8) and 4.443(8) Å, respectively (the symmetry operation code for § is $-1/2-x$, $1/2+y$, $-z$), which may bring about intermolecular magnetic coupling rather than intramolecular.

Fig. 2(a) shows the molecular structure of $[Ag(pzbisIN)]_n$. Selected bond lengths and angles are listed in Table 4. Owing to five-membered chelate formation, the pyrazole ring and IN imidazoline ring are almost coplanar. N2 and N5 also participate in another chelate ring containing a neighboring Ag ion as shown in Fig. 2(b). The torsion angles around N1–C3–C4–N3 and N2–C1–C11–N5 are 11(1) and −3.6(9)°, respectively. The

Table 4 Interatomic distances (Å) and angles (degrees) for $[Ag(pzbisIN)]_n$ [a]

Ag1–N1	2.151(5)	N1–Ag1–N2*	110.2(2)
Ag1–N2*	2.468(5)	N1–Ag1–N3	71.2(2)
Ag1–N3	2.613(5)	N1–Ag1–N5*	169.1(2)
Ag1–N5*	2.175(5)	N2*–Ag1–N3	92.4(2)
O1–N4	1.269(7)	N2*–Ag1–N5*	73.4(2)
O2–N6	1.266(7)	N3–Ag1–N5*	119.4(2)
N1–N2	1.343(8)	Ag1–N1–N2	130.4(4)
N1–C3	1.364(9)	Ag1–N1–C3	120.2(4)
N2–C1	1.357(8)	Ag1#–N2–N1	143.2(4)
N3–C4	1.290(9)	Ag1#–N2–C1	110.1(4)
N4–C4	1.390(9)	Ag1–N3–C4	103.2(4)
N5–C11	1.304(9)	Ag1–N3–C5	138.0(4)
N6–C11	1.394(8)	Ag1#–N5–C11	116.4(4)
C1–C11	1.454(9)	Ag1#–N5–C12	132.2(4)
C3–C4	1.455(9)		

[a] The symmetry operation codes for * and # are $-1/2+x$, $1/2-y$, $1-z$, and $1/2+x$, $1/2-y$, $1-z$.

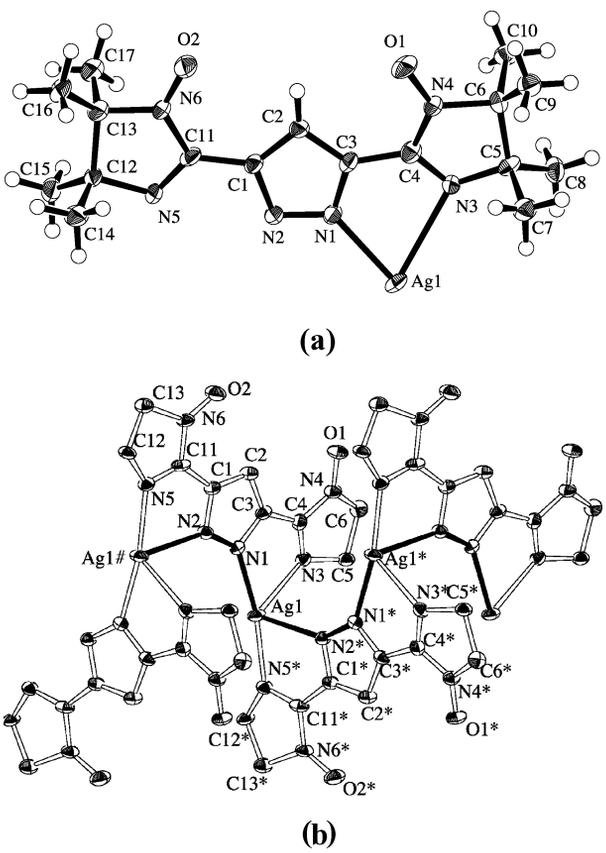

Fig. 2 (a) Ortep drawing of a repeating unit of $[Ag(pzbisIN)]_n$ at the 50% probability level. Atomic numbering is also shown. (b) Molecular packing of $[Ag(pzbisIN)]_n$. H atoms and methyl groups are omitted for clarity. Four units are drawn in an infinite chain. The polymer backbone is indicated with filled bonds. The symmetry operation codes for * and # are $-1/2+x$, $1/2-y$, $1-z$, and $1/2+x$, $1/2-y$, $1-z$, respectively.

Ag ions are tetracoordinate, but the basically linear dicoordinate structure is assigned to N1–Ag1–N5* because their bond distances, 2.151(5) and 2.175(5) Å for N1–Ag1 and N5*–Ag1, respectively, are considerably shorter than the equatorial ones, 2.613(5) and 2.468(5) Å for N3–Ag1 and N2*–Ag1, respectively (the symmetry operation code for * is $-1/2+x$, $1/2-y$, $1-z$).

The polymer backbone consists of an Ag-pzbisIN zigzag chain as indicated by the filled bonds in Fig. 2(b); the N1–Ag1–N2* angle is 110.2(2)° and the neighboring units are related by a 2_1 symmetry along the *a* axis. Owing to the steric effects of the bulky IN groups, Ag-pzbisIN could not construct trimeric macrocycles like $[Ag(pzIN)]_6$. X-ray crystallographic analyses on Ag-pz-based polymeric coordination compounds are rare;[10] while a similar zigzag chain has been reported for [Tl-(3-(2-pyridyl)pyrazolate)]$_n$,[12] the present complex is the first example of Ag-pz zigzag chain containing a *cis*-N_{pz}–Ag–N_{pz} structure. The polymeric $[Ag(3,5\text{-di}(2\text{-pyridyl})pyrazole)]_n^{n+}$ was structurally characterized, but the pyrazole ring does not work as a bridge.[29] The space group $P2_12_12_1$ of $[Ag(pzbisIN)]_6$ is non-centrosymmetric, and actually the Ag-pzbisIN chain is homochiral, as a result of spontaneous resolution.[30] Introduction of chirality to molecule-based magnetic materials is counted as a current target toward multi-functional materials.[31,32]

There is a possible through-bond spin–spin coupling along the *cis*-IN–Ag–IN moiety in $[Ag(pzbisIN)]_n$, and therefore we have to think of two spin–spin couplings along intra-ligand IN–pz–IN and inter-ligand IN–Ag–IN pathways. The IN–Ag–IN separation is indicated by the $N3_{imino} \cdots N2_{imino}$* distance of 4.141(7) Å, which is shorter than the IN–pz–IN separation (the $C4_{imino} \cdots C11_{imino}$ distance of 5.050(9) Å).

Magnetic properties

Fig. 3(a) shows the temperature dependence of $\chi_{mol}T$ and χ_{mol}^{-1} for $[Ag(pzIN)]_6$. The $\chi_{mol}T$ value at 100 K is 2.18 cm^3 K mol^{-1}

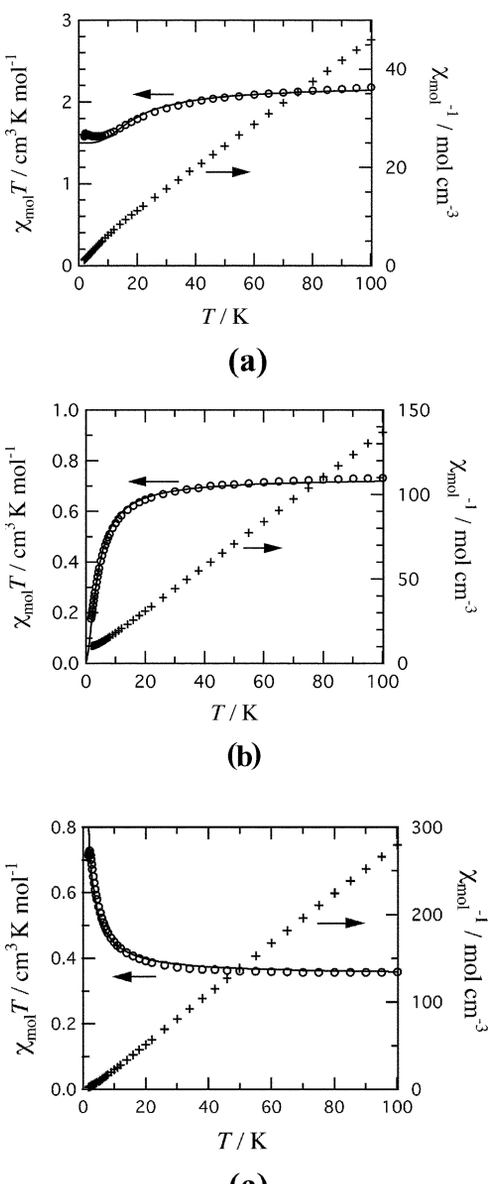

Fig. 3 Temperature dependence of $\chi_{mol}T$ and χ_{mol}^{-1} for $[Ag(pzIN)]_6$ (a), $[Ag(pzbisIN)]_n$ (b), and $[Ag(pzNN)]_n$ (c). The solid lines represent theoretical curves. For the equations and parameters, see the text.

which well agrees with the theoretical value (2.25 cm^3 K mol^{-1}) for six non-interacting $S = 1/2$ species with $g = 2.00$. With a decrease of temperature the $\chi_{mol}T$ gradually decreases and reaches a plateau of an almost 2/3 level below 10 K. This behavior is interpreted in terms of antiferromagnetic interaction between two spins plus four non-coupled spins.

Assuming antiferromagnetic coupling within a molecule, only one third of the molar magnetic susceptibility survives on lowering temperature from the molecular structure and symmetry point of view (two antiferromagnetic couplings through N3···N11′ and N11···N3′), but the experimental results are incompatible with this interpretation. We found shorter radical–radical distances among molecules (Fig. 1(c)) as described above. The observed antiferromagnetic coupling can be attributed to this geometry. Thus, the magnetic data were analyzed by a combined equation (eqn. (1)) from four ideal paramagnetic spins and two spins obeying the singlet–triplet model.[33] The spin–spin exchange Hamiltonian is defined as $H = -2JS_1 \cdot S_2$. The parameters J and g were optimized in eqn. (1), giving $2J/k_B = -36(2)$ K and $g = 1.95(3)$. The calculated curve is superimposed in Fig. 3(a).

$$\chi_{mol} = \frac{N_A g^2 \mu_B{}^2}{k_B T}\left[\frac{2}{3+\exp(-2J/k_B T)}+1\right] \qquad (1)$$

Fig. 3(b) shows the results on $[Ag(pzbisIN)]_n$ where the $\chi_{mol}T$ and $\chi_{mol}{}^{-1}$ values are plotted on the basis of a repeating unit. The $\chi_{mol}T$ value at 100 K was 0.732 cm^3 K mol^{-1}, which corresponds to the high-temperature limit of two $S = 1/2$ spins (0.750 cm^3 K mol^{-1}). On cooling, the $\chi_{mol}T$ value monotonically decreases to 1.8 K, indicating the presence of dominant antiferromagnetic coupling. The singlet–triplet model[30] reproduces the experimental data, and the introduction of a Weiss temperature into the singlet–triplet model (eqn. (2)) well improves the fitting. The optimized parameters are: $2J/k_B = -2.4(1)$ K, $\theta = -3.1(1)$ K, and $g = 2.02(2)$.

$$\chi_{mol} = \frac{N_A g^2 \mu_B{}^2}{k_B (T-\theta)}\left[\frac{2}{3+\exp(-2J/k_B T)}\right] \qquad (2)$$

The parameters obtained here indicate that the secondary interaction has an appreciable magnitude. The magnetic system of $[Ag(pzbisIN)]_n$ seems better analyzed with the alternating chain model defined by J_1 and J_2 ($= \alpha J_1$) between neighboring spins. We applied an expression of magnetic susceptibility (eqn. (3)) formulated by Hatfield,[34] where A–F are given in the literature and $x = -J/k_B T$.[34,35] We obtained $2J_1/k_B = -2.4(2)$ K, $2J_2/k_B = -2.3(2)$ K, and $g = 1.98(1)$. The calculated curve is superimposed in Fig. 3(b).

$$\chi_{mol} = \frac{N_A g^2 \mu_B{}^2}{k_B T}\left[\frac{A+Bx+Cx^2}{1+Dx+Ex^2+Fx^3}\right] \qquad (3)$$

There are two possible pathways of antiferromagnetic couplings, IN–pz–IN and IN–Ag–IN. Since two parameters (J_1 and J_2) are comparable to each other, we cannot determine the assignment of the magnetic couplings with geometrical pathways. The magnetic study on the free ligand pzbisINH showed antiferromagnetic interaction with a Weiss temperature of −8.3 K. The origin of one antiferromagnetic coupling of $[Ag(pzbisIN)]_n$ may be reasonably attributed to intramolecular coupling, *i.e.*, IN–pz–IN. The experimental results indicate that the antiferromagnetic interaction ascribable to the IN–Ag–IN pathway is simultaneously operative together with that of IN–pz–IN.

Finally, we describe the magnetic properties of $[Ag(pzNN)]_n$. The crystals of $[Ag(pzNN)]_n$ were very thin, and unfortunately we could not determine the crystal structure. The elemental analysis indicated that the Ag/pzNN ratio was 1:1. Oligomeric structures can be expected for $[Ag(pzNN)]_n$ observing from the bridging nature of the pyrazolate anion, but the value of sufix n remains unknown. Fig. 3(c) shows the $\chi_{mol}T$ *vs.* T plot for $[Ag(pzNN)]_n$. Ferromagnetic interaction was clearly observed as indicated by the monotonic increase of the $\chi_{mol}T$ with a decrease of temperature. The Curie–Weiss analysis gave $\theta = 1.8$ K, which is larger than those of the genuine organic ferromagnets *p*-nitrophenyl NN (+0.9 K)[36] and hydroquinonyl NN (+0.8 K).[37] The $\chi_{mol}T$ value at 100 K (0.358 cm^3 K mol^{-1}) agrees with the theoretical value of $S = 1/2$ species (0.375 cm^3 K mol^{-1}). At 2 K, the value of 0.73 cm^3 K mol^{-1} exceeds the theoretical value for $S = 3/2$ species (0.625 cm^3 K mol^{-1}), suggesting that more than three molecules are correlated ferromagnetically. A polymeric magnetic structure is assumed for $[Ag(pzNN)]_n$, and we applied a uniform infinite chain model. The ferromagnetic interaction was estimated as $2J/k_B = +5.7(2)$ K with $g = 1.93(2)$ from the high-temperature series expansion of Baker and co-workers (eqn. (4)).[38] The coefficients a–i are given in the literature and $y = J/2k_B T$.[38] The calculated curve is superimposed in Fig. 3(c). The optimized g value was somewhat smaller than the value determined by EPR, suggesting the presence of diamagnetic impurity. We obtained the purity factor of 93(1)% with fixed $g = 2.00$.

$$\chi_{mol} = \frac{N_A g^2 \mu_B{}^2}{4k_B T}\left[\frac{1+ay+by^2+cy^3+dy^4+ey^5}{1+fy+gy^2+hy^3+iy^4}\right] \qquad (4)$$

The satisfactory fit in Fig. 3(c) strongly suggests that $[Ag(pzNN)]_n$ does not have a triangular structure but a polymer structure. The NN group in pzNN may give a non-planar six-membered chelate owing to the steric effect, and the angle formed from the pz–Ag moiety does not meet the requirement of a triangle formation.

Summary

We have demonstrated two types of supramolecular arrays using pyrazolate-based IN radicals. The crystal of $[Ag(pzIN)]_6$ shows a dimeric structure of triangular molecules. The observed magnetic coupling is antiferromagnetic, which is ascribable to intermolecular radical–radical contacts. The crystal of $[Ag(pzbisIN)]_n$ has a polymeric structure exhibiting dominant antiferromagnetic interactions, which are ascribable to two possible exchange pathways of the first- and second-nearest neighboring radicals. Unfortunately, the observed magnetic interactions for $[Ag(pzIN)]_6$ and $[Ag(pzbisIN)]_n$ are antiferromagnetic, but the novel supramolecular architectures due to pyrazolate-substituted imino nitroxides have been developed, using the unique coordinative versatility of the pyrazole derivatives. Hierarchical self-assemblies such as dimerization of triangles (2 × 3 array) and equally-spaced polymerization of diradicals (n × 2 array) have been established toward metal–radical magnetic materials. As suggested by the results on $[Ag(pzNN)]_n$, we still have a chance to exploit ferromagnetic hybrid materials in using the pyrazolate supramolecular synthon.

In the metal–radical approach toward hybrid magnets, bulky anions such as hfac (1,1,1,5,5,5-hexafluoropentane-2,4-dionate) often insulate magnetic networks to give low T_C (or T_N) magnets due to low-dimensional structures.[1,2] Although intermolecular or interchain weak interactions are favorable for development of single-chain magnets[39] and for analysis of discrete high-spin molecules,[40] improvement of these weak interactions is usually desired for bulk, *i.e.*, three-dimensionally networked magnets. Purge of the counter anions seems a promising strategy for that purpose, and several successful results have been reported containing anionizable ligands such

as NN-substituted imidazolates.[6] Furthermore less bulky substituents (R in Scheme 1) are favorable. The present work has demonstrated a potential utility of anion radical ligands containing a relatively small pyrazolate group to construct metal–radical hybrid solids. Complexation of these ligands with transition metal ions carrying electron spins now becomes of great interest.

Acknowledgements

This work was partly supported by Grants-in-Aid for Scientific Research (Nos. 13640575, 15550115, and 15073101) from the Ministry of Education, Culture, Sports, Science and Technology, Japan.

References and notes

1 A. Caneschi, D. Gatteschi, P. Rey and R. Sessoli, *Acc. Chem. Res.*, 1989, **22**, 392.
2 T. Ise, T. Ishida and T. Nogami, *Inorg. Chem.*, 2003, **42**, 6106.
3 D. Luneau, P. Rey, J. Laugier, P. Fries, A. Caneschi, D. Gatteschi and R. Sessoli, *J. Am. Chem. Soc.*, 1991, **113**, 1245; D. Luneau, P. Rey, J. Laugier, E. Belorizky and A. Conge, *Inorg. Chem.*, 1992, **31**, 3578.
4 K. Fegy, K. E. Vostrikova, D. Luneau and P. Rey, *Mol. Cryst. Liq. Cryst.*, 1997, **305**, 69; T. Matsuyama, Y. Iwata, T. Ishida and T. Nogami, *Synth. Met.*, 2003, **133–134**, 611.
5 J. Omata, T. Ishida, D. Hashizume, F. Iwasaki and T. Nogami, *Inorg. Chem.*, 2001, **40**, 3954; J. Omata, T. Ishida, D. Hashizume, F. Iwasaki and T. Nogami, *Mol. Cryst. Liq. Cryst.*, 2002, **376**, 455.
6 K. Fegy, D. Luneau, T. Ohm, C. Paulsen and P. Rey, *Angew. Chem. Int. Ed. Engl.*, 1998, **37**, 1270; K. Fegy, N. Sanz, D. Luneau, E. Belorizky and P. Rey, *Inorg. Chem.*, 1998, **37**, 4518; K. Fegy, D. Luneau, E. Belorizky, M. Novac, J.-L. Tholence, C. Paulsen, T. Ohm and P. Rey, *Inorg. Chem.*, 1998, **37**, 4524.
7 C. Aoki, T. Ishida and T. Nogami, *Inorg. Chem. Commun.*, 2003, **6**, 1122; C. Aoki, T. Ishida and T. Nogami, *Inorg. Chem.*, 2003, **42**, 7616.
8 G. V. Romanenko, I. V. El'tsov and V. I. Ovcharenko, *J. Struct. Chem.*, 2002, **43**, 700; L. Catala, R. Feher, D. B. Amabilino, K. Wurst and J. Veciana, *Polyhedron*, 2001, **20**, 1563.
9 G. L. Monica and G. A. Ardizzoia, *Prog. Inorg. Chem.*, 1997, **46**, 151; S. Trofimenko, *Prog. Inorg. Chem.*, 1986, **34**, 115; K. Umakoshi, Y. Yamauchi, K. Nakamiya, T. Kojima, M. Yamasaki, H. Kawano and M. Onishi, *Inorg. Chem.*, 2003, **42**, 3907; P. A. Angaridis, P. Baran, R. Boca, F. Cervantes-Lee, W. Haase, G. Mezei, R. G. Raptis and R. Werner, *Inorg. Chem.*, 2002, **41**, 2219.
10 N. Masciocchi, M. Moret, P. Cairati, A. Sironi, G. A. Ardizzoia and G. L. Monica, *J. Am. Chem. Soc.*, 1994, **116**, 7668.
11 G. Yang and R. G. Raptis, *Inorg. Chem.*, 2003, **42**, 261.
12 R. G. Raptis, H. H. Murray, III and J. P. Fackler, Jr., *J. Chem. Soc., Chem. Commun.*, 1987, 737.
13 K. Singh, J. R. Long and P. Stavropoulos, *J. Am. Chem. Soc.*, 1997, **119**, 2942.
14 H. H. Murray, R. G. Raptis and J. P. Fackler, Jr., *Inorg. Chem.*, 1998, **27**, 26.
15 S. J. Kim, S. H. Kang, K.-M. Park, H. Kim, W.-C. Zin, M.-G. Choi and K. Kim, *Chem. Mater.*, 1998, **10**, 1889; L. Barberá, A. Elduque, R. Giménez, F. J. Lahoz, J. A. López, L. A. Oro and J. L. Serrano, *Inorg. Chem.*, 1998, **37**, 2960.
16 M. Enomoto, A. Kishimura and T. Aida, *J. Am. Chem. Soc.*, 2001, **123**, 5608.
17 E. F. Ullman, J. H. Osiecki, D. G. B. Boocock and R. Darcy, *J. Am. Chem. Soc.*, 1972, **94**, 7049.
18 E. F. Ullman, L. Call and J. H. Osiecki, *J. Org. Chem.*, 1970, **35**, 3623.
19 V. J. Arán, M. Kumar, J. Molina, L. Lamarque, P. Navarro, E. García-España, J. A. Ramírez, S. V. Luis and B. Escuder, *J. Org. Chem.*, 1999, **64**, 6135.
20 J. J. Lafferty and F. H. Case, *J. Org. Chem.*, 1967, **32**, 1591; R. H. Wiley and P. E. Hexner, *Org. Synth. Coll. Vol.*, 1963, **IV**, 351.
21 C. Stroh, F. M. Romero, N. Kyritsaqkas, L. Catala, P. Turek and R. Ziessel, *J. Mater. Chem.*, 1999, **9**, 875.
22 *Winepr SimFonia*, 1.25, shareware version, Bruker Analytical Instruments,Rheinstetten, Germany, 1996.
23 S. Yamada, T. Ishida and T. Nogami, unpublished results.
24 *TeXan*: Crystal Structure Analysis Package, Molecular Structure Corp., The Woodlands, TX, 1985, 1999.
25 A. Bondi, *J. Phys. Chem.*, 1964, **68**, 441.
26 F. Meyer, A. Jacobi and L. Zsolnai, *Chem. Ber. Recueil*, 1997, **130**, 1441.
27 M. K. Ehlert, S. J. Rettig, A. Storr, R. C. Thompson and J. Trotter, *Can. J. Chem.*, 1990, **68**, 1444.
28 J. A. S. Smith, B. Wehrle, F. Aguilar-Parrilla, H. H. Limbach, M. C. Foces-Foces, F. H. Cano, J. Elguero, A. Baldy, M. Pierrot, M. M. T. Khurshib and J. B. Larcombe-McDouall, *J. Am. Chem. Soc.*, 1989, **111**, 7304.
29 M. Munakata, L. P. Wu, M. Yamamoto, T. Kuroda-Sowa, M. Maekawa, S. Kawata and S. Kitagawa, *J. Chem. Soc., Dalton Trans.*, 1995, 4099.
30 L. Pérez-García and D. B. Amabilino, *Chem. Soc. Rev.*, 2002, **31**, 342.
31 K. Inoue, K. Kikuchi, M. Ohba and H. Okawa, *Angew. Chem. Int. Ed. Engl.*, 2003, **42**, 4810; K. Inoue, H. Imai, P. S. Ghalsasi, K. Kikuchi, M. Ohba, H. Okawa and J. V. Yakhmi, *Angew. Chem. Int. Ed. Engl.*, 2001, **40**, 4242; E. Coronado, C. J. Gómez-García, A. Nuez, F. M. Romero, E. Rusanov and H. Stoeckli-Evans, *Inorg. Chem.*, 2002, **41**, 4615; E. Coronado, J. R. Galán-Mascarós, C. J. Gómez-García and J. M. Martínez-Agudo, *Inorg. Chem.*, 2001, **40**, 113; M. Minguet, D. Luneau, C. Paulsen, E. Lhotel, A. Gorski, J. Waluk, D. B. Amabilino and J. Veciana, *Polyhedron*, 2003, **22**, 2349; N. Domingo, P. Gerbier, J. Gómez, D. Ruiz-Molina, D. B. Amabilino, J. Tejada and J. Veciana, *Polyhedron*, 2003, **22**, 2355.
32 K. Nakayama, T. Ishida, R. Takayama, D. Hashizume, M. Yasui, F. Iwasaki and T. Nogami, *Chem. Lett.*, 1998, 497; K. Zusai, T. Kusaka, T. Ishida, R. Feyerherm, M. Steiner and T. Nogami, *Mol. Cryst. Liq. Cryst.*, 2000, **343**, 127; T. Ishida, L. Yang and T. Nogami, *Chem. Lett.*, 2003, **32**, 1018.
33 B. Bleaney and K. D. Bowers, *Proc. R. Soc. London, Ser. A*, 1952, **214**, 451.
34 W. E. Hatfield, *J. Appl. Phys.*, 1981, **52**, 1985.
35 O. Kahn, *Molecular Magnetism*, VCH, New York, 1993, ch. 11.
36 K. Awaga and Y. Maruyama, *J. Chem. Phys.*, 1989, **91**, 2743.
37 T. Sugawara, M. M. Matsushita, A. Izuoka, N. Wada, N. Takeda and M. Ishikawa, *J. Chem. Soc., Chem. Commun.*, 1994, 1723.
38 G. A. Baker, G. S. Rushbrooke and H. E. Gilbert, *Phys. Rev. A*, 1964, **135**, 1272.
39 A. Caneschi, D. Gatteschi, N. Lalioti, C. Sangregorio, R. Sessoli, G. Venturi, A. Vindigni, A. Rettori, M. G. Pini and M. A. Novak, *Angew. Chem., Int. Ed. Engl.*, 2001, **40**, 1760.
40 Y. Kobayashi, S. Ueki, T. Ishida and T. Nogami, *Chem. Phys. Lett.*, 2003, **378**, 337.

Weak ferromagnetism with very large canting in a chiral lattice: Fe(pyrimidine)$_2$Cl$_2$

R. Feyerherm* and A. Loose
Hahn-Meitner-Institut and Berlin Neutron Scattering Center, 14109 Berlin, Germany

T. Ishida and T. Nogami
Department of Applied Physics and Chemistry, The University of Electro-Communications, Chofu, Tokyo 182-8585, Japan

J. Kreitlow, D. Baabe, F. J. Litterst, S. Süllow, and H.-H. Klauss
Institut für Metallphysik und Nukleare Festkörperphysik, TU Braunschweig, 38106 Braunschweig, Germany

K. Doll
Institut für Mathematische Physik, TU Braunschweig, 38106 Braunschweig, Germany

(Received 6 February 2003; revised manuscript received 15 December 2003; published 29 April 2004)

The transition metal coordination compound Fe(pyrimidine)$_2$Cl$_2$ crystallizes in a chiral lattice, space group $I4_122$ (or $I4_322$). Combined magnetization, Mössbauer spectroscopy, and powder neutron diffraction studies reveal that it is a canted antiferromagnet below $T_N = 6.4$ K with an unusually large canting of the magnetic moments of 14° from their general antiferromagnetic alignment, one of the largest reported to date. This results in weak ferromagnetism with a ferromagnetic component of $\sim 1\ \mu_B$. The large canting is due to the interplay between the antiferromagnetic exchange interaction and the local single-ion anisotropy in the chiral lattice. The magnetically ordered structure of Fe(pyrimidine)$_2$Cl$_2$, however, is not chiral. The implications of these findings for the search of molecule based materials exhibiting chiral magnetic ordering are discussed.

DOI: 10.1103/PhysRevB.69.134427 PACS number(s): 75.25.+z, 75.50.Ee, 75.50.Xx

I. INTRODUCTION

In recent years, the interdisciplinary field of molecule based magnetic materials has been the focus of very intense research efforts.[1–5] These are directed towards synthesizing new molecular building blocks and supermolecular aggregates, which subsequently are subject to a detailed physical characterization. Here, one major issue is to develop multifunctional compounds that combine technologically relevant magnetic properties with other physical properties, such as conductivity[6] or optical activity.[7]

In this framework, extensive efforts are undertaken to find chiral magnetic materials that exhibit magnetochiral dichroism (MChD), a phenomenon first observed by Rikken and Raupach in a chiral paramagnetic material.[8] Large MChD is expected in materials that combine chirality and magnetic order. To date, however, there is no evidence for large MChD, although a number of chiral magnetic materials have been reported.[9]

Recently, the magnetism of pyrimidine bridged transition metal complexes has been investigated in which pyrimidine ($C_4H_4N_2$) plays the role of an antiferromagnetic coupling unit.[10–13] Interestingly, the halide complexes T(pyrimidine)$_2X_2$ ($T = Co^{II}$, $X = Cl$, Br; $T = Fe^{II}$, $X = Cl$) possess a chiral three-dimensional network of T ions and exhibit weak ferromagnetism below about 5 K.[14,15] The preliminary analysis of magnetization measurements on these compounds pointed to a very large canting and an associated large ferromagnetic component of the ordered moments. It appeared possible that these compounds possess a chiral magnetically ordered structure which would be of great interest in the framework of MChD.

In order to determine the magnetic structure and to elucidate the origin of the large canting we performed magnetization measurements, Mössbauer spectroscopy and powder neutron diffraction on Fe(pyrimidine)$_2$Cl$_2$. Here, we present a complete analysis of these data together with electronic structure calculations.

The basic result of our investigation is that, in spite of its chiral structure, Fe(pyrimidine)$_2$Cl$_2$ does not exhibit a chiral magnetic ordering but an exceptionally large canting of the magnetic moments of 14° from their general antiferromagnetic alignment. This canting is one of the largest reported to date. Weak ferromagnetic behavior is associated with the canting, resulting in a ferromagnetic component of 1 μ_B. We argue that in the present case the canting is due to the interplay between the antiferromagnetic exchange interaction and the local single-ion anisotropy. This implies that the chiral symmetry is the origin of the large canting in Fe(pyrimidine)$_2$Cl$_2$. We discuss the general implications of our findings for studies in search of molecule based materials exhibiting chiral magnetic ordering.

II. EXPERIMENTAL

Microcrystalline samples of Fe(pyrimidine)$_2$Cl$_2$ were obtained by mixing aqueous solutions of Fe^{II} chloride (e.g., 10 mmol in 20 ml H_2O) with the stoichiometric amount of pyrimidine. The resulting yellow precipitates were filtered and washed thoroughly with H_2O. Mössbauer data indicate the presence of a secondary phase, which we identified as Fe(pyrimidine)Cl$_2$. The volume amount of the secondary phase increases with storage time of the samples. While a freshly prepared sample contained less than 2% secondary phase, about 22% secondary phase have been observed in the same sample stored for three years under air (see below).

This indicates that under such conditions Fe(pyrimidine)$_2$Cl$_2$ is unstable against the formation of Fe(pyrimidine)Cl$_2$.

Magnetization measurements were carried out using an MPMS Squid magnetometer (Quantum Design). Some 20 mg of freshly prepared sample was filled into a gelatine capsule and dispersed in a small amount of mineral oil. At low temperature the oil freezes, preventing the sample grains from moving in large applied fields. Similarity of the magnetization curve for the dispersed powder sample with published data for a pure sample[15] shows that Fe(pyrimidine)$_2$Cl$_2$ does not react with the mineral oil. In contrast, dispersing Fe(pyrimidine)$_2$Cl$_2$ in ethanol leads to immediate formation of Fe(pyrimidine)Cl$_2$.

^{57}Fe Mössbauer spectroscopy experiments have been performed in a standard low-temperature Mössbauer setup at temperatures ranging from 2.3 K to 300 K [source: ^{57}Co-in-Rh matrix at room temperature; emission line half width at half maximum: 0.130(2) mm/s]. The spectra have been evaluated using the Mössbauer fitting program RECOIL[16] in the thin absorber approximation. Above T_N the spectra were modeled as Lorentzian lines in the presence of an electric-field gradient. Below T_N a diagonalization of the full hyperfine Hamiltonian including electric quadrupole and magnetic Zeeman interaction is used.[17] From the eigenvalues the energy of the resonance lines and from the eigenvectors the line intensities are obtained.

Neutron powder diffraction measurements were performed using the instruments $E6$ and $E9$ at the Berlin Neutron Scattering Center. The instrument $E6$ provides a high neutron flux and medium resolution, is equipped with a 20°-multichannel detector, and covers a range of scattering angles up to about 100° at a neutron wavelength of $\lambda = 2.448$ Å. In contrast, the instrument $E9$ is a low-flux high-resolution powder diffractometer with an extended 2θ range up to 160° and $\lambda = 1.7964$ Å. Therefore, the former was used for the study of magnetic Bragg reflections, while the latter was employed for checking the crystal structure at low temperatures. The nondeuterated sample was filled into a 7 mm diameter vanadium can with 40 mm length, resulting in a sample volume of about 1.5 cm^3. An absorption correction for cylindrical samples was applied ($\mu R = 0.94$) to account for the strong incoherent scattering from hydrogen. During the refinement, no other but symmetry constraints were used for the atom positional parameters. Therefore, the validity of the crystal structure model is proven by the correct geometry of the pyrimidine molecules determined in the refinement. The Rietveld refinement of the diffraction data was carried out using the WINPLOTR/FULLPROF package.[18]

III. RESULTS

A. Crystal structure

The high-resolution powder neutron diffraction data, taken at 10 and 298 K on a freshly prepared sample, confirm that Fe(pyrimidine)$_2$Cl$_2$ is isostructural to the Co analog for which single-crystal data are available.[19] Both compounds are tetragonal with the chiral space group no. 98, $I4_122$ (or the enantiomorphic $I4_322$). The lattice parameters for

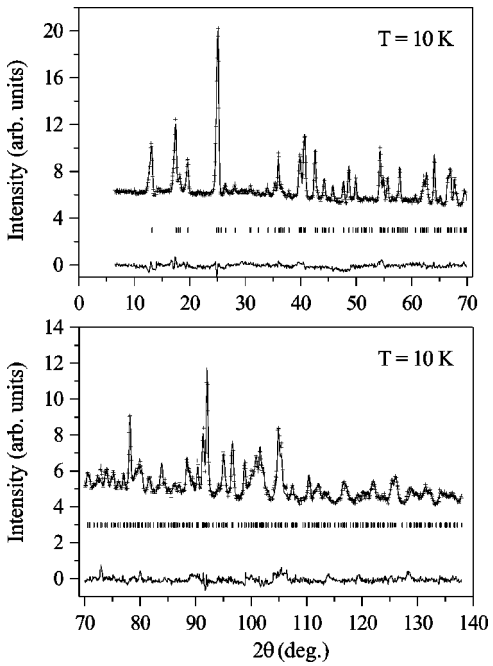

FIG. 1. High-resolution neutron powder diffractogram of Fe(pyrimidine)$_2$Cl$_2$ measured at 10 K (+). The wavelength was 1.7964 Å. The solid line through the data represents the result of a Rietveld refinement of the structural model described in the text. The difference between the measured and calculated diffractograms is shown as solid line at the bottom of each panel. Vertical bars mark expected Bragg peak positions.

Fe(pyrimidine)$_2$Cl$_2$ are $a = b = 7.3681(4)$ Å and $c = 20.339(1)$ Å at 10 K and $a = b = 7.4292(4)$ Å and $c = 20.364(1)$ Å at 298 K. At 10 K, the Fe-N and Fe-Cl distances 2.256(22) and 2.396(16) Å are determined, respectively. Due to the significantly reduced intensity of the high-angle Bragg reflections, the 298 K data are only of limited quality and therefore will not be discussed further.

Figure 1 shows the high-resolution powder diffraction pattern recorded at 10 K together with the result of the Rietveld refinement and the difference between the calculated and measured profiles. The large background signal mostly stems from the incoherent scattering from the hydrogen atoms. The thermal parameters were set equal for all atoms of the same type, because the data quality did not allow for a separate refinement for all nonequivalent atoms. The resulting crystal structure is depicted in Fig. 2 and the structural parameters are listed in Table I. No traces of any secondary phase could be identified.

The crystal structure Fe(pyrimidine)$_2$Cl$_2$ consists of a chiral three-dimensional network of Fe ions coordinated by two Cl and linked by pyrimidine molecules. Due to the 4_1 (or 4_3) screw axis, the local environment of two Fe ions in neighboring layers z and $z + 1/4$ is rotated by 90°. We will discuss below that this specific feature of the crystal structure of Fe(pyrimidine)$_2$Cl$_2$ can be regarded as the origin of the large canting observed in the magnetically ordered state.

In the local FeN$_4$Cl$_2$ geometry all nitrogen atoms of pyrimidine are equatorially coordinated. It was pointed out[13]

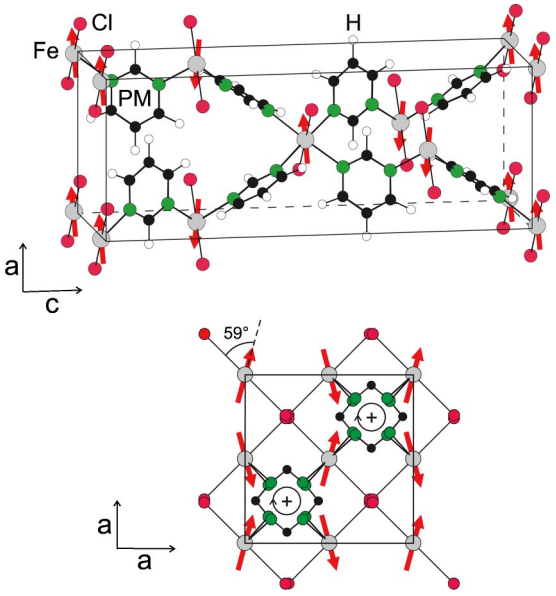

FIG. 2. The crystal and magnetic structure of Fe(pyrimidine)$_2$Cl$_2$. Lower section: A view along the c axis, with the positions of the 90° screw axes marked. The angle $\alpha = 59°$ between the magnetic moments and the local electric-field gradient is also indicated (see text).

that in this case antiferromagnetic correlations are expected to be transferred through the pyrimidine molecule.

B. Magnetization

Figure 3 depicts the M vs H hysteresis curve of a freshly prepared sample Fe(pyrimidine)$_2$Cl$_2$ measured at 1.8 K. On increasing the field from zero, we observe an initial steep increase of the magnetization in a low field region (a few 100 Oe) to a value much smaller than the full Fe^{II} moment. Subsequently, a rounded crossover around 500 Oe is followed by an almost linear field dependence up to 55 kOe. On sweeping the field down from 55 kOe, a weak hysteresis develops and

TABLE I. Structural parameters of Fe(pyrimidine)$_2$Cl$_2$ at 10 K, slightly above the magnetic transition. Space group $I4_122$ (no. 98), $a = b = 7.3681(4)$ Å, $c = 20.339(1)$ Å. The occupancy is unity for all atoms. Quality of the refinement: $R_p = 2.3\%$, $R_{wp} = 3.2\%$, $R_{expected} = 1.4\%$.

Atom[a]	x/a	y/b	z/c	B (Å^2)
Fe ($4b$)	0	0	0	0.4(1)
Cl ($8d$)	0.229(2)	−0.229(2)	0	0.2(1)
N ($16g$)	0.150(2)	0.165(2)	0.076(1)	0.3(1)
C1 ($8f$)	0.066(3)	1/4	1/8	0.3(1)
C2 ($16g$)	0.337(3)	0.168(3)	0.075(1)	0.3
C3 ($8f$)	0.431(3)	1/4	1/8	0.3
H1 ($8f$)	−0.087(7)	1/4	1/8	1.4(2)
H2 ($16g$)	0.393(5)	0.108(5)	0.032(2)	1.4
H3 ($8f$)	0.579(7)	1/4	1/8	1.4

[a]Multiplicity and Wykoff letter.

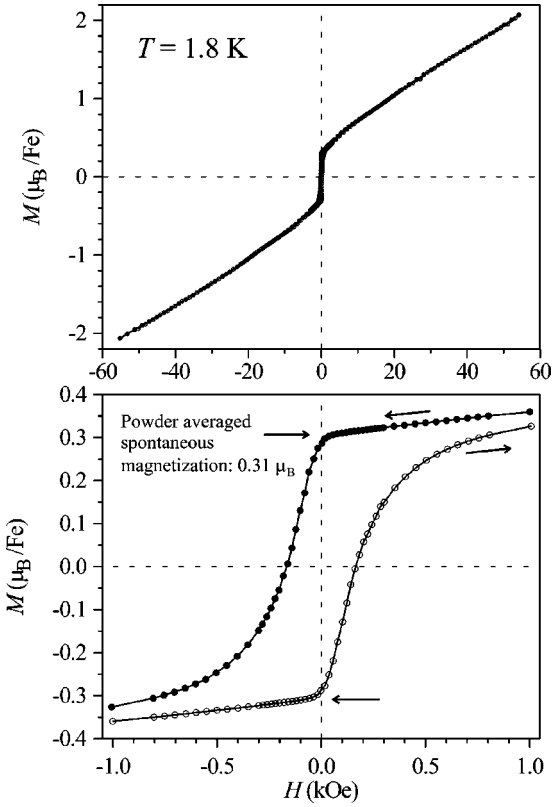

FIG. 3. Hysteresis loop of Fe(pyrimidine)$_2$Cl$_2$ measured at 1.8 K; (a) full hysteresis curve; (b) a blow-up of the low-field section.

a sharp kink is observed around $H = 0$. Upon increasing temperature the hysteresis in the $M(H)$ curves is reduced and vanishes above 6.4 K.

This behavior is typical for a weak ferromagnet, where the steep increase at low H reflects the spontaneous magnetization and the linear high-field behavior is due to the dominant antiferromagnetic interactions. The kink around $H = 0$ allows for an accurate determination of the spontaneous magnetization. We obtain a value of 0.31(1) μ_B on the powder average at 1.8 K. The coercitive field is small (~150 Oe), classifying Fe(pyrimidine)$_2$Cl$_2$ as a soft magnet.

Assuming that the ferromagnetic component in a given magnetic domain is pointing along a specific crystal direction, the measured powder average of the spontaneous magnetization has to be multiplied by a factor of three to obtain the ferromagnetic moment along this axis. Then, from the magnetization we obtain a ferromagnetic component of 0.93(3) μ_B per Fe ion in the canted antiferromagnetic state. We will show in the following that this value is in full agreement with the combined Mössbauer spectroscopy and neutron diffraction results.

C. Mössbauer spectroscopy

In Fig. 4 we plot the Mössbauer spectra of Fe(pyrimidine)$_2$Cl$_2$ at temperatures 2.3–300 K. In Fig. 4(a) data are shown for a newly made sample, while in Fig. 4(b) we display the spectra taken on the same sample after storage for two years under air.

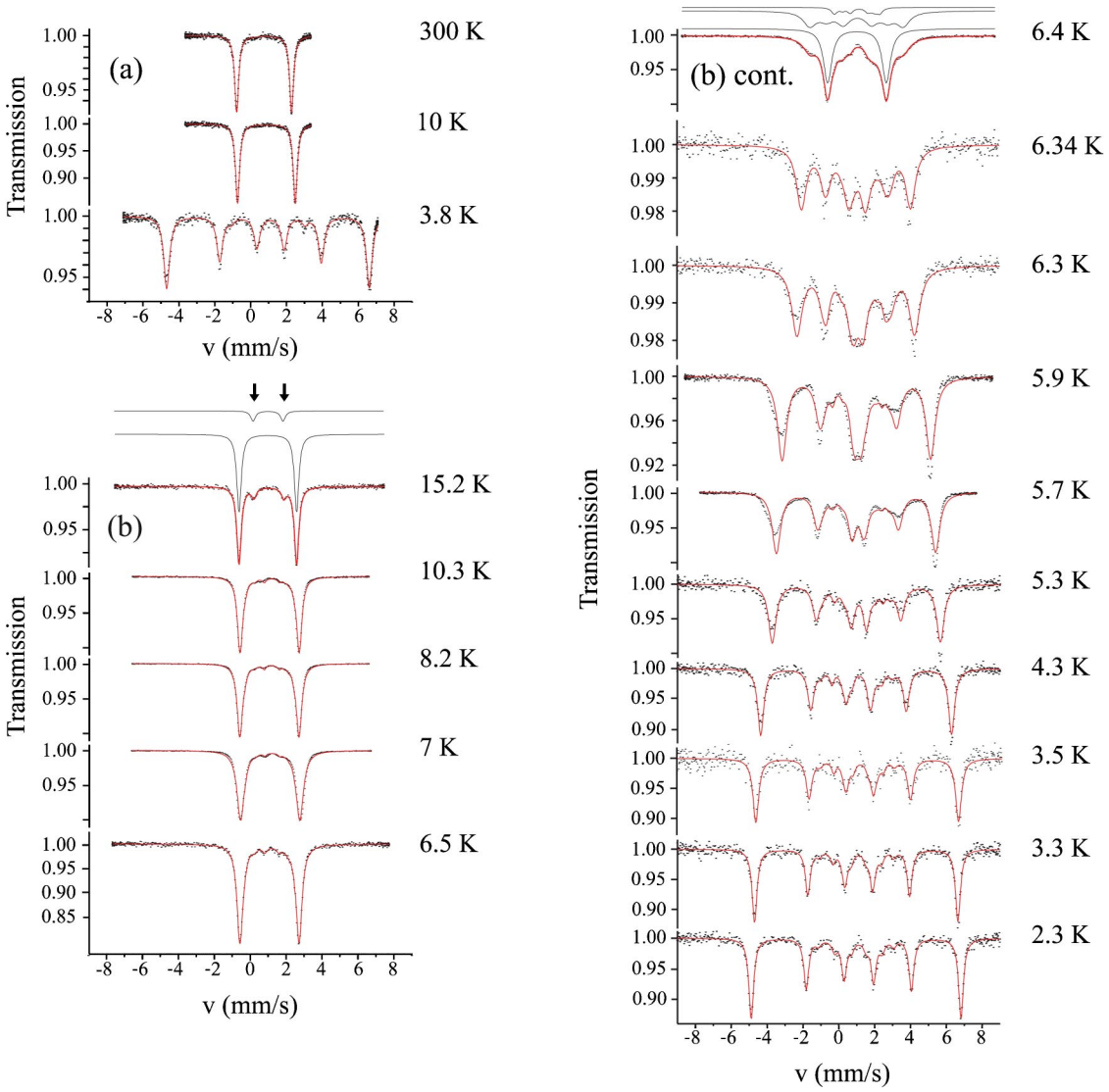

FIG. 4. Mössbauer spectra of Fe(pyrimidine)$_2$Cl$_2$ measured at various temperatures. The solid lines are fits to the data points. The data sets (a) and (b) were measured after different storage times of the sample, arrows in the left part of (b) mark the contribution from a secondary phase (for details see text).

At room temperature, for the newly made sample we observe a two line spectrum, resulting from a quadrupole splitting of $QS=3.11(1)$ mm/s and an isomer shift of $IS=1.03(1)$ mm/s (relative to α-iron foil) [Fig. 4(a) and Table II]. These are typical values for high spin Fe^{II}.[20] Upon lowering the temperature, and above T_N, both QS and IS slightly increase.

Below T_N, at 3.8 K, for the newly made sample eight separate absorption lines with an irregular intensity distribution are observed. As demonstrated by Kündig,[21] such spectra arise from the coexistence of an electric-field gradient and a hyperfine magnetic field (B_{HF}) at the Fe nucleus, whose main axes span an angle α. A fit to the data at 3.8 K based on the diagonalization of the full hyperfine Hamiltonian including electric quadrupole and magnetic Zeeman interaction as described in Ref. 21 yields values for the isomer shift $IS=1.16(1)$ mm/s, quadrupole splitting $QS=3.28(1)$ mm/s, asymmetry parameter $\eta=(V_{xx}-V_{yy})/V_{zz}=0.11(1)$, and the magnetic hyperfine field $B_{HF}=30.2(1)$ T. Moreover, from the fit we determine the angle α between the direction of the hyperfine magnetic field, B_{HF}, and the main electric field gradient component V_{zz} to 59(1)°.

After storage of the sample for two years under air we observe an additional two line spectrum resulting from quadrupole splitting of a secondary phase [arrows in Fig. 4(b) for 15.2 K]. We have chemically isolated this secondary phase and characterized it as Fe(pyrimidine)Cl$_2$.[22] A Mössbauer study above 11 K on a single phase sample of this secondary phase reveals that it can be taken into account in a fit of the data on Fe(pyrimidine)$_2$Cl$_2$ using a quadrupole split set of lines with $QS=1.73(1)$ mm/s and $IS=1.21(1)$ mm/s. In Fig. 4(b) we illustrate the decomposition of the data into two components for the spectrum at 15.2 K by including the separate absorption lines for the two chemical phases. From

TABLE II. Refined parameters from the Mössbauer spectra on Fe(pyrimidine)$_2$Cl$_2$ between 300 and 2.3 K for the newly made sample (**A**) and after storage for two years (**B**). Parameters are the isomer shift IS, quadrupole splitting QS and below T_N the hyperfine field B_{HF}, asymmetry parameter η and canting angle α, with χ^2 as measure for the fit quality.

T (K)	IS [mm/s]	QS [mm/s]	η [ ]	B_{HF} [T]	α [°]	χ^2
A						
300	1.03(1)	3.11(1)	0	0	0	1.07
10.4	1.16(1)	3.27(1)	0	0	0	1.17
3.8	1.16(1)	3.28(1)	0.11(1)	30.2(1)	59(1)	1.35
B						
15.2	1.16(1)	3.28(1)	0	0	0	1.47
10.3	1.16(1)	3.27(1)	0	0	0	4.7
8.2	1.16(1)	3.28(1)	0	0	0	8.5
7	1.18(1)	3.37(1)	0	0	0	27
6.5	1.16(1)	3.30(1)	0	0	0	1.19
6.4[b]	1.16(1)	3.34(1)	0	0	0	3.5
6.4[b]	1.16(1)	3.36(1)	0.1[a]	7.7(1)	59[a]	3.5
6.34	1.14(1)	3.30(3)	0.08(5)	11.5(1)	60(1)	1.19
6.3	1.14(1)	3.29(2)	0.09(5)	13.3(1)	59(1)	1.53
5.9	1.16 [a]	3.26(1)	0.10[a]	19.7(1)	60(1)	13
5.7	1.16 [a]	3.31(1)	0.08(3)	21.7(1)	60(1)	39
5.3	1.14(1)	3.33(2)	0.06(3)	23.4(1)	59(1)	1.73
4.3	1.15(1)	3.23(1)	0.10(1)	28.1(1)	59(1)	1.54
3.5	1.16(1)	3.25(3)	0.11(1)	30.2(1)	60(1)	1.06
3.3	1.16(1)	3.32(1)	0.10(1)	30.3(1)	59(1)	1.24
2.3	1.16(1)	3.33(1)	0.10(1)	31.5(1)	59(1)	1.01

[a]Parameters fixed to stabilize fit.

[b]Spectrum at 6.4 K has been fitted assuming 50% antiferromagnetically ordered and 50% paramagnetic sample volume.

this procedure, the relative spectral weight of the secondary phase is estimated to 14%. It increases to 22% after three year storage.

The secondary phase exhibits magnetic long range order below 11 K. Mössbauer spectra on Fe(pyrimidine)Cl$_2$ measured between 2.5 and 9 K are successfully reproduced by the full hyperfine Hamiltonian with nearly temperature independent hyperfine parameters.[22] Therefore, the parameter set evaluated at 3 K for Fe(pyrimidine)Cl$_2$ was used to describe the secondary phase signal in the measurements on Fe(pyrimidine)$_2$Cl$_2$ at 8.2 K and below. This way, we evaluate the T dependence of the parameters IS, QS, η, B_{HF}, and α for Fe(pyrimidine)$_2$Cl$_2$. The resulting fits and fit parameters are included in Fig. 4(b) and Table II, respectively.

With our procedure, we nicely reproduce the spectra on Fe(pyrimidine)$_2$Cl$_2$ at temperatures down to T_N as well as at 5.3 K and below [Fig. 4(b)]. The mismatch between fit and data in the range from T_N down to $\sim$5.7 K reflects a distribution of the transition temperature T_N of the main phase Fe(pyrimidine)$_2$Cl$_2$. This is demonstrated for the spectrum taken at 6.4 K. Here, we had to assume that 50% of the main phase volume is paramagnetic and 50% antiferromagnetically ordered. The corresponding data decomposition of the full spectrum into the three components, one from

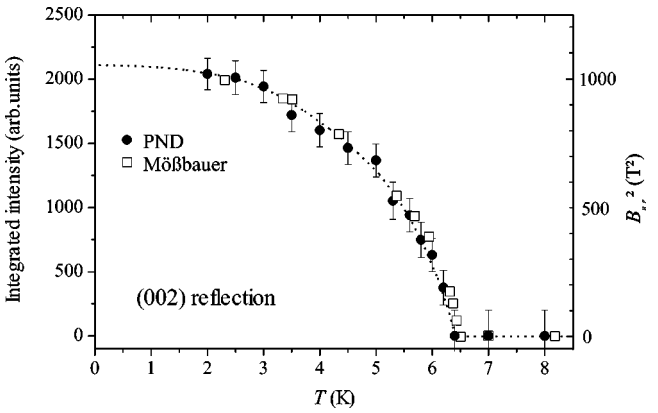

FIG. 5. Temperature dependence of the square of the hyperfine field B_{HF} observed by Mössbauer spectroscopy (data set B of Table II), together with the integrated intensity of the (002) Bragg reflection, being proportional to the square of the ordered moment. The dashed line is a guide to the eye.

paramagnetic and a second from antiferromagnetic Fe(pyrimidine)$_2$Cl$_2$, plus a third from the secondary phase, is exemplified in Fig. 4(b).

In consequence, fits of our Mössbauer spectra assuming a homogeneous antiferromagnetically ordered sample properly reproduce the data well only as long as the hyperfine field B_{HF} does not vary rapidly with temperature, i.e., sufficiently far below T_N. In contrast, close to T_N the distribution of the local hyperfine fields B_{HF} causes a larger mismatch between fit and data. These issues in mind, we find that within experimental resolution IS, QS, η, and α are temperature independent below T_N. The temperature dependence of B_{HF}^2 is displayed in Fig. 5. B_{HF}^2 vanishes at $T_N \sim 6.4$ K and exhibits a behavior typical for a magnetic second-order transition.

To derive the spatial orientation of the magnetic moment at the Fe site from the knowledge of α, one needs to know the orientation of V_{zz} with respect to the crystal lattice. Since this cannot be determined experimentally from Mössbauer experiments on a polycrystalline sample we performed electronic structure calculations as described in the following section.

D. Theoretical calculations

Electronic structure calculations were performed with a code based on a local basis set.[23] Unrestricted Hartree-Fock and density-functional calculations were performed for the periodic system. The functional was chosen as a hybrid functional with a mixture of Fock exchange, a modification of the Becke gradient corrected exchange functional, the Vosko-Wilk-Nusair local correlation functional, and the gradient corrected correlation potential by Lee, Yang, and Parr. This combination has become one of the most popular density functionals and is usually referred to as B3LYP.[24]

The basis functions were chosen as Gaussian type orbitals. The iron basis set[25] (outermost d-exponent 0.4345) is of the size $[5s4p2d]$, the chlorine basis set[26] (with one d exponent with value 0.5) of the size $[5s4p1d]$, carbon and nitrogen basis sets[27] of the size $[3s2p1d]$, and finally a

$[2s1p]$ hydrogen basis set[28] was used. To test the stability of the results, additional tight basis functions were added for the iron atoms and a diffuse sp function (exponent 0.12) was added at the nitrogen site to account for a better description of this negatively charged atom. The results were, however, found to be essentially stable with respect to the various basis sets. With these parameters, the Hartree-Fock or Kohn-Sham equations for the antiferromagnetic (Néel-like) structure are solved self-consistently, and properties such as charge distributions and field gradients can be computed. The structural data used in the calculations are taken from Table I.

From the calculations, the charges were determined to be $+1.9$ for Fe, -1.0 for Cl, -0.8 for N, between 0 and $+0.7$ for carbon, while the hydrogen atoms were found to be slightly positive charged (at most $+0.1$). The spin on the Fe site is 1.9, with a corresponding magnetic moment of 4.0 μ_B, using a g factor of 2.13.[15] Thus, there is moment reduction by about 5% due to covalency effects. The magnitude of the spin at the Cl, N, or C sites is less than 0.1 and thus negligible, the spin at the hydrogen sites virtually zero. The electric field gradient at the Fe site has components with the value $V_{xx}=-0.8$, $V_{yy}=-1.3$, and $V_{zz}=2.1\times10^{22}$ V/m^2. These numbers have an uncertainty of the order of 0.1×10^{22} V/m^2. The asymmetry parameter η is especially sensitive to this uncertainty and values in the range from 0.1 to 0.3 are obtained.

The second largest component of the tensor is identical with the crystallographic c direction, the other two components lie perpendicular in the tetragonal basal plane and are rotated by $\pm45°$ with respect to the a axis. The largest component of the tensor points into the direction of the Cl atoms. Therefore, the Fe-Cl bonds define the principal axis of the electric-field gradient measured in the Mössbauer spectroscopy experiments.

We compare the computed field gradient with the experimental value obtained from Mössbauer spectroscopy by converting according to the formula $QS=eQV_{zz}c/2E_0$, with $E_0=14.4$ keV and using the value of 0.16 barn for the quadrupole moment Q.[29] With these parameters, we obtain a computed $QS=3.5$ mm/s which is in good agreement with the experimental value.

E. Magnetic structure

In Fig. 6 we display the powder neutron diffractograms taken at 1.6 and 7 K (i.e., well below and above T_N), as well as the difference of these two diffractograms, measured on a freshly prepared sample (same sample as used for the crystal structure determination, Sec. III A). The Rietveld refinement of these data was performed, using the positional parameters, thermal factors and lattice constants from Table I, i.e., from the separate high-resolution diffraction experiment at 10 K. The only free parameters were line shape, background and scaling parameters. No additional structural information is obtained. There is no indication for any thermal variation of the structural parameters between 1.6 and 10 K.

The difference spectrum reveals additional Bragg intensities produced by the long-range magnetic ordering. All magnetic reflections can be indexed on the basis of the crystallographic unit cell. The rule $h+k+l=$ even for the observed magnetic Bragg reflections (hkl) indicates that in the magnetically ordered phase the body centering is conserved. A number of observed magnetic Bragg reflections, namely, (002), (110), (114), and (202), break the selection rules for the special position of Fe and therefore cannot be related to any ferromagnetic component. In contrast, all observed magnetic Bragg reflections, but a possible (112), can be reproduced assuming a simple antiferromagnetic ordering between moments in neighboring layers z and $z+1/4$. The presence and strength of the reflection (002) suggest that the magnetic moments lie perpendicular to the c axis.

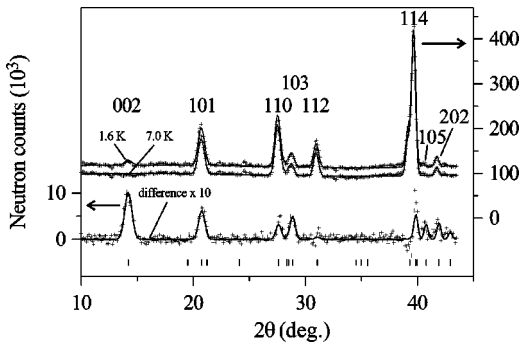

FIG. 6. The two neutron powder diffractograms measured at 1.6 K (below T_N) and 7.0 K (above T_N) for Fe(pyrimidine)$_2$Cl$_2$, offset for clarity, and the difference of the two diffractograms. The wavelength was 2.448 Å. The reflections are indexed on the basis of the crystallographic unit cell. The Rietveld refinements of all three data sets are shown as lines through the corresponding data points.

Initial refinements of the 1.6 K data based on a simple antiferromagnetic structure showed already good agreement and resulted in an ordered moment of roughly 4 μ_B.[15] However, the orientation of the moments within the basal plane as well as the angle and direction of canting can not be determined from these data. We wish to point out that the only unambiguous signature of the ferromagnetic component is the weak additional magnetic intensity expected at the (112) position, which, however, is hidden in the noise of the experimental data. We therefore use the information from the Mössbauer spectroscopy to arrive at the final magnetic structure model.

With the principal axis of the electric-field gradient parallel to the Fe-Cl bonds, as it was determined in the theoretical calculations, in the basic antiferromagnetic structure the moments have to be aligned parallel to the a axis in order to enclose an identical angle with the local electric-field gradient at each Fe. To increase this angle from 45° to 59°—as observed in the Mössbauer experiment—either a canting by 14° within the basal plane (along a') or by 45° along c needs to be introduced. However, only a canting in the basal plane gives a ferromagnetic component close to 1 μ_B, whereas a canting along c would require a ferromagnetic component of 2.8 μ_B. Comparing these values to the results from the magnetization measurements, the latter model can be ruled out. Therefore, for the final magnetic structure model, the moments were confined to the basal plane and the canting angle 14° was fixed. The fit of this final model to the

difference spectrum is shown in Fig. 6 as solid line. In this fit, the only free parameter is the magnitude of the ordered moment. All other parameters, such as lattice constants and line shapes, are fixed by the Rietveld refinements of the high-resolution diffraction data and of the low-resolution nuclear Bragg pattern recorded at 7 K.

In view of the large background noise from the hydrogen incoherent scattering, the refinement gives good agreement with the data ($R_p=0.114$, $R_{wp}=0.137$, $R_{expected}=0.118$ referring to the difference diffractogram). The fit yields an ordered moment of 4.0(3) μ_B—in agreement with the above calculated full moment on the Fe—and a ferromagnetic component of 1.0(1) μ_B. The latter value is in good agreement with the magnetization data discussed above, which resulted in a ferromagnetic component of 0.93(3) μ_B per Fe ion in the canted antiferromagnetic state.

The magnetic ordering breaks the symmetry of the lattice. The 90° screw axis symmetry is lifted as well as the tetragonal symmetry—the two basal-plane axes become nonequivalent. The magnetic structure can be represented in a two-sublattice model with the magnetic space group $I112'$ (special cell choice of space group $C2$ with c as unique axis) with one sublattice at (0,0,0) and the second at (1/2,0,1/4).

The temperature dependence of the integrated intensity of the (002) Bragg reflection is included in Fig. 5. With a temperature independent canting angle α from the Mössbauer study, the Bragg intensity is proportional to the square of the ordered moment, and thus to the hyperfine field B_{HF}^2. Figure 5 reveals a very good agreement between the T dependence of B_{HF}^2 and of the magnetic Bragg intensity in Fe(pyrimidine)$_2$Cl$_2$, thus verifying the validity of our Mössbauer and neutron diffraction analysis. The quantities represent the temperature dependence of the antiferromagnetic order parameter, decreasing continuously with rising temperature and vanishing at $T_N=6.4(2)$ K.

IV. DISCUSSION

The canting angle $\alpha=59°-45°=14°$ observed in the present measurements is extremely large, actually one of the largest reported to date for any weak ferromagnetic compound. For example, weak ferromagnetism of Fe with a canting angle of 16° has been reported for the intermetallic compound UFe_4Al_8. However, the ferromagnetic component is only 0.3 μ_B per Fe in this compound and the canting is due to an interaction between the U 5f and the Fe 3d electrons.[30] Therefore, the physics of this compound is hardly comparable to that of Fe(pyrimidine)$_2$Cl$_2$.

Large canting angles of 2°–7° have been also observed in Gd_2CuO_4-type cuprates. For these materials, a correlation between weak ferromagnetism and the crystal symmetry has been discussed in detail.[31] We believe that such a correlation is also present in Fe(pyrimidine)$_2$Cl$_2$ and that the large canting observed in this compound is a direct result of its chiral lattice symmetry. Due to this symmetry, the orientation of the local easy axis varies by 90° between nearest Fe neighbors linked by a pyrimidine molecule. Therefore, the local anisotropy would favor a 90° alignment between the moments. However, the AFM interaction favors a 180° alignment. The actual angle $180°-2\alpha=152°$ between neighboring moments therefore can be regarded as the result of the competition of the local anisotropy and the antiferromagnetic exchange. The final magnetic structure model suggests that the local easy axis lies perpendicular to c and within the equatorial plane of the local coordination octahedron of each Fe. Thus, it coincides with the axis of the smallest electric field gradient component V_{xx} calculated above. We may express this anisotropy as an additional term in the Hamiltonian of the system,

$$\mathbf{H}=\sum_{NN}\left[J\vec{S}_1\cdot\vec{S}_2+D(S_{1x}S_{2y})\right], \tag{1}$$

where the sum is over all pairs of nearest-neighbor spins $(\vec{S}_1,\vec{S}_2)$, $\vec{S}_j=(S_{jx},S_{jy},S_{jz})$, and $D<0$. The resulting angle α is related to D and J by $D/J=-2\sin 2\alpha$. With the measured α we get $D=-0.96J$. If one would assign the canting to a Dzyaloshinsky-Moriya type interaction,[32–34] the Dzyaloshinsky-Moriya vector was aligned along c as expected for symmetry reasons and the Dzyaloshinsky-Moriya term would read $D(S_{1x}S_{2y}-S_{1y}S_{2x})$. The latter term of (1) differs from the Dzyaloshinsky-Moriya term in leading to a canting towards specific axes x and y for S_1 and S_2, respectively, rather than a canting within the tetragonal basal plane in general.

It is interesting to note that magnetization data on the Co analogs of the present compound, Co(pyrimidine)$_2$Cl$_2$ and Co(pyrimidine)$_2$Br$_2$,[14] indicate even larger ferromagnetic components and therefore suggest even larger canting angles than in Fe(pyrimidine)$_2$Cl$_2$. Another example of such a large canting may be 3D-[Fe(N$_3$)$_2$(4,4′-bpy)], with bpy =4,4′-bipyridine. A microcrystalline sample of this compound was recently reported to exhibit a large spontaneous magnetization of 0.48 μ_B per Fe tentatively ascribed to ferromagnetic ordering while a canted structure was not excluded.[35,36] This tetragonal compound also forms a chiral 3D network structure, space group $P4_12_12$, which is closely related to that of Fe(pyrimidine)$_2$Cl$_2$. The negative Curie-Weiss temperature and the similarity of the magnetization data of 3D-[Fe(N$_3$)$_2$(4,4′-bpy)] with that of the T(pyrimidine)$_2X_2$ complexes suggests that also in the former a canted antiferromagnetic state with a very large canting (of roughly 20°) within the tetragonal basal plane is realized.

To our knowledge, only few other molecule based magnets with chiral crystal structures have been reported. The oxalato (ox) based compound [Co(2,2′-bpy)$_3$][Co$_2$(ox)$_3$]ClO$_4$ (Ref. 37) exhibits weak ferromagnetism with small canting ($\mu_{\mathrm{fm}}=0.009$ μ_B). The compounds of the series [Z$^{\mathrm{II}}$(2,2′-bpy)$_3$][ClO$_4$][M$^{\mathrm{II}}$Cr$^{\mathrm{III}}$(ox)$_3$][38] order ferromagnetically. Both systems crystallize in the cubic chiral space group $P4_132$. Another example is ferrimagnetic Mn(hfac)$_2$NITPhOMe, crystallizing in space group $P3_1$.[39] The other compounds discussed in the framework of chiral magnetism are based on chiral constituents and crystallize in noncentrosymmetric but achiral space groups, such as $P1$ or $P2_12_12_1$.[9]

V. CONCLUSION

We have shown that Fe(pyrimidine)$_2$Cl$_2$ is a weak ferromagnet with low coercitive field but a very large ferromagnetic component of $\sim 1\ \mu_B$, corresponding to a canting angle of 14°. This is one of the largest values reported to date. In a given magnetic domain, the antiferromagnetic component of the moments is confined to the a axis, while the canting occurs along the perpendicular direction a'. We argued that the large canting in Fe(pyrimidine)$_2$Cl$_2$ is the direct result of its chiral lattice symmetry leading to a competition between the antiferromagnetic exchange interaction and the local single-ion anisotropy. The appearance of canting rather than a chiral magnetic structure may be a general feature of the magnetic ordering in similar structures possessing 90° screw axes. This observation is of interest in view of the extensive efforts to produce a molecular magnet exhibiting chiral magnetic ordering. To date, both strategies, crystallizing (i) achiral constituents in a chiral lattice and (ii) chiral constituents in non-centrosymmetric but achiral lattices did not lead to chiral magnetic ordering.

Most of these compounds possess 90° or 180° screw axes. These lead to a $\pm 90°$ or to no alteration at all, respectively, of the local anisotropy along the screw axes and thus do not necessarily support any chirality of the ordered magnetic structure. Local anisotropy supporting chiral magnetic ordering therefore appears more likely in chiral trigonal/hexagonal lattices. We suggest that the search for chiral magnetic ordering should focus on compounds of that kind.

ACKNOWLEDGMENTS

We thank N. Stüsser and D. Toebbens for experimental support. This work has been partially supported by the Deutsche Forschungsgemeinschaft DFG under Contract No. SU229/6-1.

*Electronic address: Feyerherm@hmi.de

[1] M. Verdaguer, Polyhedron **20**, 1115 (2001), and the following articles of Issues 11–14 of this volume (Proc. ICMM 2000, San Antonio).
[2] E. Coronado Miralles, Polyhedron **22**, 1725 (2003), and the following articles of Issues 14–17 of this volume (Proc. ICMM 2002, Valencia).
[3] O. Kahn, *Molecular Magnetism* (VCH, New York, 1993).
[4] J. Miller and A. Epstein, Angew. Chem., Int. Ed. Engl. **33**, 385 (1994).
[5] D. Gatteschi, Adv. Mater. (Weinheim, Ger.) **6**, 635 (1994).
[6] E. Coronado, J.P. Galán-Mascarós, C.J. Gómez-García, and V. Laukhin, Nature (London) **408**, 447 (2000).
[7] S. Benard, P. Yu, J. Rivière, R. Clément, J. Guilhelm, L. Tchernatov, and K. Nakatani, J. Am. Chem. Soc. **122**, 9444 (2000).
[8] G.L.J.A. Rikken and E. Raupach, Nature (London) **390**, 493 (1997).
[9] E. Coronado, C.J. Gómez-García, A. Nuez, F.M. Romero, E. Rusanov, and H. Stoeckli-Evans, Inorg. Chem. **41**, 4615 (2002), and references therein.
[10] T. Ishida, S.-I. Mitsubori, T. Nogami, and H. Iwamura, Mol. Cryst. Liq. Cryst. **233**, 345 (1993).
[11] G.D. Munno, T. Poerio, M. Julve, F. Lloret, and G. Viau, New J. Chem. **22**, 299 (1998).
[12] R. Feyerherm, S. Abens, D. Günther, T. Ishida, M. Meißner, M. Meschke, and T. Nogami, J. Phys.: Condens. Matter **39**, 8495 (2000).
[13] F. Mohri, K. Yoshizawa, T. Yamabe, T. Ishida, and T. Nogami, Mol. Eng. **8**, 357 (1999).
[14] K. Nakayama, T. Ishida, R. Takayama, D. Hashizume, M. Yasui, F. Iwasaki, and T. Nogami, Chem. Lett. **27**, 497 (1998).
[15] K. Zusai, T. Kusaka, T. Ishida, R. Feyerherm, M. Steiner, and T. Nogami, Mol. Cryst. Liq. Cryst. Sci. Technol., Sect. A **343**, 127 (2000).
[16] K. Lagarec, *Reoil*, Version 1.02 (Department of Physics, University of Ottawa, Ottawa, 1998).
[17] N. Blaes, H. Fischer, and U. Gonser, Nucl. Instrum. Methods Phys. Res. B **9**, 201 (1985).
[18] T. Roisnel and J. Rodríguez-Carvajal, Mater. Sci. Forum **378-381**, 118 (2001).
[19] D. Hashizume, R. Takayama, K. Nakayama, T. Ishida, T. Nogami, M. Yasui, and F. Iwasaki, Acta Crystallogr., Sect. C: Cryst. Struct. Commun. **55**, 1793 (1999).
[20] D. Barb, *Grundlagen und Anwendungen der Mössbauerspektroskopie* (Akademie, Berlin, 1980).
[21] W. Kündig, Nucl. Instrum. Methods **48**, 219 (1967).
[22] R. Feyerherm *et al.* (2003), a full account of the properties of this material will be given elsewhere.
[23] V.R. Saunders, R. Dovesi, C. Roetti, M. Causá, N.M. Harrison, R. Orlando, and C.M. Zicovich-Wilson, CRYSTAL98 *User's Manual* (University of Torino, Torino, Italy, 1998).
[24] P.J. Stephens, F.J. Devlin, C.F. Chabalowski, and M.J. Frisch, J. Phys. Chem. **98**, 11623 (1994).
[25] M. Catti, G. Valerio, and R. Dovesi, Phys. Rev. B **51**, 7441 (1995).
[26] M. Prencipe, A. Zupan, R. Dovesi, E. Aprá, and V.R. Saunders, Phys. Rev. B **51**, 3391 (1995).
[27] R. Dovesi, M. Causá, R. Orlando, C. Roetti, and V.R. Saunders, J. Chem. Phys. **92**, 7402 (1990).
[28] R. Ditchfield, W.J. Hehre, and J.A. Pople, J. Chem. Phys. **54**, 724 (1971).
[29] P. Dufek, P. Blaha, and K. Schwarz, Phys. Rev. Lett. **75**, 3545 (1995).
[30] J.A. Paixão, B. Lebech, A.P. Gonçalves, P.J. Brown, G.H. Lander, P. Burlet, A. Delapalme, and J.C. Spirlet, Phys. Rev. B **55**, 14 370 (1997).
[31] H.M. Luo, Y.Y. Hsu, B.N. Lin, P. Chi, T.J. Lee, and H.C. Ku, Phys. Rev. B **60**, 13 119 (1999).
[32] I. Dzyaloshinsky, J. Phys. Chem. Solids **4**, 241 (1958).
[33] T. Moriya, Phys. Rev. **117**, 635 (1960).
[34] T. Moriya, Phys. Rev. **120**, 91 (1960).
[35] T. Yuen, C.L. Lin, A. Fu, and J. Li, J. Appl. Phys. **91**, 7385 (2002).
[36] A. Fu, X. Huang, J. Li, T. Yuen, and C.L. Lin, Chem.-Eur. J. **8**, 2239 (2002).
[37] M. Hernández-Molina, F. Lloret, C. Ruiz-Pérez, and M. Julve, Inorg. Chem. **37**, 4131 (1998).
[38] E. Coronado, J.P. Galán-Mascarós, C.J. Gómez-García, and J.M. Martínez-Agudo, Inorg. Chem. **40**, 113 (2001).
[39] A. Caneschi, D. Gatteschi, P. Rey, and R. Sessoli, Inorg. Chem. **30**, 3936 (1991).

Selected Paper

Single-Crystal Magnetic Study on Guest-Tunable Weak Ferromagnets [M{N(CN)$_2$}$_2$(pyrimidine)](guest) (M = Fe, Co)

Naomi Takagami,[1] Takayuki Ishida,*[1,2] and Takashi Nogami[1]

[1]Department of Applied Physics and Chemistry, The University of Electro-Communications, Chofu, Tokyo 182-8585

[2]Course of Coherent Optical Science, The University of Electro-Communications, Chofu, Tokyo 182-8585

Received November 19, 2003; E-mail: ishi@pc.uec.ac.jp

Low-temperature magnets derived from [M{N(CN)$_2$}$_2$(pm)] (M = Fe^{II}, Co^{II}) have guest molecules incorporated in the clearance of the three-dimensional framework, where pm stands for pyrimidine. A pm molecule in [Fe{N(CN)$_2$}$_2$(pm)](pm) (**1**) was characterized as a guest by means of X-ray crystallographic analysis. The guest molecules as well as the host N(CN)$_2$ skeletons are disordered in [Fe{N(CN)$_2$}$_2$(pm)](guest) (guest = EtOH (**2**), *n*-PrOH (**3**), 1/2 *n*-BuOH (**4**)) and also in [Co{N(CN)$_2$}$_2$(pm)](guest) (guest = EtOH (**5**), *n*-PrOH (**6**)). The ac and dc magnetic susceptibility measurements on randomly oriented polycrystalline samples of **1**–**6** revealed that they were weak ferromagnets (canted antiferromagnets) below T_N. The single-crystal magnetization measurements clarified the T_N's and the cant angles at 2 K as follows: $T_N = 5.6$ K, $\theta = 1.3°$ ($H \parallel c$) for **1**; $T_N = 3.3$ K, $\theta = 16°$ ($H \parallel c$) for **2**; $T_N =$ ca. 2 K, $\theta = 7.1°$ ($H \parallel b$) for **5**. The magnetic ground state seems to be related with single-ion anisotropy of the metal ions and the spin canting may take place as a combined result of the axial or in-plane anisotropy and antiferromagnetic interaction. The incorporated guest molecule tunes the single-ion anisotropy of the host metal ions, and consequently the magnetic phase transition phenomena were drastically different depending on the guest molecules.

There have been numerous reports on infinite metal–organic polymeric frameworks involving N-donor bridging ligands.[1] We have reported the magnetism of pyrimidine (pm)-bridged transition metal complexes in connection with the high-spin *m*-phenylene-bridged poly-carbenes and -radicals[2] and also the versatile utility of pm as a supramolecular synthon.[3] The role of pm as a magnetic coupler has been clarified to depend on the magnetic orbitals on the metal ions and the coordination geometries.[4,5] Various magnets have also been reported that contain d-transition metal ions and polycyano-anion bridges such as N(CN)$_2^-$.[6,7] Ternary systems attract much attention. Some peculiar crystal structures have been reported for [Mn{N(CN)$_2$}$_2$](pz)][8] and [Cu{N(CN)$_2$}$_2$(pz)],[9] where pz stands for pyrazine. We have already reported the transition metal complexes containing both pm and N(CN)$_2^-$ bridges, namely, [M^{II}\{N(CN)$_2$\}$_2$(pm)] (M = Fe,[10] Co,[10] Ni[11]) (Chart 1). Recently, we also developed the azide-bridged complexes, [M^{II}(N$_3$)$_2$(pm)] (M = Mn, Fe, Co, Ni), having a similar pillared-layer structure (Fig. 1) and a comparably higher T_N.[12] These metal dicyanamides and related ternary systems have often been characterized as canted antiferromagnets (weak ferromagnets),[6,7,10–13] and the origin of spin canting became of current interest.[14]

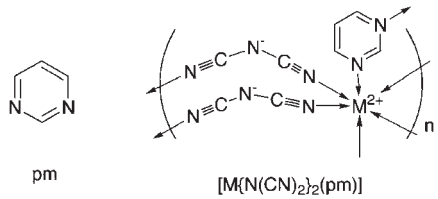

Chart 1.

Self-assembled complexes also attract attention for nano-porous materials that find potential applications in many areas (gas absorption for instance).[1] Porous magnets enable us to examine possible control of the magnetism by means of supramolecular techniques.[15] The specimen of [M{N(CN)$_2$}$_2$(pm)] prepared from an ethanol solution was revealed to contain ethanol molecules as a guest.[10] We have examined the solvent-dependence of the magnetic properties for the "solvated magnets" of [Fe{N(CN)$_2$}$_2$(pm)], since preparation from various solvents gave isomorphous compounds with only slight structural modification.[16] To investigate origins of the spin canting in [M{N(CN)$_2$}$_2$(pm)]-type compounds, we planned to study their single-crystal magnetic properties by varying the transition metal ions and guest molecules. Here we will concisely review the crystal structures of the host-guest compounds and the magnetic properties of randomly oriented polycrystalline sam-

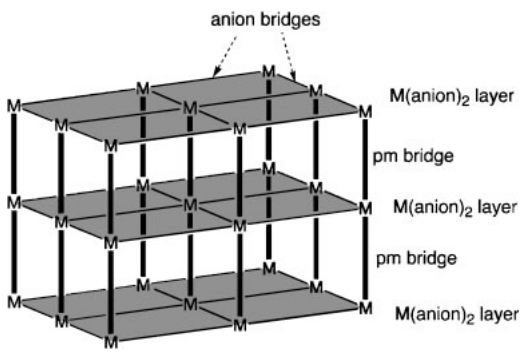

Fig. 1. Schematic drawing of the crystal structure of [M(X)$_2$(pm)] (M = Mn^{II}, Fe^{II}, Co^{II}, N^{II}; X = N(CN)$_2^-$, N$_3^-$).

Published on the web June 9, 2004; DOI 10.1246/bcsj.77.1125

ples for $[M\{N(CN)_2\}_2(pm)](guest)$.[10,11,16] A possible origin of the spin canting will be discussed after we describe the magnetic ordering phenomena on a single crystal of selected compounds.

Results

Crystal Structures. The X-ray crystal structure analysis reveals that the crystals of **1**–**6** are isomorphous, belonging to a space group orthorhombic *Pnma*. The cell parameters are summarized in Table 1, together with the composition determined from elemental analysis. Figures 2(a) and 2(b) show the ORTEP drawings of the $[Fe\{N(CN)_2\}_2(pm)]$ moiety in **1** as a host skeleton. There is only one Fe ion in an asymmetric unit. Each octahedral Fe ion resides at an inversion center and is coordinated by four nitrile N atoms at the equatorial sites and by two pm N atoms at the axial sites. The Fe^{II} and two $N(CN)_2^-$ ions construct a two-dimensional network parallel to the *ac* plane (Fig. 2(a)). The pm molecules bridge inter-sheet Fe ions along

Table 1. Cell Parameters of $[M\{N(CN)_2\}_2(pm)](guest)$ (**1**–**6**)[a)]

Compound	**1**	**2**	**3**	**4**	**5**	**6**[b)]
M	Fe	Fe	Fe	Fe	Co	Co
guest	pyrimidine	ethanol[c)]	propanol[c)]	1/2 butanol[c)]	ethanol[c)]	propanol[c)]
a/Å	13.0061(5)	12.917(1)	12.597(5)	12.9486(7)	12.8586(4)	12.768(3)
b/Å	12.3550(4)	12.0440(6)	12.001(6)	12.2052(6)	11.9268(4)	12.121(2)
c/Å	9.2235(4)	9.2575(8)	9.461(4)	9.4499(6)	9.2126(2)	9.292(2)
V/Å^3	1482.1(1)	1440.2(2)	1430(1)	1493.5(2)	1412.86(7)	1438.1(9)
D_{calcd}/g cm^{-3}	1.560	1.449	1.523	1.584	1.491	1.530
T/K	90	100	90	90	100	90

a) The space groups are orthorhombic *Pnma* with $Z = 4$ unless otherwise noted. Pm stands for pyrimidine.
b) Only the cell parameters were determined. c) Determined by elemental analysis (C, H, N).

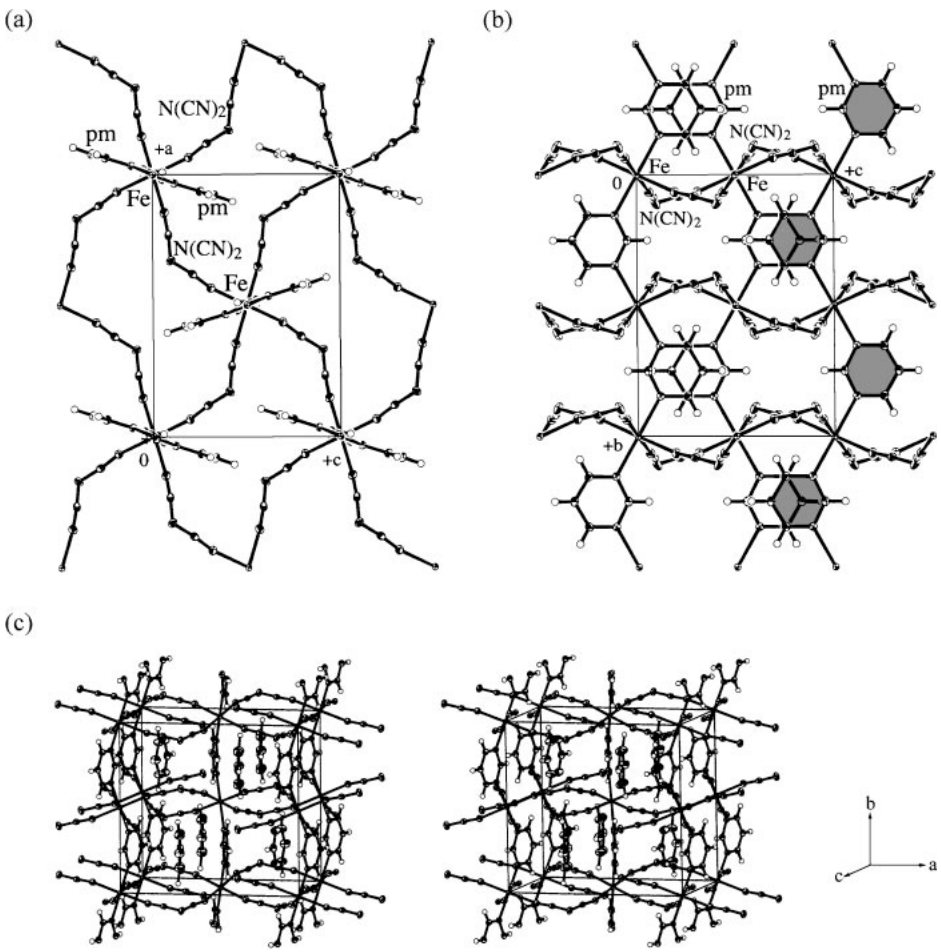

Fig. 2. (a,b) ORTEP drawings of $[Fe\{N(CN)_2\}_2(pm)](pm)$ (**1**), viewed along the *b* axis (a) and *a* axis (b). Thermal ellipsoids are drawn at the 50% probability level for non-hydrogen atoms. The guest pyrimidine molecules are omitted for the sake of clarity. A one-dimensional Fe–pm chain is shaded in (b). (c) A stereo-view of the crystal structure of **1**. Pm stands for pyrimidine.

the *b* axis to form a *trans* zigzag Fe–pm chain, as indicated by the shaded pm rings in Fig. 2(b). Thus, the $N(CN)_2^-$ and pm moieties contribute μ-1,5-bridged two-dimensional and μ-1,3-bridged one-dimensional structures, respectively, constructing a three-dimensional framework (Fig. 1).

Important geometries are described for **1**. Four nitrile nitrogen atoms are coordinated at the equatorial sites with the Fe–$N_{nitrile}$ distances of 2.126(1) and 2.141(1) Å, and by two pm nitrogen atoms at the axial sites with the Fe–N_{pm} distance of 2.219(1) Å. The $N_{nitrile}$–Fe–N_{pm} angles range from 88.87(5) to 91.13(5)°. The amide nitrogen atom does not participate in coordination. The central C–N–C angle is 120.3(1)°, the N–C≡N angles are 173.4(2) and 173.7(2)°, and the C≡N–Fe angles are 163.6(1) and 167.1(1)°. The Fe···Fe separation of 6.1775(2) Å across the pm bridge is shorter than the intra-sheet Fe···Fe separation of 7.9723(2) Å across the $N(CN)_2^-$ bridge, and accordingly the pm bridge may afford a principal magnetic exchange pathway. Owing to the strong directionality of the pm lone-pairs, the elongated octahedral axes of neighboring Fe ions are relatively inclined by 118°.

The guest molecule in **1** was characterized to be an uncoordinated pm (Fig. 2(c)). The hydrogen atoms in the guest pm were experimentally found and the positional parameters were optimized successfully. The analysis revealed no disorder of the nitrogen position. Although the *R* factors in the refinement were satisfactorily lowered, thermal ellipsoids in the guest pm are somewhat larger, even at 90 K, than those in the host. The site occupancy of the guest pm was refined to be almost unity, in good agreement of the elemental analysis.

The [Fe{$N(CN)_2$}$_2$(pm)] skeletons are essentially the same among **1**–**4**, except for the small change of the cell lengths (Table 1). The solvent molecules in **2**–**4** were found in difference Fourier maps but their positional and thermal displacement parameters could not be completely determined owing to disorder. In addition to the guest disorder, the skeletal $N(CN)_2^-$ bridges in **2**–**4** also showed disorder. The detailed crystal structure of **2** measured at 100 K was published elsewhere.[10] The equatorial Fe–$N_{nitrile}$ distances are 2.138(4) and 2.142(4) Å, and the axial Fe–N_{pm} distance is 2.202(4) Å. The $N_{nitrile}$–Fe–N_{pm} angles range from 89.6(2) to 90.4(2)°. The intra- and inter-sheet Fe···Fe separations are 7.9458(5) and 6.0220(3), respectively.

The crystal structure of **5** is also isomorphous to that of **2**.[10] The guest ethanol molecules and the host $N(CN)_2^-$ bridges are disordered. The Co–$N_{nitrile}$ bond lengths are 2.103(4) and 2.105(4) Å and the Co–N_{pm} bond length 2.154(4) Å. The slightly elongated octahedron was characterized with the pm nitrogen atoms at the axial positions, in the same way as **1** and **2**. The intra- and inter-sheet Co···Co separations are 7.9091(2) and 5.9634(2), respectively. The metal–nitrogen bond lengths for **1**, **2**, and **5** are summarized in Table 2. The Co–N bond lengths are shorter than the Fe–N bond lengths in an isomorphous series,[5] and accordingly the cell volume of **5** is smaller than that of **2**.

Magnetic Properties for Polycrystalline Samples. We measured field-cooled magnetization (FCM), remnant magnetization (RM), and zero-field-cooled magnetization (ZFCM) of randomly oriented polycrystalline specimens of **1**–**4**. The temperature dependence of the FCMs at 5 Oe showed clear upsurges at about 5.6, 3.7, 4.6, and 3.6 K for **1**–**4**, respectively, and, after the applied field was removed, the RMs disappeared at the same temperatures. The FCM results are summarized in Fig. 3(a). We measured the ac magnetic susceptibility (Figs. 3(b) and 3(c); χ_{ac}' and χ_{ac}'' for the real and imaginary parts, respectively) of **1**–**4**. As Fig. 3(b) shows, the χ_{ac}' measurements (100 Hz) exhibited peaks at 5.6, 3.3, 4.4, and 3.6 K, respectively, supporting the occurrence of the magnetic phase transition. We found no frequency dependence of T_N.

Table 2. The Metal–Nitrogen Bond Lengths (Å) of [M{$N(CN)_2$}$_2$(pm)](guest) (**1**, **2**, and **5**)

Compound	**1**	**2**	**5**
M	Fe	Fe	Co
guest	pyrimidine	ethanol	ethanol
M–$N_{nitrile}$	2.126(1)	2.138(4)	2.103(4)
	2.141(1)	2.142(4)	2.105(4)
M–N_{pm}	2.219(1)	2.202(4)	2.154(4)

In order to clarify the nature of magnetism below T_N, we measured *M*–*H* curves at 2.0 K for the polycrystals of **1**–**4**. As reported in the previous communication,[10] the Fe^{II} ion in **2** has a high-spin state ($S = 2$) and dominant antiferromagntic interactions were clarified with a negative Weiss temperature (−7.0 K) in the paramagnetic phase. Figure 4 shows that **1**–**4** behave as weak ferromagnets, as indicated by spontaneous magnetizations (M_S) in a low field region. Stepwise saturation behavior was observed, the origin of which can be proposed as spin-flip transition from a canted antiferromagnetic phase to a canted ferromagnetic phase. The smaller M_S implies a smaller cant angle in a canted antiferromagnetic phase, and after a possible spin-flip transition the saturation magnetization should be larger in a canted ferromagnetic phase. This interpretation is supported by comparison of the *M*–*H* curve of **1** with those of **2**–**4**. The M_S of **1** was the smallest and the strong antiferromagnetic nature seems responsible for the small χ_{ac}' and χ_{ac}'' peaks of **1**. The M_S's at 2.0 K were found to be 0.2×10^3 and 5.8×10^3 erg Oe^{-1} mol^{-1} for **1** and **2**, respectively, indicating that the cant angles for **1** and **2** are 0.6 and 14° at the ground state. The coercive fields were <20 Oe, indicating a soft character of **1**–**4**. Small hysteresis-like behavior was found during the metamagnetic transition, but it is not intrinsic because the single-crystal magnetic study exhibited no hysteresis behavior (see below).

The magnetic properties of **5** have been described elsewhere.[10] The antiferromagnetic interactions among the high-spin Co^{II} ions ($S = 3/2$) were characterized for **5** with a negative Weiss temperature of −4.4 K.[10] The magnetization curve measured at 2.0 K showed an M_S of 2.5×10^3 erg Oe^{-1} mol^{-1} (Fig. 5(a)), indicating the cant angle of 7°. The coercive field was <20 Oe. The transition temperature was near 2.0 K, as determined by the FCM, RM, and ZFCM measurements together with the χ_{ac}' and χ_{ac}'' measurements. The [Co{$N(CN)_2$}$_2$(pm)](guest) series also exhibited guest dependence of the magnetic phase transition phenomena. Actually, the sample prepared from propanol (**6**) showed the *M*–*H* curve with a more distinguished metamagnetic transition than that for **5** (Fig. 5(b)). The M_S of **6** at 2.0 K was almost the same as that of **5**. The transition temperature of **6** was 2.1 K, as determined by the FCM, RM, ZFCM, and ac susceptibility measurements.

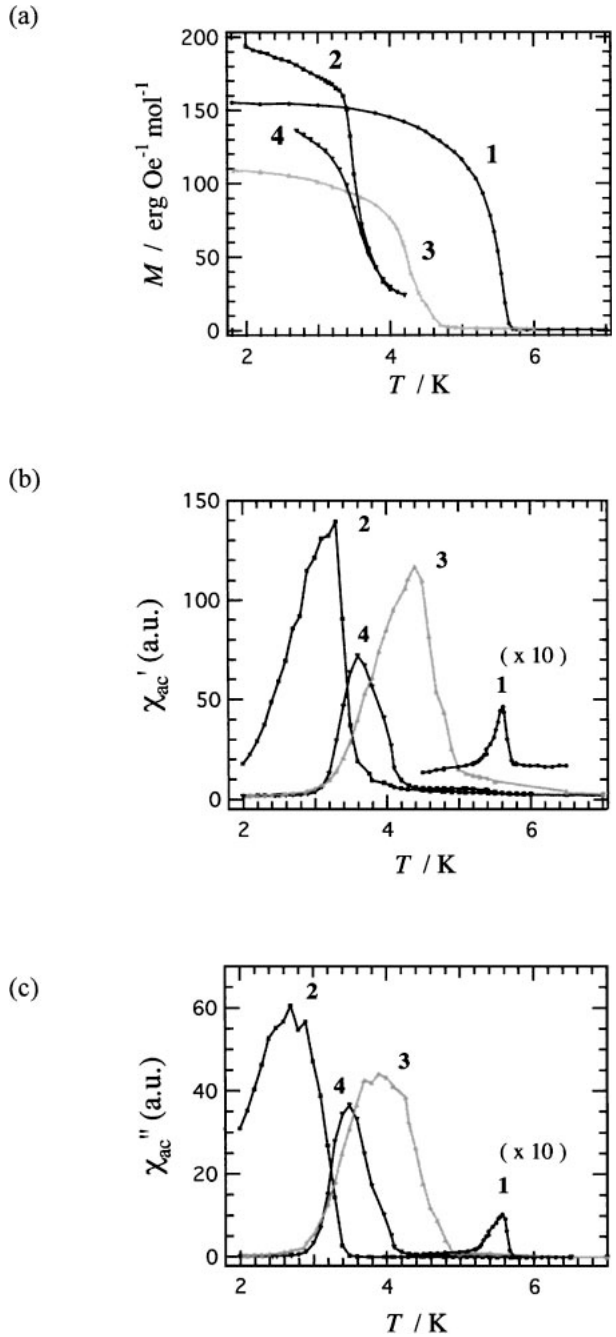

Fig. 3. (a) Field-cooled magnetization of **1**–**4** measured at 5 Oe. (b,c) Temperature dependence of χ_{ac}' (b) and χ_{ac}'' (c) for **1**–**4** ($\nu = 100$ Hz). Comparison of relative intensity is valid in the arbitrary scale.

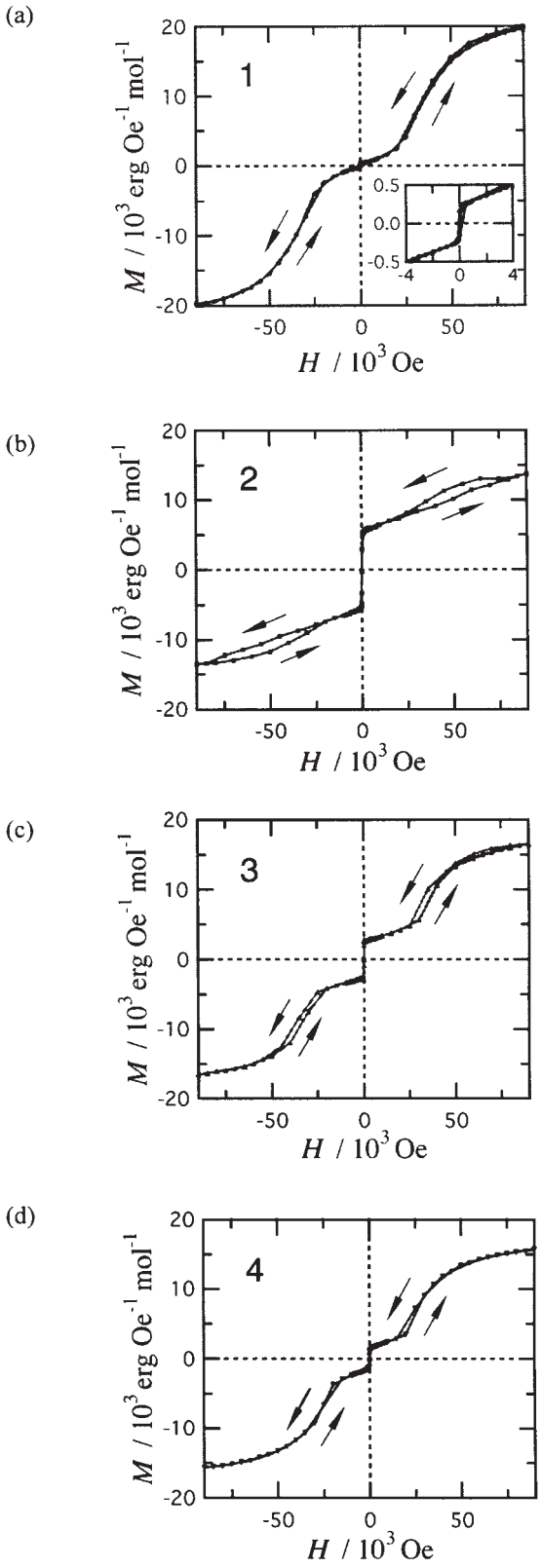

Fig. 4. (a–d) *M*–*H* curves of **1**–**4** measured at 2.0 K. Solid lines are shown for a guide to the eye.

However, the Co series is supposed to be rather inadequate for the detailed study of the guest dependence because the T_N's were too low for us to measure their magnetic properties precisely on our apparatus.

Magnetic Properties for Single-Crystal Samples. We measured FCM, RM, and ZFCM of a single crystal of **1**. As Fig. 6(a) shows, only when an external field was applied parallel to the crystallographic *c* axis did the magnetization show an obvious upsurge near T_N (5.6 K) upon cooling. The estimated mass of the single crystal specimen was 0.0475 mg. A rather large magnetic field (500 Oe) was applied because sufficient SQUID responses were recorded for the small crystal. Some biases were found for the data measured at the applied field par-

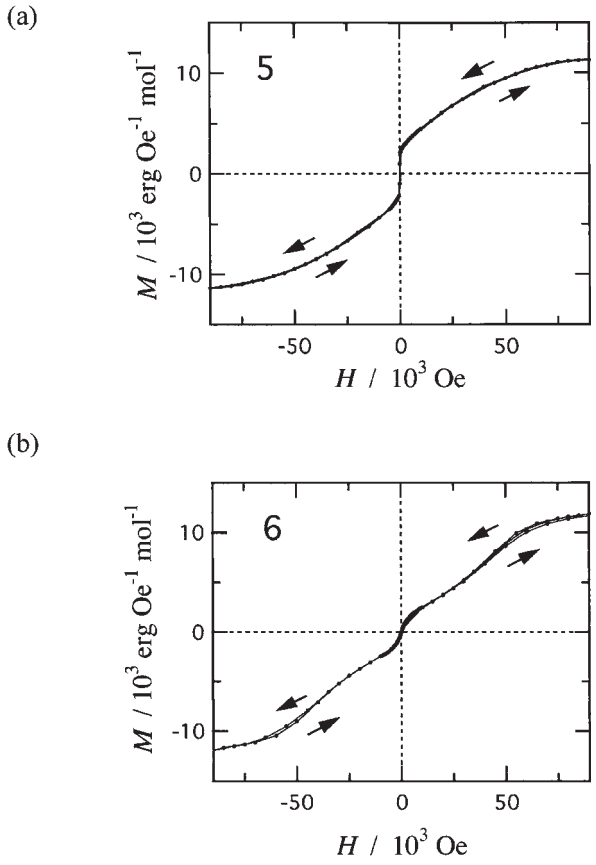

Fig. 5. (a,b) *M–H* curves of **5** and **6** measured at 2.0 K. Solid lines are shown for a guide to the eye.

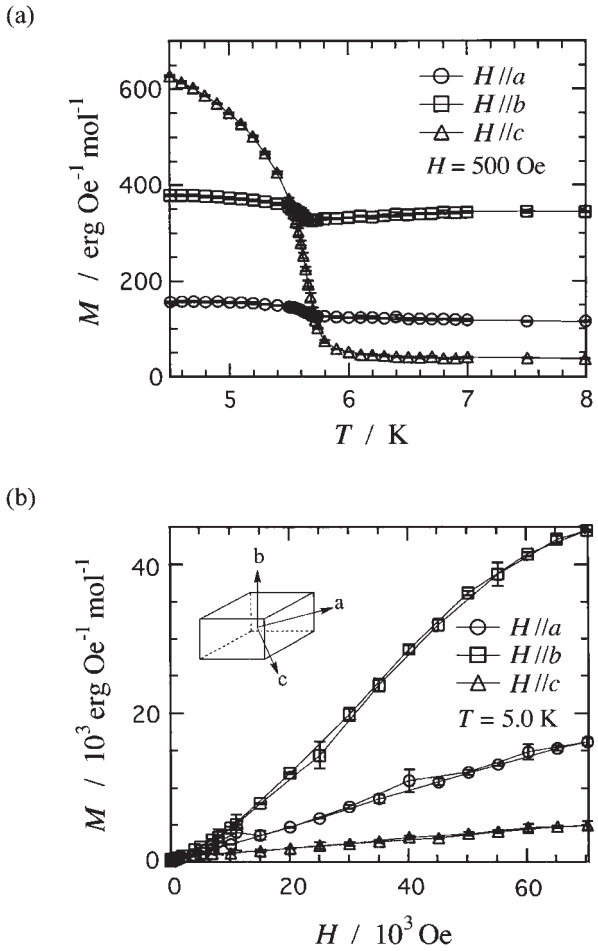

Fig. 6. (a) Field-cooled magnetization measurements of a single crystal of **1** with the applied fields of 500 Oe parallel to the *a*, *b*, and *c* axes. (b) Magnetization curves of **1** at 5 K with the applied field parallel to the *a*, *b*, and *c* axes. Solid lines are shown for a guide to the eye. Inset depicts the relation between the crystal habit and axis directions.

allel to the *b* and *a* axes and these are not essential; the magnetization upsurge is very small so that these biases seemed relatively large. Small kinks are found in the data measured with $H \parallel a$ and $H \parallel b$ but these are negligible within experimental error since the crystal was mounted manually under a microscope.

One may wonder whether the small ferromagnetic component observed for the polycrystalline samples is intrinsic in the crystal structure, especially for **1** showing the extremely small spontaneous magnetization (M_S). If we argue from the above results, however, the highly anisotropic FCM upsurge observed can be attributed genuinely to the crystal of **1** and not to impurities that contaminate.

This experiment clearly tells us that the spin canting direction is the *c* axis, and the magnetic easy axis is expected to reside perpendicular to that axis. We measured the precise angular dependence of FCM as a function of a rotation angle within the *ac* and *bc* planes. We found that they showed monotonic behavior and that the maximum and minimum were located just at the axis directions.

Figure 6(b) shows the *M–H* curves for **1** with the applied fields parallel to the *a*, *b*, and *c* axes. The magnetization along the *c* axis was the most insensitive to the applied field. This finding indicates that the magnetically hard axis should be assigned to the *c* axis, in good agreement of the canting direction determined from the FCM results. We can find an S-shaped magnetization curve in the data of $H \parallel b$. Therefore the magnetic structure of **1** at the ground state was described as a dominantly antiferromagnetic structure along the *b* axis with a small spin canting toward the *c* direction. The anisotropic bulk magnetism with respect to the magnetic unique *b* axis may be related to the Ising (S_z) spin character of the Fe^{II} ion (see Discussion section). The angle of spin canting was estimated to be 1.3° toward the *c* axis from the basal alignment on the *b* axis.

We similarly measured anisotropic properties in the FCM and *M–H* curves for **2**. Interestingly, the angular dependence of **2** was quite different from that of **1** despite the isomorphous crystals with the same metal ions. Figure 7(a) shows the FCM results on **2** at 500 Oe when the magnetic fields were applied along the *a*, *b*, and *c* axes. The magnetization due to spin canting was observed for the measurement with $H \parallel c$ just like **1**, and also relatively small magnetization for the measurement with $H \parallel b$. Practically no magnetization was observed in the measurement with $H \parallel a$. Figure 7(b) shows the *M–H* curves for **2** with the applied fields parallel to the *a*, *b*, and *c* axes. An M_S was clearly observed in the data of $H \parallel c$, and the data of $H \parallel a$ traced an S-shaped curve typical of metamagnetic behavior, obviously indicating that the *a* and *c* axes can be defined

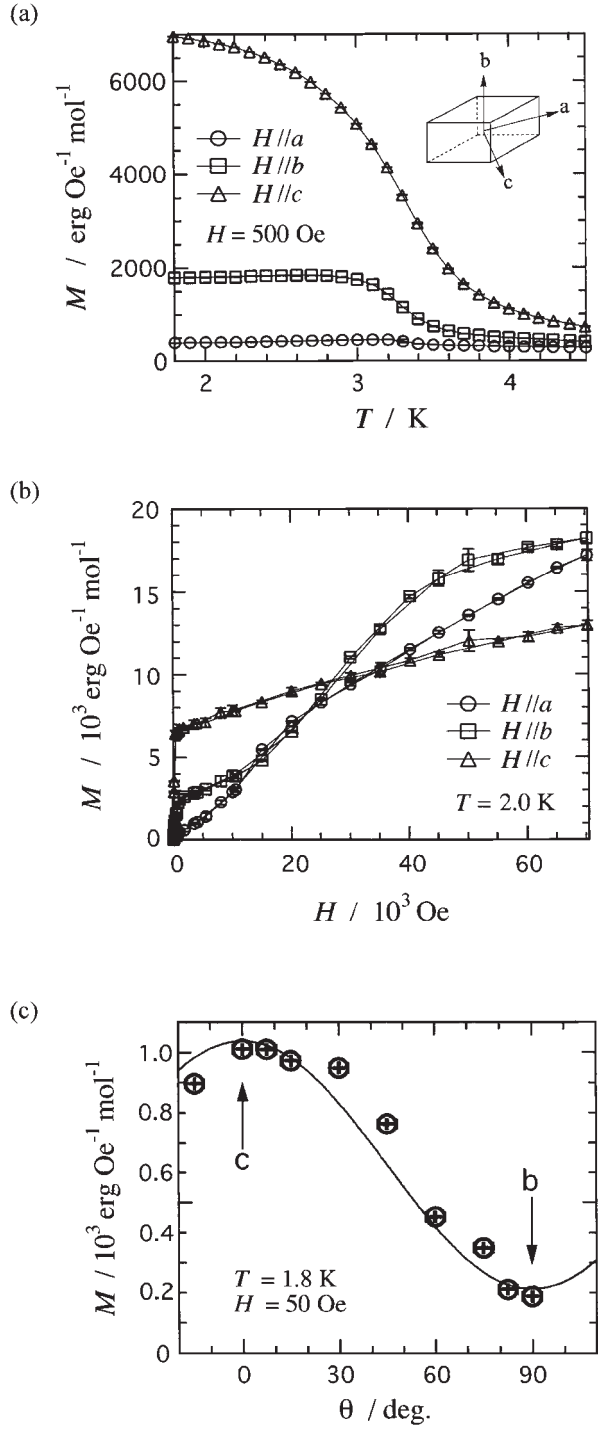

Fig. 7. (a) Field-cooled magnetization measurements of a single crystal of **2** with the applied fields of 500 Oe parallel to the *a*, *b*, and *c* axes. (b) Magnetization curves of **2** at 2.0 K with the applied fields parallel to the *a*, *b*, and *c* axes. (c) Angle dependence of the field-cooled magnetization of **2** at 1.8 K. Solid lines are shown for a guide to the eye.

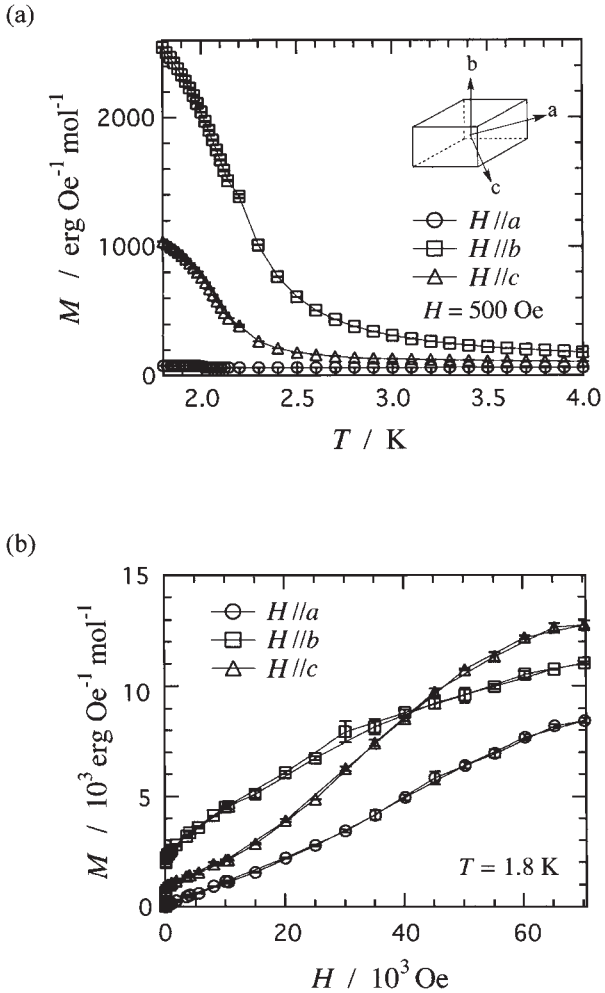

Fig. 8. (a) Field-cooled magnetization measurements of a single crystal of **5** with the applied fields of 500 Oe parallel to the *a*, *b*, and *c* axes. (b) Magnetization curves of **5** at 2.0 K with the applied fields parallel to the *a*, *b*, and *c* axes. Solid lines are shown for a guide to the eye.

as magnetically easy and hard axes, respectively. On the other hand, the data on $H \parallel b$ shows both features; i.e., the presence of M_S near 0 Oe and an S-shaped transition around 30 kOe. In general, M_S due to the spin canting should be observed in the perpendicular direction of dominant anitferromagnetic moments, but such a simple scheme can not explain the behavior of $H \parallel b$.

To clarify the magnetic structure when a magnetic field is applied along the *b* axis, we measured the angular dependence of FCM of **2**. Figure 7(c) shows the plot of the magnetization after a field-cooled process from 4.5 to 1.8 K at 50 Oe for each angle measurement. The *c* axis direction shows a maximum of magnetization and the *b* axis direction a minimum. The observed magnetization was substantial even at the minimum (parallel to the *b* axis) in the *bc* plane. Since the magnetization minima were assigned to be the *a* axis in both *ab* plane and *ac* plane, appreciable magnetization was present in any direction within the *bc* plane. This finding suggests an S_{xy} character of Fe^{II} spins in **2** (see Discussion section). Assuming that the spin is canted toward the *c* axis direction, one can estimate the cant angle to be 16°.

We investigated the FCM and *M*–*H* curves of a single crystal of **5**, which contain cobalt(II) ions in place of iron(II) ions of **2** in an isostructural crystal. Figure 8(a) shows the FCM results on **5** at 500 Oe. The magnetizations due to spin canting were

observed for the data on the *b* and *c* axes, and no magnetization was observed for the data on the *a* axis. It should be noted that the largest magnetization was found for the data in $H \parallel b$ for **5**, in sharp contrast to the largest magnetization in $H \parallel c$ for **2**. Figure 8(b) shows the *M*–*H* curves for **5**. M_S's were observed in the *b* and *c* axis directions and S-shaped magnetization curves were obtained along the *a* and *c* axes. Thus, the *a* and *b* axes can be defined as magnetically easy and hard axes, respectively. Anomalous behavior of $H \parallel c$ showing both M_S and metamagnetic behavior are found for **5**, like $H \parallel b$ in **2**, but the roles of the *b* and *c* axes are exchanged between **2** and **5**. The cant angle was estimated as 7.1° from the data of $H \parallel b$.

Discussion

We have found that the magnetic phase transition phenomena of **1**–**4**, such as the transition temperatures (T_N), metamagnetic transition critical fields, and the spontaneous magnetizations (M_S) (which correlate to the cant angles of spins), depend on the guest molecules from the experimental results on **1**–**4**. Actually, the T_N's of **1** and **2** were determined to be 5.6 and 3.3 K, respectively. The T_N difference of 2.3 K is relatively large in a liquid He temperature region. The magnetic properties are ascribed only to the host of the $[M\{N(CN)_2\}_2(pm)]$ skeleton, but the guest molecule affects the structure of the host. The coordination geometries around the metal ions are most likely deformed by the strain of the host through van der Waals repulsive or attractive interactions between the host and guests. The presence of the van der Waals interactions is supported by the disorder of the host $N(CN)_2$ skeletons in the compounds that include alcohol and by orderly arranged pm in **1**. This deformation may give rise to changes of single-ion properties (see below) as well as changes of the magnitude of spin–spin exchange coupling.

The present compounds $[M\{N(CN)_2\}_2(pm)](guest)$ are weak ferromagnets with a low coercive field and a very large ferromagnetic component (spontaneous magnetization) corresponding to a cant angle of up to 16° for **2**. This is one of the largest values reported. Such a large spin canting has been observed and well discussed for the non-centrosymmetric crystals such as $[MCl_2(pm)_2]$ (M = Fe,[17] Co[18]) and $[Fe(N_3)_2(bpy)]$ (bpy = 4,4′-bipyridyl).[19] However, the present compounds belong to a centrosymmetric *Pnma* space group. The magnetic structure might be acentric as a sublattice. Now we discuss possible origins of the spin cantings and ground spin structures in **1**, **2**, and **5** which significantly differs from each other. The difference between **1** and **2** is interesting in particular because **1** and **2** are isomorphous with the same metal ions. As described above, their single-crystal magnetic study revealed that the magnetic structures of the ground state were essentially different.

As for **1**, the anisotropy of the FCM and *M*–*H* curves may be basically interpreted in terms of the single-ion anisotropy. If we assume that Fe^{II} ions in **1** have an axial anisotropy, i.e., that the effective zero-field splitting (*D*) is negative, the moment on Fe^{II} tends to turn in the axial direction. We use the *D* parameter for convenience in discussion, though it is not accurately defined for iron(II) ions. The axial anisotropy is suggested for the canted antiferromagnet $[FeCl_2(pm)_2]$[17] and for other Fe^{II} coordination compounds.[20]

The X-ray crystallographic study indicates that the Fe^{II} ion has an elongated octahedron and that the pm nitrogen atoms are coordinated at the axial positions (Table 2). The pm bridge works as an antiferromagnetic coupler when pm nitrogen atoms are coordinated to form σ-type orbital overlaps between the metal e_g orbitals and nitrogen n orbital on both sides, leading to an antiferromagnetic superexchange through the pm molecular orbitals.[5] This interaction favors the antiparallel spin alignment between the neighboring spins. On the other hand, the pm has a rigid direction of 120° between two lone pairs and accordingly the axial anisotropy favors a 120° alignment across the pm bridge (Fig. 9(a)). As a consequence, from a balance of two contributions, $J < 0$ and $D < 0$, the spin is canted with an angle between 0 and 60°. As Fig. 2(b) shows, the pm–Fe zigzag chain is located almost on the *bc* plane, and the axial direction is nearer the *b* axis than the *c* axis. Therefore, this interpretation is consistent with the observed magnetic anisotropy; the dominant antiferromagnetic structure is defined to be the *b* axis and the spin canting direction is the *c* axis.

Table 2 shows slight changes of the metal–nitrogen bonds between **1** and **2**. In **2**, one of the equatorial Fe–$N_{nitrile}$ bonds is longer, while the axial Fe–N_{pm} bond is shorter, than those in **1**. The single-ion anisotropy of Fe^{II} may be changed by the geometrical changes around the Fe^{II} coordination sphere. The experimental results on **2** and **5** indicate that the moment can easily rotate depending on the direction of the applied magnetic field. This finding suggests the xy-character of the spin, i.e., the metal spin has an in-plane anisotropy (effectively $D > 0$) in **2** and **5**.

The spin of Co^{II} in **5** favors residing at the equatorial plane as depicted in Fig. 9(b). When an external magnetic field was applied parallel to the *a* axis, the moment can rotate and form an antiparallel alignment in the $\pm a$ directions. This situation fully satisfies the requirement, $J < 0$ and $D > 0$, and accordingly **5** behaves as a genuine antiferromagnet along the *a* axis. When an external field was applied in the *b* direction, the antiferromagnetic structure is ruled by a competition between $J < 0$ and $D > 0$. In a low field region, the antiferromagnetic structure is formed along the *a* axis, and the residual moment due to the spin canting can be observed in both *b* and *c* directions. On the other hand, with an increase of the applied field, the spin can rotate in an equatorial plane. The antiferromagnetic interaction favors the 180° alignment, but the in-plane anisotropy allows the 120° alignment. The cant angle becomes between 0° and 60°. This situation was observed as the principal antiferromagnetic structure along the *c* axis with the spin canting toward the *b* axis. Actually the experimental results on **5** can be explained by the above argument. The in-plane anisotropy of the Co^{II} ion has been discussed recently.[21]

The S_{xy}-characters were found in **2** and **5** but the roles of the *b* and *c* axes are changed. The reason is not clear so far. The *a* axis is unique and the *b* and *c* axis characters are similar to each other for **2** and **5**. Both **2** and **5** have the severe disorder of $N(CN)_2$ bridges,[10] which brings about a further deformation of the metal coordination sphere. The degree of the disorder may affect the magnitude and direction of in-plane anisotropy in **2** and **5**. One possibility is that the in-plane anisotropy of Fe^{II} ions in **2** is not located in the equatorial plane defined by the crystallographic bond lengths. Nevertheless, the experimen-

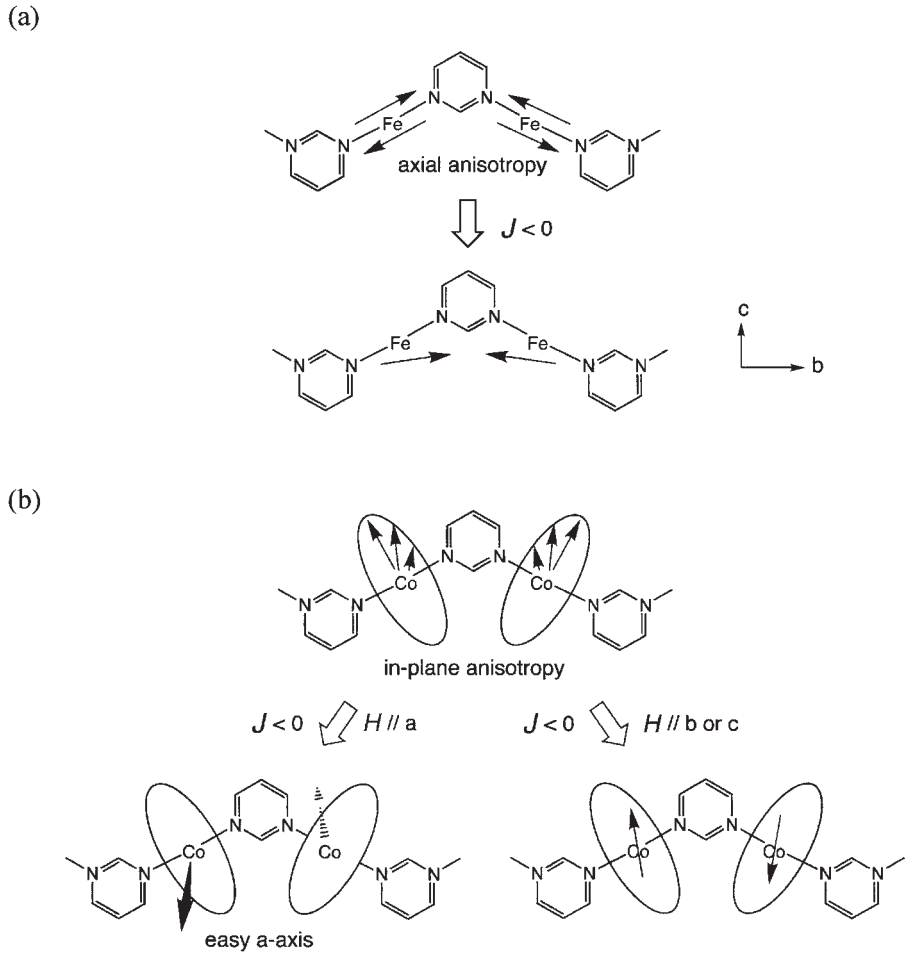

Fig. 9. Schematic drawings of the spin structures for **1** (a) and **5** (b).

tal results suggest the in-plane anisotropy of Fe^{II} in **2**, leading to the following conclusion: the guest molecule tunes the single-ion anisotropy of the host. Consequently, the magnetic phase transition phenomena were drastically different depending on the guest molecules.

The transition temperatures (T_N's) of **2**, **5**, and the nickel(II) analogue $[Ni\{N(CN)_2\}_2(pm)](H_2O)$[11] were 3.6, 2.0, and 8.3 K, respectively. We have reported another isomorphous series of $[MCl_2(pm)_2]$, whose T_N's are 6.1, 4.4, and 16 K for M = Fe,[17] Co,[18] and Ni,[17] respectively. Interestingly, the dependences of T_N upon metal ion species are parallel to each other. Furthermore, the transition temperatures of $[M\{N(CN)_2\}_2]$ (M = Fe: T_N = 18.5 K; M = Co: T_C = 9.2 K; M = Ni: T_C = 20.6 K)[6] show a similar tendency of the metal ion dependence. These findings support the conclusion that the transition phenomena are dominantly affected by the single ion properties. However, the proposed mechanism can only account for magnetic behavior within a pm-bridged zigzag chain. Problems about bulk residual moments surviving in a centrosymmetric crystal still remain.

Conclusion

Nano-porous materials generally tend to form interpenetrated structures, such as the nested rutile-like compounds,[6–8] or to include small guest molecules, as shown in the present study. In the latter case, we have a chance to control the physical properties of the host compounds by means of supramolecular techniques. We have shown that the solvated magnets $[M\{N(CN)_2\}_2(pm)](guest)$ are characterized as weak ferromagnts (canted antiferromagnets): **1** (M = Fe, guest = pm), T_N = 5.6 K, θ (cant angle) = 1.3° at 2 K with $H \parallel c$; **2** (M = Fe, guest = ethanol), T_N = 3.3 K, θ = 16° at 2 K with $H \parallel c$; **5** (M = Co, guest = ethanol), T_N = ca. 2 K, θ = 7.1° at 2 K with $H \parallel b$. The proposed mechanism of spin-canting based on the single-ion anisotropy is plausible. The S_z-character is suggested for the iron(II) ions in **1** for the definite anisotropic magnetization observed. On the other hand, the S_{xy}-character should be taken into consideration for the iron(II) ions in **2** and the cobalt(II) ions in **5** because the anisotropic magnetization measurements indicated that the spin could rotate according to the applied field. The magnetic phase transition phenomena were tuned by the guest molecules. The origin of the tuning is the variable single-ion anisotropy of the metal ions, which is susceptible to delicate coordination geometry changes.

Experimental

Preparation of Single Crystals. $[Fe\{N(CN)_2\}_2(pm)](pm)$ (1): An aqueous solution (6 mL) containing pm (0.11 g; 1.4 mmol) and $NaN(CN)_2$ (0.25 g; 2.8 mmol) was added to an aqueous solution (2 mL) containing $FeCl_2 \cdot 4H_2O$ (0.28 g; 1.4 mmol). The mixture was allowed to stand for a day at room temperature to give yellow single crystals of **1**. Elemental analysis, X-ray crystallo-

graphic analysis, and magnetic measurements of these compounds were done immediately after the isolation on a filter. In some cases practically colorless thin needles were obtained as a by-product; these were characterized as an isomeric one-dimensional compound $[Fe\{N(CN)_2\}_2(pm)_2]$.[22]

$[Fe\{N(CN)_2\}_2(pm)](EtOH)$ (2): Pm (0.080 g; 1.0 mmol) and $NaN(CN)_2$ (0.18 g; 2 mmol) were dissolved in a mixed solvent of ethanol (5 mL) and water (5 mL) and added to an aqueous solution (5 mL) containing $FeCl_2 \cdot 4H_2O$ (0.20 g; 1.0 mmol). The mixture was allowed to stand for a day at room temperature to give yellow single crystals of **2**. The single crystals of **3** and **4** were similarly prepared from *n*-PrOH–H_2O (1/4), and *n*-BuOH–H_2O (1/15) mixed solutions, respectively, by using pm/$NaN(CN)_2$/$FeCl_2$ with a ratio of 1/2/1.

$[Co\{N(CN)_2\}_2(pm)](EtOH)$ (5): Pm (0.080 g; 1.0 mmol) and $NaN(CN)_2$ (0.18 g; 2 mmol) were dissolved in a mixed solvent of ethanol (5 mL) and water (25 mL) and added to an aqueous solution (5 mL) containing $CoCl_2 \cdot 6H_2O$ (0.24 g; 1.0 mmol). The mixture was allowed to stand for two days at room temperature to give pink single crystals of **5**. The single crystals of **6** were similarly prepared from a *n*-PrOH–H_2O (1/10) mixed solvent.

Elemental Analysis. Elemental analysis (C,H,N) on a Fisons EA-1108 by a usual combustion method revealed that the composition formulae were $[Fe\{N(CN)_2\}_2(pm)](guest)$, where guest = pm, EtOH, *n*-PrOH, and $(n\text{-BuOH})_{1/2}$ for **1**–**4**, respectively, and $[Co\{N(CN)_2\}_2(pm)](guest)$ where guest = EtOH and *n*-PrOH for **5** and **6**, respectively. Anal. Calcd for **1**: C, 41.4; H, 2.3; N, 40.2%. Found: C, 40.6; H, 2.2; N, 40.8%. Calcd for **2**: C, 38.2; H, 3.2; N, 35.7%. Found: C, 38.6; H, 3.2; N, 36.6%. Calcd for **3**: C, 39.3; H, 3.4; N, 33.3%. Found: C, 40.3; H, 3.7; N, 34.2%. Calcd for **4**: C, 40.6; H, 3.4; N, 35.0%. Found: C, 39.4; H, 3.0; N, 36.7%. Calcd for **5**: C, 37.2; H, 3.4; N, 39.8%. Found: C, 37.5; H, 3.4; N, 39.9%. Calcd for **6**: C, 38.9; H, 3.3; N, 34.1%. Found: C, 39.9; H, 3.7; N, 33.8%.

X-ray Crystallographic Analysis. Diffraction data of single crystal of **1** were collected on a Rigaku R-axis RAPID diffractometer with graphite monochromated Mo Kα radiation ($\lambda = 0.71069$ Å) at 90 K. The structures were directly solved by a heavy-atom Patterson method in the teXsan program package.[23] Numerical absorption correction was used. All of the hydrogen atoms could be found in difference Fourier maps, and the parameters of the hydrogen atoms were included in the refinement. The thermal displacement parameters were refined anisotropically for non-hydrogen atoms and isotropically for hydrogen atoms. Full-matrix least-squares methods were applied using all of the unique diffraction data. The selected data for **1** are: $C_{12}H_8Fe_1N_{10}$, orthorhombic, *Pnma*, $a = 13.0061(5)$, $b = 12.3550(4)$, $c = 9.2235(4)$ Å, $V = 1482.1(1)$ Å^3, $Z = 4$, $D_{calc} = 1.560$ g cm^{-3}, $\mu = 1.033$ mm^{-1}, $R_1(I > 2\sigma(I)) = 0.0265$, and R_w(all data) = 0.0707, for 1771 diffractions ($2\theta \leq 55^\circ$) at $T = 90$ K. The crystallographic data of **1** in a cif format have been deposited with the CCDC (# 222024). The detailed results of the crystal structure analysis on **2** and **5** have been described elsewhere.[10] The analyses on **3** and **4** were also successful and their cell parameters were refined using all of the reflection data.

Magnetic Measurements. Dc and ac magnetic susceptibilities of polycrystalline samples of **1**–**6** were measured on Quantum Design MPMS SQUID and PPMS magnetometers equipped with 7 and 9 T coils, respectively, in a temperature range down to 1.8 K. The magnetic responses were corrected with diamagnetic blank data of the sample holder measured separately. The diamagnetic contribution of the sample itself was estimated from Pascal's constant. Ac magnetic susceptibilities were measured on a PPMS ac/dc magnetometer. An ac magnetic field (amplitude: 10 Oe, frequency: 100, 1000, and 10000 Hz) was applied to polycrystalline samples.

Single-crystal magnetization data of **1**, **2**, and **5** were obtained on the SQUID magnetometer. The sample was mounted inside on a probe tube with a slight amount of Apiezon H grease and the crystal axis was carefully oriented under a microscope. The crystal planes were defined with Miller indexes by means of X-ray diffraction, and the crystallographic axes could be assigned in a single crystal. The needle-like crystal was characterized with $(0\ \pm1\ 0)$ basal planes and $(\pm1\ 0\ \pm1)$ lateral faces. The sample mass was estimated from the sample dimensions and the density (D_{calc} in the X-ray diffraction study) and also from comparison of the magnetization averaged over the three axes with that of the randomly oriented polycrystalline sample.

This work was partly supported by a Grant-in-Aid for Scientific Research on Priority Areas of "Molecular Conductors" (No. 15073101) and by Grants-in-Aids for Scientific Research (Nos. 13640575 and 15550115), all from the Ministry of Education, Culture, Sports, Science and Technology.

References

1 P. J. Stang and B. Olenyuk, *Acc. Chem. Res.*, **30**, 502 (1997); O. M. Yaghi, H. Li, C. Davis, D. Richardson, and T. L. Groy, *Acc. Chem. Res.*, **31**, 474 (1998); M. Eddaoudi, D. B. Moler, H. Li, B. Chem, T. M. Reineke, M. O'Keeffe, and O. M. Yaghi, *Acc. Chem. Res.*, **34**, 319 (2001); S. Kitagawa and M. Kondo, *Bull. Chem. Soc. Jpn.*, **71**, 1739 (1998).

2 T. Ishida and T. Nogami, *Recent Res. Devel. Pure Appl. Chem.*, **1**, 1 (1997); T. Ishida, K. Nakayama, M. Nakagawa, W. Sato, Y. Ishikawa, M. Yasui, F. Iwasaki, and T. Nogami, *Synth. Met.*, **85**, 1655 (1997).

3 T. Ishida, L. Yang, and T. Nogami, *Chem. Lett.*, **32**, 1018 (2003), and references cited therein.

4 T. Ishida, S.-i. Mitsubori, T. Nogami, N. Takeda, M. Ishikawa, and H. Iwamura, *Inorg. Chem.*, **40**, 7059 (2001).

5 T. Ishida, T. Kawakami, S.-i. Mitsubori, T. Nogami, K. Yamaguchi, and H. Iwamura, *J. Chem. Soc., Dalton Trans.*, **2002**, 3177.

6 S. R. Batten, P. Jensen, B. Moubaraki, K. S. Murray, and R. Robson, *Chem. Commun.*, **1998**, 439; M. Kurmoo and C. J. Kepert, *New J. Chem.*, **22**, 1515 (1998); J. L. Manson, C. R. Kmety, Q. Z. Huang, J. W. Lynn, G. M. Bendele, S. Pagola, P. W. Stephens, L. M. Liable-Sands, A. L. Rheingold, A. J. Epstein, and J. S. Miller, *Chem. Mater.*, **10**, 2552 (1998); J. L. Manson, C. R. Kmety, A. J. Epstein, and J. S. Miller, *Inorg. Chem.*, **38**, 2552 (1999).

7 J. S. Miller and J. L. Manson, *Acc. Chem. Res.*, **34**, 563 (2001).

8 J. L. Manson, C. D. Incarvito, A. L. Rheingold, and J. S. Miller, *J. Chem. Soc., Dalton Trans.*, **1998**, 3705; J. L. Manson, Q.-Z. Huang, J. W. Lynn, H.-J. Koo, M.-H. Whangbo, R. Bateman, T. Otsuka, N. Wada, D. N. Argyriou, and J. S. Miller, *J. Am. Chem. Soc.*, **123**, 162 (2001).

9 P. Jensen, S. R. Batten, G. R. Fallon, D. C. R. Hockless, B. Moubaraki, K. S. Murray, and R. Robson, *J. Solid State Chem.*, **145**, 387 (1999).

10 T. Kusaka, T. Ishida, D. Hashizume, F. Iwasaki, and T. Nogami, *Chem. Lett.*, **2000**, 1146.

11 T. Kusaka, T. Ishida, D. Hashizume, F. Iwasaki, and T.

Nogami, *Mol. Cryst. Liq. Cryst.*, **376**, 463 (2002).

12 Y. Doi, T. Ishida, and T. Nogami, *Bull. Chem. Soc. Jpn.*, **75**, 2455 (2002); A. Escuer, R. Vicente, F. A. Mautner, M. A. S. Goher, and M. A. M. Abu-Youssef, *Chem. Commun.*, **2002**, 64.

13 E.-Q. Gao, A.-M. Wang, and C.-H. Yan, *Chem. Commun.*, **2003**, 1748; H.-L. Sun, B.-O. Ma, S. Gao, and G. Su, *Chem. Commun.*, **2001**, 2586.

14 A. Lappas, A. S. Wills, M. A. Green, K. Prassides, and M. Kurmoo, *Phys. Rev. B*, **67**, 4406 (2003).

15 For example, J. Omata, T. Ishida, D. Hashizume, F. Iwasaki, and T. Nogami, *Polyhedron*, **20**, 1557 (2001); T. Ishida, J. Omata, and T. Noagmi, *Polyhedron*, **22**, 2133 (2003).

16 T. Kusaka, T. Ishida, and T. Nogami, *Mol. Cryst. Liq. Cryst.*, **379**, 259 (2002).

17 R. Feyerherm, A. Loose, T. Ishida, T. Nogami, J. Kreitlow, D. Baabe, F. J. Litterst, S. Süllow, H.-H. Klauss, and K. Doll, *Phys. Rev. B*, in press; K. Zusai, T. Kusaka, T. Ishida, R. Feyerherm, M. Steiner, and T. Nogami, *Mol. Cryst. Liq. Cryst.*, **343**, 127 (2000).

18 K. Nakayama, T. Ishida, R. Takayama, D. Hashizume, M. Yasui, F. Iwasaki, and T. Nogami, *Chem. Lett.*, **1998**, 497.

19 T. Yuen, C. L. Lin, A. Fu, and J. Li, *J. Appl. Phys.*, **91**, 7385 (2002); A. Fu, X. Huang, J. Li, T. Yuen, and C. L. Lin, *Chem.—Eur. J.*, **8**, 2239 (2002).

20 J.-S. Sun, H. Zhao, X. Ouyang, R. Clérac, J. A. Smith, J. M. Clemente-Juan, C. Gómez-Garcia, E. Coronado, and K. Dunbar, *Inorg. Chem.*, **38**, 5841 (1999).

21 E.-C. Yang, D. N. Hendrickson, W. Wernsdorfer, M. Nakano, R. Sommer, A. L. Rheingold, M. Ledezma-Gairaud, and G. Christou, *J. Appl. Phys.*, **91**, 7382 (2002); J.-P. Costes, F. Dahan, and J. Garcia-Tojal, *Chem.—Eur. J.*, **8**, 5430 (2002).

22 The cell constants of $[Fe\{N(CN)_2\}_2(pm)_2]$: triclinic, $P\bar{1}$, $a = 6.238(1)$, $b = 7.400(2)$, $c = 9.0999(9)$ Å, $\alpha = 109.16(2)$, $\beta = 105.82(1)$, and $\gamma = 90.22(2)^\circ$ at $T = 100$ K. A preliminary analysis indicates that the Fe^{II} ions are doubly bridged with $N(CN)_2^-$ anions in a μ-1,5 manner to form a one-dimensional structure and that both pms do not work as a bridge but as a monodentate pendant.

23 teXsan: crystal structure analysis package, Molecular Structure Corp., The Woodlands, TX, 1985, 1999.

Available online at www.sciencedirect.com
SCIENCE DIRECT®
Chemical Physics Letters 392 (2004) 74–79
CHEMICAL PHYSICS LETTERS
www.elsevier.com/locate/cplett

Remarkably strong intermolecular antiferromagnetic couplings in the crystal of biphenyl-3,5-diyl bis(*tert*-butyl nitroxide)

Gentaro Kurokawa [a], Takayuki Ishida [a,b,*], Takashi Nogami [a]

[a] *Department of Applied Physics and Chemistry, The University of Electro-Communications, Chofu, Tokyo 182-8585, Japan*
[b] *Course of Coherent Optical Science, The University of Electro-Communications, Chofu, Tokyo 182-8585, Japan*

Received 8 March 2004; in final form 15 April 2004

Abstract

Magnetic susceptibility measurements of biphenyl-3,5-diyl bis(*t*-butyl nitroxide) diradical showed practically diamagnetic behavior over a temperature range 1.8–300 K. The strong antiferromagnetic couplings are ascribable to intermolecular interactions whilst intramolecular coupling could not be observed. Partly bonding nature can be pointed out in the intermolecular N–O′ contacts with the distances of 2.321(2) and 2.359(2) Å, which are 23–24% shorter than the sum of the van der Waals radii. On the other hand, the N–O bond lengths of 1.303(2) and 1.294(2) Å are somewhat longer than typical values of *t*-butyl phenyl nitroxide radicals reported.

1. Introduction

There have been numerous reports on intermolecular magnetic interactions in purely organic radical crystals in pursuit of ferromagnetic materials [1–3]. We have already developed the TEMPO-based ferromagnets, but their magnetic phase transition temperatures (T_Cs) were limited below 0.3 K [4–7], mainly because the spin delocalization in aliphatic substituents are generally very small and the intermolecular contacts are intervened with such methyl groups in TEMPO [6,7] (TEMPO = 2,2,6,6-tetramethylpiperidin-1-yloxyl). Since intermolecular magnetic interaction has been proposed to be proportional to the polarized spin densities at contacting atoms [8], we turned our attention to spin-delocalizable radicals, especially to phenyl nitroxide derivatives, to elevate T_C. Several π-conjugated nitroxide radical crystals exhibited positive Weiss temperatures [9–12] and these values were larger than those of the TEMPO derivatives. However, one may wonder whether singly occupied molecular orbitals (SOMOs) extended on π-conjugated substituents are ready to overlap in crystal packing giving rise to intermolecular antiferromagnetic couplings.

Biphenyl-3,5-diyl bis(*t*-butyl nitroxide) (**1**) was designed as a ground triplet molecule where an additional phenyl group was introduced for improving stability and intermolecular interactions. The *meta*-phenylene bridge is supposed to be a robust ferromagnetic exchange coupler, as supported by the extensive works on high-spin polycarbenes, -nitrenes and -radicals [13–15]. Contrary to our expectation, magnetic susceptibility measurements revealed that the solid of **1** was practically diamagnetic. We will report here the crystal structure and magnetic behavior of **1** and clarify the origin of strong intermolecular antiferromagnetic couplings occurring at each radical center.

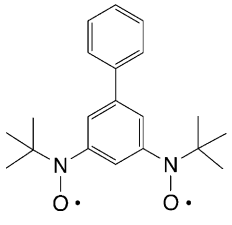

1

* Corresponding author. Fax: +81-424-43-5501.
E-mail address: ishi@pc.uec.ac.jp (T. Ishida).

0009-2614/$ - see front matter © 2004 Elsevier B.V. All rights reserved.
doi:10.1016/j.cplett.2004.04.111

2. Experimental

Diradical **1** was prepared by lithiation of the corresponding dibromo compound followed by the reaction with 2-methyl-2-nitrosopropane to give 3,5-bis(*N*-*t*-butylhydroxylamino)biphenyl (**2**). Subsequent oxidation of **2** with Ag_2O gave **1**.

To an ether solution (10 ml) containing 3,5-dibromobiphenyl [16] (1.03 g; 3.31 mmol) was added a hexane solution of *t*-butyl lithium (9.5 ml; 14 mmol) at −90 °C under nitrogen atmosphere. After the mixture was warmed to −30 °C and cooled again to −90 °C, an ether solution (15 ml) containing 2-methyl-2-nitrosopropane (0.604 g; 6.93 mmol) was added to the above mixture. The mixture was warmed to room temperature and stirred for further 1 h to complete the reaction. Aqueous NH_4Cl was added and the organic layer was separated with a separate funnel after neutralization with K_2CO_3. The organic layer was dried over $MgSO_4$, passed through a short column (silica-gel eluted with ether) and concentrated under reduced pressure, giving a colorless powder. Almost pure **2** was obtained by collection on a filter followed by washing with a small amount of CH_2Cl_2. The yield was 199 mg (0.61 mmol; 18%), m.p. 140–142 °C (chloroform). ^{1}H NMR (270 MHz, $CDCl_3$): δ 8.34 (s, 2H, hydroxyl), 7.57–7.32 (m, 5H, aromatic), 7.16–7.09 (m, 3H, aromatic), 1.11 (s, 18H, *t*-butyl).

A suspension of 199 mg of **2** (0.61 mmol) and a large excess amount of freshly prepared Ag_2O (≈2 g) in 25 ml of benzene was stirred at room temperature for 3 h. The benzene layer turned red. After passed through a short column (silica-gel eluted with CH_2Cl_2), red plates of **1** were obtained by crystallization from CH_2Cl_2–hexane. The yield was 49.8 mg (0.15 mmol; 25%), m.p. 95–97 °C. Anal. Calcd. for $C_{20}H_{26}N_2O_2$: C, 73.59; H, 8.03; N, 8.58%. Found: C, 73.64; H, 7.89; N, 8.28%. ESR (Bruker ESP-300E X-band (9.4 GHz), benzene, room temperature): $g = 2.0060$. The hyperfine splitting constants could not be determined because of line broadening (Fig. 1).

Diffraction data of a single crystal of **1** were collected on a Rigaku R-axis RAPID diffractometer with graphite monochromated Mo Kα radiation ($\lambda = 0.71069$ Å) at 100 K. The structures were directly solved and the parameters were refined in the CrystalStructure program package [17]. Numerical absorption correction was used. All of the hydrogen atoms could be found in difference Fourier maps. Thermal displacement parameters were refined anisotropically for non-hydrogen atoms and isotropically for hydrogen atoms. Full-matrix least-squares methods were applied using all of the unique diffraction data. The selected data for **1** are: $C_{20}H_{26}N_2O_2$, FW = 326.4, triclinic $P\bar{1}$, $a = 8.830(3)$, $b = 10.727(5)$, $c = 11.192(5)$ Å, $\alpha = 102.33(3)$, $\beta = 106.21(3)$, $\gamma = 110.89(3)°$, $V = 891.2(6)$ Å^3, $Z = 2$, $D_{calc} = 1.216$ g cm^{-3}, μ(Mo Kα) = 0.079 mm^{-1}, $R_{int} = 0.041$, $R(F)(I > 2\sigma(I)) = 0.049$ and $R_W(F^2)$ (all data) = 0.026 for 3985 unique reflections. CCDC reference number 232856.

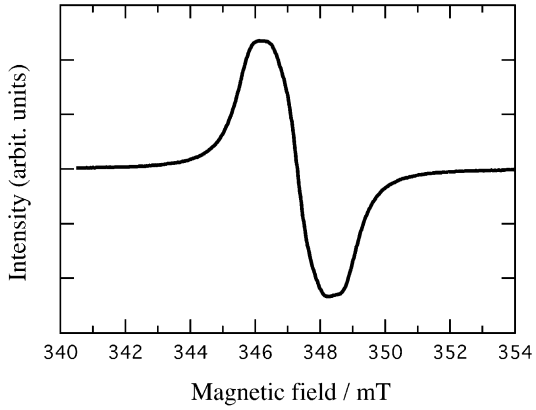

Fig. 1. X-band ESR spectrum of **1** in benzene at room temperature.

Dc magnetic susceptibilities of polycrystalline samples of **1** were measured on a Quantum Design MPMS SQUID magnetometer equipped with a 7 T coil in a temperature range of 1.8–330 K. The magnetic responses were corrected with diamagnetic blank data of the sample holder measured separately. The diamagnetic contribution of the sample itself was estimated from Pascal's constant. Owing to the computation algorithm from SQUID response to magnetization, the error bar was significantly large when the absolute SQUID response value came close to null. We applied the magnetic field of 5 kOe to 41.78 mg of **1** and found that the paramagnetic and diamagnetic contributions were accidentally balanced around 35 K. However, the data below 30 K and above 40 K are sufficiently reliable. A frozen solution of **1** was prepared by dissolving 0.92 mg of **1** in 0.2 ml of a 6/1 (v/v) ethanol–toluene mixed solvent and subsequent rapid cooling in a gelatin capsule loaded in a SQUID sample chamber.

3. Results and discussion

3.1. ESR spectrum

The X-band ESR spectrum of **1** shows an unresolved single line with a peak-to-peak line width of 20 G in a dilute and deairated benzene solution (Fig. 1). This broadening is due to intramolecular dipole–dipole and exchange interactions among the unpaired electrons and also probably to overlap of different signals and hyperfine structures of conformational isomers. Diradical **1** was found to be satisfactorily stable during the studies of X-ray diffraction and magnetic properties. The solution ESR signal showed no change at room temperature

under air for a week. After the measurements of magnetic properties, the ESR signal of **1** in a benzene solution reproduced the initial spectrum. Possible monoradicals as decomposed products were not detected since no 1/1/1 triplet lines were superimposed to the broad line of **1**.

3.2. X-ray crystal structure

The crystal structure of **1** was determined at 100 K. All of the hydrogen atoms were experimentally found and hydrogen atoms were absent around the oxygen atoms. Ortep drawing and crystal packing diagram are depicted in Fig. 2 and selected bond lengths and angles together with intermolecular atomic distances are listed in Table 1. The N–O bond distances are 1.303(2) and 1.294(2) Å, which are characteristic of *t*-butyl phenyl nitroxide groups [18–20] and significantly shorter than those of typical *N*-*t*-butyl-*N*-phenylhydroxylamines reported (1.456(4) Å [21] for example).

The *m*-phenylene group bridges two radical groups (N1–O1 and N2–O2), which have a *syn* configuration with respect to the phenylene ring. The nitroxide nitrogen atoms are pyramidalized, as indicated by the deviation from the plane defined with the surrounding C–C–O atoms (0.262(2) and 0.255(2) Å for N1 and N2, respectively). The large torsion angles of O1–N1–C1–C2 and O2–N2–C3–C2 (49.4(2)° and 45.3(2)°, respectively) indicate that the N–O groups are moderately conjugated with the phenylene ring. The biphenyl skeleton is also twisted around the C5–C7 bond with the dihedral angle of 26.19(7)° between two benzene rings.

As Fig. 2b shows, molecules of **1** are one-dimensionally arrayed in the crystallographic $a + c$ diagonal direction with very short intermolecular contacts. The neighboring molecules are related with inversion symmetry. The surroundings of the nitroxide groups are quite similar to each other, although they are crystallographically independent. Head-to-tail and face-to-face dimeric arrangements of N1–O1–N1^{i}–O1^{i} and N2–O2–N2^{ii}–O2^{ii} give almost rectangular shapes, where the symmetry operation codes for i and ii are $1 - x$, $1 - y$, $1 - z$ and $2 - x$, $1 - y$, $2 - z$, respectively. The sums of the van der Waals radii are 3.10 and 3.04 Å for N–N and O–O, respectively [22]. The observed N–N and O–O contacts are 12–14% shorter than the sum of the van der Waals radii and furthermore the N–O contacts are 23–24% shorter (Table 1).

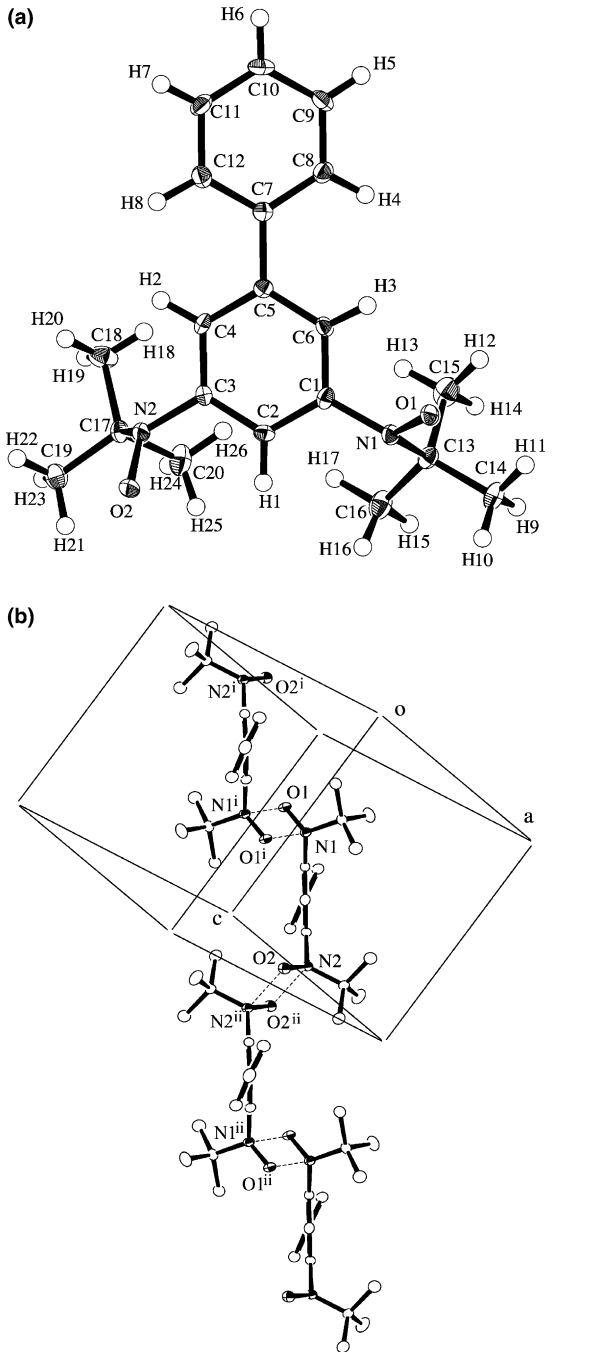

Fig. 2. (a) Ortep drawing of **1** with the thermal ellipsoids at the 50% probability level for non-hydrogen atoms. (b) Molecular arrangement in the crystal of **1** viewed along the biphenyl principal axis (C2–C10). Four molecules are drawn in a linear array along the $a + c$ diagonal direction. Hydrogen atoms are omitted for clarity. Relatively short distances are indicated with dotted lines. See Table 1 for interatomic distances and symmetry operation codes.

3.3. Magnetic properties

The polycrystalline sample of **1** was found to be practically diamagnetic over the temperature range of 1.8–300 K (Fig. 3). No intramolecular magnetic coupling is characterized, contrary to our expectation from the molecular design for a stable triplet molecule. An analysis on the Curie law ($\chi_{mol} = C/T$) gave a small Curie constant, $C = 7.2 \times 10^{-3}$ cm^3 K mol^{-1}, which corresponds to only 0.96% of the theoretical spin-only value. We assume that this paramagnetic spin originates in the lattice defect, i.e., monoradicals as impurity.

Table 1
Selected bond lengths (Å), bond angles (°), torsion angles (°) and intermolecular distances (Å) in the crystal of **1**[a]

O1–N1	1.303(2)	O2–N2	1.294(2)
N1–C1	1.450(2)	N2–C3	1.459(2)
N1–C13	1.530(3)	N2–C17	1.529(3)
C1–N1–C13	118.2(2)	C3–N2–C17	117.7(1)
C1–N1–O1	115.3(1)	C3–N2–O2	115.0(2)
C13–N1–O1	116.5(1)	C17–N2–O2	117.9(1)
O1–N1–C1–C2	−139.4(2)	O2–N2–C3–C2	45.3(2)
C13–N1–C1–C2	76.1(2)	C17–N2–C3---C2	−100.5(2)
O1---N1^{i}	2.321(2)	O2---N2^{ii}	2.359(2)
O1---O1^{i}	2.652(1)	O2---O2^{ii}	2.688(2)
N1---N1^{i}	2.672(2)	N2---N2^{ii}	2.692(2)
O1---C1^{i}	3.047(2)	O2---C3^{ii}	3.063(2)
O1---C2^{i}	3.207(3)	O2---C4^{ii}	3.137(2)
O1---H1^{i}	2.78(2)	O2---H2^{ii}	2.65(1)

[a] Symmetry operation codes for i and ii are $1-x$, $1-y$, $1-z$ and $2-x$, $1-y$, $2-z$, respectively.

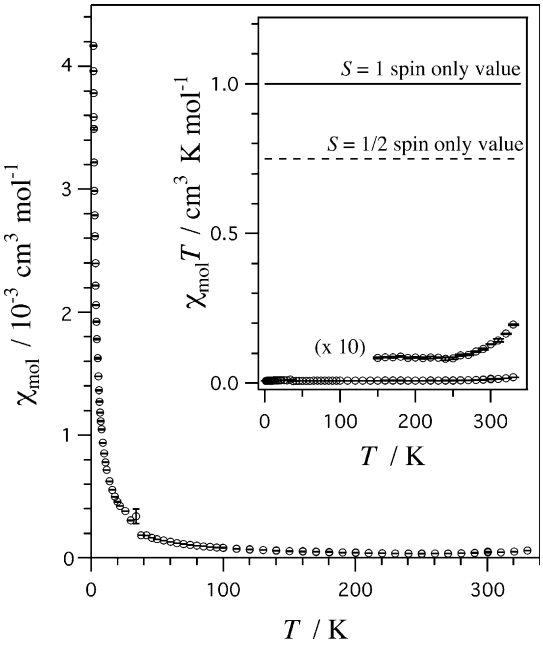

Fig. 3. Temperature dependence of the magnetic susceptibility (χ_{mol}) for **1**. Inset: temperature dependence of the product $\chi_{mol}T$. Solid and broken lines represent the theoretical spin-only values for paramagnetic species having a triplet state and two non-interacting doublet centers, respectively.

From a close look at the $\chi_{mol}T$ vs T plot (the inset of Fig. 3), a small and monotonic increase of the $\chi_{mol}T$ value is found above 250 K, which can be assigned to contribution from a thermally accessible triplet species. The energy gap between exited triplet and ground singlet states is estimated to be $2J/k_B \approx -1700$ K based on the singlet–triplet model [23]. The crystallographic analysis suggests that the singlet–triplet model is applicable to the intermolecular N–O dimers and not to the intramolecular one. The intermolecular antiferromagnetic interactions are much stronger than the intramolecular (ferro)magnetic coupling and accordingly the former buries the latter.

We have also measured the magnetic properties of **1** in a frozen solution (6/1 ethanol–toluene). The magnetization curve measured at 1.8 K is well reproduced with the theoretical Brillouin function of $S = 1$, indicating that **1** behaves as a ground triplet molecule. We need to pay attention to possible conformational changes leading to different intramolecular interaction and evaluate the intramolecular interaction for a given geometry in the crystal of **1** by the following theoretical approach.

3.4. Mechanism of antiferromagnetic couplings

The SOMO in phenyl nitroxide radicals is extended onto the phenyl group but localized at *ortho*- and *para*-positions [10]. Compound **1** is a space-sharing-type diradical; i.e., one SOMO from N1–O1 and the other from N2–O2 are expected to have appreciable $2p_z$ coefficients in common at C2, C4 and C6, and consequently **1** should be a ground triplet molecule. The spin density distribution of triplet **1** was calculated on the UB3LYP/6-31G** level [24] with the geometry determined from the X-ray diffraction study (Fig. 4). A preliminary calculation on the singlet and triplet states of isolated **1** suggested that the triplet state had lower total energy, as expected. Viewing from the magnitude of the spin density and the SOMO coefficients, the observed intermolecular antiferromagnetic interaction can be attributed mainly to the N1–O1–N1^{i}–O1^{i} and N2–O2–N2^{ii}–O2^{ii}

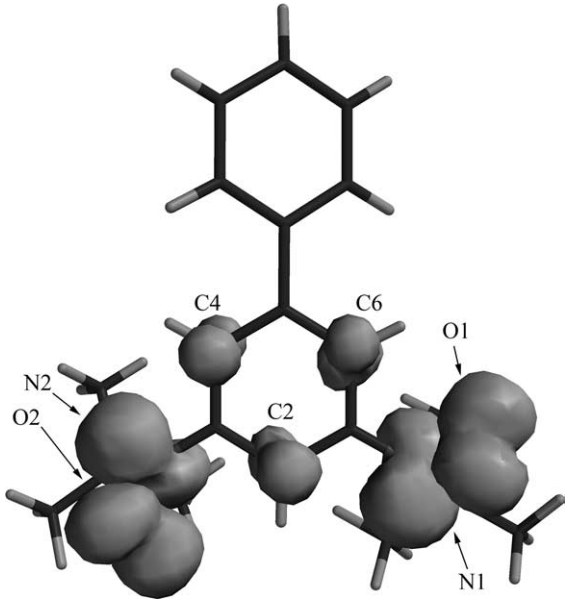

Fig. 4. Spin density surface of **1** at the triplet state calculated with UB3LYP/6-31G**. The geometry and atomic numbering were taken from the X-ray crystallographic analysis.

contacts. The O1–C2[i] and O2–C4[ii] contacts seem to bring about auxiliary antiferromagnetic contribution.

The N–O contacts affording strong antiferromagnetic couplings can be explained in terms of the canonical structures as illustrated below, but the contribution of the third form is very small because **1** still has a radical character in the solid, as indicated by the red color typical of nitroxide radicals.

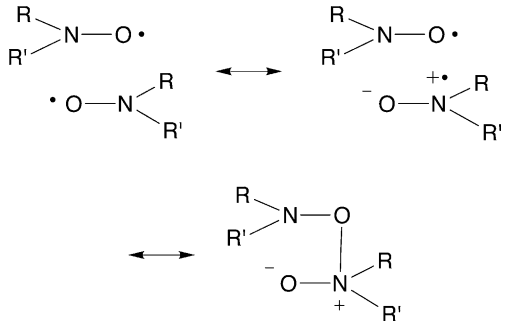

The presence of a partly bonding nature in the N–O contacts being assumed, the N1–O1 and N2–O2 bonds are expected to be elongated owing to the decrease in electron density within the N–O bonds. Actually, the N–O bond lengths of 1.294(2) and 1.303(2) Å observed in **1** are slightly longer than those in *t*-butyl phenyl nitroxides reported to be 1.258(4) Å [18], 1.271 Å (averaged on two NO groups) [19], and 1.273 Å (averaged on four NO groups) [20]. The present work implies that the N–O bond elongation would be detectable in compounds showing strong antiferromagnetic interaction and that an X-ray crystallographic analysis would be another versatile tool for evaluation of the magnitude of magnetic interaction.

Whereas the magnitude of intermolecular ferromagnetic coupling is limited and results only in the development of low T_C ferromagnets, antiferromagnetic coupling ranges in much larger magnitudes up to chemical bonding. Therefore the construction of organic ferrimagnets has become a current challenging target [25,26]. Actually, most organic–inorganic hybrid magnets exhibiting high T_Cs include ferrimagnetic couplings [27,28]. Organic ferrimagnets have been designed from assemblies of triplet diradicals and doublet monoradicals in which intermolecular antiferromagnetic interactions and intramolecular ferromagnetic interactions are simultaneously operative and competitive [25,26]. While organic solids showing $2|J|/k_B \geqslant 10^3$ K are rather rare [29], the present work has clarified that *t*-butyl phenyl nitroxides can afford such large intermolecular interactions. Although excessive intermolecular antiferromagnetic interaction seems unsuitable for the development of organic ferrimagnets, molecular complexes consisting of diradicals like **1** and appropriate *t*-butyl phenyl nitroxide monoradicals may provide organic ferrimagnetic materials.

Acknowledgements

We thank Prof. Masahiro Kako (The University of Electro-Communications) for kind assistance in performing MO calculations. This work was supported by a Grant-in-Aid for Scientific Research on Priority Areas of 'Molecular Conductors' (No. 15073101) and by Grants-in-Aids for Scientific Research (Nos. 13640575 and 15550115) from the Ministry of Education, Culture, Sports, Science and Technology, Japan.

References

[1] K. Itoh, M. Kinoshita (Eds.), Molecular Magnetism – New Magnetic Materials, Kodansha Gordon & Breach, Tokyo, 2000.
[2] J. Veciana, H. Iwamura, MRS Bull. 25 (2000) 41.
[3] J.A. Crayston, J.N. Devine, J.C. Walton, Tetrahedron 56 (2000) 7829.
[4] T. Nogami, K. Tomioka, T. Ishida, H. Yoshikawa, M. Yasui, F. Iwasaki, H. Iwamura, N. Takeda, M. Ishikawa, Chem. Lett. (1994) 29.
[5] T. Ishida, S. Ohira, T. Ise, K. Nakayama, I. Watanabe, T. Nogami, K. Nagamine, Chem. Phys. Lett. 330 (2000) 110.
[6] T. Nogami, T. Ishida, M. Yasui, F. Iwasaki, N. Takeda, M. Ishikawa, T. Kawakami, K. Yamaguchi, Bull. Chem. Soc. Jpn. 69 (1996) 1841.
[7] K. Togashi, R. Imachi, K. Tomioka, H. Tsuboi, T. Ishida, T. Nogami, N. Takeda, M. Ishikawa, Bull. Chem. Soc. Jpn. 69 (1996) 2821.
[8] H.M. McConnell, J. Chem. Phys. 39 (1963) 1910.
[9] R. Imachi, T. Ishida, M. Suzuki, M. Yasui, F. Iwasaki, T. Nogami, Chem. Lett. (1997) 743.
[10] M. Nakagawa, T. Ishida, M. Suzuki, D. Hashizume, M. Yasui, F. Iwasaki, T. Nogami, Chem. Phys. Lett. 302 (1999) 125.
[11] T. Ishida, Y. Akui, S.-y. Masaoka, M. Nakagawa, D. Hashizume, M. Yasui, F. Iwasaki, T. Nogami, Mol. Cryst. Liq. Cryst. 334 (1999) 89.
[12] M. Seino, Y. Akui, T. Ishida, T. Nogami, Synth. Met. 133–134 (2003) 581.
[13] H. Iwamura, Adv. Phys. Org. Chem. 26 (1990) 179.
[14] A. Rajca, Chem. Rev. 94 (1994) 871.
[15] T. Ishida, H. Iwamura, J. Am. Chem. Soc. 113 (1991) 4238.
[16] T.R. Kelly, G.J. Bridger, C. Zhao, J. Am. Chem. Soc. 112 (1990) 8024.
[17] CrystalStructure, Single Crystal Structure Analysis Software Version 3.5.1, Rigaku/MSC, 9009 New Trails Drive, The Woodlands, TX 77381, USA, 2003.
[18] K. Inoue, H. Iwamura, Adv. Mater. 4 (1992) 801.
[19] J. Fujita, M. Tanaka, H. Suemune, N. Koga, K. Matsuda, H. Iwamura, J. Am. Chem. Soc. 118 (1996) 9347.
[20] J. Fujita, Y. Matsuoka, K. Matsuo, M. Tanaka, T. Akita, N. Koga, H. Iwamura, Chem. Commun. (1997) 2393.
[21] K. Inoue, H. Iwamura, J. Am. Chem. Soc. 113 (1991) 9803.
[22] A. Bondi, J. Phys. Chem. 68 (1964) 441.
[23] B. Bleaney, K.D. Bowers, Proc. R. Soc. Lond. Ser. A 214 (1952) 451.
[24] Spartan '02, Wavefunction Inc., 18401 Von Karman Avenue, Suite 370 Irvine, CA 92612, USA, 2002.
[25] Y. Hosokoshi, K. Katoh, Y. Nakazawa, H. Nakano, K. Inoue, J. Am. Chem. Soc. 123 (2001) 7921.
[26] D. Shiomi, T. Kanaya, K. Sato, M. Mito, K. Takeda, T. Takui, J. Am. Chem. Soc. 123 (2001) 11823.

[27] K. Inoue, T. Hayamizu, H. Iwamura, D. Hashizume, Y. Ohashi, J. Am. Chem. Soc. 118 (1996) 1803.
[28] K. Fegy, D. Luneau, T. Ohm, C. Paulsen, P. Rey, Angew. Chem. Int. Ed. 37 (1998) 1270.
[29] K. Goto, T. Kubo, K. Yamamoto, K. Nakasuji, K. Sato, D. Shiomi, T. Takui, M. Kubota, T. Kobayashi, K. Yakusi, J. Ouyang, J. Am. Chem. Soc. 121 (1999) 1619.

GSCH 41012—6/5/2004—KREETHI—104630

Supramolecular Chemistry, 2004 VOL. 00 (0), pp. 1–5

Taylor & Francis
Taylor & Francis Group

Short Communication

Crystal Structure of a Molecular Complex from Native β-cyclodextrin and Copper(II) Chloride

GENTARO KUROKAWA[a], MIYUKI SEKII[a], TAKAYUKI ISHIDA[a,b,*] and TAKASHI NOGAMI[a]

[a]*Department of Applied Physics and Chemistry, The University of Electro-Communications, Chofu, Tokyo 182-8585, Japan;* [b]*Course of Coherent Optical Science, The University of Electro-Communications, Chofu, Tokyo 182-8585, Japan*

Received (in Southampton, UK) 23 February 2004; Accepted 25 March 2004

Reaction of β-cyclodextrin (β-CD) with $CuCl_2$ in neutral aqueous solutions gave a stable molecular complex without any side-arm support. The X-ray crystallographic analysis clarified that the copper ion was located at the bottom of the primary-hydroxy side as a $CuCl_2(H_2O)_2$ form. Hydrogen bonds were found between the Cl and H_2O ligands and β-CD hydroxy and ether groups. The copper ion is axially coordinated with a hydroxy group of a neighboring β-CD molecule, giving a one-dimensional β-CD/$CuCl_2$ array.

Keywords: β-Cyclodextrin; Copper(II) ion; Molecular complex; Coordination compound

Cyclodextrins (CDs; see Scheme 1 for β-CD) have been extensively studied for the development of catalysts and enzyme mimics [1–3]. There are several reports on CD-based catalysts for hydrolysis and hydrogenesis in the presence of transition metal ions [4–6]. These catalytic centers are usually coordinated with N-, O-, or P-donor side-arms in artificial CDs [7]. Complexes containing native CDs and simple inorganic molecules (iodine [8,9] for example) are very rare. Recently, complex formation between copper(II) and β-CD in basic solutions has been studied from the equilibrium constants point of view [10]. The deprotonated CDs can coordinate copper(II) and manganese(III) ions at high pHs [11,12] and the peculiar crystal structures of multinuclear copper(II) and lead(II) complexes have been characterized including β- and γ-CD polyanions as polydentate ligands [13,14]. To the best of our knowledge, however, there is no report on stable complexes consisting of neutral CDs and transition metal salts without any side-arm support. We report here the crystal structure of a β-CD/$CuCl_2$ complex, in which the intact β-CD plays a role in both the hydrogen-bond frame and O-donating ligand.

β-CD (238 mg, 0.21 mmol) and $CuCl_2{\cdot}2H_2O$ (434 mg, 2.54 mmol) were dissolved in hot water (20 ml). The light blue solution was concentrated on warming to a small volume (*ca.* 2 ml), and the resultant green solution was allowed to stand for a week. The precipitated light blue plates were separated on a filter, washed with a small amount of water and immediately used for further analysis. The yield was 96.9 mg (33%). The elemental analysis, magnetic susceptibility measurements, and X-ray crystallographic analysis indicated that the $CuCl_2$/β-CD ratio was typically 0.5 to 0.6 and could not be raised to unity in spite of the synthetic efforts. The elemental analysis (C, H, N) of the adduct on a Fisons EA-1108 by a usual combustion method suggests the following composition: Anal. Calcd for β-CD·$(CuCl_2)_{0.55}$·$(H_2O)_{10}$: C, 36.31; H, 6.53%. Found: C, 35.79; H, 6.42%. Magnetic properties of the β-CD/$CuCl_2$ adduct were measured on a Quantum Design MPMS SQUID magnetometer. The temperature dependence of the magnetic susceptibility obeyed the Curie law ($\chi = C/T$). The observed Curie constant of $1.80 \times 10^{-4}\,cm^3\,K\,g^{-1}$ agrees well with the proposed formula containing 0.55 moles of copper(II) spins of $S = 1/2$ and $g = 2.2$.

*Corresponding author. E-mail: ishi@pc.uec.ac.jp

ISSN 1061-0278 print/ISSN 1029-0478 online © 2004 Taylor & Francis Ltd
DOI: 10.1080/1061027042000220742

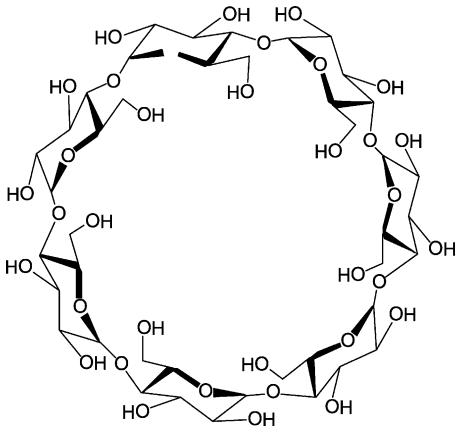

SCHEME 1 Molecular structure of β-CD.

X-Ray diffraction data were collected on a Rigaku RAPID IP diffractometer using graphite-monochromated MoKα radiation at 100 K. The structure was directly solved and expanded using Fourier techniques in the *CrystalStructure* program package.[†] Population analysis was applied for the $CuCl_2$ moiety, giving the occupancy of 0.545(4). The β-CD/$CuCl_2$ adduct crystallized in a monoclinic $P2_1$ space group,[‡] and the absolute configuration was manually assigned based on the known D-glucopyranose structure in the β-CD. Ten water solvate molecules were found in an asymmetric unit. The hydrogen atoms on the water molecules and hydroxy groups could not be located in the analysis.

Figure 1 shows the molecular structure of β-CD·$CuCl_2(H_2O)_2$. The copper ion is coordinated by two chloride ions at the *trans*-equatorial positions with Cu1–Cl1 and Cu1–Cl2 distances of 2.220(5) and 2.274(6)Å, respectively. Two water molecules are coordinated at the other *trans*-equatorial positions with the Cu1–O36 and Cu1–O37 distances of 1.96(1) and 2.007(6)Å, respectively. The copper ion has a saddle-type configuration. The Cl1–Cu1–Cl2 and O36–Cu1–O37 angles were 154.6(2) and 170.3(5)°, respectively, and each pair of the ligands is located in the opposite hemisphere of the copper(II) averaged equatorial plane.

The hydrophobic cavity of the β-CD could not accommodate $CuCl_2(H_2O)_2$ inside, but the $CuCl_2(H_2O)_2$ group was situated at almost the center of the bottom of the primary-hydroxy side. Hydrogen bonds were found between the Cl and H_2O ligands and the β-CD hydroxy and ether groups. Since most OH hydrogen atoms could not be determined experimentally, we evaluated possible hydrogen bonds by the van der Waals contacts and close interatomic distances within 3.6 Å among the non-hydrogen atoms. As Fig. 1(b) shows, there are five endohedral water molecules (Ow38–Ow42) and three exohedral ones (Ow43–Ow45). Hydrogen bonds are suggested between the β-CD primary-hydroxy groups and the ligand water oxygen or chlorine atoms (O25–O36, O20–O36, O35–Cl2 *etc.*). A hydrogen-bonding network penetrates into a cavity (O37–Ow40, Ow41–Ow42–Ow39 *etc.*).

As the side view (Fig. 1(c)) shows, the outer axial site of the copper ion was occupied with a hydroxy group of a neighboring β-CD molecule, forming a linear polymeric chain $[\beta\text{-CD}\cdot CuCl_2(H_2O)_2]_n$ along the crystallographic *b* axis. The Cu1–O3* distance is 2.398(6)Å and the O3*–Cu1–Cl1 and O3*–Cu1–Cl2 angles are 94.2(1) and 109.9(2)°, respectively.

Interestingly, the β-CD host alone crystallizes from an aqueous solution as the eleven-hydrated form in practically the same crystal packing motif belonging to a monoclinic $P2_1$ space group[¶] [15,16]. When we refined the occupancies of O36 and O37 independently from those of $CuCl_2$ group in the adduct, we obtained occupancies of nearly 1.0 and not 0.55. This finding implies that O36 and O37 are present irrespective of the $CuCl_2$ defect. The β-CD primary-hydroxy rim as well as the clusterized water framework seem to be preorganized for the $CuCl_2$ capping. The $CuCl_2$ group was intercalated to the rather rigid host lattice, only giving rise to slight *b*-axis elongation (3.1%) and cell volume expansion (2.7%). Actually we determined the β-CD·$(H_2O)_{11}$ molecular structure with the aid of the β-CD geometry in the β-CD/$CuCl_2$ adduct as an initial structure.

The copper(II) axial site facing inside the β-CD is vacant, which reminds us of the possibility of catalytic reactions within the β-CD chiral cavity by using the Lewis acidity of the copper(II) ion. Though the β-CD/$CuCl_2$ binding seems labile, we observed the color change during concentration of β-CD/$CuCl_2$ mother liquors which suggests an appreciable formation of a β-CD/$CuCl_2$ complex in concentrated solutions. This study may also provide a new supramolecular building block for CD-based polymeric rotaxanes [17] involving linear bridging ligands. We have investigated the reaction of $CuCl_2$ and β-CD in the presence of

[†]*CrystalStructure*: Single Crystal Structure Analysis Software version 3.5.1, Rigaku/MSC, 9009 New Trails Drive, The Woodlands, TX 77381, USA, 2003.

[‡]Selected crystallographic data are: $C_{42}H_{90}O_{45}Cu_{0.55}Cl_{1.1}$, FW 1389.1, $a = 20.82(1)$, $b = 10.366(6)$, $c = 14.968(9)$ Å, $\beta = 110.12(4)°$, $V = 3033(2)$ Å^3, $Z = 2$, μ(MoKα) = 0.369 mm^{-1}, $R_{int} = 0.065$, $R(F)(I > 2\sigma(I)) = 0.078$, and $R_w(F^2)$ (all data) = 0.105 for 7749 unique reflections. All of the OH hydrogen atoms were not included in the refinement and aliphatic hydrogen atoms were located at calculated positions. CCDC reference number 231760.

[¶]The cell parameters of β-CD·$(H_2O)_{11}$ were determined under the same conditions as those of the β-CD/$CuCl_2$ adduct: $a = 20.910(6)$, $b = 10.057(3)$, $c = 14.888(5)$ Å, $\beta = 109.32(1)°$, $V = 2954(1)$ Å^3 and $R_{int} = 0.056$ at 100 K.

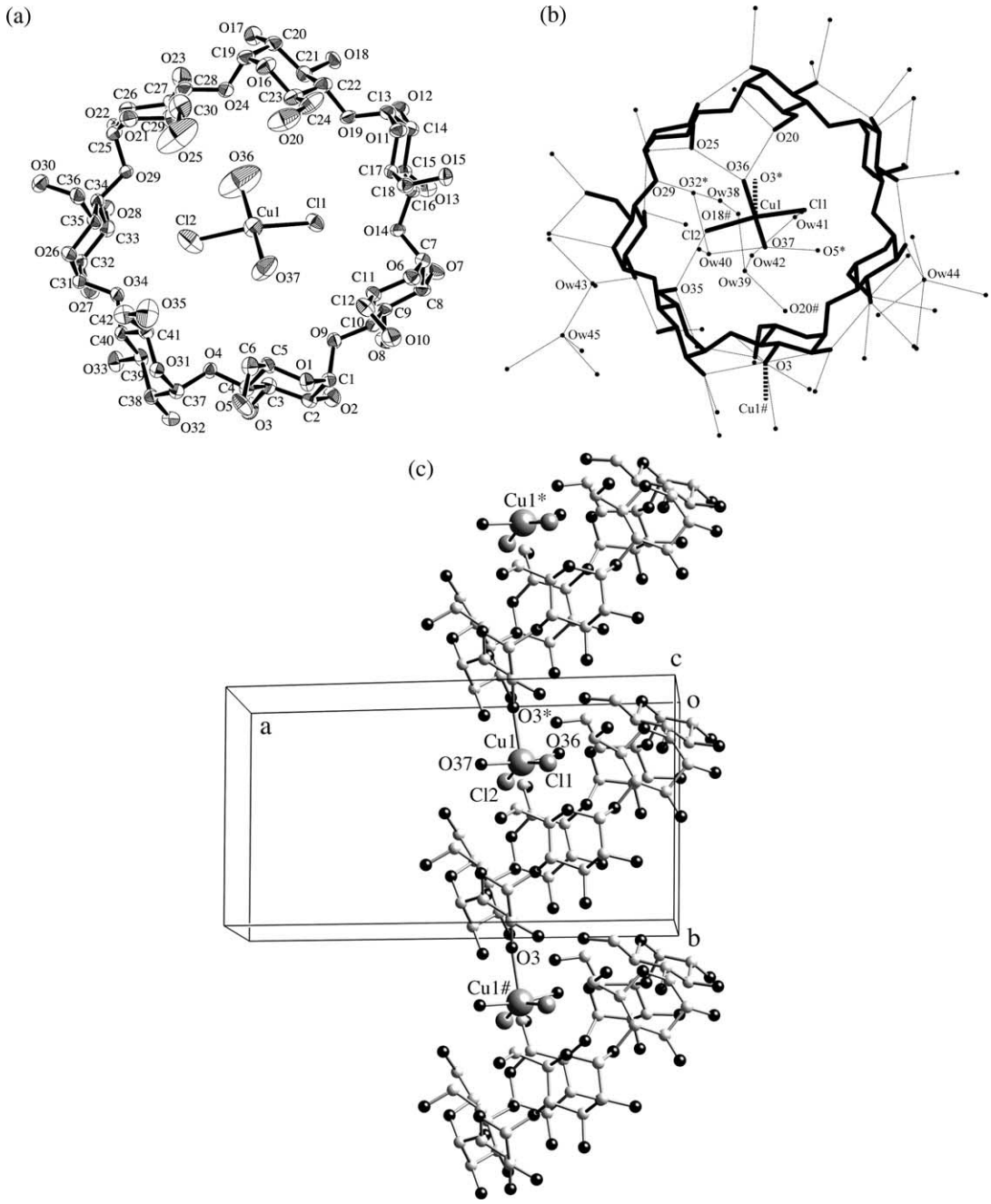

FIGURE 1 (a) ORTEP drawing of β-cyclodextrin·$(CuCl_2)_{0.55}$·$(H_2O)_{10}$ complex with the thermal ellipsoids at the 50% probability level. Uncoordinated water molecules and hydrogen atoms are omitted for clarity. (b) A stick model of β-cyclodextrin·$CuCl_2$ and water molecules (Ow36–Ow45). Selected atoms are labeled. Relatively short intermolecular O- - -O and O- - -Cl distances are indicated as thin lines. The axial coordination bonds, Cu1–O3* and O3–Cu1#, are also shown with broken lines. The symmetry operation codes for * and # are $x, y + 1, z$, and $x, y - 1, z$, respectively. (c) Three repeating units are shown in an infinite chain of β-cyclodextrin·$CuCl_2(H_2O)_2$ along the *b* axis. Cu, large gray circles; Cl, middle gray circles; O, small black circles; C, small gray circles.

1,4-diazabicyclo[2.2.2]octane (DABCO) in water, but so far we have isolated only a 1/1 β-CD·DABCO inclusion complex[§] [18]. The guest DABCO seems to disturb the complexation of β-CD and $CuCl_2$ by reorganization of the hydrogen-bond frame around the β-CD primary-hydroxy bottom.

In summary, we have clarified that the reaction of β-CD with $CuCl_2$ gave the molecular complex β-CD·$(CuCl_2)_{0.550}$·$(H_2O)_{10}$, whose structure is highly isomorphous with that of β-CD·$(H_2O)_{11}$ [15,16]. The $CuCl_2$ moiety is hydrogen-bonded at the rim of the primary-hydroxy side; *i.e.*, the present adduct is

[§]Sekii, M., Ishida, T., Nogami, T., Unpublished results. X-Ray crystallographic analysis of DABCO·β-CD·$(H_2O)_{13}$ gave the following parameters: $C_{48}H_{108}N_2O_{48}$, FW 1481.3, monoclinic, $P2_1$, $a = 15.2981(4)$, $b = 16.4407(3)$, $c = 15.3985(3)$ Å, $\beta = 62.5439(7)°$, $V = 3436.7(1)$ Å^3, $Z = 2$, μ(MoKα) $= 0.129\,mm^{-1}$, $R_{int} = 0.031$, $R(F)(I > 2\sigma(I)) = 0.043$, and $R_w(F^2)$ (all data) $= 0.068$ at $T = 100$ K for 8155 unique reflections.

not a guest-"inclusion" compound but a novel kind of capped CD compound.

Acknowledgements

This work was partly supported by Grants-in-Aid for Scientific Research (Nos. 15073101, 13640575 and 15550115) from the Ministry of Education, Culture, Sports, Science and Technology, Japan.

References

[1] Breslow, R.; Dong, S. D. *Chem. Rev.* **1998**, *98*, 1997.
[2] Tabushi, I. *Pure Appl. Chem.* **1986**, *58*, 1529.
[3] Rizzarelli, E.; Vecchio, G. *Coord. Chem. Rev.* **1999**, *188*, 343.
[4] Reetz, M. T. *J. Heterocycl. Chem.* **1998**, *35*, 1065.
[5] Barr, L.; Easton, C. J.; Lee, K.; Lincoln, S. F.; Simpson, J. S. *Tetrahedron Lett.* **2002**, *43*, 7797.
[6] Wong, Y. T.; Yang, C.; Ying, K. C.; Jia, G. C. *Organometallics* **2002**, *21*, 1782.
[7] Engeldinger, E.; Armspach, D.; Matt, D. *Chem. Rev.* **2003**, *103*, 4147.
[8] Noltemeyer, M.; Saenger, W. *J. Am. Chem. Soc.* **1980**, *102*, 2710.
[9] Betzel, C.; Hingerty, B.; Noltemeyer, M.; Weber, G.; Saenger, W. *J. Inclusion Phenom.* **1984**, *1*, 1811.
[10] Norkus, E.; Grinciene, G.; Vuorinen, T.; Butkus, E.; Vaitkus, R. *Supramol. Chem.* **2003**, *15*, 525.
[11] Matsui, Y.; Kurita, T.; Date, Y. *Bull. Chem. Soc. Jpn.* **1972**, *45*, 3229.
[12] Nair, B. U.; Dismukes, G. C. *J. Am. Chem. Soc.* **1983**, *105*, 124.
[13] Fuchs, R.; Habermann, N.; Klüfers, P. *Angew. Chem. Int. Ed. Engl.* **1993**, *32*, 852.
[14] Klüfers, P.; Schuhmacher, J. *Angew. Chem. Int. Ed. Engl.* **1994**, *33*, 1863.
[15] Zabel, V.; Saenger, W.; Mason, S. A. *J. Am. Chem. Soc.* **1986**, *108*, 3664.
[16] Lindner, K.; Saenger, W. *Carbohydr. Res.* **1982**, *99*, 103.
[17] Liu, Y.; Zhao, Y.-L.; Zhang, H.-Y.; Song, H.-B. *Angew Chem. Int. Ed.* **2003**, *42*, 3260.
[18] Oyama, S.; Miyake, K.; Yasuda, S.; Takeuchi, O.; Sumaoka, J.; Komiyama, M.; Futaba, D. N.; Morita, R.; Yamashita, M.; Shigekawa, H. *Jpn J. Appl. Phys.* **2001**, *40*, 4419.